AEC RESEARCH AND DEVELOPMENT REPORT

ORNL-1943
Progress

HOMOGENEOUS REACTOR PROJECT

QUARTERLY PROGRESS REPORT

FOR PERIOD ENDING JULY 31, 1955

OAK RIDGE NATIONAL LABORATORY
OPERATED BY
UNION CARBIDE NUCLEAR COMPANY
A Division of Union Carbide and Carbon Corporation
UCC
POST OFFICE BOX P · OAK RIDGE, TENNESSEE

DISCLAIMER

ORNL-1943

Contract No. W-7405-eng-26

HOMOGENEOUS REACTOR PROJECT

QUARTERLY PROGRESS REPORT

For Period Ending July 31, 1955

Project Director – J. A. Swartout
Associate Director – C. E. Winters

Homogeneous Reactor Test – S. E. Beall
Thorium Breeder Reactor – R. B. Briggs and J. A. Lane
Corrosion – E. G. Bohlmann
Engineering Development – J. A. Lane
Chemical Engineering Development – F. R. Bruce
Supporting Chemical Research – E. H. Taylor

Compiled by

H. F. McDuffie
D. C. Kelly

DATE RECEIVED BY INFORMATION AND REPORTS DIVISION

(AUGUST 9, 1955)

DATE ISSUED

OCT

OAK RIDGE NATIONAL LABORATORY
Operated by
UNION CARBIDE NUCLEAR COMPANY
A Division of Union Carbide and Carbon Corporation
Post Office Box P
Oak Ridge, Tennessee

HRP QUARTERLY PROGRESS REPORT

SUMMARY

PART I. HOMOGENEOUS REACTOR TEST

1. Construction

Construction of the HRT reactor shield tank was completed, and the inside surfaces were painted. The roof structure for the tank is being assembled in preparation for an acceptance pressure test. Service piping and instrument lines are being installed in the control room area by ORNL craft forces. This work is approximately 50% complete. Fabrication of all low-pressure system components, except the blanket outer storage tanks, has been completed.

A detailed project schedule has been prepared in an effort to coordinate activities of various groups. Manpower estimates covering all construction work necessary for the completion of the reactor show a total of 10,500 man-days required to complete the installation. The project is presently ten working days behind schedule.

2. Design

Approximately 80% of all drawings of the HRT equipment, building, and services have been approved for construction. Drawings approved during the reported quarter include those for fuel and blanket processing piping, cooling water piping, steam and condensate service piping, instrument cubicles, thermal shield, sampling station, line coolers, and pump installation drawings.

Detailed drawings and specifications for prefabrication of high-pressure process piping have been issued to piping fabricators for bids.

3. Reactor Analysis

The effect of fluid circulation upon HRT stability was studied for the case of a slurry blanket containing 1350 g of thorium per kilogram of D_2O. The reactor system was found stable for operating power levels in excess of 10 Mw. If D_2O is used as a reflector material, power levels greater than 100 Mw appear to be permissible.

A study was made of the reaction force arising from rupture of the fuel inlet nozzle of the pressure vessel when the initial pressure and temperature are 2000 psi and 300°C. The maximum upward distance that the pressure vessel could travel would be about 4 ft if no holding force were present. To ensure zero upward movement, a holding force of 50,300 lb is required.

The temperature of the HRT core wall was calculated to be a maximum of 18°F above that of the core fluid when the reactor is operating at 5 Mw with a D_2O blanket.

Estimates of heat generation by radiation absorption in the control room shield wall indicate that no internal cooling is required.

4. Component Development

The HRT fuel mockup pump suffered severe corrosion attack during a run in which leakage occurred around the main pump gasket. The 400A pump has completed 1000 hr of operation at 300°C and 860 hr of operation at 250°C with a solution containing 30 g of uranium per kilogram of water. Some corrosion attack was observed. The 230-gpm blanket prototype pump has operated for 1050 hr on water. Successful water injection at the back of the pump was demonstrated.

New thermal barriers are being made for the HRT fuel and blanket pumps. A new gasket design is being incorporated in the pumps. Parts of all the pumps were inspected at Westinghouse Electric Corporation.

The HRT mockup loop has received 416 hr of operation on uranyl sulfate solution ranging in concentration from 1 to 10 g of uranium per kilogram. The recommended oxygen concentration of 50 ppm was found to be too low to prevent high generalized corrosion rates and uranium precipitation in stagnant regions. Leakage past the Westinghouse pump gasket was another source of trouble. The pump was modified for the next run, which will utilize higher oxygen concentrations.

Fabrication of the HRT heat exchangers was completed. After passing hydrostatic and helium leak tests, the first unit developed leaks during the 50 thermal cycles. With extra precaution and refined welding technique the tube joint welding trouble on the second unit was eliminated. This unit is undergoing acceptance tests.

The initial phase of the HRT dump test, consisting in tests using a single-region system, was completed.

Prototypes of the isolation chamber and sample flask holder were fabricated for testing prior to mocking up a complete sampler station.

Thermal insulation, consisting of multiple aluminum sheets held in place by machined lava spacers, was tested for heat losses and effects of thermal cycles. It was found satisfactory for HRT service.

The HRT reflux condenser-recombiner assembly was tested. The original recombiner design was unsatisfactory because it allowed the production of sharp explosions; alternate designs are being tested.

5. Controls and Instruments

Detailed work on the layout and interconnection of the instrumentation within the control room area of the HRT is 80% complete. This includes complete details for the control panels, the control circuit relay cabinet, and the electrical distribution center and preliminary layout and piping of the instrument cubicles. Design approval was given for the low-pressure, 500-psi, differential pressure transmitters, and construction was started. A prototype liquid-level transmitter was assembled and tested prior to installation on the HRT mockup loop. Preliminary tests indicate satisfactory operation except for possible vibration difficulties. The cylinder-type actuator chosen for the HRT valves was shown to be unsatisfactory; so bellows-type operators will be substituted. A tight seal was obtained between the Stellite No. 6 plug and the type 347 stainless steel seat of a $\frac{1}{8}$-in. sampling valve after 200 operations in tests at 1700 psi and 300°C.

PART II. THORIUM BREEDER REACTOR

6. Reactor Analysis

A comparison of the stability of one- and two-region reactors is reported. Although the one-region reactor appeared to have a greater degree of stability, there appeared to be no distinct advantage of one type over the other, since both normally operate well within the stable region.

It was illustrated that the effect of fluid circulation could be neglected, with relatively small effect upon the stability criteria.

The TBR and similar high-power-density reactors have stable-type behavior, as do low-power-density one-region reactors.

The effect of slurry settling on reactivity in large one-region thorium breeder reactors was studied under the assumption that the reactor would remain a thermal critical assembly. It appeared that, for reactors of economic interest, the assembly would become subcritical upon slurry settling.

Neutron losses due to the use of platinum as a protective coating for a zirconium core tank were estimated. At a flux of 10^{15} neutrons/cm^2/sec, a minimum platinum cross section of 3.7 barns (2200 m/sec) would be reached in about 14 years. The average cross section over a ten-year period would be about 5 barns, representing, for a 10-mil platinum layer, a loss of 0.02 in the TBR breeding gain. At 10^{15} flux about 5% of the platinum would be converted to mercury in three years, and in eight years about 10% would be transformed.

An economic study of partial fuel costs for one-region plutonium-uranium reactors was completed. Where possible, the process characteristics and cost factors were the same as those used in a previous study of one-region thorium breeder reactors. The minimum partial-fuel-cost reactor was found to be about 12 ft in diameter, operating with about 225 g of uranium per liter, 2 g of fissionable fuel per liter, and giving a conversion ratio of 0.84 for a chemical processing cycle of 138 days. If $\eta(41)$ were 2.4, the partial fuel cost would be about 0.1 mill/kwhr higher than that for one-region thorium breeder reactors; if $\eta(41)$ were 1.9, the partial fuel cost would be about 0.7 mill/kwhr higher. The cost of power appeared to be increased by about 0.1 mill/kwhr when resonance absorption of neutrons by plutonium isotopes was included in the calculations.

7. Engineering Studies

The design concept of a 300-electrical-megawatt thorium breeder power station utilizing low-pressure gas recombination was completed. The construction and operating costs were estimated on the assumptions that a breeding gain of 0.11 would be achieved and that the maintenance of the reactor plant would not differ in unit cost from that of large modern steam plants. The total plant investment was calculated to be about $60,300,000, or a unit cost of $201 per kilowatt of installed capacity. For an assumed plant factor of 0.8 the unit cost of power was calculated to be 6.2 mills/kwhr.

Several basic design questions which became apparent during the study will have to be resolved before the design can be considered practical. The mathematical analysis of the reactor kinetics

should be extended to define the operating limitations which must be designed into the reactor from the standpoint of safety in the event of certain types of misoperation or equipment failure. A maintenance procedure must be worked out which will permit repair or replacement of failing equipment without extensive shutdown periods if the assumed plant factor is to be realized. Adequate operating experience with certain new types of equipment must be obtained to show that they work as intended. Additional information must be developed on the fission-product disposal problem and on boiler feed-water treatment under conditions of oxygen generation and exposure to radiation.

Thus, although the design study and cost estimate confirm previous studies with respect to plant size, building costs, and installation of the more conventional equipment, considerable essential engineering information must be obtained before a practical plant can be defined.

The thermal stress problem encountered in layout of the piping configurations of the main circulating loops led to a general analytical solution to the three-plane piping problem; this was coded for the Oracle.

The modification of the TBR, case A, from low-pressure to high-pressure recombination, referred to as case B, was started. Changes in component design and plant layout are being studied so that a more easily maintainable plant can be designed. Since the core vessel might have to be replaced before the reactor pressure vessel, two designs of large, high-pressure closures are being studied in an attempt to design a reactor with a removable core.

PART III. CORROSION

8. Pump-Loop Corrosion Tests

8.1 Pump-Loop Operation and Maintenance. – Operation of 12 dynamic-corrosion test loops proceeded in a routine manner with no significant changes or difficulties during the report period.

Initial dynamic-corrosion tests were made with thorium oxide slurries. Loop runs with thorium oxide slurries containing nominal concentrations of 250, 500, and 1000 g of thorium per kilogram of water at temperatures of 250 and 300°C were completed. Some difficulties were encountered in maintaining equilibrium and theoretical thorium concentrations in the loop system.

8.2 Results of Loop Tests with Solutions. – During the past quarter additional corrosion results were collected, all of which are reported in tabular form. The previously reported finding, that the addition of a soluble sulfate salt to uranyl sulfate solutions reduced their corrosiveness, was substantiated. In addition, it was found that a solution 1.34 *m* in uranyl sulfate and 1.34 *m* in lithium sulfate was phase-stable to at least 315°C. Preliminary results indicated that such a solution was less corrosive at 300°C than had been expected.

Three long-term runs, one each at 200, 250, and 300°C, in which 0.04 *m* uranyl sulfate, 0.005 *m* copper sulfate, and 0.006 *m* sulfuric acid is being circulated, were continued. The average corrosion rate in all cases was low, less than 0.1 mpy. However, at 250 and 300°C the solutions were not completely stable; slow losses of both uranium and copper from solution were noted, accompanied by a pH decrease. An attempt to remedy the situation was made by increasing the concentration of sulfuric acid in the solution.

Studies concerning the effect of Cr(VI) on the corrosion of stainless steel by uranyl sulfate solutions were continued. While the results showed qualitatively that chromium accelerated attack on the film-free metal, the results lacked quantitative significance.

8.3 Results of Loop Tests with Thoria Slurries. – Slurries were circulated in loop CS for the first time during the past quarter. Generally the concentration of thoria in the slurry was less than had been expected, which indicated that some of the oxide was retained in the system. The corrosion data that were collected are shown in tabular form.

8.4 Sedimentation Characteristics of Thorium Dioxide Slurries at Elevated Temperatures. – Sedimentation rates of thoria slurries were determined over the temperature range of 100 to 300°C. From these data the apparent particle diameters were estimated by using two different methods of calculation.

9. Radiation Corrosion

9.1 In-Pile Loop. – Two in-pile loops, EE and L-4-8, were completed during the past quarter. The operation of loop EE for radiation corrosion studies in the LITR beam hole HB-4 installation was completed. Following removal of loop EE, loop L-4-8 was installed in beam hole HB-4. Loop L-4-8 contained additional stressed specimens of stainless

steel, Zircaloy-2, and titanium, exposed to both the vapor and the liquid phases in the loop pressurizer.

An in-pile loop, for operation at 300°C and 2000 psi in beam hole HB-2, is under construction. The construction of this loop is proceeding along with construction of the replacement loop for L-4-8 in beam hole HB-4.

The circulating pumps for use in in-pile loops were redesigned to include "outboard" bearings for improved reliability. Bearing and journal material is pure sintered aluminum oxide.

During the past quarter, work was continued with an experimental in-pile slurry loop in an attempt to develop a loop assembly acceptable for in-pile operation with thorium oxide slurries. Additional runs were made with slurries of several thorium oxide concentrations, and several revisions were made to the loop design in an attempt to achieve satisfactory operation.

The third in-pile loop experiment, GG, was completed. This experiment, designed primarily for the determination of the corrosion of Zircaloy-2 under irradiation, was, in many respects, a duplicate of the previous Zircaloy-2 experiment with loop FF. Operating conditions differed from those of the previous loop in that the period of exposure to radiation and the level of radiation were both greater for loop GG. In-pile operation of the loop was for a period of 981 hr, of which approximately 897 hr was with the LITR at 3 Mw. The fission power generated in the loop, with the LITR at 3 Mw, was approximately 800 w as determined by cesium analysis. The generalized corrosion rate, indicated by oxygen consumption and the increase in nickel concentration, decreased from 7.3 mpy for the early portion of the run to 0.5 mpy in the latter portion. As before, the core coupons were attacked appreciably, and the extent of the attack increased with increasing power density. There is some indication, however, that the radiation effect levels off at the higher power densities. The highest corrosion rate measured was about 3.5 mpy, based on radiation time, at a power density of about 4.8 w/ml.

9.2 LITR Bomb Tests. – The main objective of the LITR bomb experiments has continued to be that of characterizing the radiation effect on the corrosion of Zircaloy-2 by uranyl sulfate solution. Three in-pile exposures of Zircaloy bombs were completed, and a fourth is in progress. An in-pile bomb experiment with stainless steel was also completed.

One of the Zircaloy-2 experiments was a determination of the effect of copper concentration on the radiation-induced corrosion. The solution was made 0.007 *m* in $CuSO_4$ rather than 0.02 *m* as had been the practice for most of the previous Zircaloy-2 experiments. No effect of copper concentration was apparent from the results.

Another Zircaloy-2 experiment was designed as a determination of the effect of temperature on the radiation-induced corrosion. One Zircaloy-2 bomb was exposed at four different temperatures: 225, 250, 280, and 290°C. This exposure was started at the lowest temperature and concluded with the highest. The corrosion rate indicated by the oxygen data approximately quadrupled in going from 225 to 290°C. A straight line was obtained when the logarithm of the corrosion rate at a given temperature was plotted against the reciprocal of the absolute temperature. An activation energy of 12,000 cal/mole for the corrosion reaction was indicated by the data.

The Zircaloy-2 experiment now in progress in beam hole HB-5 uses depleted uranium. The fission power in the solution is negligible. The power from absorption of gamma rays and fast neutrons is estimated at 0.5 w/ml. At 250°C the oxygen data indicated a corrosion, during exposure, of 1 to 2 mpy. Exposures at 280°C and at 300°C are in progress.

The stainless steel experiment was the first of several which are planned to determine the effects of excess H_2SO_4 on the corrosion of type 347 stainless steel by uranyl sulfate solution under irradiation. The solution employed was 0.015 *m* in H_2SO_4. Other experimental conditions, with the exception of the pressure of oxygen, were the same as those employed in the great majority of stainless steel bomb tests which have been carried out in the past. This bomb was charged with an initial oxygen pressure of about 1100 psi at temperature. Previous tests, with few exceptions, employed an initial pressure of about 250 psi. The radiation corrosion rate after 900 Mwhr of LITR operation was approximately 1 mpy. No marked "breakaway" was observed, in contrast with previous stainless steel experiments (containing no excess acid and a relatively slight excess of oxygen), which showed a rapid increase in corrosion rate after one to seven days of irradiation. The experiment was

terminated after about 1250 Mwhr because of a plugged capillary.

9.3 MTR Bomb Tests. – The first rocking-bomb experiment at the MTR was completed successfully. The bomb was of Zircaloy-2, and the solution was 0.04 *m* in UO_2SO_4 (1.7% enrichment), 0.05 *m* in $CuSO_4$, and 0.02 *m* in H_2SO_4. The exposure temperature was about 280°C. The estimated fission power density at the exposure temperature was 0.5 w/ml. The results of the experiment are being analyzed and correlated.

9.4 Van de Graaff Accelerator Tests. – Experimental studies were undertaken with regard to the effect of fast-electron irradiation on the corrosion of Zircaloy-2 by uranyl sulfate solutions. The equipment and techniques employed in this study are of the type previously used and reported by Hochanadel and Ghormley for a similar study of stainless steel. The equipment was placed in proper working condition, and preliminary irradiations were made.

10. Laboratory Corrosion Studies

Type 347 stainless steel was protected effectively against stress-corrosion cracking in an aggressive medium when it was coupled with carbon steel.

The titanium alloys A-110-AT and C-130-AM, considered for HRT core bolt service, showed acceptable corrosion behavior in simulated HRT fuel solution at 100, 250, and 300°C.

No stress-corrosion cracking of type 347 stainless steel, titanium 75A, or Zircaloy-2 was noted in HRT and in-pile loop environments in a variety of extended tests, in which temperatures ranged from 100 to 300°C.

Highly stressed specimens of partially hardened type 17-4 PH stainless steel showed no evidence of stress-corrosion cracking after 2000 hr of exposure in simulated HRT fuel solution at 100, 250, and 300°C.

Pure sintered aluminum oxide was substantially unattacked by 0.17 *m* UO_2SO_4 solution at temperatures up to 300°C.

Type 347 stainless steel and titanium 75A showed no localized attack at the water line in extended tests at 250 and 300°C in oxygenated 0.005 to 1.3 *m* UO_2SO_4 solutions.

Coupling of type 347 stainless steel with titanium 75A or Zircaloy-2 in boiling 5% HNO_3 did not affect the corrosion rate of these materials, all rates being below 0.2 mpy. Uncoupled partially hardened type 17-4 PH stainless steel corroded at about 1 mpy in this medium.

Gold-plated Iso-Elastic spring alloy was too severely pitted to be useful in boiling 0.17 *m* UO_2SO_4 solution.

The effect of sulfate additions to thorium oxide on the corrosion of type 347 stainless steel, titanium 75A, and Zircaloy-2 by circulating aqueous thoria slurries was studied, with the use of toroids. Additions of thorium sulfate up to 10,000 ppm sulfate (ThO_2 basis) to D-17 thorium oxide (ORNL Thorex product, oxalate precipitated, 650°C calcined) or Lindsay No. 8 oxide (Lindsay Chemical Co., oxalate precipitated, 900°C calcined) at slurry concentrations of 500 to 1000 g of thorium per kilogram of water produced no significant change in the corrosion rates of type 347 stainless steel at 250°C, 26 fps relative slurry velocity, and 100 psi oxygen pressure as long as the pH remained at approximately 4 or higher. Additions of calcium, magnesium, or sodium sulfates at the 1000-ppm sulfate level to slurries of 500 g of thorium per kilogram of water also gave no significant change in the corrosion rate from that obtained without the sulfate additions. Titanium and Zircaloy-2 were essentially unaffected under all the conditions studied.

The rate of attack of type 347 stainless steel, titanium 75A, and Zircaloy-2 by circulating aqueous thoria slurries appeared to be determined by the particle size of the thorium oxide as well as by its calcination temperature. Thus a high-fired (1600°C) small-sized thoria slurry gave a lower average corrosion rate for these three metals than a low-fired (650°C) larger-sized thorium oxide slurry. This particle-size influence on the corrosion rate should permit the use of higher fired thoria slurries, which may be desirable because of their improved handling.

PART IV. ENGINEERING DEVELOPMENT

11. Development of Fuel-System Components

In the Foster Wheeler Corp.–ORNL heat exchanger development program, the design of U-tube, 50-Mw exchangers was completed; as a result of studies of larger exchanger designs, design of straight-through 50-Mw units will be investigated. Feasibility of 300-Mw capacity exchangers was established; the most promising design appeared to

be one employing welded, all-stainless-steel construction for the exchanger and carbon steel for the steam drum. A method of strength-welding tubes to a tube sheet was developed and was applied to the HRT heat exchangers. Four tubing inspection devices were investigated, and two were selected for a controlled evaluation in which the HRT heat exchanger tubing was used. Seventeen out of 544 tubes were rejected and are being examined.

After modification of the electrolytic cells in the recombiner loop to dilute the hydrogen and oxygen with steam, no further explosions occurred. Stress-corrosion cracking occurred in flanges and welds.

Construction of the dump-valve test loop was completed, and preliminary runs were made with water.

A 20-cfm gas circulator is being designed by the Allis-Chalmers Mfg. Co. Layout drawing, bill of material, and fit dimensions were received and are being studied for possible revisions.

A 5-gpm ORNL pump, converted for use as a gas circulator, operated on saturated steam for 5600 hr at approximately 110 psi. The 2000-psi, 5-gpm canned-rotor pump has now operated for over 1500 hr at 300°C with water. The 1000-psi, 5-gpm canned-rotor pump has operated for about 6900 hr at 250°C with water. In order to increase stator life and pump reliability, one ORNL 5-gpm canned-rotor pump was rewired with the windings in series, rather than in parallel. The pump has accumulated 2350 hr of operation and the test is continuing.

Circulation in the 4000-gpm loop was started on April 20. After 50 hr of operation, the packing in the Milton Roy feed pump was leaking so badly that the loop had to be shut down. Scott and Williams feed pumps were installed in place of the Milton Roy pump.

A program was initiated to study titanium design and fabrication for such components as piping, heat exchangers, etc. A preliminary inquiry was sent to several industrial firms, and replies were received from eight interested firms.

12. Development of Blanket-System Components

A study of the effect of temperature and slurry concentration on the attack by ThO_2 slurry on type 347 stainless steel, zirconium, and titanium was started and is now two-thirds completed.

ORNL 5-gpm pumps are being modified to make them more usable in small slurry-circulating loops.

The Westinghouse 200-gpm slurry pump was successfully operated for 234 hr at 300°C with ThO_2 slurry at a concentration of 500 g of thorium per kilogram of H_2O.

A bypass stream to the top of the pressurizer was found to maintain automatically the concentration of the slurry in a circulating loop.

No method has been proved for keeping the solids suspended in full-size horizontal dump tanks. In a small model, bubbling steam through a sintered stainless steel plate on the bottom of the tank resuspended settled slurry and maintained the suspension but also introduced a foaming problem.

A method of characterizing the flow properties of ThO_2 slurries, regardless of concentration, was proposed.

It was found that the yield stress for some ThO_2 slurries increased as the temperature increased from 25 to 75°C.

The slurry blanket mockup system is now expected to be completed by October 1.

Based partly on previous analyses, it was concluded that 8 to 10 kw/liter can be removed as steam from a boiling system which is 10 ft high and operated at 1000 psi with a vapor fraction of 0.3. At 2000 psia, a similar system would release 15 to 20 kw/liter.

13. Metallurgy

Results of stress-corrosion tests on austenitic stainless steels in boiling 42 wt % magnesium chloride solutions showed a direct relationship between austenite stability and resistance to transgranular cracking. Threshold stresses, below which this type of failure is highly improbable, were established tentatively for types 309 SCb and 310 steel. Dynamic-corrosion tests have confirmed previous observations that, relative to the as-welded condition, a 1000°F heat treatment is beneficial and that a full anneal at 1850 to 1950°F is detrimental to the corrosion resistance of type 347 stainless steel welds exposed to uranyl sulfate solutions. Sigma-phase alloys of iron and chromium and of iron, chromium, and nickel appeared to have less corrosion resistance in uranyl sulfate solutions than ferrites of the same composition. Cathodic treatments of 100-hr duration of Zircaloy-2 in 1 *N* sulfuric acid at 30°C and 10 ma/cm^2 resulted in no change in hydrogen content, while similar treatments at 250°C raised the hydrogen content to 130 to 170 ppm.

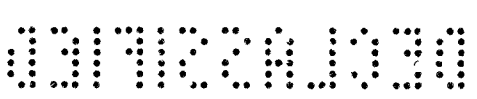

Impact tests on Zircaloy-2 specimens from in-pile loop run GG were completed. All specimens fractured completely when tested, and the impact energy values recorded at the higher testing temperatures were appreciably lower than those obtained with specimens from previous in-pile loop runs. Samples of impact specimens from run GG were analyzed for hydrogen content, and no evidence of hydrogen absorption was found.

Tests on specimens of stainless steel and carbon steels irradiated by integrated fast-neutron fluxes of 10^{19} and 10^{20} proved that the mechanical properties of both types of steel are changed appreciably by such irradiation, especially by irradiation to 10^{20} nvt. Further work is needed to determine whether fast-flux irradiations anticipated in proposed reactors will produce dangerous embrittlement in ordinary pressure-vessel steel.

PART V. CHEMICAL ENGINEERING DEVELOPMENT

14. ThO_2 Slurry Development

Slurries of thorium oxide, prepared by thermal decomposition of the oxalate at 650 and 900°C, respectively, were irradiated at 300°C in the LITR for 288 and 115 hr without apparent change in properties. A 650°C preparation, irradiated for six days in the Graphite Reactor at 300°C, also showed no apparent change. Difficulties were encountered in stirring the slurries under irradiation in the standard irradiation bomb, but a slurry of 900°C oxide was stirred at 300°C in an improved model of the dash-pot-stirred bomb in the LITR for one week without interruption.

A slurry of Thorex product oxide containing 0.09 *m* $CuSO_4$ combined stoichiometric oxygen with 2 moles of hydrogen per hour per liter of slurry at 284°C and at a hydrogen partial pressure of 500 psi. The addition of acid or the use of Ames oxide rather than Thorex product oxide increased the combination rate. Silver was a much more active catalyst than copper. A slurry containing 0.02 *m* silver combined 35 moles of hydrogen per hour per liter of slurry at 270°C and the same partial pressure. A slurry of mixed oxide, 99.5% ThO_2–0.5% UO_3, with 0.01 *m* silver gave a combination rate of 19 moles of hydrogen per hour per liter of slurry at 280°C and at a hydrogen partial pressure of 500 psi. The addition of 5000 ppm of sulfate to the mixed oxide decreased the combination rate by a factor of 2. The silver, in contrast to the copper sulfate, acts as a true heterogeneous catalyst.

In laboratory studies of the properties of thorium oxide, prepared by thermal decomposition of the oxalate, the particle size and shape depended on the oxalate precipitation temperature. The x-ray crystallite size increased, and the nitrogen adsorption surface area decreased, with increasing calcination temperature and time. The crystallite size and the surface area were related to each other. Sintering between particles did not take place to any noticeable extent up to 900°C.

The crystallite particle sizes of oxides calcined at 650, 750, 900, or 1000°C were unaffected by wet-autoclaving at 300°C, with 0, 200, 500, 1,000, 2,500, 5,000, or 10,000 ppm of sulfate both in the presence and absence of 0.005 *m* $Na_4P_2O_7$. The supernatant pH's decreased with increasing sulfate concentration. At any one sulfate concentration the density of settled solids increased with the firing temperature of the original oxide, the effect being much more pronounced in the presence of the pyrophosphate. The settled solids density observed for any one oxide depended primarily on pH rather than on additive concentration, and a minimum in settled density was observed for all oxides between pH 6 and 9.

Oxides pumped as slurries at high temperature or degraded dry at room temperature in a Micronizer reached essentially the same particle size. Only a slight increase in surface area was observed in the sample which had been "micronized," indicating that the surface areas measured by nitrogen adsorption were mainly internal.

15. Fuel Processing

The HRT chemical plant will treat the reactor fuel continuously by centrifugally removing suspended insoluble fission and corrosion products, and by adsorbing, on the hot surface of a feed preheater, those fission and corrosion products which have demonstrated a tendency to precipitate and to adsorb on hot metallic surfaces in current loop tests. Periodically, the centrifuged solids and those deposited on the hot surface will be combined, dried to recover the heavy water, and transported in a shielded carrier to a solvent extraction facility for recovery and decontamination of the associated uranium.

Fabrication and installation of the chemical processing equipment are scheduled for completion

by June 1956, with full-scale startup on reactor fuel scheduled for September 1956.

The solubility of neodymium sulfate in 0.02 *m* UO_2SO_4–0.005 *m* H_2SO_4 was 25 to 30 mg per kilogram of H_2O at 292 to 295°C when a mixture of rare-earth sulfates was being precipitated. Increasing the uranyl sulfate concentration increased the amount of neodymium sulfate retained in solution. From simulated fuel solutions containing only neodymium sulfate, and this in excess of 250 mg per kilogram of H_2O, the solid phase that separated upon heating was identified as $Nd_2(SO_4)_3 \cdot H_2O$. From solutions containing 150 mg or less of neodymium sulfate per kilogram of H_2O, the solid phase was tentatively identified as $Nd_2(SO_4)_3 \cdot 3UO_2SO_3 \cdot 10H_2O$.

Reduction of I^{5+} to I^0 was pronounced in aqueous solution exposed to Co^{60} gamma radiation at room temperature. This reduction was increased by the addition of sulfuric acid and/or copper sulfate to the solution but was depressed by the presence of uranyl sulfate.

Results of studies of the behavior of neodymium sulfate as a representative rare-earth fission product in high-pressure loops confirmed the tendency of the neodymium to adhere to metal walls that are at a higher temperature than the bulk solution flowing past. However, most of the precipitated neodymium did not adhere tightly to the hot walls. In one run, over 50% of the neodymium which precipitated in the loop preheater was withdrawn in solution samples taken from the preheater exit line. These results indicate that a heater followed by a hydroclone, as in the HRT chemical plant, should be effective in removing rare-earth fission products from the reactor system.

Neodymium sulfate precipitated in a loop that had no metal walls hotter than the solution failed to remain suspended in the circulating stream for more than a few hours. The reason for this is not known; however, tests with dilute slurries of ThO_2 (which has comparatively a very low solubility) under these conditions gave the same result. When $Nd_2(SO_4)_3$, ThO_2, or Fe_2O_3 solids were known to be suspended in the loop circulating stream, a 0.4-in.-dia hydroclone was effective in concentrating them.

Hydroclone development and parameter studies were completed, and dimensions for a hydroclone for the HRT Chemical Processing Plant were specified. Both stainless steel and titanium-lined hydroclones showed serious corrosion when they plugged. However, the corrosion resistance of a titanium-lined hydroclone was satisfactory as long as the hydroclone was operating properly.

16. Plutonium-Producer Blanket Processing

Adsorption of plutonium on titanium and Zircaloy-2 from 1.26 *m* UO_2SO_4 at 250°C was dependent on the concentration of the plutonium in the solution. After 2 liters of 1.26 *m* UO_2SO_4, containing 100 mg of plutonium per kilogram of H_2O, had passed over titanium at 250°C, a metal sample located at the solution inlet had adsorbed 0.16 mg of plutonium per square centimeter. Metal at the solution exit (solution depleted in dissolved plutonium by both adsorption and PuO_2 precipitation) had adsorbed only 0.03 mg/cm^2. Similar results were obtained when 1 liter of this solution was passed over Zircaloy-2 at 250°C. Metal at the solution inlet adsorbed 0.13 mg of plutonium per square centimeter, and metal at the outlet adsorbed only 0.013 mg/cm^2. The adsorption at the solution inlet was considerably above the saturation value of 0.05 mg/cm^2 on zirconium (not Zircaloy-2) determined in static solutions. Adsorption of plutonium on titanium and Zircaloy-2 was not uniform; small areas adsorbed large amounts of plutonium. However, as more plutonium was adsorbed, the metal surfaces became completely covered with plutonium. Adsorption of plutonium on type 347 stainless steel was erratic; no adsorption was found on the black corrosion film but occasional adsorption was noted on metallic areas from which the corrosion film had flaked.

Plutonium material balances through the hydroclone varied from 50 to 85%. It was encouraging to note that PuO_2 was always concentrated in the underflow. Concentration factors varied from 2 to 8.

Results of two irradiation experiments in the LITR, in which a solution of depleted uranyl sulfate was used, indicated the solubility of plutonium to be 0 to 10 mg per kilogram of H_2O at 250°C. These experiments were made with 1.26 *m* UO_2SO_4 solutions contained in a titanium bomb in one case and in a Zircaloy-2 bomb in the other. The PuO_2 precipitate carried about 10% of the neptunium. Adsorption of plutonium on a titanium surface of the irradiation bomb slightly cooler than the uranyl sulfate was 1.2 μg/cm^2 and on a titanium surface slightly hotter than the solution, adsorption was 2.1 μg/cm^2.

17. Thermal-Breeder Blanket Processing

Although protactinium apparently is bound within the irradiated ThO_2 particles, 94% of it was leached from 15 mg of ThO_2 (prepared by calcination at 650°C) by refluxing with 14 *N* H_2SO_4 for 2 hr and washing with hot 14 *N* H_2SO_4. The percentage of protactinium removed decreased as larger amounts of ThO_2 were leached. When 4.8 g of ThO_2 was refluxed in 14 *N* H_2SO_4 for 2 hr, only 50% of the protactinium was leached. This procedure converts most of the ThO_2 to $Th(SO_4)_2$; however, the solubility of $Th(SO_4)_2$ in 14 *N* H_2SO_4 at 90°C is only 0.008 to 0.012 mg/ml.

The sulfate content of the leached thorium oxide was reduced from 34 to 0.12% by calcining in air at 900°C for 16 hr. Sulfate removal is markedly dependent upon calcination temperature. When a residue was calcined for 2 hr, the sulfate content was reduced from 14.9 to 0.56% at 870°C but to only 7.8% at 700°C.

18. Summary of Work of Vitro Laboratory

The mole fraction of iodine in the vapor above 0.02 *m* UO_2SO_4–0.005 *m* H_2SO_4 was five times larger than in the liquid at 300°C and decreased as the pH of the liquid phase increased. Mass transfer rates ranging from "0.9 to 2.2 gram moles I_2/(min)(cm^2)(g I_2/kg H_2O)" were reported by Vitro. Garnet sand in contact with simulated fuel solution at 300°C held the cerium solubility to 0.006 g per kilogram of H_2O. Preliminary process design work for an iodine removal process is under way.

PART VI. SUPPORTING CHEMICAL RESEARCH

19. Aqueous Systems at Elevated Temperatures

19.1 Alkaline Carbonate – Uranium Trioxide Systems at 250°C. – Preliminary solubility data for the systems Na_2O-UO_3-CO_2-H_2O, Li_2O-UO_3-CO_2-H_2O, and MgO-UO_3-CO_2-H_2O were obtained at 250°C and up to approximately 1000 psi CO_2 pressure. On the basis of these data some deductions about the solid phases in equilibrium with the solutions were made, and tentative phase diagrams are presented. In addition, the order of magnitude of the solubility of UO_3 or UO_2CO_3 as a function of CO_2 gas pressure and temperature is given.

19.2 The Base-Saturated Region of the System CuO-UO_3-SO_3-H_2O at 100°C. – Study of the solid-liquid phase equilibria in the four component system CuO-UO_3-SO_3-H_2O at 100°C in the region in which the liquid is base-saturated was nearly completed. Data embracing all but a small uranium-rich region of the phase diagram from total salt concentrations as low as about 4% up to salt concentrations of about 25% are presented.

19.3 Phase Volumes in the Two-Liquid-Phase Region of the System UO_3-SO_3-H_2O. – The volumes of the liquid and vapor phases of 0.25, 0.50, 1.00, 2.00, and 3.00 *m* uranyl sulfate solutions were measured over the temperature range from 25 to 400°C at several values for the fractional filling from about 0.25 to about 0.60. Typical curves showing the relative volumes of the phases as a function of temperature are given and discussed.

19.4 Colloidal Thorium Oxide as a Reactor Blanket. – The factors involved in stabilizing a colloidal sol of thorium oxide for use in a reactor blanket are discussed. Experimental work directed to finding the conditions for maximum stability was initiated.

19.5 Adsorption of Water by ThO_2. – Measurements, at several temperatures between 150 and 360°C, of the unsaturated steam pressure of one sample of deaerated ThO_2 and water were completed. The data indicate the probable occurrence of a slow, irreversible decrease in active surface area at 360°C.

20. Adsorption on Inorganic Materials

Study of adsorption by inorganic materials from the point of view of ion exchange was continued. Adsorption of Hg(II) in 0.1 *M* HCl on the anion exchanger, zirconium hydroxide, was demonstrated. Effect of variation in preparative technique on adsorption by the cation exchanger, zirconium tungstate, was investigated. Under certain conditions, exchange on both cation and anion exchangers was found to approximate closely ideality, but a pronounced loading effect was found for zirconium tungstate. Separations of several of the alkalies and of Co(II) from Fe(III) were demonstrated on zirconium tungstate and zirconium phosphate.

21. Radiation Studies on Thorium Nitrate Solutions

The molecular nitrogen yield from the radiation decomposition of thorium nitrate solutions was found to be independent of temperature between 130 and 250°C. The reduction of nitrate ion to nitrite in sodium nitrate solutions was strongly pH dependent – the yield increasing markedly as the solution became more basic. The molecular nitrogen yield from 5 *M* $NaNO_3$ was independent of pH between 0.5 and 11.0.

CONTENTS

Part I

HOMOGENEOUS REACTOR TEST

S. E. Beall

1. CONSTRUCTION

S. E. Beall

J. J. Hairston P. N. Haubenreich S. I. Kaplan

1.1 REACTOR SHIELD TANK

Construction of the reactor shield tank, in which the reactor components will be installed, proceeded at a rapid pace during the past three months. The subcontractor completed the tank assembly and the reinforcement of the roof support columns. Approximately 500 service and instrument lines were welded through the walls of the tank, and all metal surfaces inside the tank were sandblasted and covered with five coats of Amercoat No. 74 to prevent corrosion of the permanently installed steel. This coating was chosen for its ability to withstand exposure to the environment (10^5 r/hr, 140°F, and high humidity). A photograph of the tank after it was painted is presented in Fig. 1.1. Figure 1.2 is a view of part of the inside surface of the north wall and shows a few of the many penetrations.

Fabrication of the roof beams and shielding slabs was completed, and the parts are being assembled in the tank prior to the performance of a pressure test of the entire tank structure. The tank will be subjected to successively increasing internal pressures, and data obtained from strain gage measurements will be used to estimate the

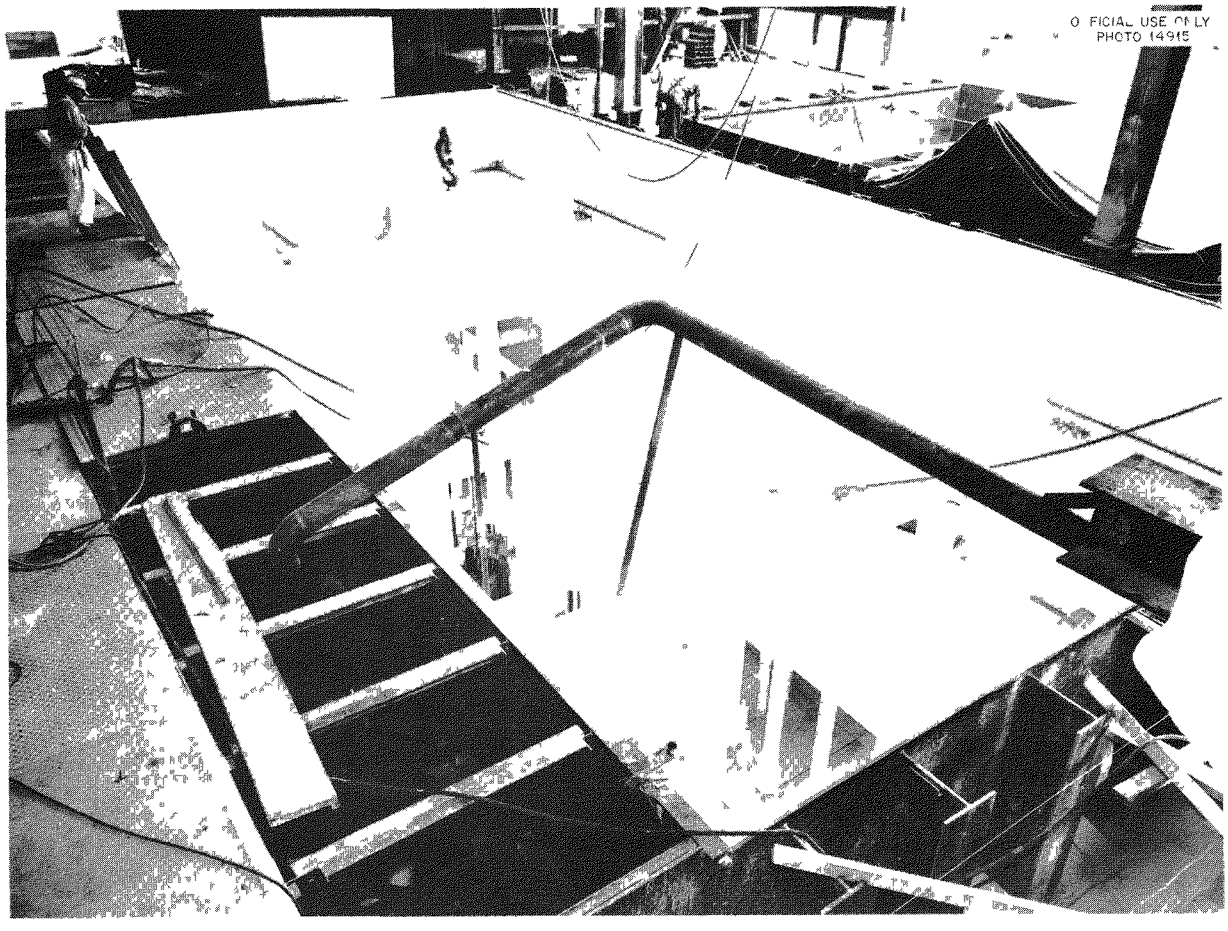

Fig. 1.1. Reactor Tank, Looking Southwest.

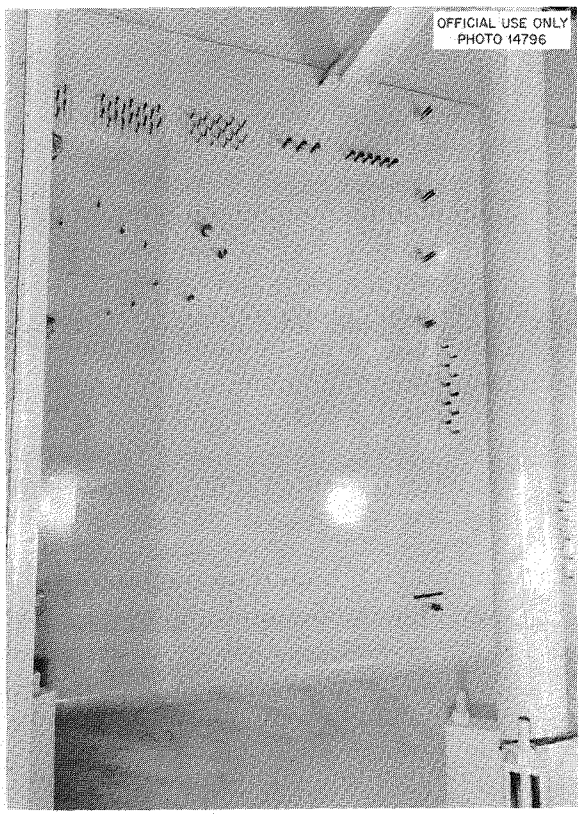

Fig. 1.2. North Wall of Reactor Tank, Showing Service-Pipe Penetrations.

maximum internal pressure which the tank can contain without rupturing. This test will be made prior to the installation of reactor components.

1.2 CONTROL ROOM AREA

ORNL craft forces are responsible for the installation of all equipment within the control room area. At the present time, approximately 75% of the service piping within this area has been completed. A portion of the cooling water feed station is shown in Fig. 1.3. Figure 1.4 is a photograph of a part of the control room side of the north wall of the reactor shield; it shows a group of air feed and exhaust lines for the remote valve motors. The auxiliary and main control panels were mounted, the electrical load center was installed, and the thermocouple scanning system was completed in other areas of the control room.

1.3 REACTOR COMPONENTS

Fabrication of all low-pressure system components, except the blanket outer storage tanks, was completed. Shop attention is now being given to the preassembly of the components and to the prefabrication of interconnecting lines and coolers. Figure 1.5 is a photograph of the completed low-pressure fuel assembly prior to its installation for operational testing. Contained in this assembly are the fuel dump tanks and evaporators, recombiner, off-gas condenser, and cold traps. An assembly of this type is also being prepared for the blanket system.

The status of high-pressure piping and components is reported in Sec. 2.3.

1.4 JOB SCHEDULING

In an effort to coordinate better the activities of the various groups concerned with design, development, procurement, fabrication, and installation, a detailed work schedule was prepared to cover the period from June 1955 through May 1956. This schedule is especially detailed with respect to shop and field craft work. According to estimates made from drawings in the 90% complete stage, approximately 3000 man-days will be required to complete the shop work at ORNL, and 7500 man-days will be required for installation of all reactor components and services. As planned on the master schedule, all this work is to be completed in March 1956. At the present time, 18% of the 10,500 man-days have been completed, whereas the schedule called for a 23% completion. Thus, the over-all work is approximately ten working days behind schedule.

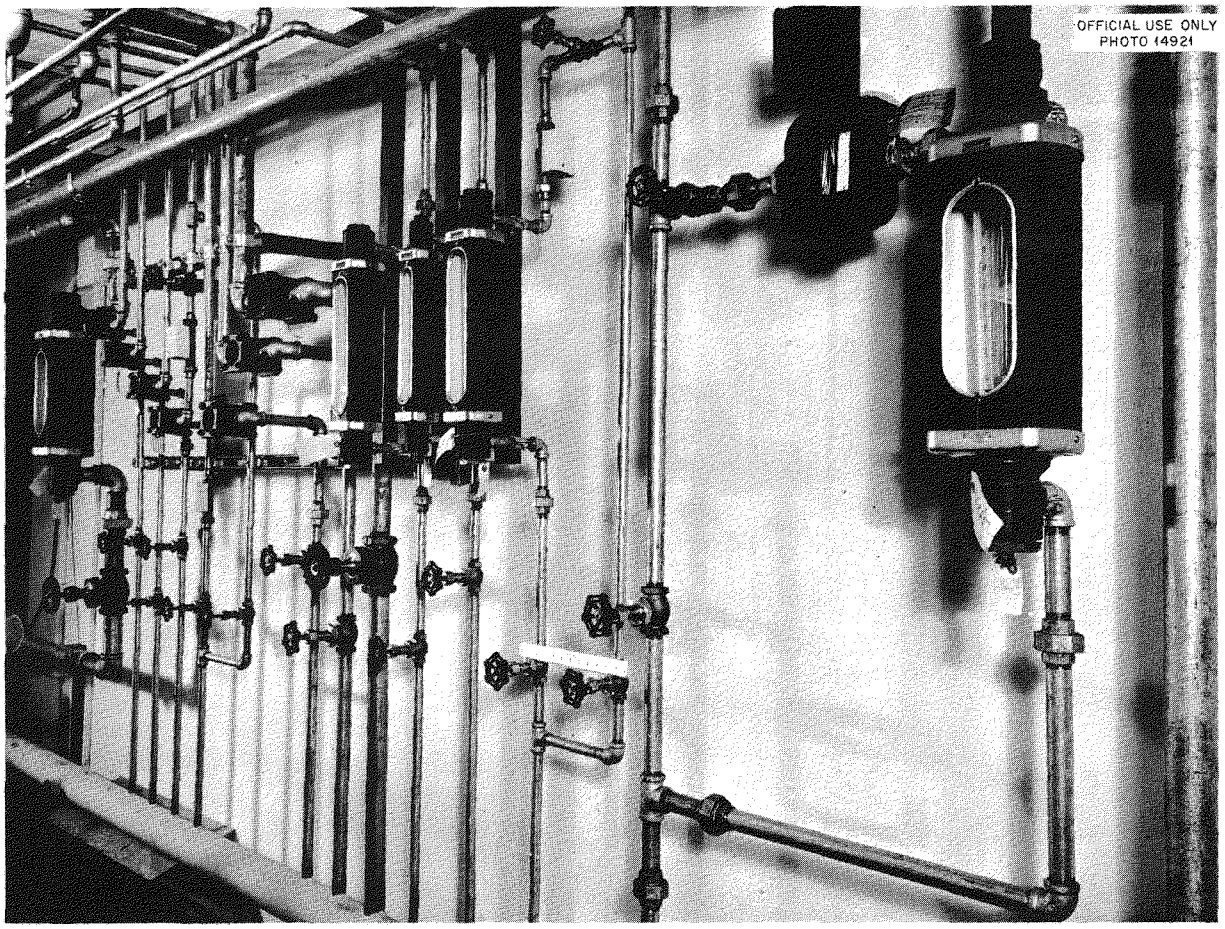

Fig. 1.3. Cooling-Water Feed Station, Control-Room Area.

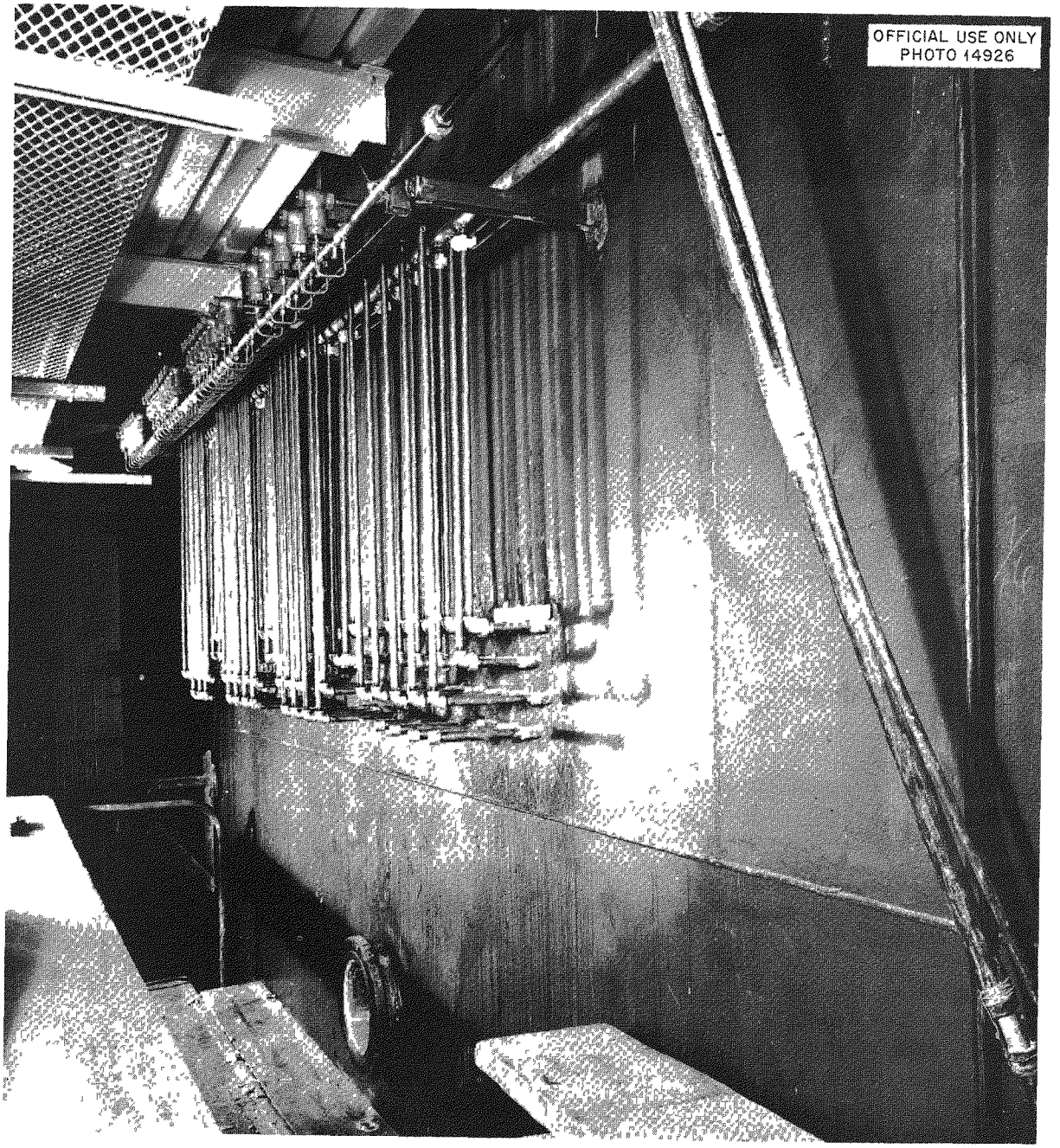

Fig. 1.4. Air Feed and Exhaust Lines Through North Wall of Reactor Tank as Seen from Control-Room Side.

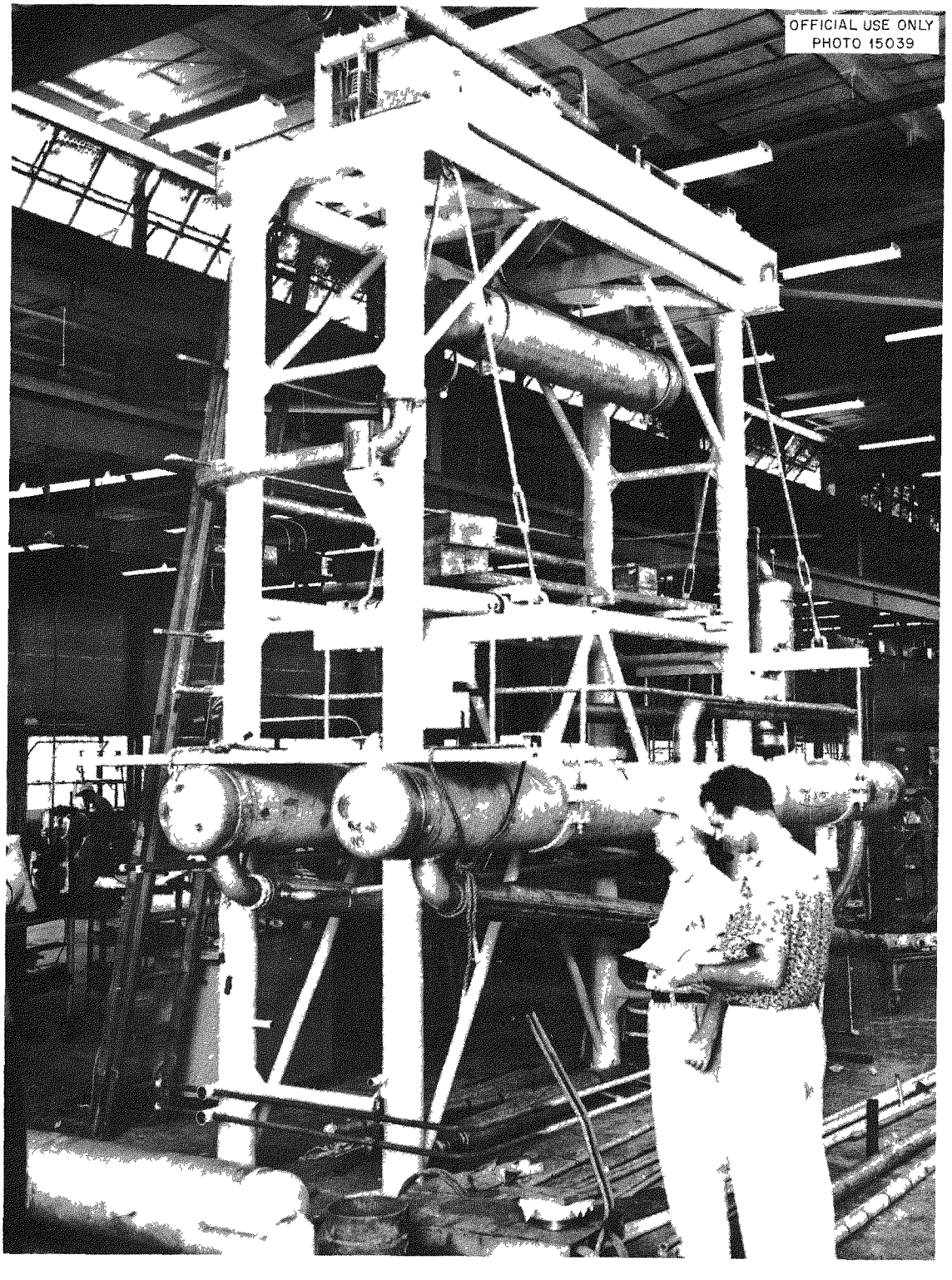

Fig. 1.5. Low-Pressure Fuel Assembly.

2. DESIGN

W. R. Gall

R. E. Aven
R. H. Chapman
C. J. Claffey
H. N. Culver[1]
J. E. Kuster[2]
M. I. Lundin
R. G. Pitkin[3]
J. N. Robinson
W. Robinson
C. L. Segaser
W. Terry
T. H. Thomas
R. VanWinkle
F. C. Zapp

2.1 GENERAL STATUS OF DESIGN

Final flow diagrams and final designs of most of the equipment for the HRT have been reported previously.[4-7] During the reported quarter, drawings were approved for construction of the following:

1. fuel and blanket process piping,
2. cooling water piping,
3. steam and condensate piping,
4. instrument cubicles,
5. thermal shield,
6. sampler,
7. circulating pump installation,
8. feed pump installation,
9. fuel and blanket line coolers.

It is estimated that 80% of all drawings of the reactor equipment, building, and services have been approved for construction.

Plan and elevation views of the fuel and blanket installations are shown in Figs. 2.1 and 2.2.

2.2 FUEL SYSTEM LINE COOLERS

In the present HRT design, cooling jackets are shown on the dump line, the sampler line, and the

[1]On loan from TVA.
[2]On loan from Maxon Construction Co.
[3]On loan from Vitro Corp.
[4]R. B. Briggs *et al.*, *HRP Quar. Prog. Rep. July 31, 1954*, ORNL-1772, p 14-29.
[5]R. B. Briggs *et al.*, *HRP Quar. Prog. Rep. Oct. 31, 1954*, ORNL-1813, p 6-18.
[6]R. B. Briggs *et al.*, *HRP Quar. Prog. Rep. Jan. 31, 1955*, ORNL-1853, p 7-13.
[7]R. B. Briggs *et al.*, *HRP Quar. Prog. Rep. April 30, 1955*, ORNL-1895, p 3-22.

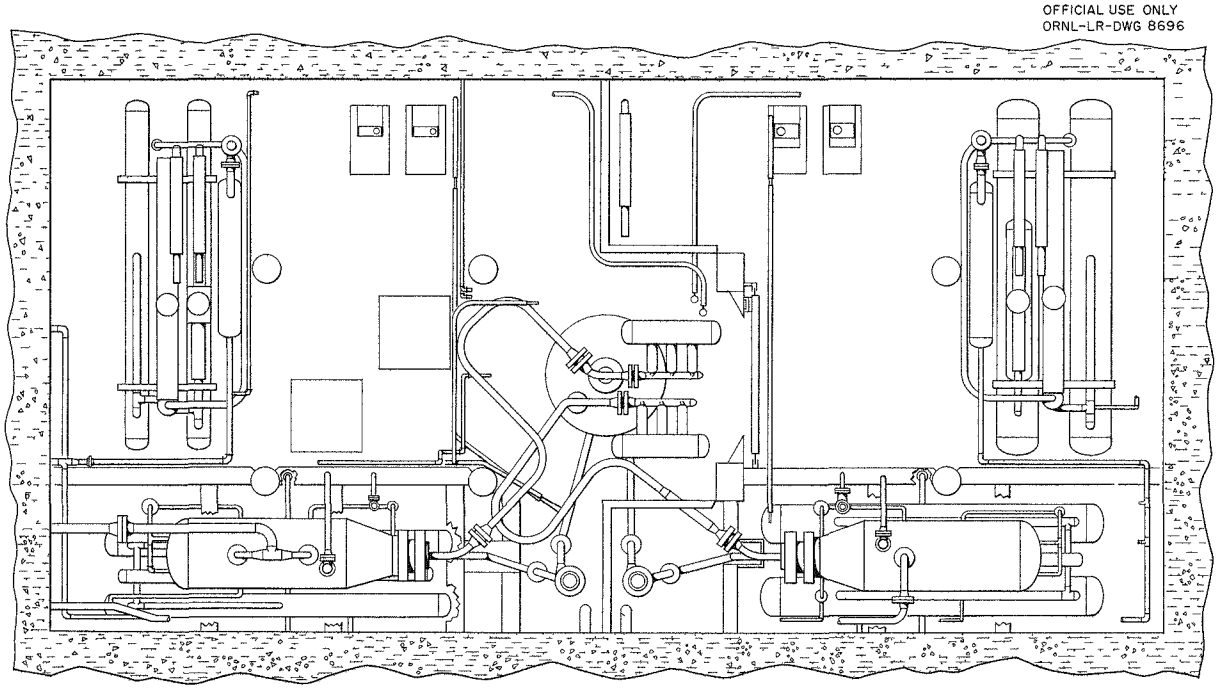

Fig. 2.1. Plan View of HRT Equipment.

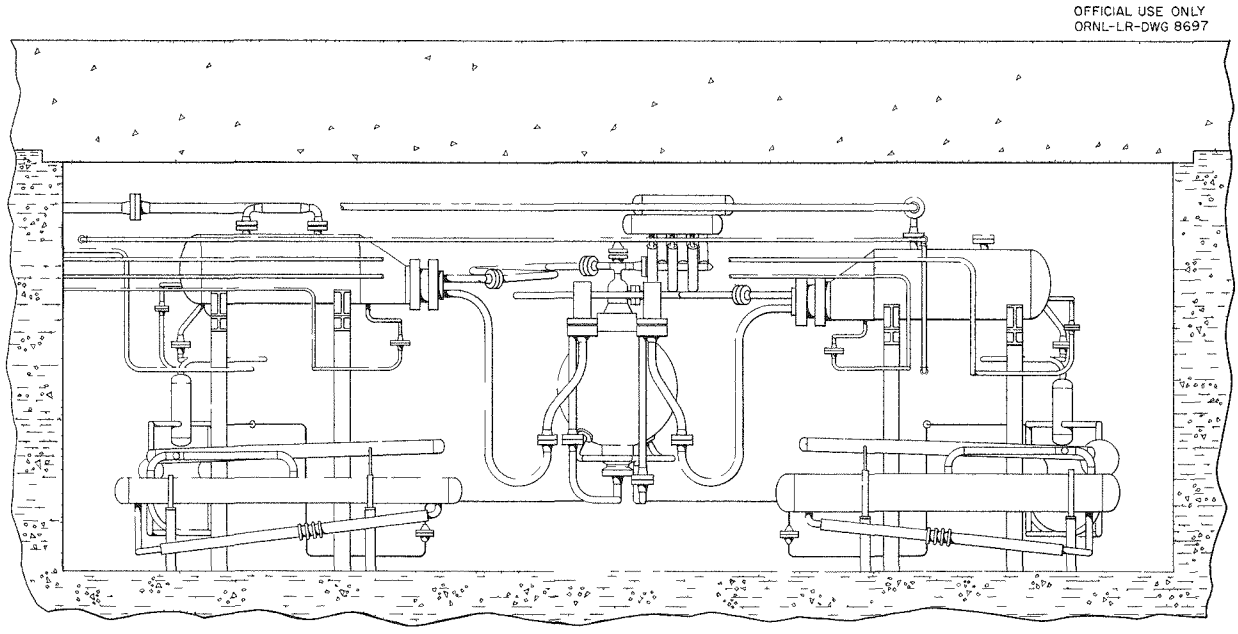

Fig. 2.2. Elevation View of HRT Equipment.

pressurizer vent line. There is a danger that uranyl peroxide may be precipitated in the dump and sampler lines if the highly radioactive fuel is cooled below 70°C soon after leaving the main circulating loop.[8] Since it is impractical to attempt to cool the solution sufficiently during a dump to protect the dump valve, the dump line jacket is intended only to maintain solution in the line at a temperature above 70°C during operation of the reactor. The sample line jacket serves to cool the solution while a sample is being drawn and also serves to maintain solution in the line above 70°C when no flow is taking place. To ensure that the fuel temperature cannot be reduced below 70°C, the cooling water circulated to these two jackets will be heated at all times to 70°C by a mixing type of steam heater in the water line.

Stress studies of both fuel and blanket dump lines were made with the use of the Oracle. The lines as originally laid out proved to be overstressed; this was caused by inclusion of a long, straight run of pipe between the pressure vessel and the valves. By relocating the valve and providing bends in the piping, the maximum combined calculated stresses were reduced to approximately 6,400 psi for the fuel line and 15,000 psi for the blanket line.

Stresses caused by heating or cooling jackets attached to the dump lines were not included in the calculations. Expansion joints will be provided on jackets to minimize these stresses. The fuel dump cooler is shown in Fig. 2.3.

2.3 HIGH-PRESSURE PROCESSING PIPING

Detail drawings of high-pressure piping for the fuel and blanket circulating systems were made and approved for construction. An investigation[9] of pipe bending and other operations used in pipe fabrication indicated that the processes and fabrication conditions must be defined accurately if close control of the metallurgical structure, physical dimensions, surface cleanliness, and other aspects of prefabricated piping is important. Specification HRP-5 was prepared in order to outline requirements for machining, bending, welding, and heat treatment of piping. Fabricators have submitted proposals based upon the drawings and specifications. Pipe and fittings meeting HRP

[8] P. M. Wood, *Possibility of Peroxide Precipitation in HRT Dump and Sampler Lines*, ORNL CF-54-11-172 (Nov. 29, 1954).

[9] R. G. Pitkin, *Trip to Crane Co., M. W. Kellogg and Vitro Corporation Regarding Pipe Fabrication*, ORNL CF-55-3-101 (March 16, 1955).

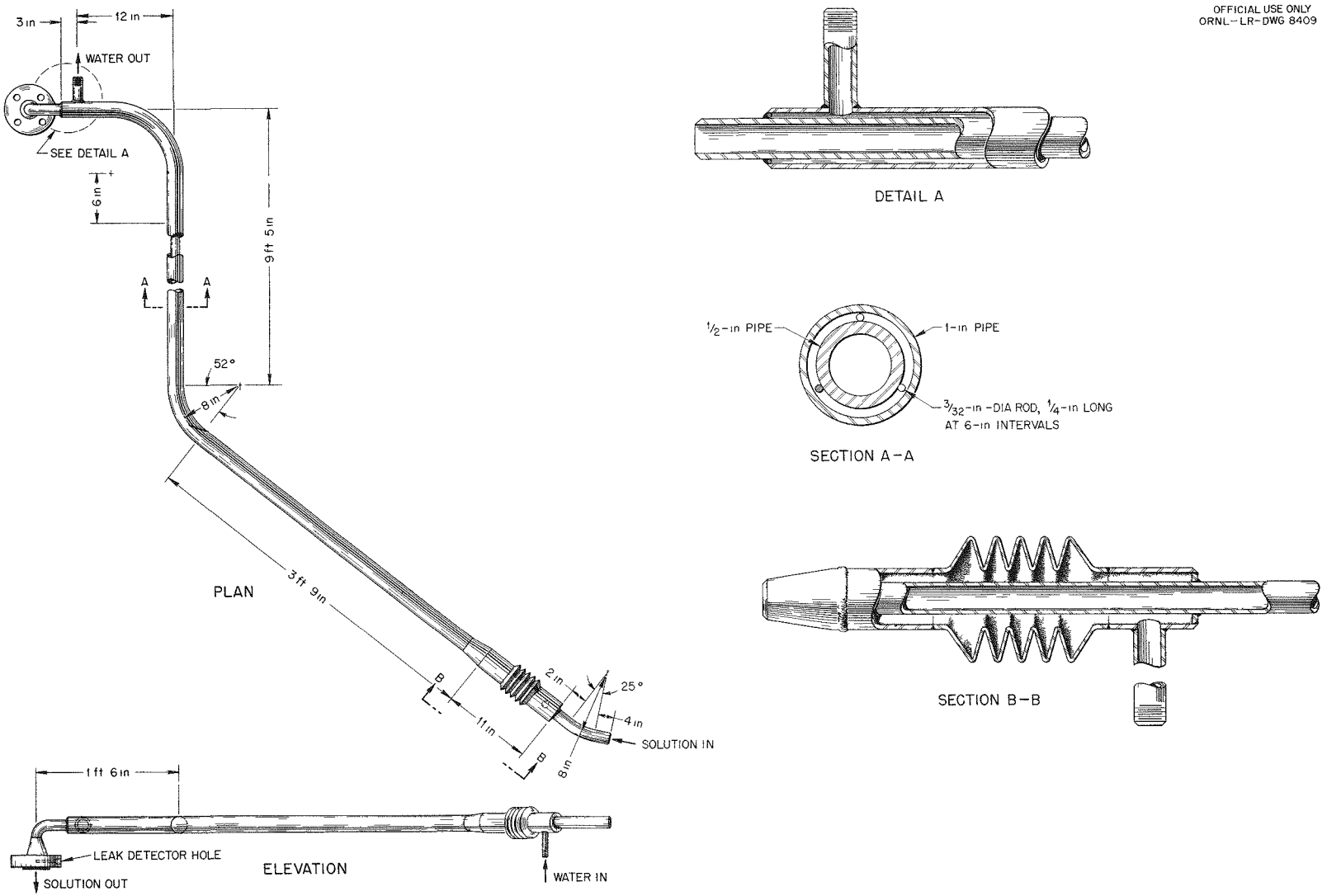

Fig. 2.3. Fuel Dump Cooler.

specifications were procured and will be supplied to the fabricator, who will cut the pipe to required lengths and bend, weld, and heat-treat it for final installation in the reactor systems.

2.4 SOURCE AND FISSION CHAMBER TUBES

In performing low-power experiments in the reactor, it may be desirable to insert a source either in the core or in the blanket region and to insert a fission chamber in the blanket. Figure 2.4 shows the arrangement of thimbles which penetrate the core and blanket for this purpose. Both thimbles may be removed after use and replaced by blank flanges or other types of penetrations. Holes in the shield plugs immediately above these tubes will enable operators to position the source and the chamber.

2.5 THERMAL SHIELD

The reactor vessel is surrounded on all sides by a thermal shield which will be cooled by water circulating through coils. The shield consists of 2 ft of a barytes sand and water mixture on all four sides and 1 ft of steel shot and water mixture at the top and at the bottom. The mixtures are contained in hollow steel walls and slabs arranged around the reactor as shown in Fig. 2.5. The bottom slab sits near the cell floor and supports the reactor. The legs connecting the vessel to this slab and the structural steel within the slab are designed to withstand an upward thrust of 50,000 lb on the reactor vessel. This is the net force which could result if the bottom nozzle were blown out of the vessel and the contents discharged in a jet impinging against the slab.[10] The entire structure of the thermal shield is designed not to exceed yield stress at an internal pressure of 25 psi. A vent area of approximately 50 ft^2 is provided in spaces between the sides and the top and bottom slabs so that the gas and vapor could escape in the event of failure of the reactor vessel. The pressure rise in the shield should be less than 25 psi, at which pressure the stresses in the structure would be less than the yield stress.

2.6 INSTRUMENT CUBICLES

Two shielded instrument cubicles are provided outside the reactor cell on the control gallery side.

[10] P. R. Kasten, *Holding Force Required for HRT Pressure Vessel*, ORNL CF-55-5-166 (May 25, 1955).

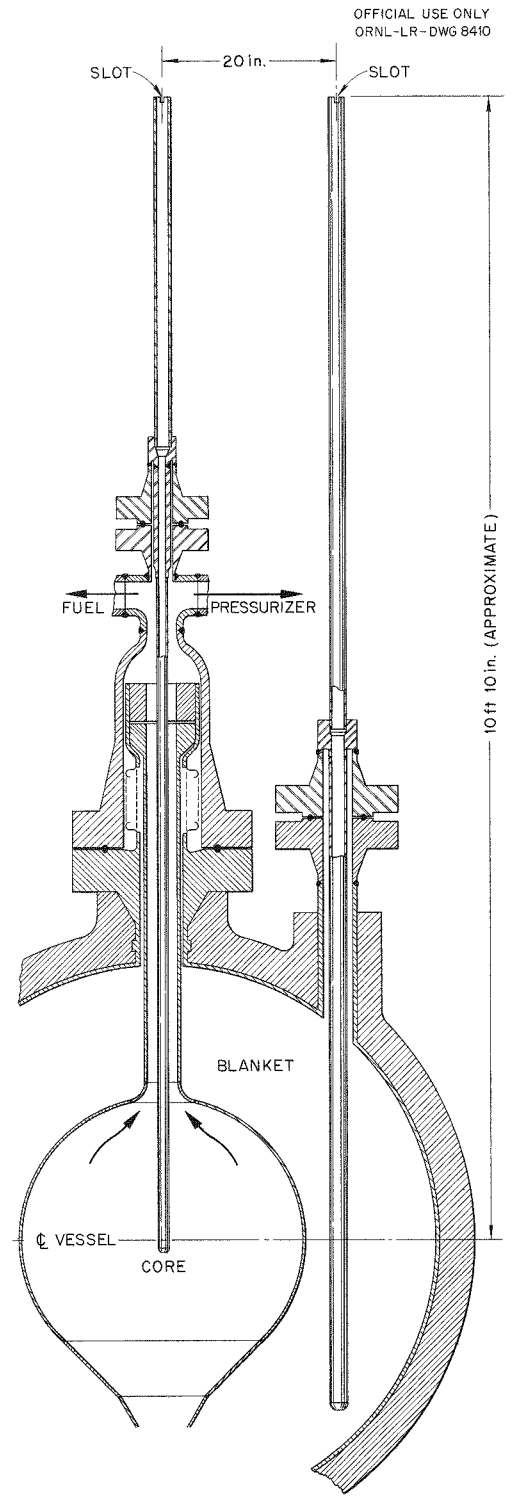

Fig. 2.4. Fission Chamber and Source Tube.

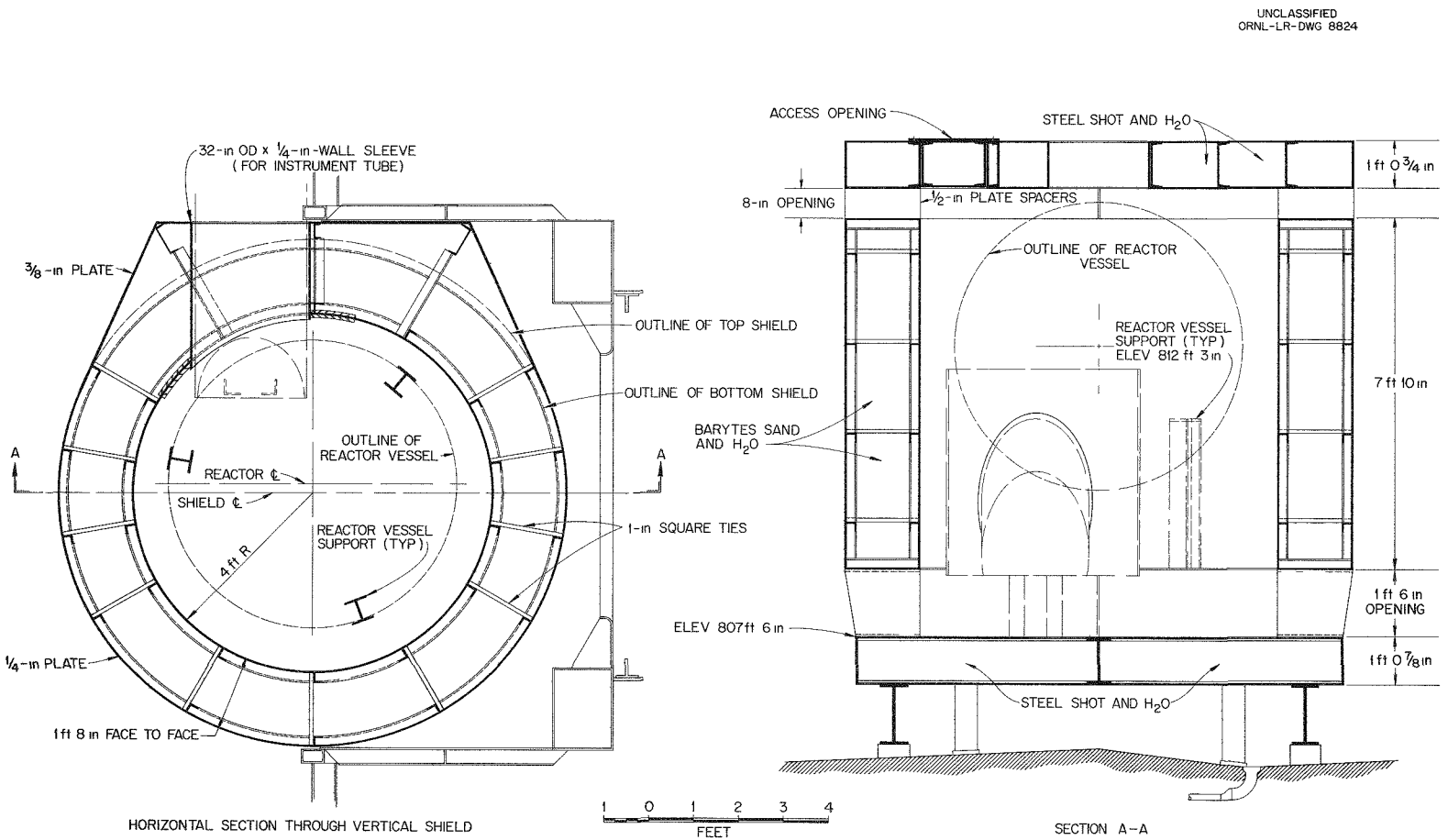

Fig. 2.5. Thermal Shield Arrangement.

They will house instruments which cannot be waterproofed or serviced under water easily and which are connected to the reactor system in such a manner that they could become contaminated in the event of a failure.

Each cubicle consists of a gastight steel tank attached to the cell wall and surrounded by concrete as shown in Fig. 2.6. Design pressure is 50 psi; if the pressure should exceed that amount, it would be relieved through a rupture disk into the reactor cell. Access is through the top by removing the shield plug and either opening the quick-opening manway or removing the entire top of the tank. The shielding provides protection from the reactor equipment so that maintenance personnel can enter the cubicles to service the instruments when the reactor is not operating.

2.7 REACTOR CELL AIR MONITOR

The HRT cell air monitors, which will provide an alarm in case of a leak in the reactor system, will be installed in the west instrument cubicle with an air circulating system as shown in Fig. 2.7.

Air will be drawn through individual 2-in. pipes from the fuel and blanket sides of the cell and will be returned through one 2-in. pipe to the fuel side of the cell. Specifications for the blower have been written to provide for a maximum time of 5 sec for air to traverse the distance through the longer (blanket side) supply line from the cell to the monitors.

2.8 SAMPLING STATIONS

Samples of liquid and suspended solids will be taken from the high- and low-pressure systems of the HRT. Locations of the four sampling points and the flow diagrams for the samplers are shown on the system flowsheet.[11] When a sample is taken from the high-pressure system, liquid will flow from high pressure through the samples to the low-pressure dump tanks. Samples will be taken from the low-pressure system by pressurizing the dump tanks and forcing liquid through the samples into a fuel transfer tank. Design of the sampler has been completed and construction of a prototype approved.

One heavily shielded sample station of the type shown in Fig. 2.8 will be provided for each of the core and blanket systems. Each station contains two isolation chambers: one for isolating samples from the low-pressure system and the other for obtaining samples from the high-pressure system. Each chamber in the station is served by a common loading and manipulating device. When a sample

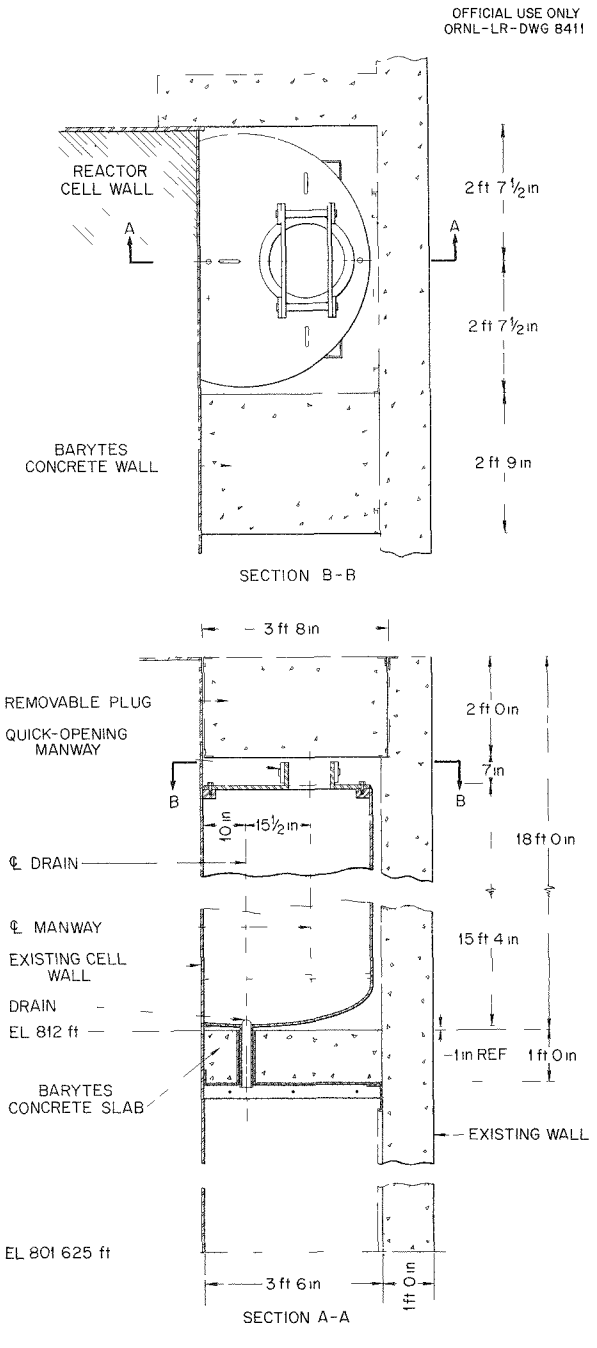

Fig. 2.6. Instrument Cubicle.

[11] R. B. Briggs *et al.*, *HRP Quar. Prog. Rep. April 30, 1955*, ORNL-1895, p 5–7.

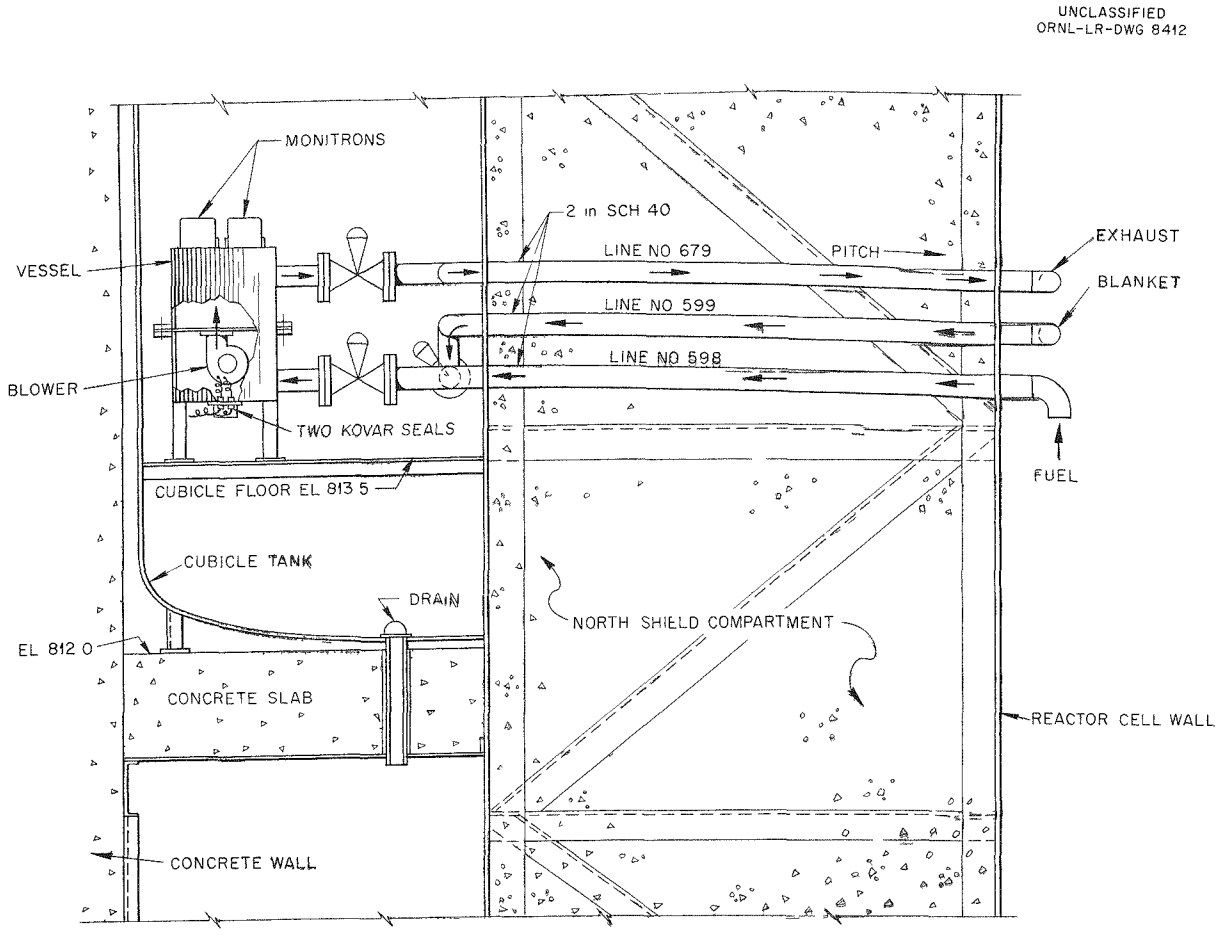

Fig. 2.7. System Cell Air Monitoring.

is being taken, solution from the desired system is allowed to flow through its isolation chamber until a fresh sample, undiluted by previous samples, is obtained. The isolation chamber is then valved off, the sample is cooled to about 80°C, and the pressure is reduced to atmospheric. A sample flask is evacuated, placed in a holder, and lowered through the loading tube to the transfer mechanism. The assembly is then indexed under the proper isolation chamber, where the flask holder is raised by an air cylinder until contact is made between the isolation chamber nozzle and the inverse cone on the carrier head (Fig. 2.9). Further lifting of the flask holder causes the hypodermic needle to puncture the rubber diaphragm and seats the carrier head against the nozzle. The sample is discharged into the flask by opening the valve on the chamber. When the sample is in the flask, the procedures are reversed and the flask holder is removed into a shielded carrier for transport to the analytical laboratory.

With the present design, the sample volume will be about 5 ml.

2.9 FISSION-PRODUCT ADSORPTION

The important design specifications for the HRT fission-product adsorption system are outlined as follows:

The Gas Stream. – The adsorption system has been designed to process gases at a rate of 500 cc (STP)/min; the gases are composed chiefly of the oxygen from the core and blanket but contain the krypton and xenon isotopes from the core produced at a 10-Mw power level. The flow time through the lines and equipment between the core and adsorber pit has been estimated to be 13,600 sec.

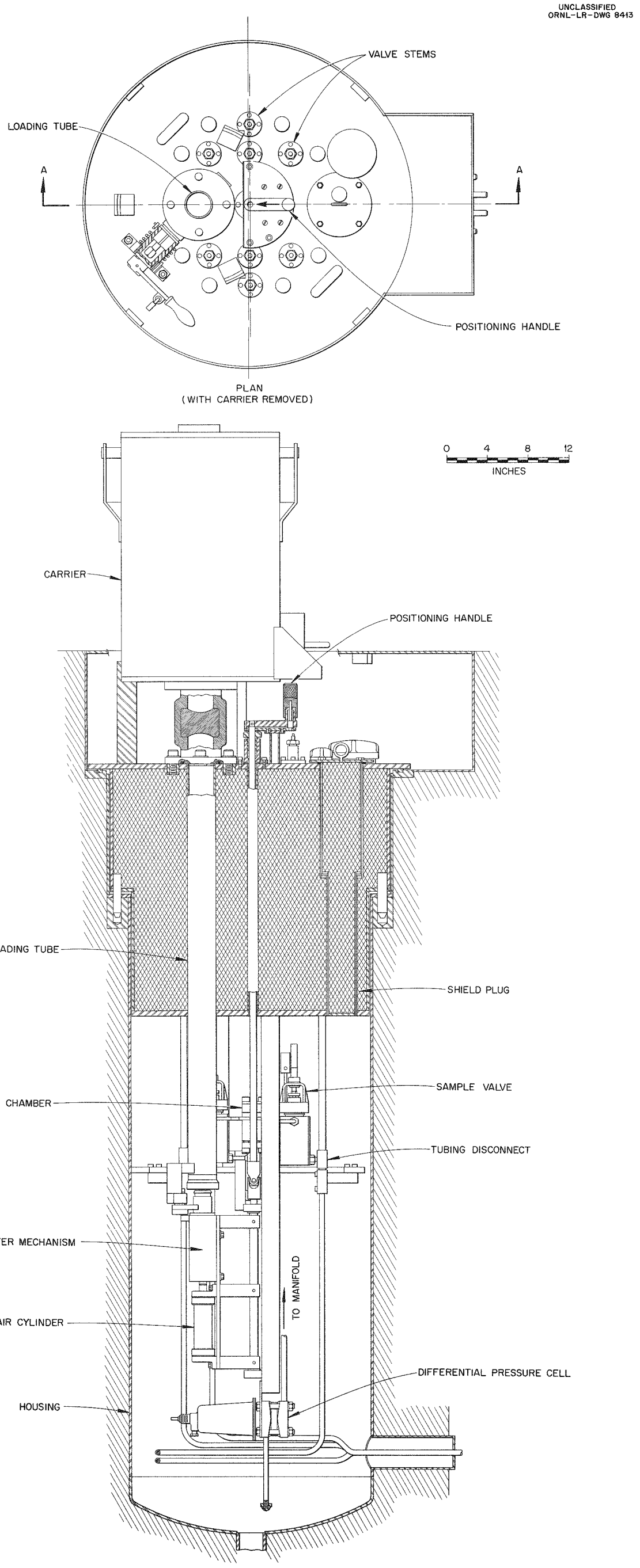

Fig. 2.8. General Assembly of Sampling Facility.

DECLASSIFIED DECLASSIFIED DECLASSIFIED

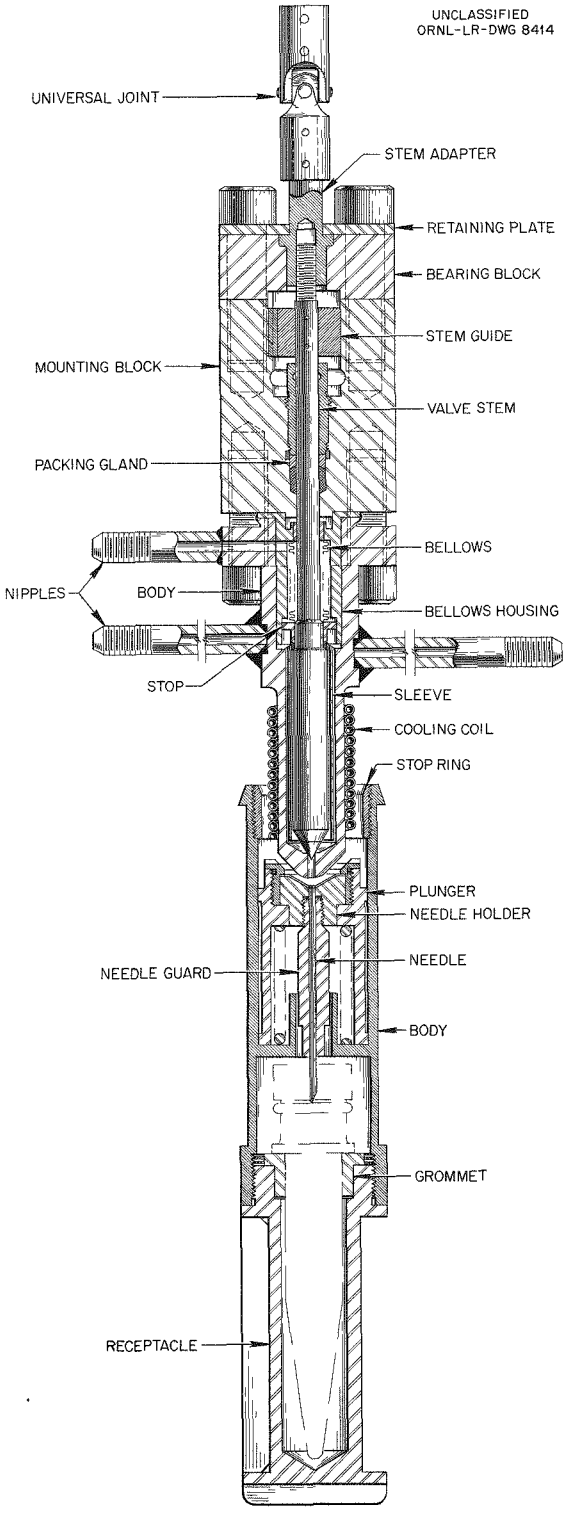

Fig. 2.9. Sample Bottle in Position to Receive Sample.

With this delay time the gas at the entrance to the adsorber pit should have the composition shown in Table 2.1.

The adsorbers are designed so that only the 6.45 curies of the 10.27-year Kr^{85} is discharged daily with the oxygen.

Additional Delay Time. – In addition to the 13,600-sec delay ahead of the adsorption pit, it is necessary to provide an additional decay period to prevent excessive temperatures in the charcoal bed. This will be done by placing 160 ft of 3-in. empty pipe in the adsorber pit just ahead of the charcoal adsorption units. The most important effect of this additional delay is to reduce the concentrations of Kr^{88} and its 17.8-min rubidium daughter, which is the greatest single contributor to the heat load in the initial portion of the bed.

Charcoal Units. – After leaving the 3-in. empty pipe, the 500 cc/min gas stream is split into two streams of 250 cc/min. Each of these 250 cc/min streams enters an identical charcoal adsorption unit. The units were designed for activated charcoal pellets of approximately 8 to 14 mesh packed in standard pipe with about 80% voids. The diameters and lengths of packed piping in the two charcoal units are shown in Fig. 2.10.

Temperatures. – The arrangement of diameters and lengths was chosen in the order shown in order to prevent the packed beds from reaching temperatures which would cause excessive oxidation of the charcoal. To remove heat, the 160 ft of empty pipe and the two charcoal units will be immersed in cooling water maintained at an estimated temperature of 30°C. The temperature in any portion of the packed sections should not exceed 100°C. Thermocouples will be installed to read the temperatures at the center of the pipe just after the beginning of the ½-, 1-, 2-, and 6-in. sections in each unit.

Safety Factors. – The degree of overdesign is indicated roughly by the safety factors shown in Table 2.2 which are based on the ratio of the charcoal volume in the specified design to the charcoal volume in units having the limiting dimensions calculated to prevent excessive activity in the exit gas and to keep the charcoal temperature just below the maximum allowable level.

2.10 CIRCULATING PUMP INSTALLATIONS

Construction drawings have been approved for the circulating pump installations for the core and

TABLE 2.1. FISSION-PRODUCT GAS COMPOSITION AT ENTRANCE TO ADSORPTION BED

Mass	Half Life	Flow Rate (atoms/sec)(10^{-15})	Partial Pressure* (mm Hg)
Krypton			
83*m*	11.4 min	0.40	0.001385
83	Stable	1.58	0.005475
84	Stable	2.95	0.010215
85*m*	4.36 hr	1.56	0.00541
85	10.27 years	1.29	0.00447
86	Stable	5.64	0.019535
87	78 min	1.21	0.00419
88	2.77 hr	4.75	0.01645
Xenon			
$131m_2$	12.0 days	0.097	0.00035
131	Stable	10.04	0.0348
132	Stable	15.05	0.05215
133*m*	2.3 days	0.525	0.00180
133	5.27 days	22.0	0.00762
134	Stable	26.4	0.09145
135	9.13 hr	14.8	0.0513
136		21.70	0.0752
	Total	131.0	0.4191

*Total pressure is 827 mm Hg.

TABLE 2.2. COMPARISON OF ACTUAL SIZE OF CHARCOAL BED WITH CALCULATED REQUIREMENT

	Calculated Limiting Design		Actual Design Specifications		
	Length (ft)	Pipe Size (in.)	Length (ft)	Pipe Size (in.)	Approximate Safety Factor
Empty pipe	106	2	160	3	3
Charcoal unit	20	½	40	½	2
	10	1	40	1	4
	10	2	40	2	4
	10	6	60	6	6

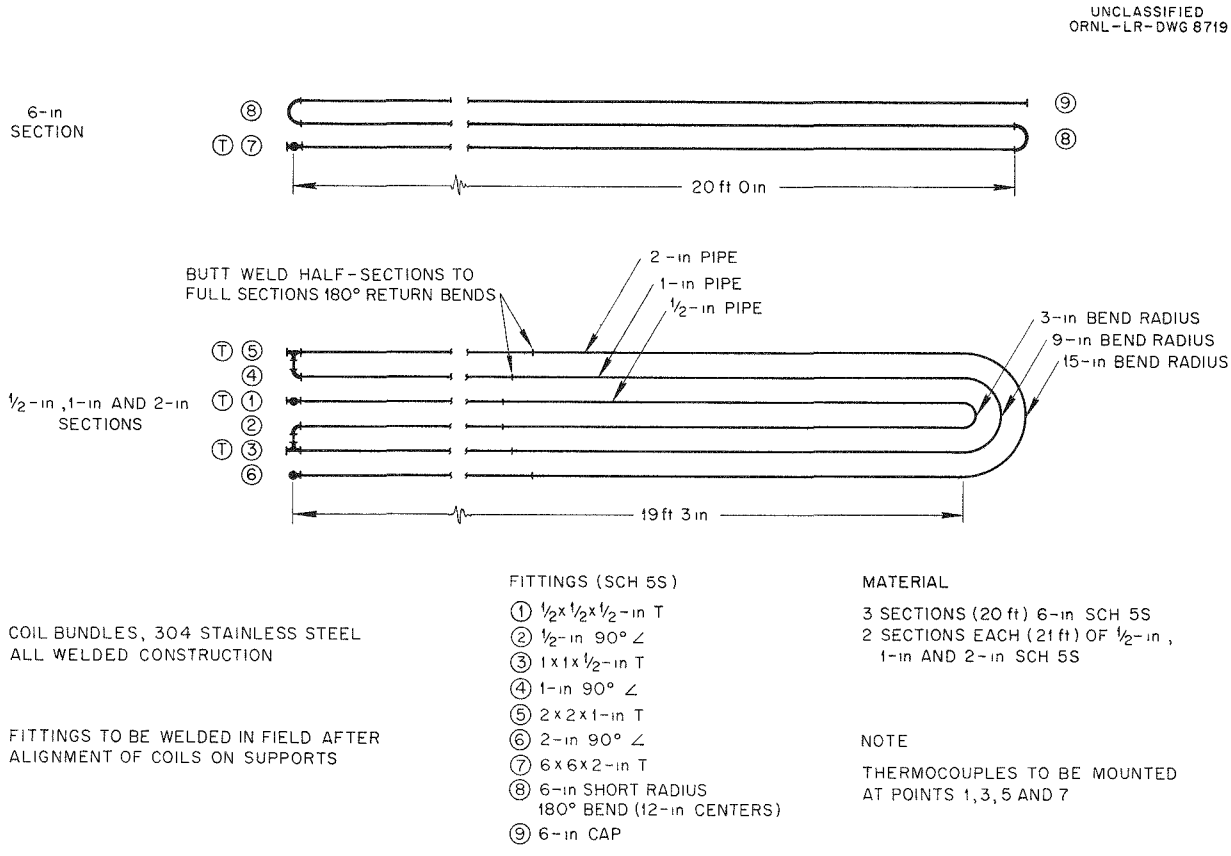

Fig. 2.10. Schematic Arrangement of Fission-Product Adsorption System.

blanket high-pressure systems. Figure 2.11 shows the pump arrangement for the fuel system. The pump base plate carries two large dowels which match with guiding holes in the top plate of the support. A jig located outside the reactor cell matches the cell pipe flange and pump dowel positions. Pump assemblies with their base plates, pipe extensions, and flanges will be fabricated on the jig so that replacements will duplicate the original equipment. Remotely operated tools will be provided to remove the flange and pump bolts and to replace them after installation of a duplicate pump assembly. Auxiliary pipes carrying cooling water and the process fluid vent extend above the pump and are provided with bolted flanges. A permanently attached bail engages the crane hook for handling.

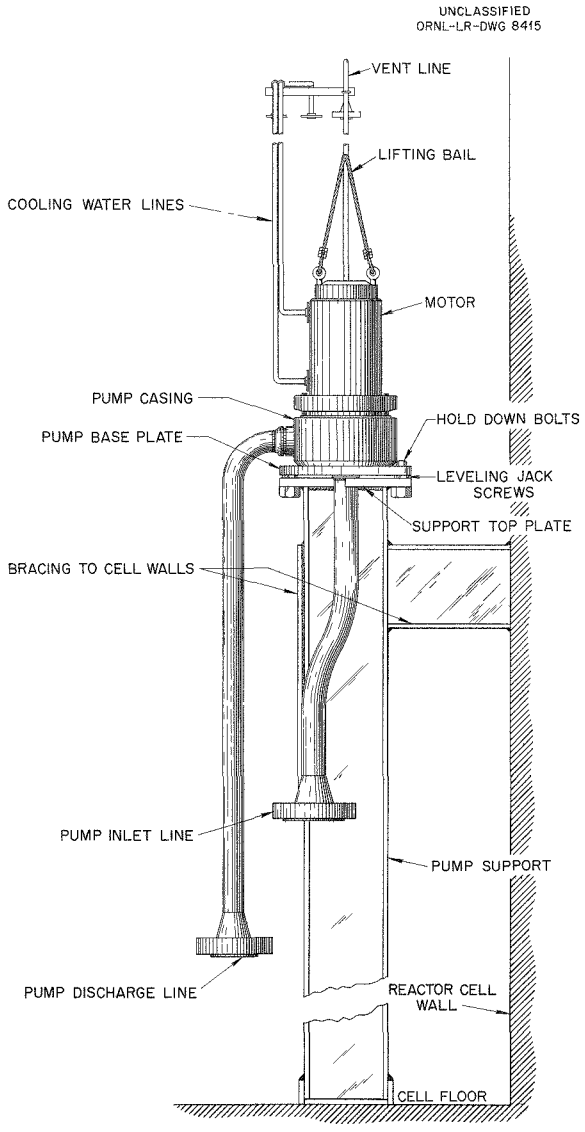

Fig. 2.11. Circulation-Pump Mount Assembly.

2.11 PURGE PUMP HEAD INSTALLATION

The installations of the purge pump heads for the fuel and blanket systems have been detailed. Drawings are ready for approval. Figure 2.12 shows the fuel purge pump installation. The pump head, which was described in an earlier report,[12] is mounted on a removable carriage, which also serves to support the attached pipes and flanges. This assembly is supported on a bracket which is welded to the cell wall; it slides out on the bracket for removal. The mating pipe flanges in the cell may be spread apart to permit clearance of the packing rings. Remote tooling will be provided to connect and disconnect bolts, to spread the flanges, and to slide the assembly. A lifting bail is provided to engage the hook of an overhead hoist for removal from the cell. Side rails on the bracket and a pin on the carrier serve to position the assembly properly when a remote installation is being made. A jig is not considered necessary for making duplicate pump head assemblies, because the cell pipes are very flexible and may be bent to match the pump flanges within the limits of manufacturing tolerances.

[12] R. B. Briggs *et al.*, *HRP Quar. Prog. Rep. Jan. 31, 1955*, ORNL-1853, p 12.

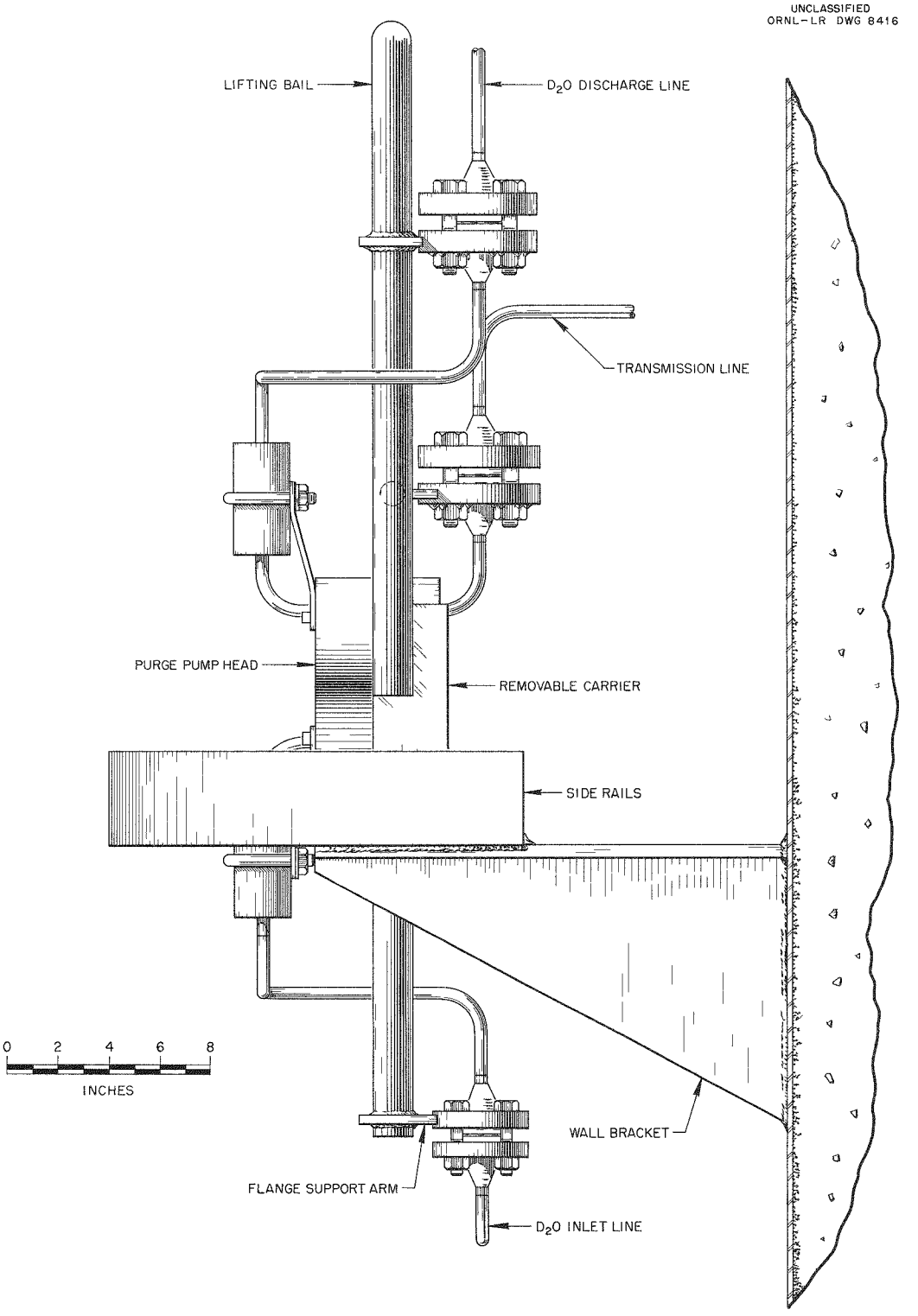

Fig. 2.12. Fuel Purge-Pump-Head Installation Assembly.

3. REACTOR ANALYSIS

P. R. Kasten P. N. Haubenreich

3.1 STABILITY OF THE HRT

The criteria for stability of a reactor system are based upon the linearized equations of motion.[1] The HRT criteria are presented in graphical form in Figs. 3.1 and 3.2, where stability is assured if the reactor operating condition lies above, or to the left of, the appropriate stability curve. In the figures, α_1 represents a normalized friction coefficient for the fluid leaving the core and entering the pressurizer; γ is the ratio of the delayed neutron fraction to the average prompt neutron lifetime; ϵ is inversely proportioned to the residence time of fluid in the core; τ is the average prompt neutron lifetime; S_s/S_c is the ratio of the fluid volume on the shell side of the heat exchanger to the fluid volume of the core; ω_n is the nuclear frequency; ω_h is the hydraulic frequency; and C_2 is related to the volume of the pressurizer vapor space. Figure 3.1 shows the HRT operating condition for the case of a slurry blanket containing 1350 g of thorium per kilogram of D_2O. The solid line ($\epsilon = 0$) is the stability criterion if the residence time of fluid in the core is infinite. If fluid flow effects are considered, the dotted curves are obtained. The relationship of the solid and dotted curves shows that fluid flow aids stability but that the $\epsilon = 0$ curve is a good approximation to the cases in which flow effects are considered. The HRT point shown is for 5-Mw operation. The operating power level appears in ω_n^2, and the curve for $S_s/S_c = 3$ in Fig. 3.1 shows that, for this case, the HRT should be stable up to a power level of 11 Mw.

If a less concentrated slurry is used, the permissible power level will increase. For the case of a D_2O reflector, the appropriate value of γ is 10 because of the increased lifetime of prompt neutrons. As shown in Fig. 3.2, the allowable $\omega_n^2/(1 + C_2)$ is 330 for an $\omega_h^2 (1 + C_2)$ of 3700; this corresponds to a permissible power level of 130 Mw.

[1] P. R. Kasten, *Stability of Homogeneous Reactors*, ORNL CF-55-5-163 (May 25, 1955).

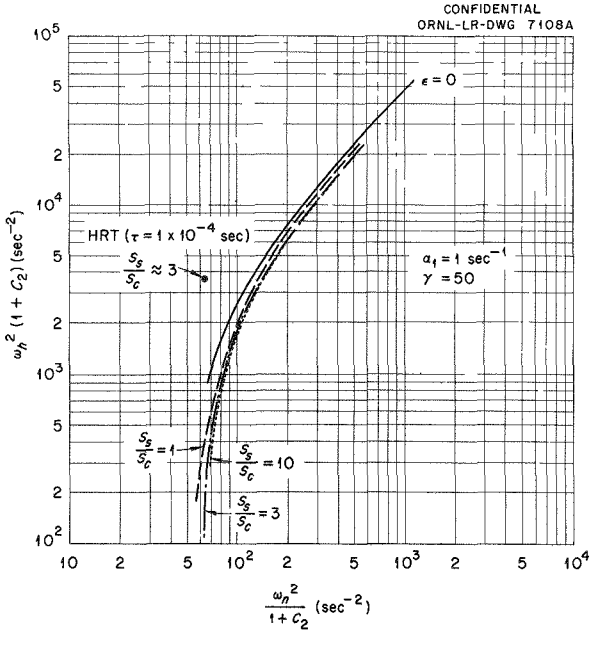

Fig. 3.1. Stability Criteria for Homogeneous Circulating Reactors.

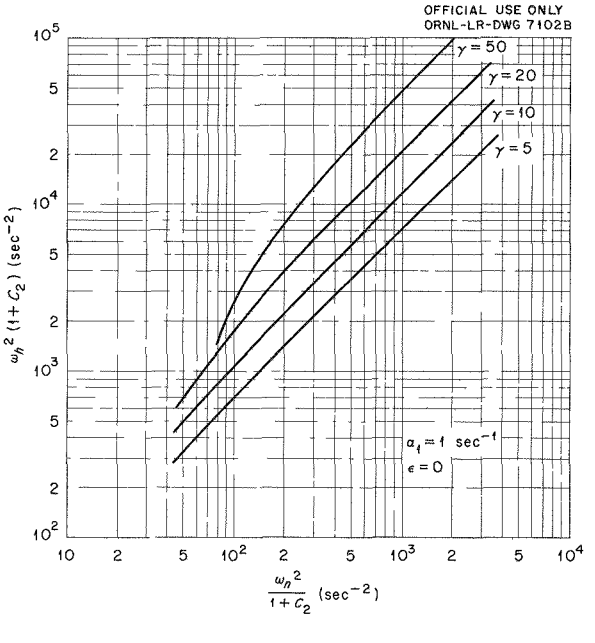

Fig. 3.2. Stability Criteria for Homogeneous Circulating Reactors.

3.2 HOLDING FORCE REQUIRED FOR HRT PRESSURE VESSEL

P. R. Kasten

Rupture of the fuel inlet nozzle on the pressure vessel would allow the reactor fluid to be ejected from the opening with high velocity. Under pessimistic conditions, the jet of fluid would be ejected in a vertical direction, and the resultant reaction force of the jet would tend to push the pressure vessel upward.

In calculating[2] the effects, a rupture was assumed with the reactor operating at 2000 psi and 300°C. The saturation pressure corresponding to 300°C is 1250 psi; therefore, the driving force for fluid ejection corresponds to 1250 psi soon after the rupture. This driving force will fall slowly as fluid is ejected, since the boiling action will cool the fluid. The pressure drop associated with the boiling action is not appreciable and was neglected.

The fluid discharge velocities and the movement of the pressure vessel were calculated from the equations of motion for the fluid and vessel. In the pessimistic case it was estimated that the fluid could be ejected with a constant velocity of 360 fps and that the vessel would rise 6 ft. When the acceleration of the fluid was included in the calculations, the estimated upward travel of the vessel was reduced to 4 ft. A force of 50,000 lb would be required to restrain the vessel.

3.3 CORE TANK TEMPERATURE

P. N. Haubenreich

It has been determined experimentally that fission products in a fuel solution tend to be deposited on a surface which is at a higher temperature than the solution. This situation exists in the core of the HRT where the walls are heated by radiation. In order to estimate the importance of this phenomenon, calculations have been made for determining the operating temperature of the core wall.[3]

The estimated temperatures of the fluid in the HRT with a D_2O reflector, operating at 5 Mw, are shown in Fig. 3.3. Under these conditions the maximum temperature difference between the wall and the fuel solution occurs near the bottom of the tank, where the wall is about 18°F above the core fluid. Temperature distributions through the wall are shown in Fig. 3.4 for operation at both 5 and 10 Mw.

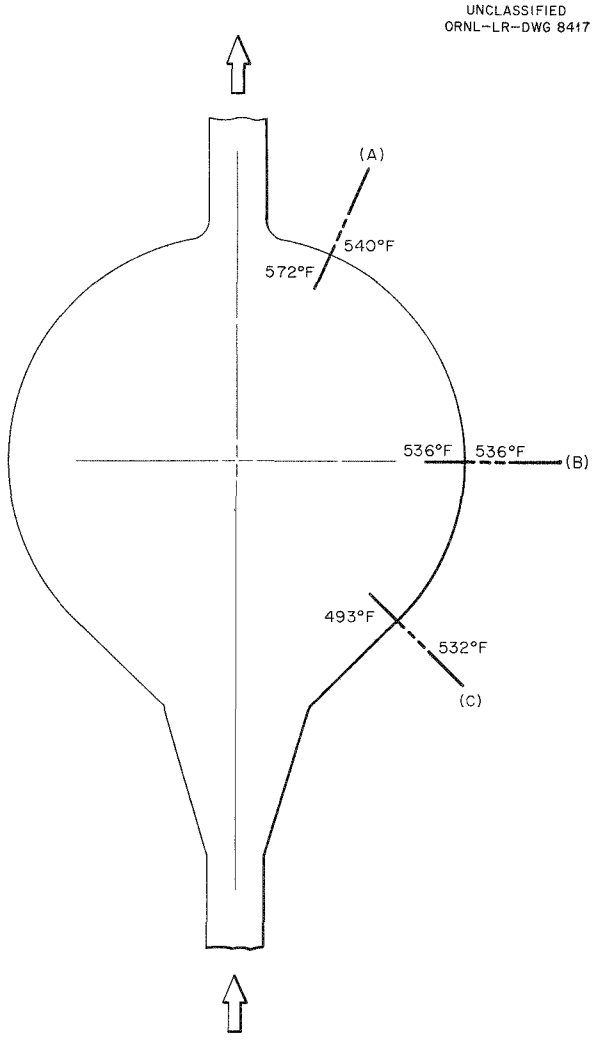

Fig. 3.3. Fluid Temperatures in HRT (D_2O Reflector, 5 Mw).

3.4 HEAT GENERATION AND TEMPERATURE DISTRIBUTION IN CONTROL ROOM AREA SHIELD

P. N. Haubenreich

The shield between the control room area and the reactor cell is a 5½-ft-thick tank, filled with a mixture of colemanite, barytes aggregate, and

[2] P. R. Kasten, *Holding Force Required for HRT Pressure Vessel*, ORNL CF-55-5-166 (May 25, 1955).

[3] P. N. Haubenreich, *HRT and TBR Core Tank Temperatures*, ORNL CF-55-7-78 (July 18, 1955).

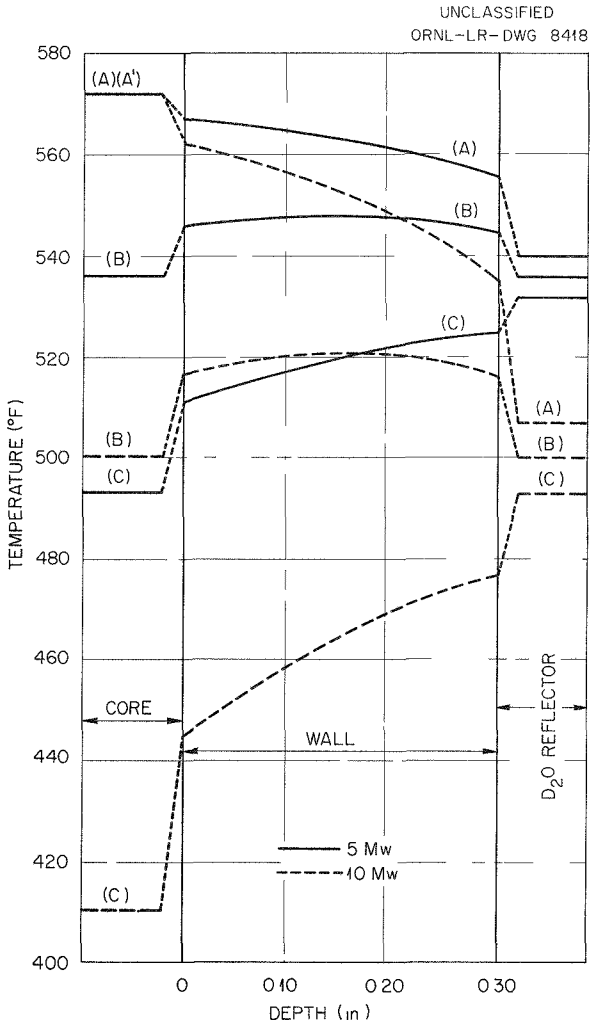

Fig. 3.4. Temperatures in HRT Core Tank Wall.

water. Heat is generated in the shield by absorption of gamma rays from the reactor and gamma rays and alpha particles resulting from neutron capture within the shield itself. Because of the thermal shield around the reactor vessel, the radiation entering the wall is not intense enough to cause a serious temperature rise. Thus there appears to be no need of internal cooling. The temperature profile through the wall in the region of greatest heat production is shown in Fig. 3.5.

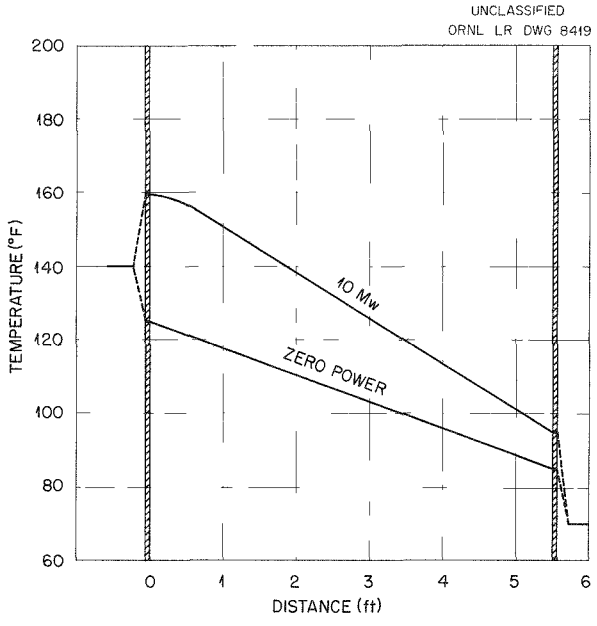

Fig. 3.5. Temperature Distribution in North Shield Wall.

4. COMPONENT DEVELOPMENT

C. B. Graham

L. J. Bell
J. S. Culver
K. E. Estes
C. H. Gabbard
L. F. Goode
J. A. Hafford
B. A. Hannaford
P. H. Harley
P. F. Pasqua[1]
W. L. Ross
J. A. Russell
I. Spiewak
D. S. Toomb
R. Van Winkle

4.1 PUMP DEVELOPMENT

Westinghouse canned-rotor pumps of types 400A, 300A, and 230A are being tested and improved for use in the high-pressure circulating system of the HRT. Separate test loops have been provided for the 400A and 230A pumps, and the 300A pump is being tested as a part of the HRT mockup. General problems and operation of the 400A and 230A loops are described here; experience with the 300A pump is reported in Sec. 4.3.

The thermal barriers of the development pumps are being replaced with a hollow-type thermal barrier[2] which should decrease the radial bearing temperature in the Kingsbury thrust-bearing assembly below 100°C according to tests run by Westinghouse. Two of these barriers were received, and the HRT mockup pump is being modified by installation of the new barrier. One 400A pump will be so modified by August 1.

Figures 4.1, 4.2, and 4.3 show the condition of parts of the 400A pump after the 1000 hr of operation on 30 g of uranium per kilogram of solution mentioned previously.[3] Corrosive attack occurred on the shaft adjacent to the thermal barrier seal rings and on both sides of the old-type thermal barrier. The temperature of the solution on the motor side of the thermal barrier was between 170 and 190°C. The metal temperature back of the wearing rings on the impeller side was unknown but was undoubtedly somewhat lower than the 300°C temperature of the main circulating solution. In addition, the solution flowing through the wearing rings was highly turbulent. The back hub of the impeller, adjacent to the wearing rings, suffered uniform local attack over about the last ¼ in. of its length. The wearing rings, shaft seal rings, and front hub of the impeller showed no attack. The bearing surfaces were in excellent condition. No other corrosion or wear was observed.

The 400A pump was reassembled, and a short water run was made to obtain 100 reverse startups (in which the pump starts in reverse rotation, runs 45 sec, and then changes to forward rotation). Subsequent inspection of the pump showed no abnormal wear. Next, the pump completed 100 reverse startups with a solution of about 0.13 *m* UO_2SO_4 with 0.005 *m* $CuSO_4$ and 10 mole % excess H_2SO_4. A run of 860 hr was then made at 250°C, and the pump was shut down to prepare for installation of the new thermal barrier. The general condition was found to be excellent except for further corrosion on the thermal barrier in the wearing ring section and on the corresponding wearing ring surface of the impeller. Corrosion damage observed previously on the motor face of the thermal barrier and on the shaft did not appear to have been increased. No other corrosion or abnormal wear was observed. Concentrations of uranium, copper, oxygen, nickel, and cobalt in solution during the test are shown in Fig. 4.4.

The 230-gpm pump loop was run only on water. A water injection system was installed which delivers 1 gph of condensate from the top of the pressurizer to the back of the pump. Installation of a new 3000-lb D/P cell eliminated the problem of D/P cell leaks. Leaks in the system have caused numerous delays. As soon as the loop is completely checked out, a slurry run will be attempted. The pump, an HRT blanket pump prototype, has accumulated 1050 hr of successful operation on water.

All the reactor development pumps have developed leaks around the hollow, metallic casing

[1] Consultant.

[2] L. J. Bell, K. E. Estes, and W. L. Ross, *HRP Quar. Prog. Rep. April 30, 1955*, ORNL-1895, p 29.

[3] *Ibid.*, p 28.

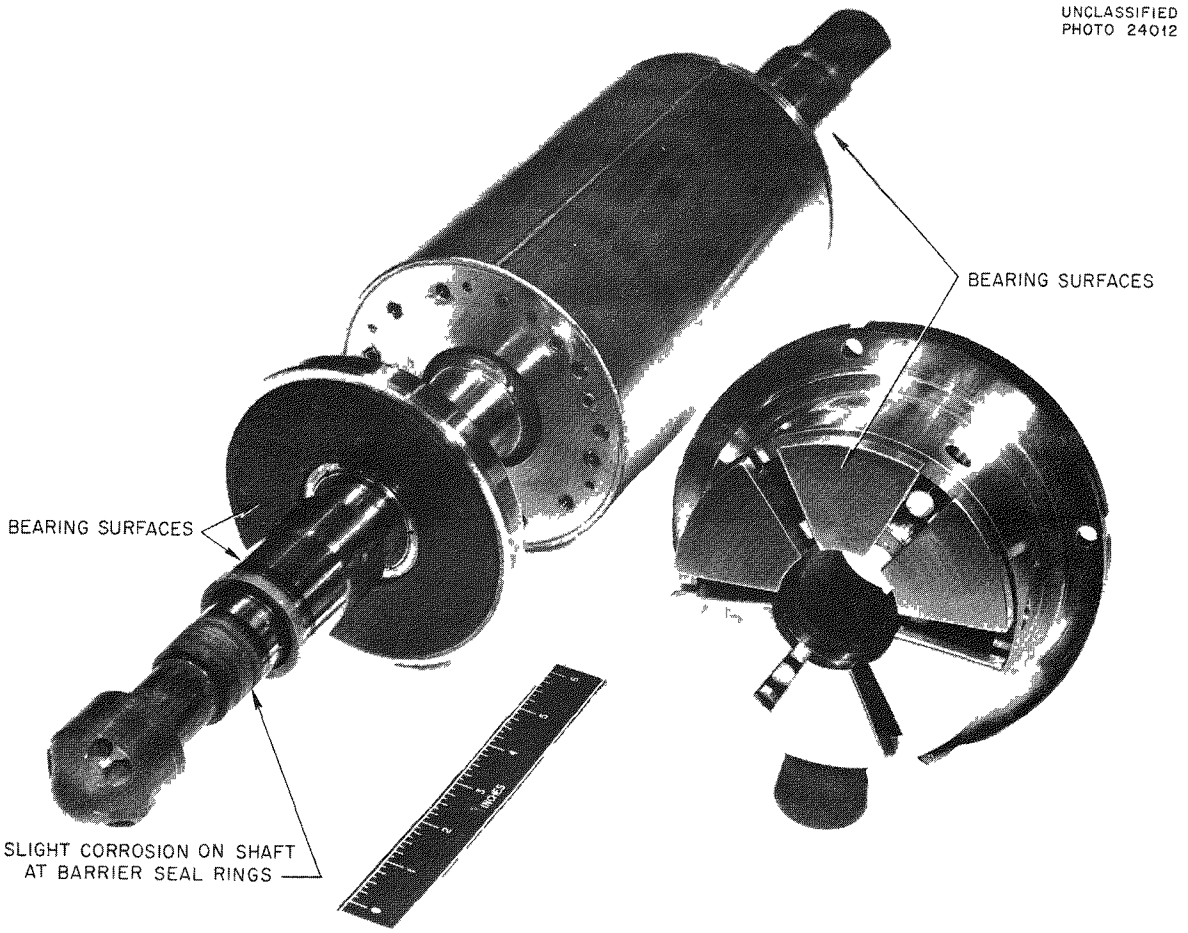

Fig. 4.1. Rotor Assembly and Kingsbury Thrust Bearing.

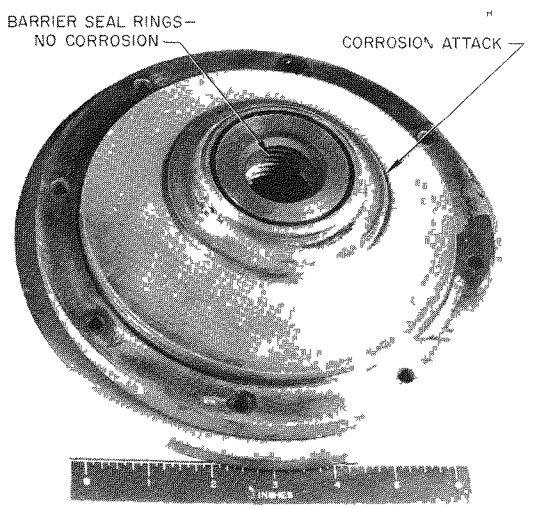

Fig. 4.2. Thermal Barrier – Motor Face.

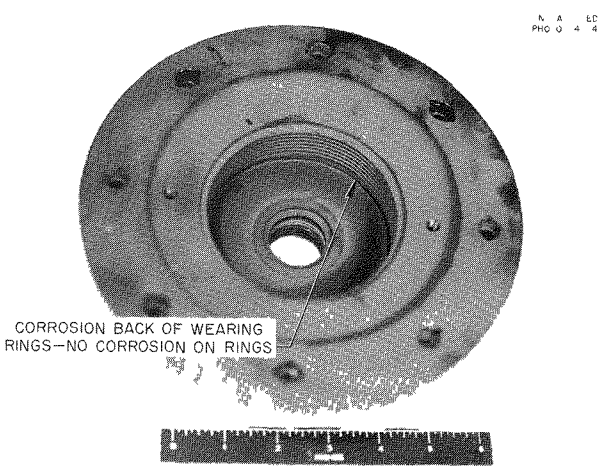

Fig. 4.3. Thermal Barrier – Impeller Face.

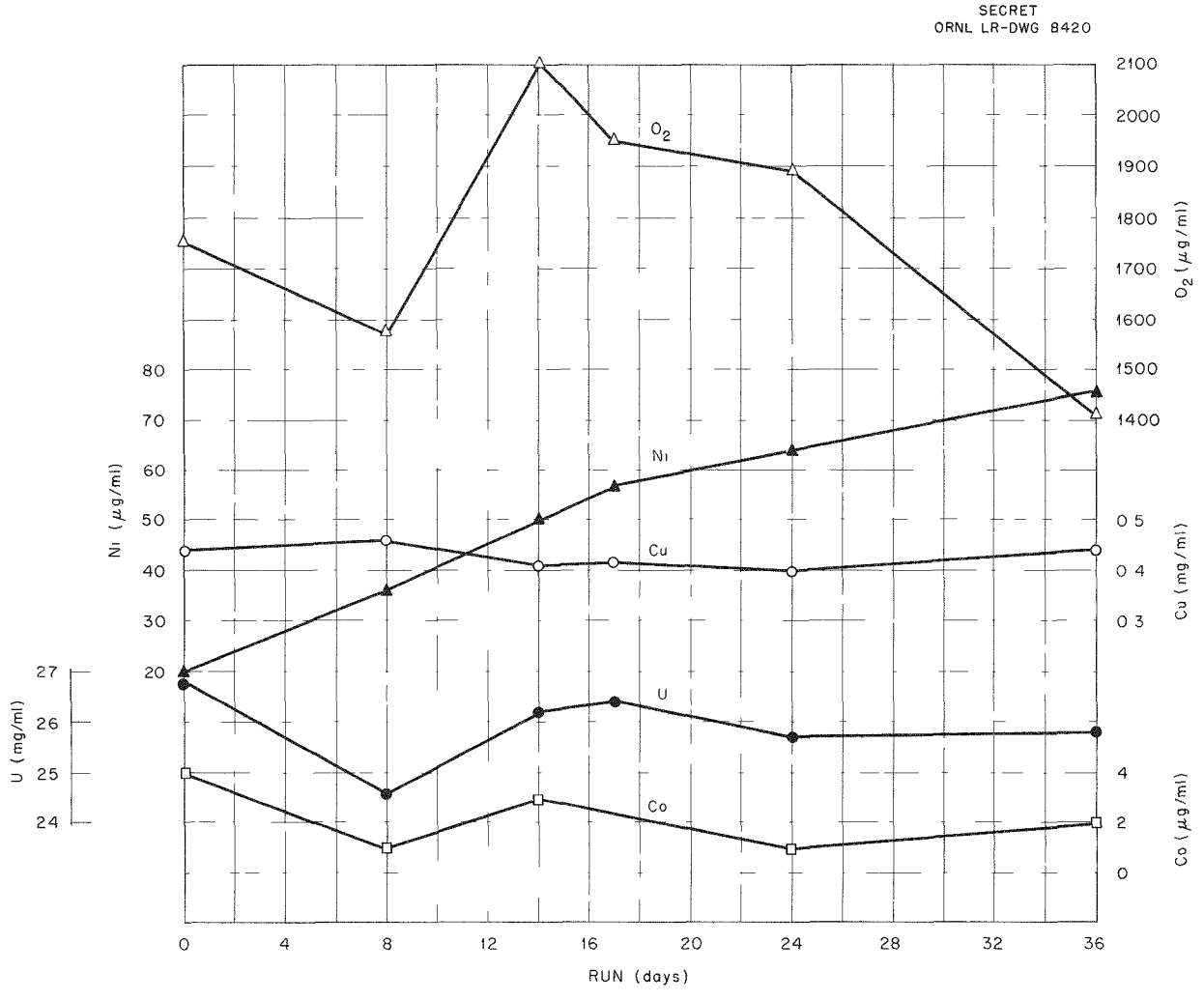

Fig. 4.4. 400A Pump Loop Run TA-9.

gasket. Such leaks usually appear after the pump has been disassembled several times. The O-ring gaskets have hard metal welds which leave little depressions in the gasket seating surfaces of the motor end and pump volute; subsequently, these depressions cause difficulty in properly seating gaskets. Some gaskets have cracked at the weld. In an attempt to attain a reliable seal, one development pump is being modified for use with a solid flat gasket. Also, consideration is being given to seal-welding the motor end and pump volute together during long runs. A custom-made seal-weld cutting machine is being investigated for use in disassembly of the pump.

4.2 FUEL AND BLANKET REACTOR PUMPS

During this period, the thermal barriers of the four pumps which are being obtained for the HRT were redesigned to incorporate a hollow air space to retard heat conduction and a metallic O-ring gasket to prevent liquid leakage around the barrier. Also, the pump design was changed to incorporate the use of a wide-face gold-plated stainless steel gasket, replacing the original proposal of a hollow O-ring type of seal on the main flange surfaces. This new gasket design will help in eliminating the high stresses in the volute and motor end shoulder bearing and the high percentage of seal

failures experienced with the various development pumps. A general inspection of the HRT pumps at Westinghouse Electric Corporation was made the week of July 11 while the first two stainless steel pumps were being machined for installation of the new thermal barriers. Inspection of the two HRT titanium-reinforced pumps showed some defects in the welding of the cooling coil to the flanges of the motor end. Evidences of porosity were found in one of the weld joints. Undercuts in the tube wall, caused by grinding weld surfaces, were unacceptable. These defects will be remedied before final acceptance of the pumps.

Procedure and specifications for inert-gas-shielded arc welding of titanium were received from Westinghouse for our review, comments, and approval. Thermal barriers and impellers of the two pumps are the only titanium parts to be welded.

4.3 HRT MOCKUP LOOP

Water operation of the HRT mockup loop has been summarized previously.[4] In the past quarter, a few additional water runs were made, and 416 hr was accumulated in three UO_2SO_4 runs.

In the water runs, two test dumps were carried out with the high-pressure loop originally at 300°C and 2000 psi. The two dumps differed only in that in the first case no gas was present and in the second the liquid in the high-pressure loop was saturated with air. Figure 4.5 shows the pressure-time behaviors which were observed when 71.5 liters of water and 58.4 liters of steam were dumped through a ½-in. dump valve and line. The two curves are parallel, but the pressure of the gas-saturated system was about 200 psi higher during most of the dump.

During recent runs, a pneumatic time-proportioning controller was used to regulate the pressurizer heaters. Its performance was as good as that of the induction regulator used formerly. Since the time-proportioner is much more compact, it will be used in the reactor.

Prior to the fuel runs, a purge water system of 25-gph capacity was added to the mockup. Flows of 10 gph and 0.75 gpm, respectively, were introduced into the pressurizer and circulating pump. Provision was also made for oxygen injection in the suction line of the injection pump.

[4] J. A. Hafford *et al.*, *HRP Quar. Prog. Rep. April 30, 1955*, ORNL-1895, p 33–37.

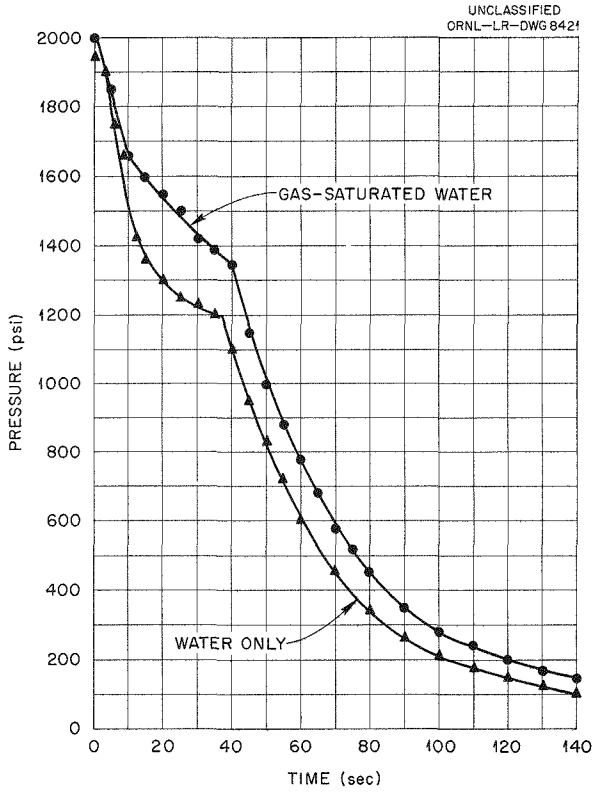

Fig. 4.5. Pressure-Time Curves of HRT Mockup Dumps.

The first fuel run, at an initial concentration of 0.004 *M* UO_2SO_4 with 50% excess acid, lasted for only 18 hr. During this period, the uranium concentration in the loop fell from 880 to 380 ppm. The trouble was traced to uranyl sulfate entrainment into the purge system and subsequent precipitation in the low-pressure part of the purge system. The cause of the precipitation has not been fully explained, but it may have been a corrosion reaction with a weld which showed localized attack. There appears to have been an oxygen deficiency involved, since the corrosion products contained considerable Fe_3O_4.

The low-pressure system was modified to minimize fuel carry-over into the purge water, and the second run was started. This run lasted for 138 hr, at which point a shutdown was forced by a serious leak in the seal ring of the 300A circulating pump and also a failure in the ORNL pump used at low pressure in connection with the purge system. The program for this run was as follows: 43 hr of

operation at 250°C with 1 g of uranium per kilogram of water, 22 hr at 300°C with 1 g of uranium per kilogram, 51 hr at 300°C with 2 g of uranium per kilogram, and 22 hr at 300°C with 5 g of uranium per kilogram. The oxygen level averaged 50 ppm in the high-pressure loop.

The uranium concentration was increased gradually in this run because it is believed that the protective film which results is superior to that obtained when starting directly with 10 g/kg solution. However, the generalized corrosion rates, based on soluble nickel, were somewhat higher than expected; 2.6 mpy was observed for the 1 g/kg portion of the run and 8.0 mpy for the 2 to 5 g/kg portion. The corrosion rate had leveled off only slightly at the end of the run.

When the pump was disassembled after the run, a fairly heavy deposit of black scale was found between the thermal barrier and the Kingsbury thrust-bearing assembly. This material was analyzed to be primarily U_3O_8, with small amounts of UO_2, Fe_2O_3, and Cr_2O_3. A fairly adherent corrosion film was noted on the pump and piping surfaces that had been in contact with high-temperature UO_2SO_4 solution. The only sign of localized attack was a small amount of pitting in and near the pump gasket seal ring which had leaked.

For the third fuel run, a gold-plated O-ring gasket was used as a seal ring. The purge flow to the pump was increased to about 1.3 gph in an effort to prevent precipitation in the thermal-barrier region. The nominal conditions of this run were 0.042 *M* UO_2SO_4 (10 g of uranium per kilogram), 15% excess H_2SO_4, and 0.005 *M* $CuSO_4$. The temperature was 300°C and the pressure was 2000 psi.

It was noted after the start of the run that solids (primarily iron and chromium oxides) were collecting in the back of the circulating pump and also that some fuel from the loop was mixing into the same region. Both these troubles were eliminated by increasing the pump purge flow to 1.8 gpm.

After about five days of operation, some uranyl sulfate leakage was again noticed at the pump seal. Since the amount of leakage was smaller than in the previous run, operation was continued to a total of 260 hr. At this point the system was shut down because chemical analyses of the fuel disclosed that uranium and copper were gradually disappearing from solution.

The uranium, copper, and SO_4 analyses indicated that a precipitation of 280 g of uranium and 14.5 g of copper, roughly 23.5% and 30%, respectively, of the total loop charge, had occurred in the loop. This precipitation had occurred gradually during the run and was accompanied by a decline in pH from 2.0 to 1.6. The soluble nickel analyses showed a constant generalized corrosion rate of 6 mpy. The mockup system was partially dismantled so that a search could be made for the missing material. The uranium was found present as U_3O_8 or UO_2; the copper was metallic or Cu_2O. Table 4.1 summarizes the distribution of precipitated uranium and copper in the loop.

The balance between the material lost and that found is better than might be expected from the accuracy of solid sampling and analysis. It is reasonable to believe that most of the missing material was found.

Two general types of solids were present in the loop. The first was a heavy, loose corrosion

TABLE 4.1. DISTRIBUTION OF URANIUM AND COPPER PRECIPITATION IN HRP MOCKUP LOOP

Location	Uranium (g)	Copper (g)
Crevices in pump thermal barrier, volute, and seal assemblies	73	0.4
Pressurizer lower header and heater legs	138	11
Piping scale, high-pressure system	40	3
Low-pressure sediment trap	0.44	0.04
Total precipitation found	251	14.4
Precipitation expected from analysis of solution	280	14.5

scale rich in Fe_2O_3 and containing about 3% uranium. This was deposited on the surfaces of the high-pressure loop and also as sediment in the pressurizer header. A small amount reached the low-pressure system and was trapped in the sedimentation tank. Based on the quantity of scale, a corrosion rate of 25 mpy is estimated, compared with 6 mpy from soluble nickel. It is believed that the heavy corrosion was caused by insufficient oxygen, because other loop experience at higher oxygen concentrations shows rates well below 1 mpy.

The second type of solid was rich in U_3O_8 and UO_2 and contained small amounts of iron, chromium, copper, and nickel oxides. It was found in the circulating pump crevices and in the pressurizer heater legs. In the pump the crevices showed severe pitting attack. This is seen in Figs. 4.6 and 4.7, which are photographs of the disassembled stator and casing. The solids in the pressurizer heater legs were associated with very light localized attack and appeared to be crystallized from the very dilute solution present. The uranium-rich solids appeared only in regions of severe oxygen deficiency, where circulating loop oxygen could not diffuse rapidly enough to satisfy the chemical demand.

Except for these chemical troubles, the HRT-type components continued to function properly. Over 1000 hr has been logged on the injection pump and 556 hr on the Westinghouse pump. The high-pressure pipe flanges have shown no leakage to date, after numerous thermal cycles in fuel as well as in water. The plug-seat clearance on valves

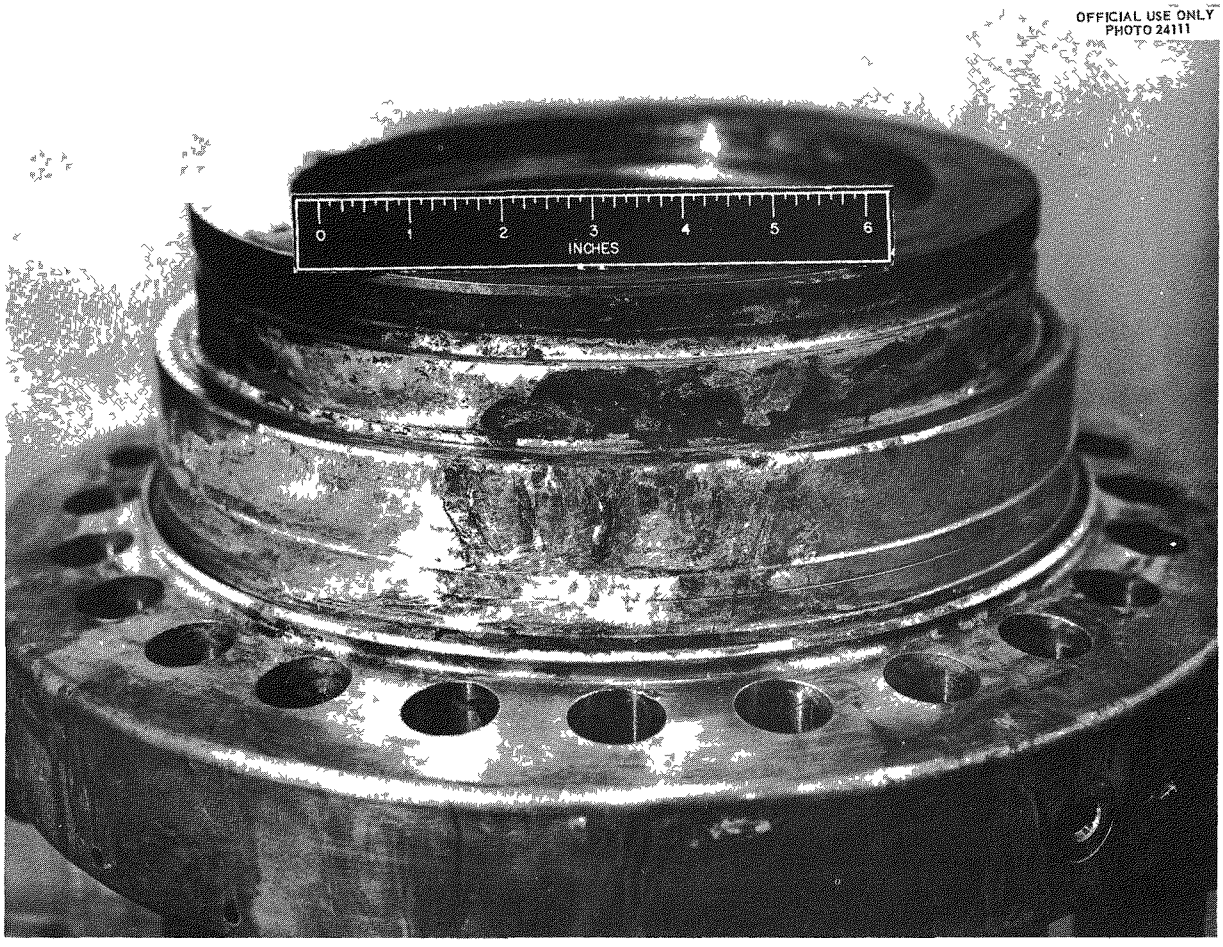

Fig. 4.6. HRT Mockup Pump Stator Assembly.

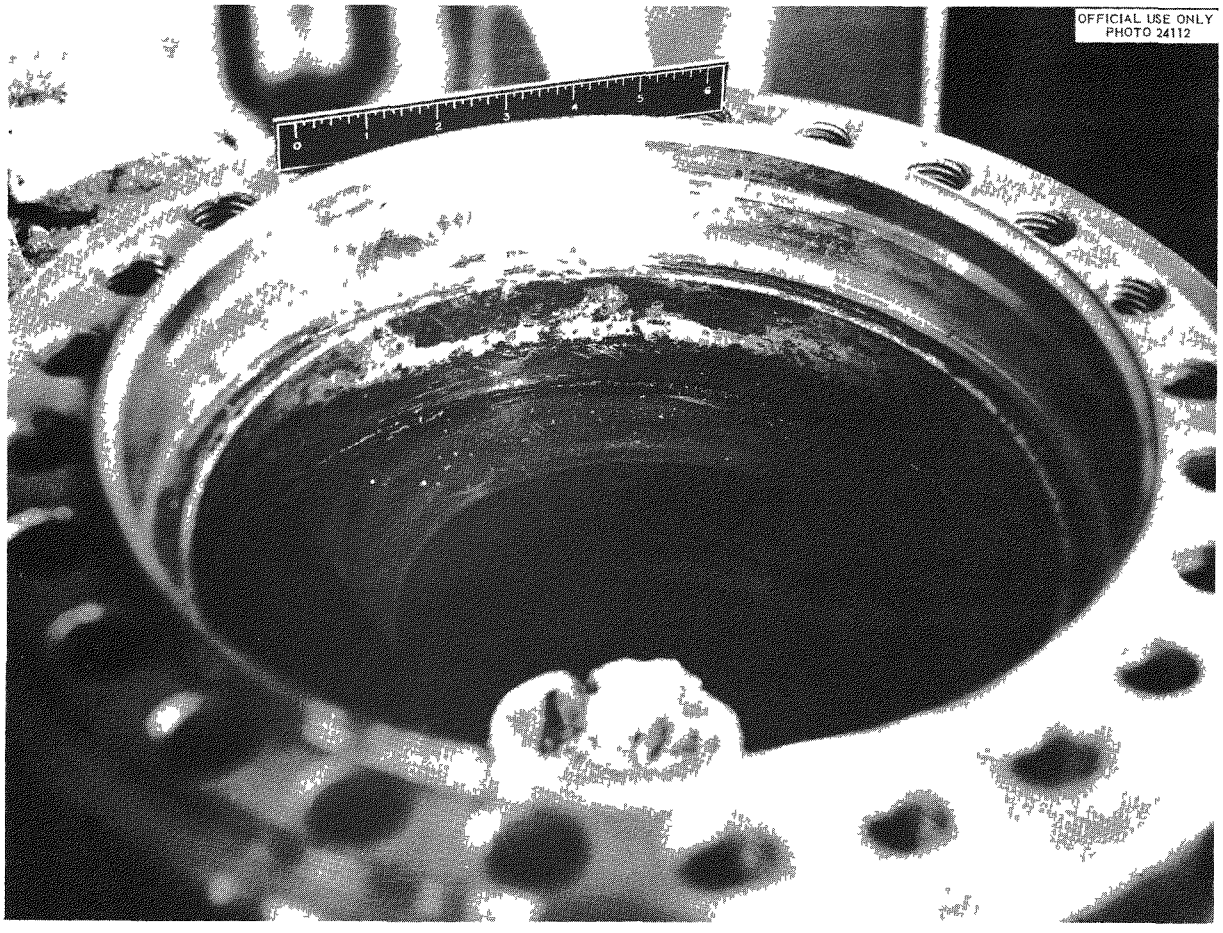

Fig. 4.7. HRT Mockup Pump Scroll.

has been increased to 0.002 in. to take care of film buildup on the surfaces, which resulted in valve sticking.

The gasket surface has been repaired, and the 300A pump has now been modified to include the new, hollow, thermal barrier and a wide flat seal gasket. This should eliminate the leakage past the thermal barrier and also reduce the volume of crevices considerably. The loop will be started up with the objective of determining the oxygen content required to stabilize the HRT solution. The HRT liquid level controller and pressurizer vent system will also be tested.

4.4 HRT HEAT EXCHANGERS

Fabrication of the HRT fuel and blanket heat exchangers was completed at the Carteret, New Jersey plant of the Foster Wheeler Corp. Both units are currently undergoing tests and inspection.

The tube-joint welding trouble encountered with the first exchanger and reported previously[5] was successfully eliminated, and similar welding on the second exchanger was satisfactory. Extra precautionary measures taken on the tube-joint welding of the second exchanger included 100% inspection, by ORNL personnel, during all welding and a requalification of the welder for each 75 first pass welds and each 25 second pass welds.

The blanket heat exchanger passed the specified 4000-psi primary side and 2500-psi secondary side hydrostatic tests with no leakage and was given a preliminary helium test with 1000-psi helium

[5] L. F. Goode and W. L. Ross, *HRP Quar. Prog. Rep. April 30, 1955*, ORNL-1895, p 29.

used in the primary side. The leakage rate from primary to secondary sides was acceptable. The seal weld between the channel and tube sheet of this unit was made successfully by Foster Wheeler and passed dye-penetrant inspection and high-pressure Freon testing. The unit was then subjected to the specified thermal-cycle test consisting of 50 cycles, wherein temperature of the incoming Dowtherm A was raised from 212 to 582°F in a period of 15 min and then lowered to 212°F in 15 min. After the second complete thermal cycle, leakage occurred across the channel gasket.

After completion of the thermal-cycle test by the first unit, the specified helium leak test between the primary and secondary sides was attempted. It was found that leakage had developed during the thermal-cycling testing. Foster Wheeler is cutting the seal weld, and an examination of the tube sheet will be made in an effort to determine the source of leakage.

The second exchanger is now undergoing the specified hydrostatic tests in preparation for the high-pressure helium test and subsequent thermal-cycling testing. A corrugated gasket made of solid stainless steel will be tested in this heat exchanger. A leak-free gasket must be developed for this unit at the Foster Wheeler Corp., since its initial operation at ORNL will be without a seal weld.

In view of the leakage problems arising as a result of the thermal-cycle testing, delivery of the two units might be delayed until September.

4.5 HRT DUMP TEST[6]

The initial phase of the HRT dump test program, consisting in tests of a single region system, was completed; a complete report of the data and results is now being written by P. F. Pasqua.

Recent tests were run to study the effect of bleeding of the reactor superpressure through the pressurizer bleed valves. The system was charged with 232 lb of water; after heating, there was 14 lb of saturated water at 236°C in the pressurizer and 218 lb at 300°C in the vessel proper. The system pressure was reduced from 2000 to 1250 psi (saturation pressure at 300°C) in 120 sec; 7.25 lb of water was removed in this period. Tests, in which nitrogen was injected into the bottom of the vessel to simulate the production of reactor gases, were inconclusive, since the amount of gas present and its location were not known accurately.

The system is now ready to be rebuilt for the second phase of the program, in which liquids will be dumped from two concentric pressure vessels. Equipment and procedures will be developed for controlling the simultaneous dumping of core and blanket of the HRT. Essentially all components are complete or available and only require assembly.

4.6 DUMP-VALVE TEST LOOP

The dump-valve test loop was completed and was put into operation with UO_2SO_4 solution.

4.7 HRT SAMPLER MOCKUP

Prototypes of the isolation chamber and sample flask holder were fabricated for testing prior to mocking up a complete sampler station.

Holdup in the isolation chamber varied from 3 to 4 ml. This is satisfactory.

The metal-to-metal (stainless steel) seal between the isolation chamber and sample flask holder was found to be unsatisfactory. A Teflon-to-stainless-steel seal was tested and proved to be effective in maintaining vacuum in the sample flask during the sampling operation. A second sample flask holder incorporating recommended changes is now being fabricated.

The ability of the isolation chamber to take a representative sample of suspended solids was determined by sampling from a circulating 0.1% slurry of thorium oxide at design flow rate of 300 lb per hour. Particle size of the ThO_2 was estimated as 1 to 10 μ. Samples taken from the isolation chamber were 10 to 20% low in ThO_2 compared with samples taken above and below the isolation chamber.

Tests presently planned will determine whether the vent valve on the isolation chamber can be eliminated and whether the holdup in the proposed bellows valves will affect the sample quality. "Memory" of the isolation chamber will be determined, and a modified sample flask holder will be tested.

Upon completion of the sample station mockup, it will be checked for mechanical reliability.

4.8 HRT THERMAL INSULATION

The conditions which must be met in the HRT thermal insulation are the following:

1. The insulation must be mechanically sound

[6] C. H. Gabbard, P. F. Pasqua, and R. VanWinkle, *HRP Quar. Prog. Rep. April 30, 1955*, ORNL-1895, p 31.

after several cycles, which include alternate water immersion and heating to 300°C.

2. Its water absorption should be small to guard against excessive contamination of the insulation if a leak occurs.

3. Fragments of insulation which might be radioactive should sink in water.

4. The insulation should have a good thermal efficiency.

One type of insulation which meets the above requirements consists of several thin aluminum sheets separated by air gaps. A 3-layer sample submitted by the Hunter Mfg. Corp. was tested on a 4-in. pipe at 620°F and showed the insulated loss to be 12% of the bare heat loss.[7]

The chief problem with the aluminum insulation is in the support material which separates the aluminum sheets. The cheapest satisfactory material appears to be unfired Lava A (trade name for machinable rock supplied by the American Lava Corp.). It has withstood several wetting-drying cycles between room temperature and 300°C with no mechanical damage and a water pickup (when wet) of 2.5% by weight.

4.9 TEST OF HRT REFLUX CONDENSER AND RECOMBINER

The HRT reflux condensers serve to remove heat after shutdown from the fuel and blanket outer dump tanks. Associated with this heating is a small amount of water decomposition gas which must be recombined and returned to the outer dump tanks.

The recombiner originally specified consisted of a platinized alumina catalyst bed between the reflux condenser and the off-gas system. Under normal operation, the condenser off-gas is a stoichiometric mixture of hydrogen and oxygen, which is quite explosive. For test purposes, a mixture of steam and stoichiometric gas, at a rate of 6.8 lb/min and 10.8 standard liters/min, respectively, was fed into the condenser-recombiner assembly. Explosions at about 2-min intervals were observed. The pressure peaks varied between 6 and 25 psi and were of $\frac{1}{25}$-sec duration according to a Baldwin cell mounted close to the recombiner. The true pressure peaks probably were considerably higher but of shorter duration. The explosions sounded like sharp hammer blows on the condenser, and over a long period might cause fatigue failures in some of the welds.

The explosions were followed by a vacuum condition of 1 to 5 psig which lasted up to 30 sec. During this period, air backed into the condenser from the off-gas line. After the pressure reached atmospheric, the gas flow resumed in the normal directions until the next explosion. Toward the end of the cycle, combustible gas was leaving the recombiner. This might be explained on the basis that the major portion of the catalyst surface was wetted during part of the cycle and not given sufficient time to be dried by the steam jacket around the recombiner section.

The originally specified recombiner was thus shown to be unsatisfactory. The following alternate systems were then considered:

1. About 1 scfm of air or argon might be circulated through the recombiner by means of a jet on the steam inlet to the condenser. This gas should serve as a diluent to prevent explosions. The only drawback to this system is the doubtful feasibility of a jet that would have to operate with about 1 psig steam in the HRT.

2. A series of catalyst baskets, steam-dried, could be used to act as "spark plugs" mounted in the condenser itself.[8] When an explosive gas mixture reaches a basket, a small explosion will result in part of the condenser. It is expected that the explosions produced in this manner would be considerably milder than those in the original design.

3. A series of platinized stainless steel tubes, steam-dried, might be used in a similar manner as the baskets (No. 2, above). In testing, it was found that a surface temperature of 325°C was required to produce ignition. The low-pressure steam, unfortunately, cools the platinized surface below this temperature. Electric heaters could be used in place of steam, but this would introduce other problems in underwater electrical leads.

Currently, catalyst baskets are being prepared for testing system No. 2. If they prove satisfactory, they will be used in the HRT.

[7] R. G. Akins and I. Spiewak, *Aluminum Insulation*, memo to C. B. Graham (June 23, 1955).

[8] W. R. Gall and R. E. Aven, *Outer Dump Tank Recombiner Program*, ORNL CF-55-5-187 (May 13, 1955).

5. CONTROLS AND INSTRUMENTS

W. P. Walker

M. C. Becker
A. M. Billings
J. R. Brown
R. L. Moore
L. R. Quarles[1]
R. E. Toucey
E. Vincens
K. W. West

5.1 GENERAL STATUS

The reported quarter was spent mainly on the detailed design of the instrumentation within the HRT control room area. This work is approximately 80% complete, including the following:

1. detailed layouts and cutouts, wiring, and auxiliary equipment mounting details for the main and auxiliary control panels;
2. approval and issuance of the functional control circuit schematic, together with all drawings necessary for construction and wiring of the relay cabinet;
3. schematic and wiring drawings for the control room area electrical distribution center;
4. preliminary drawings for the layout and piping of the instrument cubicles.

Figure 5.1 shows the front elevation of the main control panel. This panel has been designed as a semigraphic installation for ease of operation. Critical instruments are mounted in the center three panels for ease of observation. The first panel on the left side contains the "jumper board," that is, the graphic control circuit with provisions for deleting operational requirements.

The weigh cells, which were reported previously,[2] were received and were tested for sensitivity and compensation for ambient pressure. Tests showed that these units have a sensitivity of less than 0.1% and compensating errors of less than ¼% of *live* load.

5.2 DIFFERENTIAL PRESSURE TRANSMITTERS

Fabrication of the low-pressure differential pressure transmitters was started. These units are to be made of type 347 stainless steel with all-welded construction at points where they are in contact with process fluid. The output signal will be pneumatic (3 to 15 psi), derived from the standard force-balanced system provided on the Taylor[3] Model 333R transmitters. Figure 5.2 shows cross sections of the sensing portion of the 30-psia unit. In order to obtain an instrument with the range 0 to 30 psia and capable of withstanding 500 psi, a differential unit with one side evacuated will be used. The unit for 100 in. H_2O is identical except that a second pressure connection is used instead of the evacuation line.

5.3 LIQUID LEVEL TRANSMITTER

A prototype of a displacement-type liquid level transmitter was fabricated in accordance with TD-D-2713 for test on the HRT mockup loop. This unit is designed to operate at 2000 psi and 325°C, with a range of 5 in. of water, utilizing a Microformer-type pickup coil and spiral-spring suspension. The initial investigations of the coil and spring suspension were reported previously.[4]

In order to withstand the high temperature, fiber glass tape and Lavite spacers were used to insulate the coil from the body of the instrument. The coil was wound with ceramic-insulated wire and impregnated with silicone varnish. Exposure to temperatures as high as 250°C during tests produced no evidence of insulation failure. The actual operating temperature of the coil should not be this high. Tests are under way to prove the reliability of the coil with respect to temperature, radiation, and vibration.

To determine the error in the electronic circuitry as a function of temperature, the transmitter was operated at 250°C with a fixed core position. A 1% shift was observed when the temperature was changing at a rate of 3°C/min; however, this error disappeared as the temperature of the unit equalized. The increase of the null or unbalanced voltage in the instrument was negligible, indicating no appreciable phase shift.

The error due to the change in the modulus of

[1]Consultant.

[2]R. L. Moore, *HRP Quar. Prog. Rep. April 30, 1955*, ORNL-1895, p 38.

[3]Taylor Instruments Companies, 95 Ames Street, Rochester 1, New York.

[4]A. M. Billings, *HRP Quar. Prog. Rep. April 30, 1955*, ORNL-1895, p 39.

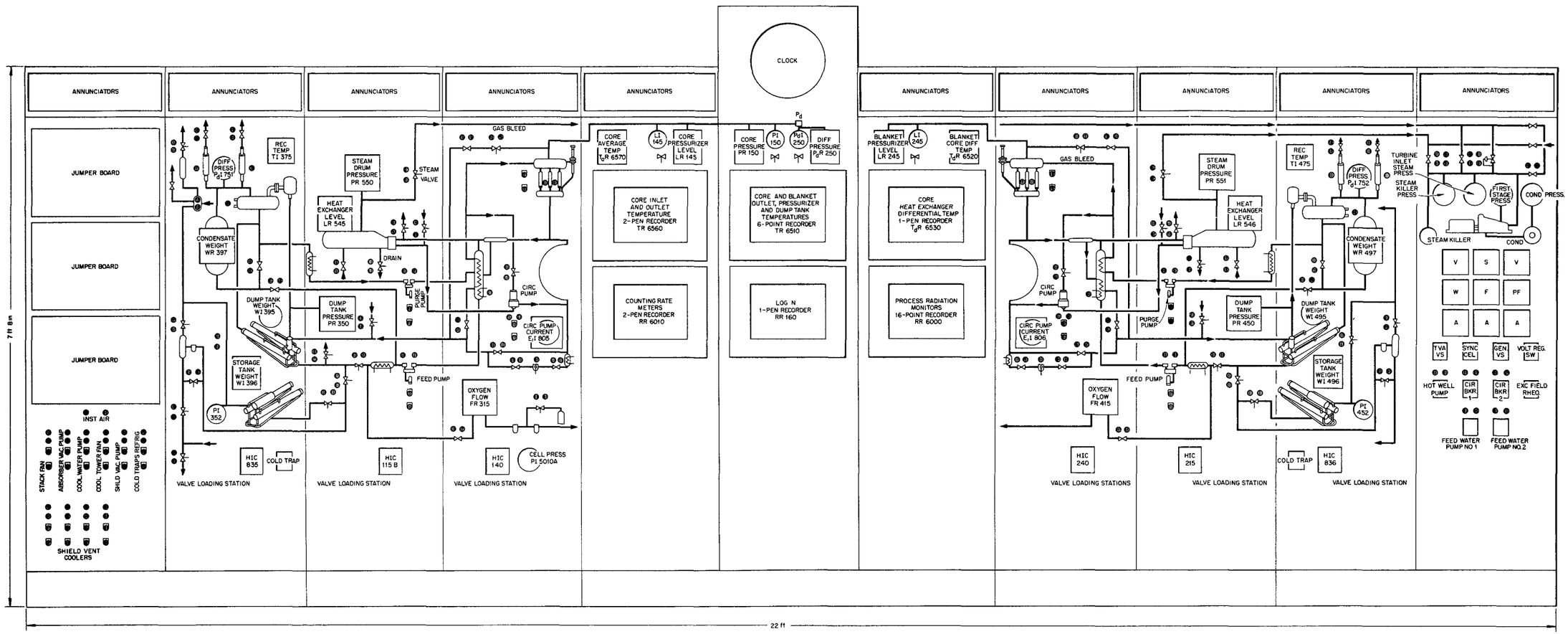

Fig. 5.1. HRT Control Panel.

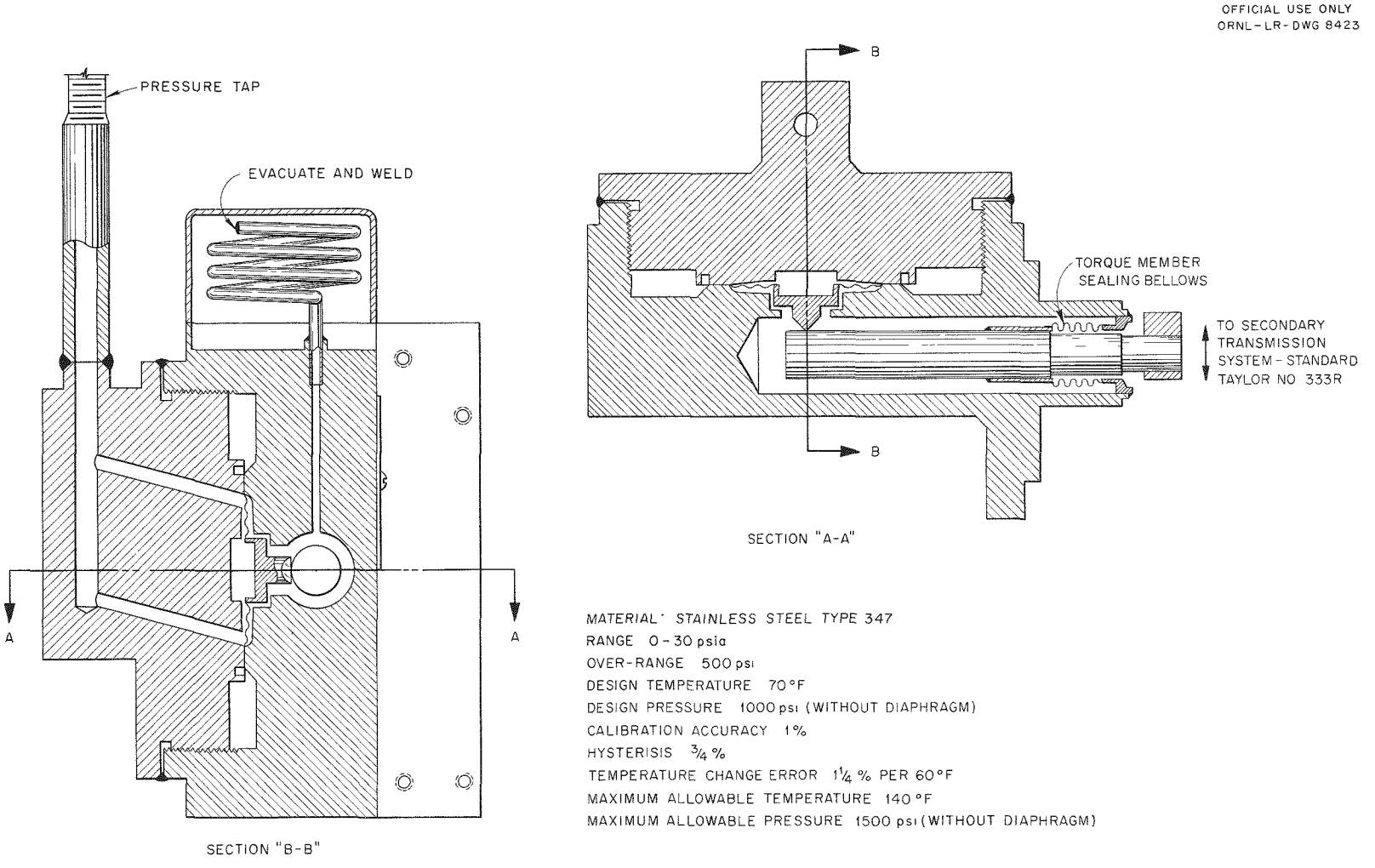

Fig. 5.2. 30-psia Differential Pressure Transmitter.

elasticity of the spring suspension was measured also. A 10% shift in zero was observed, which agreed with the calculations.

The unit, as designed, is extremely underdamped and very sensitive to vibrations. Operation on the HRT mockup loop should indicate whether this sensitivity is objectionable. Tests and design work were initiated to provide magnetic damping for the instrument and to eliminate difficulties experienced in the assembly of the present unit.

5.4 VALVES AND OPERATORS

The cylinder-type valve actuator,[4] which had previously been specified for use with the HRT valves, was abandoned by the manufacturer in favor of a metallic bellows type. Previous tests, upon which feasibility was based, involved the use of a lubricating and sealing grease with a nylon O-ring between the piston and the cylinder wall. Since the radiation dosage expected is approximately 5×10^9 r, the radiation damage to any known grease would cause it to harden and to lose its lubricating and sealing properties. Further work by the vendor indicated that it would not be feasible to operate the units using the nylon with no lubricant or even with dry lubricants, because the degree of compression required to obtain a reasonable leak rate across the piston (0.1 scfm with 100-psi pressure drop) was such that the actuator would not operate smoothly and reliably. The vendor is now constructing a prototype bellows actuator for test and evaluation.

Two bellows-sealed sampling valves similar to the HRT $\frac{1}{8}$-in., 2000-psi valve[5] were installed in a 400A pump loop for use in sampling service. These valves were fabricated with a Stellite No. 6 plug and type 347 stainless steel integral seat. After 200 operations of sampling or draining solutions at elevated temperatures, these valves were still leaktight. One half of these operations were with water, and the other half were with 10 to 30 g of uranyl sulfate per liter in the loop. Each operation consisted of withdrawing approximately 50 cc from the loop (at 1500 to 1700 psi and 300°C) into a container at atmospheric pressure. Figure 5.3 shows the stem, bellows, and plug assembly. Figure 5.4 shows the magnified view of the plug. The high pressure was applied under the seat on these valves, and it is notable that the more severe attack took place above the seating region, where the flashing or two-phase flow would be expected to be initiated.

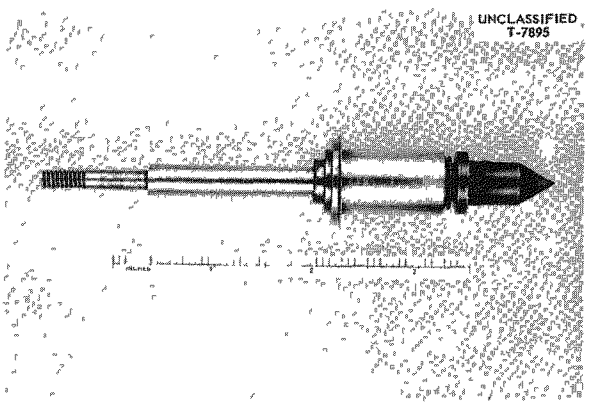

Fig. 5.3. Sampling-Valve Stem Assembly.

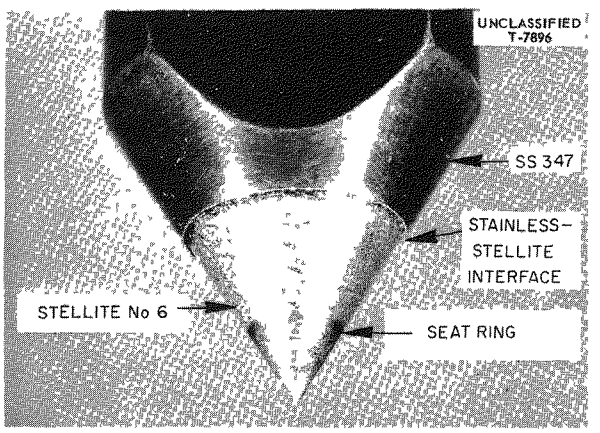

Fig. 5.4. Sampling-Valve Plug.

[5] J. N. Baird *et al.*, *HRP Quar. Prog. Rep. Oct. 31, 1954*, ORNL-1813, p 37.

Part II

THORIUM BREEDER REACTOR

R. B. Briggs J. A. Lane

6. REACTOR ANALYSIS

P. R. Kasten

H. C. Claiborne M. Tobias T. B. Fowler

6.1 STABILITY OF HOMOGENEOUS REACTORS

The stability of reactor systems is related to the reactor operating conditions and nuclear characteristics. In the present discussion it is assumed that the stability relations in a two-region reactor are determined by the core-system characteristics. Under most circumstances this will be true if a large fraction of the power is generated in the core region. The equations of motion for a one-region reactor will, therefore, be assumed applicable to both one- and two-region machines, and so differences in stability of the two types of reactors will be due to differences in operating power densities and nuclear parameter values, rather than to the criteria for stability.

6.1.1 Stability Criteria

It can be shown,[1] from the linearized equations of motion for a one-region reactor, that the conditions which have to be satisfied are given by

$$
\begin{aligned}
(1)\quad & \epsilon^3[\omega_b^2(1+C_2)+\gamma(\alpha_1+\gamma)]\alpha_1 \\
& + \epsilon^2\{(\alpha_1+\gamma)\alpha_1[\omega_b^2(1+C_2)+\gamma(\alpha_1+\gamma)]\} \\
& + \epsilon[\omega_b^2(1+C_2)+\alpha_1\gamma][\omega_b^2(1+C_2)+\gamma(\alpha_1+\gamma)]\alpha_1 \\
& + \alpha_1\gamma\omega_b^2(1+C_2)[\omega_b^2(1+C_2)+\gamma(\alpha_1+\gamma)] \\
& > \epsilon^2\omega_b^2\omega_n^2 + \epsilon[2\omega_b^2\omega_n^2(\alpha_1+\gamma)] \\
& + (\alpha_1+\gamma)^2\omega_b^2\omega_n^2 > 0,
\end{aligned}
$$

where

- ϵ is related to the residence time of fluid in the reactor core,
- ω_b is the frequency of the hydraulic system,
- C_2 is related to the pressurizer volume,
- γ is a function of the delayed neutron fraction,
- α_1 is related to the fluid friction between the core and pressurizer,
- ω_n is the frequency of the nuclear system.

If fluid-flow effects within the reactor can be neglected in Eq. 1, then $\epsilon = 0$, and the stability-criteria inequalities simplify to

$$
(2)\quad \alpha_1\gamma[\omega_b^2(1+C_2)+\gamma(\alpha_1+\gamma)] > (\alpha_1+\gamma)^2\frac{\omega_n^2}{1+C_2} > 0.
$$

Since all quantities are positive, the inequality on the right in Eq. 2 is always satisfied. By replacing the other inequality with an equals sign and fixing all parameters but one, the value of the remaining parameter (which barely fails to satisfy the inequality) can be obtained. Equation 1 (with an equality sign used in the expression) is given in Figs. 6.1 to 6.3 as a function of parameter values. Stable operating conditions are those lying above the appropriate curves in Figs. 6.1 to 6.3.

Reasonable values for ϵ lie between 0.2 and 2 sec^{-1}, corresponding to core residence times between 10 and 1 sec. As illustrated in Figs. 6.2

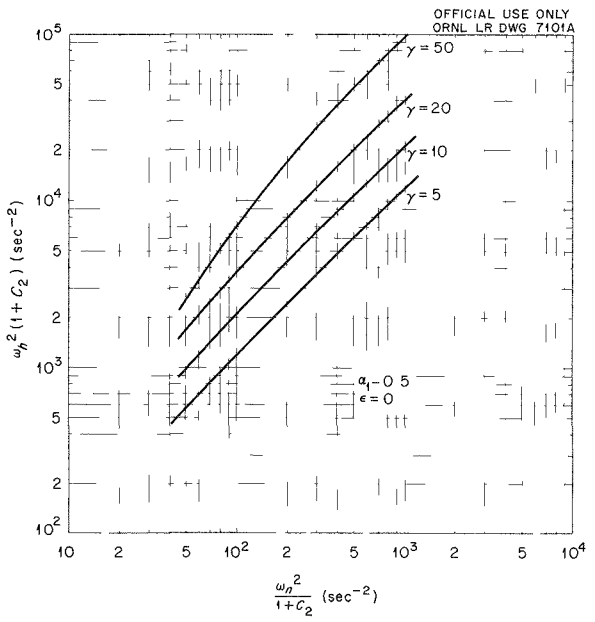

Fig. 6.1. Stability Criteria for Homogeneous Circulating Reactors. Reactor is stable if operating position lies above and to the left of the appropriate curve.

[1] P. R. Kasten, *Stability of Homogeneous Reactors*, ORNL CF-55-5-163 (May 25, 1955).

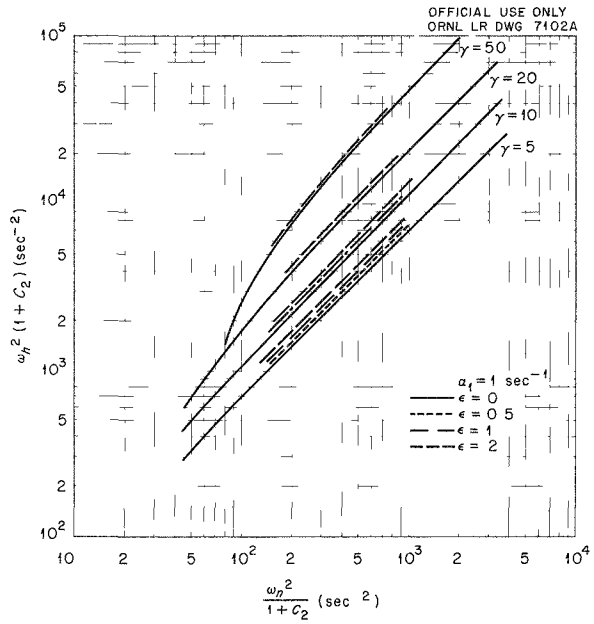

Fig. 6.2. Stability Criteria for Homogeneous Circulating Reactors. Reactor is stable if operating position lies above and to the left of the appropriate curve.

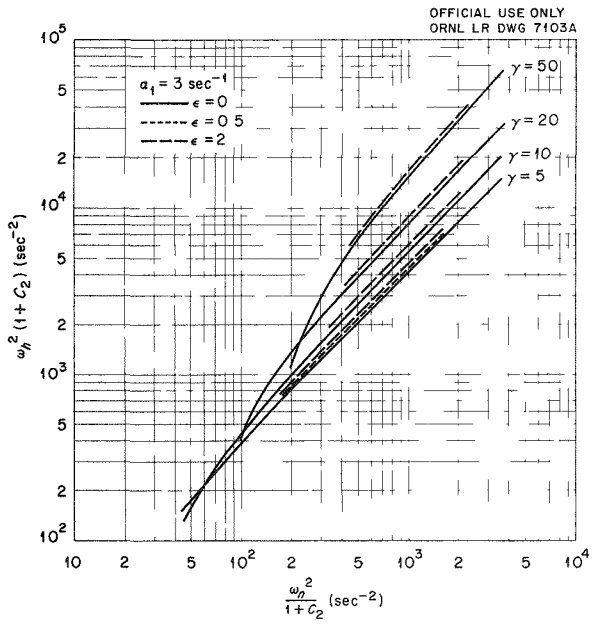

Fig. 6.3. Stability Criteria for Homogeneous Circulating Reactors. Reactor is stable if operating position lies above and to the left of the appropriate curve.

and 6.3, increasing ϵ increases the stringency of the stability condition at low values of α_1. However, as shown below, the influence of fluid circulation in the reactor system will more than compensate for the effect of flow in the reactor core alone.

6.1.2 Fluid-Circulation Effects

In obtaining Eq. 1, it was assumed that the heat exchanger would always return core fluid at a constant temperature. A more reasonable assumption would be to consider that the power removed from the shell side of the heat exchanger was constant. This would allow the temperature of the fluid entering the core to vary as a function of time.

The resultant expression of the stability criteria is more complicated than Eq. 1 and involves the ratios of the volume heat capacities of the reactor core, heat-exchanger core fluid, and cooling fluid. For numerical work the parameter values given in Table 6.1 were assumed, where S is the volume heat capacity of the fluid, the subscripts c, s, and h refer to the fluid in the core, shell side of heat exchanger, and tube side of heat exchanger, respectively, and α_2, α_3, and α_4 are functions of S_s, S_c, S_h, and the rate of heat transfer from the core side to the shell side of the heat exchanger.

The stability criteria were then obtained in terms of allowable values of $\omega_h^2(1 + C_2)$ for a chosen value of $\omega_n^2/(1 + C_2)$ as shown in Fig. 6.4.

Previous stability studies[2] showed that the effects of circulation would always tend to damp any power oscillations so long as the Fourier sine transform of $K(t)$ was greater than zero, where $K(t)$ is a weighting kernel, relating the actual power removal from the reactor to the past reactor power. In such studies, the pressurizer system was neglected. Based on the results given in Fig. 6.4, inclusion of the pressurizer system does not appear to alter the effect of fluid circulation; namely, circulation tends to damp out any pressure (or power) oscillations. The magnitude of the effect is illustrated in Fig. 6.4, which indicates that for large values of ω_n^2 little damping action is afforded by circulation. Under such circumstances, neglect of fluid circulation is justified, since such neglect introduces only small changes in the stability criteria. At lower values of ω_n^2 the effect of circulation upon the stability criteria can be appreciable

[2] W. K. Ergen and A. M. Weinberg, *Physica* 20, 413–426 (1954).

TABLE 6.1. PARAMETER VALUES CHOSEN FOR FLUID CIRCULATION STUDY

$\frac{S_s}{S_c}$	α_4 (sec^{-1})	α_3 (sec^{-1})	α_1 (sec^{-1})	γ (sec^{-1})	α_2 (sec^{-1})
1	3.3	6.33	1.0	50	3.8
3	1.1	3.80	1.0	50	3.8
10	0.33	3.10	1.0	50	3.8

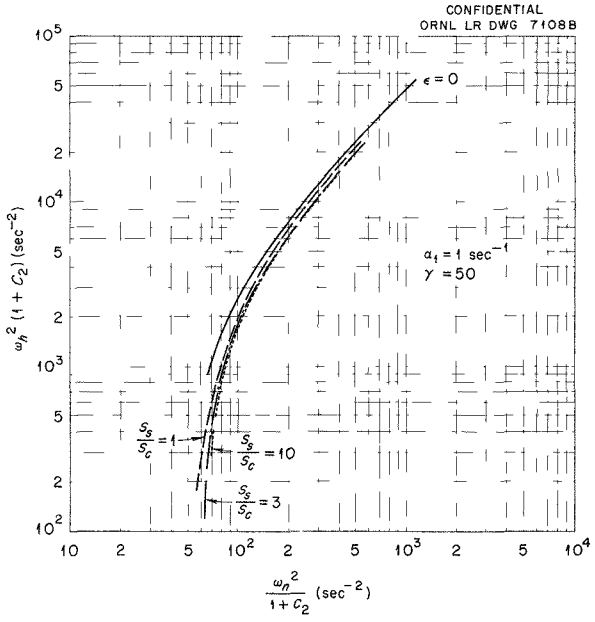

Fig. 6.4. Stability Criteria for Homogeneous Circulating Reactors. Reactor is stable if operating position lies above and to the left of the appropriate curve.

insofar as degree of stability is concerned. However, the $\epsilon = 0$ curve is reasonably accurate (and also conservative) and more convenient for design bases. Some advantage is gained in stability by increasing the value of S_s/S_c, but for the assumed conditions little is gained by increasing S_s/S_c above a value of 3.

6.1.3 One- and Two-Region Reactor Conditions

Generally, a one-region machine will operate at a power density lower than that at which the corresponding two-region reactor is operated, and the physical size of the one-region reactor will be larger. On the basis of economic studies,[3] the optimum two-region reactor will operate at a core power density of 100 to 200 kw/liter, and a one-region machine at power densities of 15 to 30 kw/liter. For the same output power, then, the total volume of the one-region reactor is roughly eight times the core volume of the two-region system. Assuming that the exit velocities, U_0, of the core fluid are about the same and that the effective length of piping between the core and pressurizer is the same, α_1 will not vary for the two reactor types.

With the same operating conditions with respect to fluid temperature and pressure, the ratio of ω_b^2 for the two reactors will be given approximately by

$$\frac{(\omega_b^2)_1}{(\omega_b^2)_2} \cong \frac{1}{8},$$

where the subscripts 1 and 2 refer to one- and two-region reactors, respectively. In the above equation it is assumed that the core-fluid temperature rise in passing through the core and the fluid exit velocity are the same for each reactor.

The ω_n^2 ratio for the two reactor types is

$$(\omega_n^2)_1 \cong \frac{1}{16} (\omega_n^2)_2 .$$

The value of $1 + C_2$ will be about the same for the two reactor types, so the net effect in going from a two-region to a one-region machine is to decrease ω_b^2 by 8 and ω_n^2 by 16 in the above case. Examination of the stability criteria given in Figs. 6.1 to 6.3 shows that such a decrease results in greater stability for the one-region reactor. About the same degree of stability would result if the product of $\omega_b^2 \omega_n^2$ remained constant in going from a one-region to a two-region reactor.

[3] H. C. Claiborne and M. Tobias, *Some Economic Aspects of Thorium Breeder Reactors*, ORNL-1810 (to be published).

Assuming that the value of $A_1/A_2 = 2$, then

$$(\alpha_1)_2 = 2(\alpha_1)_1$$

and

$$(\omega_b^2)_1 \cong \frac{1}{4}(\omega_b^2)_2 .$$

An advantage may be gained by such a change if the desirable increase in ω_b^2 is not offset by the undesirable decrease in α_1. Results given in Figs. 6.1 and 6.2 indicate that no significant advantage is gained by such a change.

To be specific, consider the TBR, which has a core power density of approximately 190 kw/liter. Reasonable values for the parameters are

$$\alpha_1 \cong 1 - 3 \text{ sec}^{-1},$$

$$\omega_n^2 \cong 70 \text{ sec}^{-2},$$

$$\omega_b^2 \cong 13{,}000 \text{ sec}^{-2},$$

$$\gamma \cong 5.$$

By comparing this operating condition with the curves shown in Figs. 6.1 to 6.3, it is seen that operation is well within the stable region.

In general, stability problems are most likely to occur in small-size high-power-density reactors (for example, in the HRT with a heavy slurry blanket, instabilities are indicated at power densities above approximately 60 kw/liter).

NOMENCLATURE

A = cross-sectional area of relief pipe, ft^2

C_2 = conversion factor = $\dfrac{144 g_c}{v_s^2}\dfrac{P_0}{\rho_0}\dfrac{V_c}{V_p}$

bA_b = heat-transfer coefficient of heat exchanger times heat-exchange area, kw/°C

g_c = dimensional constant, $\dfrac{32.2 \text{ lb mass·ft}}{\text{lb force·sec}^2}$

$\dfrac{\partial k_e}{\partial \rho}$ = density coefficient of reactivity, ft^3/lb mass

$\dfrac{\partial k_e}{\partial T}$ = absolute value of temperature coefficient of reactivity, °C^{-1}

L = length of piping between core and pressurizer surface, ft

P_0 = reactor power evaluated under initial conditions, kw

S_c = heat capacity of core fluid volume, °C/kw-sec

S_b = heat capacity of heat-exchanger fluid volume, °C/kw-sec

S_s = heat capacity of shell side fluid volume of heat exchanger, °C/kw-sec

t = time, sec

U_0 = U evaluated under initial conditions, fps

v_s = velocity of sound in core fluid, fps

$= \sqrt{\dfrac{dp}{d\rho}\, 144 g_c}$

V_c = volume of fluid in reactor core, ft^3

V_p = volume of pressurizing fluid in pressurizer, ft^3

$\alpha_1 = \dfrac{n_f U_0}{L}$ normalized friction coefficient, sec^{-1}

$\alpha_2 = \dfrac{bA}{S_s}\left(1 + \dfrac{S_s}{S_c + S_b}\right)$, sec^{-1}

$\alpha_3 = \dfrac{S_c}{S_c + S_b}$, dimensionless

$\alpha_4 = \dfrac{bA_b}{S_s}$, sec^{-1}

β = effective fraction of fission neutrons which are delayed, dimensionless, $\beta = \sum_i \beta_i$

$\gamma = \dfrac{\beta}{\tau}$, sec^{-1}

$\epsilon = 2/t_r$, where t is the average residence time of a fluid particle in the core, sec^{-1}

ρ_0 = average core fluid density, lb mass/ft^3

τ = mean lifetime of prompt neutrons, sec^{-1}

$\omega_b^2 = \dfrac{Av_s^2}{V_c L}$ = square of frequency of hydraulic systems, sec^{-2}

$\omega_n^2 = \dfrac{1}{\tau}\dfrac{\partial k_e}{\partial T}\dfrac{P_0}{S_c}$ = square of frequency of nuclear system, sec^{-2}

6.2 EFFECT OF SLURRY SETTLING ON REACTIVITY IN A ONE-REGION THORIUM BREEDER REACTOR

In a one-region reactor operating with a slurry fuel (UO_3-ThO_2-D_2O), there exists the possibility

of a reactivity increase, if rapid settling of the slurry should occur. However, the fissile material settles along with the fertile material, and, under certain conditions, the decrease in resonance-escape probability and the increase in radial leakage would more than compensate for the D_2O reflector formed at the top, in which case no reactivity increase would occur.

Two-group calculations were made to determine the order of reactivity change with uniform settling for reactor conditions in the range of economic interest[3] (10 to 12 ft in diameter, 200 to 300 g of thorium per liter). As a first approximation, the reactor was considered to be an optimum cylinder (height = 1.847 × radius). The slurry was assumed to be homogeneously distributed in the bottom portion of the reactor, with a D_2O reflector on top. The amount of fuel required for criticality was calculated and compared with the amount of fuel initially required before settling occurred.

The main results of this study are shown plotted in Fig. 6.5. It is evident that supercriticality by thermal neutrons cannot occur for the cases studied, although there is still a question as to the effect of resonance and fast fissions on criticality as the slurry settles.

The effect of uniform settling is less pronounced as the reactor diameter and poisons are increased and as the thorium concentration is decreased. Calculations made for 3-in. settling in a 20-ft reactor indicate that a slight supercriticality occurs when the fuel contains 200 g of thorium per liter.

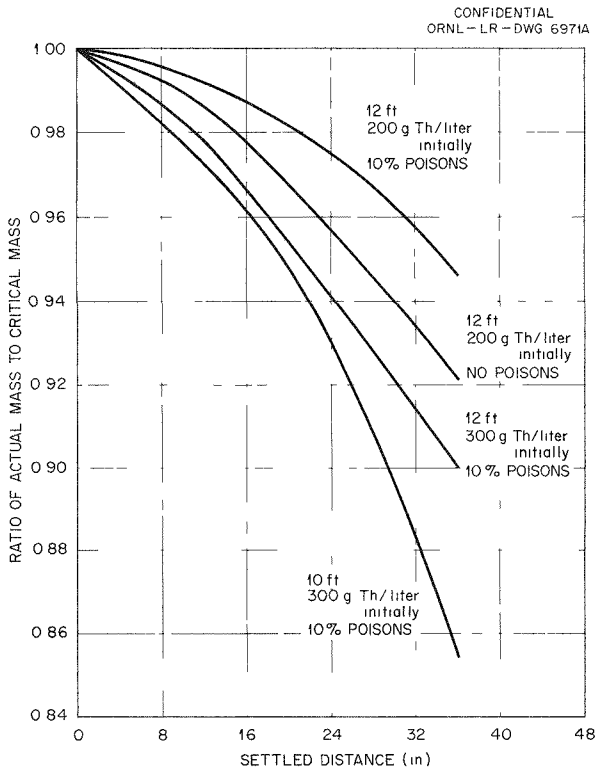

Fig. 6.5. Effect of Settling on Reactivity. Reactor is stable if operating position lies above and to the left of the appropriate curve.

6.3 NEUTRON LOSSES IN THE TBR DUE TO THE USE OF PLATINUM AS A PROTECTIVE COATING FOR THE ZIRCONIUM CORE TANK

Recent cross-section measurements of the isotopes of platinum[4] have led to the belief that this element should be re-examined, with the aim of evaluating it as a corrosion-resistant lining for reactor vessels. The flux-time variation of the average cross section of a layer of platinum covering the zirconium core tank of the TBR and the effect of this variation upon the breeding ratio are reported here.

The cross-section measurements indicate that the majority (92%) of the platinum isotopes must pass through the 196 isotope stage before conversion to other elements. A chart of the reaction processes is displayed in Fig. 6.6.

The mathematical problem of finding the isotope concentrations offers no theoretical difficulty but is too cumbersome to treat directly in practice. For present purposes, several simplifications were made which were considered valid in the flux-time range treated:

1. The macroscopic absorption cross sections of platinum isotopes 191 and 193 were assumed to be equal to those of their immediate predecessors, and their concentrations were assumed to vary according to the destruction rates of their predecessors.
2. Radioactive decay to or from the iridium isotopes was neglected.
3. The macroscopic-cross-section contribution of each of the isotopes succeeding Pt^{196} (ending with Hg^{202}) was assumed to be equal to that of Pt^{196}.

The variation of the average cross section with

[4]H. F. McDuffie and H. S. Pomerance, *Thermal Neutron Cross Sections of Platinum Isotopes*, ORNL CF-55-3-229 (March 15, 1955).

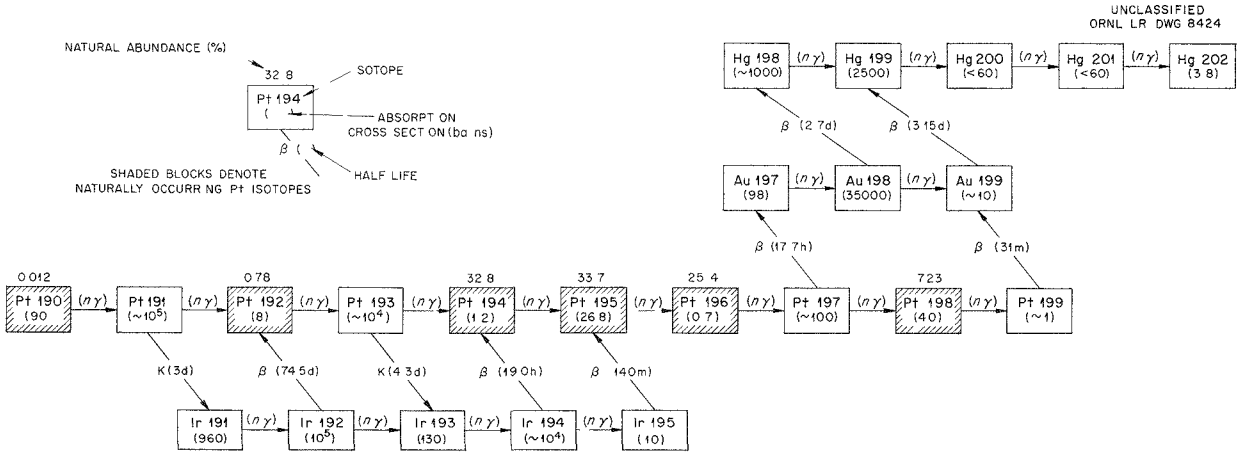

Fig. 6.6. Nuclear Processes Undergone by Platinum. Shaded blocks denote the naturally occurring platinum isotopes. Numbers in parentheses in the blocks are absorption cross sections in barns. Numbers in parentheses on arrows are half lives for the decay processes indicated. Numbers above shaded blocks indicate the natural abundance of the isotope in per cent.

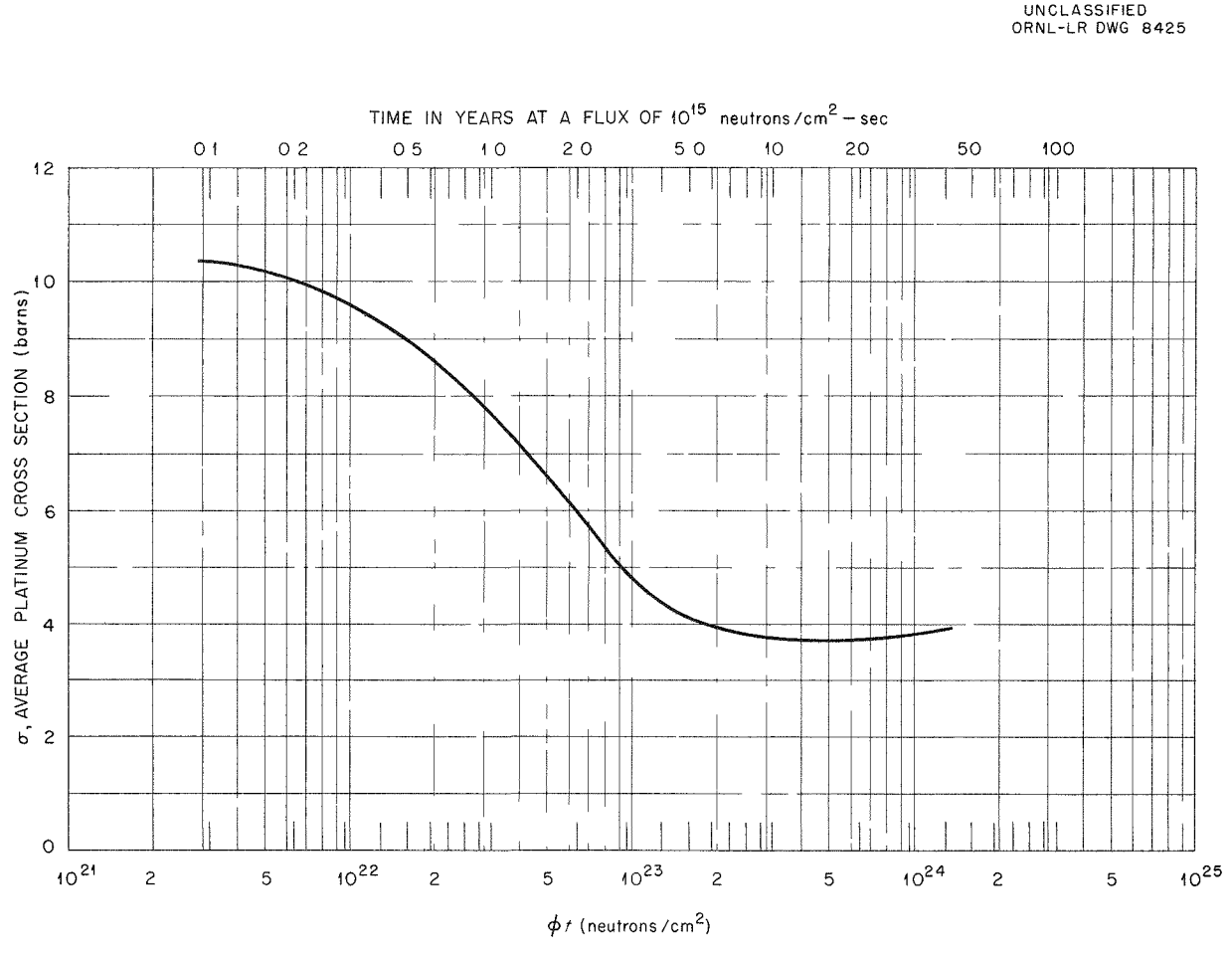

Fig. 6.7. Average Platinum Cross Section at 2200 m/sec as a Function of Flux Time.

ϕt is shown in Fig. 6.7. The flux-time range corresponds to an exposure to a flux of 10^{15} neutrons/cm^2/sec for a period of 0.1 to 40 years. A minimum of 3.7 barns (2200 m/sec) is reached in about 14 years; as can be seen, the curvature in the neighborhood of the minimum is quite small so that the 4-barn level is reached in less than seven years. The average cross section over a ten-year period is about 5 barns, representing an approximate loss of 0.02 in the breeding gain of the TBR for a layer of platinum 10 mils thick (or 0.01 and 0.03 for 5 and 15 mils, respectively). A loss of 0.02 in breeding gain corresponds to a loss of about 15% of the excess fuel production.

Another important consideration may be the buildup of mercury in the platinum. Estimates indicate that in three years at a flux of 10^{15} neutrons/cm^2/sec about 5% of the platinum will be converted into mercury, and in eight years about 10% will be transformed. It is not known at the present time just how large a conversion is permissible from the standpoint of reliability of the platinum as a protective coating.

6.4 HOMOGENEOUS PLUTONIUM-URANIUM REACTORS

Some economic aspects of one-region homogeneous power reactors fueled with PuO_2-UO_3-D_2O slurries were investigated as functions of operating conditions and nuclear characteristics. Where possible, the same bases were used as in the previously reported[5] one-region thorium breeder studies.

In the reactor system studied, the plutonium produced was fed back as reactor fuel after recovery in a Purex plant. The separated uranium was recycled to a diffusion plant for re-enrichment. Since in all cases the breeding ratio was less than unity, the additional fuel requirement was met by a uranium feed of an enrichment dictated by the operating conditions.

As a result of the feedback of plutonium, the equilibrium concentration of plutonium in the reactor was high enough for resonance absorptions and fissions to have an appreciable effect. A six-group method was used for the nuclear calculations in an effort to account for the resonance absorptions in uranium and plutonium. Although the resonance data for the plutonium isotopes are insufficient for accurate calculation of the resonance effects, the results obtained indicate the economic influence of absorption by plutonium. The most important uncertainty in the nuclear data is the value of η for Pu^{241}. Estimated values lie between 1.9 and 2.4, and so in the cases studied the extreme values were assumed.

The results obtained are for a 480-Mw one-region reactor system operated at an average temperature of 280°C and delivering 125 Mw of electrical power. The unit cost of power, as shown in Fig. 6.8, is a net partial cost composed of the following charges: inventory, net uranium feed (total feed minus credit for material returned to diffusion plant), D_2O make-

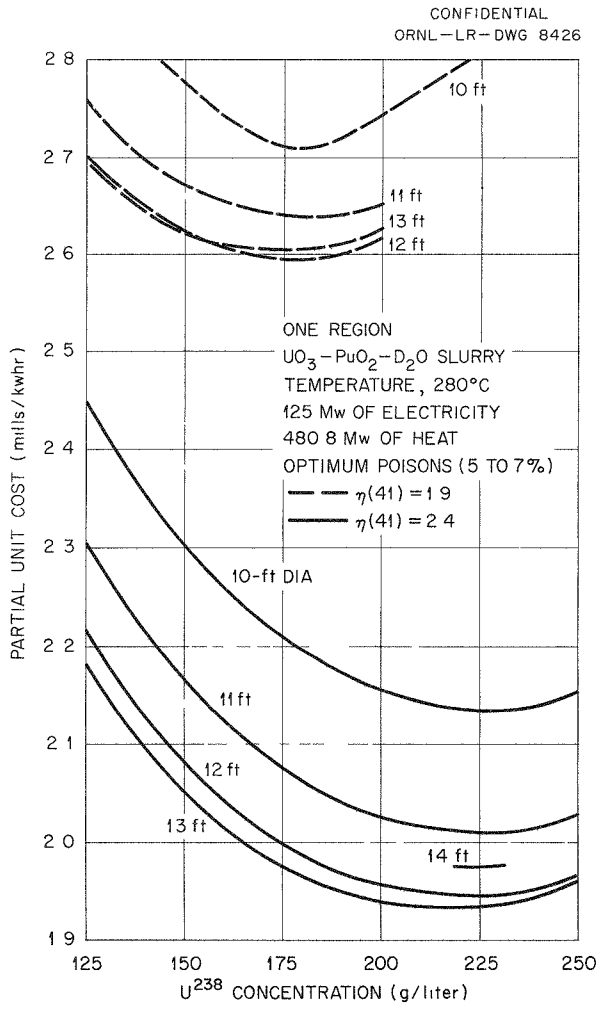

Fig. 6.8. Effect of U^{238} Concentration on Power Cost.

[5] M. C. Edlund *et al.*, *HRP Quar. Prog. Rep. April 30, 1955*, ORNL-1895, p 45–48.

TABLE 6.2. COST BREAKDOWNS AND NEUTRON BALANCES FOR REACTORS NEAR OPTIMUM CONDITIONS

Process Characteristics and Costs					
Reactor diameter, ft	10	10	12	12	10
U^{238} concentration, g/liter	175	225	175	225	175
$\eta(41)$	1.9	2.4	1.9	2.4	1.9
Resonance absorptions in plutonium considered	Yes	Yes	Yes	Yes	No
Reactor poisons, %	7.0	6.0	6.0	6.0	7.0
Total system volume, liters	38,900	38,900	49,700	49,700	38,900
Chemical process cycle time, days	155	167	151	138	159
U^{235} feed, g/day	615	479	579	430	576
Feed enrichment, % U^{235}	1.37	0.90	0.99	0.52	1.32
U^{235} concentration, g/liter	1.45	1.31	1.12	0.82	1.39
Pu^{239} concentration, g/liter	0.84	1.30	0.86	1.17	0.93
Pu^{240} concentration, g/liter	0.46	0.64	0.49	0.62	0.98
Pu^{241} concentration, g/liter	0.35	0.57	0.36	0.49	0.34
Np^{239} concentration, g/liter	0.03	0.04	0.03	0.03	0.03
U^{236} concentration, g/liter	0.15	0.11	0.10	0.06	0.15
Conversion ratio	0.68	0.79	0.74	0.84	0.68
Net partial cost of power, mills/kwhr	2.71	2.14	2.60	1.95	2.60
Fuel inventory, mills/kwhr	0.24	0.25	0.25	0.22	0.24
D_2O inventory, mills/kwhr	0.52	0.52	0.66	0.66	0.52
D_2O losses, mills/kwhr	0.22	0.22	0.27	0.27	0.22
Net uranium feed cost, mills/kwhr	1.52	0.91	1.15	0.48	1.41
Chemical processing (less fixed costs), mills/kwhr	0.22	0.31	0.27	0.32	0.21
Neutron Balances					
Absorptions and losses					
U^{235}	0.71	0.42	0.54	0.29	0.62
U^{236}	0.00	0.00	0.00	0.00	0.00
U^{238} (thermal)	0.36	0.30	0.35	0.33	0.32
U^{238} (resonance)	0.77	0.87	0.77	0.81	0.68
Np^{239}	0.00	0.00	0.00	0.00	0.00
Pu^{239} (thermal)	1.00	1.00	1.00	1.00	1.00
Pu^{239} (resonance)	0.13	0.17	0.12	0.14	0
Pu^{240} (thermal)	0.17	0.16	0.18	0.17	0.33
Pu^{240} (resonance)	0.21	0.24	0.20	0.22	0
Pu^{241}	0.38	0.40	0.38	0.39	0.33
Poisons	0.11	0.09	0.09	0.06	0.10
D_2O	0.02	0.01	0.02	0.01	0.02
Fast leakage	0.30	0.27	0.20	0.18	0.27
Slow leakage	0.19	0.12	0.13	0.10	0.17
Total neutrons absorbed and lost	4.36	4.05	3.98	3.71	3.84
Production					
Neutrons from U^{235}	1.48	0.87	1.12	0.61	1.29
Neutrons from Pu^{239} (thermal)	1.93	1.93	1.93	1.93	1.93
Neutrons from Pu^{239} (resonance)	0.23	0.30	0.21	0.25	0
Neutrons from Pu^{241}	0.73	0.95	0.72	0.93	0.63
Total neutrons produced	4.36	4.05	3.98	3.71	3.84

up, and chemical processing charges that are a function of throughput. The addition of the fixed charges for chemical processing (essentially a function of the number of reactors serviced) to this partial cost will yield the total fuel cost. The over-all results of the cost study plotted in Fig. 6.8 are for the optimum poison concentration (between 5 and 7% in all cases). Some typical results for several reactors near optimum cost are shown in Table 6.2.

7. ENGINEERING STUDIES

R. B. Korsmeyer

A. L. Gaines
P. N. Haubenreich
M. C. Lawrence[1]
M. I. Lundin
R. G. McGrath[2]
C. L. Segaser
W. F. Taylor[3]

7.1 TBR DESIGN, CASE A

7.1.1 Cost Estimates

The design of the 300-electrical-megawatt thorium breeder power station utilizing low-pressure recombination presented last quarter[4] was completed. The construction and operating costs were estimated on the assumption that a breeding gain of 0.11 would be achieved and that the reactor maintenance and operation would not differ in unit cost from that of large, modern steam plants. A summary of the estimate is presented in Tables 7.1 and 7.2. In figuring the annual charges and unit cost of power, the following materials costs and accounting rules were assumed:

Inventory	Schedule I	Schedule II
Fuel (U^{233} or U^{235}), dollars per gram	20	20
ThO_2, dollars per pound of thorium	10	10
D_2O, dollars per pound	40	28
Inventory charges		
Fuel and ThO_2, % per year	12	4
D_2O, % per year	17*	9*
Capital investment charges, % per year	15	15

* Includes 5% annual charge for losses.

7.1.2 Design Criticism

Throughout the design and estimating studies, the ultimate existence of solutions to several basic questions had to be assumed. These questions will have to be answered before a practical design can be evolved. The major unsolved problems confronting the designer at the present time, in addition to radiation damage and corrosion, are briefly indicated below.

(a) Reactor Kinetics. – A comprehensive study of the TBR kinetics has not been completed. The pressurizer surge-volume design was based on a limiting core pressure rise (relative to the blanket) of 400 psi, which corresponds to a reactivity addition rate of about 0.8% per second at source power, and it is estimated, pending detailed calculations, at 2% per second at a fission power level in excess of 1 Mw. Under normal load it is hardly conceivable that reactivity could be added at an excessive rate via rapid cooling of the circulating fluid. However, the combination of high steam pressure in the boilers, high reactor temperature, and power levels below 1 Mw would occur automatically if the electrical load on a generator were dropped without a simultaneous removal of fuel from the reactor or of water from the boilers. Similar conditions at source power could exist during startup periods. If a line should break, a safety valve stick open, or some other failure occur in the steam system at such a time, it might be possible for the rate of reactivity to be great enough to damage the core vessel. Designing safeguards to protect the reactor in the event of rapid loss of steam pressure may be difficult.

(b) Reactor Maintenance. – No scheme has yet been proved for maintenance of a large reactor once the system has become highly radioactive. The designer's dilemma is that, without knowledge of a workable maintenance procedure, he cannot design a plant with the assurance that the maintenance and operating costs will be under control. The maintenance problems must be solved by experience simulated on mockups and, finally, by reactor operation.

(c) Reactor Equipment. – Much of the reactor equipment is so new and different from anything in present commercial use that there is no standard

[1] On loan from General Dynamics Corp.
[2] On loan from Westinghouse Electric Corporation.
[3] On loan from Pioneer Service & Engineering Co.
[4] R. B. Korsmeyer *et al.*, *HRP Quar. Prog. Rep. April 30, 1955*, ORNL-1895, p 48–65.

TABLE 7.1. SUMMARY OF STATION INVESTMENT

A. Reactor plant		
1. Reactor proper (one reactor)		
High-pressure systems	$ 1,364,000	
Low-pressure systems	714,000	
Sampling systems	85,000	
Piping, valves, insulation, and installation of equipment	865,000	
Instrumentation and controls	250,000	
2. Reactor cell		
Cell vessel	350,000	
Excavation, structural, concrete shielding	575,000	
Total cost, one reactor	$ 4,203,000	
Total cost, three reactors		$12,609,000
3. Reactor station		
Cranes	$ 250,000	
Recirculating-water system	200,000	
Waste system and common facilities	1,950,000	
	$ 2,400,000	
		2,400,000
4. Station – general		
Land rights, site preparation, and auxiliaries	$ 900,000	
Maintenance facilities	1,000,000	
Chemical processing facilities	3,287,000	
	$ 5,187,000	
		5,187,000
Total basic costs		$20,196,000
Basic costs	$20,196,000	
Contingencies (25%)	5,049,000	
Subtotal	$25,245,000	
Engineering and design (10%)	2,524,500	
Fees (3%)	757,500	
Reactor plant costs	$28,527,000	
B. Turbogenerator plant		
300,000 kw × $106 per kw = $31,800,000	31,800,000	
Total station investment	$60,327,000	
Unit cost per kilowatt	$201	

TABLE 7.2. SUMMARY OF ANNUAL CHARGES AND UNIT POWER COSTS

	Schedule I	Schedule II
Charges against capital investment (15% per year)	$ 9,050,000	$ 9,050,000
Inventory charges, feed and losses	2,238,000	811,000
Net chemical-processing operating costs	334,000	334,000
Station operation and maintenance	1,335,000	1,335,000
	$12,957,000	$11,530,000
Unit cost of power, mills/kwhr	6.17	5.50

by which to estimate performance, safety in operation, and reliability of service. These questions eventually will be answered and present designs changed through continued development experience.

(d) Waste Disposal. – The gaseous waste of importance is Kr^{85}. About 600 curies per day per reactor is released, and the ten-year half life of the Kr^{85} makes storage during decay unattractive. At present it appears that this quantity probably can be discharged safely in an industrial area from a tall stack. If further investigation shows that this cannot be done, a penalty will have to be applied to the calculated cost of power in the event of unfavorable plant location or additional equipment requirements.

The solid wastes, consisting of concentrated fission products from the chemical processing plants and maintenance scrap which is not worth salvaging, are presently disposed of by permanent storage in a controlled area. It is possible that these materials might have to be shipped some distance from a power-plant site for burial, but such extra costs have not been considered in this study.

(e) Boiler Feed-Water Treatment. – In all modern boiler practice, feed-water purity control is exceedingly important, and the applicability of the more modern treatments to the TBR conditions need to be investigated. These include the possible use of hydrazine and various amines, as described elsewhere in detail.[5]

(f) Conclusions. – This design study has the value of confirming previous conceptual designs and estimates with respect to the turbogenerator facility, approximate plant size, building costs, and installation of the more conventional equipment. It differs from the former studies in that the basis is a particular plant, rather than a set of generalizations. This study, like the others, fails, for lack of essential engineering information, to depict a practical plant. Consequently, cost conclusions represent desirable goals in reactor plant investment and operating costs, rather than figures achievable today.

7.1.3 Oracle Coding for the Three-Plane Piping Problem

The general analytical solution to the three-plane piping problem,[6] which includes the effects of thermal expansion and anchor-point movements, was coded for the Oracle.[7] This code was successfully applied to the determination of piping stresses in the TBR layouts and the HRT systems.[8]

7.2 TBR DESIGN, CASE B

7.2.1 High-Pressure Gas Recombination Systems

Six variations of a high-pressure recombination system for the core were prepared for consideration. All schemes utilize a circulating fluid to dilute the radiolytic gases below explosive concentrations. The fluids considered were helium,

[5] R. B. Korsmeyer, *Chemical Treatment for the HRT Steam System*, ORNL CF-54-6-232 (June 30, 1954).

[6] M. W. Kellogg Company, *Expansion Stresses and Reactions in Piping Systems*, 1941 (out of print).

[7] Oracle code 139.

[8] M. I. Lundin, *HRT High-Pressure System Piping Stresses and Equipment Nozzle Reactions*, ORNL CF-55-6-150 (June 28, 1955).

oxygen, and steam, with the steam circulated by a mechanical pump, an evaporator, a jet pump, or natural convection. Schematic flowsheets with heat balances of the six variations are shown in Figs. 7.1 through 7.6. The corresponding material balances are given in Table 7.3. The data pertain to steady-state conditions, as the systems have not yet been investigated for startup and unsteady-state behavior.

7.2.2 Pressure-Vessel Closure

Since the probable life of the core vessel may be shorter than that of the reactor pressure vessel, the feasibility of designing the latter with a mechanical closure which would permit replacement of the core vessel is being investigated. A removable top closure appears feasible if the opening required is not too large. Because of the high pressure and large diameter of the opening, a standard bolted flange joint is out of the question, and recourse must be had to a type of design now used in high-pressure technique where the head is retained in the vessel by a shear ring. Details of two variations are shown in Figs. 7.7 and 7.8. The closure developed by the American Locomotive Co. is shown in Fig. 7.7 with dimensions applicable to the TBR pressure vessel. In this joint two gaskets are used; the inner gasket is seated by the hydrostatic force on the head, and the outer one is seated by the volts in the segmented shear rings. An adaptation of the

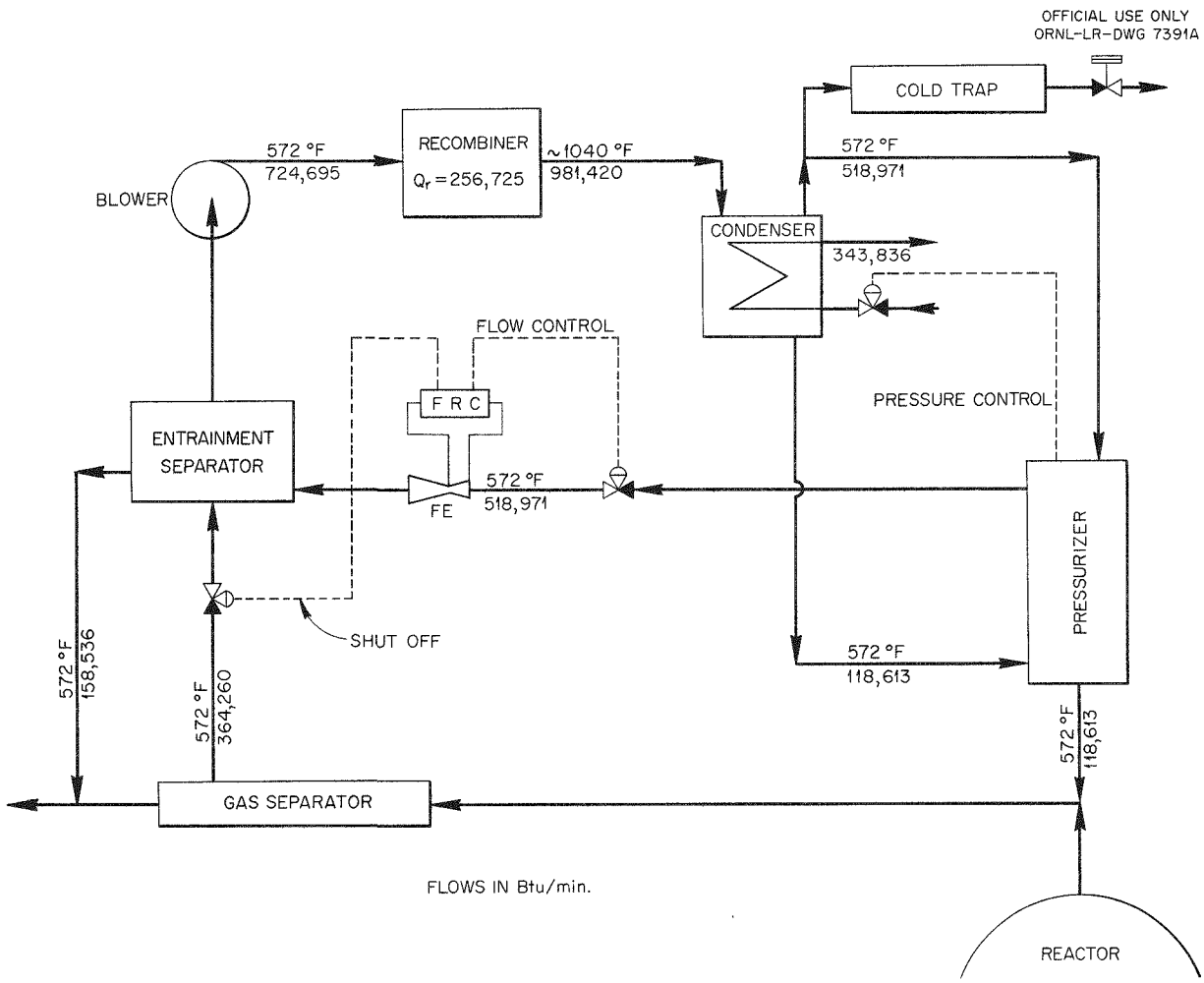

Fig. 7.1. TBR High-Pressure Recombination – Recirculated Helium Diluent.

TABLE 7.3. TBR HIGH-PRESSURE RECOMBINATIONS – PRELIMINARY MATERIAL BALANCES

	Flows (lb/min)			
	Helium, Fig. 7.1	Oxygen, Fig. 7.2	Recirculated Steam, Fig. 7.3	Evaporative Steam, Fig. 7.4
Gas separator to entrainment separator				
Steam	156	156	156	156
Oxygen	39	39	39	39
Deuterium	10	10	10	10
Solution	274	274	274	274
Entrainment separator to system				
Solution	274	274	274	274
Entrainment separator to recombiner				
Steam	555	1044	660	660
Oxygen	39	704	39	39
Deuterium	10	10	10	10
Helium	37.3	0	0	0
Recombiner to condenser				
Steam	604	1044	709	709
Oxygen	0	665	0	0
Helium	37.3	0	0	0
Condenser to pressurizer				
Steam	399	888	504*	504
Oxygen	0	665	0	0
Helium	37.3	0	0	0
Heavy water	205	205	205	205
Pressurizer to entrainment separator				
Steam	399	888	504*	504
Oxygen	0	665	0	0
Helium	37.3	0	0	0
Pressurizer to system				
Heavy water	205	205	205	205

	Steam, Jet Pumped, Fig. 7.5	Steam, Natural Recirculation, Fig. 7.6
Gas separator to entrainment separator		
Steam		156
Oxygen		39
Deuterium		10
Solution		274
Gas separator to jet pump		
Steam	156	
Oxygen	39	
Deuterium	10	
Solution	274	

* Forced-recirculation steam diluent flows directly from condenser to entrainment separator.

TABLE 7.3 (continued)

	Steam, Jet Pumped, Fig. 7.5	Steam, Natural Recirculation, Fig. 7.6
Entrainment separator to system		
Solution	274	274
Entrainment separator to recombiner		
Steam	660	660
Oxygen	39	39
Deuterium	10	10
Recombiner to jet pump		
Steam	195	
Recombiner to economizer		
Steam	514	709
Economizer to condenser		
Steam	514	709
Condenser to pressurizer		
Heavy water	205	205
Condenser to evaporator		
Heavy water		504
Condenser to economizer		
Heavy water	309	
Evaporator to economizer		
Wet steam		504
Economizer to entrainment separator		
Steam	309	504

Bridgman self-sealing gasket closure is shown applied to the TBR design in Fig. 7.8. Although the hydrostatic force is utilized to seat the gasket to prevent leakage around both sides of the shear ring, this type of gasket tends to stick to the vessel wall, making removal of the cover difficult. Further study of the closure design, with modifications for remote manipulation, is indicated.

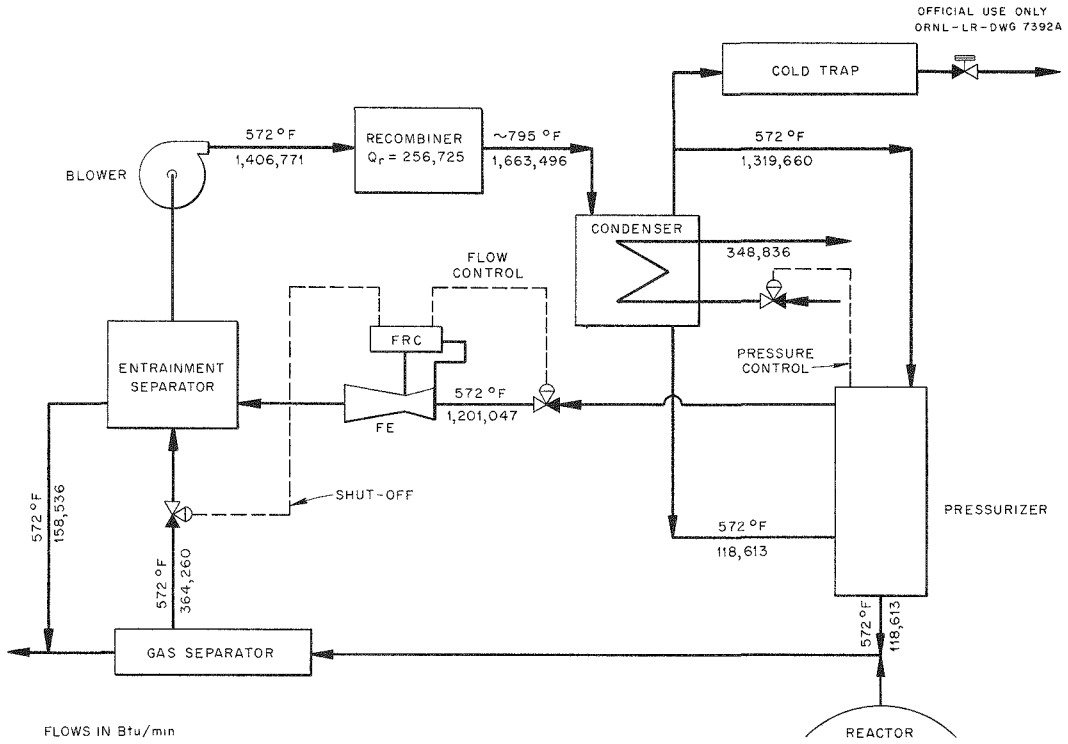

Fig. 7.2. TBR High-Pressure Recombination – Recirculated Oxygen Diluent.

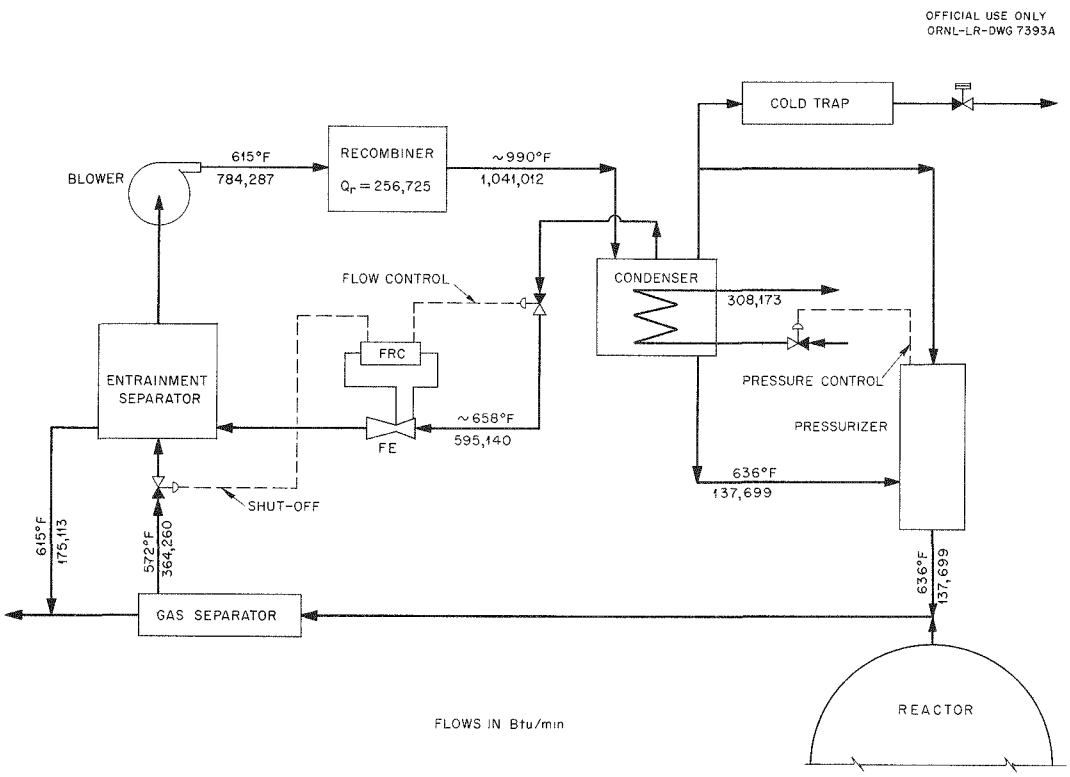

Fig. 7.3. TBR High-Pressure Recombination – Recirculated Steam Diluent.

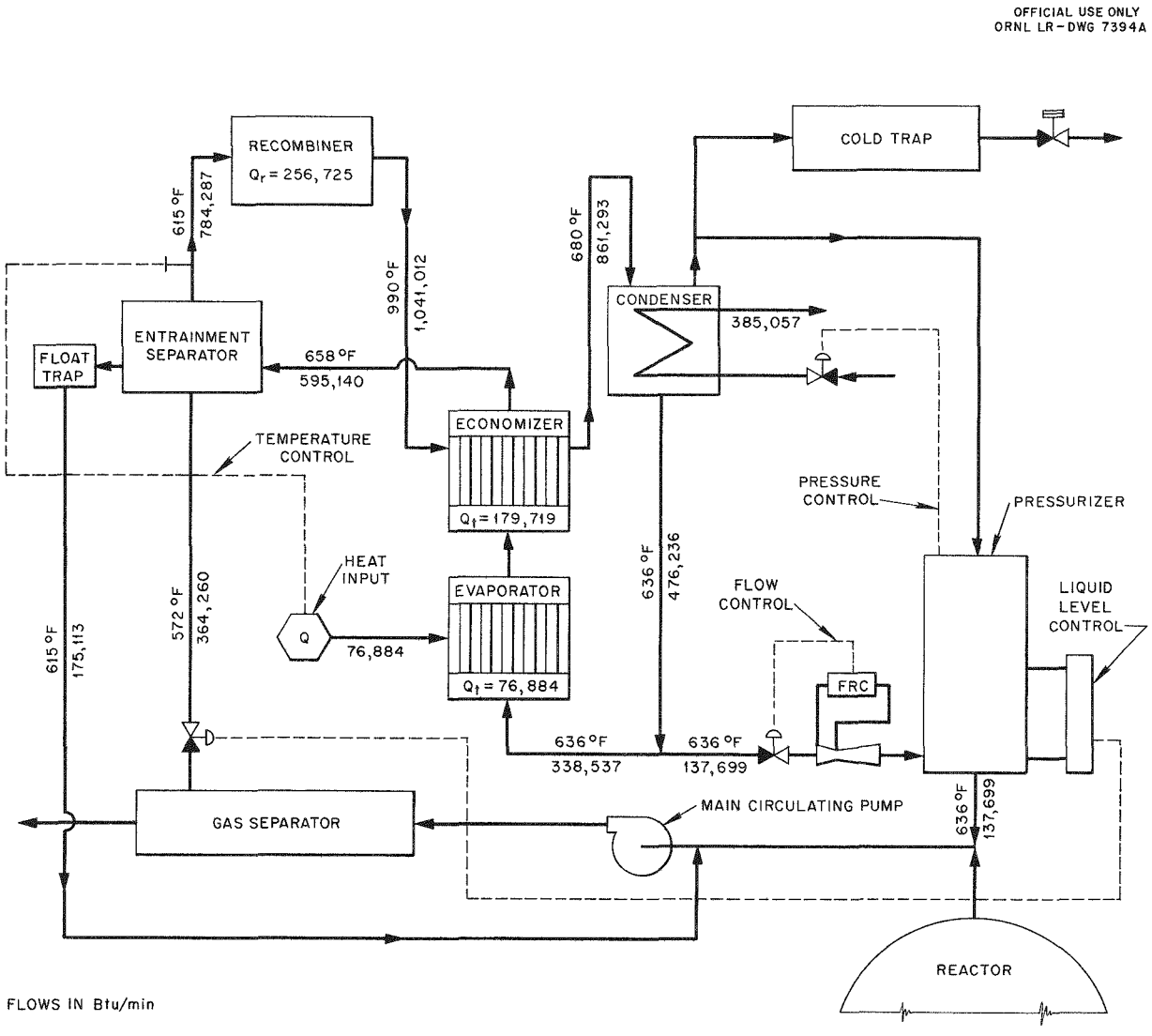

Fig. 7.4. TBR High-Pressure Recombination – Evaporative Steam Diluent.

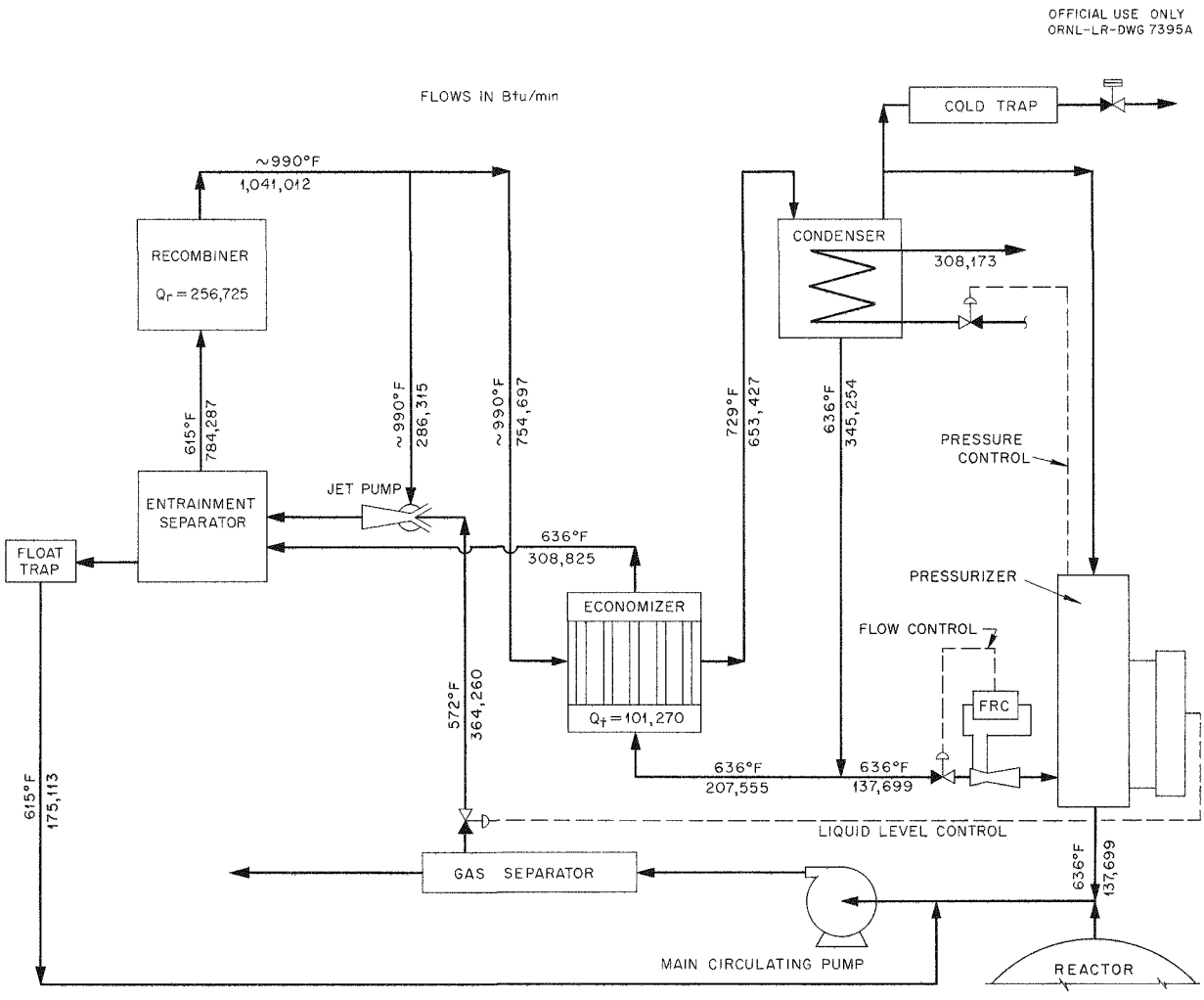

Fig. 7.5. TBR High-Pressure Recombination – Evaporative Steam Diluent with Jet Pump.

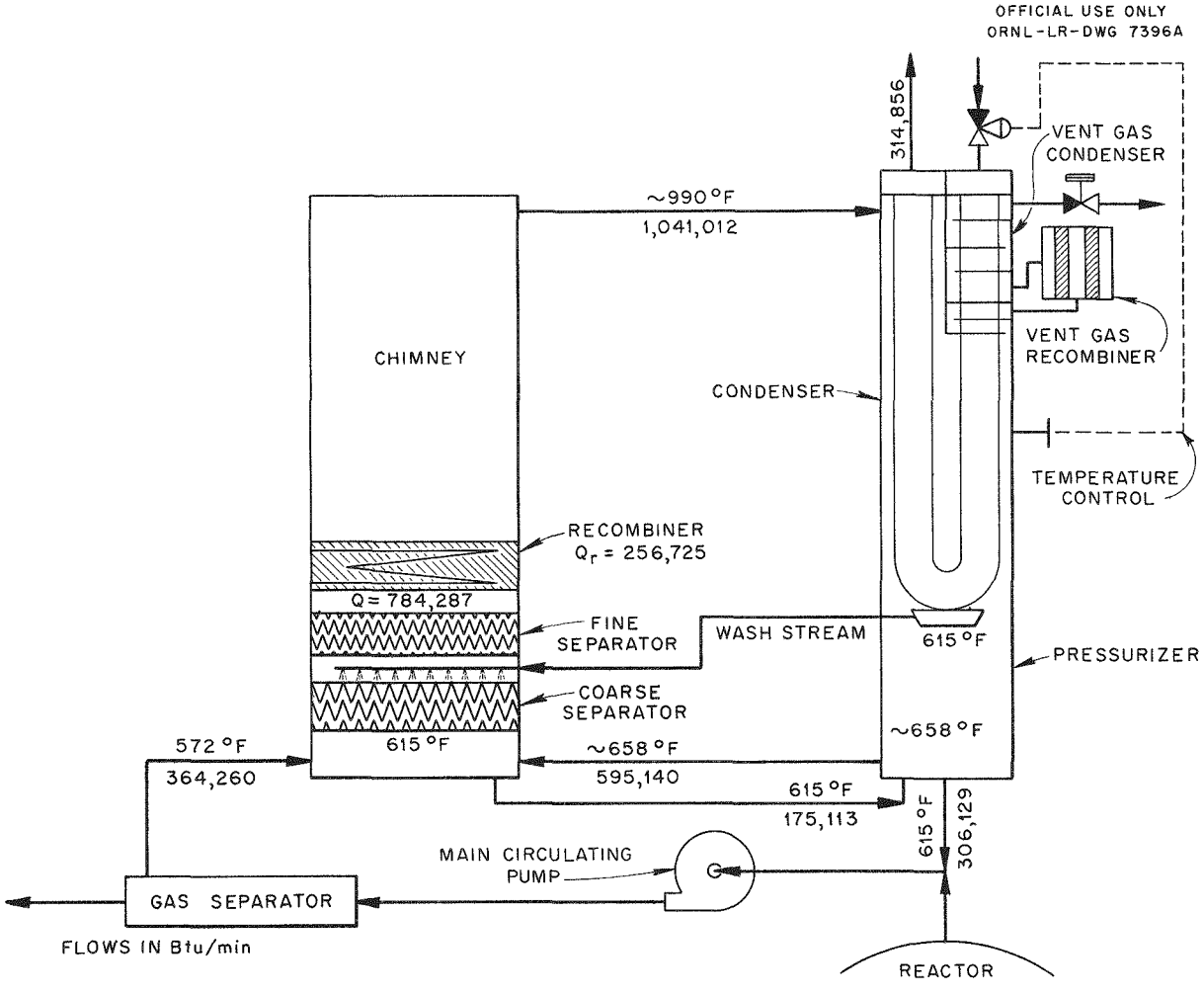

Fig. 7.6. TBR High-Pressure Recombination – Steam Diluent with Natural Recirculation.

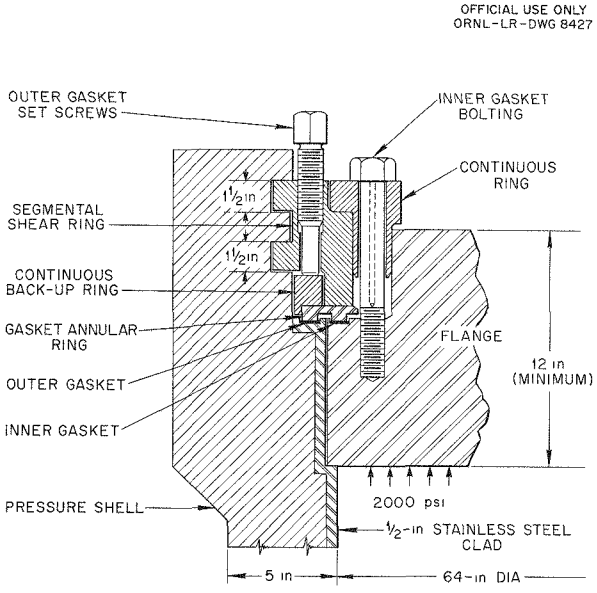

Fig. 7.7. Reactor Vessel High-Pressure Closure, American Locomotive Co. Type.

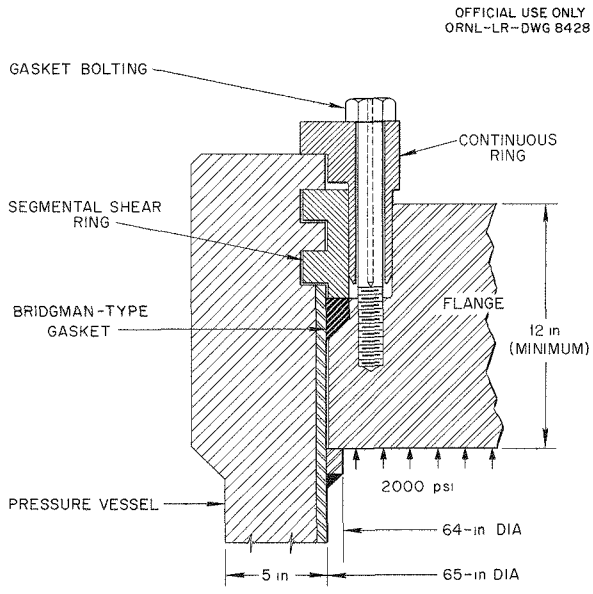

Fig. 7.8. Reactor Vessel High-Pressure Closure, Modified Bridgman Type.

Part III

CORROSION

E. G. Bohlmann

8. PUMP-LOOP CORROSION TESTS

J. C. Griess H. C. Savage
R. S. Greeley
S. A. Reed
F. J. Walter

8.1 PUMP-LOOP OPERATION AND MAINTENANCE

H. C. Savage F. J. Walter

8.1.1 Solution Loops

Operation of 12 dynamic-corrosion test loops proceeded in a routine manner, with no significant changes or difficulties. The corrosion data obtained from these loops are reported in Sec. 8.2.

In a previous quarterly report,[1] it was reported that a 1½-in. sched-80 tee in a test section from 100A loop N was rather severely corroded during 1700 hr of operation with 1.34 *m* uranyl sulfate solution at 275°C. Figures 8.1 and 8.2 are photographs of a cross section of this test section. Since the 2.2-fps flow through this section was considerably lower than the flow through the corrosion coupons (which were not severely attacked) and since no attack was observed on the smooth radius elbows in the same section, the localized

[1] J. C. Griess and R. S. Greeley, *HRP Quar. Prog. Rep. April 30, 1955*, ORNL-1895, p 83.

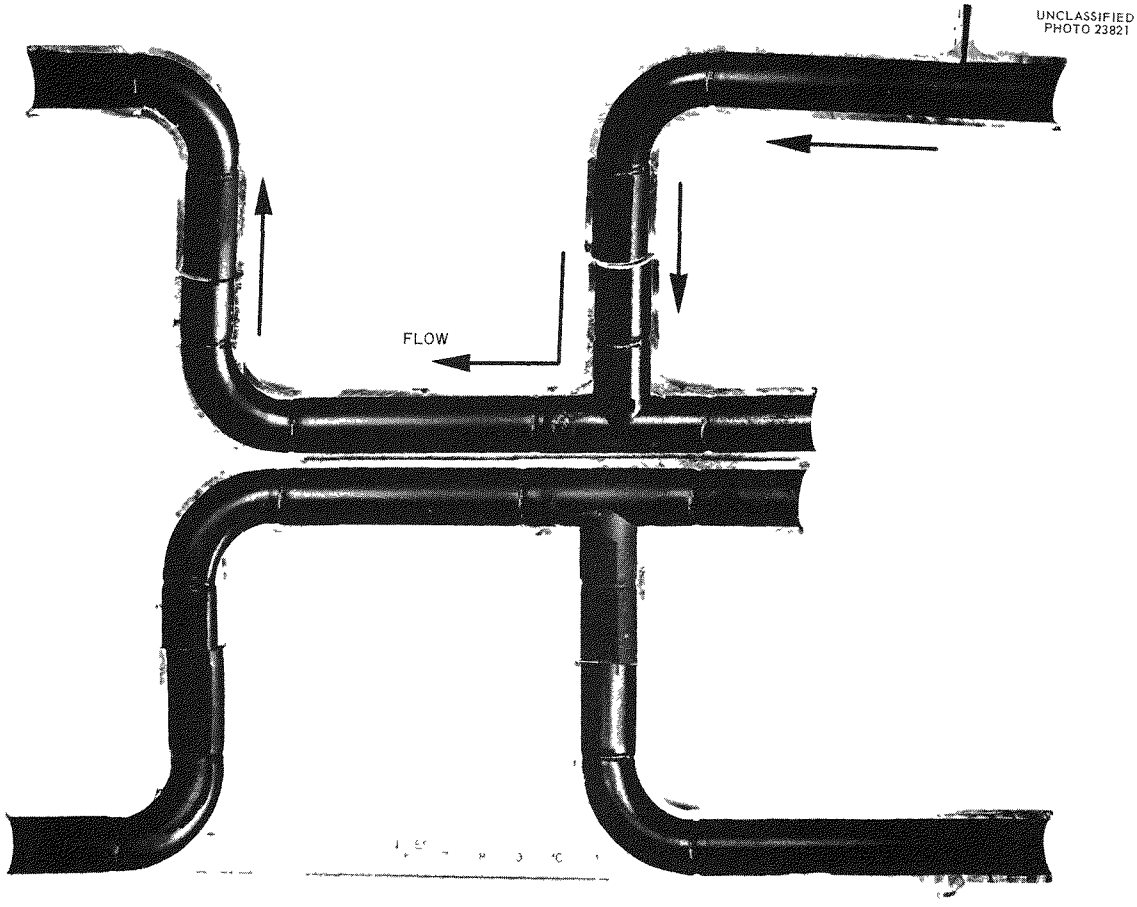

Fig. 8.1. 1½-in. Sched-80 IPS Pipe Test Section from 100A Loop N. Flow, 15 gpm, 2.2 fps. Environment, 1.34 *m* uranyl sulfate solution. Temperature, 275°C. Pressure, 1200 psig. Operating time, 1700 hr. Runs N-1 and N-2.

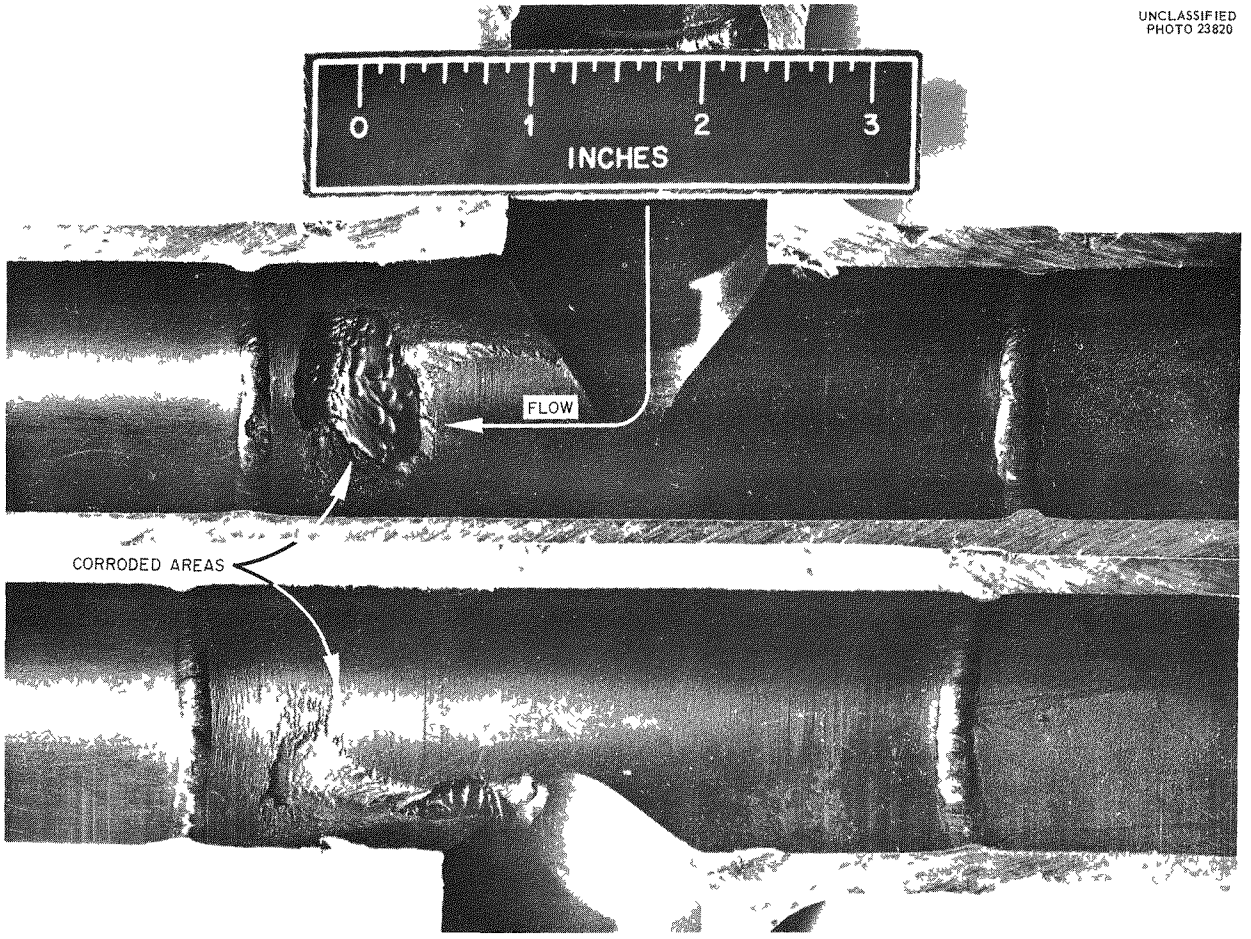

Fig. 8.2. Close-up of Corroded 1½-in. Sched-80 Pipe Tee from Test Section Shown in Fig. 8.1.

attack in the 1½-in. sched-80 IPS tee re-emphasizes the effect of geometry on critical velocity. Chemical and metallographic examination of the forged fittings in this test section showed that the fittings had been made from acceptable type 347 stainless steel.

8.1.2 Slurry Loops

Initial dynamic-corrosion tests with thorium dioxide slurries were completed in 100A pump loop CS[2] (Fig. 8.3). In all runs made to date, the system was operated isothermally; that is, the loop and pressurizer were at the same temperature, and an attempt was made to maintain a uniform concentration of thorium throughout the entire system. In all tests completed to date, the over-all mechanical operation of the loop was quite satisfactory.

The loading procedure consisted in drawing a weighed portion of thorium dioxide, previously slurried in water, into the evacuated system. Oxygen was added to the system to inhibit corrosion[3,4] and to provide the necessary overpressure for loop operation. While the loop was being heated to temperature, a Lapp CPS-1 Pulsafeeder was used to inject water into the rear of the circulating pump. Injecting water in this manner allowed the circulating pump to be operated while the loop was being heated to operating temperature, thereby preventing the slurry from settling or getting into

[2]H. C. Savage, F. J. Walter, and R. M. Warner, *HRP Quar. Prog. Rep. Oct. 31, 1954*, ORNL-1813, Fig. 3.1, p 65, and Fig. 3.2, p 66.

[3]A. S. Kitzes and R. B. Gallaher, *HRP Quar. Prog. Rep. April 30, 1955*, ORNL-1895, p 137–138.

[4]G. E. Moore and E. L. Compere, *HRP Quar. Prog. Rep. Oct. 31, 1954*, ORNL-1813, p 101–102.

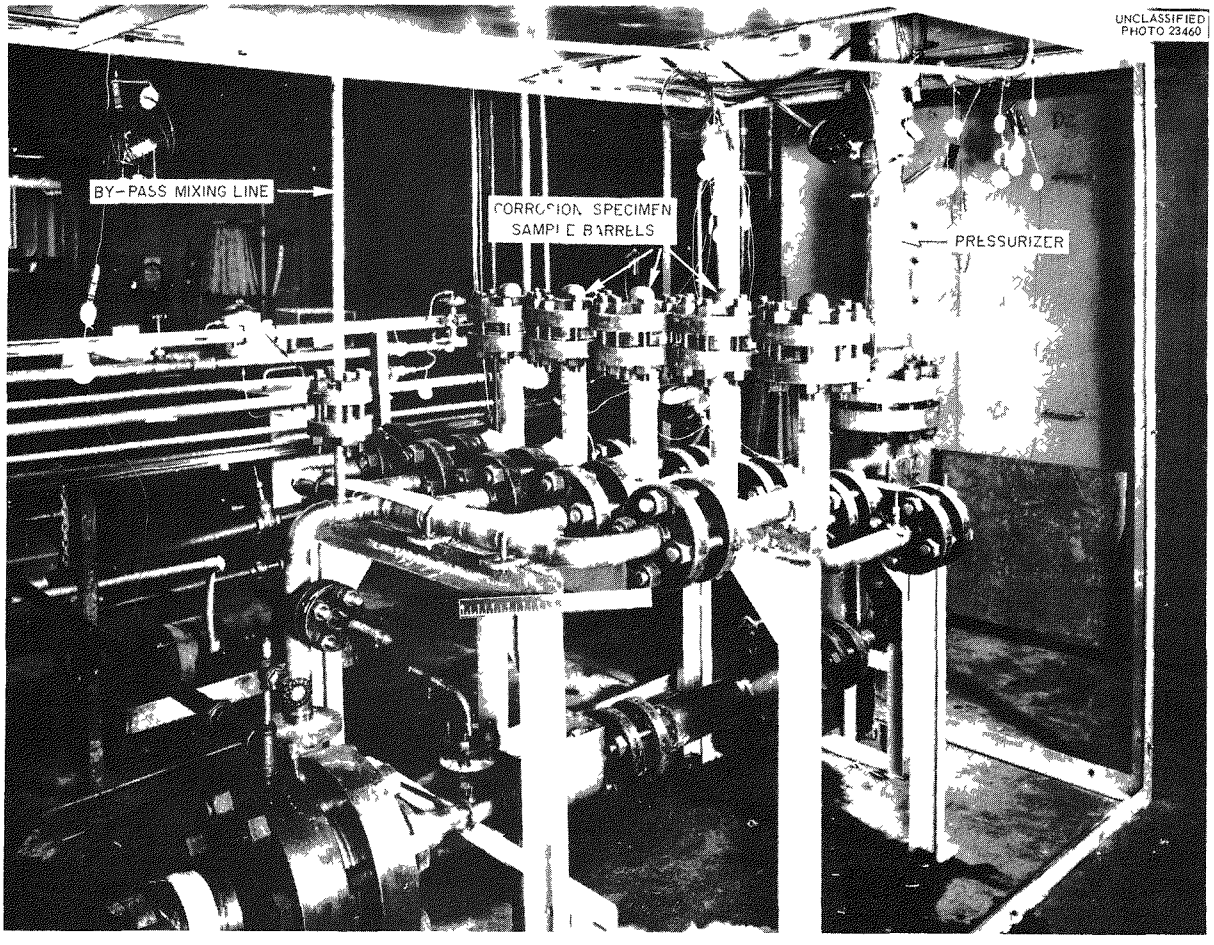

Fig. 8.3. Slurry Corrosion Test Loop CS.

the pump rotor and bearings during this period. When the loop reached operating temperature, water injection was terminated, and condensed steam from the vapor phase of the pressurizer was allowed to flow into the back of the pump to keep the pump flushed free of solids.

The purpose of the first six runs was to investigate the corrosion and/or erosion of various materials by thoria slurries. All tests were made with slurries of distilled water and ORNL production batch D-17 thorium dioxide, which was prepared by calcining thorium oxalate at 650°C. The corrosion data obtained in these runs are reported in Sec. 8.2.

As indicated in Sec. 8.2, a marked fluctuation in thorium concentration occurred during several of the runs. Thorium concentration as a function of operating time for runs CS-4 through CS-9 is presented in Fig. 8.4. Additional operating data are reported in Table 8.1.

No explanation is available for the decrease of thorium concentration from 300 to less than 200 g of thorium per kilogram of water during run CS-4. Examination of the system at the end of the run showed no cakes or large accumulations of thorium dioxide.

In run CS-8, which was charged to provide a slurry concentration of 500 g of thorium per kilogram of water, the actual sampled concentration of the loop was approximately 400 g of thorium per kilogram of water. At present, no explanation for this large deviation is apparent. Visual examination of the system after the run was terminated revealed no visible cakes or large accumulations of thorium dioxide.

TABLE 8.1. OPERATION CONDITIONS FOR RUNS CS-4 THROUGH CS-9*

Pump impeller	7-in. diameter, 347 stainless steel
Maximum flow in 1½-in. sched-80 loop piping**	85 gpm, 15.5 fps
Minimum flow in 1½-in. sched-80 loop piping (coupon holder sample bypass)	7.5 gpm, 1.3 fps
Flow through ½-in. sched-80 mixing line to pressurizer	2 gpm (runs CS-4 through CS-7) 6 gpm (runs CS-8 and CS-9)
Vertical flow down through pressurizer	0.06 fps (runs CS-4 through CS-7) 0.17 fps (runs CS-8 and CS-9)
Condensed steam to back of 100A pump	1 to 2½ liters/hr

*For temperatures and concentrations of these runs, see Fig. 8.4.
**All flows are measured as water flow at room temperature.

Although both runs CS-6 and CS-9 were charged to provide slurry concentrations of 1000 g of thorium per kilogram of water, neither run reached actual circulating concentrations in excess of 800 g of thorium per kilogram of water. This discrepancy between charged concentration and actual concentration indicates that nominal D-17 thorium oxide slurries cannot be satisfactorily circulated at the level of 1000 g of thorium per kilogram of water under the existing conditions in loop CS.

During one of the tests with a nominal concentration of 1000 g of thorium oxide per kilogram of water (run CS-6), measurements with a portable scintillation counter indicated a large accumulation of thorium in the pressurizer between the upper and lower sets of heaters. After 168 hr of operation, 200 psi of oxygen was added to the system and then suddenly vented through the high-pressure vent valve. The violent boiling induced by the resultant sudden decrease in pressure caused most of the thoria cake to break loose. The presence of large lumps of thorium oxide in the circulating stream was indicated by violent fluctuations in the circulating-pump current. Some of the lumps of thoria plugged the bypass mixing line and thus caused the termination of the run.

After the system was shut down and cooled, the 4-in. flange at the top of the pressurizer was removed to allow observation of the remnants of the thoria cake. The photograph of the cake shown in Fig. 8.5 was taken from the top of the pressurizer.

During the second test with a nominal concentration of 1000 g of thorium per kilogram of water (run CS-9), the low concentration level in the circulating loop indicated the possible presence of a cake or an accumulation of thoria. A scintillation-counter survey of the pressurizer did not, however, show any large accumulations of thorium. Visual observations after the run was terminated failed to show any large isolated accumulations of thorium dioxide. Most of the thoria was evenly distributed on the walls of the circulating loop.

During runs CS-4 through CS-9 a rather large effort was devoted to evaluating the problem of sampling thoria slurries. Several sampling procedures and mechanisms were tested on the three loop sample valves. The sampling procedures and mechanisms were evaluated on a basis of reproducibility of thorium concentrations and convenience of operation. The sampling technique finally selected consists in drawing a 70-ml flush sample into a standard steel sample bomb; immediately after the flush sample is taken, the actual sample is allowed to flow into a 50-ml quartz bottle contained in a standard Aminco autoclave (see Fig. 8.6). After cooling and allowing the excess gas pressure to escape, the quartz bottle is removed from the autoclave and submitted for analysis of the contents.

Comparison of samples taken from the probe, located in the vertical 4-in. pipe directly below the pressurizer, with samples taken from valves at the inlet and outlet of the pump indicated that the sample probe in the 4-in. pipe gave samples which were consistently lower in thorium concentration. The sample probe consists of a ¼-in. sched-80

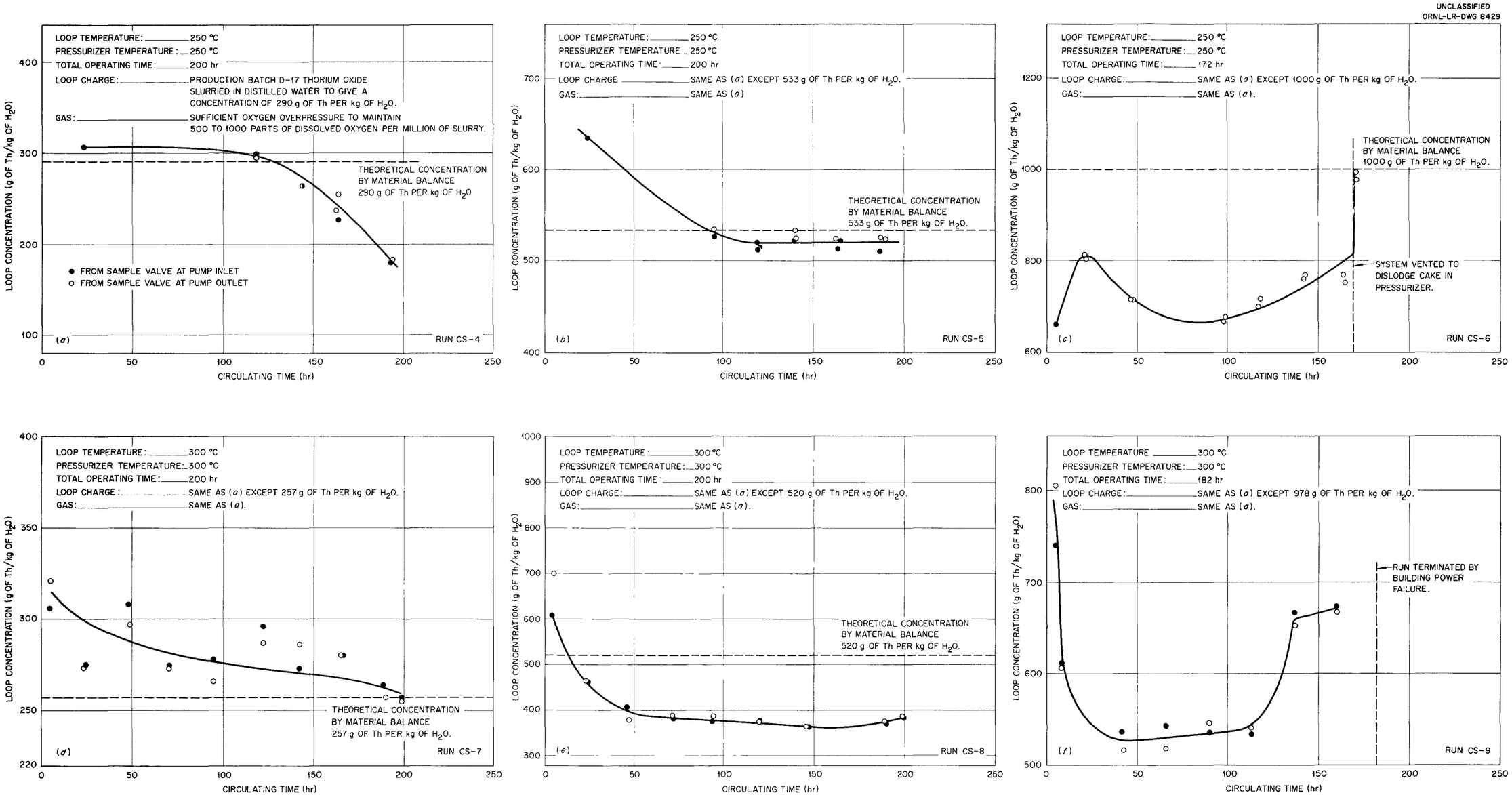

Fig. 8.4. Thorium Concentration as a Function of Time – Runs CS-4 through CS-9.

DECLASSIFIED
DECLASSIFIED

IPS pipe extending down at 60 deg to the vertical into the center of the 4-in. sched-80 IPS pipe. The sample valves at the inlet and outlet of the pump are flush with the walls of the 1½-in. sched-80 IPS main circulating pipes.

Statistical analysis of 28 paired duplicate samples taken from runs CS-7 through CS-9 showed that at the 95% confidence level there was no significant difference between the samples taken from the valves at the inlet and those taken from the valves at the outlet of the pump.

A rapid method for determining the thorium concentration in samples taken from slurry loops was needed in order that loop operation might be more closely controlled. A density method for determining thorium concentrations was developed to meet this need. A series of control samples and comparison of density-determined concentrations and chemically determined concentrations on samples taken from loop CS showed that the density method compares favorably in accuracy and precision with chemical determinations of thorium concentrations.

Construction of a second slurry corrosion test loop, loop BS, is 30% complete. Loop BS will be essentially the same as loop CS except for the modifications described below:

1. In order to obtain a more favorable volume ratio between the loop and pressurizer, the total length of the circulating loop will be reduced by 1 ft.
2. The sample probe, of questionable reliability, extending into the 4-in. pipe described above will be modified so that samples will be taken from near the wall of the 4-in. pipe.
3. Based on flow studies with water in a 0.4-scale glass model, it was decided to modify the design of the entrance of the 1½-in. main circulating

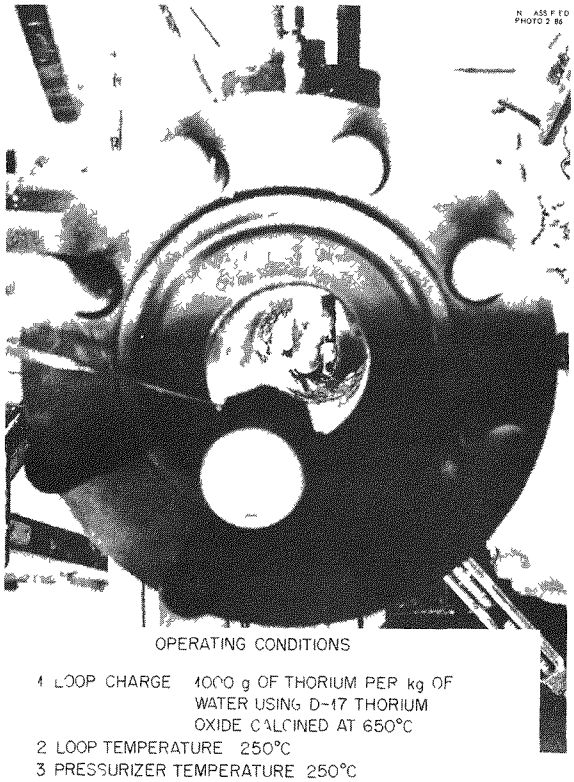

OPERATING CONDITIONS

1 LOOP CHARGE 1000 g OF THORIUM PER kg OF WATER USING D-17 THORIUM OXIDE CALCINED AT 650°C
2 LOOP TEMPERATURE 250°C
3 PRESSURIZER TEMPERATURE 250°C
4 TOTAL PRESSURE 1000 psig
5 VERTICAL FLOW DOWN THROUGH PRESSURIZER 0.066 fps
6 DURATION OF RUN 172 hr

Fig. 8.5. Thoria Cake in Pressurizer of Slurry Loop CS After Run CS-6. Loop charge, 1000 g of thorium (D-17 thorium oxide calcined at 650°C) per kilogram of water. Loop temperature, 250°C. Pressurizer temperature, 250°C. Total pressure, 1000 psig. Vertical flow down through pressurizer, 0.06 fps. Duration of run, 172 hr.

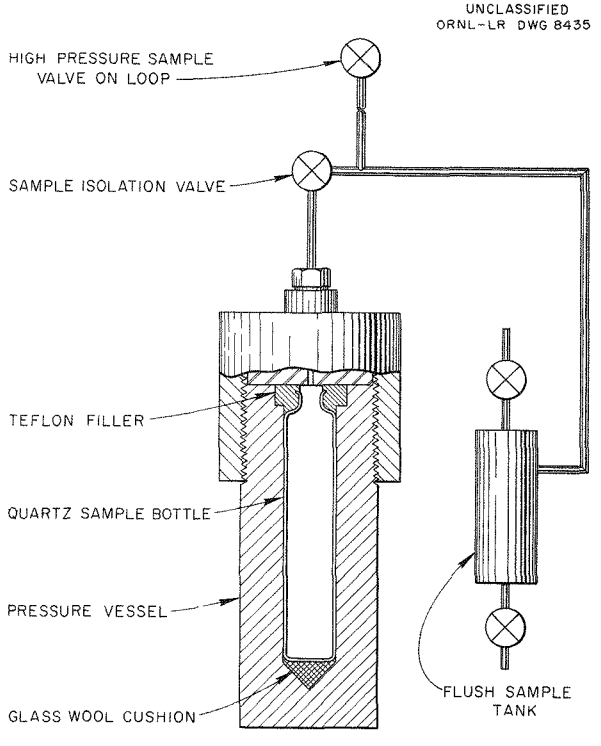

Fig. 8.6. Sampling Mechanism for Slurry Loop CS.

pipe into the 4-in. vertical pipe below the pressurizer.[5] This design change consists in extending the 1½-in. pipe into the 4-in. pipe and directing the flow down the center of the vertical 4-in. pipe by welding a 90-deg elbow on the 1½-in. pipe. It is anticipated that this change will give generally more favorable flow conditions in the pressurizer by supplementing the baffles in preventing vortexing and movement of fluid up into the pressurizer.

8.2 RESULTS OF LOOP TESTS WITH SOLUTIONS

J. C. Griess R. S. Greeley

8.2.1 Introduction

Tests of uranyl sulfate solutions containing added sulfate salts were continued. These solutions showed a decrease in the extent of corrosion both at high and low flow rates, but several of the solutions tested were unstable with respect to uranium content. Long-term runs with simulated HRT solutions also showed solution instability at 250 and 300°C. Both uranium and copper were slowly lost from solution. Two series of very short runs were made in order to investigate the formation of the oxide film or stainless steel, and a series of runs was made in the all-titanium loop in order to determine corrosion rates with very low chromium concentrations in solution.

8.2.2 Results

(a) General Corrosion Rates. – Table 8.2 lists the pin data obtained during the quarter from runs with solutions in the dynamic loops. The form of the table is the same as it has been in previous reports,[6–15] and the same precautions given before still apply.

The pin data obtained from runs in loop CS with thoria slurries are not given in Table 8.2 but are included in Sec. 8.3. Also a number of heat-treated and welded specimens were exposed to uranyl sulfate solutions, and the results of these tests are discussed in Sec. 13.

(b) Corrosion of Stainless Steel by Uranyl Sulfate Solutions Containing Added Sulfate Salts. – Additional runs were made with uranyl sulfate solutions containing either magnesium sulfate or lithium sulfate to investigate further the decreased corrosion previously reported.[15]

Run F-54 was made with 0.04 *m* uranyl sulfate, 0.04 *m* magnesium sulfate, and 0.006 *m* sulfuric acid at 250°C. As can be seen in Table 8.2, stainless steel pin corrosion rates were low, roughly only one-tenth those observed in a similar run without the added magnesium sulfate (see run D-7, ref. 16). However, the solution was not stable; the uranium concentration decreased slowly, throughout the run, from 10.6 to 9.1 g of uranium per liter.

Runs A-82, B-61, and E-43 were made with 0.13, 0.12, and 0.08 *m* magnesium, respectively, in 0.17 *m* uranyl sulfate at 250°C in efforts to find a stable solution. All solutions lost uranium slowly and their pH's decreased slowly. Two additions of magnesium sulfate were made in run A-82 in order to increase the magnesium/uranium ratio, but each time nearly all the added magnesium sulfate precipitated. One addition of dilute sulfuric acid was then made in order to dissolve some of the precipitated uranium, but some of the precipitated magnesium dissolved instead. High-velocity corrosion rates in these three runs were not so low as in a similar run, A-78, described previously,[17] but were lower than in runs without added sulfate salts. Low-velocity corrosion rates were roughly the same as they were in run A-78, being five to ten times lower than in runs without added sulfate salts. The critical velocity was not changed by the addition of the sulfate. Table 8.2 gives

[5] H. C. Savage, F. J. Walter, and R. M. Warner, *HRP Quar. Prog. Rep. Oct. 31, 1954*, ORNL-1813, Fig. 3.2, p 66.

[6] J. C. Griess, J. M. Ruth, and R. E. Wacker, *HRP Quar. Prog. Rep. Jan. 1, 1953*, ORNL-1478, p 63.

[7] J. C. Griess and R. E. Wacker, *HRP Quar. Prog. Rep. March 31, 1953*, ORNL-1554, p 49.

[8] J. C. Griess and R. E. Wacker, *HRP Quar. Prog. Rep. July 31, 1953*, ORNL-1605, p 74.

[9] J. C. Griess and R. E. Wacker, *HRP Quar. Prog. Rep. Oct. 31, 1953*, ORNL-1658, p 45.

[10] J. C. Griess and R. E. Wacker, *HRP Quar. Prog. Rep. Jan. 31, 1954*, ORNL-1678, p 50.

[11] J. C. Griess and R. E. Wacker, *HRP Quar. Prog. Rep. April 30, 1954*, ORNL-1753, p 61.

[12] J. C. Griess, *HRP Quar. Prog. Rep. July 31, 1954*, ORNL-1772, p 60.

[13] J. C. Griess and R. S. Greeley, *HRP Quar. Prog. Rep. Oct. 31, 1954*, ORNL-1813, p 67.

[14] J. C. Griess and R. S. Greeley, *HRP Quar. Prog. Rep. Jan. 31, 1955*, ORNL-1853, p 56.

[15] J. C. Griess and R. S. Greeley, *HRP Quar. Prog. Rep. April 30, 1955*, ORNL-1895, p 69.

[16] J. C. Griess and R. E. Wacker, *HRP Quar. Prog. Rep. Oct. 31, 1953*, ORNL-1658, p 48.

[17] J. C. Griess and R. S. Greeley, *HRP Quar. Prog. Rep. April 30, 1955*, ORNL-1895, p 72.

the pin data obtained in these runs. Further work aimed at stabilizing the solution with small amounts of added sulfuric acid is under way.

Solutions of 1.1 *m* uranyl sulfate with 1.1 *m* magnesium sulfate were stable at 225°C (runs H-65 and H-67) and solutions of 1.3 *m* uranyl sulfate with 1.3 *m* lithium sulfate were stable at 300°C (runs H-68 and H-74). Significantly, the lithium sulfate solution showed no phase separation at 300°C. Quartz-tube experiments with this solution showed no phase separation up to 315°C, the highest temperature to which the tubes could be subjected. Without the lithium sulfate, 1.3 *m* uranyl sulfate develops a second liquid phase at about 285°C. Low-velocity corrosion rates for these solutions were a factor of about 10 lower than those for comparison runs. High-velocity corrosion rates were lower also, but the degree varied from run to run. Figures 8.7 and 8.8 show the weight losses vs solution velocity for coupons exposed in these and comparison runs at 225 and 300°C, respectively. Table 8.2 gives the results for the pin-type specimens.

In run H-68 with added lithium sulfate at 300°C, the chromium concentration in solution increased very rapidly, reaching 4 g per liter in 100 hr; this very likely influenced the corrosion rates significantly. (Hexavalent chromium usually decreases the low-velocity corrosion rate and increases the high-velocity rate.) For this reason, run H-74 was made with a lower oxygen concentration in an effort to decrease the oxidizing power of the solution and thereby decrease the rate of Cr(VI) formation. However, the chromium concentration still was 760 ppm at the end of run H-74. Hence, further work is necessary to determine whether the reduced corrosiveness of the solution is due to the added sulfate or to the high Cr(VI) concentration.

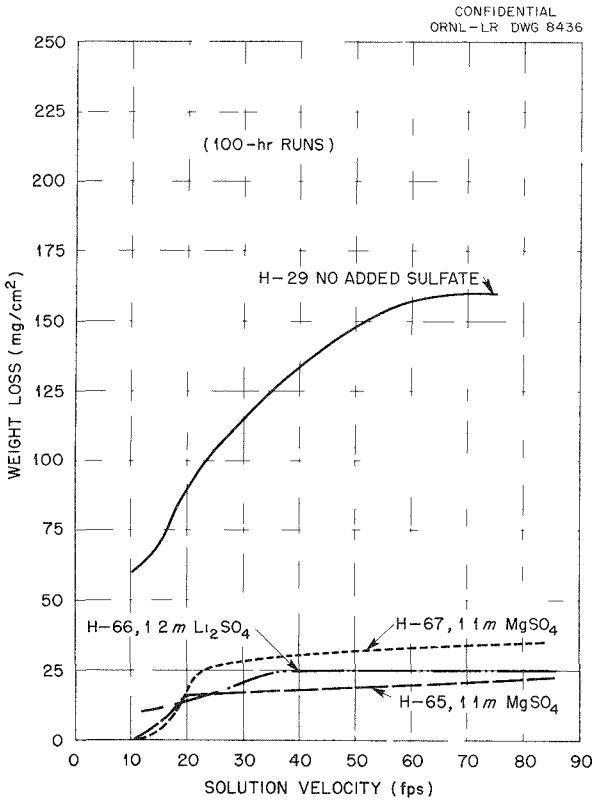

Fig. 8.7. Corrosion of Type 347 Stainless Steel Coupons in 1.2 *m* Uranyl Sulfate Solutions Containing Added Sulfate Salts at 225°C (100-hr Runs).

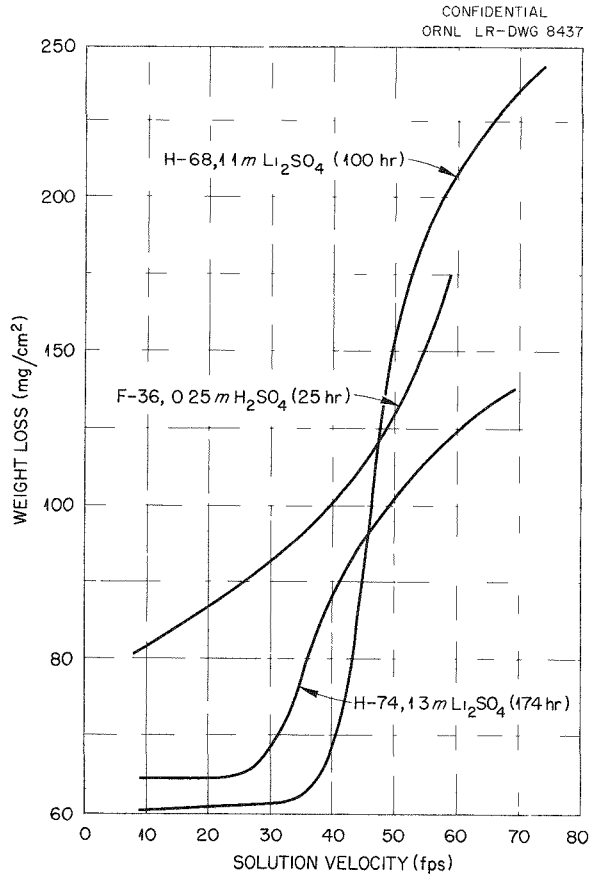

Fig. 8.8. Corrosion of Type 347 Stainless Steel Coupons in 1.3 *m* Uranyl Sulfate Solutions Containing Added Lithium Sulfate at 300°C.

TABLE 8.2. CORROSION RESULTS FOR PIN-TYPE SPECIMENS

Run No.	Test Conditions					Pin Material	Number of Pins	Corrosion Rate (mpy)		
	UO_2SO_4 Concentration (m)	Temperature (°C)	Time (hr)	Additions	Flow Rate (fps ± 10%)			Minimum	Average	Maximum
A-82	0.17	250	845	1000–2000 ppm O_2 0.13 m $MgSO_4$	17	304L SS	4	2.4	3.7	4.2
						309 SCb SS	3	2.8	3.0	3.4
						347 SS	4	4.2	4.7	5.2
						Titanium 75A	2	0.0	0.06	0.12
						Zircaloy-2	1		*a*	
					60	304L SS	5	34	75	110
						309 SCb SS	4	80	85	90
						316L SS	3	86	110	140
						321 SS	3	77	110	150
						347 SS	8	31	65	77
						Platinum	1		*a*	
						Titanium 75A	1		0.06	
						Titanium RC-55	1		0.03	
						Zircaloy-2	2		*a*	
B-61	0.17	250	396	1000–2000 ppm O_2 0.12 m $MgSO_4$	16	304L SS	4	2.5	2.7	2.8
						309 SCb SS	3	2.3	2.4	2.6
						347 SS	4	1.0	2.3	4.3
						Titanium 75A	2	0.16	0.16	0.16
						Zircaloy-2	1		*a*	
					68	304L SS	2	130	150	160
						309 SCb SS	1		160	
						316L SS	1		110	
						321 SS	3	130	170	240
						347 SS	2	140	140	140
						430 SS	1		120	
						Platinum	1		0.26[b]	
						Titanium RC-55	1		0.54	
						Zircaloy-2	1		0.11[b]	

TABLE 8.2 (continued)

Run No.	Test Conditions					Pin Material	Number of Pins	Corrosion Rate (mpy)		
	UO_2SO_4 Concentration (m)	Temperature (°C)	Time (hr)	Additions	Flow Rate (fps ± 10%)			Minimum	Average	Maximum
B-63	0.17	250	73	100 ppm O_2	16	347 SS	14	20	84	96
					68	347 SS	14	110	130	180
B-65	0.17	250	52	40–150 ppm O_2	17	347 SS	14	61	71	90
					68	347 SS	14	70	82	93
CS-2	0 (distilled water)	250	120	1000–2000 ppm O_2	16	309 SCb SS	1		0.14	
						347 SS	2	0.0	0.0	0.0
						410 SS[d]	1		[c]	
						416 SS[d]	1		0.57	
						420 SS[d]	1		0.42	
						17-4 PH SS[d]	1		0.0	
						Graphitar No. 14	1		[e]	
						Inconel X	1		4.2	
						Nickel	1		44	
						Stellite 1	1		39	
						Stellite 6	1		52	
						Stellite 25	1		19	
						Stellite 98M2	1		31	
					51	309 SCb SS	1		0.14	
						322 W SS[d]	1		0.14	
						347 SS	2	0.14	0.14	0.14
						430 SS	1		0.0	
						440C SS[d]	1		0.71	
						17-4 PH SS[d]	1		0.57	
						Carpenter 20 SS	1		0.0	
						Nickel	1		55	
						Stellite 1	1		38	
						Stellite 6	1		55	
						Titanium (3% Al–5% Cr)	1		0.28	
						Titanium (5% Al–2.5% Sn)	1		[c]	
						Titanium (6% Al–4% V)	1		[c]	

TABLE 8.2 (continued)

Run No.	Test Conditions: UO_2SO_4 Concentration (m)	Test Conditions: Temperature (°C)	Test Conditions: Time (hr)	Test Conditions: Additions	Test Conditions: Flow Rate (fps ± 10%)	Pin Material	Number of Pins	Corrosion Rate (mpy): Minimum	Corrosion Rate (mpy): Average	Corrosion Rate (mpy): Maximum
CS-3	0 (distilled water)	300	86	1500–4500 ppm O_2	16	309 SCb SS	1		0.59	
						347 SS	3	0.59	0.66	0.79
						410 SS[d]	1		1.2	
						416 SS[d]	1		1.4	
						420 SS[d]	1		0.99	
						17-4 PH SS[d]	1		0.79	
						Inconel X	1		5.5	
						Nickel	1		11	
						Stellite 1	1		5.7	
						Stellite 6	1		6.1	
						Stellite 25	1		3.2	
						Stellite 98M2	1		51	
					51	309 SCb SS	1		0.20	
						322W SS[d]	1		0.40	
						347 SS	2	0.20	0.40	0.59
						430 SS	1		0.99	
						440C SS[d]	1		1.2	
						17-7 PH SS[d]	1		0.20	
						Carpenter 20 SS	1		0.59	
						Nickel	1		24	
						Stellite 1	1		9.5	
						Stellite 6	1		6.1	
						Titanium (3% Al–5% Cr)	1		[c]	
						Titanium (5% Al–2.5% Sn)	1		[c]	
						Titanium (6% Al–4% V)	1		0.0	
E-43	0.17	250	287	1000–2000 ppm O_2 0.08 m $MgSO_4$	17	304L SS	4	2.0	5.2	6.3
						309 SCb SS	3	2.3	5.0	6.6
						347 SS	4	1.4	6.1	8.3
						Titanium 75A	2	0.32	0.32	0.32
						Zircaloy-2	1		[a]	

TABLE 8.2 (continued)

Run No.	Test Conditions					Pin Material	Number of Pins	Corrosion Rate (mpy)		
	UO_2SO_4 Concentration (m)	Temperature (°C)	Time (hr)	Additions	Flow Rate (fps ± 10%)			Minimum	Average	Maximum
E-43	0.17	250	287	1000–2000 ppm O_2 0.08 m $MgSO_4$	36	304L SS	2	130	130	130
						309 SCb SS	1		61	
						316L SS	1		120	
						321 SS	3	130	130	130
						347 SS	4	62	92	120
						Platinum	1		0.31	
						Titanium RC-55	1		0.32	
						Zircaloy-2	1		*c*	
F-54	0.04	250	200	1000–2000 ppm O_2 0.04 m $MgSO_4$ 0.006 m H_2SO_4	13	302B SS	2	0.76	0.88	1.0
						304L SS	2	1.0	1.1	1.1
						309 SCb SS	2	1.4	1.4	1.4
						316 SS	2	1.0	0.93	0.97
						347 SS	4	0.85	0.95	1.0
						Platinum	1		0.06	
						Titanium 75A	1		0.15	
					74	302B SS	2	6.3	6.6	6.9
						304L SS	2	3.7	3.9	4.0
						309 SCb SS	2	4.7	4.7	4.7
						316 SS	2	5.6	5.7	5.6
						347 SS	4	4.8	5.1	5.5
						Platinum	1		1.0	
						Titanium 75A	1		0.74	
G-17	0.02	250	200	1000–2000 ppm O_2 0.005 m H_2SO_4 60 ppm Cr(VI)	40	347 SS	1		5.4	
G-18	0.02	250	465	1000–2000 ppm O_2 0.005 m H_2SO_4 40 ppm Cr(VI)	15	347 SS	1		1.5	

TABLE 8.2 (continued)

Run No.	Test Conditions					Pin Material	Number of Pins	Corrosion Rate (mpy)		
	UO_2SO_4 Concentration (m)	Temperature (°C)	Time (hr)	Additions	Flow Rate (fps ± 10%)			Minimum	Average	Maximum
G-20	0.17	250	735	1000–2000 ppm O_2	15	347 SS	1		8.9	
G-21	0.17	250	200	1000–2000 ppm O_2	15	347 SS	1		27	
G-22	0.17	250	400	1000–2000 ppm O_2	15	347 SS	1		11	
G-23	0.04	250	100	1000–2000 ppm O_2 0.006 m H_2SO_4	70	347 SS	2	60	60	60
G-24	0.17	250	100	1000–2000 ppm O_2	70	347 SS	2	110	110	110
G-25	0.40	250	12	1000–2000 ppm O_2	70	347 SS	2	88	90	91
G-26	0.40	250	88	1000–2000 ppm O_2	70	347 SS	2	180	280	380
G-27	1.34	250	100	1000–2000 ppm O_2	70	347 SS	2	1200	1200	1200
G-28	0.11	250	100	1000–2000 ppm O_2 0.016 m H_2SO_4	70	347 SS	2	210	260	310
G-29	0.80	250	100	1000–2000 ppm O_2	70	347 SS	2	970	1000	1100
G-30	0.11	250	100	1000–2000 ppm O_2	64	347 SS	2	120	130	130
H-65	1.1	225	100	1000–2000 ppm O_2 1.1 m $MgSO_4$	15	304L SS	4	42	45	47
						309 SCb SS	3	36	39	45
						347 SS	4	27	50	68
						Titanium 75A	2	0.30	0.30	0.30
						Zircaloy-2	1		0.43[b]	
					64	304L SS	2	77	78	79
						309 SCb SS	1		75	
						316L SS	1		84	
						321 SS	3	68	72	78
						347 SS	4	91	150	210

TABLE 8.2 (continued)

Run No.	Test Conditions					Pin Material	Number of Pins	Corrosion Rate (mpy)		
	UO_2SO_4 Concentration (m)	Temperature (°C)	Time (hr)	Additions	Flow Rate (fps ± 10%)			Minimum	Average	Maximum
H-65	1.1	225	100	1000–2000 ppm O_2 1.1 m $MgSO_4$	64	Platinum	1		43	
						Titanium RC-55	1		31	
						Zircaloy-2	1		57	
H-66	1.2	225	100	1000–2000 ppm O_2 1.2 m Li_2SO_4	15	304L SS	4	41	61	93
						309 SCb SS	3	72	79	83
						347 SS	4	41	74	100
						Titanium 75A	2	0.61	1.4	1.2
						Zircaloy-2	1		0.64[b]	
					64	304L SS	2	110	120	130
						309 SCb SS	1		110	
						316L SS	1		130	
						321 SS	3	110	120	140
						347 SS	4	150	160	190
						Platinum	1		67	
						Titanium RC-55	1		63	
						Zircaloy-2	1		73	
H-67	1.1	225	100	1000–2000 ppm O_2 1.1 m $MgSO_4$[f]	15	304L SS	4	42	59	79
						309 SCb SS	3	75	100	150
						347 SS	4	31	75	90
						Titanium 75A	2	0.0	0.31	0.61
						Zircaloy-2	1		[a]	
					64	304L SS	2	120	130	130
						309 SCb SS	1		120	
						316L SS	1		350	
						321 SS	3	75	140	250
						347 SS	4	150	200	310
						Platinum	1		0.0	
						Titanium RC-55	1		0.31	
						Zircaloy-2	1		[a]	

TABLE 8.2 (continued)

Run No.	Test Conditions					Pin Material	Number of Pins	Corrosion Rate (mpy)		
	UO_2SO_4 Concentration (m)	Temperature (°C)	Time (hr)	Additions	Flow Rate (fps ± 10%)			Minimum	Average	Maximum
H-68	1.3	300	100	1000–2000 ppm O_2 1.3 m Li_2SO_4[g]	16	304L SS	4	6.1	7.7	8.7
						309 SCb SS	3	7.3	8.0	8.5
						347 SS	4	8.8	9.6	11
						Titanium 75A	2	2.1	2.3	2.5
						Zircaloy-2	1		[a]	
					64	304L SS	2	1700	1800	1800
						309 SCb SS	1		1200	
						316L SS	1		1100	
						321 SS	3	980	1000	1100
						347 SS	4	880	1000	1200
						Platinum	1		2.1	
						Titanium RC-55	1		4.3	
						Zircaloy-2	1		1.4	
H-74	1.3	300	174	150–750 ppm O_2 1.3 m Li_2SO_4 80 psi He	16	304L SS	4	4.3	19	36
						309 SCb SS	3	18	20	23
						347 SS	4	6.1	8.8	13
						Titanium 75A	2	0.7	0.8	0.9
						Zircaloy-2	1		[a]	
					64	304L SS	2	500	640	780
						309 SCb SS	1		600	
						316L SS	1		610	
						321 SS	3	380	600	1000
						347 SS	4	210	360	480
						Platinum	1		52	
						Titanium RC-55	1		2.3	
						Zircaloy-2	1		0.7	
I-27	0 (distilled water)[b]	300	95	1000–2000 ppm O_2	12	304 SS	2	0.36	0.45	0.54
						304L SS	5	0.0	0.40	0.72
						309 SCb SS	3	0.18	0.30	0.36
						316 SS	2	0.36	0.54	0.72

TABLE 8.2 (continued)

Run No.	Test Conditions					Pin Material	Number of Pins	Corrosion Rate (mpy)		
	UO_2SO_4 Concentration (m)	Temperature (°C)	Time (hr)	Additions	Flow Rate (fps ± 10%)			Minimum	Average	Maximum
I-27	0 (distilled water)[b]	300	95	1000–2000 ppm O_2	12	316L SS	2	0.54	0.63	0.72
						318 SS	2	0.18	0.45	0.72
						321 SS	3	0.18	0.30	0.54
						322W SS	2	0.36	0.36	0.36
						322W SS[d]	2	0.18	0.27	0.36
						347 SS	14	0.0	0.20	0.54
						347 SS[i]	2	0.18	0.27	0.36
						17-4 PH SS[d]	2	0.36	0.45	0.54
						17-7 PH SS	2	[c]	0.27	0.54
						17-7 PH SS[d]	2	0.18	0.45	0.72
						410 SS	1		11	
						410 SS[d]	1		0.36	
						416 SS	1		1.1	
						416 SS[d]	1		5.4	
						420 SS	1		1.6	
						420 SS[d]	1		2.7	
						430 SS	2	[c]	0.36	0.72
						440C SS	1		5.9	
						440C SS[d]	1		1.4	
						443 SS	1		0.54	
						446 SS	1		0.36	
						Carpenter 20 SS	2	0.0	0.36	0.72
						Electromet titanium	1		0.0	
						Graphitar	2		[e]	
						Inconel X	1		[c]	
						Miscro 4	2	0.89	5.4	10
						Nickel	1		9.1	
						Stellite 1	2	0.72	1.4	2.1
						Stellite 6	2	[c]	2.0	3.9
						Stellite 25	2	[c]	[c]	[c]
						Stellite 98M2	2	[c]	[c]	[c]

TABLE 8.2 (continued)

Run No.	Test Conditions					Pin Material	Number of Pins	Corrosion Rate (mpy)		
	UO_2SO_4 Concentration (m)	Temperature (°C)	Time (hr)	Additions	Flow Rate (fps ± 10%)			Minimum	Average	Maximum
I-27	0 (distilled water)[b]	300	95	1000–2000 ppm O_2	12	Titanium 75A	2	[c]	0.16	0.32
						Worthite	2	0.0	0.18	0.36
						Zircaloy-2	4		[a]	
						Zirconium–2½% Sn	2		[a]	
I-28	0 (distilled water)[j]	300	337	1000–2000 ppm O_2	12	304 SS	2	0.30	0.35	0.40
						304L SS	5	0.15	0.20	0.30
						309 SCb SS	3	0.25	0.20	0.30
						316 SS	2	0.05	0.10	0.15
						316L SS	2	0.05	0.10	0.15
						318 SS	2	0.10	0.18	0.25
						321 SS	3	0.15	0.20	0.25
						322W SS	2	[c]	0.08	0.15
						322W SS[d]	2	0.15	0.15	0.15
						347 SS	16	0.05	0.19	0.30
						347 SS[i]	2	0.15	0.15	0.15
						17-4 PH SS[d]	2	0.05	0.10	0.15
						17-7 PH SS	2	0.05	0.13	0.20
						17-7 PH SS[d]	2	0.15	0.15	0.15
						410 SS	1		0.86	
						410 SS[d]	1		0.15	
						416 SS	1		0.50	
						416 SS[d]	1		0.40	
						420 SS	1		1.7	
						420 SS[d]	1		0.61	
						430 SS	2	0.15	0.25	0.35
						440C SS	1		7.5	
						440C SS[d]	1		0.30	
						443 SS	1		0.30	
						446 SS	1		0.35	
						Carpenter 20 SS	2	0.40	0.55	0.70

TABLE 8.2 (continued)

Run No.	Test Conditions					Pin Material	Number of Pins	Corrosion Rate (mpy)		
	UO_2SO_4 Concentration (m)	Temperature (°C)	Time (hr)	Additions	Flow Rate (fps ± 10%)			Minimum	Average	Maximum
I-28	0 (distilled water)[j]	300	337	1000–2000 ppm O_2	12	Inconel X	1		5.6	
						Miscro 4	2	0.25	0.30	0.35
						Nickel	1		100	
						Stellite 1	2	54	57	60
						Stellite 6	2	41	46	51
						Stellite 25	2	27	28	28
						Stellite 98M2	2	5.8	6.7	7.6
						Titanium 75A	3	*c*	0.03	0.09
						Worthite	2	0.40	0.45	0.50
						Zircaloy-2	3	*a*	*a*	*a*
						Zirconium–2½% Sn	3	*a*	*a*	*a*
I-29	0 (distilled water)	300	350	80 psig He (at room temperature)	12	304 SS	2	0.24	0.32	0.39
						304L SS	5	0.0	0.17	0.39
						309 SCb SS	3	0.0	0.16	0.48
						316 SS	2	0.15	0.17	0.19
						316L SS	2	0.10	0.13	0.15
						318 SS	2	0.05	0.15	0.24
						321 SS	3	0.24	0.27	0.29
						322W SS	2	0.10	0.20	0.29
						322W SS[d]	2	*c*	0.17	0.34
						347 SS	16	*c*	0.13	0.29
						347 SS[i]	2	0.15	0.17	0.19
						17-4 PH SS[d]	2	0.05	0.20	0.34
						17-7 PH SS	2	0.19	0.29	0.39
						17-7 PH SS[d]	2	0.24	0.44	0.63
						410 SS	1		0.49	
						410 SS[d]	1		0.49	
						416 SS	1		0.49	
						416 SS[d]	1		*c*	
						420 SS	1		0.34	

TABLE 8.2 (continued)

Run No.	Test Conditions					Pin Material	Number of Pins	Corrosion Rate (mpy)		
	UO_2SO_4 Concentration (m)	Temperature (°C)	Time (hr)	Additions	Flow Rate (fps ± 10%)			Minimum	Average	Maximum
I-29	0 (distilled water)	300	350	80 psig He (at room temperature)	12	420 SS[d]	1		0.49	
						430 SS	2	0.0	0.46	0.92
						440C SS	1		1.4	
						440C SS[d]	1		0.0	
						443 SS	1		0.0	
						446 SS	1		0.05	
						Carpenter 20 SS	2	0.10	0.10	0.10
						Inconel X	1		0.15	
						Miscro 4	2	0.15	0.30	0.44
						Nickel	1		0.24	
						Stellite 1	2	[c]	0.15	0.29
						Stellite 6	2	[c]	[c]	[c]
						Stellite 25	2	3.2	3.4	3.5
						Stellite 98M2	2	0.87	1.4	1.9
						Titanium 75A	3	0.0	0.34	0.88
						Worthite	2	0.05	0.15	0.24
						Zircaloy-2	3	[a]	[a]	[a]
						Zirconium–2½% Sn	3	[a]	[a]	[a]
N-3	0.04	250	200	1000–2000 ppm O_2 0.005 m $CuSO_4$ 0.006 m H_2SO_4	12	321 SS	2	2.1	2.3	2.4
						347 SS	7	1.4	2.4	3.4
						Allegheny Metal 350[k]	2	1.6	2.1	2.6
						Allegheny Metal 350[l]	2	2.7	3.2	3.7
						Allegheny Metal 350[m]	2	3.5	4.0	4.5
						Allegheny Metal 350[n]	2	2.1	2.6	3.0
						Allegheny Metal 350[o]	2	2.5	3.0	3.5
						55.7% Fe–43.7% Cr[p]	2	7.4	7.6	7.7
						50.5% Fe–43.7% Cr–4.94% Ni[p]	1		9.7	
						55.7% Fe–43.7% Cr[q]	2	9.5	9.8	10
						50.5% Fe–43.7% Cr–4.94% Ni[q]	2	17	19	21
						Titanium plate[r]	2	4.7	6.2	7.6

[a] Not defilmed. Showed weight gain due to deposition of iron and chromium oxides.

[b] Not defilmed.

[c] Defilmed but still showed weight gain due to incomplete removal of oxides.

[d] Hardened by suitable heat treatment.

[e] Pin dissolved.

[f] Soup drained from H-65, filtered, and 23 ml of 20% H_2O_2 added to reduce Cr(VI) to Cr(III).

[g] Soup drained from H-66, filtered, and 24 ml of 20% H_2O_2 added to reduce Cr(VI) to Cr(III).

[h] Contaminated with UO_2SO_4.

[i] Cast.

[j] Contaminated with nitric acid.

[k] Annealed.

[l] Annealed, heated at 1350°F for 1 hr.

[m] Annealed, heated at 1350°F for 1 hr and then at 850°F for 1 hr.

[n] Annealed, refrigerated to −80 to −100°F for 10 min.

[o] Annealed, refrigerated to −80 to −100°F for 10 min, heated to 750°F for 2 hr.

[p] A special alloy prepared by HRP Metallurgy Group. Fully ferritic.

[q] A special alloy prepared by HRP Metallurgy Group. Transformed from ferrite to sigma.

[r] About 3 mils of titanium plated on type 321 stainless steel by Solar Aircraft Co.

In the hope of finding other sulfate salts having a high degree of solubility in uranyl sulfate solutions at elevated temperatures, the general solubility limits of several sulfate salts in uranyl sulfate solutions were investigated by heating the appropriate solutions in quartz tubes in a rocking furnace. In this manner it was found that magnesium sulfate was soluble on an equimolal basis in 0.04 *m* and 0.17 *m* uranyl sulfate at 250°C and in 1.3 *m* uranyl sulfate up to 230°C. Lithium sulfate, on the other hand, was not soluble on an equimolal basis in 0.04 *m* and 0.17 *m* uranyl sulfate at 250°C but was soluble in 1.3 *m* uranyl sulfate up to 315°C. The sulfates of aluminum, cadmium, cobalt, copper, manganese, nickel, and sodium were not soluble at equimolal level in 0.17 *m* uranyl sulfate at 250°C. Cesium has been reported to be very soluble in 0.17 *m* uranyl sulfate,[18] and the corrosiveness of solutions of cesium sulfate and uranyl sulfate will be investigated in the future, although the unfavorable cross section of cesium make its use in a reactor impracticable. Several of these solutions were not stable with regard to hydrolytic precipitation of uranium.

(c) Long-Term Runs with Simulated HRT Solutions. – As noted in previous reports,[19–21] three loops are in use in long-term corrosion tests with a uranyl sulfate solution similar to that proposed for use in the HRT, namely, 0.04 *m* uranyl sulfate, 0.006 *m* sulfuric acid, and 0.005 *m* copper sulfate, containing 1000 to 2000 ppm dissolved oxygen. In loop K the temperature of the solution is 300°C; in loop L, 200°C; and in loop M, 250°C. The specimens in loops K and M were removed for examination twice, and those in loop L once. In each case the specimens were examined visually, weighed, and returned to the loop. The same solution that was withdrawn from the loop, plus additional fresh solution to make up for that removed during sampling, was added, and the run was continued. Totals of 6539, 3462, and 4678 hr have been accumulated on loops K, L, and M, respectively. All runs are continuing.

(1) *Corrosion Results.* – The corrosion specimens in all loops showed very little attack, with two exceptions to be referred to below. Tables 8.3, 8.4, and 8.5 give the as-removed average weight losses for three typical stainless steels at four different flow rates. All specimens had oxide

TABLE 8.3. AS-REMOVED WEIGHT LOSSES OF STAINLESS STEEL PIN-TYPE SPECIMENS FROM LOOP K (300°C)

Type of Stainless Steel	Flow Rate (fps)	Average Weight Loss (mg/cm^2)	
		2865 hr	6539 hr
304L	9.4	0.42	0.14
309 SCb		0.79	0.59
347		0.76	0.54
304L	19	0.52	0.53
309 SCb		1.08	0.92
347		0.93	0.68
304L	33	0.58	0.40
309 SCb		1.76	1.70
347		1.18	0.89
304L	37	1.94	1.86
309 SCb		1.94	1.78
347		1.77	1.32

TABLE 8.4. AS-REMOVED WEIGHT LOSSES OF STAINLESS STEEL PIN-TYPE SPECIMENS FROM LOOP L (200°C)

Type of Stainless Steel	Flow Rate (fps)	Average Weight Loss (mg/cm^2) 3462 hr
304L	10	1.04
309 SCb		1.73
347		0.96
304L	19	1.51
309 SCb		0.08
347		1.32
304L	34	32.8
309 SCb		–0.44
347		1.20
304L	42	86.9
309 SCb		0.16
347		0.56

[18] E. V. Jones, *HRP Quar. Prog. Rep. March 15, 1952*, ORNL-1280, p 177.

[19] J. C. Griess and R. S. Greeley, *HRP Quar. Prog. Rep. Oct. 31, 1954*, ORNL-1813, p 80.

[20] J. C. Griess and R. S. Greeley, *HRP Quar. Prog. Rep. Jan. 31, 1955*, ORNL-1853, p 74.

[21] H. C. Savage and F. J. Walter, *HRP Quar. Prog. Rep. April 30, 1955*, ORNL-1895, p 69.

TABLE 8.5. AS-REMOVED WEIGHT LOSSES OF STAINLESS STEEL PIN-TYPE SPECIMENS FROM LOOP M (250°C)

Type of Stainless Steel	Flow Rate (fps)	Average Weight Loss (mg/cm^2)	
		2306 hr	4678 hr
304L	10	0.21	−0.18
309 SCb		0.86	0.57
347		0.35	−0.04
304L	19	0.25	0.02
309 SCb		1.45	1.21
347		0.45	0.21
304L	35	0.28	0.16
309 SCb		2.08	2.00
347		0.57	0.49
304L	38	0.32	0.06
309 SCb		2.16	2.00
347		0.63	0.64

scale on their surfaces so that the actual weight of metal oxidized was somewhat greater than the reported weight losses. (A weight loss of 20 mg/cm^2 is equivalent to a penetration of 0.001 in.) In all cases (except for type 304L stainless steel at 200°C at flow rates greater than 19 fps), corrosion damage was slight. It can be seen in Tables 8.3 and 8.4 that the specimens showed a weight gain between the first and second weighings. This was due to the deposition of iron and chromium oxides on the surface of the pins. Nickel analyses of solution samples indicated that corrosion of the rest of the systems (loop walls, impeller, etc.) was less than 0.1 mpy in all three cases.

In addition to pin holders, one tapered holder with coupon-type specimens was used in each run. These coupons all developed continuous black films and showed low weight losses, except those in the velocity range of 55 to 70 fps in loop K. As noted previously,[20] these coupons developed triangular pits during the first part of the run. During the second part of the run the number and the depths of pits did not increase, but the diameters became larger.

A number of different zirconium and titanium alloys were exposed. Generally, the attack on all was insignificantly slight. At 300°C, however, two Zircaloy-1 pins and one crystal-bar-zirconium pin began to develop white oxides on their surfaces. Under the same conditions, all Zircaloy-2 pins had black films, with no signs of white oxide on their surfaces.

(2) *Solution Stability Results.* – Figures 8.9, 8.10, and 8.11 illustrate how the concentration of various ions varied with time in loops K, L, and M, respectively. In Figs. 8.9 and 8.11 it can be seen that at 300 and 250°C the solution was not stable with respect to copper and uranium concentrations.

In loop K (300°C) the copper concentration in solution decreased from the time the copper sulfate was added (170 hr after the run started) until the run was first stopped after 2860 hr. During this same period the uranium concentration decreased slightly and the pH decreased. Nickel and chromium concentrations increased in the expected manner.

Before the run was started again, fresh solution, of the same composition as the original, was added to that drained from the loop to compensate for losses due to sampling. In so doing, the uranium and copper concentrations were increased, and the nickel and chromium concentrations were decreased. Within 4 hr after startup the uranium and copper concentrations had increased further. Evidently some of the material that had precipitated during the first part of the run was redissolved. However, as the second part of the run progressed, slow precipitation of uranium and copper recurred.

An increased rate of appearance of nickel in solution after about 4000 hr and a decreased rate of formation of chromium, apparent in Fig. 8.9, were both due to the pump trouble which caused shutdown at 6539 hr. Severe wear on the front Graphitar bearing allowed the rotor shaft and impeller to drag and thereby corrode badly. The Graphitar worn off the bearing was oxidized to CO_2, at least partially, by the Cr(VI) in solution, and the reduced chromium precipitated from solution.

In loop M (250°C) the copper, uranium, and hydrogen ion concentrations changed in about the same manner as they did in loop K. Unlike loop K, loop M was not a new loop at the start of the run, and this fact may have been partly responsible for the relatively large amounts of soluble Cr(VI) formed during the run. The shutdown at 4678 hr was also due to failure of the front bearing of the pump.

In loop L (200°C) the copper, uranium, and hydrogen ion concentrations remained nearly constant,

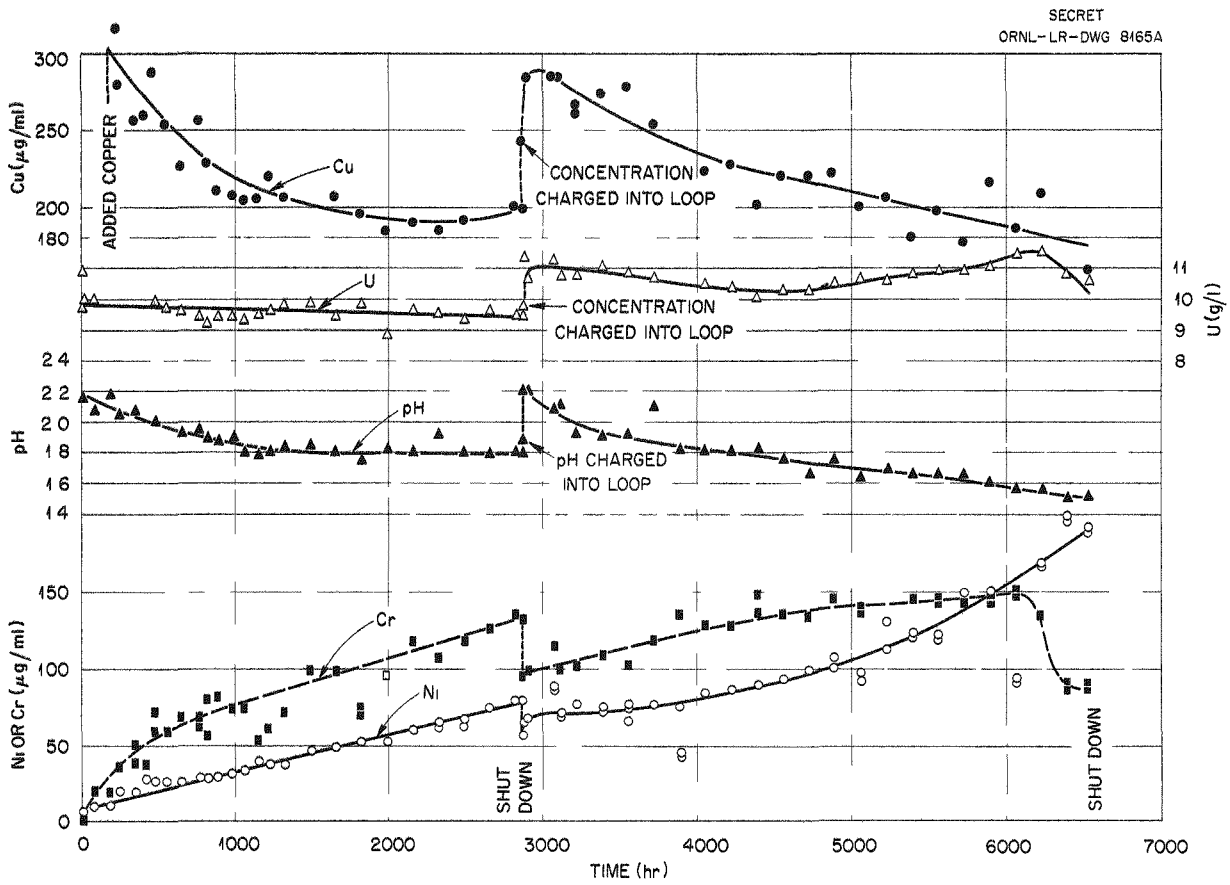

Fig. 8.9. Change in Concentration of Various Ions in Loop K. Initial concentrations: 0.04 *m* UO_2SO_4, 0.006 *m* H_2SO_4, 0.005 *m* $CuSO_4$, and 1000–2000 ppm O_2 at 300°C.

although the copper may have decreased slightly (the decrease was within the analytical spread). No pump trouble has been experienced in this loop so far; the two early shutdowns were caused by small leaks.

The mechanism by which copper and uranium ions were lost from solution at 250 and 300°C is not known, but the change in pH of the solution strongly suggests that a slow hydrolysis was involved. If this was the case, the addition of more sulfuric acid to the solution should reduce the extent of hydrolysis. A current run is being made with 0.02 *m* sulfuric acid (50 mole %) instead of 0.006 *m* (15 mole %) in order to test this hypothesis. The pH of this solution is 1.7. The solutions in loops K and M approached this pH asymptotically, as can be seen in Figs. 8.9 and 8.11, and thus this amount of acid might prevent hydrolytic precipitation. This low pH may, however, cause a substantial decrease in the critical velocity, particularly at the lower temperatures.

(d) Short-Term Runs. – A technique was devised to make very short runs in order to investigate the formation of bulk oxide films on stainless steel. In previous runs, 25 to 50 hr long, the film had already formed on surfaces exposed to uranyl sulfate at flow rates less than the critical velocity. The present series included, therefore, runs 2, 4, 8, 16, and 30 hr long.

The technique consisted in freezing a plug of solution upstream of a coupon holder in a special bypass. The loop proper was started and brought to temperature before the plug was allowed to melt. From thermocouples on the bypass the exact instant was known when hot solution reached the coupons and corrosion began. At the end of the run the pump was stopped, and cooling water was immediately sprayed on the bypass to cool it to

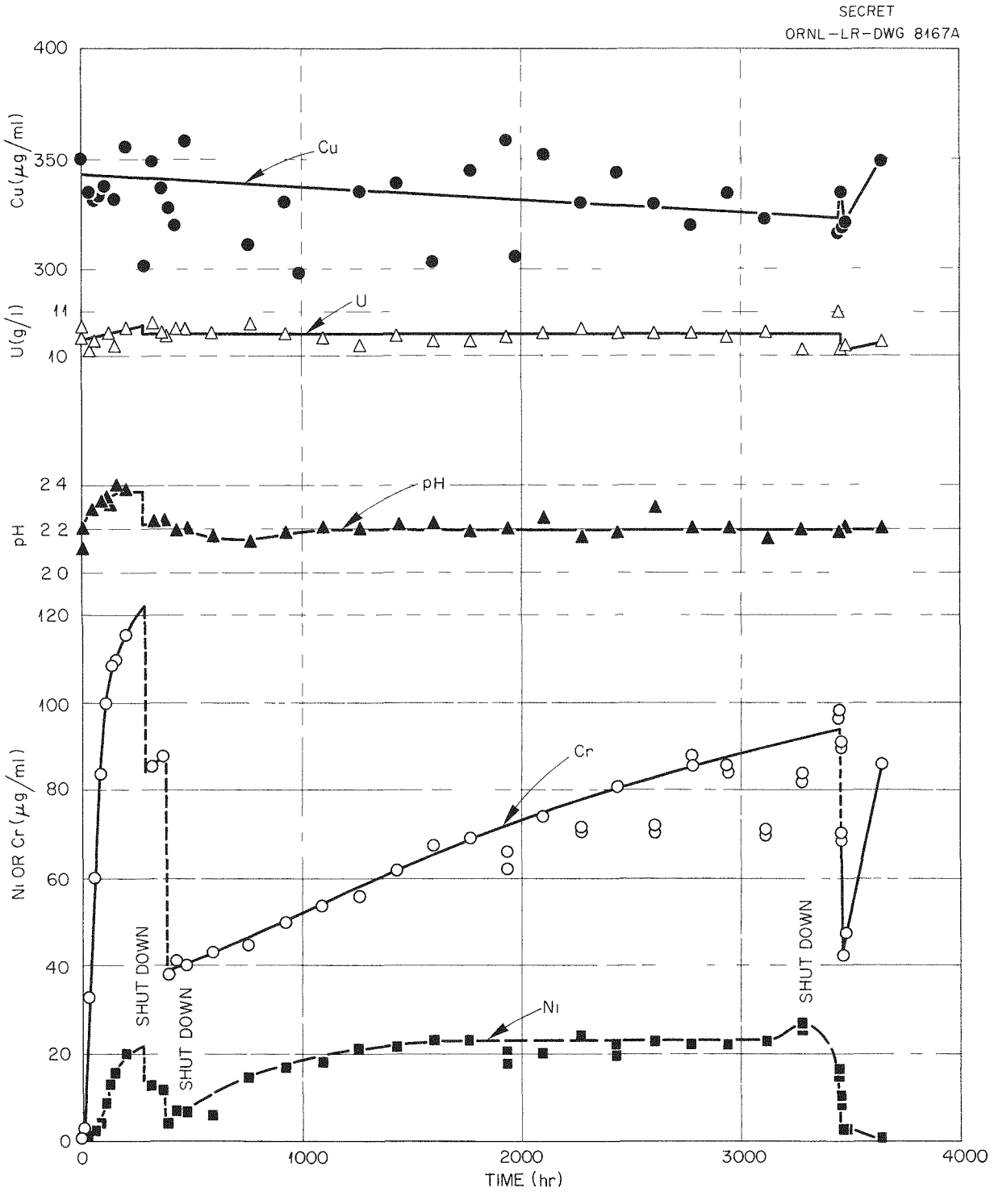

Fig. 8.10. Change in Concentration of Various Ions in Loop L. Initial concentrations: 0.04 *m* UO_2SO_4, 0.006 *m* H_2SO_4, 0.005 *m* $CuSO_4$, and 1000–2000 ppm O_2 at 200°C.

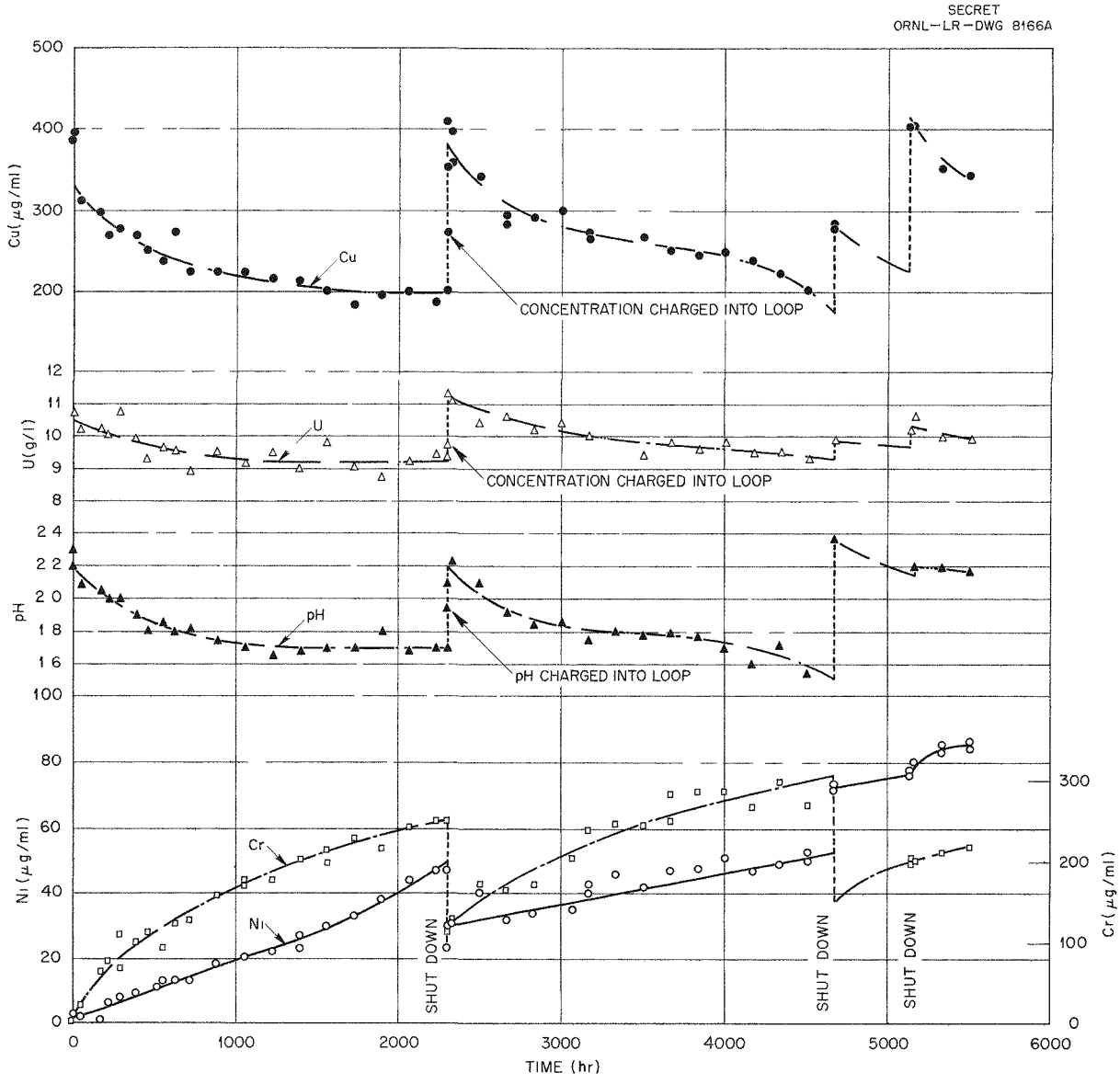

Fig. 8.11. Change in Concentration of Various Ions in Loop M. Initial concentrations: 0.04 *m* UO_2SO_4, 0.006 *m* H_2SO_4, 0.005 *m* $CuSO_4$, and 1000–2000 ppm O_2 at 250°C.

below 100°C within a few minutes.

The first set of runs with 0.17 *m* uranyl sulfate at 250°C showed that the formation of the oxide film began on the lowest-velocity coupon (10 to 11 fps) after about 12 hr. A subsequent set of runs, however, showed that this time of formation was very dependent on the Cr(VI) concentration in solution. A 2-hr run with 200 ppm Cr(VI) gave a film on the first three coupons (9 to 16 fps), whereas a 30-hr run with 2 ppm Cr(VI) gave no film on any coupon (9 to 80 fps).

The effect of Cr(VI) on the film-free corrosion rate was also marked. In the first series of runs, H-58 through H-62, an excess of oxygen (over 2000 ppm in solution) was used, and the Cr(VI) concentration increased rapidly in each run; thus the final concentration depended on the length of the run. In the second series of runs, H-69 through

H-73, very low oxygen concentration was maintained. The Cr(VI) concentration remained very low (approximately 3 ppm except in run H-69) since the oxidizing power of the solution was low. Table 8.6 shows that the film-free corrosion rates depended almost linearly on the Cr(VI) concentration.

Anomalously, run H-69 with 43 ppm Cr(VI) had a corrosion rate less than half that of run H-58 with 34 ppm Cr(VI). This fact may indicate that low oxygen concentration in itself decreases the film-free corrosion rate, since run H-69 had only 50 ppm oxygen in solution, while run H-58 had over 2000 ppm.

(e) Corrosion of Stainless Steel by Uranyl Sulfate Solutions Containing Low Cr(VI) Concentrations. – Further effects of low Cr(VI) concentrations on the corrosion of stainless steel by uranyl sulfate solutions were investigated in the all-titanium loop G at flow rates both above and below the critical velocity. By using only small stainless steel corrosion specimens in this loop, it is possible to keep the Cr(VI) concentration at a much lower level than is possible in a stainless steel loop.

Two series of runs were made at 250°C with 0.17 *m* uranyl sulfate, one with a flow rate of 15 fps, which is below the critical velocity, and one at 70 fps, which is in excess of the critical velocity. The purpose of the low-flow experiment was to determine whether a stable, protective film would form when the system contained very low concentration of Cr(VI), and the purpose of the other experiment was to determine how fast the stainless steel would corrode in a presumably film-free condition.

TABLE 8.6. FILM-FREE CORROSION RATES IN SHORT-TERM RUNS FOR TYPE 347 STAINLESS STEEL COUPONS

Run No.	Length (hr)	Final Chromium Concentration (ppm)	Average Corrosion Rate (mpy)
H-58	2	34	83
H-59	4	45	94
H-60	8	78	130
H-61	16	123	160
H-62	30	248	210
H-69	2	43	34
H-70	4	3	32
H-71	8	3	56
H-72	16	2	47
H-73	30	2	30

Three runs of different duration, runs G-20 through G-22, were made with a flow rate of 15 fps past the one stainless steel pin; the corrosion rate of the pin in each run can be seen in Table 8.2. The exposure times and weight losses were 200 hr, 12 mg/cm^2; 411 hr, 10 mg/cm^2; and 735 hr, 15.1 mg/cm^2. During these runs the Cr(VI) concentration built up to 5 to 12 ppm during the run, which may have been enough to influence results. In a stainless steel system under the same conditions except for the larger amount of Cr(VI), the weight loss after which corrosion would practically stop is 12 ± 10 mg/cm^2 (95% C.I.). Hence at low flow the low concentration of Cr(VI) in the system had no apparent adverse effect on corrosion.

Six runs, G-23, G-24, and G-26 through G-29, each about 100 hr long, were made with 0.04, 0.11, 0.17, 0.40, 0.80, and 1.3 *m* uranyl sulfate with the normal flow of 70 fps past the pins. (Run G-25 was inadvertently terminated after 12 hr and is not considered here.) Again the chromium concentration increased during each run, particularly in the runs with more concentrated solution, and probably influenced the results. Figure 8.12 shows the observed corrosion rates obtained in these runs (two type 347 stainless steel pins per run) and the film-free rates obtained in stainless steel loops, where the chromium concentration increased to an appreciable extent (100 to 500 ppm). Up to 0.17 *m* uranyl sulfate the rates were lower for the pins in these runs with relatively low Cr(VI) than they were in similar runs in stainless steel systems. At higher concentrations the chromium concentration became high and gave essentially the same results as those obtained in stainless steel loops.

Obviously, the results obtained to date concerning the influence of Cr(VI) on the corrosion of stainless steel are not conclusive. There is some evidence indicating that even very low concentrations of Cr(VI) markedly affect the results, and, to date, it has been impossible to keep the corroding solution completely free of Cr(VI). Further experiments are planned to evaluate more closely the effect of Cr(VI), as well as oxygen and hydrogen ion concentrations, on the corrosion of stainless steel by uranyl sulfate solutions.

(f) Corrosion of Selected Alloys in High-Temperature Water. – In the preparation for runs with thoria slurries in loop CS, several runs were made

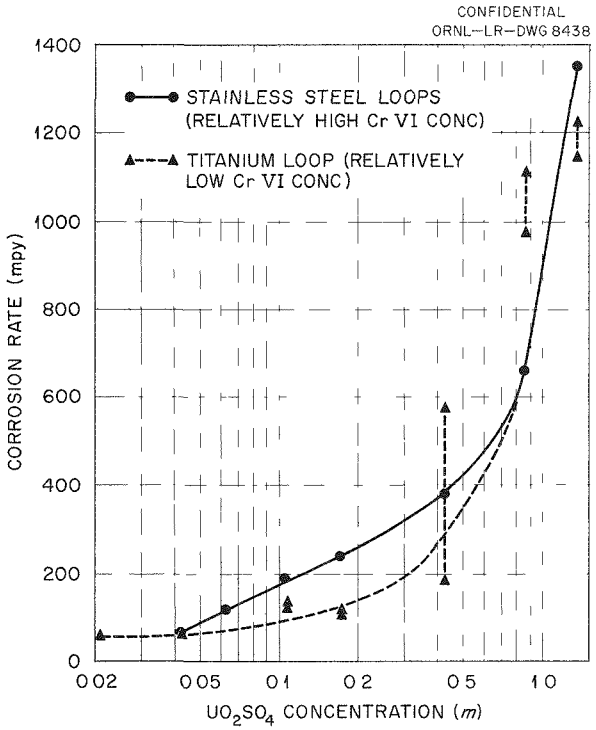

Fig. 8.12. Film-Free Corrosion Rates of Type 347 Stainless Steel Pins vs Uranyl Sulfate Concentration at 250°C.

with distilled water to obtain a base line for water corrosion prior to circulating thoria slurries. Various alloys were exposed at 250 and 300°C, and oxygen or helium pressurization was used. Table 8.2 gives the results obtained (runs I-27, I-28, I-29, CS-2, and CS-3).

In run I-27 a small amount of uranyl sulfate was detected in the water by chemical analysis; the concentration decreased from 2.0 to 0.04 g of uranium per liter during the run. Following this run, the loop was rinsed with 5% nitric acid, to remove all the uranyl sulfate, and then with water. Evidently not all the acid was rinsed, since the pH of the solution in run I-28 was low. The effect of these contaminants was slight, however, since the corrosion rates obtained were in general agreement with previous runs (M-1 and M-2).[22] The generalized corrosion rate as determined from nickel analyses in run I-28 was 0.1 mpy. No generalized rate was obtained from the other runs, since nickelous ion is insoluble in solutions with a pH above 3.5.

In general, the stainless steels tested showed excellent resistance to corrosion by the high-temperature water. Alloys which were more susceptible to attack were the Stellites, 440C stainless steel, Hastelloy C, and Inconel X. Unalloyed nickel also showed a high rate of attack. As previously reported, the susceptible alloys mentioned above showed less attack in the systems which contained no oxygen than they did in those systems pressurized with oxygen. This difference appeared to be related to the fact that in oxygen-containing systems some of the chromium of the alloys was oxidized to the hexavalent state, with an equivalent amount of hydrogen ions being formed. In systems which contained no oxygen, no chromium was found in solution and the pH remained constant.

8.2.3 Miscellaneous

Most of the data presented in Table 8.2 have been discussed or appear to be sufficiently clear to need no further discussion. However, there is one run, the significance of which is not apparent from Table 8.2 alone, that should be discussed.

Run N-3 contained a new alloy, Allegheny Metal 350 (AM-350), with nominal composition 17.0% Cr–4.2% Ni–2.75% Mo–0.60% Mn–0.40% Si–0.08% C–balance Fe, which can be precipitation-hardened or hardened by transformation to martensite at –80 to –100°F. This alloy showed a corrosion resistance in 0.04 *m* uranyl sulfate plus 0.005 *m* copper sulfate and 0.006 *m* sulfuric acid at 250°C very close to that of type 347 and other types of stainless steel. The corrosion resistance in the above solution was independent of the heat treatment.

Run N-3 also contained specimens, supplied by the Solar Aircraft Co. to the HRP Metallurgy Group, of type 321 stainless steel plated with about 3 mils of titanium. After the run it could be seen that, along the sheared edges, the titanium tended to peel from the base metal. Microscopic examination of the flat surfaces showed that small areas of titanium had been removed from the steel and that the steel had corroded, with the formation of many small pits.

Also tested in run N-3 were two alloys, one of composition 50.5% Fe–43.7% Cr–4.94% Ni and the other 55.7% Fe–43.7% Cr. Four pins of each alloy

[22] J. C. Griess and R. E. Wacker, *HRP Quar. Prog. Rep. July 31, 1953*, ORNL-1605, p 84–86.

were heat-treated by the HRP Metallurgy Group; two of each were transformed entirely into the ferritic state and two of each entirely into the sigma phase. During the run all the sigma-phase pins were broken into two pieces. Both pieces of all pins, however, remained in the holder, and the corrosion rates listed in Table 8.2 were obtained by weighing the two pieces. Table 8.2 shows that the sigma pins corroded slightly more than the ferritic pins (although the difference may be due to the break in the sigma pins), and the Fe-Cr-Ni alloy corroded slightly more than the Fe-Cr alloy.

8.3 RESULTS OF LOOP TESTS WITH THORIA SLURRIES

J. C. Griess S. A. Reed

A series of six runs with various concentrations of thorium oxide slurry at 250 and 300°C was completed in loop CS during the past quarter. In each of the runs both pin- and coupon-type corrosion specimens were exposed; slurry samples were withdrawn from the loop and analyzed both chemically and physically.

In all tests the slurries were prepared from batch D-17 ThO_2 (Sec. 14.4). No additions were made to the slurries, other than the gaseous oxygen injected into the loop to maintain approximately 1000 ppm of dissolved oxygen at the selected temperature.

Because these were the initial corrosion tests made with ThO_2 slurry in loop CS, particular emphasis was given to following the concentration of thorium and of corrosion ions throughout each 200-hr run. Chemical analyses were performed on both solid and liquid phases of each sample. In all runs the corrosion ions, iron, chromium, and nickel, were found associated solely with the solid phase, and their relative concentrations were in good agreement with the ratios of these constituents in type 347 stainless steel, indicating a uniform attack of the stainless steel loop. The chemical analyses of samples withdrawn during each test are shown in Table 8.7.

At room temperature, samples of slurry taken from loop CS during the six runs appeared to become creamier in consistency, and the rate of sedimentation decreased markedly during the first 40 hr. Particle-size distribution determined by sedimentation and electron microscopy indicated a gradual degradation of ThO_2 particles during this same period.

Because of the wide fluctuations in slurry concentration that occurred in these six tests, it is probable that the corrosion data which were obtained have little more than a qualitative significance.

Over-all loop corrosion rates calculated from nickel analyses were from 1 to 3 mpy. The average corrosion rates of pin-type corrosion specimens exposed in the tests are presented in Table 8.8. Of the materials tested, the Stellites, nickel, and Hastelloy C were most severely attacked. Graphical representations of the average corrosion rate vs slurry velocity, obtained from weight losses of type 347 stainless steel coupons, are given in Fig. 8.13 through Fig. 8.15. Thin oxide films, approximately 0.01 mg/cm^2, were formed on coupons at both temperatures. Coupons exposed to velocities ranging from approximately 8 to 60 fps showed no indication of a sharp critical velocity. In general, the weight losses seemed to be proportional to the flow rate and slurry concentration.

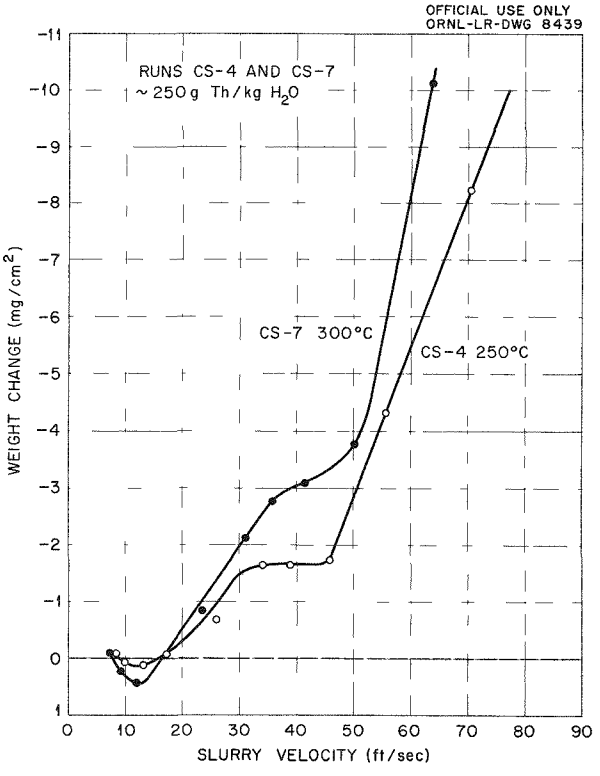

Fig. 8.13. Corrosion Rate of Type 347 Stainless Steel vs Slurry Velocity. Runs CS-4 and CS-7; approximately 250 g of thorium per kilogram of H_2O.

TABLE 8.7. CHEMICAL ANALYSES OF SLURRY SAMPLES FROM RUNS CS-4 THROUGH CS-9

Run No.	Temperature (°C)	Concentration of Loop Charge (g of Th per kg of H_2O)	Solid Phase				Aqueous Phase		Pumping Time (hr)
			Thorium (g per kg of H_2O)	μg per g of Slurry			Conductivity ($\times 10^{-5}$ mohs/cm)	pH	
				Fe	Cr	Ni			
CS-4	250	285	306					7.5	2.5
			273					7.6	24
			248					7.4	48
			263					7.3	70
			236					7.0	100
			166	284	58	40		7.0	150
			181	266	65	42		7.1	200
CS-5	250	500	619	120	26	19		7.1	6
			490	230	60	43		6.4	24
			521	282	75	50		7.0	50
			530	325	80	54		7.1	72
			525	358	100	65		7.0	100
			520	411	101	70		7.3	200
CS-6	250	1000	654	18	7	6	7.1	6.9	5
			806	53	14	12	3.5	7.0	22
			713	110	25	19		7.3	50
			666	233	46	34	3.9	7.0	75
			718	254	59	46	7.8	6.8	100
			750	295	71	55	4.4	7.9	150
			998	284	72	55	4.4	8.0	172*
CS-7	300	276	321	33	8	5	2.3	7.4	4
			275	92	19	13	2.9	7.3	20
			229	182	36	26	3.1	7.0	48
			273	207	53	29	3.1	7.0	72
			296	279	80	43	3.3	6.7	100
			280	334	77	57	3.6	7.2	150
			260	364	87	59	3.6	6.6	200
CS-8	300	530	718	42	10	10	3.3	6.4	4
			464	121	28	22	3.2	6.0	20
			312	189	46	38	2.3	6.6	44
			388	230	63	52	4.0	6.2	68
			377	367	79	66	4.3	6.8	100
			368	435	102	75	4.2	7.3	150
			384	487	112	84	3.9	7.1	200
CS-9	300	1000	806	44	6	5	4.5	6.1	4
			612	95	12	6	5.1	6.4	20
			535	190	37	38	9.0	7.2	44
			544	272	59	53	5.4	7.0	69
			536					7.1	100
			667	398	103	69		7.2	181**

*The loop was sparged with oxygen before this sample was taken.

**Run terminated because of power failure.

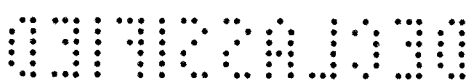

TABLE 8.8. CORROSION RATE OF PIN-TYPE SPECIMENS (RUNS CS-4 THROUGH CS-9)

Run No.	Test Conditions					Pin Material	Number of Pins	Corrosion Rate (mpy)		
	ThO_2 Slurry Concentration (g of Th per kg of H_2O)	Temperature (°C)	Time (hr)	Additions	Flow Rate (fps ± 10%)			Minimum	Average	Maximum
CS-4	166–306[a]	250	200	1000 ppm O_2	17	309 SCb SS	1		0.34	
						347 SS	3	0.60	0.66	0.68
						410 SS[b]	1		1.1	
						416 SS[b]	1		1.2	
						420 SS[b]	1		1.0	
						17-4 PH SS[b]	1		0.94	
						Inconel X	1		5.1	
						Nickel	1		16	
						Stellite 1	1		[c]	
						Stellite 6	1		0.09	
						Stellite 25	1		[c]	
						Stellite 98M2	1		2.6	
					40	302B SS	2	4.8	5.2	5.5
						304L SS	2	3.9	4.2	4.4
						309 SCb SS	2	4.9	4.9	4.9
						316 SS	2	4.2	4.6	5.0
						321 SS	2	4.7	4.8	4.8
						347 SS	3	2.2	3.4	4.3
						Platinum	1		[c]	
					50	309 SCb SS	1		8.8	
						322W SS[b]	1		8.7	
						347 SS	2	5.9	6.7	7.4
						440C SS[b]	1		13	
						17-4 PH SS[b]	1		9.3	
						Carpenter 20 SS	1		11	
						Nickel	1		34	
						Stellite 1	1		25	
						Stellite 6	1		51	
						Titanium (3% Al–5% Cr)	1		[c]	
						Titanium (5% Al–2.5% Sn)	1		[c]	
						Titanium (6% Al–4% V)	1		[c]	

TABLE 8.8 (continued)

Run No.	Test Conditions					Pin Material	Number of Pins	Corrosion Rate (mpy)		
	ThO_2 Slurry Concentration (g of Th per kg of H_2O)	Temperature (°C)	Time (hr)	Additions	Flow Rate (fps ± 10%)			Minimum	Average	Maximum
CS-5	490–619[a]	250	200	1000 ppm O_2	16	309 SS	1		2	
						347 SS	3	1.4	2	2.2
						410 SS[b]	1		3.1	
						416 SS[b]	1		3.1	
						420 SS[b]	1		3.1	
						17-4 PH SS[b]	1		2.5	
						Inconel X	1		6.3	
						Nickel	1		21	
						Stellite 1	1		1.7	
						Stellite 6	1		2.6	
						Stellite 25	1		6.4	
						Stellite 98M2	1		18	
					36	302B SS	2	7.6	8	8.3
						304L SS	2	8.7	8.7	8.7
						309 SCb SS	2	7.6	8.1	8.6
						316 SS	2	7.8	8.3	8.8
						321 SS	2	7.7	7.6	8.1
						347 SS	3	4.9	7	8.0
						Platinum	1		1.1	
					47	309 SCb SS	1		17	
						322W SS[b]	1		12	
						347 SS	2	9.3	10.7	12
						430 SS	1		16	
						440C SS[b]	1		15	
						17-7 PH SS[b]	1		13	
						Carpenter 20 SS	1		15	
						Nickel	1		39	
						Stellite 1	1		110	
						Stellite 6	1		74	
						Titanium (3% Al–5% Cr)	1		[c]	
						Titanium (5% Al–2.5% Sn)	1		[c]	
						Titanium (6% Al–4% V)	1		[c]	

TABLE 8.8 (continued)

Run No.	Test Conditions					Pin Material	Number of Pins	Corrosion Rate (mpy)		
	ThO_2 Slurry Concentration (g of Th per kg of H_2O)	Temperature (°C)	Time (hr)	Additions	Flow Rate (fps ± 10%)			Minimum	Average	Maximum
CS-6	654–998[a]	250	172	1000 ppm O_2	15	309 SCb SS	1		4.2	
						347 SS	3	4.5	4.6	4.7
						410 SS[b]	1		4.3	
						416 SS[b]	1		5.8	
						420 SS[b]	1		4.3	
						17-4 PH SS[b]	1		5.5	
						Inconel X	1		12	
						Nickel	1		31	
						Stellite 1	1		9.9	
						Stellite 6	1		8.1	
						Stellite 25	1		16	
						Stellite 98M2	1		140	
					35	302B SS	2	8.5	8.6	8.6
						304L SS	2	12	12.5	13
						309 SCb SS	2	11	11.5	12
						316 SS	2	11	11	11
						321 SS	2	10	10.5	11
						347 SS	3	7.7	10.2	12
						Platinum	1		2	
					45	309 SCb SS	1		17	
						322W SS[b]	1		16	
						347 SS	2	16	16	16
						430 SS	1		18	
						440C SS[b]	1		20	
						17-7 PH SS[b]	1		16	
						Carpenter 20 SS	1		21	
						Nickel	1		51	
						Stellite 1	1		120	
						Stellite 6	1		110	
						Titanium (3% Al–5% Cr)	1		[c]	
						Titanium (5% Al–2.5% Sn)	1		[c]	
						Titanium (6% Al–4% V)	1		[c]	

TABLE 8.8 (continued)

Run No.	Test Conditions					Pin Material	Number of Pins	Corrosion Rate (mpy)		
	ThO_2 Slurry Concentration (g of Th per kg of H_2O)	Temperature (°C)	Time (hr)	Additions	Flow Rate (fps ± 10%)			Minimum	Average	Maximum
CS-7	229–321[a]	300	200	1000 ppm O_2	15	309 SCb SS	1		1.1	
						347 SS	2	1.4	1.5	1.5
						347 SS[d]	1		1.8	
						443 SS	1		2.6	
						446 SS	1		2.9	
						Inconel X	1		3.1	
						Nickel	1		1.7	
						Stellite 1	1		2.0	
						Stellite 3	1		5.5	
						Stellite 6	1		2.0	
						Stellite 25	1		0.77	
						Stellite 98M2	1		15	
						Titanium 75A	1		0.31	
					35	304L SS	2	4.6	5.2	6.0
						309 SCb SS	1		5.7	
						322W SS[b]	1		5.1	
						322W SS[e]	1		5.5	
						347 SS	2	6.4	6.4	6.4
						347 SS[d]	1		6.2	
						17-7 PH SS[b]	1		6.1	
						17-7 PH SS[e]	1		6.2	
						Platinum	1		0.02	
						Titanium (3% Al–5% Cr)	1		0	
						Titanium (5% Al–2.5% Sn)	1		0.31	
						Titanium (6% Al–4% V)	1		0.31	
					44	322W SS[e]	1		9.7	
						347 SS	2	7.9	8.1	8.3
						347 SS[d]	1		8.1	
						Carpenter 20 SS	1		13	
						Nickel	1		8.8	
						Platinum	1		0.15	

TABLE 8.8 (continued)

Run No.	Test Conditions					Pin Material	Number of Pins	Corrosion Rate (mpy)		
	ThO_2 Slurry Concentration (g of Th per kg of H_2O)	Temperature (°C)	Time (hr)	Additions	Flow Rate (fps ± 10%)			Minimum	Average	Maximum
CS-7	229–321[a]	300	200	1000 ppm O_2	44	Stellite 1	1		51	
						Stellite 3	1		16	
						Stellite 6	1		32	
						Stellite 98M2	1		8.3	
						Titanium 75A	1		0.22	
						Zircaloy-2	1		2.2	
						Zirconium[f]	1		2.3	
CS-8	312–718[a]	300	200	1000 ppm O_2	15	309 SCb SS	1		2.7	
						347 SS	2	3.4	3.5	3.5
						347 SS[d]	1		3.5	
						443 SS	1		5.5	
						446 SS	1		5.9	
						Inconel X	1		10	
						Nickel	1		4.2	
						Titanium 75A	1		2.0	
						Stellite 1	1		2.4	
						Stellite 3	1		3.9	
						Stellite 6	1		2.6	
						Stellite 25	1		3.1	
						Stellite 98M2	1		8.8	
					34	304L SS	2	5.5	6	6.5
						309 SCb SS	1		5.9	
						322W SS[b]	1		6.3	
						322W SS[e]	1		6.6	
						347 SS	3	6.2	6.3	6.5
						17-7 PH SS[b]	1		6.5	
						17-7 PH SS[e]	1		6.3	
						Platinum	1		1.2	
						Titanium (3% Al–5% Cr)	1		2.9	
						Titanium (5% Al–2.5% Sn)	1		3.5	
						Titanium (6% Al–4% V)	1		3.5	

TABLE 8.8 (continued)

Run No.	Test Conditions					Pin Material	Number of Pins	Corrosion Rate (mpy)		
	ThO_2 Slurry Concentration (g of Th per kg of H_2O)	Temperature (°C)	Time (hr)	Additions	Flow Rate (fps ± 10%)			Minimum	Average	Maximum
CS-8	312–718[a]	300	200	1000 ppm O_2	42	304L SS	2	11	11.5	12
						309 SCb SS	1		11	
						347 SS	2	11	11	11
						347 SS[d]	1		10	
						Carpenter 20 SS	1		11	
						Nickel	1		18	
						Platinum	1		3.7	
						Synthetic sapphire	1		520	
						Titanium 75A	1		4.6	
						Titanium 150A	1		4.6	
						Zircaloy-2	1		5.1	
						Zirconium[f]	1		4.9	
CS-9	535–806[a]	300	181.6	1000 ppm O_2	15	309 SCb SS	1		3.8	
						347 SS	2	5.3	5.4	5.4
						347 SS[d]	1		4.6	
						443 SS	1		11	
						446 SS	1		11	
						Inconel X	1		15	
						Nickel	1		6.4	
						Stellite 1	1		0.93	
						Stellite 3	1		6.1	
						Stellite 6	1		4.2	
						Stellite 25	1		3.4	
						Stellite 98M2	1		16	
						Titanium 75A	1		0.51	
					36	304L SS	2	7.6	8.8	9.9
						309 SCb SS	1		8.3	
						322W SS[b]	1		11	
						322W SS[e]	1		12	
						347 SS	3	9.2	9.2	9.3
						17-7 PH SS[b]	1		11	

TABLE 8.8 (continued)

Run No.	Test Conditions					Pin Material	Number of Pins	Corrosion Rate (mpy)		
	ThO_2 Slurry Concentration (g of Th per kg of H_2O)	Temperature (°C)	Time (hr)	Additions	Flow Rate (fps ± 10%)			Minimum	Average	Maximum
CS-9	535–806[a]	300	181.6	1000 ppm O_2	36	17-7 PH SS[e]	1		12	
						Platinum	1		2.9	
						Titanium (3% Al–5% Cr)	1		1.3	
						Titanium (5% Al–2.5% Sn)	1		2.4	
						Titanium (6% Al–4% V)	1		2.9	
					46	304L SS	2	20	22	24
						309 SCb SS	2	20	21	22
						347 SS	2	21	21	21
						347 SS[d]	1		17	
						Carpenter 20 SS	1		20	
						Nickel	1		26	
						Platinum	1		7.2	
						Titanium 75A	1		2.7	
						Titanium 150A	1		2	
						Zircaloy-2	1		9.2	
						Zirconium[f]	1		8.5	

[a] See Table 8.7, column 3.
[b] Hardened.
[c] Showed slight weight gain.
[d] Cast.
[e] Annealed.
[f] Crystal bar.

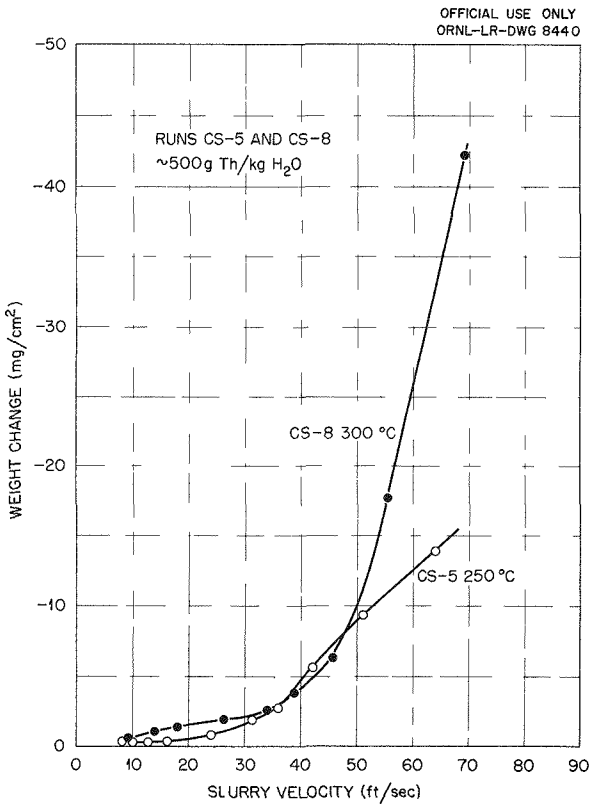

Fig. 8.14. Corrosion Rate of Type 347 Stainless Steel vs Slurry Velocity. Runs CS-5 and CS-8; approximately 500 g of thorium per kilogram of H_2O.

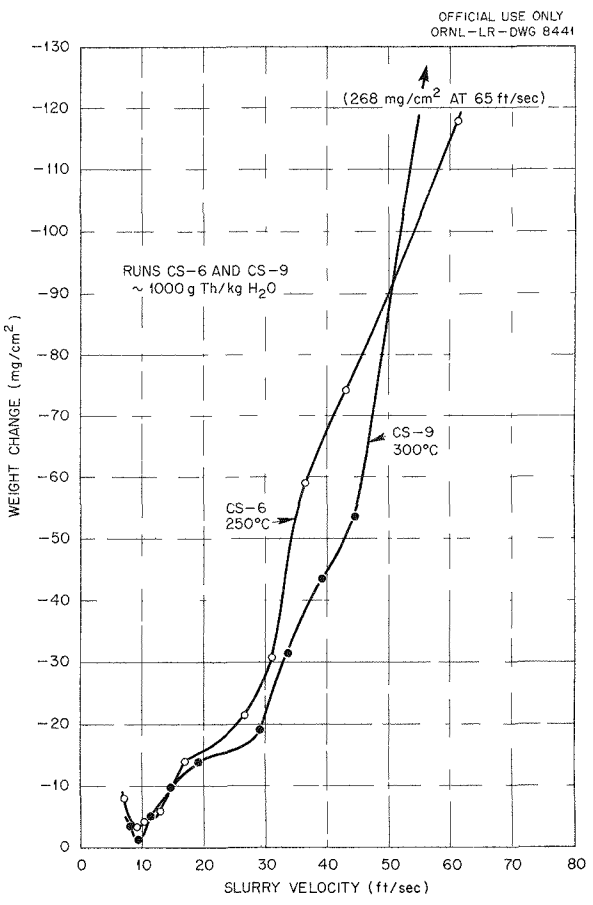

Fig. 8.15. Corrosion Rate of Type 347 Stainless Steel vs Slurry Velocity. Runs CS-6 and CS-9; approximately 1000 g of thorium per kilogram of H_2O.

There were no significant differences in corrosion rate between comparable runs at 250 and 300°C except at the higher velocities. Type 347 stainless steel coupons exposed to velocities of 60 to 70 fps at 300°C appeared to be more abraded or eroded than specimens in the same velocity region at 250°C.

In each run platinum pins were exposed to the slurries at approximately 40 fps. Since little or no chemical attack of platinum would be expected under the test conditions, the weight losses should serve as an index to abrasion or erosion by the slurry. Weight losses of the platinum pins indicated an attack rate of 0.02 to 7.2 mpy.

8.4 SEDIMENTATION CHARACTERISTICS OF THORIUM DIOXIDE SLURRIES AT ELEVATED TEMPERATURES

S. A. Reed

Previous tests to investigate the sedimentation characteristics of thorium dioxide slurries were extended to include studies at 100 and 150°C, and additional sedimentation data were collected for slurry preparations described previously.[23,24]

[23] S. A. Reed, *HRP Quar. Prog. Rep. Jan. 31, 1955*, ORNL-1853, p 83–85.

[24] S. A. Reed, *HRP Quar. Prog. Rep. April 30, 1955*, ORNL-1895, p 92–93.

Sedimentation rates were determined for one new thoria slurry, prepared from batch D-17 ThO_2 currently being used in dynamic-loop-corrosion studies (see Secs. 14.4 and 8.3 of this report). A series of calculations, in which these data were used, was made to estimate the effective particle size of slurries at temperature.

8.4.1 Sedimentation at 100 and 150°C

As noted in a previous report,[23] a rather marked change in the general characteristics of the slurries under test occurred in the temperature range 100 to 180°C. In preliminary tests the slurries in this temperature range appeared to become creamy in consistency, adhered quite tenaciously to the walls of the quartz tubes, and ceased to be free flowing. Particular emphasis was therefore given to studying the rate of sedimentation of each slurry sample when heated to 100 and 150°C. At 150°C several of the preparations containing 250 g of thorium per kilogram of water were found to be in the hindered settling region, while others gave rates indicative of compaction settling. However, at 100°C the sedimentation of these same preparations was quite erratic. While no hindered settling was expected, a measurable compaction rate should have been observed. Often this was not the case. During studies with the same sample at 100°C, a measurable compaction rate was observed in one test, while in the next test no settling was observed in a 4- to 6-hr period. A closer inspection of the sample showed that considerable gas or steam was entrapped in the slurry. When the tube was gently agitated, some of the gas was slowly expelled, the slurry appeared to be more fluid, and settling occurred. If the samples were then heated to 250 or 300°C without agitation, additional gas was released and further settling was noted. In similar tests conducted at room temperature, air mixed into the slurries with a laboratory blender was held so tenaciously that it did not escape until the solids were centrifuged. The phenomenon was most pronounced with the low-calcined oxides having the larger surface areas. The higher fired oxides, such as Lindsay batch 8 (L-8) material, settled more uniformly at room temperature and at 100 to 150°C and appeared to retain much smaller quantities of gas.

One new thoria slurry, prepared from batch D-17 ThO_2, was examined during the quarter. Sedimentation rates were determined at 250 and 300°C on samples of the slurry both before and after pumping in loop C and after treatment in a high-shear laboratory blender for 4 hr. A portion of the pumped material was also resuspended in D_2O and tested. The sedimentation rates obtained for these preparations, and additional data collected for the preparations previously reported, are presented in Table 8.9.

8.4.2 Estimation of Particle Size

To date, three different methods have been described by other investigators[25-27] for estimating the particle size of thorium dioxide: the electron-diffraction method, which, in general, affords an estimation of the size of the particles and aggregates; nitrogen surface-area measurements, from which the average size of the thoria crystallites may be estimated; and sedimentation techniques in which dilute suspensions of thoria at room temperature are used. From the last method, the distribution of particles, as well as the apparent Stokes' diameters of the particles, has been calculated.

While it is questionable that the sedimentation rates shown in Table 8.9 are appropriate for estimating particle size, a series of calculations was made to ascertain whether any agreement existed when particle diameters calculated from these data were compared with those found when the three methods noted above were used.

The rates at elevated temperatures were determined by following the settlement of the top surface of the ThO_2 suspensions and therefore describe the average downward movement of the meniscus of solids through the liquid column before the solids reached a state of compaction. Particle diameters calculated from the rates, then, can represent only an average size. If particle diameters are calculated by using Stokes' law, with corrections for the viscosity and density of water, the values are severalfold greater than those given by the other methods. This is to be expected, however, since in the concentration range 250 to 500 g of thorium per kilogram of water the porosities of the slurries are much lower than in very dilute

[25] D. E. Ferguson *et al.*, *ThO_2 Slurry Development: Quarterly Report for Period Ending April 31, 1955*, ORNL CF-55-5-198 (May 20, 1955).

[26] G. W. Leddicotte and H. H. Miller, *Anal. Chem. Semiann. Prog. Rep. Oct. 20, 1954*, ORNL-1788, p 21–23.

[27] R. E. Druschel, G. W. Leddicotte, and H. H. Miller, *Anal. Chem. Div. Semiann. Prog. Rep. April 20, 1955*, ORNL-1880, p 17.

TABLE 8.9. SEDIMENTATION RATES OF ThO_2 SLURRIES AT ELEVATED TEMPERATURES

Slurry Identification[a]	Approximate Concentration (g of Th per kg of H_2O)	Rate of Sedimentation (cm/sec)				
		100°C	150°C	200°C	250°C	300°C
D-10[b]	250	c	c	0.17	0.23	0.30
H-5-A[b]	250	c	c	0.10	0.14	0.17
	1000	c	c	c	c	c
D-17[b]						
Raw	250				0.61	0.81
Blended	250				0.36	0.43
Pumped	250				0.21	0.33
Pumped and resuspended in D_2O	250				0.20	0.33
	500				0.18	0.28

[a] See Sec. 14.4.

[b] D-10 and D-17: ORNL production batches, two-stage calcination (650°C maximum); H-5-A: ORNL experimental batch, contained 7800 ppm SO_4^{--}.

[c] In compaction (no hindered settling was apparent).

suspensions, where Stokes' law would apply. Because of this obvious variable, an equation suggested by J. M. Dallavalle[28] was used:

$$D_s = \frac{u\mu}{0.006g(\rho_s - \rho_0)} \cdot \left(\frac{1 - \epsilon}{\epsilon^3}\right)^{1/2},$$

where

D_s = apparent particle diameter, μ,
u = observed velocity, cm/sec,
μ = viscosity of water,
g = gravitational factor, cm/sec^2,
ρ_s = density of a solid, g/cc,
ρ_0 = density of a fluid, g/cc,
ϵ = porosity.

The equation is a modification of the classical Poiseuille equation and offers a means of correcting for the porosity of the slurries by including the term $(1 - \epsilon)/\epsilon^3$. The value 0.006 is an empirical constant found by plotting the Froude values as a function of the Reynolds numbers, which are derived from experimental data. With the appropriate corrections for changes in density and viscosity due to temperature, the calculated diameters closely approximate those found from surface-area measurements for both pumped and blended samples of the slurries. A comparison of these data is given in Table 8.10. The diameters calculated by this method for the D-17 raw sample, which received no prior treatment, indicate average diameters several-fold greater than those for the pumped material, while the blended samples give diameters intermediate between the two. This was attributed to aggregation and is in agreement with results obtained by other investigators who concluded that untreated thoria slurries consisted of particle aggregates which were partially degraded by blending or "micronizing."

A second series of calculations was also performed to estimate the effective particle diameter and apparent particle density on the assumption that the particles were aggregated or agglomerated and had associated with them an amount of water which would vary with the temperature during settling. Although the calculations have not been completed for all the slurries tested, some of the preliminary data are presented in Table 8.10 for comparison.

If by interaction of water and thoria the particles form agglomerates and if these agglomerates act as individual particles during the process of sedimentation, an estimate of the effective diameters may be calculated when corrections are made for

[28] Consultant.

TABLE 8.10. ESTIMATED PARTICLE SIZES OF ThO_2 SLURRIES AT ELEVATED TEMPERATURE

Slurry Preparation	Approximate Concentration (g of Th per kg of H_2O)	Temperature (°C)	Sedimentation Rate (cm/sec)	Average Particle Diameter		Calculated Average Particle Diameter		Values Calculated by Use of Steinour's Equation		
				Calculated from N_2 Surface Area (Å)	Room-Temperature Sedimentation* (μ)	By Use of Stokes' Equation (μ)	By Use of Modified Poiseuille Equation (μ)	Porosity, ϵ	Apparent Agglomerate Density	Agglomerate Diameter (μ)
D-17										
Raw				200	2.4					
	250	250	0.71			12	16			
	250	300	0.81			12	14			
Blended					0.6–1.0					
(4 hr)	250	250	0.36			9	10			
	250	300	0.43			10	10			
	500	250	0.23			7		0.863	3.7	24
	500	300	0.27			7		0.867	3.2	21
Pumped					0.2–0.4					
(200 hr)	250	250	0.21			6	3			
	250	300	0.33			6	3			
	500	250	0.18			6	4	0.943	8.1	8
	500	300	0.25			7	4	0.969	9.6	8
L-8										
Raw				900	4					
	250	300	0.82			12	16			
Blended					1.5					
(4 hr)	250	200	0.16			6	7			
	250	250	0.24			7	7			
	250	300	0.33			6	7			
	500	200	0.10			6	7	0.851	1.7	28
	500	250	0.17			7	7	0.870	2.5	20
	500	300	0.24			7	7	0.880	3.6	12

*See D. E. Ferguson *et al.*, *ThO_2 Slurry Development: Quarterly Report for Period Ending April 31, 1955*, ORNL CF-55-5-198 (May 20, 1955).

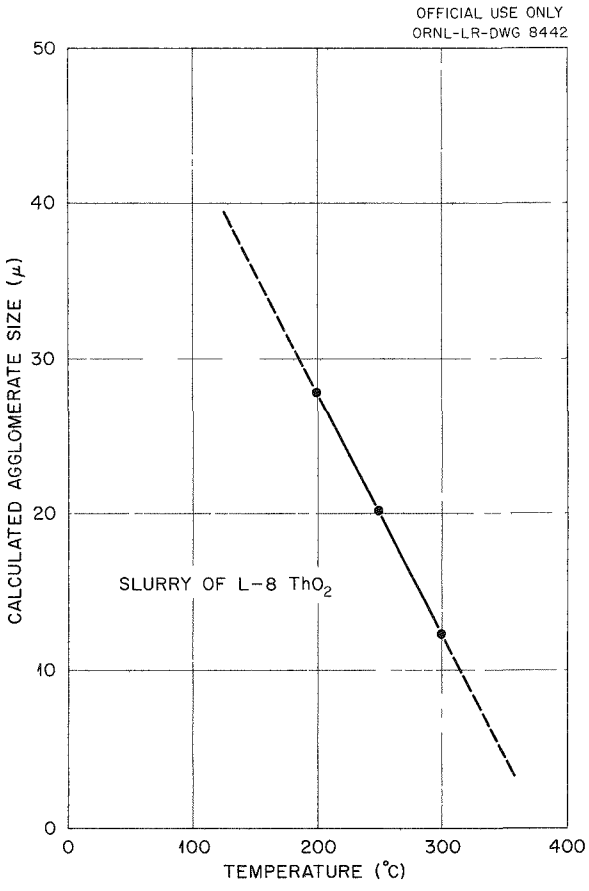

Fig. 8.16. Variation of Calculated Agglomerate Diameter with Temperature. Slurry of L-8 ThO_2.

the alteration in particle density and the corresponding change in porosity at each temperature.

With the use of the experimentally determined rates Q for any two concentrations of the same slurry at a given temperature, the adjusted porosities, ϵ, and apparent Stokes' velocities V_s were calculated by using the Steinour equation,

$$Q = V_s \epsilon^2 10^{-1.82(1-\epsilon)} .$$

The calculated values for V_s were then used to estimate the apparent particle diameter by the Stokes' equation. A typical plot of the agglomerate diameters vs temperature for one of the slurries is shown in Fig. 8.16. However, the data are presented at this time to exemplify the correlations that exist when the particulate properties of thoria slurries at elevated temperatures are compared with those properties observed at room temperature.

9. RADIATION CORROSION

G. H. Jenks

A. L. Bacarella
J. E. Baker
W. N. Bley
N. C. Bradley
W. E. Clark
R. J. Davis
H. O. Day
H. A. Fisch
B. O. Heston
D. T. Jones
H. C. Savage
R. A. Lorenz
J. R. McWherter
A. R. Olsen
M. D. Silverman
H. H. Stone
R. M. Warner
K. S. Warren
L. F. Woo
W. C. Yee

9.1 IN-PILE LOOP

H. C. Savage
G. H. Jenks

W. N. Bley
N. C. Bradley
D. T. Jones
J. E. Baker
R. A. Lorenz
A. R. Olsen
R. M. Warner

9.1.1 Development and Construction

(a) HB-4 Mockup. – The fabrication of in-pile circulating loops for radiation corrosion studies continued during the past quarter. Loop assembly EE was completed and was installed in beam hole HB-4 of the LITR. This was the fourth loop assembly installed and operated in the LITR. The corrosion specimens consisted of coupons in Zircaloy-2 tapered-channel holders, stressed specimens, and coupled specimens. These specimens were made of type 347 stainless steel, Zircaloy-2, and titanium 55AX. Detailed information on these corrosion specimens was given in a previous report.[1]

Since it is planned that in-pile loops will be installed in beam hole HB-2 of the LITR in addition to HB-4 and since other reactor facilities might be used for future in-pile loops, a new system of in-pile loop identification has been devised. This system consists of three parts, which designate the reactor in which the loop is to be installed, the reactor test facility, and the loop number (numbered consecutively). Identification of the reactor is by letter and is first in order; the second number or letter designates the particular reactor test hole to be used; and the third number is the loop number. Loops will be numbered in sequence. For example, the in-pile loop installed after removal of loop EE was identified as L-4-8. The "L" indicates that the loop is to be installed in the LITR; the "4" designates beam hole HB-4; and the "8" indicates that this loop is the eighth in-pile type of loop that has been built.

Loop L-4-8 was completed and was then installed in beam hole HB-4 at the LITR following removal of loop EE. Corrosion coupons in Zircaloy-2 tapered holders were installed in both the in-line and core positions. These coupons were of three materials: type 347 stainless steel, Zircaloy-2, and titanium. The arrangement of the coupons in the holders was identical to that of the coupons for loop EE described previously.[1] Two rod-and-sleeve assemblies containing uncoupled coupons of types 347 and 309 SCb stainless steel were installed in the core position, replacing the coupled specimens used in loop EE. These assemblies were mounted around the coupon holder in the core position along with stressed specimens of Zircaloy-2, hardened type 17-4 PH stainless steel, and type C-130-AM titanium. The type C-130-AM titanium and hardened type 17-4 PH stainless steel are materials with high yield strength that are under consideration for use as bolting material for the fuel-contacting joint between the HRT core and pressure vessel. These two materials are also under investigation to determine their corrosion resistance under static out-of-pile conditions.

In addition to the usual core and in-line corrosion specimens, loop L-4-8 contained stressed specimens in a second in-line holder for comparison with the stressed specimens in the core. This second in-line holder contained three stressed-specimen assemblies – one each of Zircaloy-2, hardened type 17-4 PH stainless steel, and type C-130-AM titanium – as shown in Fig. 9.1. A third set of eight stressed-specimen assemblies – two each of Zircaloy-2, type 347 stainless steel, type 17-4 PH stainless steel, and type C-130-AM titanium – was installed in the pressurizer. The assemblies were so arranged that one stressed assembly of each afore-mentioned material would be exposed to the liquid and one to the vapor phase

[1] G. H. Jenks, H. C. Savage, *et al.*, *HRP Quar. Prog. Rep. April 30, 1955*, ORNL-1895, p 94–95.

in the pressurizer. The temperature in the pressurizer is 280°C, whereas the in-line and core temperature is 250°C. The arrangement of the stressed specimens in the pressurizer is shown in Fig. 9.2.

The circulating pump in loop L-4-8 is a modified ORNL 5-gpm model with pure sintered aluminum oxide bearings and journal bushings. The pump is discussed later in this section under the heading of "In-Pile Pumps."

Fig. 9.1. In-Line Stress Specimen Holder – Loop L-4-8.

Loops L-2-10 and L-4-11 (to be installed following the removal of L-4-8) are now under construction. Loop L-2-10 is designed for operation up to 300°C and 2000 psia. The present in-pile loop packages are limited to 250°C and 1000-psia operation.

(b) LITR HB-2 Installation. – *(1) Loop Package.* – As mentioned above, in-pile loop L-2-10 is under construction. The corrosion coupons in loop L-2-10 are $\frac{1}{4} \times \frac{1}{2} \times 0.060$ in. thick. Twenty-four of these coupons are installed in each tapered coupon holder in the in-line and core position. Coupons of each of three materials – Zircaloy-2, type 347 stainless steel, and titanium – are arranged in the holder. The coupon holders in loop L-2-10 are made of type 347 stainless steel instead of Zircaloy-2, which was used in all previous in-pile loops. This change in holder material, as well as a change in the arrangement of the coupons of the three metals, was made in an effort to evaluate galvanic couple effects under radiation. Specimens of Zircaloy-2 for impact and tensile-strength measurements after operation of the loop in the LITR are included in both the in-line and core positions. The impact and tensile specimens are shown in Fig. 9.3.

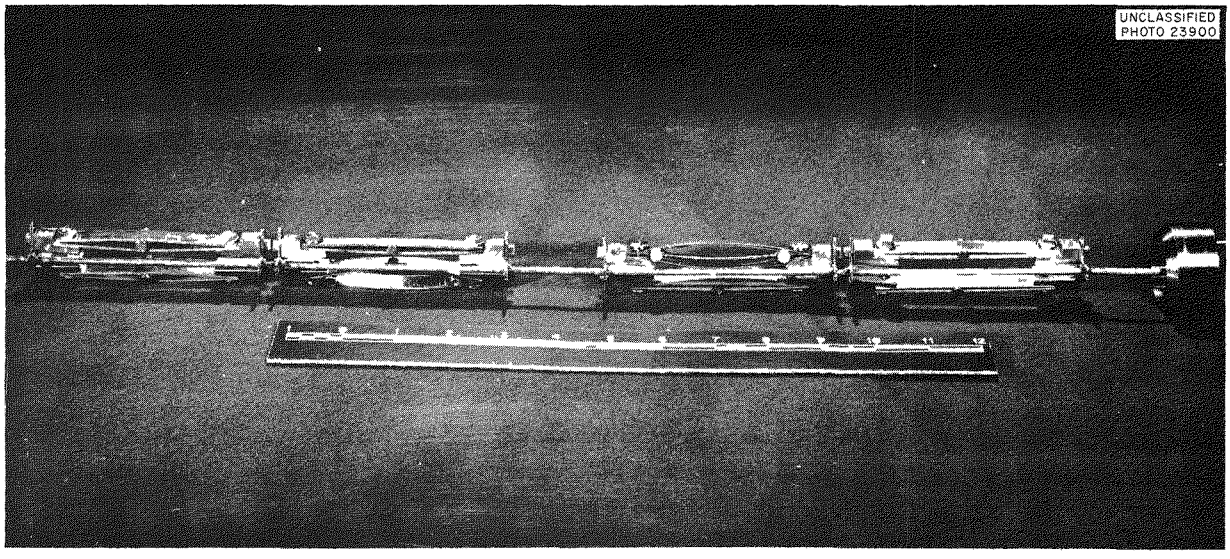

Fig. 9.2. Pressurizer Stress Specimens – Loop L-4-8.

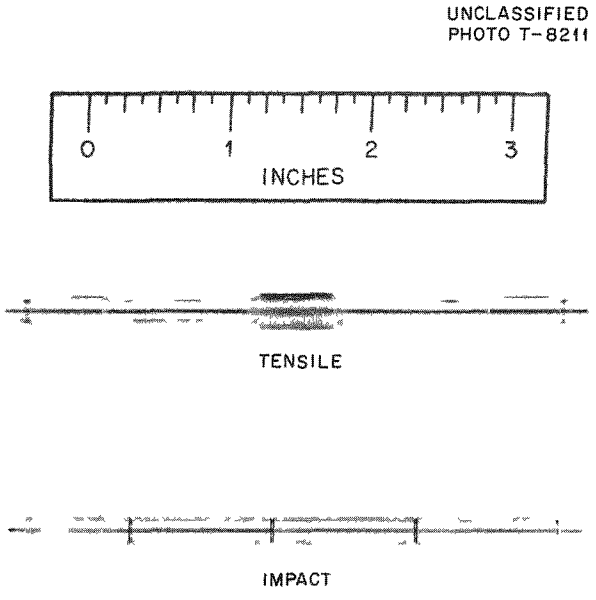

Fig. 9.3. Zircaloy-2 Impact and Tensile Specimens.

An in-pile test loop was constructed which is capable of operating at 300°C and 2000 psia. This loop is being used to test components, instrumentation, and control for the beam hole HB-2. A 2000-psia model of the present ORNL 5-gpm pump will be used in the HB-2 loop packages, pending delivery and testing of the Byron Jackson pumps originally planned for use in the loops in HB-2. The loop package for use in HB-2 of the LITR should be completed and tested by September 15, 1955.

(2) LITR Equipment. – This loop facility is scheduled for completion by October 15. The completion date is predicated on the arrival of the instrument panel by September 20. All drawings, except overhead-services drawings, were issued to field forces. The final drawings will be issued by August 1. The service lines under the floor were installed, and the floor was repoured with a heavier concrete slab. The valve boxes are under construction. Installation of valves and interconnecting piping is scheduled to start August 15.

(c) In-Pile Pumps. – As reported previously,[2] the pumps for use in the in-pile loops were modified to include outboard bearings. With the new design it is possible to obtain better dynamic balance of the rotor assembly and also to reduce the axial thrust load to a minimum, thereby eliminating one of the major causes of bearing failure encountered on the single-bearing pump design formerly used.

The pump in loop L-4-8 is of the new type, fitted with sintered aluminum oxide bearings and journals.[2]

Oxygen is used in the in-pile loops to maintain solution stability. In addition, measurements of the partial pressure of oxygen during loop operation give an indication of oxygen consumption and a measure of corrosion. The oxygen inventory in an in-pile loop is very small, and, in order to maintain accurate measurements of corrosion due to oxygen consumption, it is desirable to eliminate any other means whereby oxygen is consumed. The aluminum oxide bearings are in the form of the stable oxide, while the Graphitar No. 14 formerly used as bearing material is pure carbon and did consume oxygen in the formation of carbon dioxide. Substitution of aluminum oxide as a bearing material eliminates this source of oxygen consumption in the in-pile loops.

Before this pump was used in an in-pile loop, it was operated for 500 hr in a test loop circulating a solution containing 0.17 *m* uranyl sulfate, 0.03 *m* copper sulfate, and 0.04 *m* sulfuric acid at 250°C and 1000 psi. At the end of the test period no visible corrosion attack or measurable wear could be observed, and the pump was installed in loop L-4-8. Satisfactory operation of the pump is continuing at the LITR.

The test model of the Byron Jackson canned-rotor pump for use in in-pile loops is now under test in development loop DV-9. After a few hours of operation at 300°C and 2000 psia, a light drag or rubbing was detected in either the bearing or the impeller region. Upon partial disassembly of the pump, there was some evidence of interference between the impeller hubs and housing (the bearings were not examined, since this would require cutting open seal welds). This drag was not noticeable during operation at temperatures and pressures below approximately 250°C and 1000 psia. After consultation with the Byron Jackson Co., it was decided to increase the clearances between the impeller hubs and housing by a few thousandths of an inch in an attempt to eliminate this rubbing. Further testing revealed that the difficulty probably is in the pump bearings.

[2] G. H. Jenks, H. C. Savage, *et al.*, *HRP Quar. Prog. Rep. Jan. 31, 1955*, ORNL-1853, p 86–87.

The pump will be returned to the Byron Jackson Co. for inspection and any necessary repair.

(d) In-Pile Slurry Loop. – During the past quarter, work was continued with the experimental in-pile slurry loop[3] in an attempt to develop an assembly acceptable for in-pile operation. Additional runs were attempted with slurries of several thorium oxide concentrations, and several revisions were made to the loop design in an attempt to improve loop operation.

Run HT-12 was performed with a slurry containing 250 g of thorium per kilogram of water (prepared from the D-17 oxide; see Sec. 14.4) by stirring in a small Waring Blendor for 2 hr. At the start of this run a flow-calibration measurement showed the main loop slurry flow rate to be 5.8 gpm, based on a value of 1.36 g/cc for the slurry density. Operating conditions, for this run and all subsequent runs reported below, were 250°C in the line and 255 to 265°C in the pressurizer, with oxygen overpressure. The thorium concentration of the circulating stream had decreased to approximately 70 g of thorium per kilogram of water after 264 hr of operation, as the result of an accumulation of solids behind the thermal spacer of the 5-gpm pump. A sample was taken after 90 hr of operation that indicated a satisfactory thorium concentration of 261 g of thorium per kilogram of water. Although the flow of condensed vapor from the pressurizer to the rear of the pump was not measured during this run, it was estimated to be less than 10 cc/hr. This flow rate appears to be too low to prevent an accumulation of solids in the pump rotor region.

Following run HT-12, two unsuccessful attempts were made to circulate a slurry with the thorium concentration increased to 500 g of thorium per kilogram of water (prepared from D-17 material). The first of these runs was terminated after 5 hr because of a tight plug in the $\frac{3}{8}$-in.-dia side inlet line to the pressurizer at the point where the line enters the pressurizer. At this time, a $\frac{13}{32}$-in.-dia flow restrictor was installed in the $\frac{3}{8}$-in.-dia bottom inlet line to the pressurizer, thereby causing an increased flow in the side inlet line which had plugged. The second D-17 thorium oxide run at the same concentration was terminated after 43 hr because of a plug in the same location described above. With the exception of the plugs, the slurry was easily removed from the loop, and the pump parts showed no appreciable wear following each of these unsuccessful runs. It was concluded that the 650°C calcined thorium cannot be satisfactorily pumped in the present experimental loop.

The next run, HT-13, was made with a slurry containing 500 g of thorium per kilogram of water (prepared from D-26 oxide; see Sec. 14.4) to compare its characteristics with the 650°C calcined material. As had happened in run HT-12 with a concentration of 250 g of thorium (D-17 oxide) per kilogram of water, the thorium oxide concentration of the circulating stream decreased during operation because of the accumulation of solids behind the thermal spacer in the 5-gpm pump. The initial liquid sample, taken after 50 hr of operation, contained 350 g of thorium per kilogram of water, and it is doubtful that the concentration of the circulating stream ever approached the theoretical concentration charged to the loop.

Examination of the pump at the end of the run showed that some thorium oxide solids had worked in between the front end of the Graphitar bearing insert and the journal bushing, causing severe radial wear of the Graphitar at that point. No appreciable wear could be detected on other surfaces of the bearing or journal. Measurements obtained during operation indicated that the flow rate of condensed vapors from the pressurizer to the rear of the pump was a maximum of 10 cc/hr.

At this time the 5-gpm ORNL pump was replaced with a 5-gpm canned-rotor double-bearing pump containing 17-4 PH journals and Graphitar No. 14 bearings. The 5-gpm double-bearing pump has proved to be more reliable than the single-bearing model. Also, revisions were made to the loop to increase the flow of condensed vapor from the pressurizer vapor space to the pump rotor chamber.

Following satisfactory preliminary runs with water at 250°C, a slurry of 500 g of thorium per kilogram of water was prepared from D-17 oxide which had been pumped for several hundred hours at 250°C in the 100A slurry loop CS and then dried in a furnace. Extreme difficulty was experienced in charging the loop in the usual manner through the $\frac{1}{4}$-in. sample line because of plugging, and the major portion of the charge had to be added to the loop through the top of the pressurizer. Evidence of partial plugging in both the pressurizer and the core sample holder was noted while the

[3] G. H. Jenks, H. C. Savage, *et al.*, *HRP Quar. Prog. Rep. April 30, 1955*, ORNL-1895, p 95–96 and Fig. 4.2.

loop was being heated. Once at temperature, operation with an oxygen overpressure of approximately 100 psia at room temperature resulted in gas binding the pump when an attempt was made to establish a flow of condensed vapors to the rear of the pump. Repeated efforts to degas the pump failed, and the run was discontinued. This slurry was viscous and difficult to remove from the loop.

The next run was attempted with a slurry containing 500 g of thorium per kilogram of water (prepared from D-17 oxide which had been recalcined at 800°C). An oxygen overpressure of 60 psia at room temperature was charged to the loop. With this particular slurry and overpressure it was possible to establish a maximum flow rate of 800 cc of condensed vapor per hour to the rear of the pump without gas binding. However, after 45 hr practically no solids remained in the loop circulating stream. Examination of the loop after shutdown showed the thorium oxide to be concentrated in a porous cake in the pressurizer, probably as the result of the high condensed-vapor flow rate to the pump. The rear of the pump was found to be completely free of solids.

At present, the primary problem in the development of the in-pile slurry loop is concerned with the flow of condensed vapor from the pressurizer to the rear of the pump can to prevent thorium oxide accumulation in the pump bearing region. If this condensed-vapor feed could be eliminated, loop operation would be greatly simplified. Results of preliminary work along this line have not been encouraging. If additional investigation indicates that the flow of condensed vapor to the pump is necessary for satisfactory pump and loop operation, a system which would maintain the flow within the required limits and a pressurizer capable of producing sufficient quantities of vapor for this flow without malfunction must be developed.

9.1.2 LITR Operation – In-Pile Loop Corrosion Test GG

9.1.2.1 Introduction

The third in-pile loop experiment was completed. This experiment, designed primarily for the determination of the corrosion of Zircaloy-2 under irradiation, was, in many respects, a duplicate of the previous Zircaloy-2 experiment with loop FF. Operating conditions differed from those for the previous loop in that the period of exposure to radiation and the level of radiation were both greater for GG. In addition, 320 ppm chromium as CrO_3 was added to the solution for this loop. The methods and procedures which were followed in this experiment were similar to those previously reported for the first and second experiments, and reference is made to the previous reports for details not included here.[4,5]

9.1.2.2 Construction and Preparation of Loop

Structure of the loop, specimen types, and specimen locations were identical with those for loop FF.[5] Summaries of the loop and sample specifications are presented in Tables 9.1 and 9.2.

The loop preparatory operations are summarized in Table 9.3. The results of solution analyses during these operations are presented in Table 9.4.

9.1.2.3 In-Pile Operation

(a) General Operating Conditions and Procedures. – The solution which was initially charged to the loop for in-pile operation was of the following composition:

UO_2SO_4	0.17 *m* (U^{235}/total U = 0.89)
$CuSO_4$	0.31 *m*
H_2SO_4	0.43 *m*
CrO_3	320 ppm Cr

A solution of the same composition (with the exception of chromium, which was 482 ppm) was used to replace liquid withdrawn from the loop during sampling operations. As in the last experiment, the large excess of H_2SO_4 was added to the solution in anticipation of a long exposure period.

In-pile operation of the loop with enriched solution was for a period of 987 hr. The total circulation time for this solution was 1064 hr. The energy output of the LITR during this time was 2692 Mwhr. Essentially all this energy was liberated at full reactor power. The reactor operating schedule for the exposure is shown in Fig. 9.4.

The schedule for solution sampling is also shown in Fig. 9.4. One sample of about 2 ml was

[4] G. H. Jenks, H. C. Savage, *et al.*, *HRP Quar. Prog. Rep. Jan. 31, 1955*, ORNL-1853, p 88.

[5] G. H. Jenks, H. C. Savage, *et al.*, *HRP Quar. Prog. Rep. April 31, 1955*, ORNL-1895, p 99.

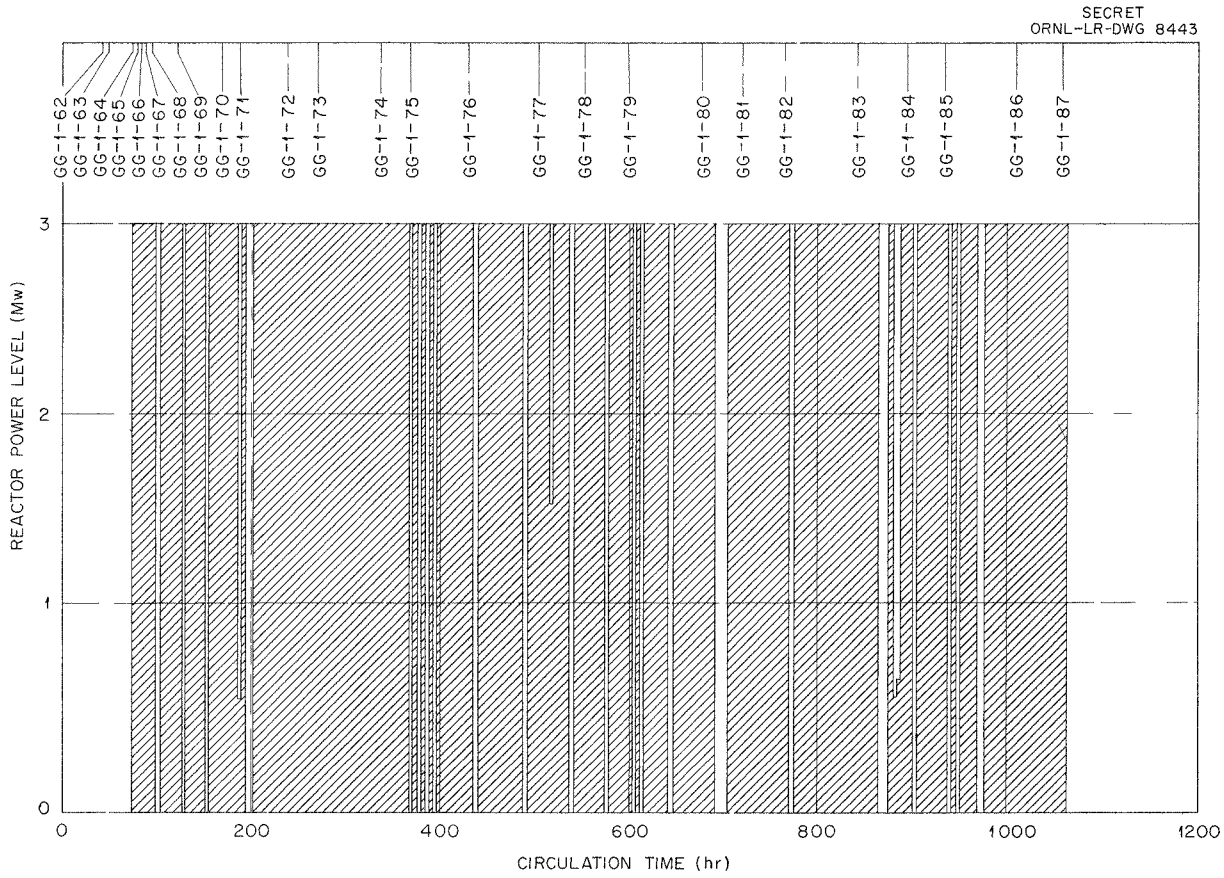

Fig. 9.4. Reactor Operating Schedule During In-Pile Operation.

taken on the occasion of each sampling. With the exception of sample GG-1-75, the samples were withdrawn while the reactor was at power. Sample GG-1-75 was withdrawn after the reactor had been at zero power for 9.3 hr.

No difficulty was encountered with the instrumentation during this experiment.

(b) Results. – In-pile loop corrosion measurements and results are given in the numbered paragraphs that follow.

(1) Solution Analyses. – The results of solution analyses for constituents other than products of irradiation are presented in Table 9.5. As observed during the previous two experiments, the reported values for the uranium content of the samples from this loop were found to be erratic, and the majority were appreciably lower than the calculated values. This discrepancy has been attributed to dilution of the sample with wash water during sampling.[4] During the latter portion of this experiment, the extent of dilution was determined quantitatively by adding a known amount of lithium sulfate to the wash water and analyzing for lithium in the samples. Lithium was found in all samples for which the tracer was employed (GG-1-79 and all subsequent samples). When the results were corrected for dilution, as indicated by the amount of lithium, the uranium concentration in each case was in fair agreement with the calculated concentration for the loop solution. The reported, corrected, and calculated values of uranium concentrations are compared graphically in Fig. 9.5.

The sample dilution factors listed in Table 9.5 are in each case, through sample GG-1-78, the ratio of the calculated uranium concentration to the reported concentration in the sample. Factors for the balance of the samples were calculated

TABLE 9.1. LOOP SPECIFICATIONS

Loop volume (including pressurizer), cc	1611
Pressurizer volume, cc	514
Flow rates	
Pressurizer, cc/sec	6.5
Core, gpm	6.4
Pump bearing material	Graphitar No. 14
Pump journal material	17-4 PH stainless steel
Pressure at which system was checked, psi	1200
Corrosion-sample units	
Specimen materials	Zircaloy-2
In-line holder	Zircaloy-2 (No. 16)
Core holder	Zircaloy-2 (No. 17)
Minimum clearance, in.	
Core holder	0.047
In-line holder	0.046
Impact-sample units	
Material	Zircaloy-2
Identification numbers	74, 76, 78, 80, 82, 84, 86, 88

TABLE 9.2. LOOP AREAS EXPOSED TO HIGH-TEMPERATURE SOLUTION

Component		Area Exposed (cm^2)
Stainless Steel		
Total main circulation lines (not including pump and core)		1553
Pressurizer		
Total		(706)
Area wetted when filled with 300 ml of solution		414
Pressurizer lines		300
Core		445
Pump		
Scroll		272
Impeller		159
	Total	3143
Zircaloy-2		
Core holder		162
In-line holder		162
Specimens		
12 core specimens		34
12 in-line specimens		34
8 impact specimens		134
	Total	526

TABLE 9.3. SUMMARY OF PREPARATORY OPERATIONS

Time (hr)	Conditions
4.5	3 wt % tribasic sodium phosphate + He, 100°C
12.0	5 wt % HNO_3 + He, 100°C
33.2	Distilled H_2O + O_2, 250°C
105.0	0.17 *m* UO_2SO_4 (normal) + 0.031 *m* $CuSO_4$ + 0.043 *m* H_2SO_4 + O_2, 250°C

TABLE 9.4 ANALYSES OF SAMPLES FROM LOOP INVENTORY DURING PREPARATORY OPERATIONS*

Solution	Total Circulation Time for Each Solution (hr)	Inventory at Time of Sampling (ml)	Uranium		Sulfate		Copper		Nickel		Iron		Chromium		Aluminum		Chlorine		Cobalt		pH
			Conc (mg/ml)	Total (g)	Conc (mg/ml)	Total (g)	Conc (μg/ml)	Total (mg)	Conc (μg/ml)	Total (mg)	Conc (μg/ml)	Total (mg)	Conc (μg/ml)	Total (mg)	Conc (μg/ml)	Total (mg)	Conc (μg/ml)	Total (mg)	Conc (μg/ml)	Total (mg)	
3% TSP, He, 100°C	4.5	1300							<1	1	3	4	<1	1							
5% HNO_3, He, 100°C	12.0	1300							17	22	65	85	7	9	9	12	<1	1	2	3	
H_2O, O_2, 250°C	33.2	1300					<1	1.3	<1	1	<1	1	2	3	<1	1	<1	1	2	3	
Natural-uranium UO_2SO_4, O_2, 250°C	41.7	1160	37.7	43.7	21.8	25.3	1980	2300	103	120	18	21	7	8	21	24	4	5	<1	1	1.3
Natural-uranium UO_2SO_4, O_2, 250°C	63.3	1160	39.0	45.2			1980	2300	53	62	6	7	24	28	23	27	4	5	9	10	1.3

*Constituent concentrations and totals shown are not cumulative but represent the quantities present for operation with each solution.

TABLE 9.5. ANALYSES OF SAMPLES FROM LOOP INVENTORY DURING ENRICHED-SOLUTION OPERATION[a]

Sample	Total Circulation Time (hr)	Accumulated LITR Energy (Mwhr)	Inventory Volume at Time of Sample, 25°C (ml)	Lithium (mg/ml)	Sample Dilution Factor[b]	Uranium		Sulfate			Copper			Chromium		Nickel		Chlorine		Iron		Zirconium		Aluminum		Manganese		pH	Specific Gravity
						Rep (mg/ml)	Calcd[c] (mg/ml)	Rep (mg/ml)	Cor[d] (mg/ml)	Calcd[e] (mg/ml)	Rep (mg/ml)	Cor[d] (mg/ml)	Calcd[e] (mg/ml)	Rep (mg/ml)	Calcd Total[f] (g)	Rep (mg/ml)	Calcd Total[g] (g)	Rep (mg/ml)	Calcd Total[g] (g)	Rep (mg/ml)	Calcd Total[f] (g)	Rep (mg/ml)	Calcd Total[f] (g)	Rep (mg/ml)	Calcd Total[g] (g)	Rep (mg/ml)	Calcd Total[g] (g)		
Original solution GG-1-60	0	0	1039			39.79	39.79	23.54	23.54	23.54	1.745	1.745	1.745	0.320	0.333	(ND)	(ND)	(ND)	(ND)	(ND)	(ND)	(ND)	(ND)	(ND)	(ND)			1.25	1.055
Make-up solution GG-1-61	0	0				39.43	39.43	23.54	23.54	23.54	1.806	1.806	1.806	0.482		(ND)	(ND)	(ND)	(ND)	(ND)	(ND)	(ND)	(ND)	(ND)	(ND)			1.25	1.055
GG-1-62	45.2	0	1039		1.14	34.9	39.8	22.7	25.8	23.5	1.74	1.99	1.75	0.182	0.216	(ND)	(ND)	(ND)	(ND)	(ND)	(ND)	(ND)	(ND)	(ND)	(ND)			1.3	
GG-1-63	47.2	0	1015		1.10	36.1	39.8	22.0	24.2	23.5	1.63	1.79	1.75	0.133	0.149	(ND)	(ND)	(ND)	(ND)	(ND)	(ND)	(ND)	(ND)	(ND)	(ND)			1.3	
GG-1-64	77.8	5.2	1035		0.98	40.8	39.8	23.4	22.9	23.5	1.94	1.90	1.75	0.089	0.090	0.058	0.059	0.001	0.001	0.024	0.024	0.039	0.040					1.3	
GG-1-65	80.1	12.2	1016		0.97	40.9	39.8	23.2	22.5	23.5	1.78	1.72	1.75	0.053	0.052	0.103	0.102	0.001	0.001	0.032	0.032	0.037	0.037					1.3	
GG-1-66	83.1	21.4	1001		1.10	36.3	39.8	21.4	23.6	23.5	1.68	1.85	1.75	0.035	0.039	0.082	0.092	0.001	0.001	0.018	0.020	0.042	0.046					1.45	
GG-1-67	85.3	27.9	986		1.11	35.7	39.8	21.4	23.7	23.5	1.57	1.75	1.75	0.038	0.042	0.091	0.103	0.001	0.001	0.023	0.025	0.037	0.041					1.50	
GG-1-68	98.6	67.6	1033		1.22	32.7	39.8	20.9	25.5	23.5	1.72	2.10	1.75	0.032	0.040	0.188	0.241	0.001	0.001	0.012	0.015	0.029	0.037	0.001	0.001			1.50	
GG-1-69	120.6	120.6	1032		1.19	33.3	39.8	22.9	27.2	23.5	1.55	1.84	1.74	0.028	0.034	0.263	0.332	0.001	0.001	0.014	0.017	0.027	0.033					1.50	
GG-1-70	169.2	253.6	1034		1.14	34.9	39.7	21.8	24.8	23.5	1.62	1.85	1.74	0.012	0.014	0.470	0.569	0.001	0.001	0.029	0.034	0.073	0.086					1.60	
GG-1-71	190.8	309.2	1036		1.17	34.2	39.7	20.0	23.4	23.5	1.79	2.09	1.74	0.011	0.013	0.440	0.559	0.001	0.001	0.025	0.030	0.057	0.069					1.60	
GG-1-72	239.5	427.5	1032		1.27	31.1	39.7	20.6	26.1	23.5	1.46	1.86	1.74	0.001	0.001	0.746	1.013	0.001	0.001	0.014	0.018	0.043	0.056					1.60	
GG-1-73	269.7	518.1	1032		1.12	35.5	39.7	21.6	24.2	23.5	1.41	1.58	1.74	0.001	0.001	0.520	0.655	0.001	0.001	0.027	0.031	0.037	0.043	0.001	0.001			1.65	
GG-1-74	337.3	719.8	1032		1.16	34.1	39.7	22.0	25.5	23.5	1.51	1.75	1.74	0.026	0.031	0.854	1.088	0.001	0.001	0.005	0.006	0.033	0.040	0.001	0.001			1.70	
GG-1-75[h]	365.3	774.7	1034		1.20	33.1	39.6	22.9	27.5	23.4	1.79	2.15	1.74	0.025	0.031	0.684	0.934	0.001	0.001	0.005	0.006	0.032	0.040	0.001	0.001			1.70	
GG-1-76	433.1	949.6	1037		1.24	31.9	39.6	20.9	25.9	23.4	1.39	1.72	1.73	0.005	0.006	0.698	0.999	0.001	0.001	0.007	0.009	0.017	0.022	0.001	0.001			1.70	
GG-1-77	504.9	1156.6	1038		1.19	33.4	39.5	21.8	25.9	23.4	1.35	1.60	1.73	0.006	0.007	0.791	1.095	0.001	0.001	0.017	0.021	0.031	0.038	0.001	0.001			1.70	
GG-1-78	553.0	1289.3	1040		1.28	30.8	39.5	20.4	26.1	23.4	1.52	1.94	1.73	0.001	0.001	0.984	1.446	0.001	0.001	0.015	0.020	0.040	0.053	0.001	0.001			1.70	
GG-1-79[i]	603.5	1567.8	1037	0.79	1.09	34.9	39.5	28.6	25.2	23.4	1.44	1.57	1.73	0.010	0.011	0.905	1.184	0.001	0.001	0.020	0.023	0.028	0.032	0.001	0.001			1.70	
GG-1-80[i]	678.4	1638.0	1034	1.24	1.15	33.6	39.5	30.9	25.7	23.4	1.41	1.62	1.73	0.005	0.006	0.833	1.171	0.001	0.001	0.017	0.020	0.020	0.024	0.001	0.001			1.75	
GG-1-81[i]	721.0	1802.2	1034	1.84	1.24	30.6	39.5	35.0	27.6	23.4	1.34	1.66	1.73	0.001	0.001	0.939	1.403	0.001	0.001	0.021	0.027	0.050	0.064	0.001	0.001			1.85	
GG-1-82[i]	769.0	1949.2	1033	1.78	1.23	33.8	39.5	33.4	25.9	23.4	1.32	1.62	1.73	0.001	0.001	1.046	1.551	0.001	0.001	0.021	0.027	0.030	0.038	0.001	0.001			1.88	
GG-1-83[i]	842.5	2155.9	1034	1.36	1.17	33.3	39.5	30.2	24.3	23.4	1.39	1.62	1.73	0.005	0.001	0.749	1.153	0.001	0.001	0.021	0.025	0.034	0.041	0.001	0.001	0.151	0.183	2.15	
GG-1-84[i]	894.2	2268.0	1035	1.86	1.24	30.4	39.5	34.5	26.7	23.4	1.34	1.66	1.73	0.001	0.001	0.923	1.450	0.001	0.001	0.018	0.023	0.033	0.042	0.001	0.001	0.182	0.237	1.95	
GG-1-85[j]	936.6	2394.1	1034	0.28	1.42	29.6	39.5	23.8	31.1	23.4	1.35	1.91	1.73	0.001	0.001	0.929	1.650	0.001	0.001	0.049	0.072	0.032	0.047	0.001	0.001	0.140	0.213	2.0	
GG-1-86[j]	1009.5	2579.6	1036	0.15	1.19	38.9	39.5	22.9	26.0	23.4	1.41	1.68	1.73	0.001	0.001	0.954	1.488	0.001	0.001	0.014	0.017	0.020	0.025	0.001	0.001	0.133	0.176	1.9	
GG-1-87[j]	1057.8	2676.4	1035	0.13	1.16	34.4	39.5	22.7	25.3	23.4	1.51	1.76	1.73	0.001	0.001	1.572	1.637	0.001	0.001	0.015	0.018	0.031	0.037	0.001	0.001	0.168	0.217	1.7	
	1063.0	2692.3	1035																										
	1063.7	2692.3	1035																										

[a] Where no values are given, either an analysis was not requested or the analytical results were not reliable. ND, not detected.

[b] Dilution factors calculated through sample GG-1-78 on uranium basis; balance calculated on lithium concentration found in sample.

[c] Determined from calculated uranium and inventory balance.

[d] (Reported concentration) × (dilution factor); samples GG-1-79 to GG-1-87 corrected for SO_4 from Li_2SO_4.

[e] Original concentration × calculated uranium concentration/original uranium concentration.

[f] (Reported concentration) × (dilution factor) × (inventory volume).

[g] (Reported concentration corrected for sample dilution and amounts withdrawn in previous samples) × (inventory volume).

[h] Sample taken with reactor down.

[i] Wash water contained Li_2SO_4 at 0.688 *M*.

[j] Wash water contained Li_2SO_4 at 0.684 *M*.

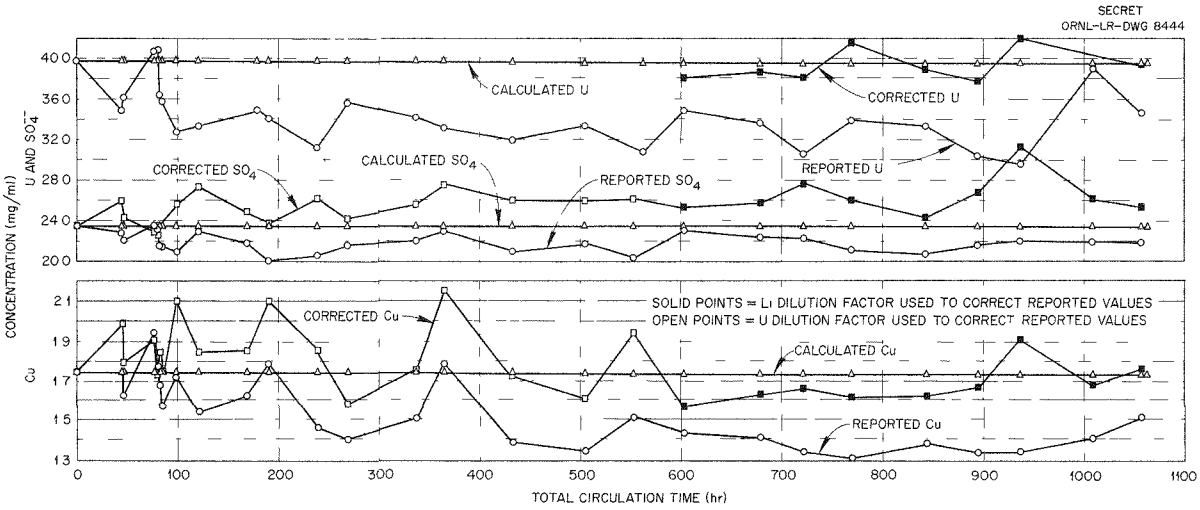

Fig. 9.5. Concentration of U, SO_4^{--}, and Cu in Solution Samples.

from the amount of lithium found in each sample. These factors were used to obtain the "corrected concentrations" for sulfate and copper which are listed. Reported, corrected, and calculated concentrations of these two solution constituents are also presented in Fig. 9.5. The copper values corrected on the basis of the lithium dilution factors are in good agreement with the calculated concentrations, lending support to the accuracy of the dilution factor. The reported and corrected values for sulfate are about in equal agreement with the calculated values. The calculated values for the other elements listed in the table were obtained through use of the listed dilutions. The values for nickel, chlorine, aluminum, and manganese were also corrected for the amount of material withdrawn in sampling. No correction was applied to pH measurements.

(2) Oxygen Consumption. – The results of oxygen depletion measurements are shown in Table 9.6. For conversion from gas volumes to pressures in the loop at operating temperature, the factor 100 psi = 1475 cc at STP is applicable.

(3) Fission Power in Loop. – Values for fission power generated in the loop, calculated from total fissions observed in the loop solution samples, are presented in Table 9.7. A sample cooling period of three months preceded these analyses, so that only about 1 to 2% of the observed cesium can be attributed to 15-day Cs^{136}. Each reported value was corrected by the appropriate sample dilution factor and was also corrected for the amount of Cs^{137} withdrawn from the loop in sampling. The values for fission power were calculated from the corrected cesium analytical results. Thus the values represent the average power from the start of irradiation to the time of sampling.

The difference between the electrical power required to maintain loop temperature with and without the reactor at power averaged 1080 w. No significant change in the power was observed throughout the operation. The maximum deviation from the average was about 3.7%.

The neutron flux at a given specimen position in the core was determined, as before, from comparison between the induced Zr^{95}-Nb^{95} activity in the specimen and that in a control specimen which was irradiated for a known nvt in the ORNL Graphite Reactor.[5] The solution used for surface decontamination of the specimens prior to counting was a mixture of 50% HF, 70% HNO_3, and H_2O in the volume ratio 8:46:46. Five washings were given each specimen, and fresh solution was used for each wash.

The results of the analyses for induced activity are shown in Table 9.8. The control specimen was irradiated for 315 hr in an average flux of 6.15×10^{11} neutrons/cm^2/sec. The elapsed time between termination of exposure and counting was 2064 hr. For the loop specimen, 1680 hr elapsed between termination of exposure and counting.

TABLE 9.6. OXYGEN CONSUMPTION IN LOOP GG

Remarks	Sample No.	LITR Energy (Mwhr)	Total Solution Circulation Time (hr)	O_2 Additions to Loop (cc at STP)	O_2 Withdrawn from Loop* (cc at STP)	Total O_2 Charged to Loop Less O_2 Withdrawn in Sampling (cc at STP)	O_2 Volume at Time of Sample (cc at STP)	O_2 Consumed Since Last Sample (cc at STP)	Total O_2 Consumed (cc at STP)	Calculated Corrosion Penetration of Type 347 Stainless Steel (mils)
Original O_2 fill GG-1 started circulation		0	0	1165		1165		0	0	0
		0	0	0		1165		0	0	0
	GG-1-62	0	45.2	0	5	1160		0	0	0
	GG-1-63	0	47.2	0	5	1155		0	0	0
Reactor on		0	76.1	0		1155		0	0	0
	GG-1-64	5.2	77.8	0	6	1149		49	48	0.003
	GG-1-65	12.2	80.1	0	4	1145		62	111	0.006
	GG-1-66	21.4	83.1	0	4	1141		81	192	0.01
	GG-1-67	27.9	85.3	0	4	1138		59	251	0.01
	GG-1-68	67.6	98.6	0	3	1135		358	609	0.03
		68.7	100.6	0		1135	471		663	
O_2 addition GG-2		68.7	100.6	1521		2656	1993		663	
	GG-1-69	120.6	120.6	0	8	2648		576	1185	0.06
			151.7	0		2648	647		2000	
O_2 addition GG-3			151.7	985		3633	1632		2000	
	GG-1-70	253.6	169.2	0	5	3628		1089	2274	0.12
	GG-1-71	309.2	190.8	0	3	3625		352	2626	0.14
			193.3	0		3625	949		2675	
O_2 addition GG-4			193.3	740		4365	1689		2675	
	GG-1-72	427.5	239.5	0	3	4365	1400	338	2964	0.16

TABLE 9.6 (continued)

Remarks	Sample No.	LITR Energy (Mwhr)	Total Solution Circulation Time (hr)	O_2 Additions to Loop (cc at STP)	O_2 Withdrawn from Loop* (cc at STP)	Total O_2 Charged to Loop Less O_2 Withdrawn in Sampling (cc at STP)	O_2 Volume at Time of Sample (cc at STP)	O_2 Consumed Since Last Sample (cc at STP)	Total O_2 Consumed (cc at STP)	Calculated Corrosion Penetration of Type 347 Stainless Steel (mils)
O_2 addition GG-4	GG-1-73	518.1	269.7	0	3	4362	1269	128	3092	0.17
			310.0	0		4359	1091		3268	
	GG-1-74	719.8	337.3	0	3	4359	1039	228	3320	0.18
			360.8	0		4356	991		3364	
O_2 addition GG-5			360.8	707		5064	1699		3364	
	GG-1-75	774.7	365.3	0	4	5064	1680	63	3383	0.18
	GG-1-76	949.6	433.1	0	4	5060	1456	220	3603	0.19
	GG-1-77	1156.6	504.9	0	4	5056	1263	189	3792	0.20
	GG-1-78	1289.3	553.0	0	4	5051	1158	201	3893	0.21
	GG-1-79	1567.8	603.5	0	4	5048	1055	99	3992	0.21
	GG-1-80	1638.0	678.4	0	3	5045	906	146	4138	0.22
	GG-1-81	1802.2	721.0	0	2	5042	844	59	4197	0.22
	GG-1-82	1949.2	769.0	0	2	5040	777	165	4262	0.23
	GG-1-83	2155.9	842.5	0	1	5039	711	65	4327	0.23
	GG-1-84	2268.0	894.2	0	1	5038	661	49	4376	0.23
	GG-1-85	2394.1	936.6	0	1	5037	623	38	4414	0.24
O_2 addition GG-6			942.2	915	0	5951	1533		4417	
	GG-1-86	2579.6	1009.5	0	–3	5948	1218	315	4729	0.25
Shut down reactor	GG-1-87	2676.4	1057.8	0	0	5948	1088	130	4859	0.26
Shut down pump	End of run	2676.4	1063.7	0	0	5948	1072	16	4875	0.26

*Calculated amount removed as O_2 dissolved in sample.

TABLE 9.7. FISSIONS IN LOOP SOLUTION

Sample No.	Accumulated LITR Energy (Mwhr)	Inventory Volume at Time of Sample (ml at 25°C)	Calculated Uranium Concentration (mg/ml)	Total Fissions per ml × 10^{-15}		Total Fission Power in Loop Solution at 3 Mw (w)
				Analysis	Corrected*	
GG-1-64	5.2	1035	39.8	0.150	0.147	775
65	12.2	1016	39.8	0.316	0.310	688
66	21.4	1001	39.8	0.544	0.605	754
67	28.0	986	39.8	0.708	0.802	755
68	67.6	1033	39.8	1.65	2.04	830
69	120.6	1032	39.8	2.85	3.46	788
70	253.6	1034	39.7	5.60	6.51	706
71	309.2	1036	39.7	7.18	8.65	771
72	427.5	1032	39.7	8.94	11.8	759
73	518.1	1032	39.7	12.1	14.2	753
74	719.8	1032	39.7	17.1	20.6	786
75	774.7	1034	39.6	17.2	21.9	778
76	949.6	1037	39.6	22.8	29.9	869
77	1156.6	1038	39.5	26.8	34.1	815
78	1289.3	1040	39.5	30.4	41.7	895
79	1567.8	1037	39.5	36.1	42.8	754
80	1638.0	1034	39.5	37.5	47.3	795
81	1802.2	1034	39.5	36.7	50.7	775
82	1949.2	1033	39.5	37.3	51.9	732
83	2155.9	1034	39.5	48.7	63.8	815
84	2268.0	1035	39.5	44.6	63.2	768
85	2394.1	1034	39.5	50.4	80.6	926
86	2579.6	1036	39.5	54.9	75.7	809
87	2676.4	1035	39.5	59.5	80.5	829

*Corrected to include amounts withdrawn in previous samples and for sample dilution.

Values for the power density were calculated from the determined values for neutron flux. A uranium concentration of 39.6 mg/ml, 88.8% enriched, was the basis for the calculation.

The intensities of reactor radiation for this experiment were appreciably higher than those for the preceding experiment, FF.[5] This increase is ascribed to a rearrangement of the fuel elements in the LITR between experiments. In this rearrangement, a fuel element was placed directly in front of the loop experimental hole, HB-4. The additional fuel elements in front of the adjacent hole, HB-5, which were mentioned previously,[5] were undisturbed.

(4) Uranium Balance. — Amounts of uranium charged to, and removed from, the loop are shown in Table 9.9. As with the preceding loops, the resulting value for the total weight of uranium

TABLE 9.8. INDUCED Zr-Nb ACTIVITY IN CORE SPECIMENS

Coupon Position	Cleaned Weight When Counted (g)	Zr-Nb Activity (0.76-Mev gamma)		Neutron Flux at 3 Mw (neutrons/cm^2/sec $\times 10^{-12}$)	Power Density at 3 Mw (w/ml)
		Counts/min/coupon $\times 10^{-6}$	Counts/min/g $\times 10^{-6}$		
		Core Specimens			
A	1.56	2.08	1.34	3.62	4.83
C	1.56	1.76	1.13	3.05	4.07
D	1.56	1.47	0.943	2.55	3.40
E	1.56	1.32	0.846	2.29	3.05
F	1.56	1.25	0.802	2.17	2.89
H	1.57	0.927	0.591	1.60	2.13
I	1.55	0.800	0.517	1.40	1.87
J	1.57	0.725	0.461	1.25	1.67
L	1.56	0.578	0.369	1.00	1.33
		Control Specimen			
	1.60	0.128	0.0798		

removed is greater than the value for the charged weight.[4,5] The material balance for the loop was 4% high.

(5) Radiolytic-Gas Pressures. – The steady-state pressures of radiolytic gas which were observed during the initial portion of the irradiation were in the range 12 to 15 psi and were in line with the pressures observed in previous tests. However, a gradual decrease in this pressure commenced shortly after the start of this run and continued for about 300 hr of operation. At the end of this period the pressure leveled off at about 5 psi and remained fairly constant at this pressure for the rest of the run.

A decrease in the rate of flow of the solution through the pressurizer was also noted during the experiment. The amount by which the flow decreased was roughly a factor of 2, and the period in which the change occurred was roughly the same as that in which the gas pressure changed. It is believed that the observed drop in pressure was, to a large extent, a result of the drop in flow.

(c) Corrosion Indicated by Nickel, Oxygen, and Manganese Data. – Values for corrosive penetration of type 347 stainless steel were calculated which correspond to the amount of nickel and manganese found in the loop solution samples, Table 9.5, and to the oxygen depletion data, Table 9.6. All three methods of calculation were based on the assumption that all steel surfaces in contact with high-temperature solution corroded uniformly and that steel surfaces in the cool rotor region of the pump did not corrode. It was also assumed that oxygen was consumed only in the oxidation of steel. Calculated values are plotted against circulation time in Fig. 9.6. Other quantities of interest are shown on additional scales. The curves are of the same general type as those obtained for the two previous experiments, showing a high initial corrosion rate which leveled off to a much lower and fairly constant rate after the first 200 hr of exposure in the reactor.[4,5] As calculated from the oxygen data, the corrosion rate during the first 200 hr after reactor startup was 7.3 mpy. During the following 500 hr, the average rate was 1.5 mpy. The rates which were observed in the previous experiment were 6.5 mpy and 2.2 mpy for like periods. The average rate for the present loop from 700 to 940 hr was 0.5 mpy. No like period exists for the preceding loop experiment, since it was terminated after 700 hr of operation.

About 115 hr before the termination of this experiment, excessive pump wear was indicated by

TABLE 9.9. URANIUM BALANCE

Source	Solution Weight (g)	Specific Gravity	Solution Volume (ml)	Uranium Concentration by Analysis (mg/ml)	Weight of Uranium (g)
Charged to Loop					
Original solution charged to system	1102.3	1.055	1044.9	39.79	41.58
Solution additions during operation			510.0	39.43	20.11
Total					61.69
Recovered from Loop					
Loop-inventory samples sent to laboratory			52.7	29.6 to 39.8	1.78
Weigh tank emptied to hot drain after sample GG-1-63			30.5 cc	39.8 (calcd)	1.21
From weigh tank after sampling contents (sample purges and flushes through sample GG-1-86)	7650[a]	1.0[b]	7650	2.0	15.30
From weigh tank after sampling contents (purges from sample GG-1-87 plus loop contents and rinse)	7300[a]	1.0[b]	7300	6.27	45.77
Weigh-tank samples sent to laboratory[c] Sample GG-1-1 and GG-1-2 (sample purges and rinses through sample GG-1-86)			4.2	2.0	0.01
Samples GG-1-3, GG-1-4, GG-1-5, and GG-1-6 (purge from GG-1-87, loop inventory, purges, etc.)			4.8	5.64 to 6.67	0.03
Total					64.11

[a]From weigh-tank reading.

[b]Assumed.

[c]Weigh tank was drained of sample purges and flushes after sample GG-1-86. Therefore the second weight inventory (before sampling) includes sample purges and flushes for sample GG-1-87 plus loop inventory and loop rinses.

an increase in the power drawn by the pump. The power demand of the pump continued to increase until the termination of the experiment. Following the reactor shutdown and after the UO_2SO_4 solution had been drained from the loop, the pump failed by stalling while wash water was being circulated through the loop. The corrosion rate, based on oxygen consumption shown in Fig. 9.6, increased markedly during the period in which the pump power was increasing.

(d) Performance of Equipment. – With the exception of the pump noted previously, the performance of the equipment was satisfactory.

[6]G. H. Jenks, H. C. Savage, *et al.*, *HRP Quar. Prog. Rep. April 30, 1955*, ORNL-1895, p 109.

9.1.3 Remote Dismantling and Inspection

(a) Dismantling, Loop GG. – Operations in the dismantling cell were very satisfactory. The new handling clamp[6] for lowering the loop into the dismantling cell proved to be successful in aligning the loop package properly in the decanning chuck and in permitting easier withdrawal of the can end after cutting. Attachment of the clamp involved essentially no radiation exposure to operating personnel despite the 4 r/hr beam through the open end of the carrier. The major source of this activity was undoubtedly the fission products which could not be completely washed out of the stalled pump at the LITR.

As with previous loops, various portions were

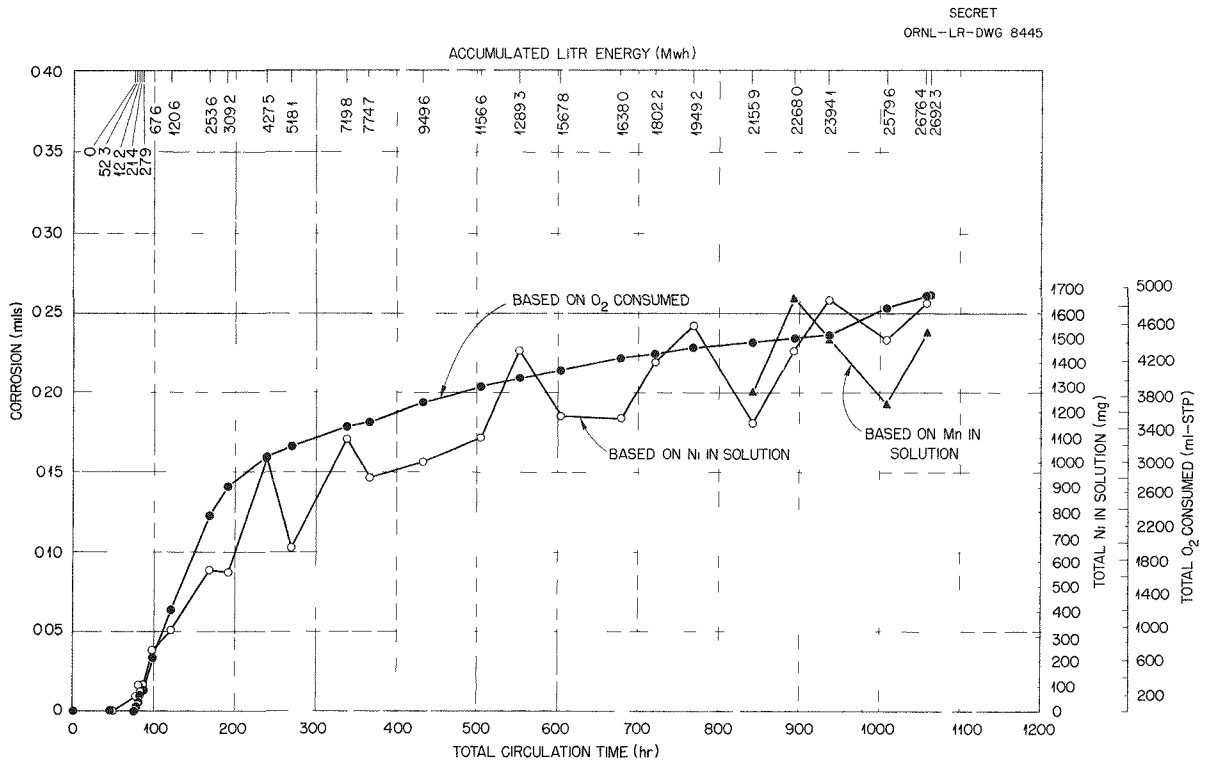

Fig. 9.6. Over-all Type 347 Stainless Steel Corrosion Penetration During Enriched-Solution Operation.

removed in the dismantling facility and transferred to the Solid State Division hot cells for further disassembly and inspection. The sections removed were the core, in-line sample holder, pressurizer, pressurizer heater, a sample of the piping including the sample line filter, and the pump. The remainder of the loop was transferred to the burial ground. An effort was made in the dismantling cell to extract the pump rotor from the stator. It was hoped that some indication of the cause of the pump failure might be found. Unfortunately, the force which could be applied with the equipment in the dismantling cell was not sufficient to overcome the frictional forces holding the thermal spacer. A further attempt at disassembly of the pump will be made when the corrosion-examination facility is available.

Disassembly, sectioning, and examination of the various components in the Solid State facilities were somewhat delayed because of other work in progress. However, the actual operations have become less time-consuming with each loop handled to date.

(b) Results of Inspection and Evaluation. – *(1) Qualitative.* – As with the previous loops,[6,7] all surfaces outside the core area were covered with a heavy rustlike scale. There was no apparent localized attack on any components inspected. Figure 9.7 is a view of coupons and interior tapered surface of the in-line coupon holder in the as-removed state. The loose, flaky nature of the bulk scale on the Zircaloy-2 coupons and holder is quite evident in this photograph. In the core region, all stainless steel surfaces appeared to be covered with a similar, but somewhat less bulky, rustlike scale. Figure 9.8 is a photograph of the core assembly in the as-removed condition. The stainless steel clamping bands on each end and the stainless steel "spiders" which held the impact samples were covered with a rustlike scale. As with loops DD and FF, the Zircaloy-2 impact specimens and holder surfaces appeared to be free from bulk-scale deposits in the higher flux region. Only on the extreme

[7] G. H. Jenks, H. C. Savage, *et al.*, *HRP Quar. Prog. Rep. Jan. 31, 1955*, ORNL-1853, p 99–106.

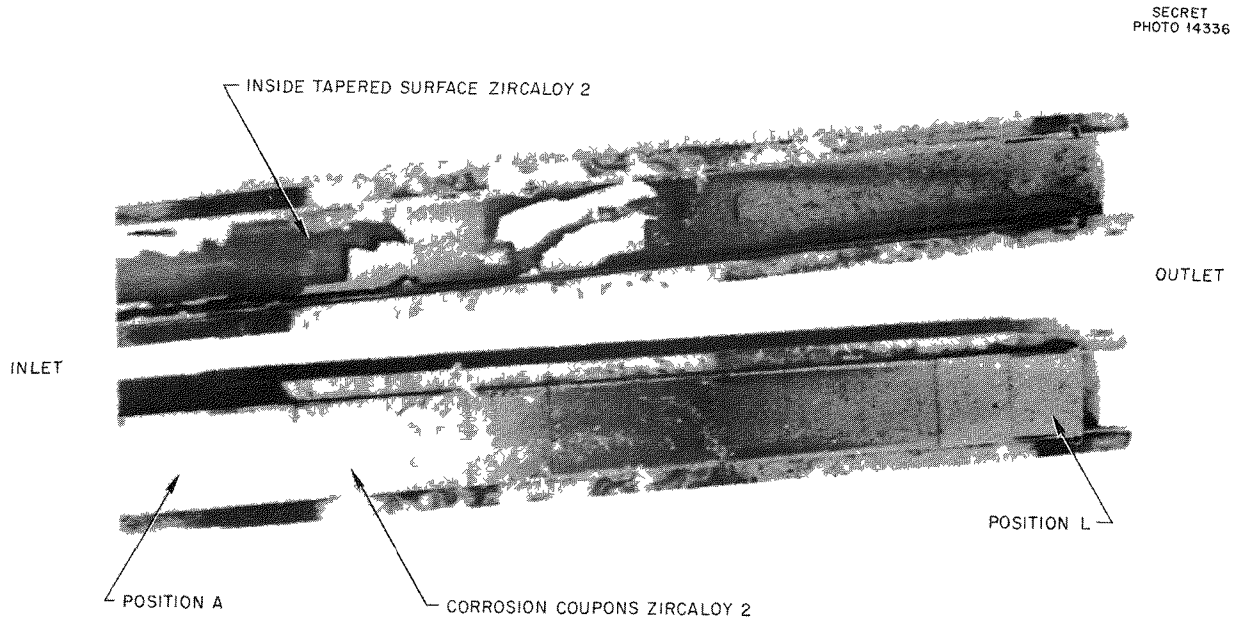

Fig. 9.7. In-Pile Loop GG In-Line Coupon Assembly.

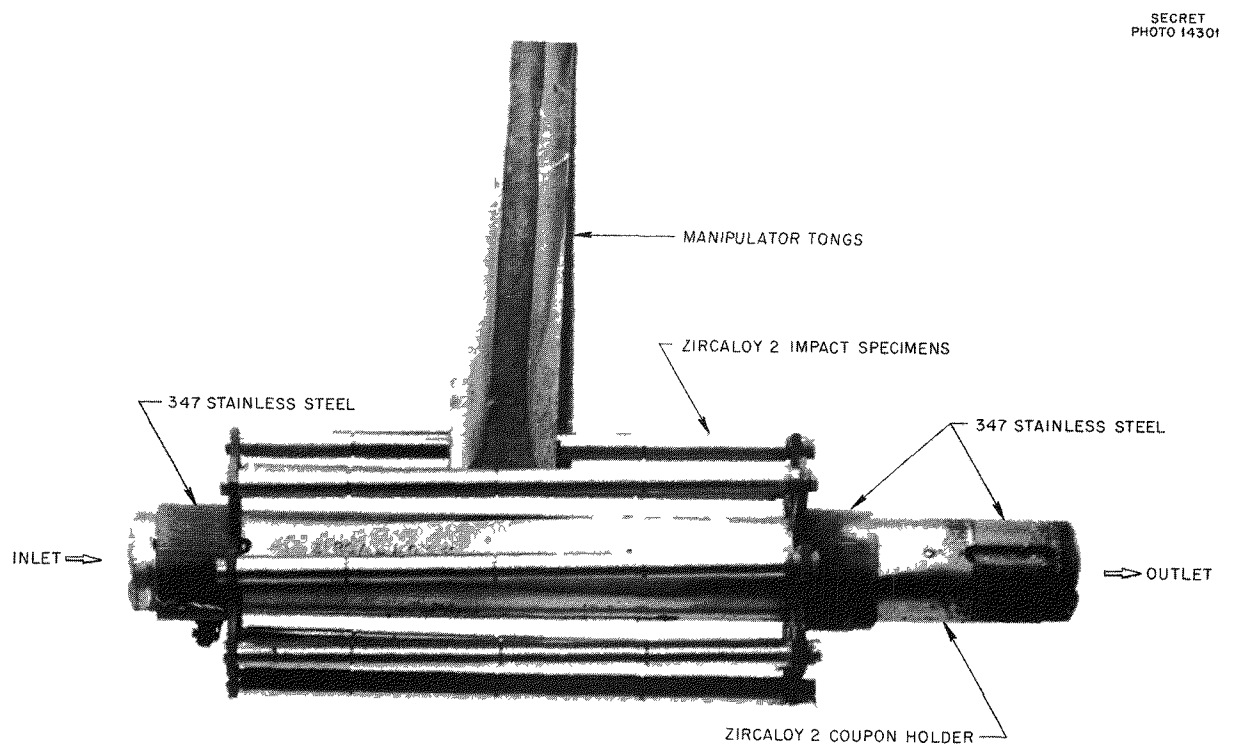

Fig. 9.8. In-Pile Loop GG Core Specimen Assembly.

outlet, or low-flux, end of the core coupon holder was there any apparent buildup of scale. Closer examination under the remote microscope revealed that there was some film on all Zircaloy-2 surfaces. The thickness of the film was apparently inversely proportional to the flux at which the surface was exposed. A detailed description of the surface appearance of the coupons is included in Table 9.10.

The core specimens were defilmed completely by cathodic treatment in 5% H_2SO_4. However, the in-line specimens, as before, could not be defilmed completely. Some of the scale was again removed by pulling it from the surface with Scotch tape, but this was only partially effective and did not remove any of the underlying film. Very extensive defilming of one in-line coupon, 939A, was attempted. Even after many repetitions of the treatment with Scotch tape and of cathodic cleaning at current densities higher than usual, the coupon still showed a 0.1-mg weight gain. Flakes of scale and a uniform coating of dark-gray film were still visible under the microscope.

Coupons from positions A, G, and K of the core array, together with coupons from positions G and K of the in-line array, were retained for x-ray analysis and metallographic examination. The remainder of the core coupons, together with coupons 935A and 942A from the in-line group, were decontaminated as described previously and transferred to the Analytical Chemistry Division for activation analyses.

A sample of the rustlike bulk scale from the in-line Zircaloy-2 holder was submitted for chemical analysis. The following composition by weight was reported: iron, 32%; uranium, 32%; zirconium, 7%; sulfate, 11%; copper, 1%; nickel, 2%; and chromium, 0.1%. Additional portions of this bulk scale were transferred to the Solid State Division for x-ray analysis and to the Analytical Chemistry Division for electron-diffraction examination. To date, it has not been possible to identify the patterns obtained.

In addition to the Zircaloy-2 coupons previously mentioned, additional metallographic samples were obtained from various stainless steel components. The metallography will be done by the Remote Metallography Group of the Solid State Division as soon as their installation is in operation.

(2) Quantitative. — Sample-weight data for in-line and core specimens, with calculated values for rate of corrosion, are presented in Table 9.10.

The values for corrosion rate of the core specimens are shown in Fig. 9.9 plotted vs the power density to which the specimen was exposed when the reactor was operating at 3 Mw. The rate values plotted are those calculated with radiation time as a basis. Comparable rate data from the previous experiment, FF, are included for comparison. The line is the estimated best line through the GG points only. The rate values which were calculated with total circulation time as a basis are plotted in Fig. 9.10 in the same fashion. The line in this case is the estimated best line for all the data. In general, the results of the two experiments are in fair agreement.

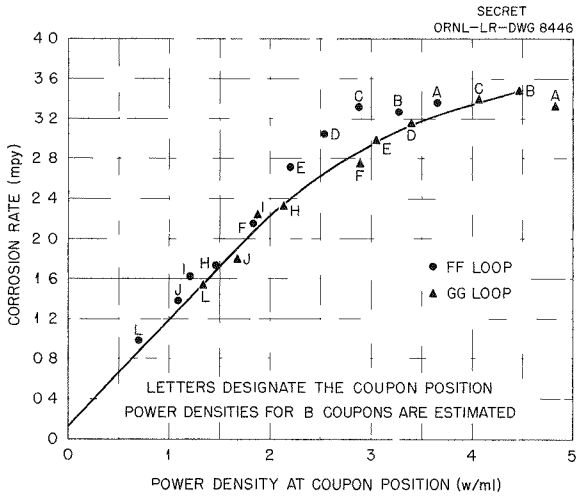

Fig. 9.9. Zircaloy-2 Core Coupon Corrosion Rates Based on Radiation Time vs Power Density at Coupon Position.

Specimens in position A apparently are protected by some unknown means, to some extent, from the irradiation effect. The same probably is true for specimens in position B. However, in addition to this effect for specimens in the highest flux, the results of loop GG indicate a leveling-off of the irradiation effect at the higher power densities.

Attention is directed to the weight losses recorded for two of the in-line specimens. The corrosion rates which are calculated from these

TABLE 9.10. CORROSION DATA FOR ZIRCALOY-2 CORROSION SPECIMENS

Sample No.	Position	Exposed Coupon Area (cm^2)	Flow Velocity at Leading Edge (fps)	Initial Weight (g)	As-Removed Weight (g)	Defilmed Weight (g)	Weight Change (mg)	Corrosion Penetration (mil)	Corrosion Rate* (mpy)		Surface Appearance, As-Removed	Surface Appearance, After Defilming
									1064 hr	897 hr		
Core Coupons												
947A	A	3.00	10.7	1.5730	1.5564	1.5561	−16.9	0.341	2.80	3.32	Etched surface covered with thin flaky scale	Dull etched appearance
948A	B	2.80	12.5	1.5691	1.5532	1.5526	−16.5	0.357	2.93	3.48	Etched surface covered with thin flaky scale	Dull etched appearance
949A	C	2.80	15.1	1.5723	1.5570	1.5562	−16.1	0.348	2.86	3.39	Etched surface covered with thin flaky scale	Dull etched appearance
950A	D	2.80	18.9	1.5750	1.5609	1.5600	−15.0	0.324	2.66	3.15	Etched surface covered with thin flaky scale	Dull etched appearance
951A	E	2.80	25.3	1.5735	1.5604	1.5594	−14.1	0.305	2.50	2.97	Lightly etched surface covered with thin flaky scale	Dull lightly etched appearance
952A	F	2.80	39.5	1.5724	1.5601	1.5594	−13.0	0.281	2.31	2.74	Lightly etched surface covered with thin flaky scale	Dull lightly etched appearance
953A	G	2.80	45.8	1.5576	1.5472	1.5458	−11.8	0.255	2.09	2.48	Faint machine marks in areas where scale has not been retained	Faint machine marks; lightly etched appearance; some very thin film visible
954A	H	2.80	55.7	1.5778	1.5694	1.5668	−11.0	0.238	1.95	2.32	Heavy flaky scale; machine marks visible	Faint machine marks; lightly etched appearance; some very thin film visible
955A	I	2.80	31.1	1.5582	1.5492	1.5476	−10.6	0.229	1.88	2.23	Some scale along clamping edges; machine marks visible	Faint machine marks; very lightly etched appearance
956A	J	2.80	22.0	1.5804	1.5720	1.5719	−8.5	0.184	1.51	1.79	Thin scale on all surfaces	Machine marks visible
957A	K	2.80	16.8	1.5810	1.5735	1.5717	−9.3	0.201	1.65	1.96	Scale on all surfaces	Machine marks visible
958A	L	3.00	13.4	1.5726	1.5658	1.5648	−7.8	0.157	1.29	1.53	Thin scale on all surfaces	Machine marks visible
In-Line Coupons												
935A	A	3.00	10.7	1.5733	1.6035	1.5744	+1.1				All surfaces covered with a heavy brown rustlike scale	Film on all surfaces; some scale retained particularly along edges
936A	B	2.80	12.5	1.5820	1.6080	1.5837	+1.7				All surfaces covered with a heavy brown rustlike scale	Film on all surfaces; some scale retained particularly along edges
937A	C	2.80	15.1	1.5800	1.6034	1.5814	+1.4				All surfaces covered with a heavy brown rustlike scale	Film on all surfaces; some scale retained particularly along edges
938A	D	2.80	18.9	1.5760	1.5982	1.5780	+2.0				All surfaces covered with a heavy brown rustlike scale	Film on all surfaces; some scale retained particularly along edges
939A	E	2.80	25.3	1.5817	1.6013	1.5840	+2.3				All surfaces covered with a heavy brown rustlike scale	Film on all surfaces; some scale retained particularly along edges
940A	F	2.80	39.5	1.5800	1.5996	1.5818	+1.8				All surfaces covered with a heavy brown rustlike scale	Film on all surfaces; some scale retained particularly along edges
941A	G	2.80	45.8	1.5842	1.6010	1.5858	+1.6				All surfaces covered with a heavy brown rustlike scale	Film on all surfaces; some scale retained particularly along edges
942A	H	2.80	55.7	1.5735	1.5928	1.5755	+2.0				All surfaces covered with a heavy brown rustlike scale	Film on all surfaces; some scale retained particularly along edges
943A	I	2.80	31.1	1.5737	1.5923	1.5756	+1.9				All surfaces covered with a heavy brown rustlike scale	Film on all surfaces; some scale retained particularly along edges
944A	J	2.80	22.0	1.5843	1.5985	1.5829	−1.4	0.030	0.25	0.29	All surfaces covered with a heavy brown rustlike scale	Film on all surfaces; some scale retained particularly along edges
945A	K	2.80	16.8	1.5573	1.5708	1.5548	−2.5	0.054	0.44	0.53	All surfaces covered with a heavy brown rustlike scale	Film on all surfaces; some scale retained particularly along edges
946A	L	3.00	13.4	1.5787	1.6004	1.5790	+0.3				All surfaces covered with a heavy brown rustlike scale	Film on all surfaces; some scale retained particularly along edges

*Two corrosion rates are presented: one based on the total operation time of 1064 hr and the other based on the total radiation time of 897 hr (3 Mwhr of reactor time equivalent to 1 hr of total radiation time).

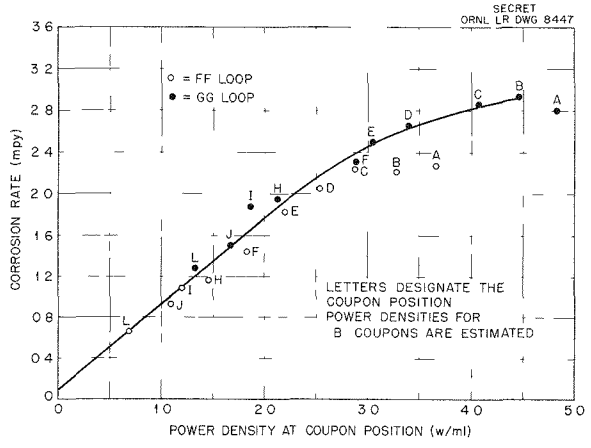

Fig. 9.10. Zircaloy-2 Core Coupon Corrosion Rates Based on Total Circulation Time vs Power Density at Coupon Position.

weight data are in excess of those found in comparable out-of-pile tests.

Weight data for the in-line and core specimen holders and for the impact specimens are shown in Table 9.11. No attempt was made to defilm these pieces, and it was apparent from visual inspection that some oxide film remained on the core pieces. The in-line holder was heavily covered with oxide. Average corrosion rates, which were calculated from these as-removed weight data, are included for the impact specimens. These rates are somewhat less than the average rates for the core specimens.

(c) Status of Design and Construction. – *(1) Corrosion Examination Facility.* – The second cutting bridge will be installed by July 29. A period of cold runs and testing will follow. At the conclusion of this test period, the cell will be ready for full-scale operation. A program of designing and building special tools for this facility is in progress.

(2) Bomb-Opening Cell. – Completion of the bomb-opening cell continues to be delayed by postponement of delivery of the lead-glass windows.

(d) Metallographic Examination of Stainless Steel Specimens from In-Pile Loop FF. – The metallographic examination, by the Remote Metallography Group of the Solid State Division, of portions from the stainless steel components of in-pile loop FF was completed.[8] The details of operation and corrosion examination of loop FF were reported previously.[9]

TABLE 9.11. WEIGHT DATA FOR ZIRCALOY-2 SAMPLE HOLDERS AND IMPACT SPECIMENS, AS-REMOVED

Identification	Weight Change (mg)	Corrosion Rate for 897 hr (mpy)
Core holder		
17-A	−259	
17-B	−369	
In-line holder		
16-A	+307	
16-B	+191	
Impact samples		
74	−54.2	1.90
76	−52.9	1.85
78	−59.2	2.07
80	−53.8	1.88
82	−54.5	1.91
84	−55.5	1.94
86	−44.6	1.56
88	−46.2	1.62

The results of the metallographic examination are summarized below:

1. There was no evidence of corrosion in sections from the pressurizer heater or in the pipe near the pump outlet.
2. Sections from the inlet end of the pressurizer and from the thermocouple well near the outlet showed no evidence of corrosion. A section of the pressurizer wall near the outlet did show slight corrosion in the grain-boundary areas. It is not known whether this section was from the liquid- or vapor-phase area, since, after sectioning, these areas could not be distinguished.
3. The core cap, which is the area exposed to the highest flux, also showed some corrosive penetration at the grain boundaries. This was not true in the case of loop DD reported previously.[10]
4. A section from the core area, which included

[8] M. J. Feldman *et al., Metallographic Examination of HRP In-Pile Loop "FF" Components,* ORNL CF-55-5-154 (May 16, 1955).

[9] G. H. Jenks, H. C. Savage, *et al., HRP Quar. Prog. Rep. April 30, 1955,* ORNL-1895, p 99–118.

[10] G. H. Jenks, H. C. Savage, *et al., HRP Quar. Prog. Rep. April 30, 1955,* ORNL-1895, p 118.

the core-body-to-reducer weld, showed evidence of surface roughening in the heat-affected zones. Either a peculiar etching effect or an intergranular attack was indicated on the core-body side of the weld. This will be checked further when the new facilities are available.

5. The cause of the large pit in the reducer section of the core is still unknown; however, the examination of the area showed the entire pit to be located in weld metal.

9.2 LITR BOMB TESTS

G. H. Jenks

A. L. Bacarella
W. E. Clark
R. J. Davis
H. O. Day
H. A. Fisch
D. T. Jones
J. R. McWherter
M. D. Silverman
H. H. Stone
K. S. Warren
L. F. Woo
W. C. Yee

9.2.1 Introduction

The main objective of the LITR bomb experiments continued to be the characterization of the effect of radiation on the corrosion of Zircaloy-2 by uranyl sulfate solutions. Three in-pile exposures of Zircaloy bombs were completed, and a fourth is in progress. An in-pile bomb experiment with stainless steel was also completed.

Two of the above-mentioned radiation exposures were carried out in the new facility in beam hole HB-5 of the LITR. The other exposures were in the beam hole HB-6 facility, which has been employed for a majority of the previous bomb tests. Details of methods, techniques, and equipment for experiments in beam hole HB-6 have been described previously.[11-13] Experiments in beam hole HB-5 are similar in most respects to those in beam hole HB-6. However, the bomb presently used in beam hole HB-5 is not of the type used in beam hole HB-6 but is of the type which was originally developed for the MTR bomb experiments and which was described and pictured previously.[14] It is equipped with a pin rack which can accommodate a total of six pin corrosion specimens.

The intensities of reactor radiations at the bomb-exposure position in beam holes HB-5 and HB-6 are listed in Table 9.12. The values for thermal-neutron flux are those determined from measurements with cobalt monitors. The values for gamma-ray intensity are given in terms of the power generated from the absorption of the reactor radiations in graphite. The contribution of fast neutrons to the power is included. These values were estimated from the measurements of others.[15,16] The higher value in beam hole HB-5 is a result of the location of three fuel elements directly in front of it. Beam hole HB-6 is separated from the active lattice by 6 in. of beryllium.

TABLE 9.12. INTENSITIES OF REACTOR RADIATIONS IN HB-5 AND HB-6 AT 3 Mw

Facility	Thermal-Neutron Flux (neutrons/cm^2/sec)	Gamma-Ray Intensity (w/g)
HB-5	1.0×10^{13}	0.5
HB-6	4.8×10^{12}	0.05

As before, each bomb was pressure-tested before use, filled with solution, and pretreated by out-of-pile operation at temperature for 15 to 30 hr prior to insertion.[13]

The bomb-dismantling facility has not been in operation, and hence only oxygen data from the experiments are available.

9.2.2 Experimental Conditions and Results

The experimental conditions and data for the various in-pile experiments are listed in Table 9.13. A brief explanation of this table will be sufficient. The experiment number and the LITR facility in which the exposure was made are shown in the first column. The temperatures maintained during the exposures are shown in the fourth column. For several experiments, the given bomb was exposed at more than one temperature. The experimental data pertinent to a given temperature

[11] C. H. Secoy *et al.*, *HRP Quar. Prog. Rep. April 30, 1954*, ORNL-1753, p 139.

[12] G. H. Jenks *et al.*, *HRP Quar. Prog. Rep. Oct. 31, 1954*, ORNL-1813, p 82.

[13] G. H. Jenks *et al.*, *HRP Quar. Prog. Rep. Jan. 31, 1955*, ORNL-1853, p 107.

[14] G. H. Jenks *et al.*, *HRP Quar. Prog. Rep. Jan. 31, 1955*, ORNL-1853, Fig. 4.22, p 116.

[15] J. J. Hairston and F. H. Sweeton, *γ-Heating after Shutdown in the Center West Horizontal Beam Hole of the LITR*, ORNL CF-51-8-201 (Aug. 31, 1951).

[16] J. H. Buck and C. F. Leyse, *MTR Project Handbook*, ORNL-963, p 4.26 (May 7, 1951).

TABLE 9.13. SUMMARY OF IN-PILE BOMB CORROSION STUDIES, APRIL 3, 1955, TO JULY 6, 1955

Bomb No. and LITR Facility	Bomb Material	Solution Composition (m)	Exposure Temperatures (°C)	Fission Power Density (w/ml)	Exposure Period (days)*	Corrosion Rate (mpy)*
Z-9, HB-6	Zircaloy-2	0.17 UO_2SO_4 (93.2% U^{235}) 0.007 $CuSO_4$	250 280	5.8 5.4	4.22 2.53	8.3 15.8
Z-10, HB-6	Zircaloy-2	0.17 UO_2SO_4 (44.1% U^{235}) 0.02 $CuSO_4$	225 250 280 290	3.0 2.9 2.7 2.7	7.87 4.55 6.62 1.65	3.1 5.7 10.0 12.2
Z-12, HB-5	Zircaloy-2	0.043 UO_2SO_4 (93.2% U^{235}) 0.05 $CuSO_4$ 0.02 H_2SO_4	280 300	3.2 3.1	9.79 5.41	9.7 ~10
Z-13, HB-5	Zircaloy-2	0.17 UO_2SO_4 (0.03% U^{235}) 0.02 $CuSO_4$	250	5×10^{-3}	19.4 (continuing)	~2
H-85, HB-6	Type 347 stainless steel	0.17 UO_2SO_4 (93.2% U^{235}) 0.01 $CuSO_4$ 0.015 H_2SO_4	250	5.8	12.8	<1

*Based on radiation time with 3 Mwhr of LITR energy equivalent to 1 hr.

are, in each case, on a line with the temperature datum. The values for the fission power density were calculated from the solution composition and from the neutron flux which prevailed when the reactor was operating at 3 Mw. Values for the exposure period, shown in the sixth column, were computed by setting 3 Mwhr of LITR energy equivalent to 1 hr. Values for the over-all corrosion rates are those calculated from the oxygen depletion data and the radiation exposure period.

The results of the oxygen depletion measurements for each experiment are plotted in Fig. 9.11, with corrosion penetration as the ordinate and radiation exposure time as the abscissa. This radiation time was obtained as described above.

Each experiment is described in more detail below.

(a) Experiment Z-9. – Without exception, the HRP in-pile bomb and loop corrosion studies have employed solutions which contained dissolved copper. In the case of the Zircaloy-2 bomb experiments, essentially all the solutions were at the particular copper concentration of 0.02 m. Experiment Z-9 employed a solution 0.007 m in copper and was carried out with the objective of determining whether the copper concentration has any influence on the radiation-induced corrosion of Zircaloy-2. Except for this difference in copper concentration, the experimental conditions for this experiment reproduced those of the prior experiment, H-58.[12]

The corrosion rate at 250°C, which was determined both for this experiment and for the prior experiment, was 8.3 mpy. No effect of copper concentration on the radiation corrosion of Zircaloy-2 is apparent from these results.

However, it is believed that, in order to obtain an unequivocal answer as to the influence of copper, it will be necessary to carry out an experiment in which copper is completely absent from the solution. Experiments are planned in which the copper catalyst will be replaced with a heterogeneous catalyst.

(b) Experiment Z-10. – This experiment was performed to determine the effect of temperature on the radiation-induced corrosion of Zircaloy-2. As shown in Table 9.13, one Zircaloy-2 bomb was exposed at four different temperatures: 225, 250, 280, and 290°C. The exposure was started at the lowest temperature and concluded with the highest.

The corrosion rates which were observed are plotted in Fig. 9.12, with the logarithm of the rate as the ordinate and the reciprocal of the absolute

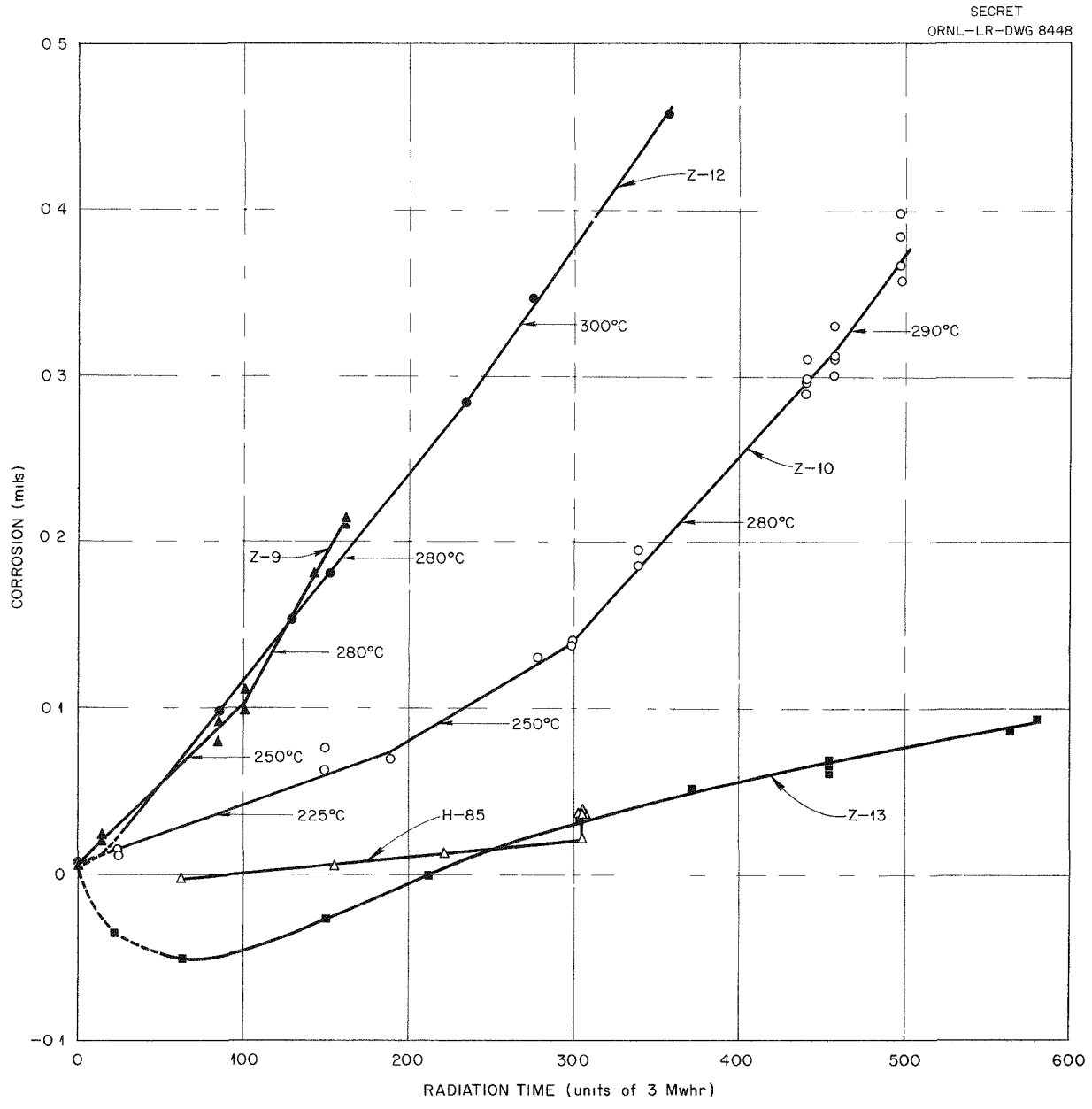

Fig. 9.11. In-Pile Bomb Corrosion Data.

temperature as the abscissa. The rate values plotted here were adjusted for differences in the power density which prevailed at the different exposure temperatures. The assumption was made that, under a given set of conditions, the rate under irradiation was directly proportional to the power density. The power density at 250°C was chosen as standard. A straight line can be drawn through the points obtained at the four temperatures. An activation energy for the corrosion reaction of 12,000 cal/mole is indicated by the data.

Data from experiments Z-5[17] and Z-9, both of which were exposed at two temperatures, 250 and

[17] G. H. Jenks *et al.*, *HRP Quar. Prog. Rep. April 30, 1955*, ORNL-1895, p 119.

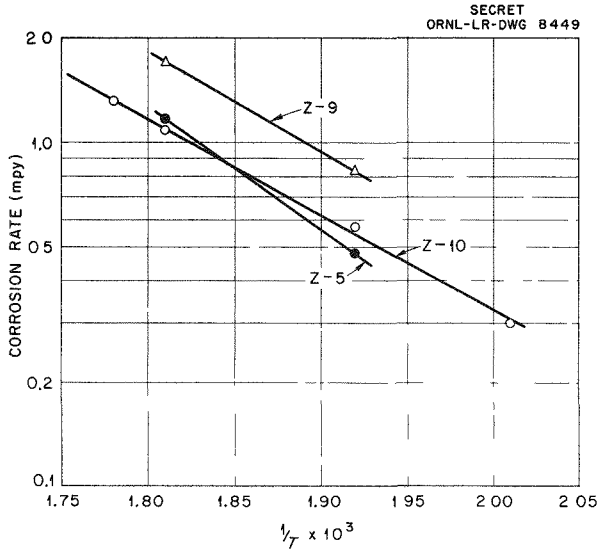

Fig. 9.12. Radiation-Induced Corrosion of Zircaloy-2 at Several Temperatures.

280°C, are also plotted in Fig. 9.12. Good agreement exists between the temperature coefficients indicated by these three experiments. It should be emphasized, however, that the coefficient may not be the same for other solutions or for other temperature ranges. Indeed, the coefficient observed in experiment Z-12, which is described below, was quite different. Exposure in experiment Z-12 was at 280 and 300°C, and the corrosion rates observed at the two temperatures were not significantly different.

(c) Experiment Z-12. – The primary objective of this experiment was to obtain control information for the MTR bomb experiments, the first of which is described in Sec. 9.3. The solution composition, except for enrichment, was the same as that presently employed in the MTR experiments. The corrosion rate observed at 280°C was not significantly different from that determined in experiment Z-10, which was performed with a solution of the composition usually employed in the LITR tests. The 300°C data are the first to be obtained at this high temperature. As shown in Table 9.13, the corrosion at 300°C was roughly equal to that at 280°C.

(d) Experiment Z-13. – The solution for this experiment contained depleted uranium, and the fission power density in the solution was negligible. The estimated power from absorption of gamma rays and fast neutrons was 0.5 w/ml.

As can be seen from the plot of the experimental data in Fig. 9.11, there was an initial increase of oxygen pressure in the bomb. The pressure reached a maximum and then decreased in a fairly regular fashion with continuing irradiation.

One possible explanation of this phenomenon is that radiolytic hydrogen diffuses into the bomb wall under exposure to reactor radiations, leaving excess oxygen behind. Small increases in pressure have been observed during the early stages of irradiation in some previous in-pile bombs, but they were limited to the first point or two at most. If the increases were due to hydrogen diffusion, they may have been overridden in previous bombs by the rapid loss of oxygen accompanying a more rapid oxidation. This experiment is continuing at an exposure temperature of 280°C. A later exposure at 300°C is planned.

(e) Experiment H-85. – This experiment was the first of several which are planned to determine the effects of excess H_2SO_4 on the corrosion of type 347 stainless steel by uranyl sulfate solution under irradiation. As shown in Table 9.13, the solution was 0.015 *m* in H_2SO_4. Otherwise the solution was of the same composition as that employed in a great majority of the steel bomb tests which have been carried out in the past. The bomb was charged with an initial oxygen pressure of about 800 psi, measured at the test temperature. This charge was several times greater than that used in previous tests, which, with few exceptions, employed an initial pressure of about 250 psi.

A marked increase in the corrosion rate after one to seven days of exposure to radiation has been characteristic of the results of previous steel bomb tests.[18] In the present experiment, as shown in Fig. 9.11, no such increase was apparent during a total of 13 days of irradiation. The experiment was terminated at the end of this period because of a stoppage in the capillary which connects the bomb with the Baldwin cell. The average corrosion rate during the exposure was less than 1 mpy.

These results indicate that the corrosion resistance of the present system under irradiation is superior to that of previous steel bomb systems. Further experiments are planned to check these

[18] S. F. Clark *et al.*, *HRP Quar. Prog. Rep. July 31, 1954*, ORNL-1772, p 161.

results and to determine whether the improvement is due to the excess acid or to the increased oxygen pressure, or to both.

9.3 MTR BOMB TEST

G. H. Jenks

R. J. Davis J. R. McWherter
D. T. Jones H. H. Stone

The first rocking-bomb experiment at the MTR, ORNL-15-1, was successfully completed. The conditions for this first experiment were as follows:

UO_2SO_4	0.04 *m* (1.7% enrichment)
$CuSO_4$	0.05 *m*
H_2SO_4	0.02 *m*
Bomb material	Zircaloy-2
Test temperature	280°C

As is indicated, the uranium employed was of low enrichment. The estimated power density from fission in this solution under the test conditions was 0.5 w/ml. However, an appreciable power was generated by the absorption of gamma rays and fast neutrons from the reactor. The power from this source was estimated to be 3 to 5 w/ml when the reactor was at 30 Mw.

The bomb assembly was inserted in beam hole HB-3 of the MTR on June 21, and operation of the reactor at 30 Mw was started three days later. The experiment was exposed to the high-flux region or retracted into a cadmium shield for periods of time as shown in Fig. 9.13. The corrosion in mils, based on oxygen consumption vs time of operation, is also shown in this figure. The rate calculated from these data is approximately 8 mpy.

The results of the experiment are being analyzed and correlated. The next experiment for the MTR will be at a fission power density of about 40 w/ml and is scheduled for insertion in the reactor in August.

Figure 9.14 shows the assembly of the experiment at the MTR prior to the installation of the outer concrete shielding doors in the HB-3 hole.

9.4 VAN DE GRAAFF ACCELERATOR TESTS

G. H. Jenks

W. E. Clark B. O. Heston
M. D. Silverman

Experimental studies of the effect of fast-electron irradiation on the corrosion of Zircaloy-2 by uranyl sulfate solutions were undertaken. The equipment and techniques employed in this study were previously used and reported by Ghormley and Hochanadel[19] for a similar study of stainless steel. The equipment was placed in proper working condition, and preliminary irradiations were made.

[19] J. A. Ghormley and C. J. Hochanadel, *Chem. Semiann. Prog. Rep. Dec. 20, 1953*, ORNL-1674, p 76.

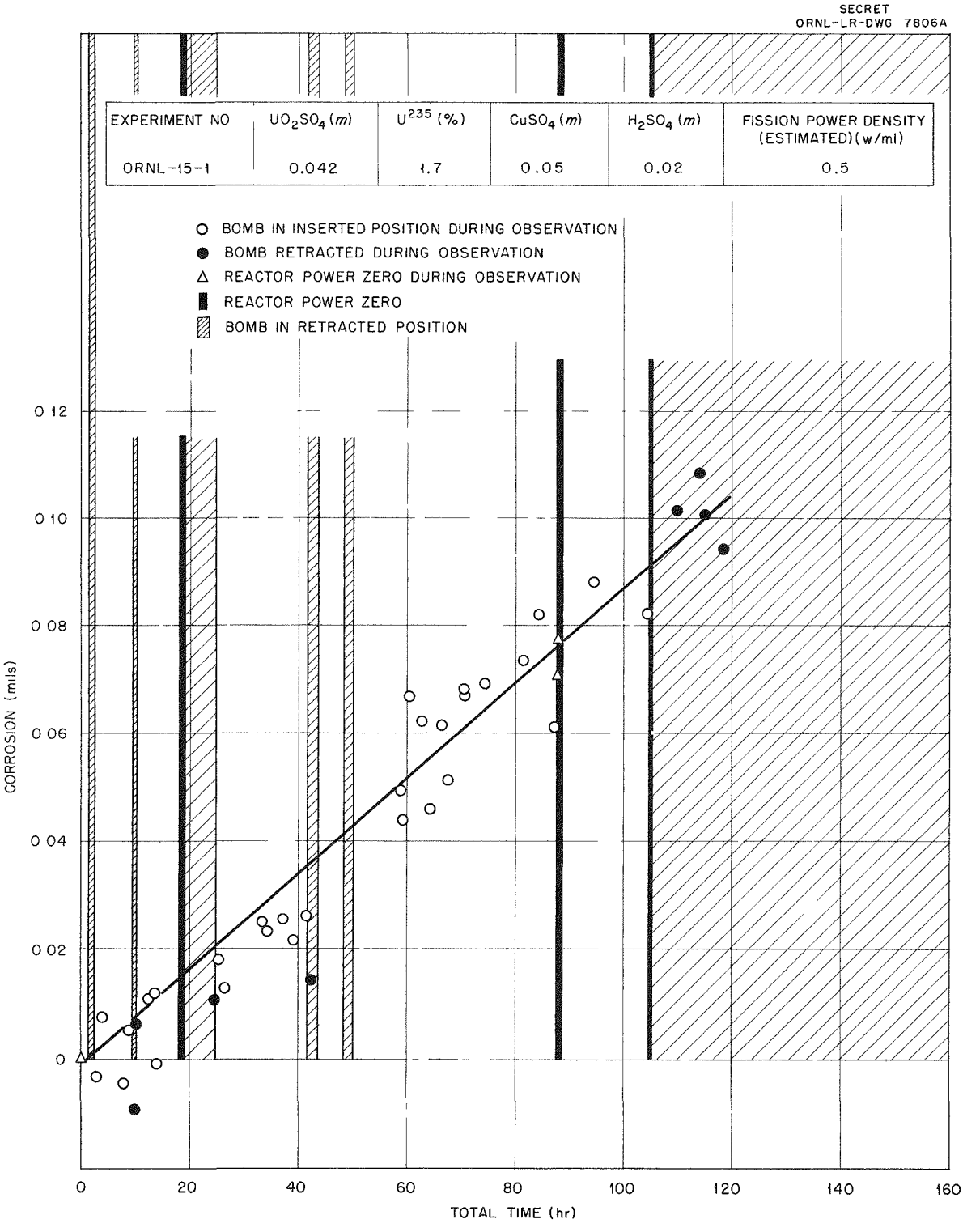

Fig. 9.13. Corrosion Data for MTR Bomb Experiment.

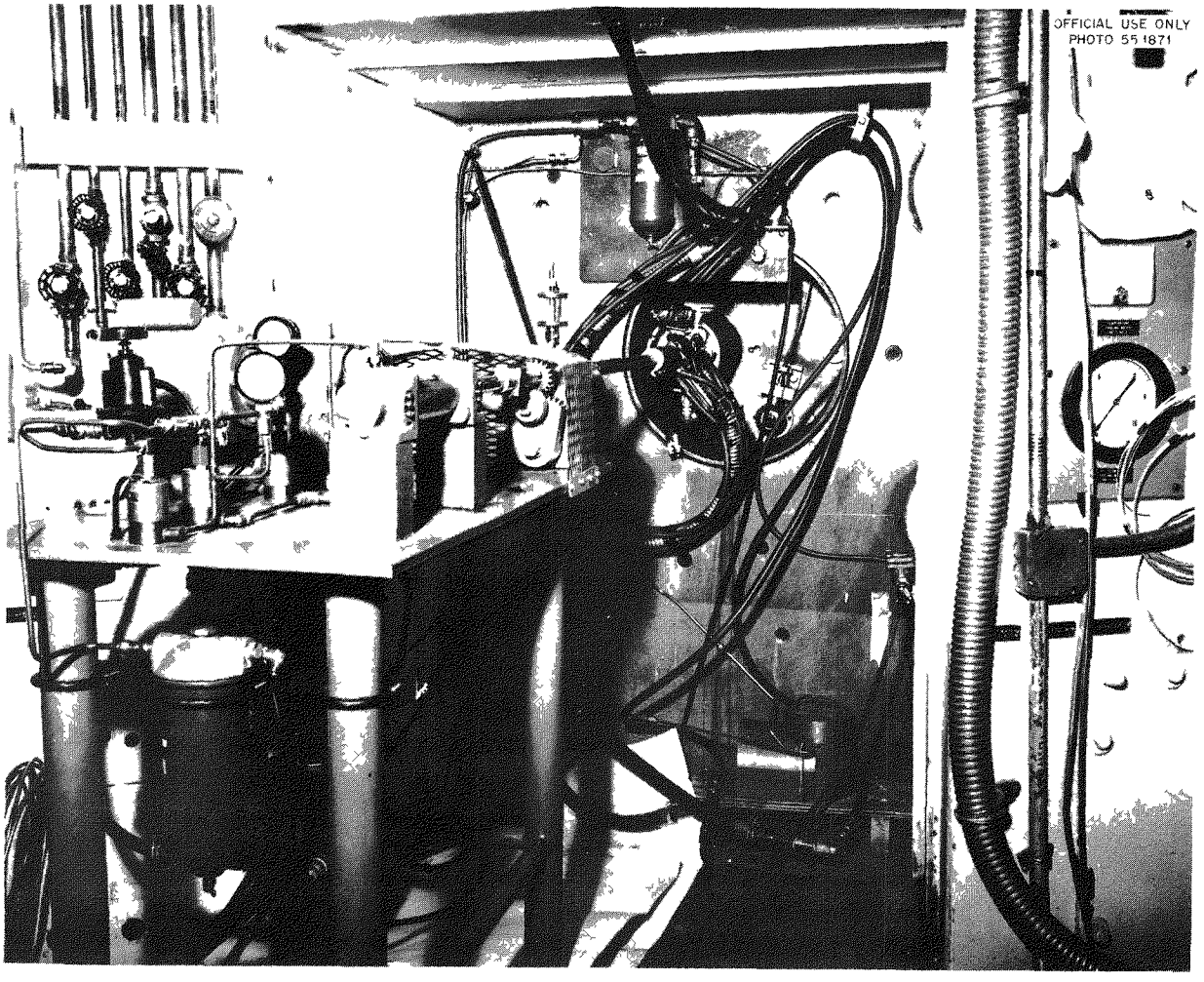

Fig. 9.14. Bomb Assembly Installed in MTR.

10. LABORATORY CORROSION STUDIES

E. L. Compere
J. L. English G. E. Moore

10.1 PREVENTION OF STRESS-CORROSION CRACKING OF TYPE 347 STAINLESS STEEL BY CATHODIC PROTECTION

E. L. Compere

Recent discussion with R. A. U. Huddle, of the British Atomic Energy Research Establishment at Harwell, suggested that the presence of carbon steel or other material anodic to type 347 stainless steel should assist in preventing the stress-corrosion cracking of the stainless steel.

As a first experiment in the development of this idea, four twin-strip stress specimens of type 347 stainless steel, stressed to 40,000 psi, were prepared. The strips were $3\frac{1}{2} \times \frac{5}{8} \times \frac{1}{8}$ in. On two of the specimens, however, a carbon-steel strip replaced one of the type 347 stainless steel strips.

The specimens were placed in 42% $MgCl_2$ solution, boiling at 154°C. On the all-stainless-steel specimens, a number of cracks were noted on the flats over the fulcrum, in the 15- to 20-hr interval, and complete strip breakage was noted in either the 30- to 45-hr interval or the 45- to 60-hr interval.

The specimens with one stainless steel and one carbon-steel strip have shown no cracks at all on the stainless steel during 160 hr of exposure. The carbon steel has been fairly severely attacked at the same time, as would be expected under such conditions. The data are summarized in Table 10.1.

It thus appears that a considerable degree of protection against stress-corrosion cracking was afforded the stainless steel in this very aggressive medium, as a result of coupling with a more anodic material. Such protection might be of value in a number of regions in the HRT, such as in the heat exchanger and steam system.

10.2 TITANIUM ALLOYS FOR HRT CORE BOLTS

E. L. Compere

Among the materials under consideration for use in fabricating HRT core bolts are the titanium alloys Ti A-110-AT and Ti C-130-AM. Alloy Ti A-110-AT is an alpha phase, 110,000-psi yield strength, aluminum-tin alloy, whereas alloy Ti C-130-AM is a mixed alpha- and beta-phase, 130,000-psi yield strength, aluminum-manganese alloy.

These alloys were exposed for several hundred hours to simulated HRT fuel solution at 100, 250, and 300°C and to simulated blanket solution (1.3 *m* UO_2SO_4). Results are given in Table 10.2. Only interference colors resulted, along with trivial attack, which was less than 0.1 mpy (undefilmed) except in the case of 1.3 *m* UO_2SO_4 at 250°C. In this case a slight dull-gray film was noted, generally along with larger, but still slight, weight changes.

Thus these materials would appear to be acceptable – within the limits of these tests – for HRT core-bolt application.

TABLE 10.1. EFFECT OF CARBON STEEL ON STRESSED TYPE 347 STAINLESS STEEL IN $MgCl_2$ (42%)

Test temperature: 154°C
Solution: 42% $MgCl_2$
Specimen type: Twin-strip stress assembly; 40,000-psi stress

Test No.	Steel Type	Duration (hr)	Specimen Condition
HS-3-AB	347	45 to 60	Cracked and broken
HS-3-CD	347	30 to 45	Cracked and broken
HS-2-AB and HS-2-CD	One strip 347; one strip carbon steel	160	No cracks; unbroken

10.3 STRESS-CORROSION STUDIES

E. L. Compere J. L. English

No stress-corrosion cracking in HRT environments has been noted experimentally in any case. However, because of the potentially dangerous character of this kind of attack, studies of it have been continued, both with various materials in HRT solutions and also in the aggressive test solution, 42% $MgCl_2$ at 154°C. Generally the twin-strip stress assembly[1] has been used, with strips of various sizes.

Stressed specimens, similar to those used in the in-pile loop, of titanium 75A, Zircaloy-2, and type 347 stainless steel were exposed to 0.17 *m* UO_2SO_4 with 0.04 *m* H_2SO_4 and 0.03 *m* $CuSO_4$ at 250°C with 150-psi oxygen. No cracking or unusual attack, attributable to the stressed condition, was observed on any of these materials after an exposure of 1070 hr. Results are shown in Table 10.3.

Type 347 stainless steel specimens stressed to 40,000 psi were exposed for 1560 hr at 300°C and with 150-psi oxygen to simulated HRT core solutions containing 0.04 *m* UO_2SO_4 with 0.006 *m* H_2SO_4. In addition, one solution contained 0.005 *m* $CuSO_4$. No cracking or unusual attack

[1] E. L. Compere, *HRP Quar. Prog. Rep. Jan. 31, 1955*, ORNL-1853, p 123–127.

TABLE 10.2. CORROSION OF TITANIUM ALLOYS IN SIMULATED HRT SOLUTIONS

Test No.		Test Conditions						
Alloy Ti A-110-AT (Rem Cru)	Alloy Ti C-130-AM (Rem Cru)	Temperature (°C)	Solution (*m*) UO_2SO_4	Solution (*m*) H_2SO_4	Solution (*m*) $CuSO_4$	Atmosphere	Specimen Type	Duration (hr)
HB-11	HB-16	100	0.04	0.006	0.005	Aerated	Coupon	660
HB-12	HB-17	250	0.04	0.006	0.005	150-psi O_2	Coupon	325
HB-13	HB-18	300	0.04	0.006	0.005	150-psi O_2	Coupon	325
HB-14	HB-19	105	1.3			Aerated	Coupon	660
HB-15	HB-20	250	1.3			150-psi O_2	Coupon	325

Test No.	Test Results		
	Total Attack* (mg/cm^2)	Average Rate* (mpy)	Specimen Condition*
HB-11	0.01		Slight lustrous yellow tarnish
HB-12	0.02	0.06	Golden tarnish
HB-13	0.03	0.1	Purple-gray film
HB-14	0.04	0.06	Lustrous
HB-15	0.46; gain 0.18**	1.0	Dull-gray film over golden tarnish
HB-16	Gain		Slight lustrous yellow tarnish
HB-17	0.02	0.04	Golden tarnish
HB-18	Gain 0.02		Purple film
HB-19	0.04	0.05	Lustrous
HB-20	Gain 0.05		Dull gray-black film over golden tarnish

*Undefilmed.

**Bomb leaked during run; furthermore, specimen undefilmed.

was observed on this material. The cracking of this material in boiling 42% $MgCl_2$ in 40 hr with 40,000 psi stress confirms the susceptibility of the material to attack in aggressive environments and indicates that uranyl sulfate solutions do not provoke stress-corrosion cracking. Results are shown in Table 10.4.

Stress specimens of type 347 stainless steel were exposed in duplicate to the liquid and vapor phases of boiling uranyl sulfate solutions contained in a steam-heated small-scale stainless steel evaporator[2,3] for a total of 4600 hr, 2600 hr since last reported. The last 3100 hr of the test were accumulated in a solution 0.04 *m* in UO_2SO_4

[2]E. L. Compere and J. L. English, *HRP Quar. Prog. Rep. July 31, 1954*, ORNL-1772, p 94–95.

[3]J. L. English, *HRP Quar. Prog. Rep. Jan. 31, 1955*, ORNL-1853, p 123.

TABLE 10.3. EFFECT OF FUEL SOLUTIONS ON STRESSED SPECIMENS OF IN-PILE TYPE LOOP

Temperature: 250°C
Solution
UO_2SO_4 0.17 *m*
H_2SO_4 0.04 *m*
$CuSO_4$ 0.03 *m*
Atmosphere: 150-psi O_2
Specimen type: In-pile loop modification of twin-strip stress specimen
Duration: 1070 hr

	Type 347 Stainless Steel	Titanium 75A	Zircaloy-2
Stress, psi	27,000	25,000	22,000
Total attack,* mg/cm^2	0.56	Gain 0.04	0.233
Average rate,* mpy	0.22		0.1
Rate range,* mpy	0.14–0.31		0.10–0.03
Rate trend	Diminishing		Diminishing
Specimen condition	No cracks; gray-black film	Purple film; no cracks	No cracks; gray-white film

*Undefilmed.

TABLE 10.4. STRESSED TYPE 347 STAINLESS STEEL IN HRT FUEL AND OTHER SOLUTIONS

Temperature, °C	300	300	154
Solution			
UO_2SO_4, *m*	0.04	0.04	
H_2SO_4, *m*	0.006	0.006	
$CuSO_4$, *m*	0.005		
$MgCl_2$, %			42
Atmosphere, psi	150, oxygen	150, oxygen	150, oxygen
Steel type	347	347	347
Stress, psi	40,000	40,000	40,000
Duration, hr	1560	1560	40
Total attack,* mg/cm^2	0.03	0.06	0.05
Specimen condition	No cracks; gray-black film	No cracks; black film	Broke (2 specimens)

*Undefilmed.

which contained 0.005 *m* $CuSO_4$ and 0.004 *m* H_2SO_4; the initial 1500-hr exposure period was made in 0.17 *m* UO_2SO_4 solution.

Microscopic examination of the constant-strain type of stress specimens disclosed no indications of a susceptibility of the stainless steel alloy to stress-corrosion cracking in either the liquid- or the vapor-phase environments. Generalized undefilmed corrosion rates for the complete stress assemblies were exceedingly low and ranged between 0.01 and 0.02 mpy.

The tests are being continued, with examination of specimens scheduled at 500-hr intervals.

10.4 STRESSED TYPE 17-4 PH STAINLESS STEEL IN SIMULATED HRT SOLUTIONS

E. L. Compere

Type 17-4 PH stainless steel has been proposed for use as HRT core-bolt material, a use in which very high stresses are to be encountered. It has been shown previously that partially hardened type 17-4 PH stainless steel was preferable. The first 1000 hr of testing of this material in various environments was described in a previous report.[1] Results after a total of 2000 hr are given in Table 10.5. No cracks or other effects attributable to the 80,000-psi stress have been observed in simulated HRT fuel solution containing 0.04 *m* UO_2SO_4 and 0.006 *m* H_2SO_4 at 100, 250, and 300°C or in 1.3 *m* UO_2SO_4 at 100°C.

10.5 CORROSION OF ALUMINUM OXIDE BY URANYL SULFATE AND OTHER SOLUTIONS

J. L. English

The interest in the use of pure sintered aluminum oxide for bearings and journals in canned-rotor pumps, for in-pile circulating corrosion test loops, warranted continued examination of the corrosion behavior of the material in uranyl sulfate solution and other solutions associated with in-pile loop operation. Previous work indicated that synthetic sapphire[4] (fused Al_2O_3) possessed good corrosion resistance to oxygenated 0.17 *m* UO_2SO_4 solution at 250°C, as did sintered aluminum oxide in tests up to 150°C in oxygenated 0.17 *m* UO_2SO_4 solution.[5] The present study was concerned with the behavior of sintered aluminum oxide at temperatures up to 300°C in uranyl sulfate solutions. Tests were also run in boiling 5% HNO_3 and in boiling 3% Na_3PO_4.

Sintered aluminum oxide specimens were supplied by the Kearfott Company, Inc., of Clifton,

[4] J. L. English, *HRP Quar. Prog. Rep. March 31, 1953*, ORNL-1554, p 69–72.

[5] E. L. Compere and J. L. English, *HRP Quar. Prog. Rep. July 31, 1954*, ORNL-1772, p 102–103.

TABLE 10.5. STRESSED TYPE 17-4 PH STAINLESS STEEL IN SIMULATED HRT SOLUTIONS

Temperature, °C	100	105	300	250
Solution				
UO_2SO_4, *m*	0.04	1.3	0.04	0.04
H_2SO_4, *m*	0.006		0.006	0.006
Atmosphere	Aerated	Aerated	150-psi O_2	150-psi O_2
Steel type	17-4 PH	17-4 PH	17-4 PH	17-4 PH
Stress, psi	80,000	80,000	80,000	80,000
Source	Armco heat 34434	Armco heat 34434	Armco heat 34434	Armco heat 34434
Duration, hr	2010	2010	2007	2007
Total attack, mg/cm^2	0.36	1.15	+0.236	0.16
Average rate, mpy	0.08	0.25		0.03
Rate range, mpy		0.04–0.4		
Rate trend		Slow rise		
Specimen condition	No crack; black film	No crack; black film	No crack; blue-black film	No crack; blue-black film

New Jersey, in the form of wafers $\frac{1}{4}$ in. thick by $1\frac{3}{16}$ in. in diameter. The corrosion media included: 0.17 *m* UO_2SO_4 solution, with and without 0.01 *m* $CuSO_4$; 5 wt % HNO_3; and 3 wt % Na_3PO_4 solution. Only the uranyl sulfate solutions were used for tests above boiling temperature, and in these tests the solutions were pressurized with 150 psi of oxygen.

A summary of the corrosion data from the uranyl sulfate tests is included in Table 10.6. At the completion of each run, the aluminum oxide specimens were washed repeatedly in distilled water and dried to constant weight.

No appreciable difference in corrosion behavior of the aluminum oxide was noted in the 0.17 *m* UO_2SO_4 solutions with and without 0.01 *m* $CuSO_4$ at temperatures up to 250°C. Specimens exposed in these solutions showed decreasing rates of attack with increased exposure times up to 300 hr. The aluminum oxide specimen exposed in the copper-free 0.17 *m* UO_2SO_4 solution continued to exhibit a decreasing rate of attack with increased exposure time as the test temperature was increased by 25°C increments from 150 to 250°C. The final observed corrosion rate for a total period of 1015 hr over the above temperature range was 0.6 mpy. An additional 100-hr run at 300°C resulted in an over-all weight gain of 0.1 mg/cm^2 for the specimen. The appearance of the aluminum oxide specimen at the conclusion of the 300°C run suggested that the weight gain may have been due to the deposition of corrosion products from solution attack on the stainless steel test container. Chemical identification of the rust-colored deposit on the aluminum oxide will be made at the completion of the corrosion study.

In addition to the uranyl sulfate tests, small specimens of pure sintered aluminum oxide – broken from a canned-rotor pump bearing – were subjected to 100-hr runs in boiling 3% Na_3PO_4 and 5% HNO_3 solutions. These two solutions are used in the preliminary cleaning of in-pile corrosion test loops prior to their operation with uranyl sulfate solutions. The aluminum oxide specimens appeared to be completely resistant to the solutions, as indicated by negligible weight changes and by unchanged physical appearances

TABLE 10.6. CORROSION OF PURE SINTERED ALUMINUM OXIDE IN OXYGENATED 0.17 *m* UO_2SO_4 SOLUTIONS

Run No.	$CuSO_4$ (*m*)	Temperature (°C)	Cumulative Time (hr)	Total Weight Loss (mg/cm^2)	Corrosion Rate (mpy)		Specimen Appearance
					Run	Cumulative	
				First Specimen			
1	0.01	200	100	0.4	3.8	3.8	No change; smooth cream color
2	0.01	200	200	0.7	2.5	3.2	No change
3	0.01	250	300	0.8	1.1	2.5	No change
				Second Specimen			
1		150	118	0.3	2.4	2.4	No change
2		150	218	0.5	1.7	2.1	No change
3		150	315	0.7	1.7	2.0	No change
4		150	415	0.8	1.1	1.8	Nonuniform brown stain
5		150	515	0.9	1.0	1.6	Nonuniform brown stain
6		175	615	0.9	0.2	1.4	Nonuniform red-brown stain
7		200	715	1.0	0.5	1.3	Uniform red-brown stain
8		225	815	0.8	+	0.9	Mottled light purple-brown
9		225	915	0.9	0.7	0.9	Mottled light purple-brown
10		250	1015	0.6	+	0.6	Mottled light purple-brown
11		300	1115	+0.1	+	+	Heavy nonuniform red-colored stain

during the first 100-hr run. The tests are being continued.

10.6 WATER-LINE CORROSION OF TYPE 347 STAINLESS STEEL AND TITANIUM 75A BY URANYL SULFATE SOLUTIONS AT ELEVATED TEMPERATURES

J. L. English

Strip-type specimens of type 347 stainless steel and titanium alloy 75A were exposed to the solution-vapor interface of simulated reactor solutions at elevated temperatures for a period of 3800 hr to examine water-line corrosion behavior of the two alloys. The solution-temperature combinations which have been tested include: 0.02 *m* UO_2SO_4 + 0.005 *m* H_2SO_4 at 300°C, 0.06 *m* UO_2SO_4 + 0.006 *m* H_2SO_4 at 300°C, 0.17 *m* UO_2SO_4 at 250 and 300°C, and 1.34 *m* UO_2SO_4 at 250 and 300°C. All solutions were pressurized with approximately 150 psi of oxygen, introduced into the system by the thermal decomposition of hydrogen peroxide.

The tests were run without solution replacement in 225-ml-capacity stainless steel autoclaves. The 40-cm^2 duplicate specimens were positioned in the autoclaves in such a manner that approximately 75% of the total surface area was immersed in the test solution.

No specimen of either alloy exhibited any localized corrosion attack at or around the solution-vapor interface in the test media. Corrosion rates, based upon scrubbed weight losses and calculated for the total surface area of the individual specimens, did not exceed 0.1 mpy in any case for the 3800-hr exposure. In general, the vapor-formed films on specimens of the two alloys were mottled in appearance and fairly thin. The solution-formed films on the type 347 stainless steel specimens were of a more uniform nature and were considerably thicker than vapor-formed corrosion films. The solution-formed films on the titanium 75A specimens were quite thin, varicolored, and exhibited a high degree of luster. The tests will be continued for an indefinite period.

10.7 CORROSION OF DISSIMILAR-METAL COUPLES BY BOILING 5% NITRIC ACID SOLUTIONS

J. L. English

A study was made to examine the possibility of galvanic corrosion effects between type 347 stainless steel and either titanium alloy 75A or Zircaloy-2 coupled with the stainless steel during exposure in boiling 5 wt % HNO_3 solution. The corrosion behavior of uncoupled and partially hardened type 17-4 PH stainless steel was examined also.

The study originated as the result of some difficulties encountered during the preliminary cleaning of a type 347 stainless steel in-pile corrosion test loop with 5% HNO_3 at a temperature below 100°C. Discoloration of the nitric acid solution indicated a corrosion attack in some portion of the test loop. Prior to the preliminary cleaning operation, test specimens and test-specimen holders of different metals and alloys had been inserted in the test loop, which was then sealed by welding. Thus the possibility was presented of an accelerated corrosion attack at some point in the system during the nitric acid cleaning as a result of dissimilar-metal contact. The present investigation was planned to explore this possibility with titanium 75A and Zircaloy-2 coupled with type 347 stainless steel.

The test couples consisted of pin-type specimens of titanium 75A or Zircaloy-2 placed between two pieces of type 347 stainless steel. The assembly was then tightened by means of a stud-and-nut combination at each end of the rectangular-shaped stainless steel specimens. The relative area ratio of either titanium 75A or Zircaloy-2 to the type 347 stainless steel was 0.1 : 1.

The tests were run with oxygen sparging and with helium sparging of the nitric acid solution. A summary of the observed results for 1015 hr of operation appears in Table 10.7.

No acceleration of corrosion attack due to galvanic effects was observed on the specimens in the bimetallic couples of type 347 stainless steel with titanium 75A and Zircaloy-2. Metal contact points in the couples were slightly stained in a few cases, but otherwise there was no localization of corrosion at these areas. Gas sparging with helium or oxygen resulted in no effect on the corrosion behavior of the couples. With either type of sparging, corrosion rates for titanium 75A and Zircaloy-2 were less than 0.1 mpy, and type 347 stainless steel was corroded at rates between 0.1 and 0.2 mpy.

Single specimens of the partially hardened type 17-4 PH stainless steel underwent a generalized type of attack in boiling 5% HNO_3 solution, and the rate of attack accelerated with increasing

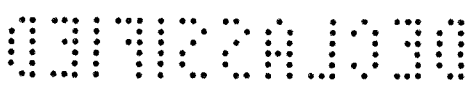

TABLE 10.7. CORROSION OF DISSIMILAR-METAL COUPLES FOR 1015 hr BY BOILING 5 wt % HNO_3 SOLUTION

Test No.	Couple Material	Type of Sparging	Corrosion Rate (mpy)	
			Control	Couple
H-79	Ti-75A,	Oxygen	0.04	0.04
	347 SS		0.15	0.15
H-80	Ti-75A,	Helium	0.07	0.03
	347 SS		0.16	0.15
H-81	Zircaloy-2,	Oxygen	0.04	0.01
	347 SS		0.15	0.14
H-82	Zircaloy-2,	Helium	0	0
	347 SS		0.14	0.14
H-83	17-4 PH SS*	Oxygen	0.8	Not tested
H-84	17-4 PH SS*	Helium	1.2	Not tested

*Type 17-4 PH was partially hardened to 36 Rockwell C by heating for 2 hr in air at 1000°F, followed by air cooling to room temperature. The 17-4 PH specimens showed an accelerating rate of corrosion attack with time.

exposure time. The specimen surfaces became covered with a lustrous, thin, black film. The observed corrosion rate in the oxygen-sparged test was 0.8 mpy, as compared with a rate of 1.2 mpy for the specimen in the helium-sparged test. The tests are being continued.

10.8 CORROSION OF GOLD-PLATED ISO-ELASTIC SPRING ALLOY BY BOILING 0.17 *m* UO_2SO_4 SOLUTION

J. L. English

A 0.030-in.-thick flat spiral spring of gold-plated Iso-Elastic alloy (a low-creep, low-temperature-coefficient spring alloy with nominal chemical composition of 36% nickel, 8% chromium, 0.5% molybdenum, and balance iron – John Chatillon & Sons, New York) was received for exposure in boiling 0.17 *m* UO_2SO_4 solution. The spring was designed for use in a displacement-type liquid-level controller operating in the vapor region of the HRT pressurizer.[6] Although the spring would be contacted by saturated steam above a uranyl sulfate solution during operation, it was decided to subject the spring to a more drastic test such as exposure in uranyl sulfate solution. This exposure served as an accelerated test for determining the effectiveness of the 3-mil-thick gold plate in preventing corrosion attack on the poorly resistant Iso-Elastic alloy.[7]

Gold plating on the spring alloy was performed by the Y-12 Plating Department. The spring was first given a flash copper plate, which was followed by gold plating to a thickness of approximately 3 mils.

The plated spring was immersed in aerated and boiling 0.17 *m* UO_2SO_4 solution for a total of 120 hr. The estimated corrosion rate at the end of this period was 57 mpy. The surface of the spring was black, blistered, and heavily roughened after the exposure. Microscopic examination at a power of 30X showed that the bulk of the gold plate had flaked from the surface, probably as the result of an undercutting action by the uranyl sulfate solution on the Iso-Elastic alloy. The flaking of the gold from the surfaces of the spring was apparent after the first 24 hr of exposure. Figures 10.1 and 10.2 show the final appearance of the specimen.

[6] A. M. Billings, *HRP Quar. Prog. Rep. April 30, 1955*, ORNL-1895, p 39–41.

[7] Previous unreported work showed that unplated Iso-Elastic alloy was corroded at a rate of 220 mpy after 72 hr in boiling 0.17 *m* UO_2SO_4 solution; the attack was characterized by massive and deep pitting.

UNCLASSIFIED
PHOTO 1312-1

Fig. 10.1. View of Gold-Plated Iso-Elastic Spring Showing Corrosion Damage After 120 hr in Boiling 0.17 *m* UO_2SO_4 Solution. 2X. Reduced 29%.

UNCLASSIFIED
PHOTO 1312-2

Fig. 10.2. Enlarged View of Section of Gold-Plated Iso-Elastic Spring Showing Blister Formation After Exposure in Boiling 0.17 *m* UO_2SO_4 Solution. 5X. Reduced 32%.

10.9 THORIUM OXIDE SLURRY CORROSION STUDIES

G. E. Moore E. L. Compere

10.9.1 Introduction

Study of the corrosion of type 347 stainless steel, titanium 75A, and Zircaloy-2 by circulating aqueous thorium oxide slurries in toroids continued.

The effect of sulfate additions to the thoria on the corrosion rates of these metals was investigated. Additions of sulfate salts of thorium, calcium, magnesium, or sodium were made to thorium oxide from two sources, distinguished primarily by their maximum calcination temperature. These sulfate-enriched, aqueous thorium oxide slurries showed little difference in behavior when compared with normal slurries to which no sulfate had been added. However, when very large amounts of thorium sulfate were used with high-fired thoria, increased attack on type 347 stainless steel was observed; this attack was attributed to the sulfuric acid in the solution formed by the hydrolysis of thorium sulfate. Some improvement in the dispersion of the slurry was observed when sodium sulfate was used, but, other than this, no beneficial effects could be attributed to sulfate under the conditions of these experiments.

It was believed that the basic factors affecting the behavior of the slurry would necessarily include the calcination temperature and particle size of the thorium oxide. It had been observed that thoria slurries showed improved handling characteristics when calcined at temperatures higher than 650°C. Although increasing the calcination temperature of the oxide improved the handling of the slurry, it also increased the rate of metal attack. However, results presented below showed that the attack on type 347 stainless steel, titanium 75A, and Zircaloy-2 was dependent on the particle size of the thoria as well as on its maximum calcination temperature. Investigations into the behavior of slurries prepared from high-fired thorium oxide would thus appear to be useful. A limitation to a maximum calcination

temperature may not necessarily be required by the erosion-corrosion of the structural metals, since this attack may be minimized through control of the particle size of the thoria.

10.9.2 Effect of Sulfate

Two runs, in which the sulfate content of the thorium oxide was varied by the addition of one of several sulfate salts, were completed. These runs were carried out with the 20-toroid rotator at 250°C and with 26 fps relative slurry velocity for approximately 140 hr. Slurry concentrations of 500 and 1000 g of thorium per kilogram of water, oxygen concentrations of 0 and 100 psi (at 250°C), and added sulfate concentrations from 100 to 10,000 parts sulfate per million parts ThO_2 were used in each run. The two runs differed only in the sources of the thorium oxide which was used to make up the slurries: Lindsay No. 8 and D-17 thoria were used. These oxides are characterized in Table 10.8.

For each run the weighed, dry, thorium oxide and sulfate salt were mixed and added to the stainless steel toroid; the proper volume of distilled water was then added. A quantity of 30% hydrogen peroxide which would yield the desired oxygen concentration by thermal decomposition was added to those toroids in which excess oxygen was desired. In the experiments in which oxygen was to be absent, the vapor space of the toroids was flushed with nitrogen for approximately 5 min to provide an inert-gas blanket. Four as-machined corrosion pin specimens – two of type 347 stainless steel, one of titanium 75A, and one of Zircaloy-2 – were exposed in each toroid.

The determination of the temperature of operation was somewhat indirect. The furnace in which the toroids were rotated was maintained at a temperature such that the wall temperature of two representative toroids was about 250°C. This temperature was determined by means of a Chromel-Alumel thermocouple welded to the toroid wall; since the rotation had to be stopped in order to connect the thermocouple leads, a curve of cooling of the toroid wall was obtained and was extrapolated to give the wall temperature at the time rotation and heating were stopped. This extrapolated temperature was taken as the operating temperature.

Table 10.9 summarizes the results of the Lindsay No. 8 experiment. All slurries were readily poured from the toroids at room temperature at the end of the run. The slurries were cream-colored, did not wet glass, and were not thick or creamy. With a concentration of 500 g of thorium per kilogram of water, the corrosion of type 347 stainless steel was practically independent of the sulfate concentration, except at

TABLE 10.8. CHARACTERIZATION OF THORIUM OXIDES

Code name	Lindsay No. 8	D-17	Ames
Source	Lindsay Chemical Co.	ORNL, Thorex	Ames Laboratory
Precipitated as	Oxalate	Oxalate	Oxalate
Maximum calcination temperature, °C	900	650	>650
Particle-size distribution,* wt %			
0 to 1 μ	5	23	7
1 to 3 μ	30	36	15
3 to 10 μ	46	26	43
Greater than 10 μ	19	15	35
Surface area, m^2/g	6.6 **	35.4	
Milligrams of sulfate per gram of thorium	0.2	<0.1	6.4

*Particle-size distributions determined by Activation Analysis Group, Analytical Chemistry Division, using gravitational sedimentation in 0.005 *M* $Na_4P_2O_7$.

**Values supplied by D. E. Ferguson and J. P. McBride, *ThO_2 Slurry Development: Quar. Rep. for Period Ending April 30, 1955*, ORNL CF-55-5-198, p 20 (May 20, 1955).

TABLE 10.9. EFFECT OF SULFATE ON THE BEHAVIOR OF CIRCULATING AQUEOUS THORIUM OXIDE SLURRIES PREPARED FROM LINDSAY NO. 8 THORIUM OXIDE

Temperature: 252 ± 5°C
Relative velocity: 27 fps
Duration of test: 137 hr

Toroid	Nominal Conditions				Chemical Analysis				Corrosion Rates (mdd)[c]			
									Type 347 Stainless Steel		Titanium Scrubbed Pins	Zircaloy-2 Scrubbed Pins
	g of Th per kg of H_2O	O_2 at 250°C (psi)	mg of SO_4 per kg of ThO_2	Form in Which Sulfate Was Added	g of Th per kg of H_2O	mg of SO_4 per kg of ThO_2[a]	Slurry pH[b]	Solution (mg of SO_4 per liter)	Toroid, As-Run	Defilmed Pins		
A	500	100		None added	170[d]	<720	6.0	<10	−3.3	−5.4, −5.9	+1.0	0.0
K					530	<430	6.5	<10	−2.8	−7.1, −7.9	−3.2	+0.7
C	500	100	10,000	$Th(SO_4)_2$	260[d]	6500	2.6	1100[e]	−3.3	−27, −29	−0.8	−1.6
M					240[d]	7600	2.4	1000[e]	−5.6	−51, −58	−1.9	+3.6
D	500	100	1,000	$Th(SO_4)_2$	270[d]	1800	5.1	30	−2.1	−6.0, −7.4	−0.8	−1.2
N					500	1200	5.7	10	−2.1	−5.2, −7.5	−2.7	−1.7
E	500	100	100	$Th(SO_4)_2$	260[d]	<470	6.4	<10	−2.7	−7.3, −7.8	−1.0	−3.3
O					530	600	5.9	15	−3.0	−6.6, −7.9	−0.7	−0.3
F	500	100	1,000	$CaSO_4$	510	1200[f]	5.9	150[g]	−1.9	−6.8, −8.0	+1.6	−1.8
P					500	1400[h]	6.5		−1.9	−7.4, −7.5	−1.2	−8.7
G	500	100	1,000	$MgSO_4$	530	1200[i]	7.2		−1.6	−3.7, −4.4	−1.1	−2.0
Q					510	1400[i]	6.0		−1.9	−8.2, −8.3	−1.6	+0.3
H	500	100	1,000	Na_2SO_4	480	750[j]	5.7	390[k]	−3.1	−4.6, −5.6	−1.5	+1.5
R					500	670[j]	6.6	460[k]	−2.4	−11, −14	−3.5	+2.1
J	500	N_2	1,000	$Th(SO_4)_2$	510	1400	7.3	20	−2.5	−9.7, −11	−2.0	−3.0
T					530	1300	7.5	24	−2.1	−10, −12	0.0	+3.0
B	1000	100		None added	630[d]	720	6.2	<10	−4.5	−11, −12	−3.1	−3.4
L					760[d]	400	6.2	40	−4.4	−12, −13	−2.5	+0.3
I	1000	100	1,000	$Th(SO_4)_2$	1100	1000	5.6	26	−1.9	−10, −14	−3.8	−4.2
S					1030	1200	5.5	22	−3.5	−12, −13	−2.8	−2.0

[a] Calculated ratio on basis of amount of sulfate contained in the solid thorium oxide.

[b] The pH of the centrifuged supernatant liquid averaged 0.3 pH units more basic than the slurry pH. Maximum deviations from the slurry pH were +1.7 and −0.9 pH units.

[c] Conversion factors. Type 347 stainless steel (mdd) × 0.181 = mpy.
Titanium (mdd) × 0.320 = mpy.
Zircaloy-2 (mdd) × 0.222 = mpy.
Estimated weighing precision: ±2.5 mdd.

[d] The cause for the low slurry concentration (if real) is unknown.

[e] Corresponds to approximately 0.01 mole of sulfate per liter of solution.

[f] Also approximately 19 mg of calcium per kilogram of thorium oxide.

[g] Corresponds to approximately 0.0016 mole of sulfate per liter of solution.

[h] Also less than 64 mg of calcium per kilogram of thorium oxide.

[i] Also approximately 90 mg of magnesium per kilogram of thorium oxide.

[j] Also no detectable amount of sodium associated with the thorium oxide.

[k] Corresponds to approximately 0.0045 *M* Na_2SO_4 on the basis of both sodium and sulfate analyses.

the highest level of 10,000 ppm added as thorium sulfate. A greater attack occurred under these conditions, as determined both by weight loss and by microscopic examination of the corrosion pin specimens, than under any of the other conditions. It appeared, however, that this attack was most likely due to dilute sulfuric acid, formed by the hydrolysis of the added thorium sulfate, since the pH of duplicate slurries was 2.4 and 2.6 at the end of the run. A concentration of 0.06 *M* H_2SO_4 (pH approximately 1.2) would be expected for the complete hydrolysis of all the thorium sulfate present, assuming that all the acid was in solution. These results were in accord with the observations of Ferguson and McBride,[8] who also found increased acidity at high thorium sulfate concentrations with high-temperature-calcined thoria and pronounced attack on stainless steel equipment under these conditions. The presence of 1000 ppm sulfate at a concentration of 1000 g of thorium per kilogram of water showed no effect over that observed in the absence of added sulfate. Under all conditions, titanium 75A and Zircaloy-2 remained unaffected, with weight changes generally within the estimated weighing error.

The experiment in which D-17 thorium oxide was used is summarized in Table 10.10. All slurries were readily drained from the toroids at room temperature after the run and were white-to-cream-colored. The slurries containing 1000 g of thorium per kilogram of water were very creamy and viscous and wet glass very strongly; the presence of sulfate did not affect these properties of the slurry. The presence of sulfate produced no significant change in the corrosion rate of type 347 stainless steel, titanium 75A, or Zircaloy-2. A sulfate concentration of 10,000 ppm, added as thorium sulfate, produced no such apparent increase in the corrosion rate of the type 347 stainless steel by the D-17 thoria slurry as it did with the Lindsay No. 8 slurry. However, there was considerably less free acid in the slurry of D-17 thoria than there was in the Lindsay No. 8 slurry. This was not expected, since the surface area of the D-17 thoria was more than five times greater than that of the Lindsay No. 8 thoria (Table 10.8). Thus at this highest sulfate level the D-17 slurry contained more sulfate in the solid and less sulfate and less acid in solution than did the Lindsay No. 8 slurry under similar conditions.

Of the sulfate salts added, only the sodium sulfate gave a noticeable change in slurry behavior. Slurries in both runs settled quite rapidly, except in the presence of sodium sulfate, which produced a more dispersed and slower settling slurry.

Thus these results indicate that sulfate additions to thorium oxide produced little effect on the corrosion rates of type 347 stainless steel, titanium 75A, and Zircaloy-2 under the conditions of the experiments, except as they influenced the pH of the system. Except for the improvement in dispersion effected by sodium sulfate, no other benefits of sulfate were revealed in these experiments.

10.9.3 Effect of Thoria Calcination Temperature and Particle Size

During the investigations of corrosion by circulating aqueous thoria slurries, two factors appeared to be of basic importance in the behavior of the slurry: the maximum calcination temperature of the thorium oxide and the particle size of the oxide. Experiments were initiated toward studying these two variables, and the results are summarized in this section.

Two experiments were completed, and a third is currently being analyzed. These experiments were carried out in the usual manner: the slurries were circulated in type 347 stainless steel toroids in which corrosion pin specimens of type 347 stainless steel, titanium 75A, and Zircaloy-2 were exposed. Excess oxygen was supplied by the thermal decomposition of hydrogen peroxide. The experimental conditions were the same in all cases: slurry concentrations were 1000 g of thorium per kilogram of water, temperatures were maintained near 250°C, relative velocities of 26 fps were used, and excess oxygen, at about 90 psi pressure, was present.

The thorium oxide was recalcined at temperatures up to 1200°C in small quartz evaporating dishes in a Lindberg electric muffle furnace for 5 to 6 hr. The thoria bed was less than 2 cm deep and was stirred several times during the calcination. Calcinations at 1600 and 1800°C were also carried out by the Ceramics Laboratory of the ORNL Metallurgy Division. (We are indebted to

[8] D. E. Ferguson and J. P. McBride, *ThO_2 Slurry Development: Quar. Rep. for Period Ending April 31, 1955*, ORNL CF-55-5-198, p 20 (May 20, 1955).

TABLE 10.10. EFFECT OF SULFATE ON THE BEHAVIOR OF CIRCULATING AQUEOUS THORIUM OXIDE SLURRIES PREPARED FROM D-17 THORIUM OXIDE

Temperature: 253 ± 5°C
Relative velocity: 26 fps
Duration of test: 145 hr

Toroid	Nominal Conditions				Chemical Analysis				Corrosion Rates (mdd)[c]			
	g of Th per kg of H_2O	O_2 at 250°C (psi)	mg of SO_4 per kg of ThO_2	Form in Which Sulfate Was Added	g of Th per kg of H_2O	mg of SO_4 per kg of ThO_2[a]	Slurry pH[b]	Solution (mg of SO_4 per liter)	Type 347 Stainless Steel: Toroid, As-Run	Type 347 Stainless Steel: Defilmed Pins	Titanium Scrubbed Pins	Zircaloy-2 Scrubbed Pins
A	500	100		None added	500	<270	6.5	<1	−2.4	−4.6, −4.7	+3.8	+1.2
K					520	400	6.5	<10	−2.0	−8.2, −9.9	+0.2	+0.6
C	500	100	10,000	$Th(SO_4)_2$	520	10,000	3.8	30	−0.8	−0.5, −2.6	+1.2	+1.1
M					520	10,000	3.9	40	−0.7	−3.2, −6.6	−0.9	+0.9
D	500	100	1,000	$Th(SO_4)_2$	500	1,500	5.8	<1	−2.0	−6.0, −7.0	−0.7	+0.6
N					520	1,400	6.2	<10	−1.6	−7.6, −7.9	+0.1	−0.2
E	500	100	100	$Th(SO_4)_2$	500	1,500	6.2	<1	−1.7	−5.4, −7.8	+0.8	+0.7
O					550	300	6.8	<10	−2.0	−6.1, −7.6	+1.3	−1.5
F	500	100	1,000	$CuSO_4$	490	1,500[d]		10[d]	−2.5	−6.8, −7.0	+2.4	−0.2
P					510	1,100[d]	6.4	<10[d]	−1.9	−7.1, −9.0	−1.5	+2.7
G	500	100	1,000	$MgSO_4$	490	1,300[e]	6.8	40[f]	−2.0	−2.0, −6.0	+1.1	−0.2
Q					550	820[e]	6.8	70[g]	−2.3	−4.4, −7.8	−3.7	−1.6
H	500	100	1,000	Na_2SO_4	540	680[h]	7.0	330[i]	−5.6	−6.8, −7.1	−0.1	+0.9
R					230	950[j]	7.0	320[i]	−3.0	−15, −15	−2.7	−3.2
J	500	N_2	1,000	$Th(SO_4)_2$	520	1,200	6.7	<10	−1.2	−8.7, −9.4	+1.1	−1.5
T					510	1,600	7.4	<10	−0.2	−6.4, −8.8	0.0	−0.6
B	1000	100		None added	1000	340	6.6	<1	−2.7	−7.3, −10	+1.7	+1.3
L					1040	250	6.4	<1	−3.4	−11, −17	−2.8	−0.6
I	1000	100	1,000	$Th(SO_4)_2$	1060	1,040	6.5		−2.2	−4.7, −11	+0.9	−0.2
S					1120	740	6.1	<10	−2.8	−15, −18	−1.9	−3.2

[a] Calculated ratio on basis of amount of sulfate contained in the solid thorium oxide.

[b] The pH of the centrifuged supernatant liquid averaged 0.3 pH units more basic than the slurry pH. Maximum deviations from the slurry pH were +1.7 and −0.9 pH units.

[c] Conversion factors: Type 347 stainless steel (mdd) × 0.181 = mpy.
Titanium (mdd) × 0.320 = mpy.
Zircaloy-2 (mdd) × 0.222 = mpy.
Estimated weighing precision: ±2.5 mdd.

[d] The cause for the low slurry concentration (if real) is unknown.

[e] Corresponds to approximately 0.01 mole of sulfate per liter of solution.

[f] Also approximately 19 mg of calcium per kilogram of thorium oxide.

[g] Corresponds to approximately 0.0016 mole of sulfate per liter of solution.

[h] Also less than 64 mg of calcium per kilogram of thorium oxide.

[i] Also approximately 90 mg of magnesium per kilogram of thorium oxide.

[j] Also no detectable amount of sodium associated with the thorium oxide.

C. E. Curtis of the Ceramics Laboratory for carrying out these calcinations and ball-milling the oxides.)

The particle-size distribution of the thoria was determined by gravitational sedimentation in 0.006 M $Na_4P_2O_7$ by using the neutron activation technique (performed by the Activation Analysis Group of the Analytical Chemistry Division). Weight fractions of the sample in a given size range may be computed from the amount settling at a given rate. Stokes' law is assumed, the sizes being those of spheres of equivalent settling rate.

The first experiment compared the effect of calcination temperature on two different oxides, D-17 and Ames (Ames Laboratory oxalate precipitated, calcined above 650°C; see also Table 10.8). These results are summarized in Table 10.11.

The second completed experiment investigated the effect of both calcination temperature and particle size of the thorium oxide; these results are summarized in Table 10.12. The thoria used in this experiment was basically D-17, the ORNL Thorex product precipitated at 40°C as the oxalate and calcined in stages, reaching a maximum temperature of 650°C (Sec. 14.4). Some of this material was recalcined at 1000°C to yield a product which had been calcined at a higher temperature than the original oxide and yet had approximately the same particle-size distribution.

In order to study the effect of the particle size of the thorium oxide on the slurry behavior, material identified as CS-4 was also used. This oxide was the pumped D-17 slurry resulting from the initial slurry run in the 100A loop CS, which was operated for 200 hr at a slurry concentration of 285 g of thorium per kilogram of water (charged as D-17 thorium oxide) at 250°C with 1000 ppm oxygen. Such pumping has been shown to result in smaller sized thoria particles. Similar production of small-sized thoria particles in the toroids has also been observed.

A portion of this pumped D-17 slurry (CS-4) was also recalcined at 1000°C to provide thoria of relatively small particle size and of higher maximum calcination temperature. Some sintering occurred during this process, as evidenced by the change in particle-size distribution (Table 10.12).

A third experiment has just been completed, and, as yet, not all analyses have been received; the results so far available are summarized in Table 10.13. This experiment was designed to study the effect of the calcination temperature of the thorium oxide on the corrosion-erosion of circulating aqueous thoria slurries. D-17 thorium oxides having maximum calcination temperatures of 650 (normal oxide), 800, 1000, and 1600°C were employed. In order to reduce the particle size, the oxide, which had been calcined at 1600°C (for 1 hr), was also ball-milled for 70 hr as an aqueous suspension, with the use of aluminum oxide balls.

The results summarized in Tables 10.11, 10.12, and 10.13 showed three important facts:

1. Increased attack on type 347 stainless steel, titanium 75A, and Zircaloy-2 by circulating aqueous thoria slurries was obtained as the calcination temperature of the thorium oxide was increased.

2. This attack was not solely governed by the calcination temperature of the thoria but depended equally as well on the particle size of the oxide. Thus thorium oxide calcined at 1600°C but subsequently treated in a ball mill to reduce the particle size gave a slurry that showed a lower average corrosion rate for the type 347 stainless steel, titanium, and Zircaloy-2 than the rate shown by a slurry of thorium oxide which had been calcined at only 650°C.

However, slurries of the higher calcined oxides produced localized (impingement) attack at the end of the corrosion pins closest to the outside toroid wall. This attack accounted for much of the weight loss experienced by the pin. Since it was precisely at this location where the heavier solids would be concentrated because of the centrifugal forces created in the eccentric rotation of the toroid, it is believed that removal of large-sized particles from the thoria would eliminate the attack entirely. Interestingly, it has been estimated[9] that, for the conditions existing in the toroids, thorium oxide particles of less than 3 μ in diameter would follow liquid flow lines and so would not strike the surface of the corrosion pins.

3. Calcination of thorium oxide at temperatures above 650°C imparted certain desirable properties to the oxide, such as greater fluidity at room temperature after circulation. This effect was most noticeable with the 1600°C thoria and to a somewhat lesser extent with the small-sized oxide calcined at 1000°C.

[9]D. G. Thomas, *Comments on the Erosiveness of ThO_2 Slurries*, ORNL CF-55-4-36 (April 5, 1955).

Thus the results presented in this section indicate that thorium oxide calcined at temperatures greater than 650°C improved the room-temperature handling properties of circulated thoria slurries. In addition, the extent of attack by thorium oxide slurries was not solely determined by the maximum calcination temperature of the thoria but also depended strongly on the particle size of the oxide. These observations support the view stated earlier that the particle size and the calcination temperature of the thorium oxide were basic factors in the behavior of thoria slurries.

TABLE 10.11. EFFECT OF CALCINATION TEMPERATURE OF THORIUM OXIDE ON THE BEHAVIOR OF AQUEOUS THORIA SLURRIES CIRCULATED IN STAINLESS STEEL TOROIDS

Slurry concentration: 1000 g of thorium per kilogram of water
Relative velocity: 26 fps
Temperature: 243 to 269°C
Oxygen pressure: 90 psi (at 250°C)
Duration of test: 162 hr

	Toroid			
	I	J	K	L
Thorium oxide	D-17[a]	D-17-1000	Ames[a]	Ames-1000
Treatment	As received	D-17 calcined 5 hr at 1000°C	As received	Ames calcined 5 hr at 1000°C
Particle-size distribution,[b] wt %				
0 to 1 μ	23	[c]	7	6
1 to 3 μ	36		15	13
3 to 10 μ	26		43	40
Greater than 10 μ	15		35	41
Carbon, mg per g of thorium	1.84	0.25		
Sulfate, mg per g of thorium			7.05	1.66
Per cent thorium drained at room temperature after run	71	85	56	73
Per cent thorium in first water wash	23	14	24	19
Slurry appearance after run	Creamy, thick	Brown, thick	White, thick	Gray, thick
Pin corrosion rate, average (mdd)[d]				
Type 347 stainless steel[e]	−11, −16 −16	−19, −20 −21	−18, −21 −21, −22	−54, −57 −58, −66
Toroid corrosion rate, (mdd)[d]				
Type 347 stainless steel[f]	−6.6	−8.5	−4.2	−24

[a] Characterized in Table 10.8.
[b] As determined by gravitational sedimentation in 0.005 *M* $Na_4P_2O_7$. Stokes' law assumed.
[c] Other preparations (see Table 10.12) showed little change in the particle-size distribution of D-17 when recalcined at 1000°C.
[d] Conversion factor; type 347 stainless steel (mdd) × 0.181 = mpy.
[e] Defilmed.
[f] As run (not defilmed).

TABLE 10.12. EFFECT OF CALCINATION TEMPERATURE AND PARTICLE SIZE OF THORIUM OXIDE ON THE BEHAVIOR OF AQUEOUS THORIA SLURRIES CIRCULATED IN STAINLESS STEEL TOROIDS

Slurry concentration: 1000 g of thorium per kilogram of water
Relative velocity: 26 fps
Temperature: 247 to 255°C
Oxygen pressure: 90 psi (at 250°C)
Duration of test: 208 hr

	Toroid			
	I	J	K	L
Thorium oxide	D-17[a]	D-17-1000	CS-4	CS-4-1000
Treatment	As received	D-17 calcined 6 hr at 1000°C	D-17 circulated in 100A loop CS	CS-4 calcined 6 hr at 1000°C
Particle-size distribution,[b] wt %				
0 to 1 μ	23	20	87	70
1 to 3 μ	36	40	9	15
3 to 10 μ	26	28	2	8
Greater than 10 μ	15	12	2	7
Per cent thorium drained at room temperature after run	12	86	72	91
Per cent thorium in water wash				
First wash	26	17	17	9
Second wash	17	3	1	0.2
Third wash	16	1		
Slurry appearance after run	White, thick	Black, thick	White, thick	Light gray, less viscous
Pin corrosion rate, average (mdd)[c]				
Type 347 stainless steel[d]	−64[e]	−177, −161	−10.0, −10.5	−16, −18
Titanium 75A[f]	−5.4[g]	−30	−4.6	−15
Zircaloy-2[f]	−6.7[h]	−7.0	−1.7	−1.8
Toroid corrosion, mdd[c]				
Type 347 stainless steel[i]	−3.8	−31	−1.6	−3.2

[a] Characterized in Table 10.8.
[b] As determined by gravitational sedimentation in 0.005 *M* $Na_4P_2O_7$. Stokes' law assumed.
[c] Conversion factors: Type 347 stainless steel (mdd) × 0.181 = mpy.
Titanium (mdd) × 0.320 = mpy.
Zircaloy-2 (mdd) × 0.222 = mpy.
[d] Defilmed.
[e] Single value only. For type 347 stainless steel in previous runs, 13 values averaged −16 mdd (minimum −11 mdd, maximum −26 mdd).
[f] Scrubbed.
[g] Three previous runs gave +0.6, −5.3, and −2.2 mdd.
[h] Three previous runs gave −3.7, −5.1, and −8.8 mdd.
[i] As run (not defilmed).

TABLE 10.13. EFFECT OF CALCINATION TEMPERATURE AND PARTICLE SIZE OF THORIUM OXIDE ON THE BEHAVIOR OF AQUEOUS THORIA SLURRIES CIRCULATED IN STAINLESS STEEL TOROIDS

Slurry concentration: 1000 g of thorium per kilogram of water
Relative velocity: 26 fps
Temperature: 249 to 271°C
Oxygen pressure: 90 psi (at 250°C)
Duration of test: 241 hr

	Toroid			
	I	J	K	L
Thorium oxide	D-17[a]	D-17-800	D-17-1000	D-17-1600
Treatment	As received (650°C calcined)	D-17 calcined 4.5 hr at 800°C	D-17 calcined 6 hr at 1000°C	D-17 calcined 1 hr at 1600°C, ball-milled in distilled water
Particle-size distribution,[b] wt %				
0 to 1 μ	23		20	45
1 to 3 μ	36		40	44
3 to 10 μ	26		28	8
Greater than 10 μ	15		12	3
Per cent thorium drained at room temperature after run	0	47	31	~80
Per cent thorium in water wash				
First wash	33	48	61	
Second wash	7	2	5	
Third wash	2	1	4	
Fourth wash	1		1	
Slurry appearance after run	White, very thick	White, thick	Black, thick	White, less viscous
Pin corrosion rate, average mdd[c]				
Type 347 stainless steel[d]	−49	−43, −44	−196, −202	−25, −47
Titanium 75A[e]	−11	−23	−39	−4.6
Zircaloy-2[e]	−6.1	−8.7	−9.1	0.0
Toroid corrosion, mdd[c]				
Type 347 stainless steel[f]	−1.8	−4.4	−56	[g]

[a] Characterized in Table 10.8.
[b] As determined by gravitational sedimentation in 0.005 *M* $Na_4P_2O_7$. Stokes' law assumed.
[c] Conversion factors: Type 347 stainless steel (mdd) × 0.181 = mpy.
Titanium (mdd) × 0.320 = mpy.
Zircaloy-2 (mdd) × 0.222 = mpy.
[d] Defilmed.
[e] Scrubbed.
[f] As run (not defilmed).
[g] Data not yet available.

Part IV

ENGINEERING DEVELOPMENT

J. A. Lane

11. DEVELOPMENT OF FUEL-SYSTEM COMPONENTS

C. B. Graham

J. S. Culver
L. F. Goode
B. A. Hannaford
P. H. Harley
I. K. Namba
W. L. Ross
J. G. Smith
I. Spiewak
D. S. Toomb
L. R. Weissert[1]

11.1 DEVELOPMENT OF LARGE HEAT EXCHANGERS

The status of the Foster Wheeler Corp.–ORNL heat exchanger development program is summarized below.

11.1.1 50-Mw Heat Exchanger and Gas Cooler Designs

Designs were completed and a final report covering the work is being written. All the several basic designs evolved and previously reported adhered to the specified use of U-tubes as in the HRT heat exchanger. In view of studies subsequently made on exchangers ranging in capacities up to 300 Mw, it now appears desirable to investigate a 50-Mw exchanger employing the straight-through type of design.

11.1.2 Large Heat Exchanger Design

The design studies carried out by the Foster Wheeler Corp. indicate that exchangers up to 300-Mw capacity are feasible, based on either stainless-clad carbon steel or all-stainless-steel designs. All the larger capacity heat exchanger designs are of the straight-through, separate steam drum type because of size and material limitations on such items as tube sheets and exchanger shells. The most promising design appeared to be that using an all-stainless-steel construction for the heat exchanger and carbon steel for the steam drum. The transition between stainless steel and carbon steel would probably take place in the connecting risers and downcomers. The stainless steel exchanger design eases the problem of differential thermal expansion that exists in an exchanger containing stainless steel tubes and a carbon steel exchanger shell. The heat exchanger heads would be attached by welding, with tube sheet access provided either through the flow nozzles or suitable hand holes.

[1]On loan from The Babcock & Wilcox Co.

11.1.3 Tube Joint Welding Development

A method of welding tubes to a tube sheet was developed by the Foster Wheeler Corp. in conjunction with the fabrication of heat exchangers for the HRT. The method, described below, proved to be successful in laboratory tests and was applied to two HRT heat exchangers. A report covering this work to date is being compiled. The procedure is for a tungsten-arc, inert-gas-shielded weld and uses a Linde Heliarc torch mounted in a rotating jig as shown in Fig. 11.1. The rate of travel is controlled manually. A J-type of joint preparation is used, and the fillet weld is deposited in two separate passes. Welding wire is formed into rings which are preplaced. The welding is initiated with a high-frequency starter and progresses through an arc of approximately 400 deg (1.1 revolutions), at which point the welding arc is tapered off by use of a crater eliminator. Between passes the weld is thoroughly cleaned and the crater area ground to sound metal. The copper pilot inserted in the tube facilitates heat removal from the tube wall. Figures 11.2 and 11.3 show the tube joint details and sample welds.

Although the above welding procedure proved successful on a laboratory scale, first-pass crater cracking appeared when the procedure was applied to the first HRT heat exchanger. This difficulty was completely eliminated on the second heat exchanger by the manual addition of bare filler wire to the crater region of the first pass as the arc was being tapered. A problem, not recognized until Boroscopic examination was undertaken during the tube joint welding of the second exchanger, was that of occasional melt-through of the tube wall in the weld area. Sample welds containing melt-through were examined and found to be structurally sound, containing no microfissures or voids. Although the weld fusion line extended through to the inside of the tube, the ferritic content of the deposit was low and well within known corrosion requirements. Several fissures, however,

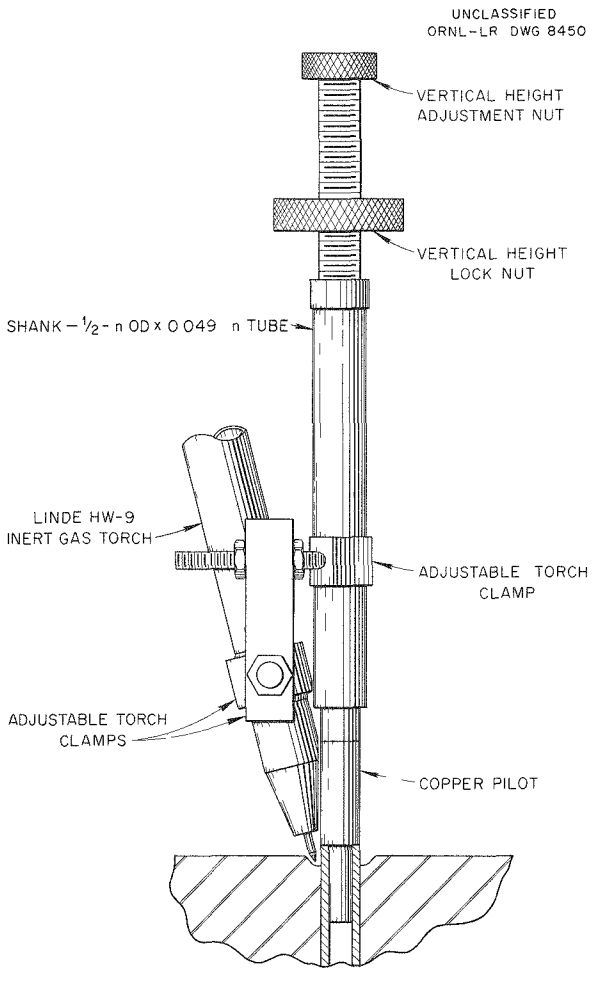

Fig. 11.1. Rotating Heliarc Torch Jig.

were found in the melt-through region when the exchangers were fabricated. They were repaired, and methods of eliminating this trouble in the future are being investigated.

11.1.4 Tube Inspection Development

Because a 300-Mw heat exchanger would carry up to 300,000 ft of small-diameter tubing, the need for thorough and economical tubing inspection becomes apparent. Standard mill inspection has been found to be inadequate.

In a study of nondestructive tubing inspection methods and equipment, an ultrasonic reflectoscope (Sperry Products, Inc.), a magnetic eddy current Probolog (Shell Development Co.), a high-frequency flaw detector (Magnetic Analysis Corp.), and x-ray fluoroscopic television equipment (RCA)

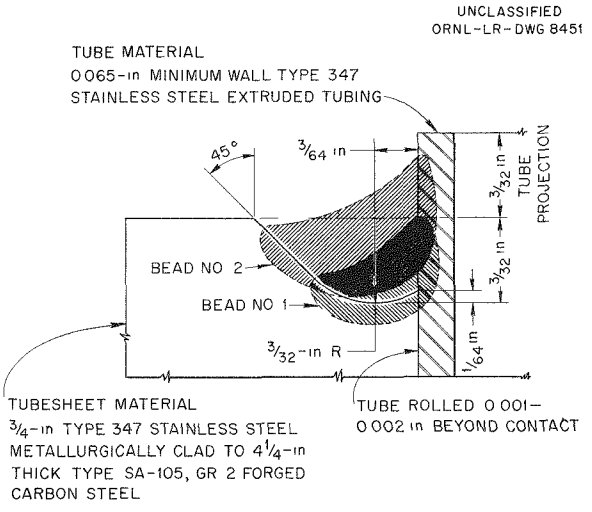

BEAD NO	TUNGSTEN DIA (in)	ARGON (cfh)	AMPS	VOLTS	WIRE DIA (in)	FERRITE (%)
1	1/16	15	72–75	10–12	1/16	12–14
2	1/16	15	82–85	10–12	3/32	5–6

Fig. 11.2. Tube-Joint Details.

have been investigated. In evaluating the four devices, the Shell equipment was not considered suitable for our application, the RCA equipment was not sufficiently developed, and the Sperry and Magnetic Analysis equipment were relatively untried in small-diameter tube-inspection applications. HRT heat exchanger tubing was used for a controlled evaluation of the reflectoscope and Magnetic Analysis equipment. The tubing rounds, which were 1-in. OD × 1.20-in. wall thickness before drawing to final size, were subjected to reflectoscope examination, but, since this method had not yet been fully developed, only eccentricity in the tube rounds was detected. All rounds passing the reflectoscope examination and two reflectoscope rejected rounds were redrawn into finished ⅜-in.-dia × 0.065-in. minimum wall tubing and processed through the Magnetic Analysis equipment. A preliminary evaluation of the Magnetic Analysis inspection results revealed three major flaws in the tubing as reported previously.[2] In all, out of 544 tubes, 17 were rejected by the Magnetic Analysis equipment, including one from the reflectoscope rejected stock. These tubes were

[2] L. F. Goode and W. L. Ross, *HRP Quar. Prog. Rep. April 30, 1955*, ORNL-1895, p 134.

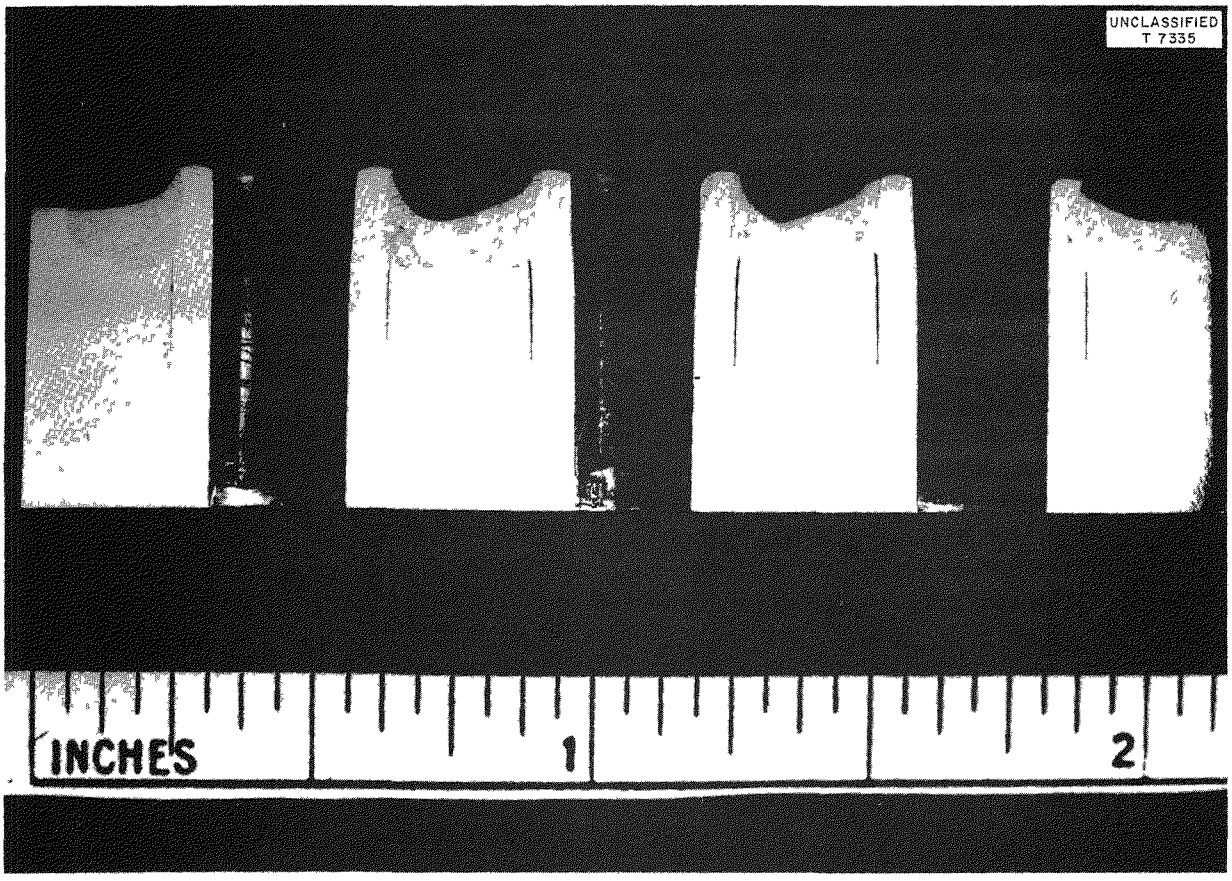

Fig. 11.3. Sample Tube-Joint Welds.

reinspected by the Magnetic Analysis equipment and sent to General Electric Company for reflectoscope examination. Test results will be correlated, and the tubing will be metallographically examined by ORNL.

To explore the minimum size defect detectable by the Magnetic Analysis equipment, a sound piece of tube containing an inside-diameter notch and a similar outside-diameter notch with depths approximately 3% of the wall thickness was used. Both these manufactured defects were readily detected. In comparing the reflectoscope and the Magnetic Analysis unit for the above application, the latter demonstrated greater operational simplicity and much higher testing speeds with comparable sensitivity. Inspection speeds of the order of 200 fpm are obtainable, and, as no direct contact through the use of a liquid coupling medium is required between the inspected piece and the inspection apparatus, as is the case with the reflectoscope, cleanup is eliminated. The Magnetic Analysis inspection becomes, within limits, more sensitive with decreasing tube diameters, whereas with the reflectoscope the difficulty of interpretation of the inspection increases substantially as the diameter of the inspected piece decreases. The flaws identified thus far, two of which are shown in Figs. 11.4 through 11.7, appear to have been produced in the redrawing operations and therefore require that ultimate inspection be on the finished product rather than at an intermediate point in the drawing process.

11.2 RECOMBINER DEVELOPMENT

After modification of the electrolytic cells to dilute the hydrogen and oxygen with steam, no further explosions occurred. Excessive caustic entrainment from the cells to the recombiner was found. It is believed that this difficulty can be

remedied with the use of wire mesh entrainment separators.

A more serious difficulty appears to be the occurrence of cracks in flanges and welds operated in contact with the hot vapors. These cracks seem to be caused by stress corrosion. In the next series of runs an attempt will be made to eliminate the chloride content in the charge to the loop to ascertain whether the stress corrosion is typical of the steam-hydrogen-oxygen system at high temperatures.

The thermal convection recombiner[3] was completed and preliminary testing carried out at 100 psia. The results indicated that the unit will work, but more quantitative information is necessary to evaluate its capacity and reliability.

11.3 DUMP-VALVE TEST LOOP

The construction of the dump-valve test loop[4] was completed, and preliminary runs were made

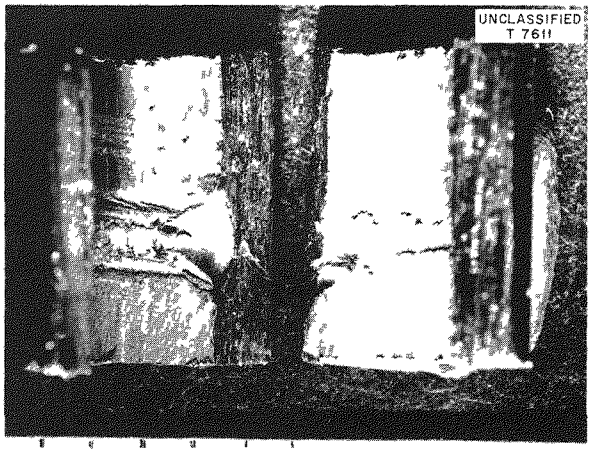

Fig. 11.4. Split Section of Defective Heat-Exchanger Tube. The $\frac{3}{8}$-in.-dia tubing was cut to show circumferential gouge in inside surface. Flaw was detected by Magnetic Analysis inspection and confirmed by x ray. 8X. Reduced 33%.

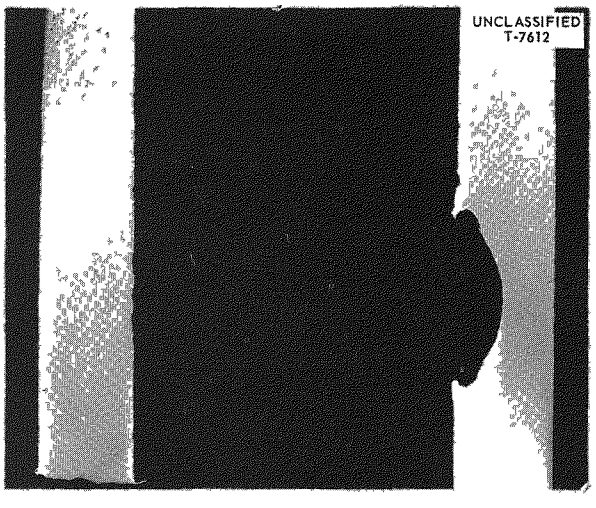

Fig. 11.5. Mounted Half of Split Section Shown in Fig. 11.4. 10X. Reduced 27%.

[3] D. M. Eissenberg *et al.*, *HRP Quar. Prog. Rep. Jan. 31, 1955*, ORNL-1853, p 135–136.

[4] J. G. Smith, I. Spiewak, and D. S. Toomb, Jr., *HRP Quar. Prog. Rep. Oct. 31, 1954*, ORNL-1813, p 109–110.

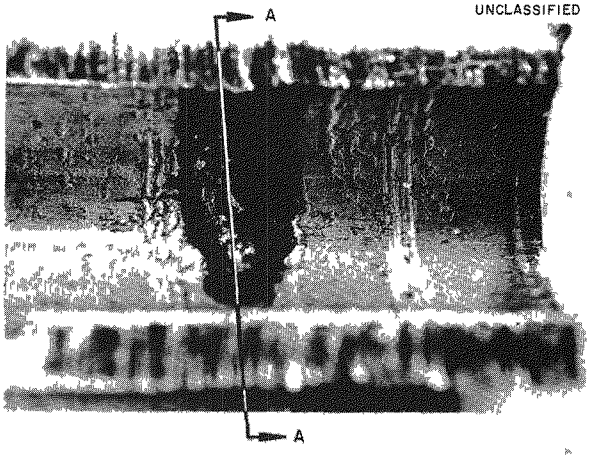

Fig. 11.6. Inside-Diameter Flaw in Heat-Exchanger Tube. Flaw was detected by Magnetic Analysis inspection and confirmed by x ray. 8X. Reduced 33%.

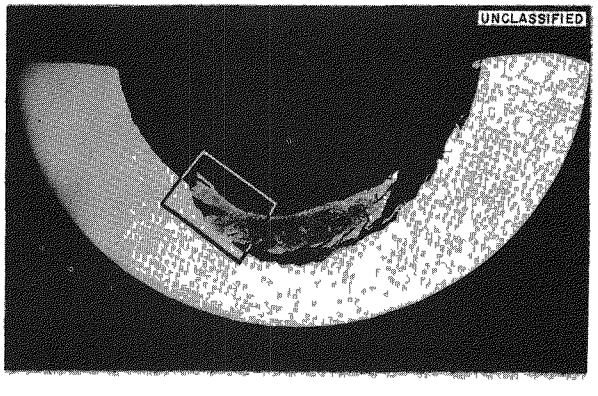

Fig. 11.7. Mounted Cross Section of Flaw Shown in Fig. 11.6. 12X. Reduced 35%.

with water. Only one problem remains to be solved before the system is ready for tests with uranyl sulfate solutions. The pressure transmitter, which opens the test valve at 2000 psi and closes it at 150 psi for the next cycle, has repeatedly shifted its zero, disrupting the cycle. A snubber, which protects the instrument, has been installed. If this does not work, some other type of control to open and close the test valve will have to be installed.

The first tests were made with the use of an HRT prototype dump valve.

11.4 SMALL REACTOR COMPONENTS

11.4.1 20-cfm Canned Rotor Blower

A 20-cfm gas circulator, suitable for operation in the HRT (or larger reactors) to supply forced circulation in high-pressure recombiner systems, is being designed in detail by the Allis-Chalmers Mfg. Co. A layout drawing, bill of materials, and fit dimensions were received and are being studied for possible revisions. After drawing approval, Allis-Chalmers will proceed with detailed drawings and fabrication of the unit.

11.4.2 ORNL Gas Circulator

A 5-gpm ORNL pump, converted for use as a gas circulator, operated on saturated steam at approximately 110 psi for 5600 hr. It has accumulated about 4100 hr of operation since the stator was repaired after an electrical failure.

11.4.3 Small Circulating Pumps

The 2000-psi, 5-gpm, canned-rotor pump has accumulated over 1500 hr of operation at 300°C with water. Operation was interrupted repeatedly by leaks in the test loop and in the gasket joint of the pump flange. Examination of pump parts has shown no excessive wear, malfunction, or corrosion.

A 1000-psi, 5-gpm, ORNL canned-rotor pump has operated about 6900 hr at 250°C with water. It has accumulated about 2000 hr since the stator was repaired after an electrical failure.

In order to increase stator life and pump reliability, one ORNL, 5-gpm, canned-rotor pump was rewired with the windings in series rather than in parallel. In effect, this makes significant reductions in input power and current at a slight sacrifice in developed head. The pump has accumulated 2400 hr of operation and the test is continuing.

11.5 4000-gpm LOOP[5]

Circulation in the 4000-gpm loop was started on April 20 with distilled water, and UO_2SO_4 was added until the concentration reached 1 g/liter. After 50 hr of operation, the packing in the Milton Roy feed pump was leaking so badly that the loop was shut down, drained, and flushed with trisodium phosphate and dilute HNO_3.

Scott and Williams feed pumps were installed in place of the Milton Roy pump, and the necessary modifications to the piping are being made, after which the loop will again be started with UO_2SO_4 solution.

11.6 TITANIUM PROGRAM

In order to take advantage of the corrosion resistance of titanium and yet keep the cost of equipment to a minimum, a program was initiated to study titanium-lined or -clad carbon steel for such components as piping, heat exchangers, etc.

A preliminary inquiry was sent to several industrial firms for proposals on test lengths of 20-in. pipe, 3½-in. pipe, and a small heat exchanger. Replies indicating interest in part or all of the program were received from eight firms. The proposals varied from fixed price bids on fabrication only, with no guarantee of performance, to extensive cost-plus development programs involving metallurgical, welding, and cladding studies.

At present, the Lukens Steel Company and the Chicago Bridge & Iron Co. have developed methods of cladding titanium on steel; however, neither firm feels that its method has been developed sufficiently to make fabricated structures from the composite material. Chicago Bridge & Iron Co. uses the Horton clad process, which is a vacuum brazing method using silver alloys as the brazing material, and has produced a ductile bond with high shear strength, on a laboratory basis. This company is working steadily on its method and hopes to have a commercial product within a year.

[5] J. S. Culver and C. W. Keller, *HRP Quar. Prog. Rep. Nov. 15, 1951*, ORNL-1221, p 47.

12. DEVELOPMENT OF BLANKET-SYSTEM COMPONENTS

R. N. Lyon

R. V. Bailey[1]
P. R. Crowley
D. G. Davis
R. B. Gallaher
W. Q. Hullings
A. S. Kitzes
B. A. Kress
C. G. Lawson
L. F. Parsly
J. D. Perret
L. E. McTaggart
R. H. Nimmo
M. Richardson
J. A. Russell
D. S. Toomb
P. C. Zmola

12.1 SLURRY CIRCULATION STUDIES

A. S. Kitzes R. B. Gallaher

12.1.1 100A Loops

The investigation of the attack on type 347 stainless steel, zirconium, and titanium by circulating aqueous thoria slurries in loop S was continued. A program was initiated to determine quantitatively the effect of circulation temperature and slurry concentration on the resistance of these three metals to the attack of thorium oxide slurries in the ranges pertinent to HRT operation. Previous studies[2] indicated that the attack appears to be controlled by the rate of formation of a protective oxide film on these metals. Qualitatively, it was found that the attack on these three metals was less severe at 300°C than at 250°C, all other conditions being the same.

Slurries prepared from oxide calcined at 800°C and containing 500 or 1000 g of thorium per kilogram of water are being circulated for two-week periods at 250, 275, and 300°C with oxygen additions. Before the slurry is loaded into the loop, thorium sulfate (1000 ppm) is added to the oxide and the mixture is agitated for 24 hr to lower the pH of the slurry and partially disperse the oxide agglomerates.

The rate of attack is measured by determining the weight changes in specimens of the three metals suspended axially by means of two spiders through the throat of a venturi.

A summary report will be issued at the termination of the program, which is now two-thirds complete.

12.1.2 5-gpm Loops

Circulation studies in the 5-gpm loops were temporarily suspended because of excessive wear on the thrust faces of the Graphitar pump bearings. In order to increase the life of the bearings, the stator cans were redesigned so that the thrust load on the Graphitar bearings can be checked and set for a given value. Also, the rotors were modified slightly to permit checking the hydrodynamic balance of the pump.

Circulation studies will be resumed in the 5-gpm loops as soon as the new cans have been installed and the balancing jig has been tested.

12.2 SLURRY COMPONENT DEVELOPMENT

W. Q. Hullings J. D. Perret
A. S. Kitzes M. Richardson
B. A. Kress J. A. Russell
C. G. Lawson D. S. Toomb

12.2.1 Westinghouse 200A Slurry Pump

W. Q. Hullings

The Westinghouse 200A pump, designed specifically to pump slurries, operated satisfactorily at 300°C for 234 hr with a slurry containing 500 g of thorium per kilogram of H_2O. At the end of the run, the pump was disassembled and inspected. Although the impeller lost 9.5 g in weight, there were no visible signs of wear, and it was coated with a thick, golden-brown oxide film – typical of slurry runs in which oxygen is present. Both the radial and thrust bearings showed no wear, indicating that the radial vanes on the back of the impeller and the water injection through the motor end of the pump were effective in keeping the bearings free of solids.

Present plans include a long-term run in which additional operational data will be accumulated. A slurry containing 1000 g of thorium per kilogram of H_2O will be circulated at 300°C for six months or more. In addition to accumulating service time on the pump, gross corrosion-abrasion rates for

[1] Tulane University.

[2] R. N. Lyon *et al.*, *HRP Quar. Prog. Rep. April 30, 1955*, ORNL-1895, p 137.

stainless steel will be determined, and the problems of maintaining concentration during prolonged circulation at elevated temperatures will be studied.

12.2.2 Dump Tank–Evaporator Tests

C. G. Lawson J. D. Perret
M. Richardson

The short-term slurry tests in the 14- and 24-in. mockups of the HRT solution dump tanks were completed. At a concentration of 500 g of thorium per kilogram of H_2O, a slurry could not be circulated by boiling convection without a decrease in concentration. Approximately 20 to 30% of the solids settled out during circulation and could not be resuspended.

Several modifications to the system were tried but with no success. They were: increasing the number of baffles from four to eight, doubling the number of thermal cycle legs, removing the baffles, varying the steam pressure on the thermal cycle leg from 40 to 80 psi, using 950°C oxide instead of 650°C pumped material, using an under-belly steam jacket in addition to the thermal cycle leg, using external vibration, and increasing the diameter of the downcomer legs.

Modifications to the present dump tanks and other dump tank systems are still being surveyed in small steel prototypes. One system which looks promising is being investigated further; in this system, a stainless steel, Micro Metallic Corp. filter is welded to the bottom of the dump tank to form a steam chest. At a pressure of 2 to 3 psi, sufficient steam passes through the filter plate to keep the solids suspended as they are circulated by boiling convection. A 24-hr run was completed in which a slurry containing 1000 g of thorium per kilogram of H_2O was circulated continually without a change in concentration. Calgon was added to minimize foaming, but some other method would be required to reduce foaming in a reactor blanket dump tank.

12.2.3 Pressurizer Studies

B. A. Kress

In the high-temperature loop studies, variations in concentrations are often observed. These variations in concentration have been shown to be dependent upon the steam withdrawal rate.[3] In the system previously described,[4] almost one-half of the fluid in the loop was held in a relatively stagnant condition in the pressurizer. However, there was a net vertical upward flow of water as a result of the removal of steam from the top of the pressurizer to provide water for flushing the pump bearings. In Table 12.1 it can be seen that the concentration of solids in the circulating loop and the level of solids in the pressurizer should be dependent upon the rate of steam removal when the main circulating stream enters the bottom of the pressurizer.

By installing a bypass stream from the main circulating loop to the pressurizer about 1 ft below the normal liquid level,[5] in addition to normal entry at the bottom of the pressurizer, uniform distribution of the solids could be maintained between the pressurizer and the main circulating loop. In addition, the level of solids in the pressurizer was no longer dependent upon the steam removal rate.

During run T-54, the bypass stream entered the pressurizer 37 in. above the main circulating loop.

[3] *Ibid.*, p 153.

[4] R. N. Lyon *et al.*, *HRP Quar. Prog. Rep. Oct. 31, 1953*, ORNL-1658, p 127.

[5] R. N. Lyon *et al.*, *HRP Quar. Prog. Rep. Jan. 31, 1955*, ORNL-1853, p 149.

TABLE 12.1 ACCUMULATION OF SOLIDS IN PRESSURIZER AS A FUNCTION OF STEAM WITHDRAWAL RATE

	Bypass Stream			No Bypass Stream		
	Steam Withdrawal Rate (lb/hr)			Steam Withdrawal Rate (lb/hr)		
	2	4	5.5	4	6	8.5
Concentration of thorium circulated, as sampled (g of Th per kg of H_2O)	378	373		514	411	353
Height of solids in pressurizer above circulating stream (in.)	43	43	43	27	33	43

Data in Table 12.1 indicate that, even with the bypass stream, solids accumulated in the pressurizer 6 in. above the bypass stream, probably as a result of eddying of the entering stream. The concentration of solids in the pressurizer and the main circulating stream was, however, the same and appeared to be independent of the steam removal rate.

It may be concluded from these tests that the concentration of the slurry in the circulating part of the loop can be maintained either by using a bypass stream to the pressurizer or by controlling the steam withdrawal rate when no bypass stream is in the system. In either case, sufficient water to flush the pump bearing could be obtained by condensing steam from the pressurizer. Steam rates as high as 8 lb/hr were obtained without entraining solids in the condensate stream.

12.3 RHEOLOGICAL PROPERTIES OF SLURRY SYSTEMS

P. R. Crowley

12.3.1 Characterization of ThO_2 Slurries

A relationship between the yield stress at 25°C and the concentration of a slurry was developed which can be used to classify slurry preparations as to their rheological properties. The relationship is shown in Eq. 1 and plotted in Fig. 12.1:

$$(1) \qquad \tau_y = X\left[\left(\frac{5120}{C} + 0.6\right)^{1/3} - 1\right]^{-5.35},$$

where

X = characterization number, a property which is essentially independent of concentration,

τ_y = yield stress, lb/ft^2,

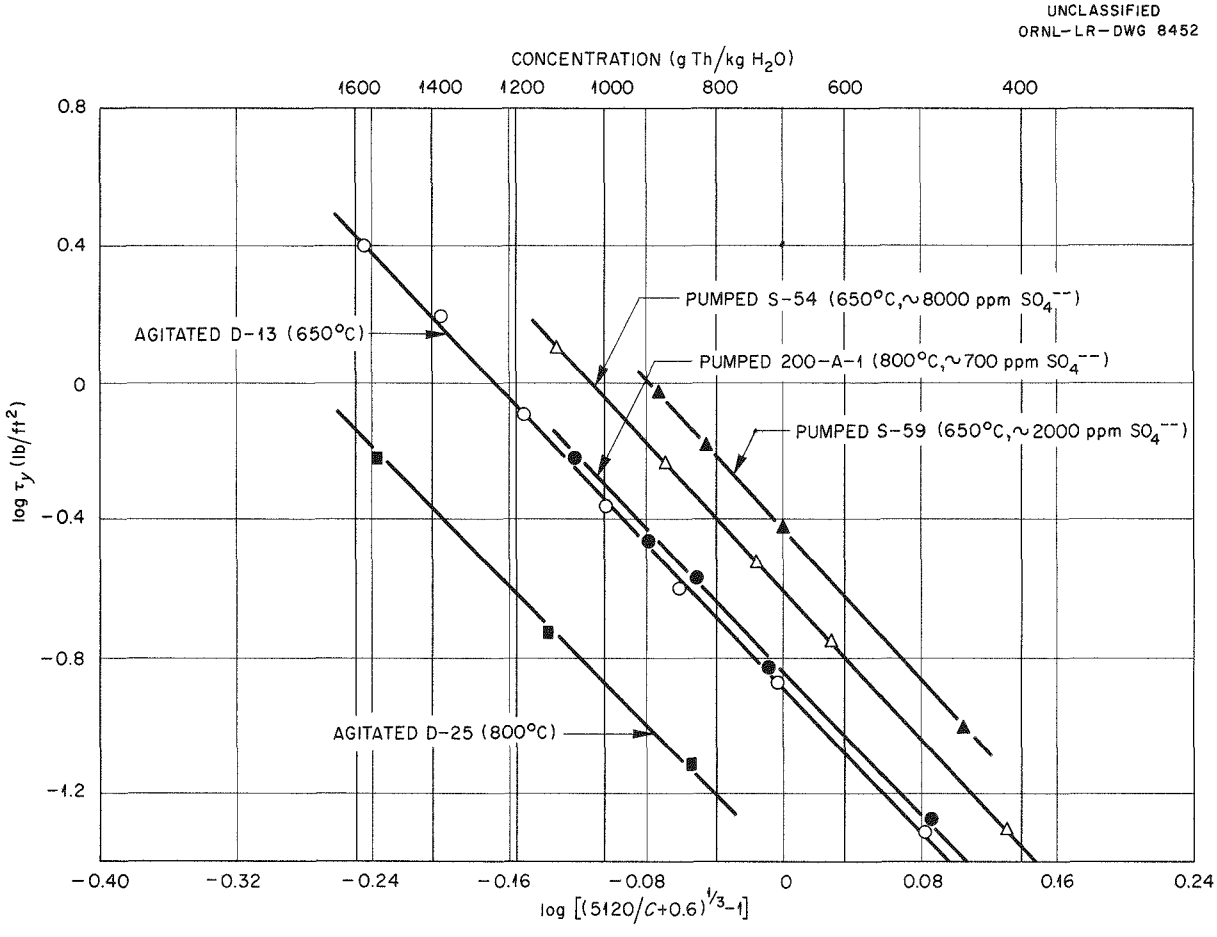

Fig. 12.1. Characterization Number for ThO_2 Slurries.

C = concentration, g of thorium per kilogram of H_2O.

A complete development of Eq. 1 is given in a memorandum.[6] In Fig. 12.1 it can be seen that a family of parallel lines is obtained. At the same concentration, slurries having the higher values for X will, in general, have higher yield values and higher viscosities for a given rate of shearing strain. Typical values for X are shown below.

Slurry Preparation	X
Oxide calcined at 800°C; laboratory agitated	0.039
Oxide calcined at 650°C; laboratory agitated	0.132
800°C oxide (containing 700 ppm SO_4) pumped at 300°C	0.145
650°C oxide (containing 8000 ppm SO_4) pumped at 250°C	0.257
650°C oxide (containing 2000 ppm SO_4) pumped at 300°C	0.380

12.3.2 Pressure Drop in Slurry Systems

Preliminary data indicated that the yield stress of a pumped slurry increased with temperature between 25 and 75°C for all concentrations of slurry between 500 and 1000 g of thorium per kilogram of H_2O. The data shown in Table 12.2 were obtained at 25, 45, 55, and 75°C in a pipe line viscometer for a slurry prepared from 800°C oxide which had been pumped at 300°C for 230 hr.

TABLE 12.2 EFFECT OF TEMPERATURE ON THE YIELD STRESS OF A PUMPED SLURRY

Concentration of Slurry (g of Th per kg of H_2O)	Temperature (°C)	Approximate Yield Stress (lb/ft^2)
500	25	0.055
	45	0.095
	55	0.115
	75	0.125
850	25	0.350
	45	0.390
	55	0.480
	75	0.575
1000	25	0.50
	45	0.730
	55	0.75
	75	0.815

12.4 SLURRY BLANKET MOCKUP

D. G. Davis, L. E. McTaggart, R. H. Nimmo, L. F. Parsly

Construction of the mockup loop is approximately 60% complete. It is now expected that construction will be completed by October 1. No significant design changes and no construction difficulties were encountered.

The main circulating loop is complete except for installation of the pump, which is being tested in another loop until needed. Construction of the slurry feed, let-down, and service piping was started. Most of the individual instruments were tested, and installation of panel-mounted instruments was begun.

12.5 BOILING STUDIES

R. V. Bailey P. C. Zmola

In the previous progress report,[7] a method for calculating the density distribution in a boiling system was presented in which the velocity of the liquid, relative to the vapor, was taken into consideration explicitly. Performance charts for several reactor arrangements in which power is generated uniformly were constructed on the basis of this "slip flow" model.[8] These charts can be used to determine the power removal capabilities of both solid- and fluid-fuel boiling reactors as a function of core geometry and operating conditions.

A boiling homogeneous reactor 10 ft high, operating with a vapor fraction of about 0.3, would be expected to produce 8 to 10 kw/liter for operation at 1000 psia and 15 to 20 kw/liter for operation at 2000 psia. A rough but convenient scaling rule is

$$\text{Power density} \sim \left(\frac{\bar{f}}{1-\bar{f}}\right)(Z^{-2/3}),$$

where $\bar{f}$ is the average vapor fraction and Z is the

[6] P. R. Crowley, *A Possible Characterization Number for Thorium Oxide Slurries*, ORNL CF-55-5-33 (May 5, 1955).

[7] R. N. Lyon *et al.*, *HRP Quar. Prog. Rep. April 30, 1955*, ORNL-1895, p 156–160.

[8] P. C. Zmola and R. V. Bailey, *Power Removal from Boiling Nuclear Reactors*, ORNL CF-55-7-43 (July 28, 1955); also ASME paper 55-SA-80 (unclassified).

core height. The estimates given above were based on uniform heat generation. To determine the power output of a specific unit more accurately, it would be necessary to determine the fission density, which, in turn, would depend upon the fuel mixture density distribution. The equations upon which the performance charts are based can be employed for such a determination.

13. METALLURGY

J. L. Gregg

R. G. Berggren
G. E. Elder
J. I. Federer
W. J. Fretague
W. O. Harms
W. J. Leonard
G. B. Wadsworth
J. C. Wilson

13.1 METALLURGY OF CORROSION

J. I. Federer
W. J. Leonard
W. O. Harms
G. B. Wadsworth

13.1.1 Stress-Corrosion Cracking of Austenitic Stainless Steels

Operation of the stress-corrosion apparatus described in previous reports[1,2] was continued during the report period, and additional specimens of six types of annealed commercial austenitic stainless steels were tested. These tests were performed on 0.050-in.-dia specimens under direct loading in boiling, 42 wt %, magnesium chloride solutions at stresses of approximately 20,000, 28,000, 36,000, and 40,000 psi. The results of these and previous tests appear in Figs. 13.1 and 13.2.

In Fig. 13.1, the time to failure is plotted against the austenite stability index, S, for the four stress levels studied. This index is calculated from a relation which is based on the assumption that the instability of austenite in a given stainless steel, with respect to its transformation to martensite, is directly proportional to the M_d temperature for that steel. The M_d temperature is defined as that temperature above which martensite will not form from austenite as the result of plastic deformation. The M_d values for the six steels under investigation, as well as the limitations of this type of representation, have been reported and discussed previously.[2] The relation used for establishing this index,

$$S = \frac{-M_d + 469}{1747} \times 100 \ ,$$

was arranged so that type 310, the most stable steel under study, would assume an index of 100. Indices for the six steels are given in Table 13.1, along with the room temperature mechanical properties as determined on 0.050-in. specimens.

It is seen that at all stress levels the more stable austenites were less susceptible to failure by stress corrosion. Tests involving type 310 ran without failure for periods ranging from 100 to 150 hr at all stress levels except 40,000 psi; type 309 SCb behaved similarly at 20,000 psi. All the other steels broke in less than about 20 hr at all stresses.

[1] W. O. Harms, J. I. Federer, and G. B. Wadsworth, *HRP Quar. Prog. Rep. Jan. 31, 1955*, ORNL-1853, p 155–157.

[2] W. O. Harms, J. I. Federer, and G. B. Wadsworth, *HRP Quar. Prog. Rep. April 30, 1955*, ORNL-1895, p 161–166.

TABLE 13.1. PROPERTIES OF AUSTENITIC STAINLESS STEELS USED IN STRESS-CORROSION STUDIES

AISI Type of Alloy	Room Temperature Mechanical Properties		Austenite Stability Index, S
	Tensile Strength (psi)	Yield Strength at 0.2% Offset (psi)	
304L	107,000	38,000	6
347	104,000	43,500	17
321	93,000	40,500	19
316L	96,000	37,500	28
309 SCb	111,000	51,500	53
310	94,000	43,000	100

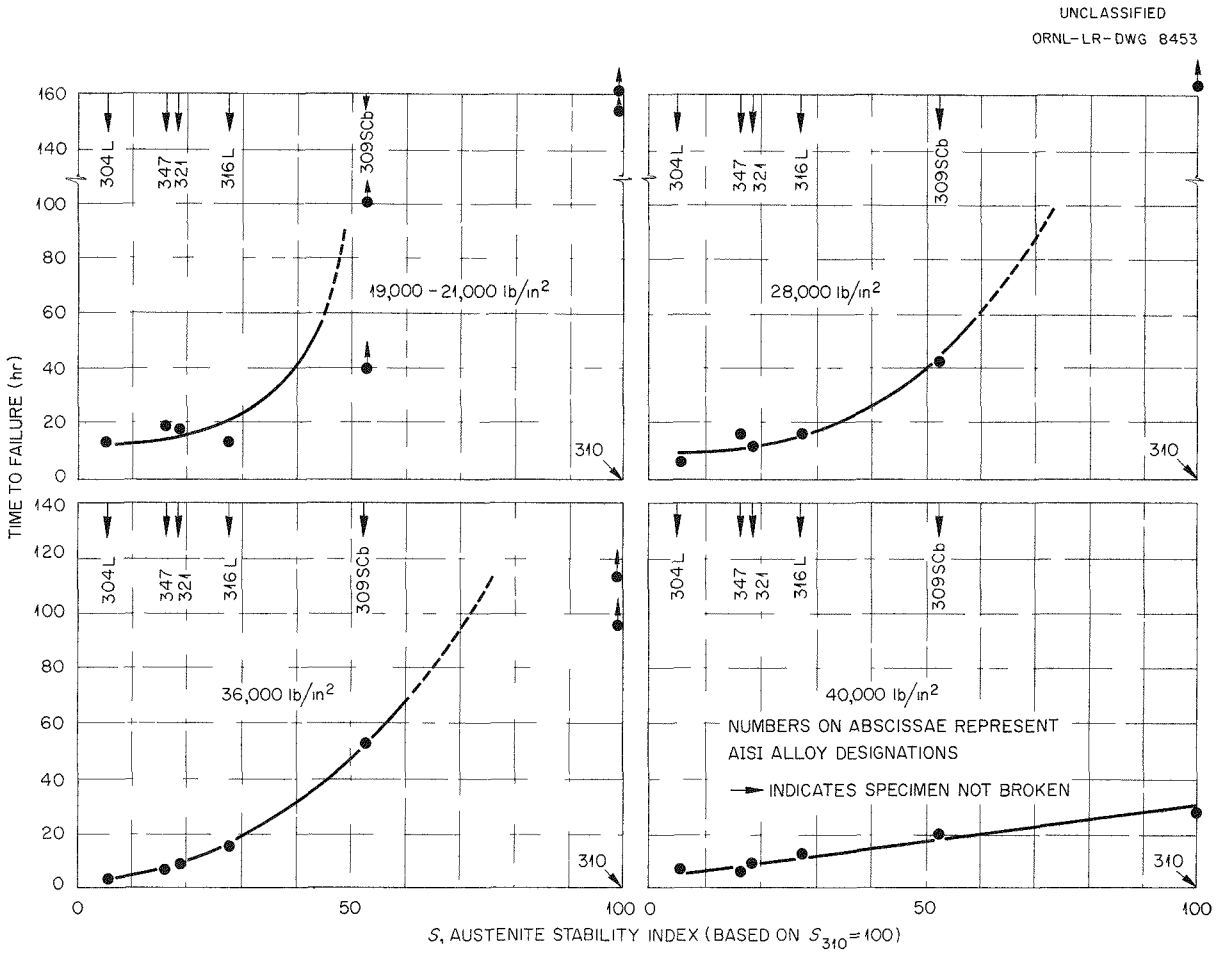

Fig. 13.1. Time to Failure vs Relative Austenite Stability for Six Austenitic Stainless Steels Tested in Boiling 42 wt % Magnesium Chloride Solutions. Each datum represents the average of from two to five determinations.

These data may be construed as indirect support for the hypothesis that propagation of transgranular stress cracks occurs along martensite plates during local yielding under applied stress. The fact that careful metallographic examination failed to reveal any evidence of martensite plates near the fracture paths does not rule out the possibility that they had formed ahead of the cracks which ultimately led to failure. The stresses at the root of a crack once begun are extremely high and could conceivably lead to localized transformation and subsequent corrosion attack on the local anodes thus created. To investigate the martensite hypothesis further, it is planned to undertake some electrode potential studies with the use of various martensites formed by subzero deformation and the undeformed austenites of similar composition. The type of stress corrosion under consideration can be inhibited by cathodic protection and is therefore an electrochemical phenomenon.

When stress vs time to failure is plotted as in Fig. 13.2, the possibility of engineering application of these data presents itself. It has been suggested that the designation of a threshold stress, below which there could be reasonable certainty that a material would not fail because of stress corrosion, would be of interest as a design criterion for such vulnerable components as heat exchangers and associated equipment.

If it is agreed that boiling 42 wt % magnesium chloride is the most severe transgranular stress corrodant for austenite stainless steels and that some correspondence could be established between the stress systems of this test and a practical situation, it appears that the threshold stress as indicated by data of the type shown in Fig. 13.2 could be used for design purposes. The severity of the environment should eliminate the necessity for any additional safety factors. It is evident that lower stress levels will have to be investigated in order to establish threshold stresses for materials such as types 304L and 347 stainless steel.

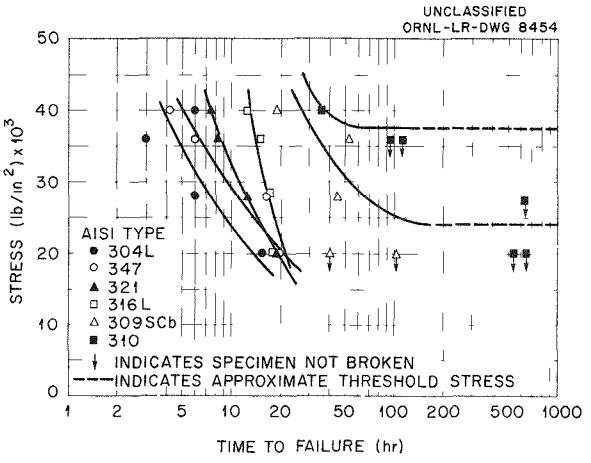

Fig. 13.2. Stress vs Time to Failure for Six Austenitic Stainless Steels Tested in Boiling 42 wt % Magnesium Chloride Solutions. Each datum represents the average of from two to five determinations.

13.1.2 Dynamic-Corrosion Study Factors Associated with Grain Size and Sigma Phase in Wrought Austenitic Stainless Steels

The preparation[2] of dynamic-corrosion specimens of types 304L and 347 stainless steel having grain sizes ranging from ASTM 2 to 8 was completed, and the pins were submitted to the HRP Dynamic Corrosion Group for testing in uranyl sulfate solutions.

Table 13.2 lists the heat treating temperatures used and the grain sizes obtained after cold reductions of 71 and 84%, respectively, of the types 304L and 347 steel. Temperatures higher than 1950°F were used for obtaining large grains in the type 347, since grain growth could not be promoted in this alloy at the lower temperatures in any reasonable length of time (300 hr at 1900°F yielded a grain size of only 4 in type 347). It was observed that a growth treatment at 2450°F, which is some 100°F higher than the temperature at which columbium carbides go into solution, led

TABLE 13.2. HEAT TREATMENT AND RESULTING GRAIN SIZES FOR TYPES 304L AND 347 STAINLESS STEEL*

	Heat Treating Conditions**			ASTM Grain Size
	Temperature (°F)	Time	Method of Cooling	
Type 304L stainless steel	1950	3 min	Water quench	8 and smaller
	1950	4 min	Water quench	6
	1950	13 min	Water quench	4
	1950	98 hr	Water quench	2
Type 347 stainless steel	1950	10 hr	Water quench	7–8
	1950	32 hr	Water quench	6–7
	2200	2½ hr	Furnace cool, to 1950°F	
	1950	½ hr	Water quench	3–4
	2300	26 hr	Furnace cool, to 1950°F	
	1950	½ hr	Water quench	2–3

*The types 304L and 347 material had been cold reduced 71 and 84%, respectively.

**All heat treating performed in dry hydrogen atmosphere.

to the formation of from 5 to 7% delta ferrite. This appeared in the microstructure as a nearly continuous network and prohibited extensive grain growth, just as the columbium carbides had done previously. Recourse to treatments at the lower temperatures of 2300 and 2200°F gave the desired results with no delta ferrite formation. These specimens were furnace-cooled to 1950°F and held for ½ hr following the high-temperature growth treatments to reprecipitate any columbium carbides which might have gone into solution.

The preparation of dynamic-corrosion pins from iron-chromium and iron-chromium-nickel alloys having compositions corresponding to sigma phase was described in the last progress report.[2] It was reported that the transformation of metastable ferrite to sigma phase occurred readily for the iron-chromium-nickel alloy; Magne-Gage measurements indicated that no ferrite remained in the microstructure after heating to 800°C for 15 hr. The transformation of the iron-chromium alloy, however, appeared to be more sluggish, since Magne-Gage measurements indicated that 8.5 to 10.5% remained after heating to 700°C for 32 hr. Subsequent heating to 650°C for 92 hr lowered the ferrite content to a value of less than 3%, in which condition the iron-chromium alloy, along with the iron-chromium-nickel alloy, was submitted for corrosion testing. For comparison, pins of each alloy were corrosion-tested in the ferritic condition, the latter being produced by heat treating at 1100°C, where the equilibrium phase is ferrite for both alloys.

The results of dynamic-corrosion tests in 0.04 *m* uranyl sulfate at 250°C and 12 fps for 200 hr which have been completed to date are given in Table 13.3. These data reveal that specimens in the sigma condition lost more weight than did the same composition in the ferritic state. However, all the brittle sigma phase specimens were broken into two pieces during testing, and the difference in weight loss may have been due to loss of material during or after fracture. It is to be noted that sigma phase and ferrites of similar composition were inferior to wrought type 347 under these test conditions.

13.1.3 Dynamic Corrosion of Austenitic Stainless Steel Weld Specimens

The results of dynamic-corrosion tests on welded coupon and pin-type stainless steel corrosion specimens, respectively, appear in Figs. 13.3 and 13.4. The heat treatment is shown in Table 13.4.

After run A-79 the specimens were refinished by light abrasion and tested in run A-81. For comparison, specimens of the type 347 base metal were tested in the various heat-treated conditions.

There are two significant features evident in the data: the lowest weight losses for welded specimens occurred for specimens given the 1000°F heat treatment; and a very high weight loss, at least in run A-79, occurred for the type 347 base metal heat treated at 1300°F.

The first point mentioned above was demonstrated previously, and it appears that the 1000°F heat

TABLE 13.3. DEFILMED WEIGHT LOSS OF 56% Fe–44% Cr AND 51% Fe–44% Cr–5% Ni CORROSION PINS (HRP DYNAMIC LOOP RUN N-3)

Alloy	Weight Loss (mg)	
	Sigma Phase	Ferrite
Fe-Cr	11.7	9.1
	11.2	8.7
Fe-Cr-Ni	24.6	
	20.1	11.4
Wrought type 347, average		2.3

TABLE 13.4. HEAT TREATMENT FOR PINS AND COUPONS OF WELDED TYPE 347 STAINLESS STEEL USED IN DYNAMIC-CORROSION TESTS

	Temperature (°F)	Time (hr)	Method of Cooling
Coupons	As-welded		
	1000	6	Air cool
	1300	8	Air cool
	1650	2	Water quench
	1900	½	Water quench
Pins	As-welded		
	975	4	Air cool
	1200	1	Air cool
	1500	1	Air cool
	1650	1	Air cool
	1850	1	Air cool

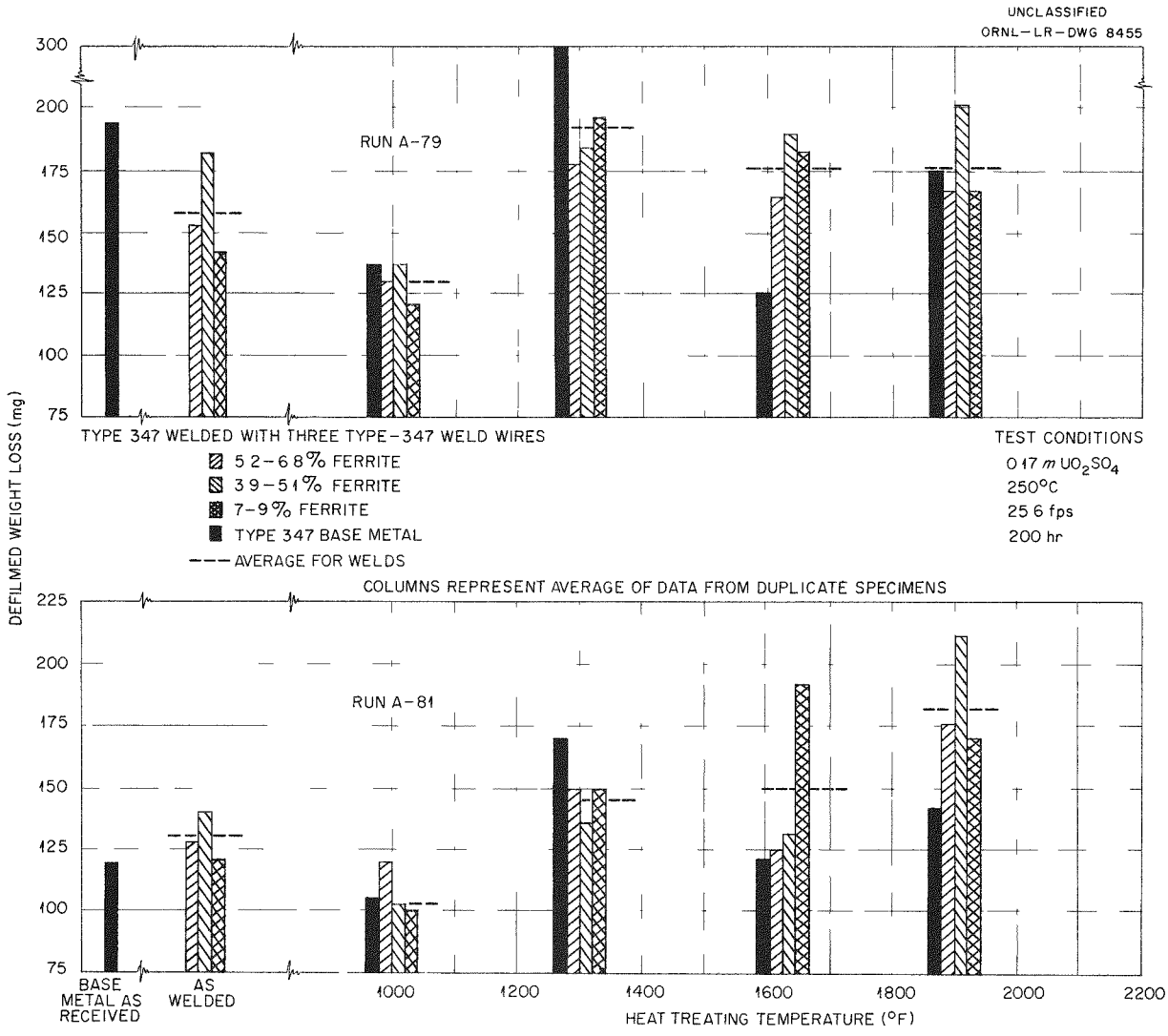

Fig. 13.3. Corrosion of Austenitic Stainless Steel Welds (Coupon-Type Specimens).

treatment definitely had a beneficial effect on the corrosion resistance of welds of this type. An explanation of this behavior is not apparent from metallographic examination of heat-treated specimens.

The data suggest that there is not a marked difference in the corrosion of as-welded specimens and specimens heat treated at temperatures up to and including 1650°F. The specimens having welds with 4 to 5% ferrite generally appeared a little more corrosion resistant than the other two, although a definite trend in this direction was not apparent. High weight losses of specimens treated at 1850°F are consistent with previous data obtained from dynamic-corrosion tests.

Thus the full-anneal heat treatment appears to have a detrimental effect on these welds, and none of the heat treatments used seemed to improve substantially the corrosion resistance over that of the as-welded condition.

13.1.4 Role of Oxide Films on Rate of Hydrogen Absorption by Zirconium and Its Alloys

Specimens of Zircaloy-2 were cathodically treated in 1 *N* sulfuric acid for 100 hr at 10 ma/cm^2 and at temperatures of 30 and 250°C in equipment

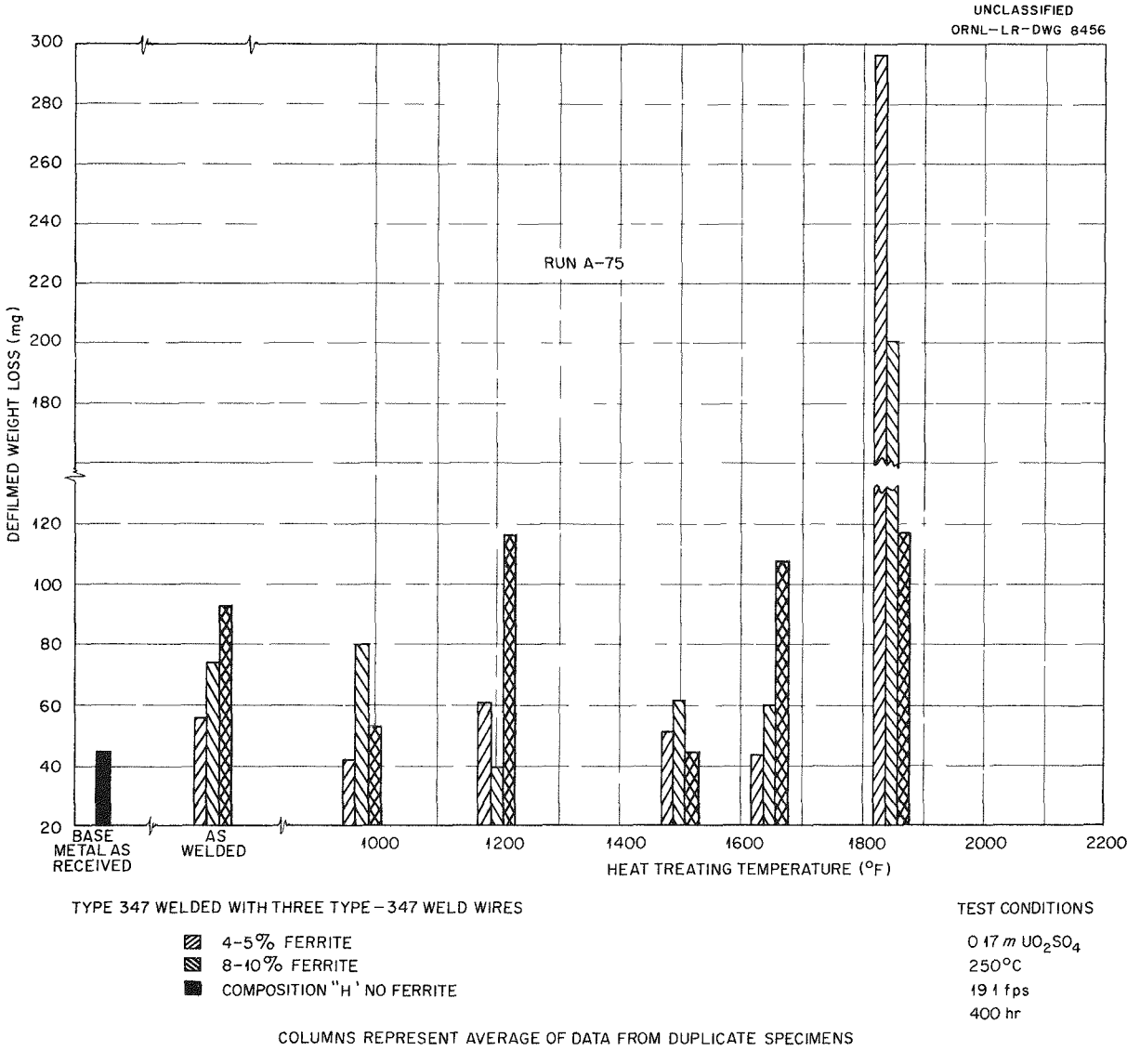

Fig. 13.4. Corrosion of Austenitic Stainless Steel Welds (Pin-Type Specimens).

described in the previous progress report.[2]

Erratic and high values of hydrogen content as determined by vacuum extraction analysis on Zircaloy-2 which had been outgassed at 10^{-6} mm Hg for 2 hr at 750°C prompted an investigation of the effectiveness of this treatment for removal of hydrogen. The results of this study are shown in Table 13.5, where it is seen that higher temperatures and longer times than previously recommended were necessary for obtaining "hydrogen-free" starting material. An exposure for 24 hr at 850°C and less than 10^{-5} mm Hg was adopted as the standard vacuum annealing treatment for this study.

Vacuum extraction analysis of four specimens cathodically treated at 30°C indicated that essentially no change in the hydrogen content had occurred as the result of this treatment. On removal from the cell, these specimens had no visible film or scale.

Considerable difficulty was encountered in the 250°C runs in the modified autoclave during this period. Four runs were terminated prematurely because of leakage in pressure fittings and

TABLE 13.5. EFFECT OF TIME AND TEMPERATURE ON REMOVAL OF HYDROGEN FROM ZIRCALOY-2

Vacuum Annealing Conditions*		Hydrogen Content (ppm)
Temperature (°C)	Time (hr)	
750	2	97
750	2	54
800	24	35
800	48	3
850	24	5
850	48	8

*Pressure, $<10^{-5}$ mm Hg.

gaskets or because of corrosion of stainless steel resulting from seepage of the acid through crevices in the zirconium protective lining. These defects were corrected by modification of the bomb design, including the use of a $\frac{1}{8}$-in. Teflon gasket and Teflon protective tubing for electrical leads, and the insertion of a Teflon spacer under the zirconium liner to force the liner against the zirconium cap.

The results of three successful runs at 250°C are given in Table 13.6. It appears that whether the specimens are previously outgassed or not, the hydrogen content increases to 130 to 170 ppm under the conditions of these runs. Metallographic examination revealed no hydride needles either near the surface or in the bulk material. The specimens have not been impact-tested for determination of transition temperatures.

13.2 EFFECT OF HEAT TREATMENT ON THE CORROSION RESISTANCE OF TYPE 347 WELD METAL

J. I. Federer
W. J. Leonard
W. O. Harms
G. B. Wadsworth

Plate and pin-type specimens of welds in type 347 stainless steel plate were exposed for 200 hr in a loop containing 0.17 *m* UO_2SO_4 operated at 250°C with 200 psi oxygen pressure.[3] The plate-type specimens were tested in a low-velocity region, 11 fps, and the pin-type specimens in a high-velocity region, 25 fps. All specimens contained weld metal plus adjacent base material. All specimens were electropolished prior to exposure.

TABLE 13.6. RESULTS OF CATHODIC TREATMENT OF ZIRCALOY-2 IN 1 *N* SULFURIC ACID AT 250°C AND 10 ma/cm^2 FOR 100 hr

Specimen No.	Hydrogen Content (ppm)	
	Before	After
Z-2F2501	75	130
Z-2F2502	<5	140
Z-2F2503	<5	170

Specimens from one weldment contained between 8 and 10% ferrite, and those from another weldment contained between 5 and 6% ferrite. Half the specimens from each weldment were heated at 1250°F for 48 hr; this treatment decreased the amount of alpha phase and probably formed some sigma phase. Photomicrographs of the weld metal, as deposited and after heat treatment, are shown in Figs. 13.5*a* and *b* and 13.6*a* and *b*.

At high velocities all specimens corroded at substantially the same rate, approximately 175 mpy. At lower velocities the corrosion rates of the as-welded materials were 8.5 and 17 mpy for the high-ferrite and the low-ferrite materials, respectively. Corresponding corrosion rates for the heat-treated materials were 3 and 7 mpy.

These data give some indication that the corrosion resistance is not greatly influenced by small changes in ferrite content or by conversion of ferrite to sigma.

13.3 PHYSICAL METALLURGY OF TITANIUM AND ZIRCONIUM ALLOYS

W. J. Fretague

13.3.1 Zirconium Alloys

Multiple-break impact specimens of irradiated Zircaloy-2 from in-pile loop run GG were tested over the temperature range from −196 to 285°C. The data obtained are plotted in Fig. 13.7, together with those obtained previously[4] for control specimens from the same lot of material.

[3] J. C. Griess *et al.*, *HRP Dynamic Corrosion Studies Summary of Run F-56*, ORNL CF-55-6-20 (June 1, 1955).

[4] W. J. Fretague, *HRP Quar. Prog. Rep. April 30, 1955*, ORNL-1895, p 167 and Fig. 8.6.

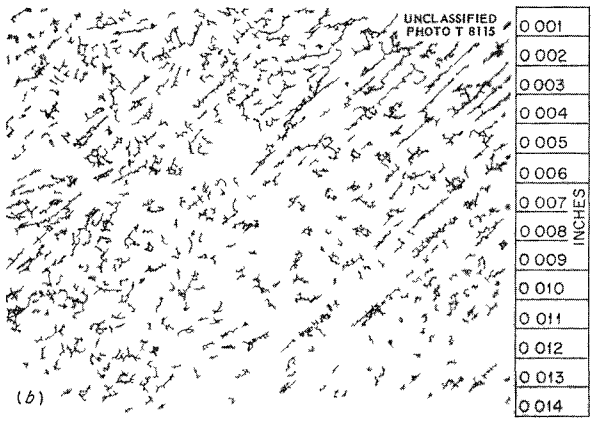

Fig. 13.5. (*a*) As-Welded Type 347 Stainless Steel Containing 8 to 10% Ferrite. (*b*) Original 8 to 10% Ferrite Heat Treated at 1250°F, 48 hr; Less Than 2% Ferrite Remaining.

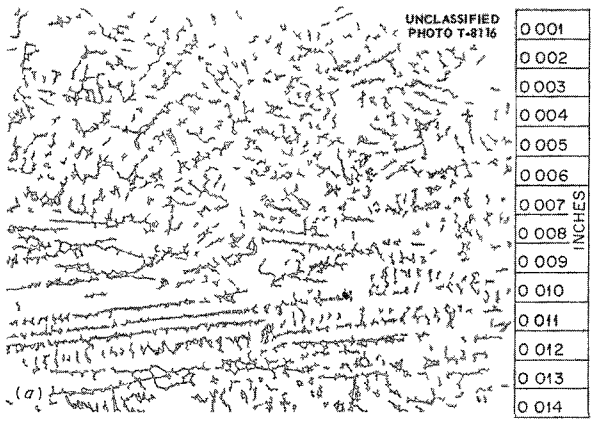

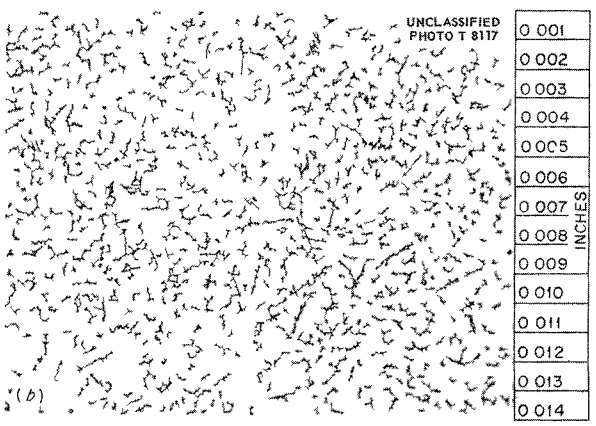

Fig. 13.6. (*a*) As-Welded Type 347 Stainless Steel Containing 5 to 6% Ferrite. (*b*) Original 5 to 6% Ferrite Heat Treated at 1250°F, 48 hr; Less Than 1% Ferrite Remaining.

It was noted that all the irradiated specimens fractured completely on impact even at the highest testing temperature employed. In addition, the energy values recorded at the elevated testing temperatures were appreciably lower than those obtained in previous tests of irradiated Zircaloy-2 specimens.

Impact specimens of Zircaloy-2 irradiated in the MTR were not damaged. Analyses of specimens from loop GG indicated hydrogen contents of 37 and 41 ppm, as compared with 35 ppm for control specimens. Microscopic examination indicated that a second phase present in the alloy seemed to be concentrated in the grain boundaries of the specimen from the loop to a greater extent than in the control specimen.

13.4 EFFECTS OF RADIATION ON STRUCTURAL METALS AND ALLOYS

R. G. Berggren J. C. Wilson

The "yield point" phenomenon and strain rate dependence of yield stress observed in irradiated austenitic stainless steels and previously reported[5] were investigated further. A series of type 304 ELC stainless steel specimens were irradiated in the HB-3 beam hole facility of the LITR to an integrated fast flux of 7×10^{18} nvt, approximately one-tenth the dose received by the specimens exposed in the MTR and reported earlier.[5] These specimens were tested over a

[5]R. G. Berggren and J. C. Wilson, *HRP Quar. Prog. Rep. April 30, 1955*, ORNL-1895, p 168.

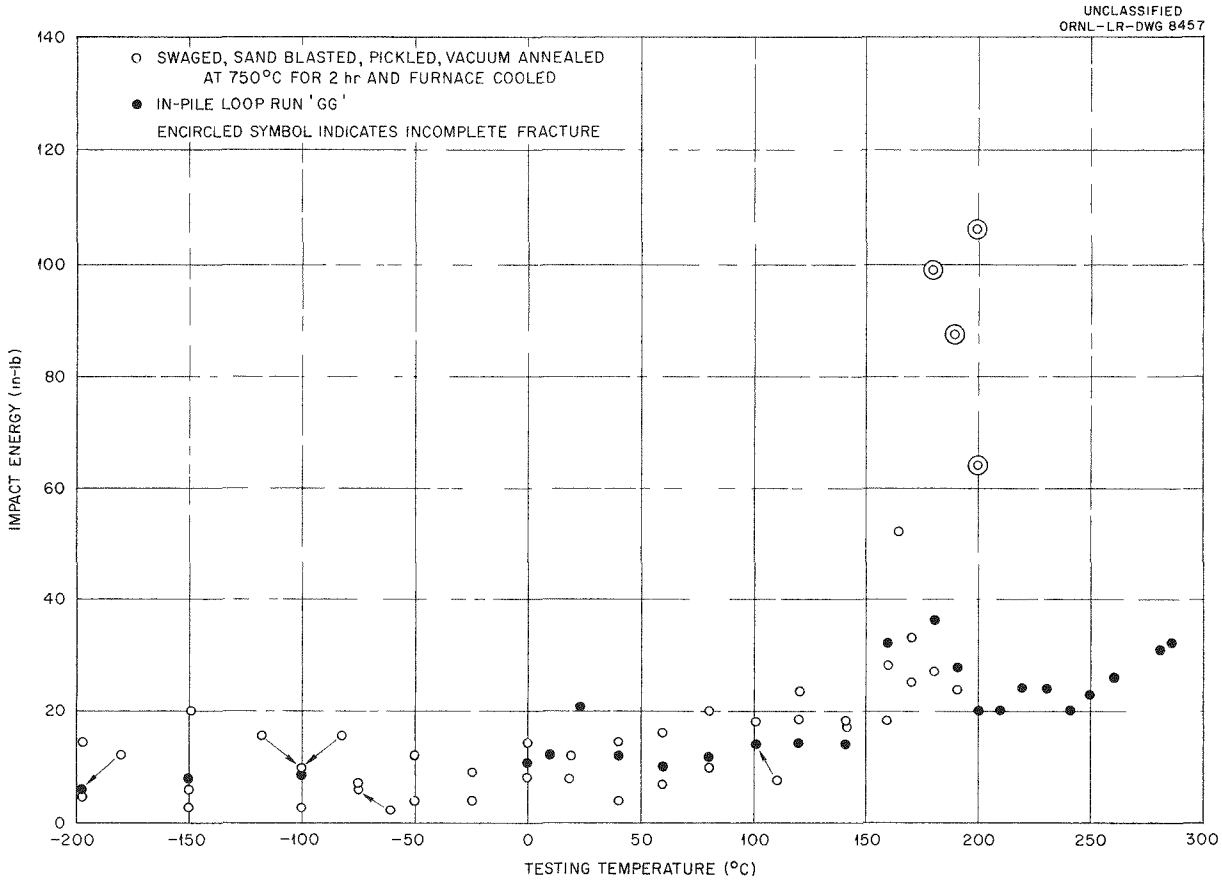

Fig. 13.7. Impact Energy vs Testing Temperature for Zircaloy-2.

40 to 1 range of strain rates. The results, shown in Fig. 13.8, indicate that the yield stress of the irradiated steel was dependent on strain rate over this range. Only the irradiated specimens tested at a strain rate of 2 in./in./min showed a "yield point." The irradiated specimens tested at lower strain rates showed points of inflection in the load-elongation curves. The unirradiated specimens showed no unusual behavior or strong strain-rate dependence. No additional notch-bar impact tests were made on these steels, but slow notch bend tests are planned for further investigation.

Tensile and notch-bar impact tests were made on carbon steels meeting ASTM A-212 Grade B specifications and two experimental heats meeting ASTM A-106 specifications, one of which was aluminum-killed to secure a fine grain size. The

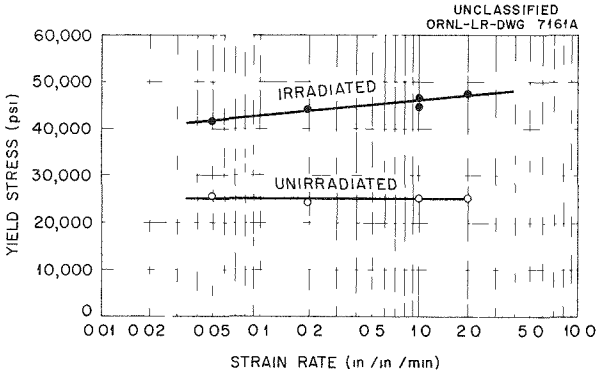

Fig. 13.8. Effect of Strain Rate on the Yield Stress of Control and Irradiated (nvt = 1×10^{19}) Tension Specimens of Annealed Type 304 ELC Stainless Steel.

results of tensile tests on these steels after normalizing and subsequent irradiation in the LITR or MTR are summarized in Table 13.7. Yield and ultimate tensile strengths increased because of irradiation; the ultimate tensile strengths increased less than the yield strengths. Ductilities, as measured by reduction of area and uniform elongation, decreased rather markedly. Comparison of specimens of the A-212B steel, irradiated to 10^{19} nvt at 140 and 570°F indicated that exposure at 570°F resulted in less increase in the yield strength but greater increase in the ultimate tensile strength. Neither the unirradiated or irradiated carbon steels exhibited a strong strain-rate dependence of yield stress.

All the unirradiated specimens of this steel showed the usual yield point. The yielding behavior was modified by irradiation, and the load-elongation curves showed points of inflection at about 1% elongation, where the rate of work hardening was very small.

Notch-impact tests on the irradiated ASTM-A-212B steel are summarized in Figs. 13.9 and 13.10. The energy absorption results are shown in Fig. 13.9, and results of measurements of lateral contraction below the root of the notch are shown in Fig. 13.10. Irradiation to a dose of 10^{19} nvt resulted in a slight rise in the fracture-transition temperature, and a dose of 10^{20} nvt produced a very marked increase in transition temperature. The control specimens in Fig. 13.10 appeared to show evidence of the ductility transition below about −60°F. Any evidence of a ductility transition in the irradiated specimens could not be resolved.

It will be noted that the shift in transition temperature in the impact tests was much more sensitive to integrated flux, at the higher inte-

TABLE 13.7. MECHANICAL PROPERTIES OF IRRADIATED CARBON STEELS

Integrated Fast Neutron Flux (nvt)	Irradiation Temperature (°F)	Strain Rate (in./in./min)	Yield Strength (psi)	Ultimate Tensile Strength (psi)	Reduction of Area (%)	Uniform Elongation* (%)
		ASTM-A-212B – Normalized from 1900°F				
0		0.05	50,000	75,400	64	22
0		0.5	51,200	77,800	61	22
1×10^{19}	140	0.05	65,400	80,800	68	18
1×10^{19}	570	0.05	56,800	83,900		
1×10^{20}	140	0.05	93,800	97,000	26	5
1×10^{20}	140	0.5	96,500	99,000	34	8
		ASTM-A-106 Coarse Grain – Normalized from 1700°F				
0		0.05	50,400	85,000	67	20.2
1×10^{19}	140	0.05	71,600	89,500	68	16.0
2×10^{18}	570	0.05	53,900	86,400	68	17.7
		ASTM-A-106 Aluminum Killed, Fine Grain – Normalized from 1700°F				
0		0.05	57,700	75,400	67	18.8
1×10^{19}	140	0.05	72,600	78,400	70	23.2
5×10^{18}	570	0.05	62,500	78,100	69	20.2

*Determined from diameter change outside the "necked" region.

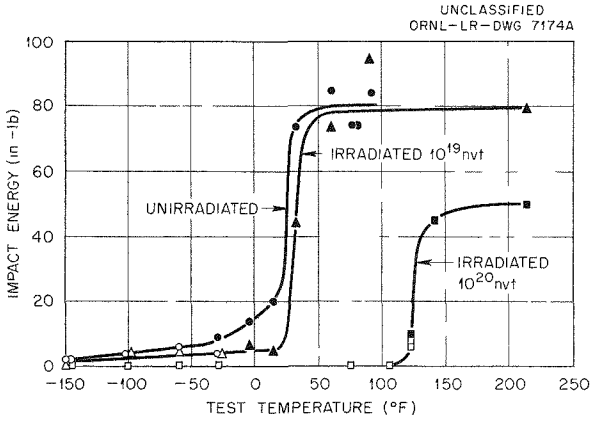

Fig. 13.9. Effect of Radiation on Impact Energy of A-212B Carbon-Silicon Steel Normalized from 1900°F.

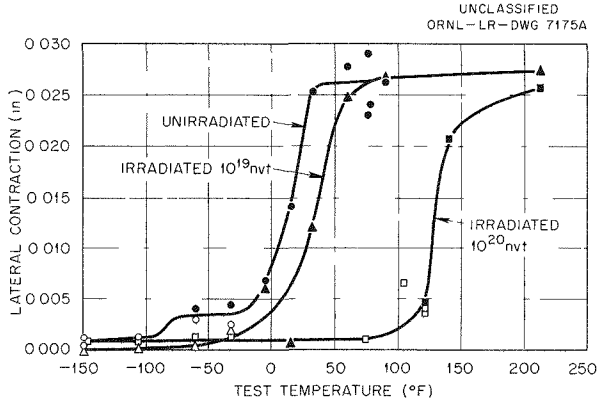

Fig. 13.10. Effect of Radiation on Lateral Contraction in the Notch Impact Test of A-212B Carbon-Silicon Steel Normalized from 1900°F.

grated fluxes, than were any of the other properties measured for this steel. In Fig. 13.11 the various mechanical properties of the steel are plotted against integrated flux. Although the data are

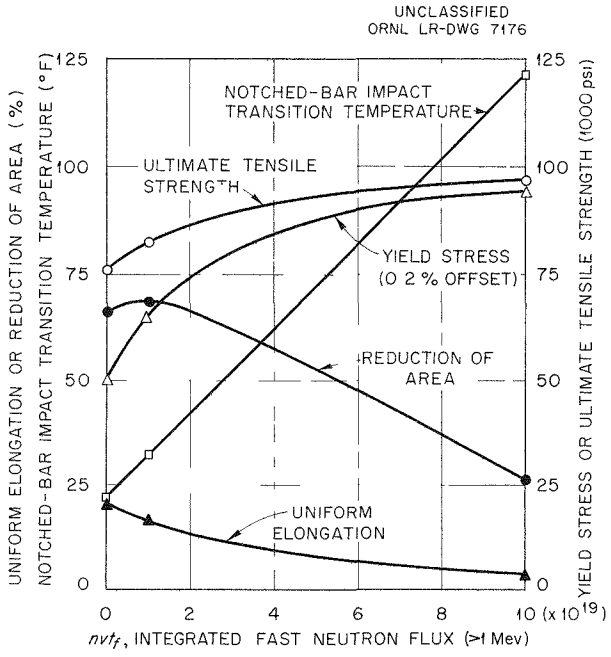

Fig. 13.11. Integrated Fast-Neutron Flux Dependence of Several Mechanical Properties of A-212B Carbon-Silicon Steel.

scanty, it is readily apparent that the transition temperature was much more integrated-flux dependent than even the elongation or the reduction of area. The transition temperature appeared to increase linearly with increasing integrated flux, while the yield stress and ultimate tensile strength were much less flux-sensitive at the higher integrated fluxes.

The tests on the two heats of the ASTM-A-106 steels confirmed many of the observations made on the A-212B steel. But, due in part to the scatter of the results and in part to variations in irradiation conditions, differences in properties of the coarse- and fine-grain steels were not apparent.

Part V

CHEMICAL ENGINEERING DEVELOPMENT

F. R. Bruce

14. THORIUM OXIDE SLURRY DEVELOPMENT

D. E. Ferguson H. K. Jackson J. P. McBride
V. D. Allred N. A. Krohn
S. R. Buxton L. E. Morse
W. H. Carr C. E. Schilling
A. R. Jones D. G. Thomas
E. V. Jones W. M. Woods

Chemical studies on development of a thorium oxide slurry for use as the blanket of the HRT have continued. Pure ThO_2 slurries apparently were unaffected by irradiation in the LITR and the ORNL Graphite Reactor. Silver was shown to be a good heterogeneous catalyst for the recombination of radiolytic gases in thorium oxide slurries. Progress has been made in the characterization of oxide products and slurries by x-ray, nitrogen adsorption surface area, thermogravimetric, and gaseous adsorption techniques, sedimentation particle size analyses, and bulk density measurements. The principal variable studied was the final calcination temperature used in preparing the oxide.

14.1 THORIUM OXIDE SLURRY IRRADIATIONS

A. R. Jones J. P. McBride
N. A. Krohn W. M. Woods

Studies to determine the effect of in-pile irradiation on the properties of thorium oxide slurries and to demonstrate slurry radiation stability have continued. Five in-pile irradiations of pure thorium oxide slurries were carried out at 300°C, one in the Graphite Reactor and four in the LITR. In addition, six settled slurries and six oxygen-sparged slurries were irradiated for one month at room temperature in the Co^{60} source. The pure thorium oxide slurries apparently were unaffected by irradiation, but slurries containing 8% U^{235} (based on the weight of thorium) were adversely affected. Studies to determine the effect of using lower uranium concentration are under way. Efforts to stir a slurry during an extended irradiation period with a simple dash-pot type of stirrer were unsuccessful. However, an improved model, employing dual solenoids to give power strokes in both directions, was used in a one-week irradiation of a slurry of 900°C calcined oxide, during which period no stirring difficulties were encountered.

14.1.1 Slurry Irradiations in the LITR

Two thorium oxide slurries, containing 500 g of thorium per kilogram of H_2O, which were irradiated in the LITR and recovered for examination, apparently were not affected by the irradiation, although the stirring mechanism in the irradiation bomb failed during each irradiation. One of the slurries was prepared with Lindsay No. 8 oxide (oxalate calcined at 900°C) and one with D-16 oxide (see Sec. 14.4). Both irradiations were carried out in hole C-44, at a flux of 3×10^{13} neutrons/cm^2/sec, at 300°C, in the dash-pot-stirred irradiation bomb described previously.[1] The total irradiation times were 115 hr for the Lindsay oxide and 288 hr for the D-16 oxide. The crystallite sizes of the irradiated materials not containing uranium appear to have been increased, but the magnitudes of the actual changes and their significance are still somewhat obscure (see Table 14.1). Such changes in size would not ordinarily be expected to cause an appreciable effect on the bulk properties of the slurries. The settled densities of the recovered slurries were 1330 and 1500 g of thorium per liter, respectively, for the Lindsay and D-16 oxides.

Additional irradiations were carried out at 300°C with slurries (500 g of thorium per kilogram of H_2O) of the D-16 oxide and of D-16 oxide recalcined at 900 and 1100°C, but these irradiated slurries have not yet been examined. Each slurry was thoroughly mixed before being loaded into the irradiation bomb, and all experimental setups were pretested at temperature before insertion in the reactor. A stirring failure, coincidental with a power failure or a reactor shutdown, occurred during each irradiation.

Out-of-pile and in-pile tests on the single-solenoid type of bomb used in the irradiation studies indicate that the stoppages in-pile were more likely the result of a mechanical failure

[1] D. E. Ferguson *et al.*, *HRP Quar. Prog. Rep. Jan. 31, 1955*, ORNL-1853, p 173.

TABLE 14.1. AVERAGE CRYSTALLITE DIAMETER OF IRRADIATED THORIUM OXIDE

Experiment	Slurry Solid	Crystallite Diameter* (Å)	
		Initial	Final
LITR-2	Lindsay No. 8	(545)	900 ± 100
LITR-3	D-16	111	195 ± 20
Graphite Reactor 1	650°C from oxalate	~100	205 ± 20
Graphite Reactor 3	Pyrohydrolyzed + 8% UO_3		220 ± 20
Graphite Reactor 4	Pyrohydrolyzed + 8% UO_3 + basic copper carbonate		180 ± 20
Graphite Reactor 5	D-12	(110)	230 ± 20

*Determined by x-ray diffraction line broadening. Values in parentheses are estimated from the surface areas of similar preparations (see Sec. 14.3.2).

than of a radiation effect. Improvements in the bomb design are being studied (see Sec. 14.1.4). In preliminary testing of one bomb employing dual solenoids and giving power strokes in both the up and down directions, a 900°C oxide slurry was irradiated in the LITR at 300°C for one week, during which period no stirring difficulties were encountered.

14.1.2 Slurry Irradiations in the ORNL Graphite Reactor

A 10-ml slurry of D-12 oxide, prepared from Thorex product by 650°C calcination, containing 500 g of thorium per kilogram of H_2O, was irradiated for six days at 300°C at a flux of 7×10^{11} neutrons/cm^2/sec. Steam pressure decreased during irradiation, indicating a leak. Approximately 2 ml of H_2O was added to the slurry when the capillary connecting the irradiation bomb to the pressure-recording system was pressurized with nitrogen. The recovered slurry contained very little water (3 to 4 ml total volume) but appeared unchanged by the irradiation after dilution. Its settled density was 1270 g of thorium per liter, and its crystallite diameter, determined by x-ray measurements, was 230 ± 20 Å (see Table 14.1).

A slurry with a thorium concentration of 500 g per kilogram of H_2O, made from mixed oxides (90% thorium–8% U^{235}–2% copper), which was irradiated for two weeks at 300°C in the ORNL Graphite Reactor, was recovered. No gas pressure in excess of steam was observed during the irradiation, and stirring stopped during the first 24 hr. The irradiated slurry was gray-green in color, presumably from reduced uranium, and a large fraction of the material was lumpy. The crystallite diameter, as determined by x-ray measurements, was 180 ± 20 Å, typical of the pyrohydrolyzed oxide used in preparing the original slurry. In a control experiment in which there was no irradiation, there was no stirring difficulty, and the recovered slurry was tan colored and showed no deterioration of slurry properties. It is presumed that the uranium reduction and the deterioration of slurry properties in the irradiated material resulted from a net accumulation of hydrogen, appearing as a consequence of the efficient catalytic recombination of the radiolytic gas and the consumption of oxygen by film formation and corrosion. Uranium reduction and gross particle growth were observed in the laboratory when a mixed oxide slurry of thorium and uranium was subjected to a hydrogen overpressure at 250°C.

14.1.3 Slurry Irradiations in the Co^{60} Source

Settled and oxygen-sparged slurries were irradiated at room temperature in a Co^{60} source at 7×10^5 and 3×10^5 r/hr, respectively, for a period of one month. The materials underwent no apparent change. Particle size distribution analyses employing Stokes' law showed no

radiation-induced change in particle size (Table 14.2).

14.1.4 Development of Facilities for Irradiation Studies

An effort is being made to develop small-scale devices, suitable for in-pile use, to study, at least qualitatively, the changes occurring in properties of slurries, primarily viscosity, while under irradiation. Extensive out-of-pile testing of the dash-pot-stirred irradiation bomb demonstrated its utility in measuring the changes in viscosity of water and water-glycerin mixtures as they were heated to 300°C. Consistent and reliable results were not obtained with thorium oxide slurries, however, and it was not possible with present bombs to stir successfully slurries containing 1000 g of thorium per kilogram of water. Modifications in both stirrer and bomb proportions are being made which should permit operation with slurries of higher thorium concentrations.

Improved models of the dash-pot-stirred irradiation bomb for use in beam hole C-44 of the LITR, which have dual-coil activation arrangements to give power strokes in both the up and down directions and, in one version, a self-timing principle for the measurement of viscosity, are currently under test with slurries. Initial tests of the self-timing device with water and water-glycerin mixtures showed the stirring rate to be very sensitive to viscosity.

Arrangements have been made with the Engineering and Mechanical Division for assistance in the design and development of radically different in-pile bombs for use with slurries and in improvement of the present irradiation facilities at the LITR and Graphite Reactor. Under development for in-pile use are a bellows-type flow-tube viscometer, a magnetic-impulse reciprocating-plunger viscometer, and a rotating cylinder viscometer. Consideration is being given to canning the experimental equipment for the LITR and fitting the can to a lattice position. A handling rod would project through a seal in the LITR top-plug, and the service and instrument connections would be introduced through a flexible tube. This arrangement would permit extended irradiations to be carried out independently of the operating schedule of the LITR.

The shielded hood for use in the remote opening and handling of the radiation bombs was completed and was used in recovering the irradiated

TABLE 14.2. EFFECT OF Co^{60} IRRADIATION ON PARTICLE SIZE DISTRIBUTION OF ThO_2

Slurry, 500 g of thorium per kilogram of H_2O, irradiated at room temperature

Slurry		Settled Sample*		Oxygen-Sparged Sample*	
Oxide	Suspending Medium	dg (μ)	σg	dg (μ)	σg
650°C D-16	H_2O	2.8	3.5	2.2	3.2
900°C D-16	H_2O	2.8	3.6	3.6	3.3
650°C D-16	0.1 m $CuSO_4$	2.6	3.9	2.6	3.9
D-16 + 8% U	H_2O	2.2	4.5	1.9	4.0
D-16 + 8% U	0.1 m $CuSO_4$	2.1	4.9	2.3	4.7
650°C D-16	0.1% $Na_2O{\cdot}SiO_2$	2.7	4.5	2.7	4.5
Unirradiated D-16		dg = 2.2, σg = 4.3			

*dg = geometric mean diameter; σg = geometric standard deviation [see T. Hatch and S. P. Choate, *J. Franklin Inst.* 207, 369–387 (1929)].

slurries discussed above. A shielded unit for removing bombs from the LITR was constructed for use with this facility. It permits a bomb to be removed from the reactor and transported to the hood without the use of an additional shielded carrying container.

The slurry abrasion tester is being modified for use with irradiated slurries. The metal foil used as the target has been incorporated into an evacuated pressure cell, which permits the penetration time to be detected by a pressure change.

14.2 GAS RECOMBINATION

L. E. Morse J. P. McBride

Studies on development of an internal catalyst to effect recombination of the radiolytic gases in a thorium oxide slurry blanket have continued. A catalyst capable of recombining the stoichiometric amount of oxygen with 10 moles of hydrogen per hour per liter of slurry at 280°C and at a hydrogen partial pressure of 500 psi is considered satisfactory. It should be chemically compatible with the slurry and should have low neutron-capture characteristics.

Out-of-pile gas combination studies included additional experiments with copper sulfate, an investigation of the use of silver as a catalyst, and studies with oxide prepared from Thorex product by calcination at 650°C (Sec. 14.4). Results indicate that 0.01 *m* silver with such thorium oxide should be more than sufficient for both TBR and HRT recombination requirements.

The addition of 0.09 *m* $CuSO_4$ alone to an Ames oxide slurry with a thorium concentration of 660 g per kilogram of H_2O resulted in a combination rate of 14 moles of H_2 per hour per liter at 292°C and at a hydrogen partial pressure of 500 psi. With the same catalyst concentration and hydrogen partial pressure, but at 284°C, a slurry containing oxide prepared from the Thorex product gave a combination rate of 2 moles of H_2 per hour per liter. The addition of 0.0025 *m* H_2SO_4 along with the $CuSO_4$ markedly increased the combination rates for both oxides (see Table 14.3).

Mole for mole, silver was catalytically more active than copper sulfate in oxide slurries. In an Ames oxide slurry with a thorium concentration of 660 g per kilogram of H_2O, 0.03 *m* silver combined 10 moles of H_2 per hour per liter of slurry at 300°C and at a hydrogen partial pressure of 500 psi (Table 14.4). Slurries prepared from the D-16 oxide were much more reactive with silver present, 0.02 *m* silver combining 35 moles of H_2 per hour per liter at 270°C and at the same hydrogen partial pressure (Table 14.5). The addition of 0.5% uranium, as $UO_3 \cdot H_2O$, to a slurry of D-16 oxide containing 0.01 *m* silver resulted in a combination rate of 19 moles of H_2 per hour per liter at 280°C and at a hydrogen partial pressure of 500 psi. Adding 5000 ppm of sulfate as $Th(SO_4)_2$ to this slurry reduced the rate by

TABLE 14.3. COMBINATION RATES OF STOICHIOMETRIC HYDROGEN AND OXYGEN MIXTURES IN THORIUM OXIDE SLURRIES CONTAINING COPPER SULFATE

Slurry thorium concentration: 660 g per kilogram of H_2O
Initial gas pressures: 960 psi H_2, 500 psi O_2 (at 25°C)

Oxide	Catalyst	Temperature (°C)	k_π (hr^{-1})	H_2 Combination Rate, P_{H_2} = 500 psi (moles/hr/liter)
Ames	0.09 *m* $CuSO_4$ + 0.0025 *m* H_2SO_4	293	76	22
	0.09 *m* $CuSO_4$	292	55	14
D-16*	0.09 *m* $CuSO_4$ + 0.0025 *m* H_2SO_4	263	7.5	3
	0.09 *m* $CuSO_4$ + 0.0025 *m* H_2SO_4	292	23.1	7
	0.09 *m* $CuSO_4$	284	6.3	2

*See Sec. 14.4.

TABLE 14.4. COMBINATION RATES FOR STOICHIOMETRIC HYDROGEN AND OXYGEN MIXTURES IN AMES THORIUM OXIDE SLURRIES CONTAINING SILVER

Slurry thorium concentration: 660 g per kilogram of H_2O
Initial gas pressures: 960 psi H_2, 500 psi O_2 (at 25°C)

Silver Concentration (m)	Temperature (°C)	k_π (hr^{-1})	H_2 Combination Rate, P_{H_2} = 500 psi (moles/hr/liter)	Final pH at 25°C
0.0019	250	1.2	0.55	5.7
	278	1.56	0.63	5.7
	289	1.69	0.63	5.7
0.031	265	8.8	3.7	6.2
	300	30.1	9.95	6.2
0.08	185	26.3	15.8	6.2
	196	33.2	18.9	6.2
	201.5	42.0	23.2	6.2

TABLE 14.5. COMBINATION RATES FOR STOICHIOMETRIC HYDROGEN AND OXYGEN MIXTURES IN D-16* THORIUM OXIDE SLURRIES CONTAINING SILVER

Slurry thorium concentration: 660 g per kilogram of H_2O
Initial gas pressures: 960 psi H_2, 500 psi O_2 (at 25°C)

Silver Concentration (m)	Additive	Temperature (°C)	k_π (hr^{-1})	H_2 Combination Rate, P_{H_2} = 500 psi (moles/hr/liter)	Final pH at 25°C
0.04	None	162	4.8	3.4	
0.02	None	201	8.6	4.9	
		220	10.9	5.5	6.7
		260	43.5	16.3	
		270	96.0	34.7	
0.01	0.5% U	280	56.2	19.0	
0.01	0.5% U, 5000 ppm SO_4^{--}	278	27.7	9.5	

*See Sec. 14.4.

approximately a factor of 2 (Table 14.5). Combination rates with slurries of the pure D-16 oxide alone were three times those obtained with Ames oxide under the same conditions but were still much too low for such slurries to be used without an additional catalyst (Table 14.6).

Experimental details and methods of analyses have been described previously.[2,3] The reaction rate constant, k_π, and the rate of hydrogen combination with oxygen in moles per hour per liter listed in the tables were obtained from the observed decrease in gas pressure with time, perfect gas

[2]D. E. Ferguson *et al.*, *HRP Quar. Prog. Rep. Oct. 31, 1954*, ORNL-1813, p 143.

[3]H. F. McDuffie *et al.*, *Reactor Sci. Technol.* 4, No. 2, 23 (1954) (TID-2013).

behavior being assumed. First-order dependence of the rate on the hydrogen partial pressure and, in effect, total gas pressure was demonstrated. Combination rates calculated in this manner do not consider gas solubility in the slurry and therefore may be 10 to 20% lower than the actual rates.

The lowered catalytic activity of copper sulfate in the absence of added acid and the additional decrease in activity observed when the D-16 oxide, which had a surface area larger than that of the Ames oxide, was substituted for the Ames material (Table 14.3) further emphasize the complex nature of the reaction when copper sulfate is used as a catalyst in a slurry. Since copper sulfate functions best as a solution catalyst, a decrease in concentration of the catalytically active ionic species occasioned by hydrolysis or surface adsorption results in a decreased gas combination rate. In the experiments on Ames oxide slurries with copper sulfate without added acid, the amount of copper in solution was less than in similar experiments with added sulfuric acid (Table 14.7). In addition, the increase in the SO_4/Cu ratio and the rise in pH suggest that the decrease in catalytic activity was associated not only with a decrease in soluble copper but also with an increase in the relative concentration of less active but soluble hydrolytic products[4] such as $Cu(HSO_4)^+$. Decreases in activity associated with the use of the larger-surface-area D-16 oxide or with increasing thorium oxide concentration noted previously[5] are probably the result of adsorption phenomena.

The silver catalysts were prepared by heating silver carbonate with the oxides at 280°C for 2 to 3 hr in the presence of oxygen. The slurry

[4]H. F. McDuffie, L. F. Woo, and C. H. Secoy, *HRP Quar. Prog. Rep. Oct. 31, 1953*, ORNL-1658, p 105.

[5]D. E. Ferguson *et al.*, *HRP Quar. Prog. Rep. Jan. 31, 1955*, ORNL-1853, p 173.

TABLE 14.6. EFFECT OF OXIDE PREPARATION ON THE COMBINATION RATE OF STOICHIOMETRIC HYDROGEN AND OXYGEN MIXTURES IN THORIUM OXIDE SLURRIES

Slurry thorium concentration: 660 g per kilogram of H_2O
Initial gas pressures: 960 psi H_2, 500 psi O_2 (at 25°C)

Preparation	Temperature (°C)	k_π (hr^{-1})	H_2 Combination Rate, P_{H_2} = 500 psi (moles/hr/liter)
Thorium oxalate* calcined at 600°C	300	0.13	0.04
Thorium oxalate calcined at 650°C (D-16)	297	0.06	0.02
Thorium oxalate calcined above 650°C (Ames)	300	0.023	0.007

*Prepared from mantle-grade thorium nitrate.

TABLE 14.7. CHEMICAL PROPERTIES OF AMES THORIUM OXIDE SLURRIES CONTAINING $CuSO_4$ AFTER COMBINATION EXPERIMENTS

Slurry thorium concentration: 660 g per kilogram of H_2O
0.09 *m* $CuSO_4$

H_2SO_4 Added (*m*)	Copper Adsorbed on ThO_2 at 25°C (% of total Cu)	SO_4/Cu Mole Ratio in Liquid Phase	pH	
			Initial	Final
0	77.3	1.59	3.10	3.41
0.0025	71.3	1.38	2.51	3.43

solids were recovered and were washed with water. With the Ames oxide only 10 to 30% of the original silver added stayed with the slurry solids. However, essentially 100% of the silver added to the D-16 oxide was adsorbed. The low adsorption encountered with the Ames oxide, and possibly the lower activity of silver catalysts prepared from it, may be associated with its significant sulfate impurity (7.55 mg of sulfate per gram of thorium). Almost stoichiometric amounts of sulfate and silver ions were found in the supernatants from the silver–Ames oxide catalyst preparation and combination experiments.

Prior to the use of the silver–thorium oxide in the combination runs, the silver could be leached from the solid with cold dilute nitric acid. However, after the combination experiment, the silver could be removed only by heating with concentrated nitric acid, and the evolution of nitrogen oxides during the dissolution indicated that at least a partial reduction of the silver to the metallic state had taken place.

Investigation of metallic oxide catalysts other than silver has been initiated. Preliminary experiments with a slurry of Thorex product oxide containing 1200 ppm of PdO indicate the PdO to be the most active catalyst yet studied. The combination rate was appreciable at room temperature (4 moles of hydrogen per hour per liter) and was explosively fast at 160°C.

14.3 LABORATORY STUDIES

V. D. Allred J. P. McBride

To support the in-pile irradiation studies and the slurry development program, laboratory studies on thorium oxide slurries were directed toward the development of methods and techniques for the study of slurries and the establishment of physical and chemical criteria for the evaluation of thorium oxide products and their aqueous suspensions. An investigation was made of the effect of preparation variables on the chemical purity and properties of thorium oxide. Oxide products were characterized by x-ray diffraction techniques, sedimentation particle size analyses, and surface area and activity measurements. The effects of additives on slurry properties were delineated. Variations in particulate properties with mechanical handling were investigated. Apparatus for the measurement of slurry viscosities at elevated temperatures was developed and is currently under test.

14.3.1 Preparation of High-Purity Thorium Oxide

E. V. Jones

Laboratory-scale preparations were carried out with the pure, essentially sulfate-free thorium nitrate product solution from the Thorex process. The method consisted in precipitating the oxalate at 40°C with 10% excess solid oxalic acid, drying the oxalate at 110°C, and decomposing to oxide by heating for 4 hr at 370°C and for 4 hr at either 650, 750, or 900°C. Table 14.8 gives the chemical composition data for the laboratory preparations and for D-16 oxide, a large-scale preparation from Thorex product solution set aside as a stock of standard oxide for use in laboratory studies on thorium oxide (see Sec. 14.4).

14.3.2 Characterization of Thorium Oxide Products

V. D. Allred S. R. Buxton

Progress was made toward the physical and chemical characterization of thorium oxide, in particular the oxide produced by the thermal decomposition of thorium oxalate. The effects of oxalate precipitation temperature, calcination temperature, and calcination time on the nitrogen adsorption surface area, x-ray crystallite size, and sedimentation particle size of oxide products were determined. A relationship between the surface area and average crystallite size was established. Thermogravimetric and CO_2 and H_2O adsorption studies were carried out with D-16 (see Sec. 14.4).

(a) Effects of Temperature and Time on the Properties of Oxide Prepared by Thermal Decomposition of Thorium Oxalate. – Thorium oxides with a considerable range of physical properties were prepared by the thermal decomposition of thorium oxalate. The size and shape of the relic oxide particles, as determined with an electron microscope, depended on the temperature at which the oxalate was precipitated and was independent of calcination temperature. However, the nitrogen adsorption surface areas and x-ray crystallite sizes were independent of the precipitation temperature; the crystallite size increased with increasing calcination temperature and time, while the nitrogen surface area decreased (see Figs. 14.1 and 14.2).

TABLE 14.8. TYPICAL CHEMICAL COMPOSITION DATA*

	Thorex Product, Thorium Nitrate	Oxalic Acid	Thorium Oxide*			
			D-16	Th-650	Th-750	Th-900
Loss on ignition (%)			1.16	0.83	0.39	0.08
Composition						
Th (%)	24.79		86.82	86.83	87.30	87.40
NO_3^- (%)	4.08		<4 ppm	0.0019	0.0018	0.0018
CO_3^{--} (%)	0.06		0.55	0.52	0.13	<0.05
SO_4^{--} (ppm)	10	12	65	<10	<10	10
Cl^- (ppm)	6	435	40	10	10	<10
F^- (ppm)	70		25	295		
PO_4^{---} (ppm)	4		100	60	45	25
Fe (ppm)	33	<5	25	13	30	60
Cr (ppm)	<5	<5	<10	<10	<10	<10
Ni (ppm)	<5	<5	<10	<10	<10	<10
Pb (ppm)	<10	<10	<10	<10	<10	<10
Ba (ppm)	<10		<10			
Ca (ppm)	45		120	90	105	90
Mg (ppm)	25		300	<400	<400	<400
Na (ppm)	9		23			
K (ppm)	<5		<10			
Li (ppm)	<5		<10			
Si (ppm)	<5		20	15	10	10

*The "D" indicates a pilot-plant preparation of the oxide, which in this case was calcined at 650°C; the "Th" indicates a laboratory-scale preparation, and the number following indicates the temperature (°C) at which the oxide was calcined.

Precipitating the oxalate at 10 and 40°C and decomposing at 400°C yielded nearly cubic oxide particles 1 to 2 μ in size. Increasing the precipitation temperature to 70 or 100°C and decomposing at 400°C gave platelike oxide particles approximately 6 μ in average size. Refiring at 500, 650, 750, or 900°C did not change the shape or size of the original oxide but increased the average crystallite size and decreased the surface areas.

The thorium oxalates were prepared by precipitation from Thorex product thorium nitrate solution (1 M) by dropwise addition, with vigorous stirring, of excess 1 M oxalic solution. The precipitates were washed, dried, calcined for 4 hr at 375°C, and then fired for 16 hr at 400°C. The resulting oxides were used as stock materials for firings at higher temperatures. Final firings were for 24-hr periods.

Figure 14.3 shows a series of electron photomicrographs of the oxides produced at the different precipitation and calcination temperatures. A marked increase in particle size was noted as the precipitation temperature was increased from 40 to 70°C. No change in particulate properties was seen on increasing the firing temperature. Shadowing techniques indicated that the particles were platelets with an edge-to-thickness ratio of about 3 to 2 for the oxide from the 10°C precipitation and a ratio of 6 to 1 for that from the 100°C precipitation.

TABLE 14.9. EFFECT OF OXALATE PRECIPITATION TEMPERATURE AND CALCINATION TEMPERATURE ON SELECTED PROPERTIES OF ThO_2

Oxalate Precipitation Temperature (°C)	Surface Area, S (m^2/g)	Average X-Ray Crystallite Diameter, D (Å)	Average Particle Size Sedimentation Analysis (μ)	$K = SD \times 10^{-3}$	Loss on Ignition[a] (wt %)
		Final Firing Temperature – 400°C[b]			
10	35.3	61	1.2	2.2	1.27
40	41.7	69	1.3	2.9	
70	45.6	57	5.6	2.6	
100	51.0	56	4.2	2.9	1.47
		Final Firing Temperature – 500°C[c]			
10	40.1	78	1.1	3.1	1.09
40	40.9	74	1.6	3.0	
70	36.9	89	5.2	3.3	
100	48.0	92	3.9	4.4	0.85
		Final Firing Temperature – 650°C[c]			
10	25.4	143	1.4	3.6	0.41
40	27.4	127	1.4	3.5	
70	21.3	166	5.2	3.5	
100	16.7	185	4.2	3.1	0.54
		Final Firing Temperature – 750°C[c]			
10	12.8	250	1.1	3.2	0.1
40	16.7	231	1.5	3.9	
70	14.2	325	8.5	4.6	
100	6.9	350	4.2	2.4	0.37
		Final Firing Temperature – 900°C[c]			
10	6.3	550	1.3	3.5	0.1
40	8.5	616	2.4	5.2	
70	7.0	696	7.2	4.8	
100	3.3	775	5.1	2.6	0.20

[a]Dried at 200°C and heated to 1000°C.
[b]Stock preparation.
[c]Fired at temperature for 24 hr.

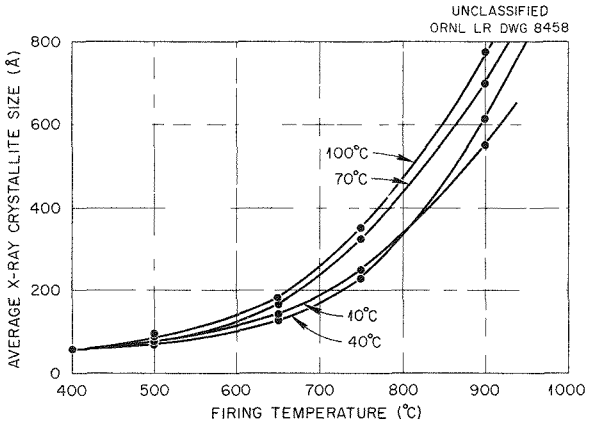

Fig. 14.1. Effect of Firing Temperature on Average X-Ray Crystallite Size of ThO_2 Fired at Temperature for 24 hr After Precipitation at Temperatures Indicated on Curves.

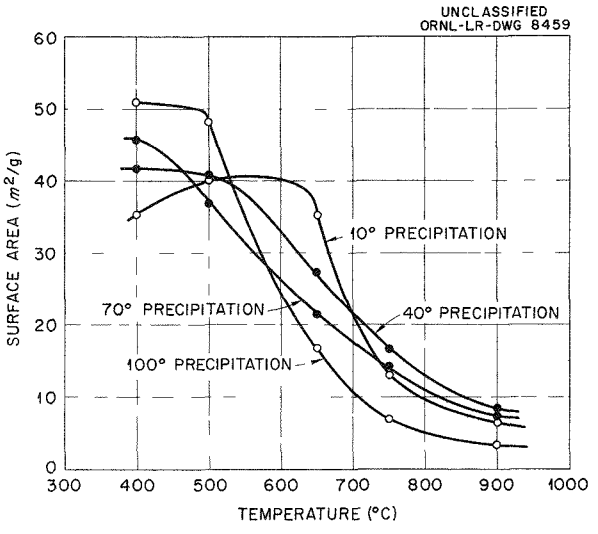

Fig. 14.2. Effect of Firing Temperature on Surface Area of ThO_2 Fired at Temperature for 24 hr.

Sedimentation particle size analyses showed excellent agreement with the electron photomicrographs.[6] Data for the 10 and 100°C precipitated material are shown in Figs. 14.4 and 14.5. Composite curves showing the effect of all precipitation temperatures on the particle size distribution of oxide products are given in Fig. 14.6.

Table 14.9 summarizes the average sedimentation particle size values together with the nitrogen adsorption surface areas and the average x-ray crystallite sizes of the oxide products. The effect of firing time on the oxide crystallite size is given in Table 14.10, and a logarithmic relation is illustrated in Fig. 14.7. From these data it can be concluded that the calcination time and temperature should be defined in order to characterize a preparation by its nitrogen adsorption surface area or its average x-ray crystallite size.

The following conclusions may be drawn concerning the temperature-time effects in the preparation of thorium oxide by oxalate decomposition:

1. The primary particle size depends on the precipitation temperature and is independent of the final calcination temperature up to 900°C.

2. The specific surface area and the crystallite size are initially independent of the precipitation temperature.

TABLE 14.10. EFFECT OF FIRING TIME ON ThO_2 CRYSTALLITE DIAMETER

Time	Temperature (°C)	Crystallite Diameter* (Å)
0		57
10 min	650	97
30 min	650	98
1 hr	650	114
7 hr 50 min	650	141
100 hr	650	209
672 hr	650	293
24 hr	650	166
24 hr	750	325
24 hr	900	696

*Determined by x-ray diffraction line broadening.

3. The x-ray crystallite size increases and the surface area proportionally decreases with either increasing calcination temperature or calcination time, or both.

4. Sintering between particles does not take place to any noticeable extent even at temperatures up to 900°C. Therefore the crystallite

[6] G. W. Leddicotte and H. H. Miller, *Anal. Chem. Semiann. Prog. Rep. Oct. 20, 1954*, ORNL-1788, p 21.

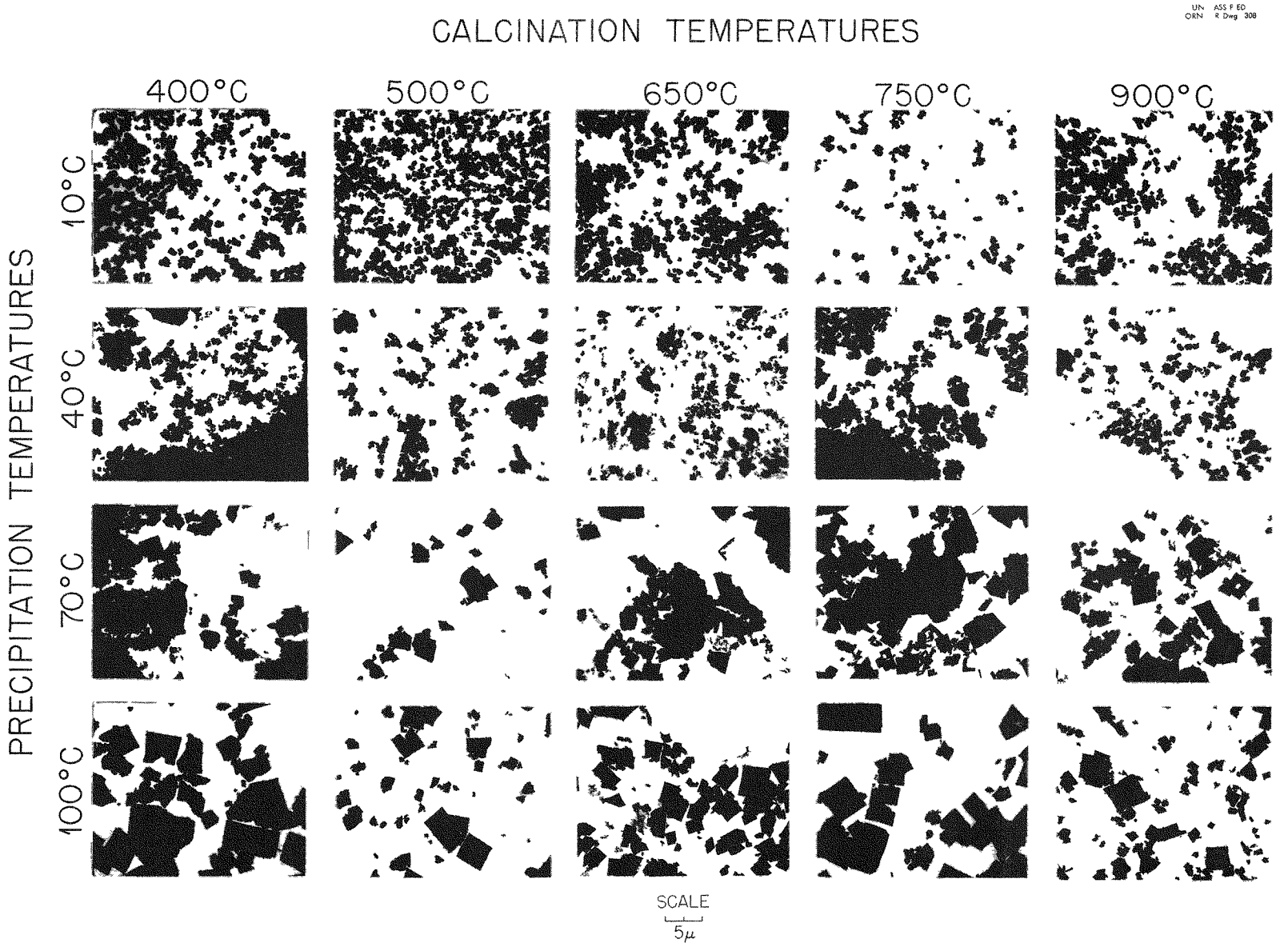

Fig. 14.3. Particle Size of ThO_2 as a Function of Calcination and Precipitation Temperatures.

growth process will probably be confined to the individual particles.

(b) Relation Between Surface Area and Crystallite Size of Oxides Prepared by Thermal Decomposition of Thorium Oxalate. – The fact that the nitrogen adsorption surface area of thorium oxide from oxalate decomposition varies inversely and the crystallite size directly with the firing temperature suggests a fundamental relation between them. For a cube or sphere the specific surface area is related to an edge or diameter by the equation

$$S = \frac{6}{\rho}\frac{1}{D},$$

where S is the area, ρ the density, and D the edge or diameter.

Figure 14.8 shows a plot of the theoretical equation, together with the data obtained with D-16 oxide and D-16 oxide recalcined at higher temperatures. The experimental curve fits an equation of the form

$$S = \left(\frac{6}{\rho}\frac{1}{F}\right)\frac{1}{D},$$

where F is a factor which involves the crystallite area not available for nitrogen adsorption as a

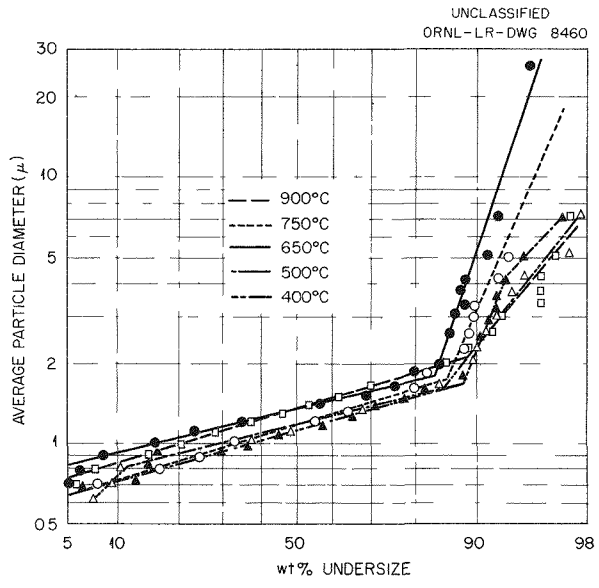

Fig. 14.4. Particle-Size Distribution of Thorium Oxides Prepared from Oxalate Precipitated at 10°C and Calcined at Elevated Temperatures.

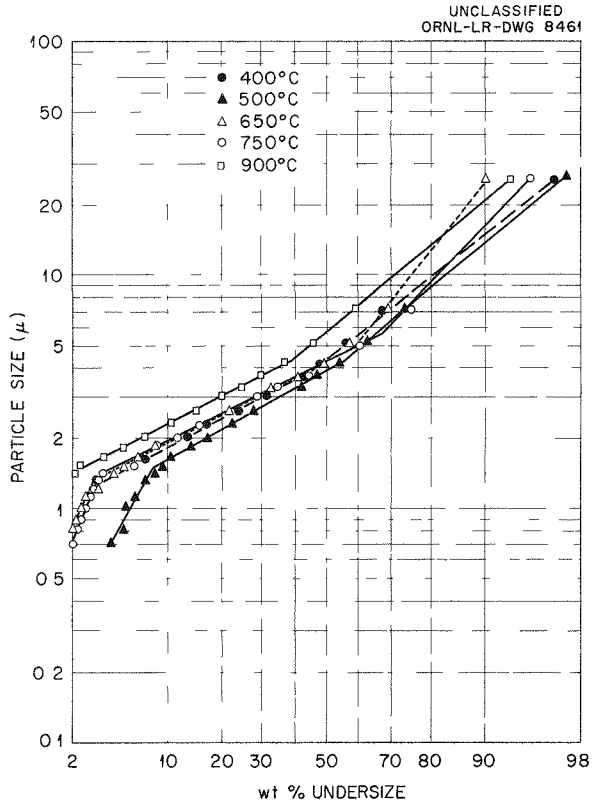

Fig. 14.5. Particle-Size Distribution for Thorium Oxides Prepared from Oxalate Precipitated at 100°C and Calcined at Elevated Temperatures.

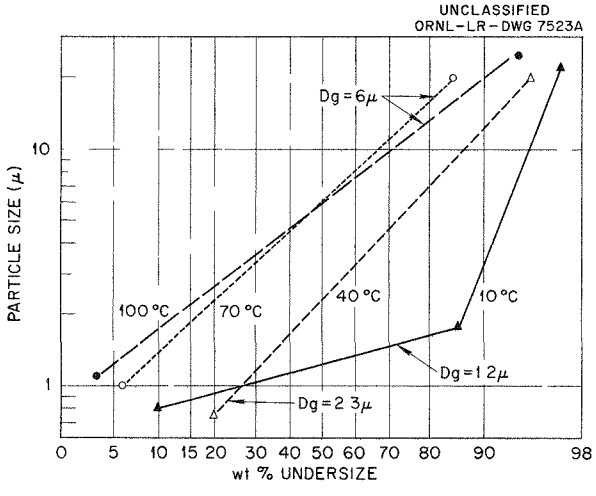

Fig. 14.6. Particle-Size Distribution vs Precipitation Temperature.

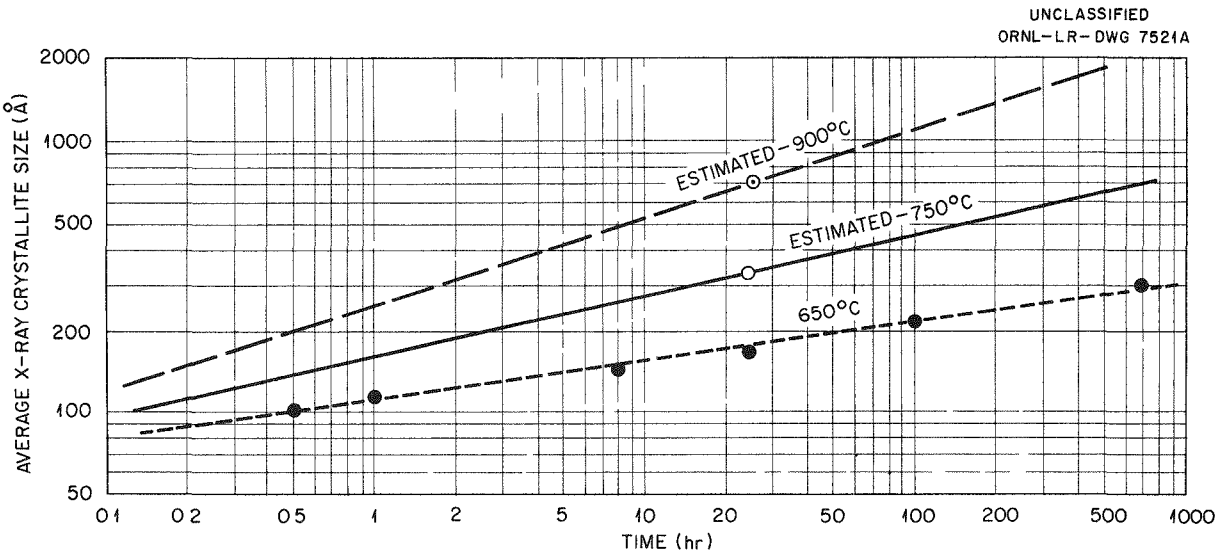

Fig. 14.7. Effect of Firing Time on Crystallite Size of ThO_2.

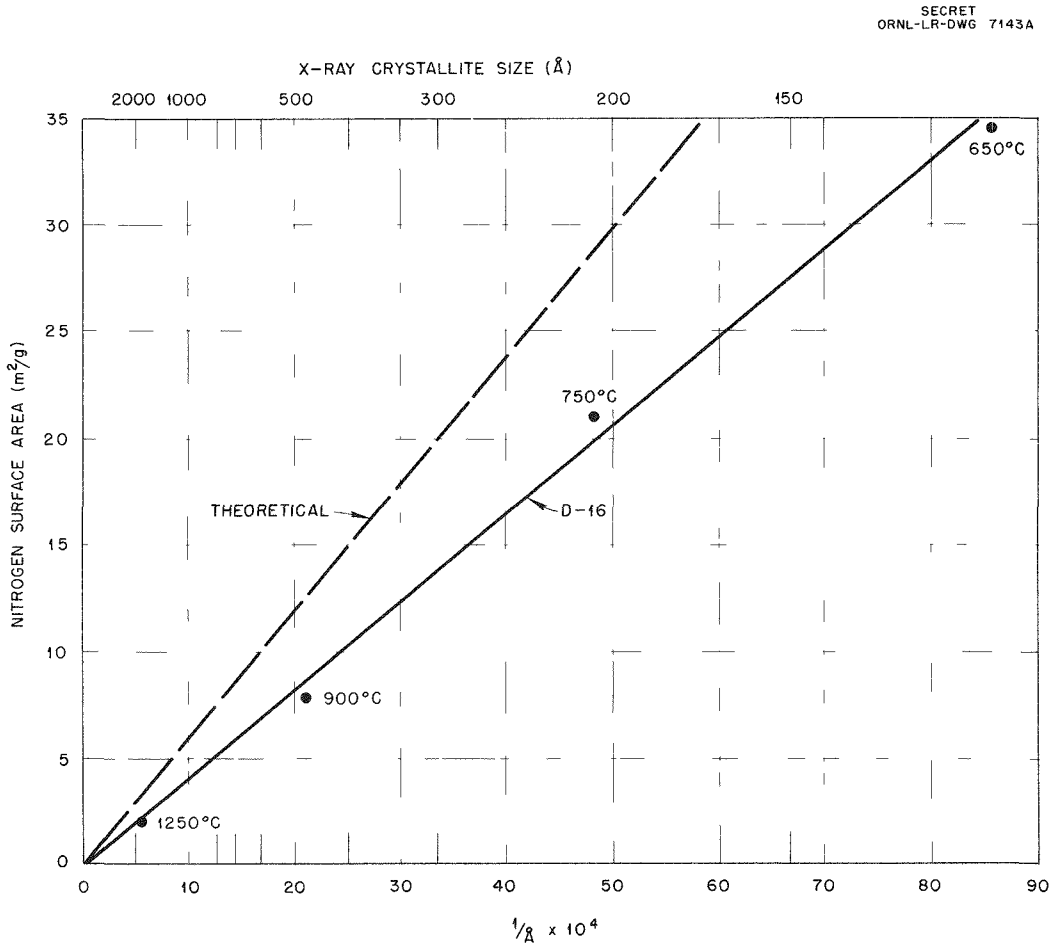

Fig. 14.8. Variation in Specific Surface Area with Variations in Average Crystallite Size of Recalcined D-16 Oxide.

result of packing, less the area contributed by roughness and deviation from the assumed perfect shape. Substituting K for the term $[(6/\rho)(1/F)]$ and solving for K gives $K = SD$. The K values have been calculated for some of the oxide products studied and are shown in Table 14.11. By using the average value for K, the approximate surface area (in square meters per gram) of an oxide from oxalate decomposition may be calculated from the x-ray crystallite size (in angstroms) by the equation $S = 3.6 \times 10^3/D$. Figure 14.9 shows the surface area–crystallite size relation.

(c) Thermogravimetric and Adsorption Properties of D-16 Oxide. – The steady-state ignition weight loss for D-16 oxide is illustrated in Fig. 14.10. Water vapor and carbon dioxide adsorption isobars are also shown for this material after it had been heated to 940°C.

The break in the curve at about 650°C is typical of the thermogravimetric data for thorium oxides and is indicative of the temperature to which the material had been previously heated. The break probably results from an increased loss of strongly adsorbed gases because of a decrease in surface area at the higher temperature.

The adsorption of CO_2 and/or H_2O on ThO_2 apparently is reversible only to the extent that a given quantity can be driven off for each temperature reached. The temperature required to degas a solid completely has not yet been established.

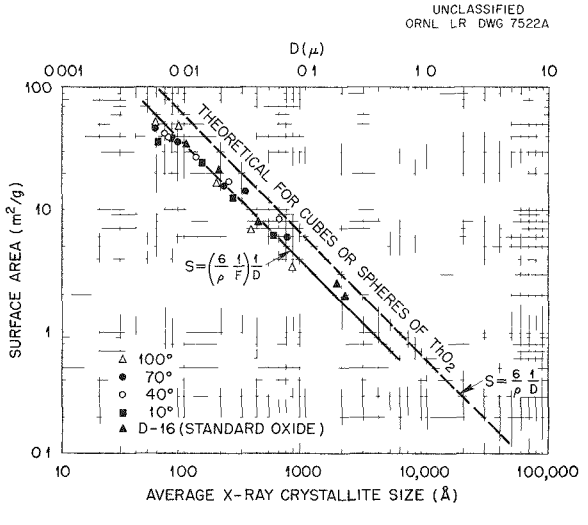

Fig. 14.9. Average X-Ray Crystallite Size vs Surface Area.

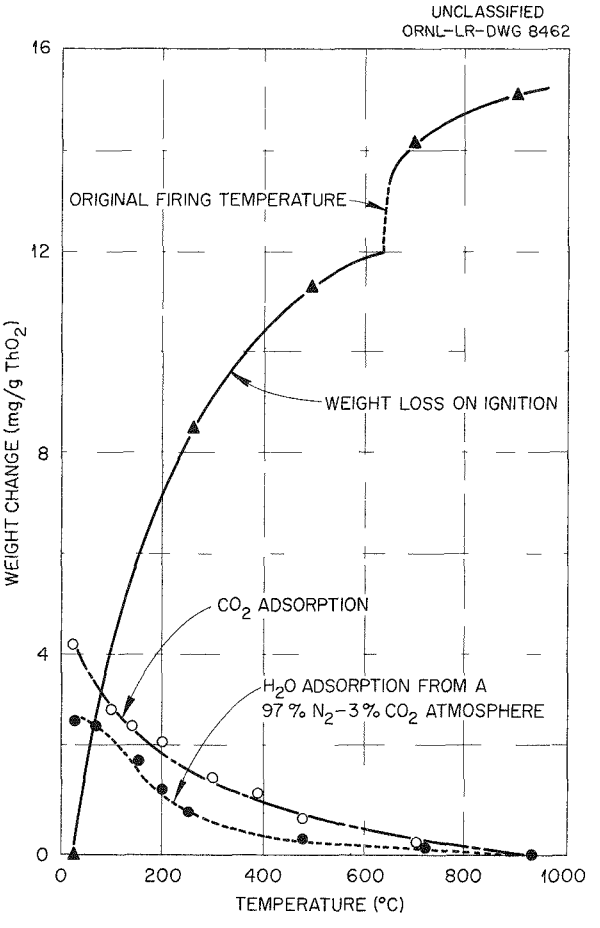

Fig. 14.10. Thermogravimetric Properties of D-16 Oxide; CO_2 and H_2O Adsorption Curves for D-16 Oxide Recalcined at 940°C.

However, loss-on-ignition data indicate that the amount of gas irreversibly adsorbed at a given temperature is related to the total surface area.

14.3.3 Effect of Sulfate on Properties of Thorium Oxide Slurries

E. V. Jones

The effect of autoclaving at 300°C in the presence of 0 to 10,000 ppm of sulfate on some of the chemical and physical properties of thorium oxide slurries was determined as a function of the firing temperature of the original oxide (650 to 1000°C). Parallel studies in which 0.005 m $Na_4P_2O_7$ was added along with the sulfate were also carried out.

TABLE 14.11. SELECTED PROPERTIES OF OXIDE PRODUCTS

Material	Final Firing Temperature (°C)	Time at Temperature (hr)	Nitrogen Adsorption Surface Area, S (m^2/g)	Average X-Ray Crystallite Diameter, D (Å)	$K = SD \times 10^{-3}$
ThO_2 from formate	650[a]		16.6		
ThO_2 from formate	650[b]		22.5		
Lindsay No. 8	900[c]		6.6		
Lindsay No. 11	650[a]		13.0	261 ± 6	3.4
Lindsay No. 12	650[b]		26.2	144 ± 5	3.8
Lindsay No. 13	650[b]		18.0	184 ± 5	3.3
ThO_2 pyrohydrolyzed	350	70	44.0		
ThO_2 pyrohydrolyzed	500	115	30.6		
ThO_2 pyrohydrolyzed	900	16	8.3		
Lab-prep Th-602[d]	650[e]	4	35.3	131 ± 13	4.6
Lab-prep Th-701[d]	750[e]	4	21.9	236 ± 36	5.2
Lab-prep Th-901[d]	900[e]	4	12.3	441 ± 80	5.4
Lab-prep Th-1000[d]	1000[e]	4	8.3	858 ± 66	7.1
H5A[d]	650[e]		31.9		
D-10[d]	650[e]	8.5	31.9		
D-12[d]	650[e]	4.5	32.7		
D-12 (pelletized at 40,000 psi)	650		33.1		
D-12[c]	650[e]		32.3		
D-15[c]	650[e]		35.6		
D-15	800		17.6		
D-15	850		13.5		
D-16	650[e]	3.4	34.7	103 ± 4	3.6
D-16 – 750[d]	750[e]	16.5	21.1	191 ± 6	4.0
D-16 – 900[d]	900[e]	16	7.9	412 ± 10	3.3
D-16 – 1250[d]	1250–1300[e]		2.0	2162 ± 46	4.3
D-17[d]	650[e]		35.4		
D-18[d]	650[e]	4.3	36.0		

TABLE 14.11 (continued)

Material	Final Firing Temperature (°C)	Time at Temperature (hr)	Nitrogen Adsorption Surface Area, S (m^2/g)	Average X-Ray Crystallite Diameter, D (Å)	$K = SD \times 10^{-3}$
D-19[d]	650[e]		33.9		
D-20[d]	650[e]	8.5	35.6		
D-21[d]	650[e]	3	35.0		
D-31[d]	800[e]	4.75	15.7		
ThO_2 from thorium nitrate	700		57.0	101 ± 3	5.76
S-64-C loop run			30.7		
X-12-C loop run			20.0		
X-12-3 loop run			18.7		
3434-55 (D-16)	1300		2.5	1783 ± 91	4.5
D-16	1100		5.96	898 ± 40	5.4
1C National Lead[c]			20.2		
9DE-238-02 National Lead[c]		0.3	29.5	110 ± 3	3.2
FMPC-6-28[c]			32.6	115 ± 4	3.8
FMPC-6-28[c]	800	4	16.0	202 ± 15	3.2

[a]Single stage hot furnace.
[b]Placed in cold furnace.
[c]Oxalate precipitated at 80–100°C.
[d]Oxalate precipitated at 40°C.
[e]Multiple-stage calcination.

In the presence of sulfate alone, the pH decreased and the density of settled solids (bulk density) for all oxides increased with increasing sulfate concentration. With pyrophosphate added, the pH also decreased, more or less regularly, with increasing sulfate concentration of all oxides, but the settled-solids densities showed marked maxima and minima, the effect becoming more pronounced with oxides that had been fired at the higher temperature (see Figs. 14.11 to 14.14). The treatment with either sulfate alone or sulfate plus pyrophosphate did not change the x-ray crystallite size or gross particle size of the original oxide (see Tables 14.12 and 14.13).

The materials used in the study were D-16 oxide (Sec. 14.4) and oxides prepared by refiring the D-16 oxide for 4 hr at 750, 900, and 1000°C. Slurries of the oxides, containing 500 g of thorium per kilogram of H_2O, were autoclaved at 300°C for 22 hr with 0, 200, 500, 1,000, 2,500, 5,000, or 10,000 ppm of SO_4^{--}, added as $Th(SO_4)_2$, in the absence and presence of 0.005 m $Na_4P_2O_7$. After cooling, the slurries were allowed to settle for more than 48 hr, and the supernatant pH and the volume of settled solids were measured. The solids were then redispersed by vigorous agitation and sampled for x-ray and sedimentation particle size analyses. The settled-solids

TABLE 14.12. EFFECT OF SULFATE ION ON PROPERTIES OF ThO_2 SLURRIES

Slurries containing 500 g of thorium per kilogram of H_2O autoclaved for 22 hr at 300°C

Experiment Number	Initial Sulfate Concentration (mg per kg of ThO_2)	Supernatant pH	Density of Settled Solids (g of Th per liter)	Average Crystallite Diameter (Å)	Average Particle Size (μ)	Average Surface Area (m^2/g)
			650°C Oxide			
X-1	0	8.3	1295	111	2.1	
X-3	200	7.6	1300	116	2.1	
X-5	500	8.0	1300	115	2.1	
X-7	1,000	7.4	1295	126	2.5	
X-9	2,500	6.5	1240	119	2.1	
X-11	5,000	5.9	1290	114	2.3	
X-13	10,000	4.1	1515	119	2.1	
						30.8
			750°C Oxide			
X-21	0	9.7	1510	228	2.2	
X-23	200	9.6	1375	204	2.0	
X-25	500	8.6	1405	213	2.0	
X-27	1,000	8.5	1410	204	2.0	
X-29	2,500	7.1	1415	204	2.9	
X-31	5,000	5.2	1540	203		
X-33	10,000	4.6	1590	227		
						17.0
			900°C Oxide			
X-41	0	8.7	1548	474	2.4	
X-43	200	8.5	1490	418	2.1	
X-45	500	8.9	1505	429	2.3	
X-47	1,000	7.0	1560	422	2.1	
X-49	2,500	5.8	1730	433	2.4	
X-51	5,000	2.5	1840	452	2.4	
X-53	10,000	4.0	1920	426	2.9	
						8.26
			1000°C Oxide			
X-61	0	8.9	1590		3.1	
X-63	200	7.3	1545	627	2.3	
X-65	500	6.5	1530	684	3.0	
X-67	1,000	5.8	1565	589		
X-69	2,500	5.0	1685	780		
X-71	5,000	5.0	1785	871		
X-73	10,000	3.9	2010			
						5.07

TABLE 14.13. EFFECT OF SULFATE PLUS SODIUM PYROPHOSPHATE ON PROPERTIES OF ThO_2 SLURRIES

Slurries containing 500 g of thorium per kilogram of H_2O autoclaved for 22 hr at 300°C

Experiment Number	Initial Sulfate Concentration (mg per kg of ThO_2)	Supernatant pH	Density of Settled Solids (g of Th per liter)	Average Crystallite Diameter (Å)	Average Particle Size (μ)	Average Surface Area (m^2/g)
			650°C Oxide			
X-2	0	10.3	1745	127	2.5	
X-4	200	9.5	1760	122	2.4	
X-6; X-6r	500	9.7; 10.1	1755; 1800	114	2.2	
X-8; X-8r	1,000	8.7; 9.2	1370; 1525	123	3.0	
X-10	2,500	7.6	1370	118	2.4	
X-12	5,000	7.2	1355	123	2.3	
X-14	10,000	4.8	1580	135	3.0	
						29.2
			750°C Oxide			
X-22	0	11.6	1740	211	3.2	
X-24r	200	11.4	1610	206		
X-26	500	11.6	1615	203		
X-28	1,000	11.1	1495	218	2.9	
X-30	2,500	10.0	1520	205	4.3	
X-32	5,000	6.8	1620	200		
X-34; X-34r	10,000	2.9	2400; 2300	209; 220		
						17.4
			900°C Oxide			
X-42	0	11.5	2500	415	2.2	
X-44	200	11.3	2530	424	2.6	
X-46	500	11.2	2315	367	2.1	
X-48	1,000	9.7	2300	345	2.2	
X-50	2,500	7.3	1990	370	2.2	
X-52	5,000	3.2	2720	394	2.6	
X-54	10,000	2.8	2205	453	3.2	
						9.07
			1000°C Oxide			
X-62	0	11.2	2860	600	2.9	
X-64	200	11.3	2800	684	3.2	
X-66	500	11.0	2770	760		
X-68	1,000	10.3	2770	801		
X-70	2,500	6.4	2760	711		
X-72	5,000	2.5	3135			
X-74	10,000	2.7	2405			
						5.02

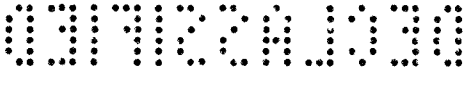

density, expressed as grams of thorium per liter, was calculated from the total thorium content and the volume of settled solids.

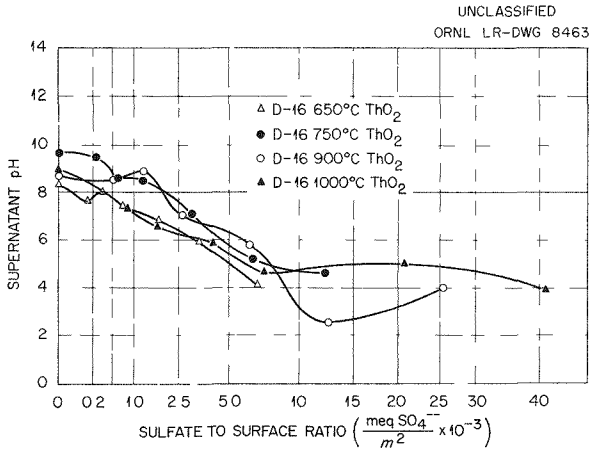

Fig. 14.11. Supernatant pH in Autoclaved (300°C) ThO_2 Slurries Containing SO_4^{--}.

The data are summarized in Tables 14.12 and 14.13. Plots of the supernatant pH and density of settled solids vs the ratio of sulfate concentration to oxide surface are shown in Figs. 14.11, 14.12, 14.13, and 14.14. The surface areas were calculated from the x-ray crystallite sizes of the oxides (see Sec. 14.3.2). The similarity in the bulk density curves obtained for all oxides suggests that sulfate-to-surface ratio is more important than sulfate concentration alone in determining the relative effect of sulfate additions on the bulking properties of slurries.

The settled-solids densities obtained in all experiments are plotted against the corresponding supernatant pH in Fig. 14.15. The dispersing action of $Na_4P_2O_7$ is illustrated by the marked increase in bulk density obtained in its presence. In addition, all oxides show a low bulk density or high flocculation characteristic at pH 6 to 9 and a relatively higher dispersion (high bulk density) in both the low and high pH regions, indicating

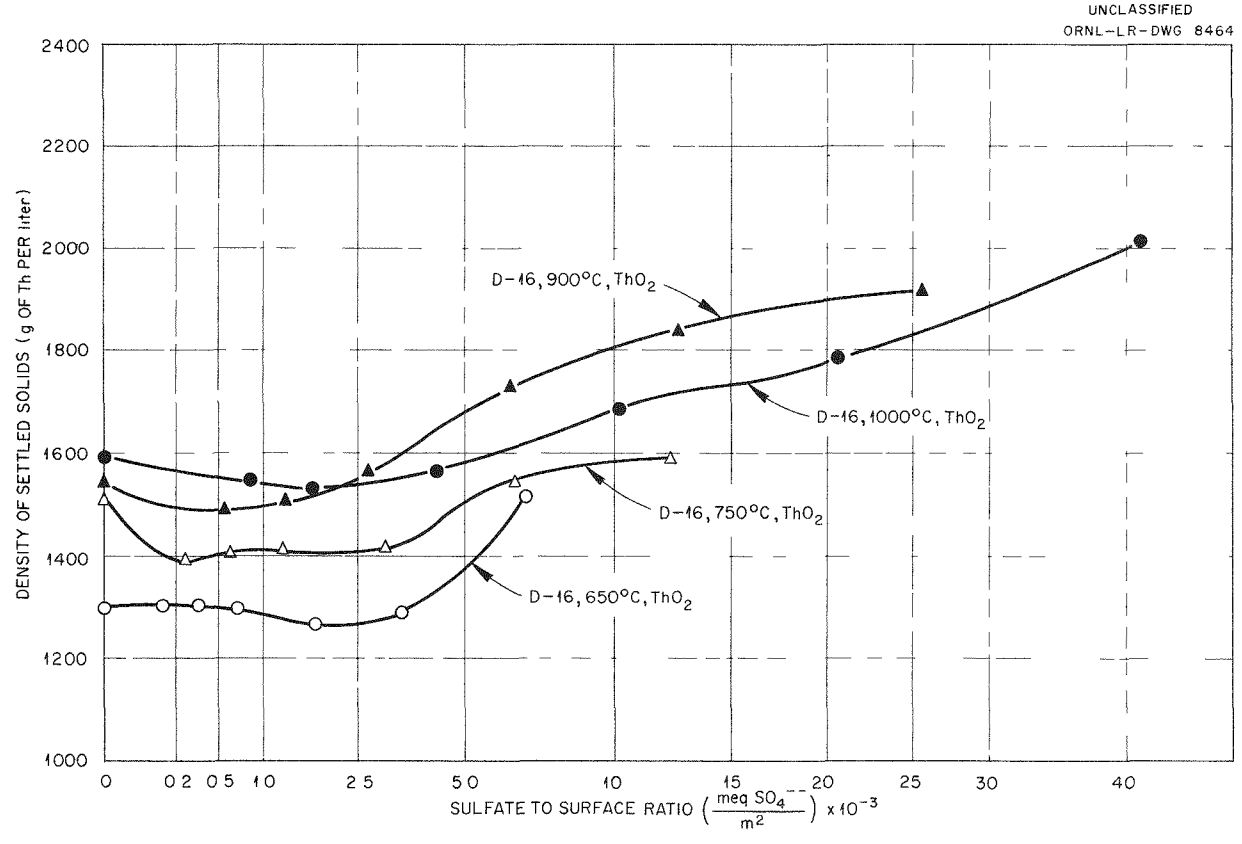

Fig. 14.12. Bulking Properties of Autoclaved (300°C) ThO_2 Slurries Containing SO_4^{--}.

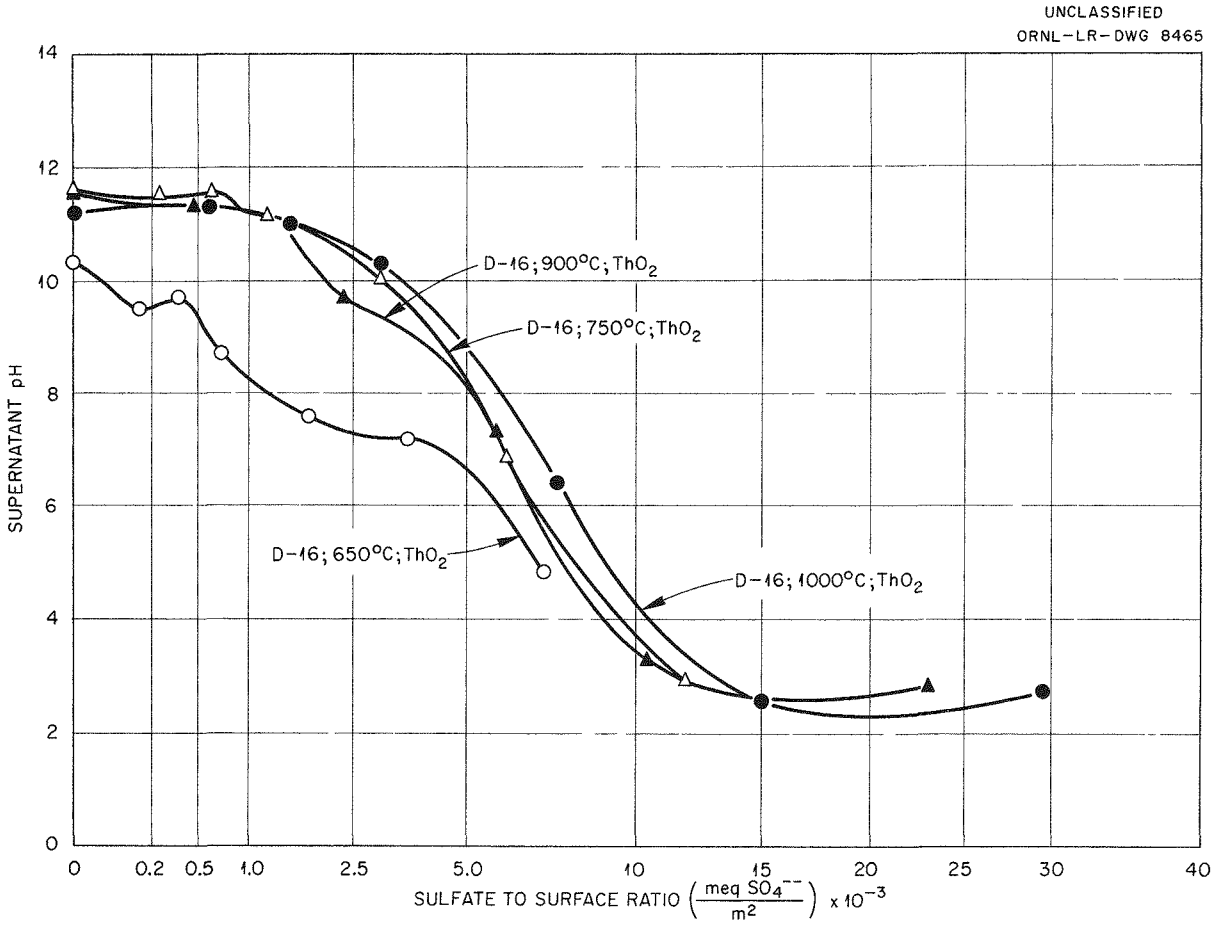

Fig. 14.13. pH of Supernatant Autoclaved (300°C) ThO_2 Slurries Containing Sulfate and 0.005 *M* $Na_4P_2O_7$.

the importance of supernatant pH in determining bulk slurry properties.

14.3.4 Particulate Properties of Thorium Oxide Slurries

C. E. Schilling

A study was initiated with the objective of developing the particle size concepts and the methods of particle size analysis of importance in the study of thorium oxide slurries and determining the effect of particle size on the characteristics of thorium oxide slurries. Particle sizes, as determined by sedimentation rate in the presence of a dispersing agent (0.005 *m* $Na_4P_2O_7$), vary with methods of preparation and slurry handling and appear to be important in the characterization of oxide solids and their suspensions. Oxides that had been pumped as a slurry at elevated temperatures reached approximately the same average particle size as those degraded dry at room temperature in a Micronizer. Preliminary results of experiments with Waring and Brookfield blenders to simulate the effect of pumping on slurry properties indicate that the observed increases in slurry viscosity are not the result of particle degradation alone.

Sedimentation particle sizes obtained with D-10 pilot plant oxide as prepared, after pumping, and after "micronizing" are shown in Fig. 14.16. Figure 14.17 is a similar plot of another pilot plant product, D-16, as prepared, after being blended for 2 hr in a Waring Blendor, and after being micronized. The degradation occasioned by mechanical handling is obvious, and the effects of the three different methods used to degrade the sample are similar. The surface area of the D-10

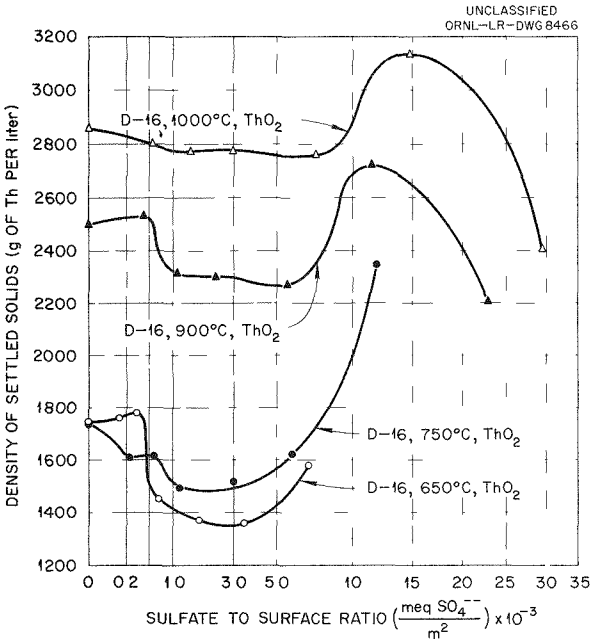

Fig. 14.14. Density of Settled Solids of Autoclaved (300°C) ThO_2 Slurries Containing SO_4^{--} and 0.005 *M* $Na_4P_2O_7$.

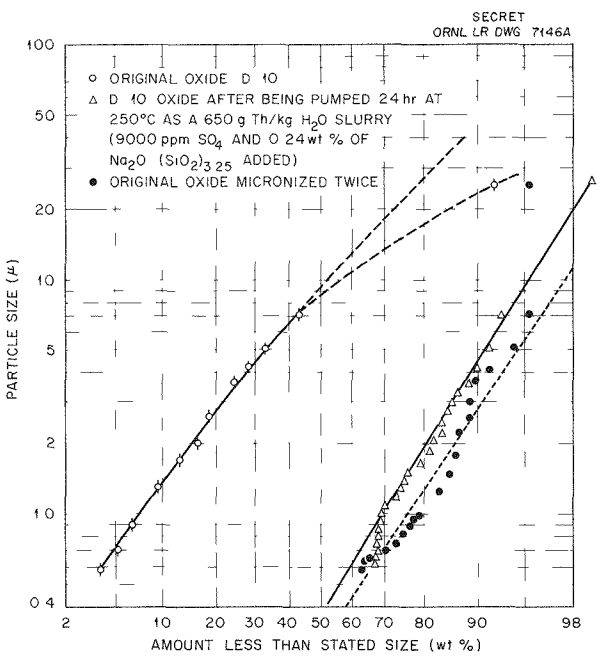

Fig. 14.16. Effect of Pumping and "Micronizing" on ThO_2 Sedimentation Particle Size.

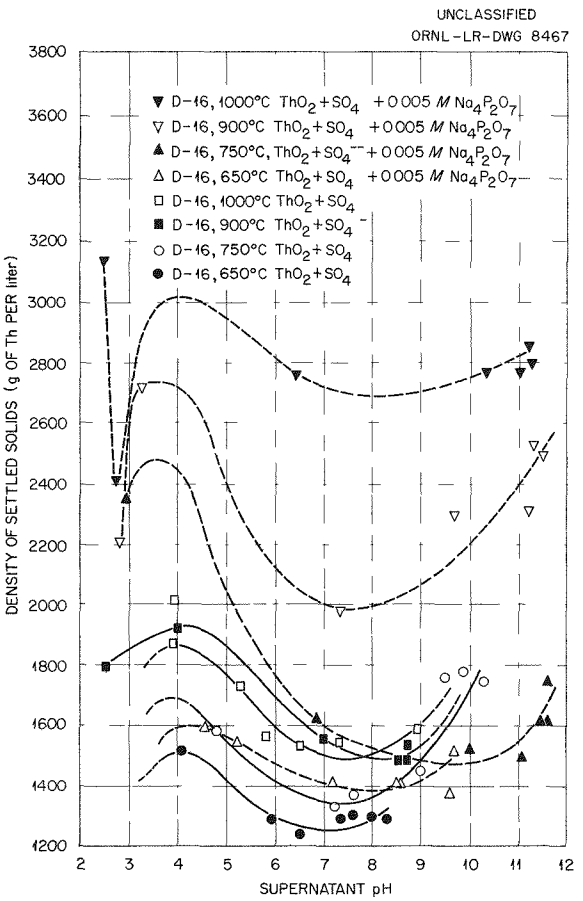

Fig. 14.15. Density of Settled Solids vs Supernatant pH for Autoclaved (300°C) ThO_2 Slurries Containing SO_4^{--} and SO_4^{--} Plus 0.005 *M* $Na_4P_2O_7$.

oxide was increased from 32.4 to only 37.9 m^2/g by micronizing, indicating that N_2 adsorption is measuring essentially internal surface area and that little change in total surface area will be brought about by prolonged pumping in a loop system.

Several samples of D-16 oxide and D-16 oxide recalcined at 750 and 950°C were made into slurries containing 1000 g of thorium per kilogram of H_2O. One sample of the D-16 oxide slurry was shaken briefly at room temperature, and a second was tumbled for one week at room temperature. A third sample of the D-16 oxide slurry and slurries of the recalcined materials were blended in a Waring Blendor at 8°C for 2 hr. Apparent Brookfield

viscosities were obtained for all the samples and for a slurry of the micronized D-16 material containing 1000 g of thorium per kilogram of H_2O (see Table 14.14). Little increase in apparent viscosity is noted for the micronized sample over the unmicronized material despite the fact that its particles had been degraded from an average size of 3.1 to 0.8 μ. The blended material, on the other hand, showed a pronounced increase in apparent viscosity even though its particles were not degraded to so small a size. The higher temperature calcined materials showed a relatively smaller increase in viscosity on blending but were degraded to nearly the same extent as the original D-16.

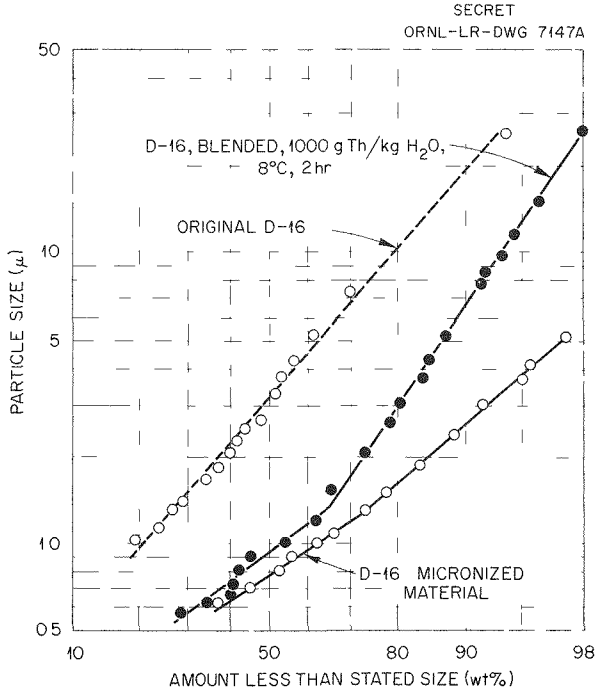

Fig. 14.17. Effect of Blending and "Micronizing" on Thorium Oxide Sedimentation Particle Size.

14.3.5 Slurry Viscosity Measurements at Elevated Temperatures

D. G. Thomas

In studies of the viscosity of thorium oxide slurries it has been shown that at room temperature and constant rates of shearing strain the apparent viscosity varies by factors of 10^3 to 10^4, depending on the electrolyte atmosphere in the slurry.[7] It has also been shown that, at room temperature and with a constant electrolyte atmosphere, the apparent viscosity varies by a factor of 10^4 as the rate of shearing strain is varied.[8] It appeared that a measurement of viscosity of thorium oxide slurries would be useful in the characterization of various preparations of thorium oxide. Since no information is

[7] R. N. Lyon *et al.*, *HRP Quar. Prog. Rep. Oct. 31, 1954*, ORNL-1813, p 123.

[8] R. N. Lyon *et al.*, *HRP Quar. Prog. Rep. Jan. 31, 1955*, ORNL-1853, p 147.

TABLE 14.14. EFFECT OF PRETREATMENT ON VISCOSITY OF THORIUM OXIDE SLURRIES

Starting material: D-16 ThO_2, calcined at 650°C
Slurry thorium concentration: 1000 g per kilogram of H_2O

Pretreatment	Apparent Brookfield Viscosity (centipoises)				Final Mean Particle Diameter (μ)
	At 6 rpm	At 12 rpm	At 30 rpm	At 60 rpm	
Shaken by hand to disperse	600	900	680	430	3.1
Tumbled for one week	700	850	580	540	3.1
Micronized dry, shaken	1500	850	700	500	0.79
Blended for 2 hr	7000	4000	2500	2600	0.92
Calcined at 750°C, blended for 2 hr		2000	2000	2100	0.95
Calcined at 900°C, blended for 2 hr	3500	1500	900	500	1.1

available on the viscosities of thorium oxide slurries at elevated temperatures, it also appeared desirable to be able to make measurements over a range of temperatures from ambient to 300°C.

A capillary viscometer,[9,10] now being used to measure the viscosity of molten salts, seemed to possess many desirable features; namely, operation required small quantities of material; with simple modifications the system could be operated at 2000 psi and 300°C; and the geometry of the system permitted rigorous analysis of the data. A stainless steel capillary viscometer, incorporating these features and suitable for use with slurries at elevated temperatures, was designed and constructed (Fig. 14.18). The slurry is made to flow either from the inner reservoir to the outer or vice versa under the action of a differential pressure. The differential pressure is measured, and the equalization of pressure between the two reservoirs indicates the end of a cycle. The inner reservoir is stirred with a dash-pot stirrer and the outer with a magnetic stirrer. The viscometer is shown disassembled in Fig. 14.19. It is now being calibrated with water.

The accuracy of the experimental results will depend on an evaluation of end and kinetic effects, as well as slippage at the wall of the capillary and slippage between the particles and the fluid. Slippage at the wall could cause an erroneous interpretation of the data in that a

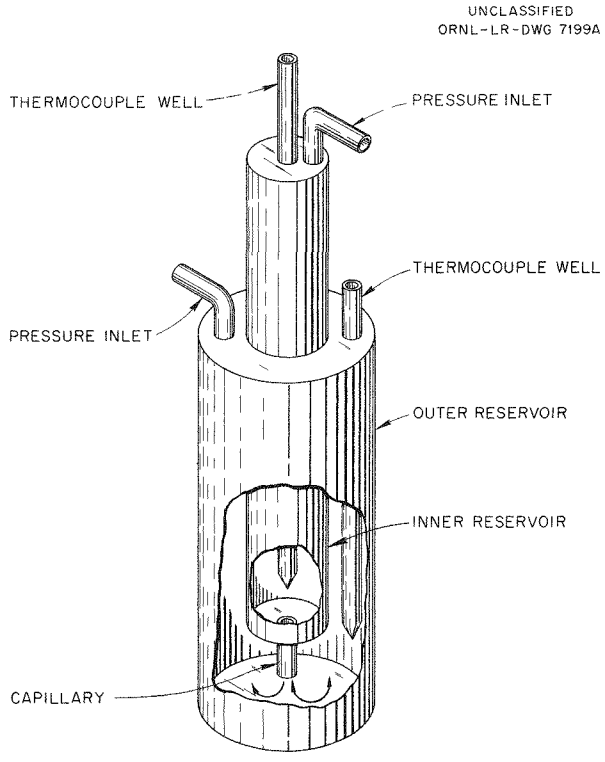

Fig. 14.18. Capillary Viscometer.

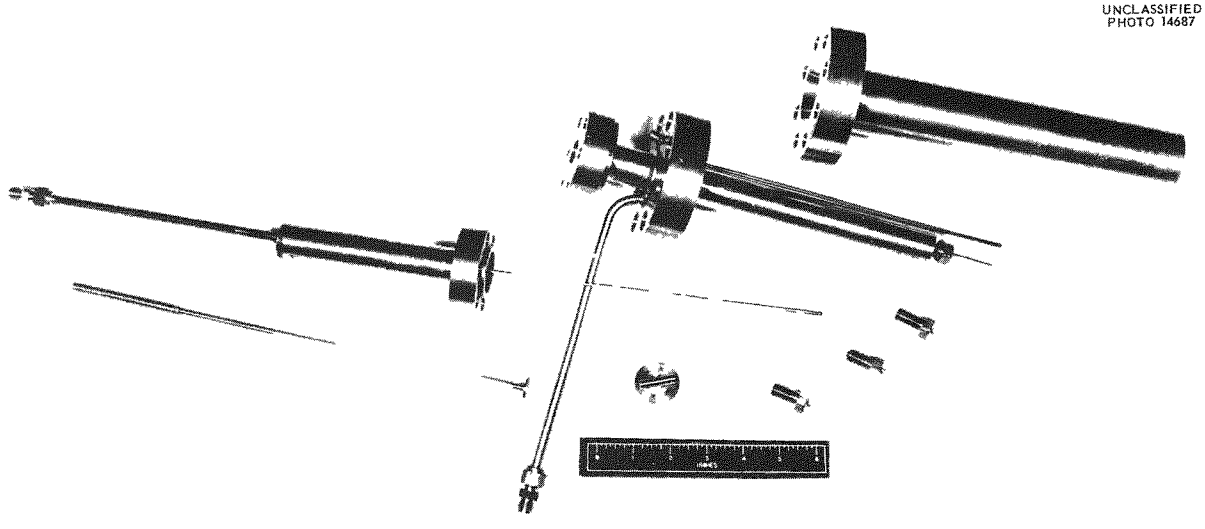

Fig. 14.19. Capillary Viscometer – Disassembled.

[9] F. A. Knox, N. V. Smith, and F. Kertesz, *ANP Quar. Prog. Rep. Sept. 10, 1952*, ORNL-1375, p 145.

[10] F. A. Knox, N. V. Smith, and F. Kertesz, *ANP Quar. Prog. Rep. Dec. 10, 1952*, ORNL-1439, p 176.

Bingham plastic would appear to behave as a pseudoplastic.

The viscosity of ThO_2 slurries at elevated temperatures was estimated in order to choose the proper range of capillary sizes for the viscometer. Guth and Simha[11] have proposed the following relation for the viscosity of concentrated suspensions of solid spheres in liquids:

$$\eta_{sp} = \eta_0 (1 + 2.5\,\phi + 14.1\,\phi^2 + \cdots) ,$$

where

η_{sp} = apparent viscosity of suspension, centipoises,

η_0 = viscosity of pure liquid, centipoises,

ϕ = volume concentration of particles.

The calculated viscosities of a slurry containing 1800 g of ThO_2 per kilogram of H_2O are plotted in Fig. 14.20 for temperatures up to 300°C. The validity of the calculated viscosity curve for ThO_2 slurry depends upon there being no interaction between ThO_2 and H_2O. At room temperatures a pronounced interaction has been shown.[7,8] However, hindered settling data taken at elevated temperatures[12] show a sharp change in the viscosity-temperature relation at temperatures in the range 150 to 200°C, indicating that the interaction of ThO_2 and H_2O may be small above 200°C. Therefore, for the temperature range 200 to 300°C, it is expected that the viscosities of all ThO_2 slurries will be approximated by a relation similar to that of Guth and Simha. At lower temperatures the viscosities are expected to be characteristic of the particular slurry preparation, and thus one of the principal uses of the viscometer will be in the study of slurries below 200°C.

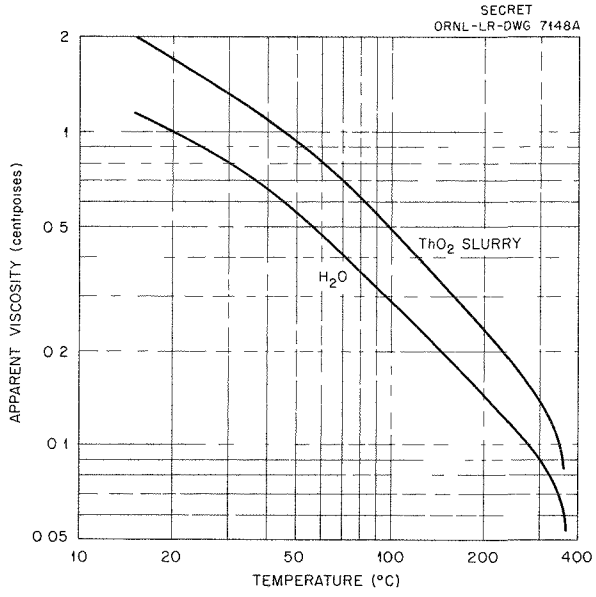

Fig. 14.20. Calculated Viscosities of Thorium Oxide Slurry (1800 g of ThO_2 per kilogram of H_2O) at Various Temperatures. The experimentally determined viscosities of water are given for comparison.

14.4 LARGE-SCALE PREPARATION OF THORIUM OXIDE

W. H. Carr

The availability of a large quantity of pure, essentially sulfate-free thorium nitrate product solution from the nonradioactive Thorex process runs prompted its utilization in the large-scale preparation of pure thorium oxide for use as a standard material in the laboratory and engineering development of a blanket slurry. The method consisted in precipitating the oxalate at 40°C by adding 15% excess solid oxalic acid to a 1 *M* solution of the Thorex product and subsequently thermally decomposing the washed and air-dried oxalate to oxide by heating for 2 hr at 370°C, 2 hr at 520°C, and 4 hr at 650, 800, or 950°C, depending on the specification of the various slurry development groups. More than 3000 lb of oxide was produced in 160-lb lots. The batches were designated by the letter "D". Lot D-16, an oxide prepared with final calcination at 650°C, was set aside as a stock of standard oxide for use in laboratory slurry studies.

[11] E. Guth and R. Simha, *Kolloid-Z.* 74, 266 (1936).

[12] S. A. Reed, *HRP Quar. Prog. Rep. Jan. 31, 1955*, ORNL-1853, p 83.

15. FUEL PROCESSING

D. E. Ferguson E. O. Nurmi W. E. Unger

R. K. Adams
W. L. Carter
J. R. Engel
C. E. Guthrie[1]
P. A. Haas
R. W. Horton
J. K. Langsdon
R. B. Lindauer
C. S. Lisser
F. C. McCullough
R. A. McNees
S. Peterson
A. M. Rom
H. E. Williamson
R. H. Winget
H. O. Weeren
M. E. Whatley

15.1 HRT CHEMICAL PLANT

R. K. Adams
W. L. Carter
C. E. Guthrie
R. B. Lindauer
C. S. Lisser
F. C. McCullough
A. M. Rom
H. O. Weeren
H. E. Williamson
R. H. Winget

The HRT fuel processing plant is an experimental facility designed to remove the insoluble fission and corrosion products from 0.25 gpm of fluid which bypasses the reactor heat exchanger. The separation will be accomplished by a 0.25-in.-dia hydroclone, a hydraulic adaptation of the familiar gas cyclone. The plant will operate for 48 hr each week and will reduce the insoluble rare-earth concentration from 70 to approximately 50 mg/liter. Corrosion products – iron, chromium, and zirconium – which hydrolyze and precipitate will also be removed.

The plant will be located in Building 7500 in a sealed, shielded cell, similar to the reactor cells, designed to contain 50 psi internal pressure. The cell liners have been installed and welded, and the surrounding barytes concrete shielding walls will be poured as soon as the cells have been leak-tested. Startup of the plant is currently scheduled for September 1956, three months after the initial startup of the reactor. The plant will be operated under a variety of conditions in order to develop information required for the design of a continuous processing plant for thermal breeder reactor fuel. The efficiency of the hydroclone as a centrifugal separator will be determined from a comparison of the rare-earth concentration in the underflow receiver to that in the clarified overflow stream return to the reactor system. Variables affecting the hydroclone efficiency are largely limited to the flow rate through the hydroclone, which is accurately indicated by the pressure drop across it. Thus the combined effect of particle size, density, and shape factors on the separability of the precipitates will be inferred from the apparent efficiency of the hydroclone.

The proposed arrangement of the equipment in the cell is shown in Fig. 15.1. The fuel stream to the hydroclone will pass through a surface heater (H-3), which will raise the feed temperature to decrease the amount of rare earths in solution (there is an approximately twofold reduction in rare-earth solubility for each 25°C increase in temperature) and will provide a hot surface to encourage the deposition of the fission products. The fuel will then go through a screen with the mesh sized to retain particles larger than the hydroclone orifices, through the hydroclone, through the fuel pump (P-1), and then back to the reactor system. The energy for centrifugation is manifest as a pressure drop across the hydroclone, supplied partly by the pressure drop across the reactor heat exchanger and partly by a canned-rotor pump in the overflow line returning the clarified fuel solution to the reactor system. The solids separated by the centrifugal action of the hydroclone collect in the underflow receiver (T-1).

At the conclusion of an operating period (about 48 hr) the feed and return lines will be closed by valves located in the reactor cell, and the pressure in the underflow pot will be reduced by lowering its temperature. The low-temperature fuel (approximately 80°C) will redissolve the rare-earth solids in the underflow receiver and from the surfaces of the heater and screen. The fuel pump may be employed to recirculate the fuel during redissolution by means of a bypass from the pump discharge to the return line, normally closed by a freeze plug.

The contents of the underflow pot will then flow to the evaporator decay tank (E-1), where the heat from radioactive decay can be dissipated and the heavy water partially recovered by evaporation.

[1] Atlantic Refining Company.

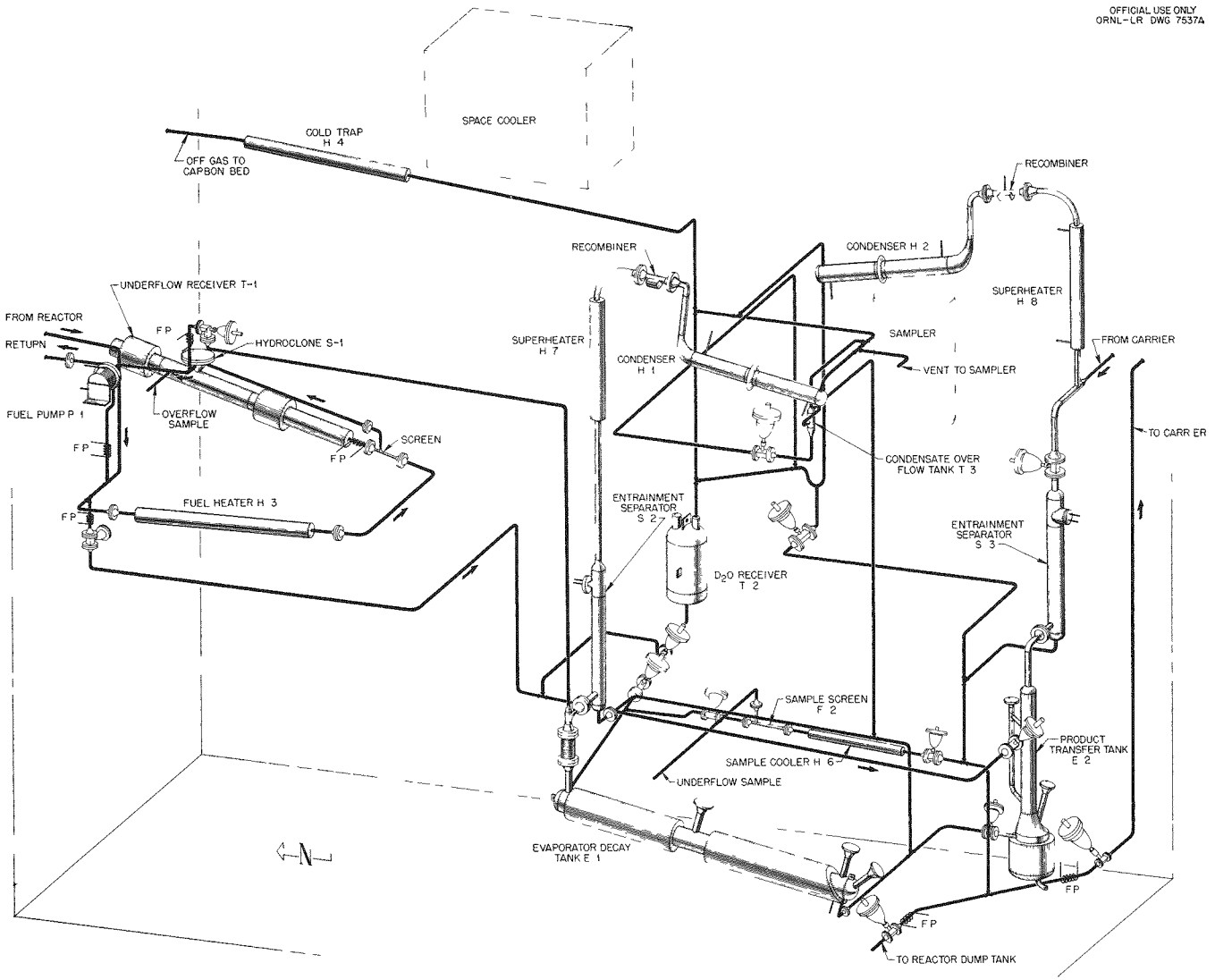

Fig. 15.1. Proposed Arrangement of Equipment in HRT Chemical Plant.

The evaporator contents, after decay and concentration, will flow to the transfer tank. The transfer tank contents may be discharged either to a shielded carrier outside the cell or to the reactor dump tank, or they may be recycled back into the evaporator. The transfer is to be accomplished by isolating the tank and increasing its temperature with its steam jacket until sufficient vapor pressure is developed to make the transfer.

Charges, transferred to the shielded carrier, will be evaporated to dryness in the carrier; the heavy vapor will be condensed and returned to the transfer tank. Periodically, the carrier, containing the dried fission and corrosion products and a small quantity of associated uranium, will be transported to a processing plant for decontamination and for recovery of the uranium by solvent extraction.

Deuterium and oxygen, produced by radiolytic dissociation of heavy water, will be recovered by catalytic recombination and condensation. A steam-jacketed superheater (H-7) is included to maintain the inlet temperature well above the dew point. A constant flow of heavy-water vapor from the evaporator will be maintained to dilute the deuterium gas below its explosive concentration. However, the process tanks and piping are designed to contain a deuterium explosion as a safety precaution.

The off-gas from the plant, comprised almost entirely of fission-product gases and oxygen, will pass through a water-cooled cold trap for recovery of heavy-water vapor, and thence to carbon beds for the adsorption of radioactive gases. The effluent from the carbon beds will be vented through a mercury seal pot to the HRT off-gas stack.

An HRT-design two-sampler unit will be located in the roof plug of cell C in Building 7500. One sampler will be in series with the transfer tank and the evaporator and can sample any solutions during transfer from the tank to the evaporator. The other sampler will be connected as a bypass between the hydroclone overflow return line and the reactor dump tank, so that samples of the overflow may be taken while the plant is in operation.

The weighing system previously outlined for the determination of evaporator and decay tank liquid level has been found to be impractical because of inherent inaccuracies introduced by the tank suspension. The evaporator and decay tank and the D_2O storage tank will be weighed by strain-gage-type load cells to determine the mass of liquid they contain.

A workable design for a conductivity probe, to sense uranium concentration in the evaporator, utilizing the principle of the alternating current transformer, is now being tested. This design involves the use of concentric cylindrical surfaces as parallel plates connected to the secondary of a transformer. The conductivity of the liquid between plates is reflected in the primary of the transformer as a change in electrical loading on the primary and is detected by standard electrical methods. The design of the transformer is such that only stainless steels are in contact with the fluid. The insulating effects of deposited solid particles on the surfaces of the concentric cylinders will be ascertained by testing with simulated fuel solutions in an evaporator mockup. Development is continuing on the toroid-type conductivity probe outlined previously.

15.2 FISSION-PRODUCT CHEMISTRY

R. A. McNees S. Peterson

15.2.1 Neodymium Sulfate Precipitation from Fuel Solution

When simulated fuel solutions (0.02 *m* UO_2SO_4, 0.005 *m* H_2SO_4) containing 250 mg or more of neodymium sulfate per kilogram of H_2O were heated until precipitation occurred, only $Nd_2(SO_4)_3 \cdot H_2O$ precipitated. However, when such solutions containing 150 mg or less per kilogram of H_2O were heated to precipitation (310 to 320°C), a yellowish solid phase containing large amounts of uranium was formed.

Some of the faintly pink crystalline precipitate from the more concentrated solutions was collected and analyzed. The analyses correspond to $Nd_2(SO_4)_3 \cdot H_2O$ and show only 1 atom of uranium per 20 atoms of neodymium. Since the method of separation did not permit washing the crystals free of uranyl sulfate solution, it is believed that the uranium found in the pinkish crystals was due to contamination. Spectrographic analysis of some of the yellow crystals obtained from dilute solutions in quartz tubes showed the crystals to contain large amounts of both neodymium and uranium. Quantitative analysis of approximately 1 mg of similar crystals obtained from a run in metal equipment showed the presence of 14.2% neodymium and 38.2% uranium. If the crystals were a sulfate salt

with water of hydration, this analysis would correspond to the formula $Nd_2(SO_4)_3 \cdot 3UO_2SO_4 \cdot 10H_2O$.

15.2.2 Neodymium Sulfate Precipitation on Hot Surfaces

In previous studies[2] only about 0.5% of the neodymium sulfate present was deposited from a solution onto a clean Zircaloy-2 surface, but the presence of corrosion products increased the deposition. In further studies on this problem, with simultaneous deposition of corrosion products, 20% (previously reported as 4 to 8%) of the neodymium present was deposited. When a film of corrosion products was already on the hot surfaces, 12 to 13% of the neodymium was deposited even though additional corrosion products were not being deposited.

The experiments were carried out in a rocking bomb. A simulated fuel solution, 0.02 *m* UO_2SO_4–0.005 *m* H_2SO_4, containing 1000 mg of neodymium sulfate per kilogram of H_2O at room temperature, was placed in the bomb and heated to about 285°C. A Zircaloy-2 finger inserted in the solution was maintained 20 to 25°C hotter than the solution. A stainless-steel-lined bomb was used for the experiment on simultaneous deposition of corrosion products. After these tests the finger was washed, without disturbing the corrosion film, and then used in a similar experiment in a bomb lined with platinum so that corrosion products would not be deposited simultaneously with the neodymium sulfate.

[2]D. E. Ferguson *et al.*, *HRP Quar. Prog. Rep. April 30, 1955*, ORNL-1895, p 173.

15.2.3 Effect of Other Rare Earths on Neodymium Sulfate Solubility

The solubility of neodymium sulfate in 0.02 *m* UO_2SO_4–0.005 *m* H_2SO_4 solutions at 292 to 295°C was only 25 to 30 mg per kilogram of H_2O when other rare-earth sulfates were being precipitated along with neodymium sulfate. This value is about half the solubility reported[2] (60 to 80 mg per kilogram of H_2O) when neodymium sulfate was being precipitated alone. For these tests Lindsay Code 302 mixed rare-earth sulfates were spiked with Nd^{147} tracer and heated in a container in such a fashion that the wall temperature of the container was not more than 3°C hotter than the solution.

15.2.4 Effect of Uranyl Sulfate Concentration on Neodymium Sulfate Solubility

In preliminary experiments, when mixed rare-earth sulfates were precipitated from 0.02 *m* UO_2SO_4–0.005 *m* H_2SO_4, the amount of nebdymium sulfate retained in solution increased as the uranyl sulfate concentration was increased (see Table 15.1).

15.2.5 Iodine Chemistry

In preliminary experiments the reduction of iodine from the pentavalent to the elemental form by Co^{60} gamma radiation was pronounced in aqueous solutions at room temperature. This reduction did not occur in pure uranyl sulfate solutions but did occur to a moderate extent when copper sulfate was added to the uranyl sulfate solution (see Table 15.2).

TABLE 15.1. EFFECT OF UO_2SO_4 CONCENTRATION ON $Nd_2(SO_4)_3$ SOLUBILITY

Temperature (°C)	UO_2SO_4 Concentration (g of U per kg of H_2O)	$Nd_2(SO_4)_3$ Solubility (mg per kg of H_2O)
292–295	6.65	31.4
292–295	7.30	32.6
292–295	8.00	35.1
292–295	15.30	66.4
282–285	10.0	51
282–285	17.8	80

TABLE 15.2. REDUCTION OF I^{5+} TO I^0 IN THE PRESENCE OF GAMMA RADIATION

Initial IO_3^- concentration, 10^{-5} *m*

Solution	Irradiation (r, $\times 10^5$)	Reduction (%)
H_2O	9.6	15
H_2O + 0.005 *m* H_2SO_4	9.6	11
H_2O + 0.005 *m* Cu^{++} + 0.005 *m* H_2SO_4	9.6	41
UO_2SO_4 (5 g of U per kg of H_2O)	8.3	0
UO_2SO_4 (5 g of U per kg of H_2O) + 0.005 *m* Cu^{++} + 0.005 *m* H_2SO_4	8.3	3

15.3 FUEL-PROCESSING-LOOP STUDIES

P. A. Haas R. W. Horton

Loops operating at temperatures and pressures expected for the HRT are being used to determine the behavior of fission- and corrosion-product solids in circulating fuel solutions. Chemical development studies have established that the majority of the fission and corrosion products resulting from HRT operation will be insoluble under reactor operation conditions (300°C and 2000 psi). Loop tests have, in general, confirmed the solubility limits determined in the laboratory experiments. The loop tests also have shown that there is a marked tendency for rare-earth fission products to adhere to metal surfaces hotter than the solution. Similar behavior is postulated for iron oxide and thorium oxide from attempts to circulate them in the loops. In addition, insoluble neodymium sulfate, thorium dioxide, and ferric oxide, which were circulated in the B-2 loop with no metal surfaces hotter than the solution, remained suspended in the circulating stream for only a few hours.

The hydroclones on the loops separated the solids whenever it was evident that particles were circulating in the loops. From these observations a scheme for processing the reactor core solution has evolved which includes a heated section of pipe for reducing the solubility and removing part of the rare-earth fission products, followed by the use of a hydroclone for removing the solid fission and corrosion products that pass the heated section. Engineering studies to evaluate the variables controlling these processes are reported here.

15.3.1 Behavior of Neodymium Sulfate in Loop A

Neodymium is the most important rare-earth product of a reactor, from the standpoint of neutron absorption cross section, after extended periods of operation. The behavior of neodymium sulfate in simulated reactor fuel at high temperature has been studied in loop A, which is heated electrically so that metal surfaces in contact with the fuel solution containing neodymium sulfate can be raised as much as 60°C above the loop solution temperatures.

In these tests more than 80% of the neodymium sulfate which precipitated during solubility tests was found in the preheater system (see Table 15.3). Samples drawn from the preheater exit line during one test showed concentrations of neodymium sulfate up to 60 times the observed solubility. This result seems to indicate that neodymium sulfate particles precipitated in the preheater were carried out into the exit line and accumulated in the sampling line. When solids were not removed in sampling, deposits in the preheater ranged from 6,000 to 19,000 mg/ft^2, and the deposit on the main loop heating section was 30 to 40 mg/ft^2. The two areas are 0.11 and 0.72 ft^2, respectively, in loop A. The total amount of deposit depended on the amount of neodymium sulfate fed to the system and the amount removed in sampling, which in turn depended on the solubility at the operating temperature.

Recent tests indicated a neodymium sulfate solubility of approximately 65 mg per kilogram of H_2O at 310°C and approximately 50 mg per kilogram of H_2O at 328°C under loop A conditions.

The loop A preheater is a $\frac{1}{8}$-in. sched-80 pipe, cast in aluminum and heated by clamshell elements clamped around the aluminum casting. Heat transfer calculations (see Table 15.4) indicate an overall heat transfer coefficient of about 700 Btu/hr·ft^2·°F for this preheater with no rare-earth precipitate. As neodymium sulfate precipitates, the coefficient decreases. The U_i values ranging from 275 to 455 Btu/hr·ft^2·°F were calculated for units on which scale had deposited.

TABLE 15.3. DISTRIBUTION OF NEODYMIUM SULFATE IN LOOP A

	Run Number		
	29	31	33
1. Preheater temperature (°C)	310	310	328
2. Average $Nd_2(SO_4)_3$ concentration in loop, solution (mg per kg of H_2O)	60.5	62	50
3. Total $Nd_2(SO_4)_3$ fed to loop (mg)	1298	1631	1425
4. Total $Nd_2(SO_4)_3$ removed from loop in samples (mg)	185	259	743
5. Total $Nd_2(SO_4)_3$ in drainage from loop at end of run (mg)	139	221	102
6. Total $Nd_2(SO_4)_3$ remaining in system after draining (mg) [line 3 minus (line 4 + line 5)]	974	1151	580
7. $Nd_2(SO_4)_3$ from preheater system, solids (mg)	700	781	236*
8. $Nd_2(SO_4)_3$ from main loop system, solids (mg)	82	180	21
9. Total $Nd_2(SO_4)_3$ removed as solids (mg) (line 7 + line 8)	782	961	257
10. Solids from preheater (% of total) (100 × line 7 ÷ line 9)	90	81	92
11. Solids from preheater [% of $Nd_2(SO_4)_3$ fed] (100 × line 7 ÷ line 3)	54	48	18
12. Per cent recovery, over-all [100 × (line 4 + 5 + 9) ÷ line 3]	85	88	78
13. $Nd_2(SO_4)_3$ deposit in preheater (mg/ft^2)	6400	7100	2140
14. $Nd_2(SO_4)_3$ deposit in main loop (mg/ft^2)	114	250	29

*This run was sampled from the preheater exit line removing solids which would have otherwise been found in the preheater system (cf. line 4 for run 33 with runs 29 and 31).

15.3.2 Behavior of Neodymium Sulfate in Loop B-2

Loop B-2 can be heated exclusively with the mechanical energy imparted by the type 30A pump used to circulate the solution, thereby avoiding any heated metal surfaces in contact with the circulating solution. A photograph of the loop without insulation is shown in Fig. 15.2. Studies of hydroclone performance and rare-earth behavior at 300°C and 2000 psi, which were started in development loop B, have been continued in loop B-2.

In loop B-2, a 30A pump circulated fuel around a simple loop, part of which was $\frac{3}{4}$ in. in diameter, part 1.5 in. in diameter, and part 4 in. in diameter. The loop was made from IPS sched-80 pipe with an oxygen overpressure-surge space in the 4-in.-dia pipe. A 0.40-in.-dia titanium-lined hydroclone was installed between the pump suction and discharge.

Loop temperatures up to 245°C were obtained when the pump was used as the only source of heat. Resistance heaters installed on the outer surfaces of the insulation to cut down heat losses actually supplied a heat input of 0.25 kw or 0.04 kw/ft^2 to the loop core before 290°C could be obtained. This amount of heat input heated the wall less than 2°C above the temperature of the solution. Loops A and B operated with heat inputs of up to 14 kw/ft^2.

The neodymium sulfate concentrations under the conditions existing in loop B-2 appeared to be limited by the fuel temperature independently of whether this temperature was increasing or decreasing. The presence or absence of a wall with a temperature 2°C above that of the solution did

TABLE 15.4. HEAT TRANSFER COEFFICIENTS FOR LOOP A PREHEATER

Preheater made of $\frac{1}{8}$-in. sched-80 pipe (type 347 stainless steel) cast in an aluminum cylinder 2.5-in. OD, internal heating surface 0.11 ft^2, in runs 29, 30, and 31, heated with an integral cast Calrod element, in run 33 heated by ceramic clamshell elements, temperature of aluminum casting used to compute Δt_m

	Run Number			
	29	30	31	33
Flow (gpm)	0.105	0.15	0.15	0.10
Velocity (fps)	0.95	1.35	1.35	0.90
Final temperature of liquid (°F)	590	591	590	622
Δt of liquid (°F)	106	76	77	77
Heat absorbed (Btu/hr)	4790	4980	4840	3470
(Btu/hr·ft^2)	43,500	45,200	44,000	31,400
Δt_m, heater to liquid (°F)	119	66	97	115
U_i (Btu/hr·ft^2·°F)	365	685	455	275
h_{wall} (Btu/hr·ft^2·°F)	1870	1870	1870	1870
h_{scale}* (Btu/hr·ft^2·°F)	450	1075	600	320

*Scale is the normal oxide film plus neodymium sulfate deposits except in run 30, where no neodymium sulfate was present.

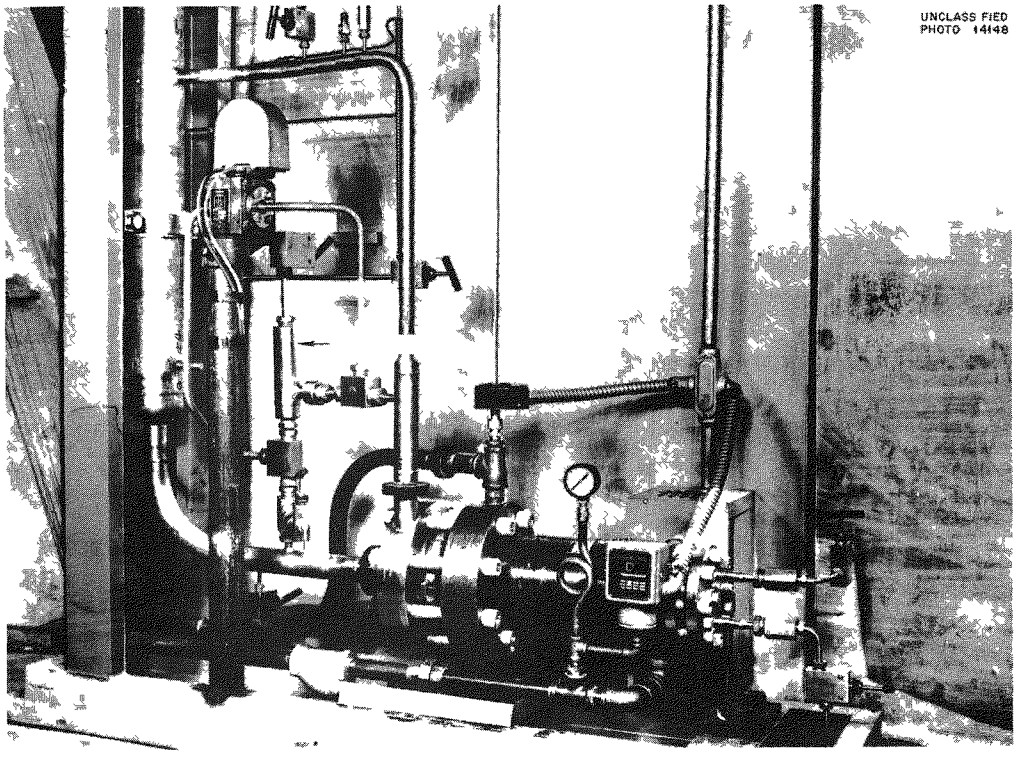

Fig. 15.2. Development Loop B-2 Without Insulation.

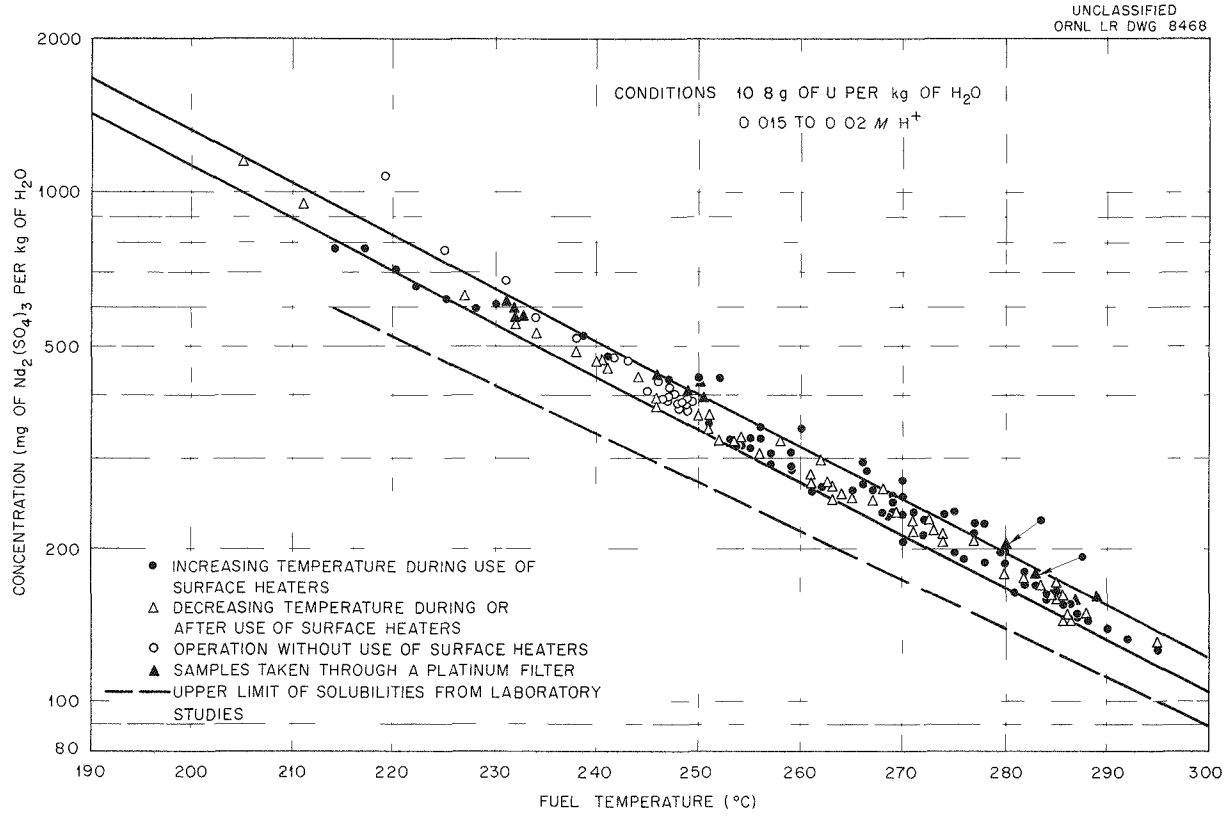

Fig. 15.3. Neodymium Sulfate Concentrations vs Fuel Temperature in Loop B-2.

not detectably affect the concentration of neodymium sulfate in the circulating fuel (see Fig. 15.3). The concentrations of the filtered samples were no lower than those of unfiltered loop samples at the same temperature. The loop B-2 neodymium sulfate concentrations were 130% or more of solubilities reported from laboratory studies. However, during the period when the loop was heating up or cooling down, there was an appreciable concentration of neodymium sulfate solids in the circulating stream. The presence of the solid phase was detected during these periods by an increased neodymium concentration in the underflow of a 0.4-in.-dia hydroclone installed on the loop.

15.3.3 Behavior of Iron Oxide

When ferric sulfate, dissolved in simulated fuel solutions, was added to loops B and B-2, only 3% of the expected concentration of iron oxides appeared in the circulating stream; the small amount which did appear initially disappeared after 4-hr periods of circulation. After the runs, washes of demineralized water and 0.01 to 0.1 *N* H_2SO_4 were heated in the loops to recover the iron which had disappeared.

In the initial loop B test with iron, about 6.2 g of iron (200 mg per kilogram of H_2O) was added to the loop as ferric sulfate solution. About 2.5 g of iron was recovered in fuel removed from the loop, and 5 g was found in water and dilute sulfuric acid washes. In the second test, in which 2.0 g (65 mg per kilogram of H_2O) of iron was added, about 1 g of iron was removed in the fuel and about 0.5 g in water and dilute sulfuric acid washes. Additional iron continued to appear in some samples throughout the next four tests, which were made without iron addition.

15.3.4 Behavior of Thorium Dioxide

Essentially all the thorium dioxide added to loop B-2 for low-temperature (below 80°C) hydroclone efficiency and ThO_2 behavior studies remained circulating. After shutdowns of 4 and 48 hr, the ThO_2 all came back into circulation within a few

minutes. After the loop was sealed and heated to above 100°C, the hydroclone underflow line plugged (see Sec. 15.3.5) and all but 1% of the ThO_2 disappeared from the circulating water.

In the experiment discussed above, about 13 g of thorium, as the oxide suspended in water, was added to loop B-2. About 3 g was recovered in samples, 2 g in water drained at the end of the run, 2 g in a dilute sulfuric acid wash, and 1 g in two water washes. The remaining 5 g, 40% of the total, was not recovered.

15.3.5 Hydroclone Performance

The 0.4-in.-dia hydroclones attached to loops B and B-2 effectively concentrated iron oxides suspended in simulated fuel solution. More than 99.9% of the iron oxide particles concentrated by a 0.4-in.-dia hydroclone attached to loop B were 0.5 μ or less in diameter (see Table 15.5).

In the iron oxide experiments none of the hydroclone overflow samples contained detectable iron oxides. When loop samples contained 2 ppm of iron or more, the underflow iron concentrations were usually in the range 5 to 30 ppm. However, four samples had iron concentrations of 38, 80, 115, and 210 ppm, respectively. The underflow rates were 10 and 2.4% of the feed flow rates for loops B and B-2, respectively.

Suspended neodymium sulfate was concentrated by factors of 2 to 30 (see Fig. 15.4 and Table 15.6) for short intervals of operation in loop B-2 with a 0.4-in.-dia hydroclone operating with an underflow rate of 1 to 2% of the feed rate. Otherwise, during the rest of the operation, no concentration was observed. This compound rapidly disappeared from the circulating fuel when the system was operated continuously.

TABLE 15.5. SIZE OF IRON OXIDE PARTICLES IN UNDERFLOW FROM A 0.4-in.-dia HYDROCLONE

Feed flow rate of 0.5 gpm; underflow rate 10% of feed; 15 psi pressure drop; iron oxide suspended in uranyl sulfate solution, 9 g of uranium per liter; 280°C

Size (μ)	Numerical* Distribution (%)	Volume** Distribution (%)
>0.5	<0.1	
0.5	0.3	34.1
0.4	0.6	34.9
0.3		
0.2	2.2	16.0
0.1	10.1	9.2
0.05	40.5	4.6
<0.05	46.3	1.1

*As reported by T. E. Willmarth, Analytical Chemistry Division, from electron microscope measurements made at 12,500X.

**Calculated by assuming that the volume of a particle is proportional to the cube of the average diameter.

15.4 COMPONENT DEVELOPMENT

J. R. Engel, J. K. Langsdon, P. A. Haas, M. E. Whatley

15.4.1 Hydroclone Development

Studies to determine the optimum dimensions of the hydroclone to be used in the HRT chemical processing plant have been completed. The recommended design dimensions are as follows:

Feed inlet	0.063 in. high, 0.033 in. wide
Cone	1.50 in. long, 0.25-in. ID at top
Vortex finder	0.053 in. dia, 0.25 in. long
Underflow port	0.075 in. dia

The hydroclone will be mounted on a 2.5-gal underflow pot.

A topical report on hydroclone development studies is in preparation.

15.4.2 Hydroclone Corrosion

Previously reported[3] studies with stainless steel hydroclones indicated that a more corrosion-resistant material would be needed for processing homogeneous reactor fuel. Results of preliminary tests on titanium-lined 0.4-in.-dia hydroclones indicate that titanium may be a satisfactory material of construction for the hydroclones in the HRT chemical processing plant. As long as the hydroclone is operating properly, the corrosion rate of the titanium exposed to uranyl sulfate solution is negligible, even in the very high velocity regions. However, if an abnormally high concentration of solids is allowed to build up in the body of the unit, the abrasive action of the solids on the

[3]D. E. Ferguson *et al.*, *HRP Quar. Prog. Rep. April 30, 1955*, ORNL-1895, p 173.

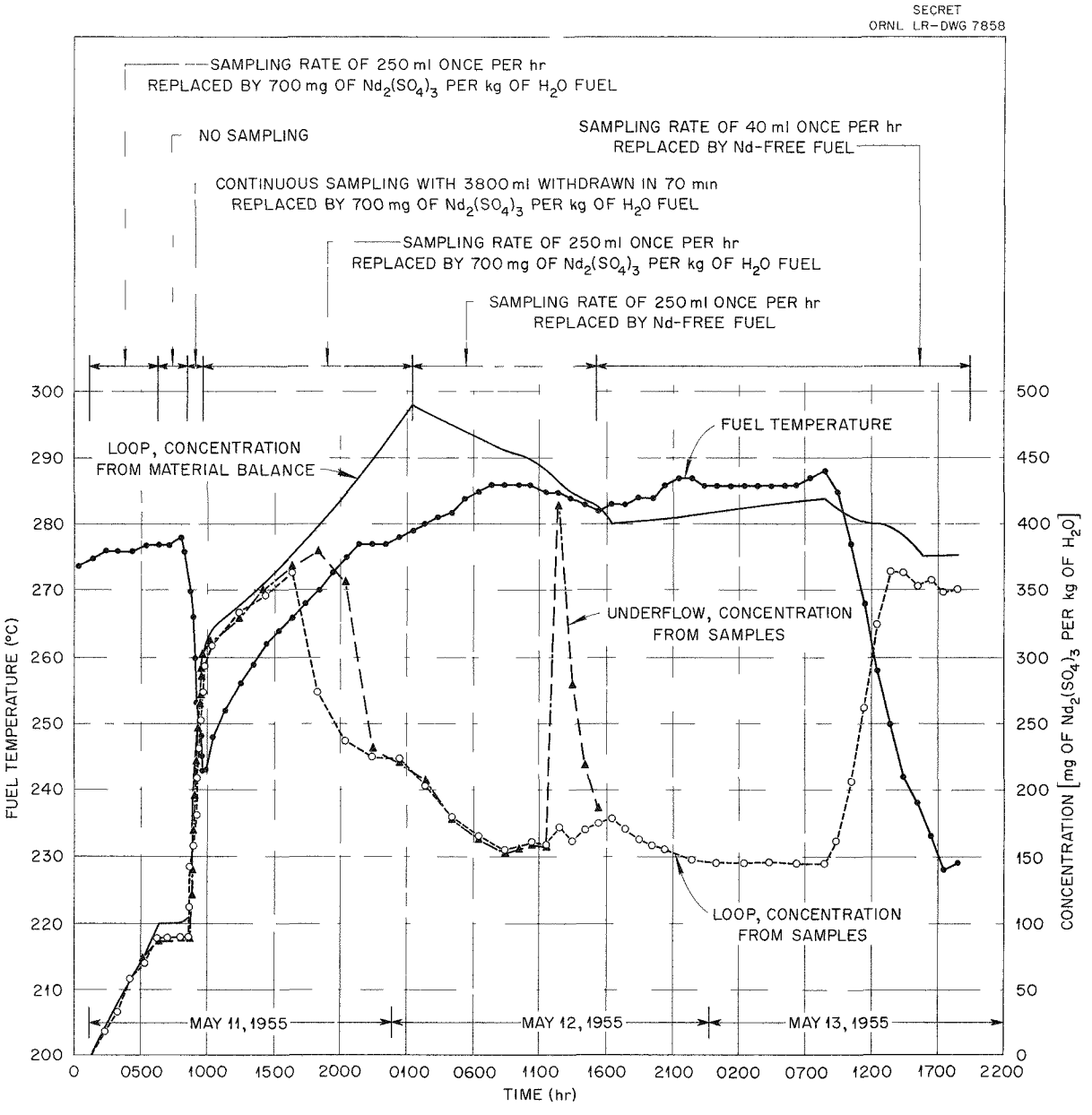

Fig. 15.4. Temperature and $Nd_2(SO_4)_3$ Concentrations for Loop B-2 Experimental Run No. 1.

protective titanium oxide film results in excessive corrosion rates. Tests were conducted on two hydroclones, one with a continuous underflow stream initially 6% of the feed stream and another with an underflow pot taking advantage of the induced underflow principle.

In the first arrangement (see Fig. 15.5*a*) a plate with a 0.030-in.-dia orifice was placed in the underflow line to restrict the flow through it to 6% of the feed rate. The underflow stream, containing the solids removed by the hydroclone, was combined with the overflow and returned to the main circulating loop. This hydroclone was operated for 200 hr on a uranyl sulfate–water solution (uranium concentration 15 g per kilogram of H_2O, 0.005 *m* in H_2SO_4) at 250°C. The total system pressure was

TABLE 15.6. CONCENTRATIONS AND CONDITIONS DURING SHORT PERIODS OF HYDROCLONE OPERATION FOR CONCENTRATION OF SUSPENDED NEODYMIUM SULFATE

Hydroclone feed rate: 0.55 gpm (2.1 liters/min)

Fuel: Uranyl sulfate solution, uranium concentration 10.8 g per kilogram of H_2O; 0.015 to 0.02 *M* H^+

Run No.	Underflow Rate (% of feed rate)	Fuel Temperature (°C)	$Nd_2(SO_4)_3$ Concentration (mg per kg of H_2O)	
			Loop	Underflow
1	2.4	285	172	415
		284	161	279
		270	273	378
2	2.4	264	255	675
3	2.4	244	437	680
		251	363	478
5	1.0*	211	1,281	16,350
		211	1,200	32,250
		212	1,100	2,640
		213	1,000	5,820
		214	786	2,200
			Gamma Activity (counts/min/ml)	
9**	2.4	180	40,200	253,000
		184	23,600	160,000
		190	18,700	41,400
		197	16,100	24,400

*A continuous underflow of 20 ml/min was desired, but maintaining a uniform flow at this rate with a loop to atmospheric pressure drop was difficult and large flow variations occurred.

**This run used mixed rare earths and both Ce^{144} and Nd^{147} tracer. Therefore, the gamma activities rather than the neodymium concentrations are given. The decreasing gamma activity with increasing temperatures is considered to be a time-dependent as well as a temperature-dependent phenomenon. The significance of the time element is being investigated further.

1000 psi, and the feed rate to the hydroclone was 1 gpm. The particles of loop scale which reported to the underflow failed to pass through the orifice and filled the underflow line and part of the hydroclone itself. However, temperature measurements indicated that some liquid flow was maintained in the underflow line throughout the run.

After 200 hr the hydroclone was removed for inspection. Considerable difficulty was encountered in removing the accumulated solids from the hydroclone and the underflow line. Measurements on the underflow port indicated a corrosion rate of 0.48 in./year. The vortex finder, which is in the highest velocity region, showed no measurable corrosion. However, there were essentially no solids in the vicinity of the vortex finder. From this it is apparent that the high corrosion rate at the underflow port occurred when the accumulated solids removed the protective oxide film from the titanium. Figure 15.6 is a photograph of a vertical section through the hydroclone showing the extent of the corrosion at the underflow port. The dotted lines indicate the original dimensions.

In the second arrangement (Fig. 15.5*b*), in which the induced underflow system was employed, there was no net flow out of the pot, and no flow restrictors were required. In this case, the underflow pot was designed to contain all the solids

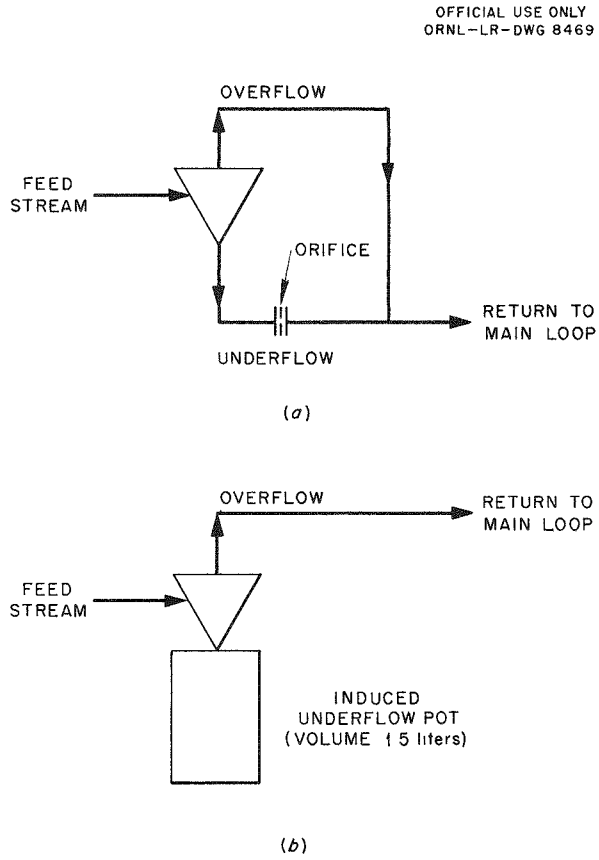

Fig. 15.5. Experimental Hydroclone Test Arrangements. (*a*) System for a continuous underflow stream initially 6% of feed stream. (*b*) System with an underflow pot.

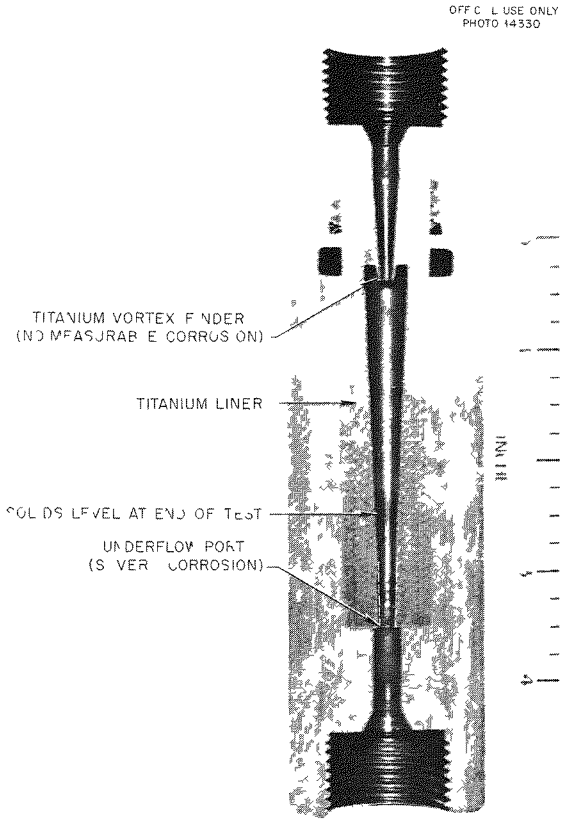

Fig. 15.6. Corrosion of 0.4-in. Titanium-lined Hydroclone.

removed from the feed stream by the hydroclone. This hydroclone was operated for 391 hr with no measurable corrosion at either the vortex finder or the underflow port. The unit was first operated for 200 hr under the same conditions as those used in the previous test. During this time, 29 g of solids, mostly Fe_2O_3, was collected in the pot. The pressure drop through the hydroclone was measured as a function of throughput, and a decrease of 15 to 20% was observed (Fig. 15.7).

Operation of the hydroclone was resumed at a temperature of 300°C, a pressure of 1500 psi, a uranium concentration of 10.2 g per kilogram of H_2O, and a throughput of 1 gpm. This part of the test was terminated after 191 hr by an operational failure in the test loop, which also prevented measurement of the accumulated solids. No measurable changes in the dimensions of the hydroclone were found, and the plots of pressure drop vs throughput followed the same line as after the first 200 hr. The initial change in pressure drop may be due to the slight roughening of the metal surface by the formation of the oxide film. Rough surfaces reduce the tangential velocity of the fluid in the hydroclone, thereby reducing the pressure drop across the centrifugal field. Operation of this hydroclone will be continued until appreciable corrosion can be detected.

Additional tests will be made on the 0.25-in.-dia hydroclone with an induced underflow pot which has been recommended for use in the HRT.

15.4.3 Pump Development

Operation of the hydroclone in the HRT chemical processing plant requires a pump capable of delivering relatively high heads at flows of less than

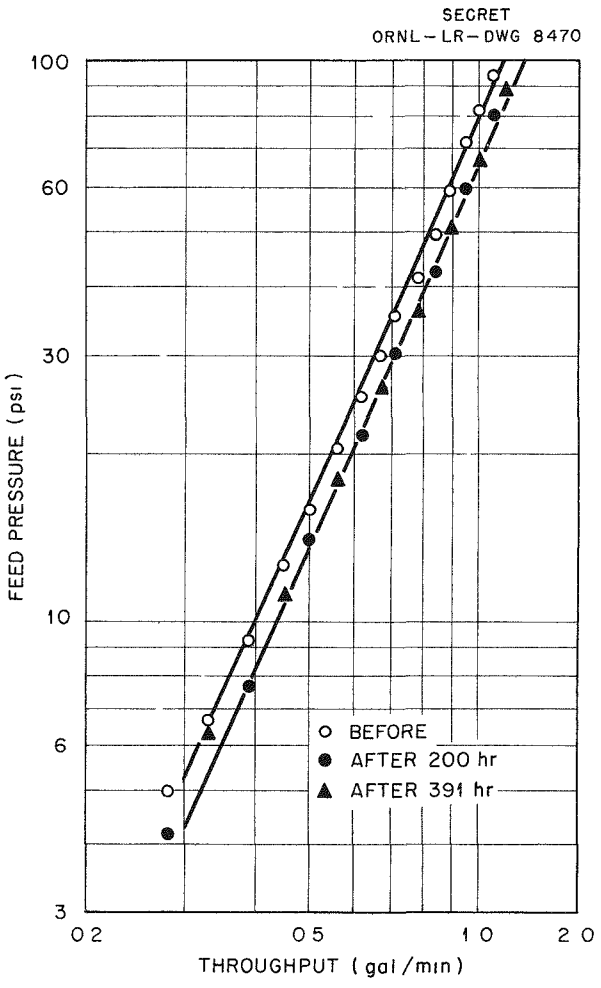

Fig. 15.7. Effect of Operation on Capacity of 0.4-in.-dia Titanium-lined Hydroclone. Equipment operated with uranyl sulfate in water (uranium concentration 15 g per kilogram of H_2O); flow rate 1 gpm; 200-hr operation at 250°C and 1000 psi pressure followed by 191 hr at 300°C and 1500 psi pressure.

1 gpm. From the standpoint of hydroclone performance, the steady pressure developed by a centrifugal pump is extremely desirable. To fill this need, two prototype pumps have been ordered, one from the Westinghouse Electric Corporation and one from the Byron-Jackson Co. These pumps will deliver 100 ft of head at 1 gpm with a 220-v 60-cycle power supply.

Since 100 ft of head may not produce sufficient flow through the hydroclone to separate efficiently the solids from the reactor fuel solution, the pumps will be operable over a frequency range of 30 to 80 cps in the power supply. By varying the frequency over this range, the head developed by the centrifugal pump can be varied from 25 to 177 ft.

In order to check the operability of a pump over this range in frequency, tests were made on an ORNL 5-gpm canned-rotor pump. Previous attempts to operate such a pump with a single-phase stator at frequencies other than 60 cps resulted in serious overheating of the stator windings. Therefore, the test pump was equipped with a three-phase 208-v stator similar to those of the prototype pumps. The pump was then operated at 40, 60, and 80 cps with no evidence of overheating. The voltage was varied directly with the frequency, using as a basis 208 v at 60 cps.

The head developed by the pump was measured as a function of flow rate for each of the above frequencies (Fig. 15.8). The head did not increase in exact proportion to the square of the frequency, as was predicted by theory. Apparently the electrical slip of the motor increases slightly with an increase in frequency.

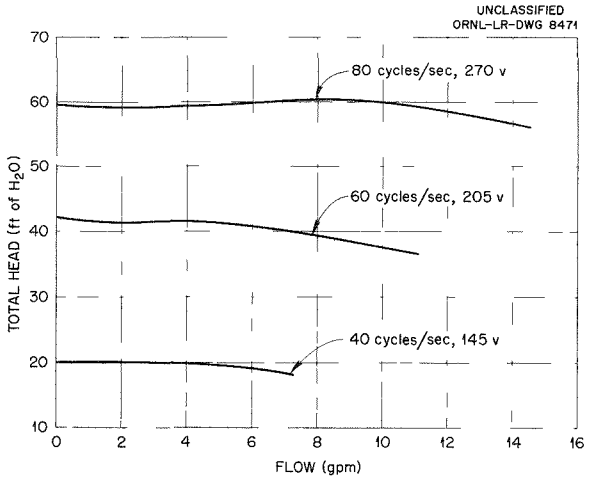

Fig. 15.8. Total Head Developed by ORNL 5-gpm 2000-psi Pump at Various Frequencies with Three-Phase Power Supply.

15.4.4 Evaporator Development

Experimental studies, designed to obtain information required for design and operation of the D_2O recovery evaporator for the HRT chemical plant, have shown that a clean fuel can be evaporated to a uranium concentration of 875 g per

kilogram of H_2O without splashing, entrainment, or foaming difficulties.

The evaporator uranium concentration was increased from 10 to 875 g per kilogram of H_2O and the sulfate concentration from 0.051 to 3.71 *M* in 66 evaporations. The uranium concentrations in the condensate were 0.001 g per kilogram of H_2O or less. This degree of separation was obtained with a very simple entrainment separator of about 6 in. of York mesh type 421 in a 4-in.-dia vapor line. There was no splattering of solution under any of the operating conditions. Foaming did not occur with heat input rates up to the design rate of 7 kw total (0.7 kw/liter).

When the uranium concentration of the liquid was about 850 g per kilogram of H_2O and the heat input was 7 kw, there was turbulence and varisized bubble formation without foaming or splashing (Fig. 15.9). When the same liquid was evaporated with a total heat input of 11 kw (1 kw/liter) or more, there was a layer of foam about 1 in. thick over the two end quarters, or over about 50% of the evaporator surface. Steam escaped from this foam without splattering or entrainment.

In normal operation of the experimental evaporator the total electrical energy input was 6 kw and the condensate takeoff rate was 120 to 130 ml/min. Heat losses to the atmosphere were 1.1 kw for the evaporator as originally installed and 1.4 and 1.6 kw with insulation removed from one and then both ends to permit replacement of leaking gaskets.

About 0.8% of the uranium in the final evaporator product was tetravalent. This U(IV), 1150 ppm of iron and 320 ppm of nickel, caused the final charge to be dark green in color. Investigation is under way to discover whether corrosion is a serious problem or whether the tetravalent uranium, iron, and nickel resulted from the a-c resistance heating.

Because of the sulfuric acid present in the original feed, the evaporator feed and the final product contained about 20 mole % excess sulfate compared with the uranium. With this excess of sulfate, the electrical resistance of the liquid was 55% or less of literature values reported for pure uranyl sulfate in water. Observed resistances were 5.5, 0.81, and 0.27 ohm-ft when the uranium concentrations were 10, 100, and 800 g per kilogram of H_2O, respectively.

The experimental evaporator body was a 6-ft length of 6-in.-dia pyrex pipe to permit use of electrical resistance heating to simulate the volume heating of fission products. The use of glass also permitted visual observation of the behavior of the boiling liquid. The geometry resembled the 6-in.-dia and 7-ft length of the "pipe tank" evaporator to be used in the HRT chemical processing plant. The experimental evaporator was operated in a horizontal position with 6-in.-dia and 6-in.-long stainless steel adapter end plates used as electrodes (Fig. 15.10). The adapter end plates were covered with insulation, and the equipment was surrounded by a barricade to protect personnel from

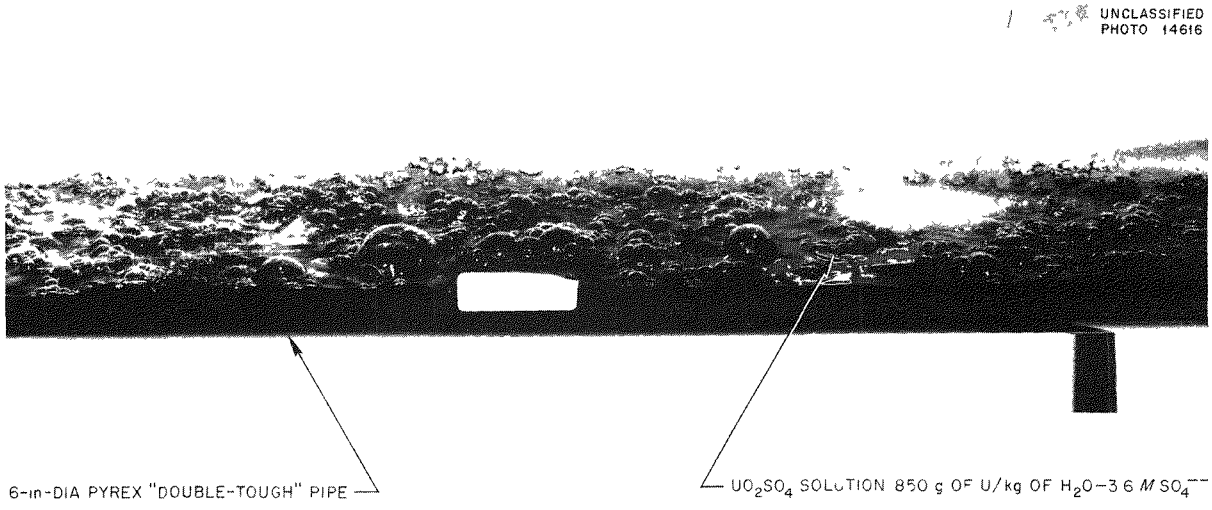

Fig. 15.9. Evaporation of Concentrated UO_2SO_4 Solution by Volume Heating.

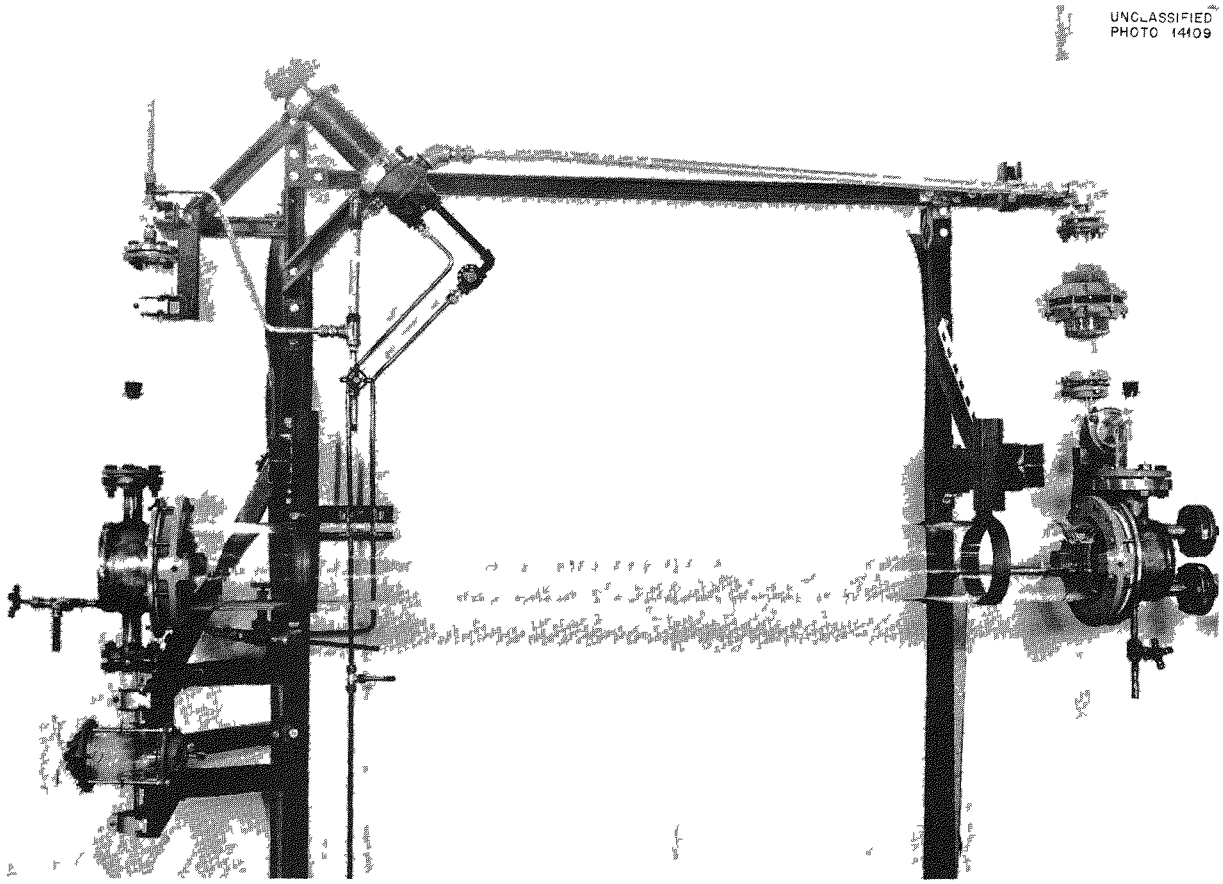

Fig. 15.10. Experimental Evaporator as Installed, Without Insulation.

the high voltages used. The electrical supply was 60 cps alternating current through *isolation* transformers and Variacs which supplied 0 to 900 v and were rated at 7 kva.

15.4.5 Freeze Plug Development

In development studies on the use of freeze plugs for normal and emergency line closures in the HRT chemical plant, such plugs held against large pressure differences. However, they could be formed only when the solution to be frozen was at rest or was flowing at a very slow rate.

Pressure differences of 16,000 psi were held for 5 min or more by $1\frac{1}{4}$-in.-long plugs frozen from stagnant water in $\frac{1}{8}$-in.-dia sched-80 pipe, and by $1\frac{7}{8}$-in.-long plugs in 0.5-in.-dia pipe. In the same pipes, plugs $\frac{7}{8}$ to $1\frac{1}{4}$ in. long frozen from a water solution of uranyl sulfate (uranium concentration of 9 g per kilogram of H_2O) held 8000-psi pressure differences for 10 min or longer. The uranyl sulfate solution plugs failed with pressure differences of 13,000 to 16,000 psi. All plugs lost their ability to hold any pressure difference within 15 to 45 sec after the refrigerant flow was stopped.

A flow of 8 ml/min maintained by an atmospheric-to-vacuum pressure drop of less than 14 psi in a $\frac{1}{8}$-in.-dia sched-80 pipe was not stopped when a 2-in.-long refrigerant jacket was used to freeze a plug, but a 5-ml/min flow was stopped. The length of the plug that can be used is limited by the danger of line ruptures.

16. PLUTONIUM-PRODUCER BLANKET PROCESSING

D. E. Ferguson

R. E. Leuze R. H. Rainey

The primary objective of processing the uranyl sulfate solution blanket of the plutonium producer is to remove plutonium and neptunium as rapidly as possible in order to minimize Pu^{240} buildup. Studies of plutonium chemistry under simulated reactor conditions included experiments on plutonium adsorption on metals and separation of PuO_2 with a hydroclone. Uranyl sulfate solutions were irradiated in the LITR to determine plutonium and neptunium behavior under intense irradiation.

16.1 ADSORPTION OF PLUTONIUM ON METALS

Adsorption of plutonium on Zircaloy-2, titanium, and type 347 stainless steel metal surfaces at 250°C from a flowing stream of 1.26 *m* uranyl sulfate solution was studied. A schematic diagram of the equipment used is shown in Fig. 16.1. It consisted essentially of three pressure vessels connected to a gas supply system and of an external solution receiver at atmospheric pressure.

CONFIDENTIAL
ORNL-LR-DWG 8472

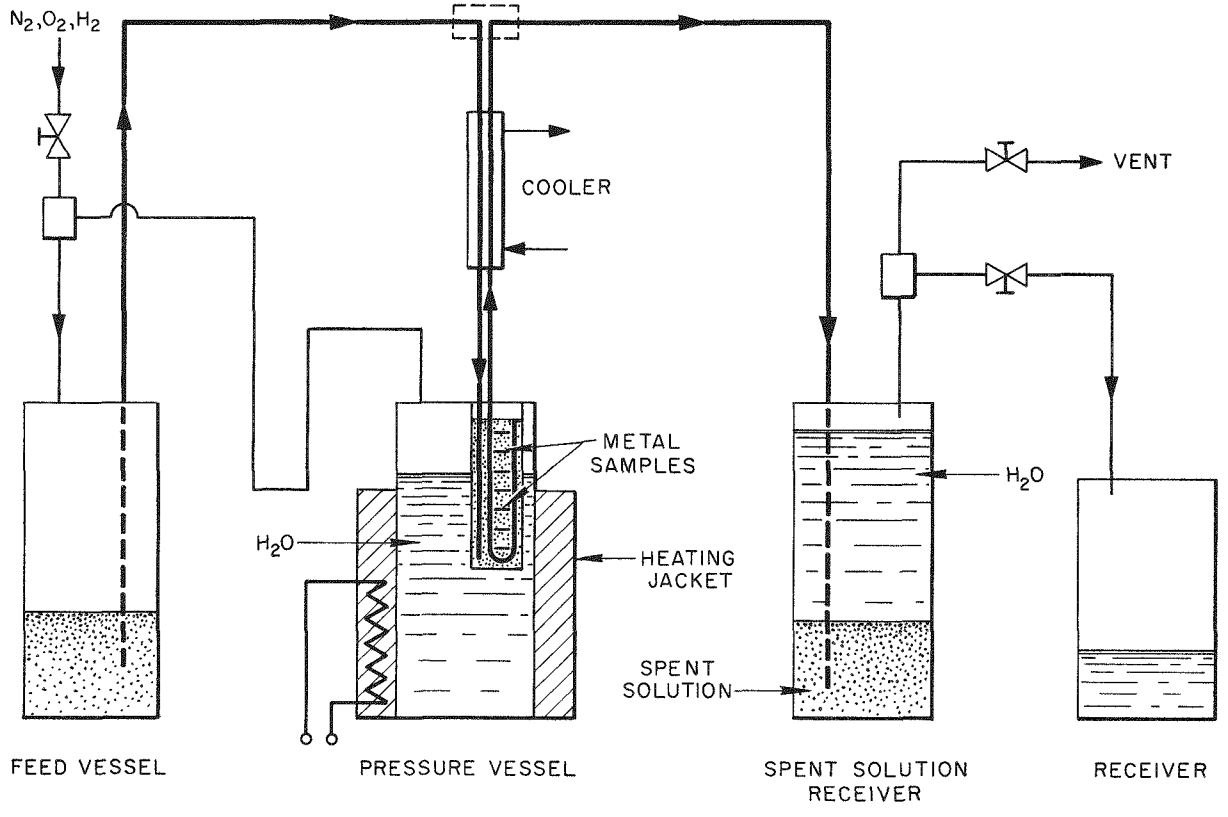

Fig. 16.1. Schematic Diagram of Equipment Used in the Study of Adsorption of Plutonium on Metals.

All equipment was stainless steel except the titanium reactor vessel, which fitted into a heated pressure vessel to hold the metal disks being studied. About 1 liter of uranyl sulfate solution, containing dissolved plutonium, was placed in the feed vessel. This was kept at room temperature, and the solution was saturated with oxygen and hydrogen by an overpressure of 80 psi of oxygen and 160 psi of hydrogen. Nitrogen gas was used to bring the total gas pressure to approximately 1000 psi and also to displace the solution through the vessel holding the metal disks. This vessel was suspended in a heated autoclave filled with water. As the solution entered the reactor, it was heated to 250°C and passed over the metal disks. The solution then passed out of the reactor through a cooler and then into a receiver. In this receiver the uranyl sulfate displaced water, which was metered through a flow control valve (this was to reduce corrosion on the valve), into an external receiver.

The uranyl sulfate solution flowed in the bottom of the vessel holding the test metal specimens and out the top. The metal specimens were mounted in the vessel to serve as baffles, thus causing the solution to flow over all the surfaces (see Fig. 16.2).

After the 1-liter solution had been passed through the reactor, the temperature and pressure were lowered and the disks removed. The plutonium adsorbed on the metal was determined by placing the disks in an alpha counter. It is known that the values obtained are low owing to shielding of the counter from some of the activity by the corrosion film; however, the relative values should be approximately correct. Actual adsorption values will be determined by descaling the metal and counting the activity of the solutions when the experiments have been completed.

After 1 liter of 1.26 *m* UO_2SO_4 containing 100 mg of plutonium per kilogram of water had been passed over a set of titanium disks, the average plutonium adsorption was 0.04 mg/cm^2. This is slightly more than the amount adsorbed in one of the batch passes described previously.[1] When a second 1-liter amount of this solution had been passed over the titanium, approximately the same amount was adsorbed, and a definite distribution pattern

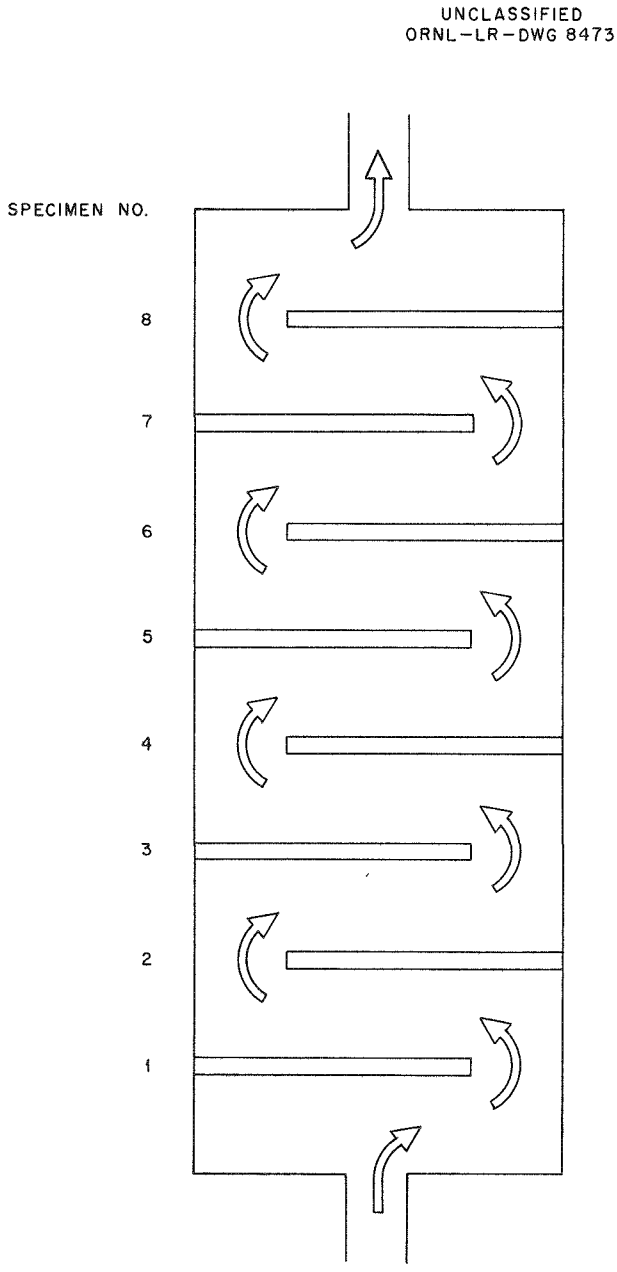

Fig. 16.2. Flow Pattern of Uranyl Sulfate Solution over Adsorption Test Specimens.

was noted (see Fig. 16.3). Considerably more plutonium was adsorbed on the bottom of each specimen (upstream side) than on the top. The plutonium on the bottom of the disk, where fresh solution entered, was 0.16 mg/cm^2 compared with 0.089 mg/cm^2 adsorbed on the top. Furthermore, there was a decrease of adsorbed plutonium from

[1] D. E. Ferguson, R. E. Leuze, and R. H. Rainey, *HRP Quar. Prog. Rep. April 30, 1955*, ORNL-1895, p 185.

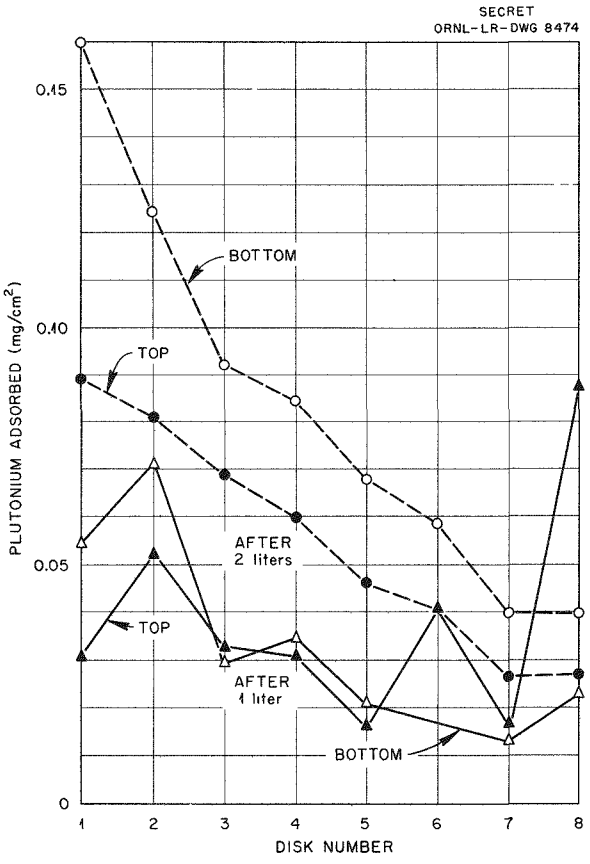

Fig. 16.3. Adsorption of Plutonium on Titanium Metal Disks from 1.26 *m* UO_2SO_4 Solution Containing 100 mg of Plutonium per Kilogram of H_2O. Temperature, 250°C.

0.16 mg/cm^2 where the solution entered to 0.027 mg/cm^2 at the exit. This apparently was a result of the decrease in plutonium in solution owing to adsorption and PuO_2 precipitation as it passed through the vessel. Autoradiographs of these disks (Fig. 16.4) showed the same change in plutonium adsorption as the solution passed from the inlet to the exit. The autoradiographs also showed that the plutonium was not uniformly adsorbed on the metal surfaces but that certain areas contained very high concentrations. However, as the amount of plutonium increased, the metal surfaces appeared to become completely covered with plutonium.

After 1 liter of 1.26 *m* UO_2SO_4 containing 100 mg of plutonium per kilogram of H_2O had been passed over Zircaloy-2 disks at 250°C, the same characteristics were noted as with titanium. In general, the bottoms of the disks had adsorbed more plutonium than the tops. Metal at the solution inlet had adsorbed 0.13 mg of plutonium per square centimeter, and this decreased to 0.013 mg/cm^2 at the exit (Fig. 16.5). It is important to note that the 0.13 mg/cm^2 value is considerably higher than the 0.05 mg/cm^2 determined as the equilibrium value on zirconium in static tests.[1] Further tests are needed to determine whether even larger amounts of plutonium may be adsorbed on Zircaloy-2. Autoradiographs (Fig. 16.6) showed that plutonium deposition was not uniform on Zircaloy-2.

Type 347 stainless steel disks were also exposed to the plutonium-containing solution in this equipment. After exposure, the disks were found to be partially covered with a heavy black corrosion film or scale, which flaked off readily. Autoradiographs (Fig. 16.7) of the disks indicated no plutonium adsorbed on the black corrosion film but, in some spots from which the scale had been removed, substantial adsorption of plutonium on the shiny metallic surface. No explanation has been advanced for the failure of plutonium to exhibit consistent behavior with respect to adsorption on shiny metallic surfaces from which corrosion film has flaked.

16.2 SEPARATION OF PuO_2 BY A HYDROCLONE

Results of experimentation on the use of a ¼-in.-dia hydroclone to concentrate PuO_2 from a water slurry at room temperature were encouraging. Concentration factors varied from 2 to 8; however, material balances were poor and varied from 50 to 85%. When the hydroclone overflow was recycled through the hydroclone as many as five times, the same separation efficiency was obtained each time. This indicates that if satisfactory removal is not obtained in a single hydroclone, additional plutonium removal can be obtained by operating several hydroclones in series.

Feed for the hydroclone tests was prepared by precipitating PuO_2 from 1.25 *m* UO_2SO_4 at 250°C, centrifuging, washing with water, and reslurrying in fresh water.

16.3 IN-PILE CHEMISTRY OF PLUTONIUM AND NEPTUNIUM

Irradiation of depleted uranyl sulfate solution in the LITR at 250°C indicated the solubility of

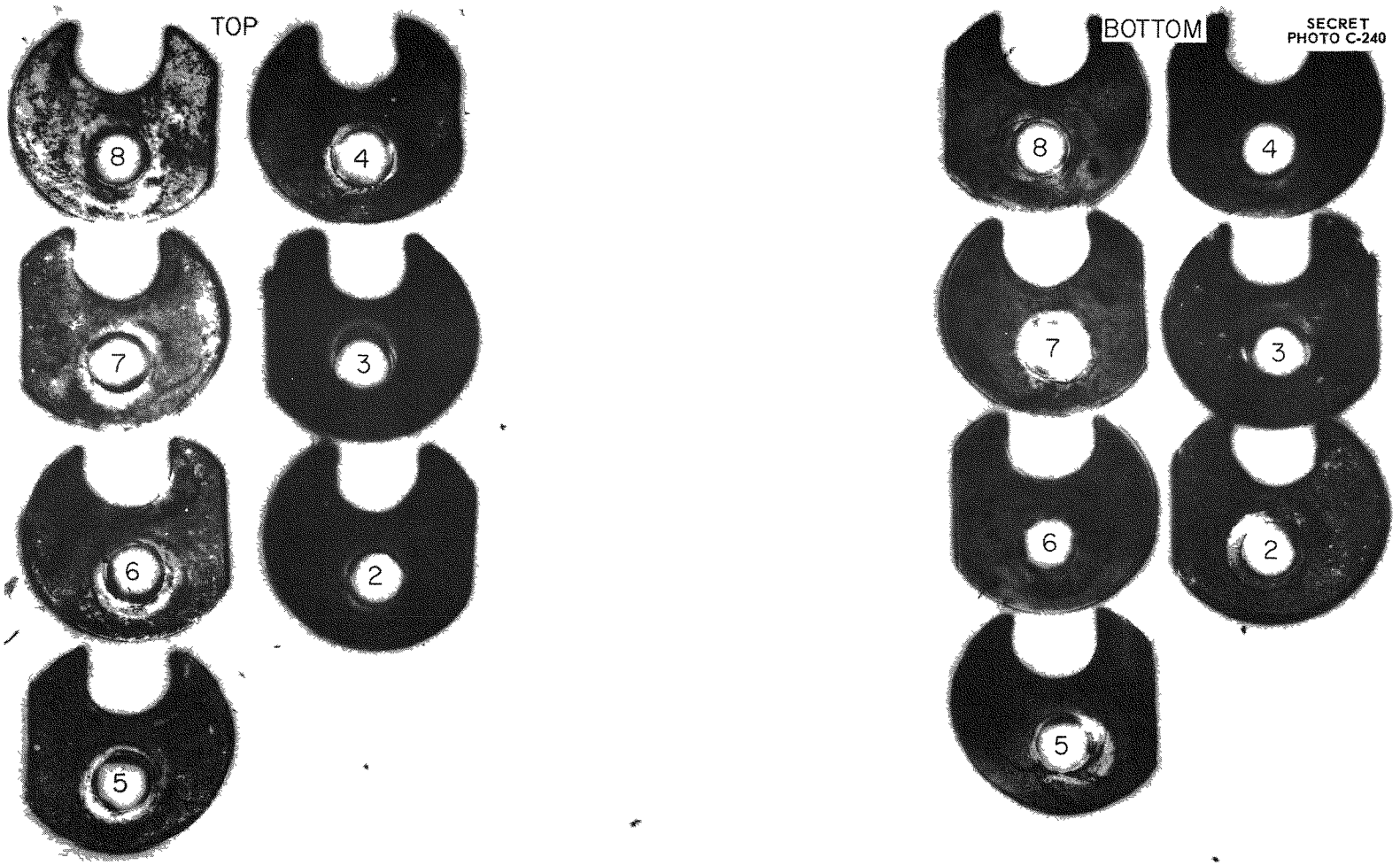

Fig. 16.4. Autoradiographs (15-min Exposure) of Titanium Metal Samples After Contact at 250°C with 2 Liters of 1.26 *m* UO_2SO_4 Containing 100 mg of Plutonium per Kilogram of H_2O. Sample 1 (not included here) was at the solution inlet (see Fig. 16.2).

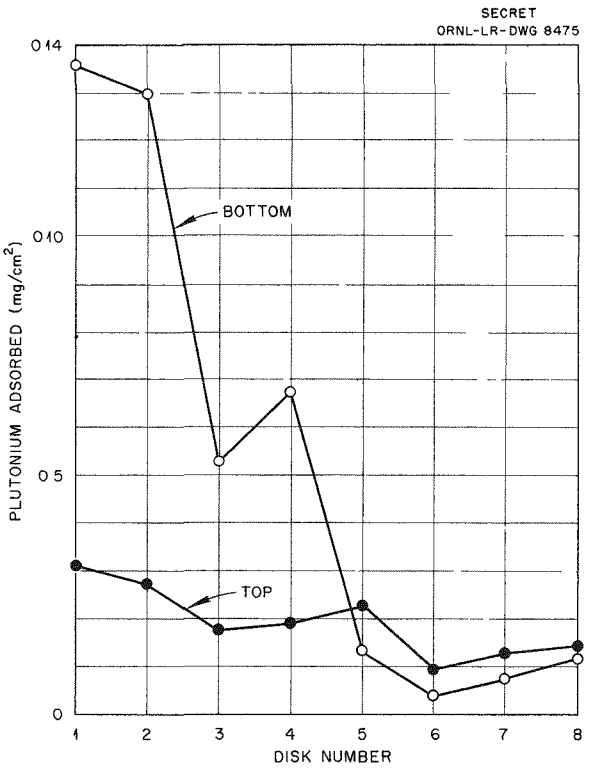

Fig. 16.5. Adsorption of Plutonium on Zircaloy-2 Metal Disks from 1.26 *m* UO_2SO_4 Solution Containing 100 mg of Plutonium per Kilogram of H_2O. Temperature, 250°C.

plutonium to be 0 to 10 mg per kilogram of H_2O. The PuO_2 which was precipitated carried 5 to 10% of the neptunium.

A titanium bomb was loaded with 5 ml of 1.26 *m* UO_2SO_4 (0.38% U^{235}) containing 0.1 *m* $CuSO_4$ and was irradiated in the LITR for 5.9 days. The temperature was maintained at about 250°C, and the resulting pressure was 770 psi. After standing at room temperature for several days to allow the short-lived radioisotopes to decay, the solution and precipitate were analyzed. From these analyses it was calculated that, at the time of removal from the reactor, the solution contained 10 mg of plutonium and 47 mg of neptunium per kilogram of H_2O. The precipitate contained 8.6 mg of plutonium and 4.4 mg of neptunium per kilogram of H_2O. Several weeks later, after all the neptunium had decayed, the bomb was descaled. The scale on the bomb contained plutonium equivalent to 7.9 mg per kilogram of H_2O. The ratio of total neptunium to total plutonium was too high to be consistent with the irradiation history of the system. However, it was interesting that the PuO_2 precipitate appeared to have carried with it about 10% of the neptunium, since removal of the PuO_2 precipitate from the blanket region of a reactor might, in this way, remove Np^{239} from additional exposure to the neutron flux and so decrease the production of Np^{240}.

The titanium bomb was air-cooled while in the LITR; thus, the walls were cooler than the solution. However, an internal thermocouple well was slightly hotter than the solution. When the bomb was descaled, 1.2 μg of plutonium per square centimeter was found adsorbed on the cooler walls and 2.1 $\mu g/cm^2$ on the hotter thermocouple well. This may indicate preferential adsorption on hot walls. Gamma spectroscopy showed that the fission-product radioactivity on the cooler walls was about two-thirds Zr^{95}-Nb^{95}, one-third ruthenium, and one-thirtieth lanthanum. Activity on the thermocouple well was 90 to 95% Ba^{140}-La^{140}.

This experiment was repeated in a Zircaloy-2 bomb. After being irradiated in the LITR for 4.6 days at 250°C, the bomb was held at room temperature for several days to allow the short-lived activity to decay. Analyses indicated that there was no plutonium but that there was 32 mg of neptunium in solution per kilogram of H_2O at the time the bomb was removed from the LITR. The precipitate contained 2.7 mg of plutonium and 1.5 mg of neptunium per kilogram of H_2O. The bomb has not yet been descaled, and the neptunium-plutonium ratio, on the material thus far recovered, was again higher than is consistent with the irradiation history of the system. It is interesting that, again, about 5% of the neptunium appeared to be carried on the PuO_2 precipitate.

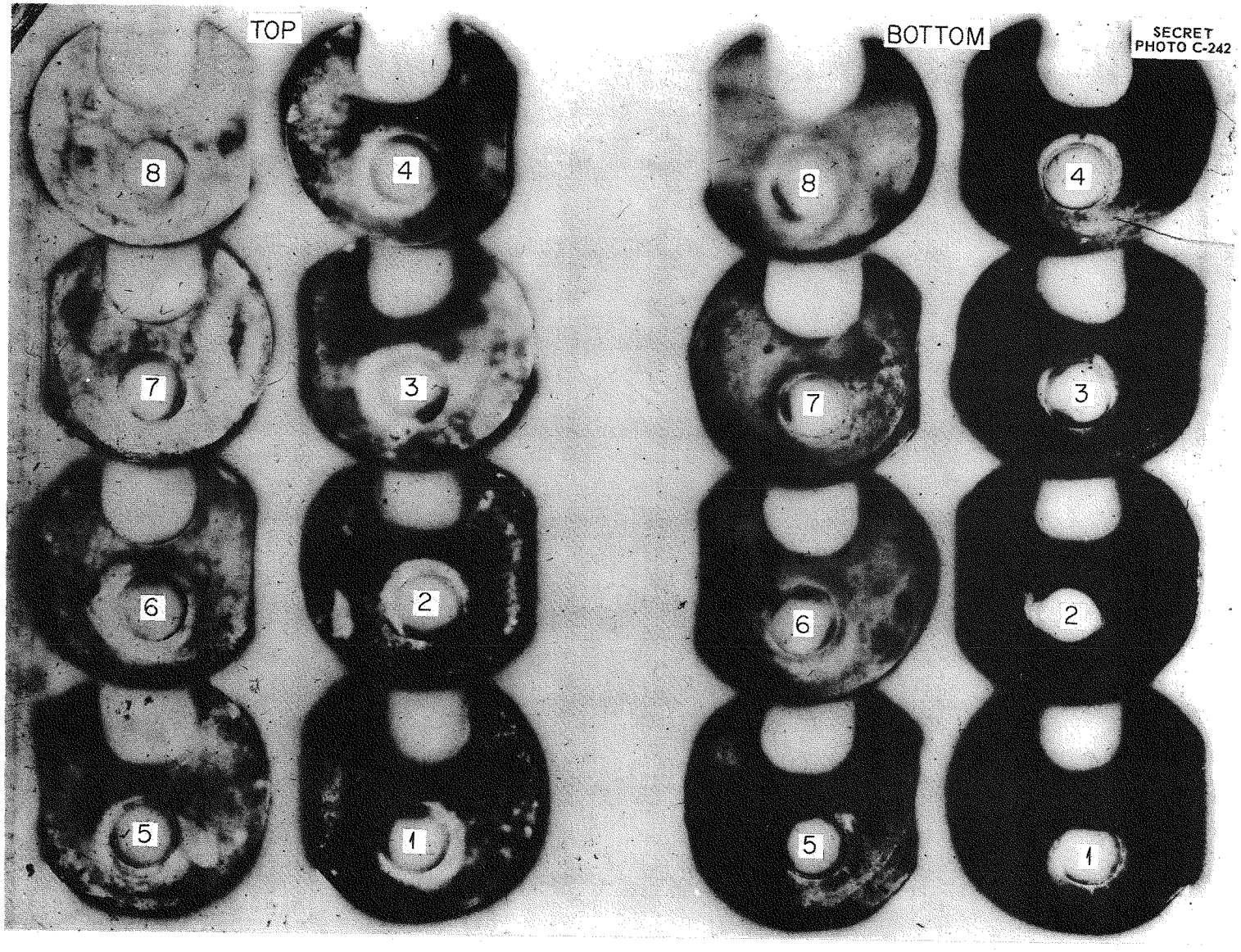

Fig. 16.6. Autoradiographs (15-min Exposure) of Zircaloy-2 Metal Samples After Contact at 250°C with 1 Liter of 1.26 *m* UO_2SO_4 Solution Containing 100 mg of Plutonium per Kilogram of H_2O. Sample 1 was at the solution inlet (see Fig. 16.2).

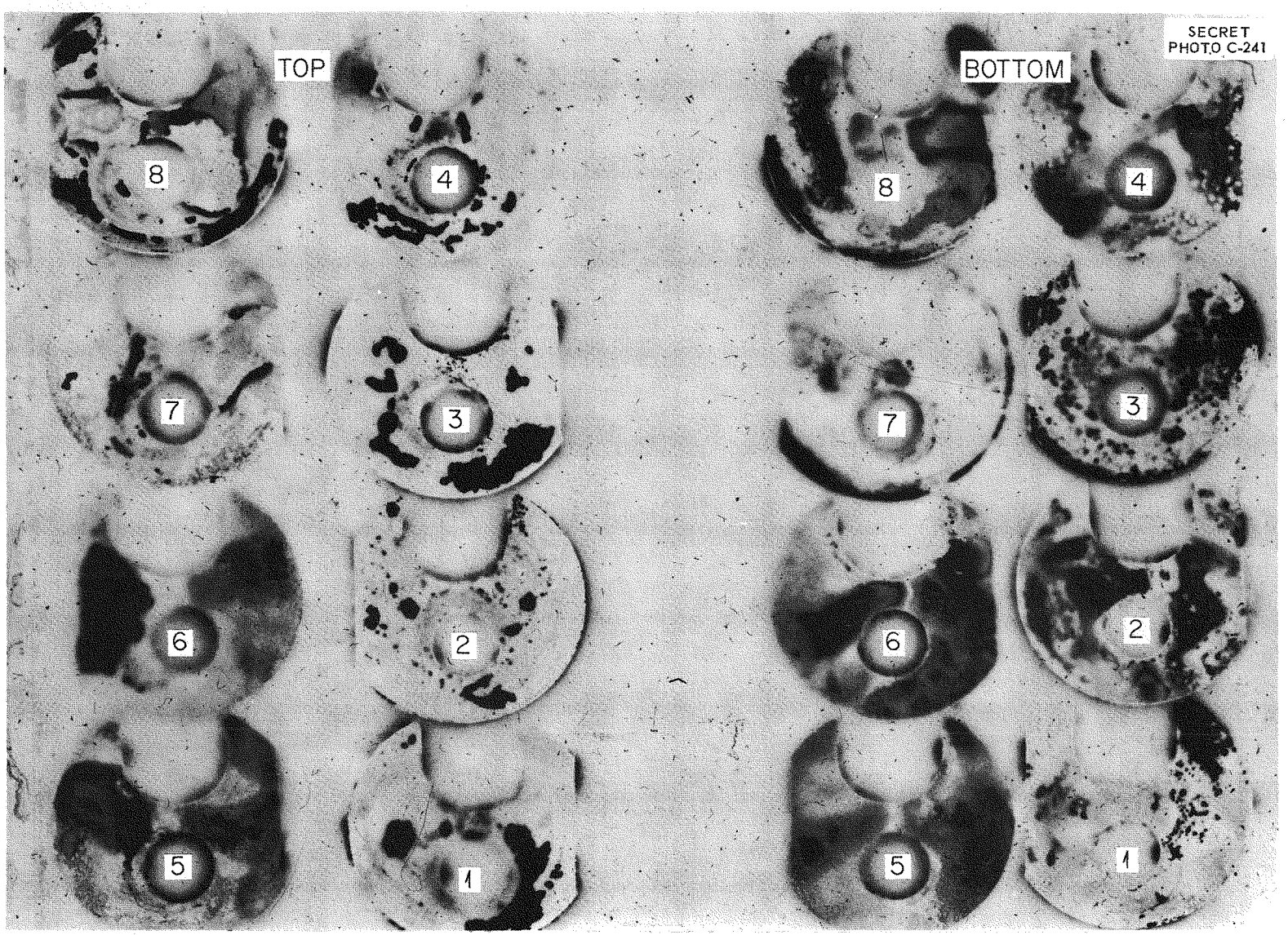

Fig. 16.7. Autoradiographs (1-hr Exposure) of Type 347 Stainless Steel After Contact at 250°C with 1 Liter of 1.26 *m* UO_2SO_4 Solution Containing 100 mg of Plutonium per Kilogram of H_2O. Sample 1 was at the solution inlet (see Fig. 16.2).

17. THERMAL-BREEDER BLANKET PROCESSING

D. E. Ferguson

R. E. Leuze W. E. Tomlin

Removal of protactinium and uranium from a ThO_2 slurry by leaching is being investigated as an alternate method to complete dissolution and solvent extraction for processing the ThO_2 blanket of the thorium-breeder reactor.

17.1 LEACHING OF IRRADIATED THORIUM OXIDE

Although protactinium apparently is bound within irradiated ThO_2 particles, up to 94% of it was leached by refluxing with 14 *N* H_2SO_4 for 2 hr and washing with another portion of 14 *N* H_2SO_4. Essentially all the ThO_2 was converted to $Th(SO_4)_2$ when refluxed in 12 to 14 *N* H_2SO_4; however, because of the low solubility of $Th(SO_4)_2$ in hot sulfuric acid, only small amounts (less than 1%) of the thorium followed the protactinium.

When 15 mg of irradiated ThO_2 (calcined at 650°C) was refluxed in 10 ml of 14 *N* H_2SO_4 for 2 hr, the mixture filtered while hot, and the residue washed with 10 ml of hot 14 *N* H_2SO_4, 94% of the protactinium and about 1.2% of the thorium were dissolved. The residue, primarily $Th(SO_4)_2$ with some remaining ThO_2, contained 6% of the protactinium originally present. However, when larger amounts of irradiated ThO_2 were processed, the percentage of protactinium leached was smaller (Table 17.1), only 50% being dissolved in 2 hr from 4.775 g of ThO_2. The decrease in protactinium leaching appeared to result primarily from the increased amount of ThO_2 processed, although the reduction in the amount of excess sulfuric acid may have had some effect. Results of analyses of the filtrates and washes indicate that the solubility of $Th(SO_4)_2$ in 14 *N* H_2SO_4 at about 90°C is 0.008 to 0.012 mg/ml. This solubility is low enough to ensure that insignificant amounts of thorium (much less than 0.5%) will follow the protactinium if satisfactory leaching of protactinium can be realized with smaller volumes of sulfuric acid.

A 417-mg sample of irradiated ThO_2 (prepared by calcination of thorium oxalate at 650°C – original protactinium content 1.4×10^9 beta counts/min/mg of ThO_2) was refluxed with 25 ml of 12 *N* H_2SO_4 to determine the rate of leaching of protactinium. The protactinium removal rate approximated a first order reaction, but decreased slightly with time (Fig. 17.1). After 2 hr, 69% of the protactinium was leached. It should be noted that the rate of removal also depended on the amount of ThO_2 processed, as discussed above.

A scouting test showed that only 15% of the protactinium was leached from 26 mg of ThO_2 by refluxing with 5 ml of 0.9 *M* oxalic acid for 2 hr. When 20 mg of ThO_2 was refluxed with 10 ml of 16 *N* HNO_3 for 3 hr, most of the thorium and protactinium were dissolved. Precipitation of the thorium with oxalic acid carried 50% of the dissolved protactinium.

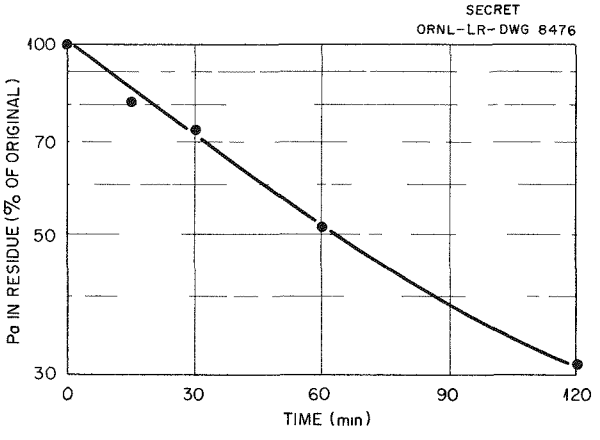

Fig. 17.1. Rate of Leaching of Protactinium from Irradiated ThO_2 by 12 *N* H_2SO_4.

TABLE 17.1. LEACHING OF PROTACTINIUM FROM IRRADIATED ThO_2

ThO_2 prepared by calcination of thorium oxalate at 650°C

Irradiated ThO_2 refluxed for 2 hr in sulfuric acid; residue filtered and washed at ~90°C

ThO_2 (g)	H_2SO_4			Protactinium (%)		
	Normality	Amount (ml)	Excess	Leach	Wash	Residue
0.015	14	10	620 ×	87	7	6
0.106	14	50	440 ×	75	4	21
0.417	12	25	48 ×	69	*	*
4.775	14	250	48 ×	46	4	50

* Not analyzed.

17.2 CONVERSION OF $Th(SO_4)_2$ TO ThO_2

Sulfate can be removed from the residue resulting when ThO_2 is leached with sulfuric acid by calcining it in air at 900°C. Calcination at 900°C for 16 hr reduced the sulfate in one such residue from 34 to 0.12%. When another residue containing 14.9% sulfate was calcined at 920°C, the sulfate was reduced to 0.59% in 2.5 hr, 0.36% in 3.5 hr, 0.32% in 4.5 hr, and 0.21% in 5 hr. It can be seen from these data that the rate of removal becomes quite slow when the sulfate is about 0.5%.

The rate of removal of sulfate is markedly dependent on the calcination temperature. When a residue was calcined for 2 hr at 700°C, the sulfate content was reduced from 14.9 to 7.8%; at 760°C, to 3.4%; at 815°C, to 0.87%; and at 870°C, to 0.56%. Although sulfate can be removed from these residues by calcination in air, it has not yet been determined whether the resulting ThO_2 will form a satisfactory slurry for re-use in the TBR blanket.

18. SUMMARY OF WORK OF VITRO LABORATORY[1]

Experiments to determine a mass-transfer coefficient for the vaporization of iodine from acidified uranyl sulfate solutions have given values ranging from 0.9 to 2.2 gram moles $I_2/(min)(cm^2)(g\ I_2/kg\ H_2O)$.[1] In these tests metallic silver was present in the vapor phase, and it was assumed that diffusion of iodine to, and reaction with, the silver was rapid with respect to the volatilization process. The mass-transfer coefficient, K, was then defined as

$$K = \frac{N}{Ax},$$

where

N = moles of iodine vaporized per minute,
A = area of gas-liquid interface in square centimeters,
x = concentration of free iodine in liquid, g/kg.

Consideration of processes involving stripping with an inert gas as a means of accelerating the desorption of iodine from fuel solution has been given secondary importance owing to the anticipated difficulty in separating the xenon daughter from the stripping gas in an economically sized unit. Emphasis has therefore been removed from the contemplated study of stripping rates[2] and placed instead on the measurement of the relative volatility of iodine and water in an acidified uranyl sulfate solution.

An apparatus has been assembled which permits liquid and vapor samples to be taken simultaneously from a bomb system and is now being used to measure the vapor-liquid distribution of iodine at temperatures up to the two-liquid-phase limit. Equilibrium data on the vapor-liquid distribution of iodine will be applied to the development of separation processes in which the first step is a partial evaporation of fuel solution to provide an iodine-bearing D_2O vapor stream, also carrying radiolytic gases and other volatile fission products.

Preliminary data from this apparatus suggest that the mole percentage of iodine in the vapor phase is about five times greater than in the liquid phase when that liquid phase is 0.02 m UO_2SO_4–0.005 m H_2SO_4. These preliminary results also indicate that this distribution is very dependent on the pH of the solution and that an increased pH in the solution results in a less favorable distribution of iodine to the vapor phase.

As presently conceived, an iodine removal process would consist of several steps, and process design, as well as laboratory investigation work, is under way in order to define areas in which specific information is needed. The steps in the process would include removing iodine from the fuel solution, concentrating and fixing of iodine within the high-pressure system, removing the fixed iodine, storing it to permit decay to xenon, and fixing the radioactive xenon.

In a single batch test, 74% of the cerium sulfate in a simulated (uranyl sulfate) fuel solution at 300°C was adsorbed by garnet sand in 1 hr. The cerium was initially present as 50% of a mixture of rare-earth sulfates, the total concentration of which was 0.026 g of rare-earth sulfates per kilogram of H_2O. Cerium may be the only one of the rare earths amenable to this adsorption owing to the relative ease of its oxidation to the tetrapositive state. A similar test with neodymium sulfate is planned.

[1] Abstracted from: W. A. Bain, *HR Fuel Reprocessing Quar. Prog. Rep. June 30, 1955*, KLX-10006.

[2] W. A. Bain, *HR Fuel Reprocessing Quar. Prog. Rep. March 31, 1955*, KLX-10000.

Part VI

SUPPORTING CHEMICAL RESEARCH

E. H. Taylor

19. AQUEOUS SYSTEMS AT ELEVATED TEMPERATURES

C. H. Secoy

F. E. Clark
S. F. Clark
G. M. Hebert
F. J. Loprest
W. L. Marshall
D. M. Richardson
D. W. Sherwood
R. Slusher
F. H. Sweeton

19.1 ALKALINE CARBONATE–URANIUM TRIOXIDE SYSTEMS AT 250°C

F. J. Loprest W. L. Marshall

19.1.1 Introduction

An investigation was started on the phase equilibria, at high temperature, in the systems: alkali or alkaline-earth oxide–uranium trioxide–carbon dioxide–water. The purpose of this work was to explore the various alkaline uranium systems and to evaluate their potentialities as suitable aqueous homogeneous reactor fuels; the results reported herein are preliminary. It was desired to survey several systems before obtaining extensive data on a specific one.

Among the systems investigated were Na_2O-UO_3-CO_2-H_2O, MgO-UO_3-CO_2-H_2O, and Li_2O-UO_3-CO_2-H_2O. Emphasis at the present is placed on the lithium system, since it appears to be the most promising of the three as a fuel solution for a reactor. Systems involving the other alkali or alkaline-earth oxides did not appear desirable either because the neutron absorption cross section of the metal oxides is high or work at low temperature indicated that low solubilities would be expected at high temperature.

There have been a few exploratory studies made on the Na_2O-UO_3-CO_2-H_2O system at high temperature (100 to 250°C) by Wright and Gill,[1] Blake *et al.*,[2] and a cursory examination by Bidwell *et al.*[3] The sodium system did not appear feasible for dissolving appreciable quantities of uranium at high temperature.

Several recent rather thorough investigations[4–6] have dealt with these systems at low temperature. Blake *et al.* have reported that as much as 320 g of uranium per liter can be dissolved at 25°C in the Na_2O-UO_3-CO_2-H_2O system. Bachelet *et al.* have studied the Li_2O-UO_3-CO_2-H_2O and MgO-UO_3-CO_2-H_2O systems, among others, and state that appreciable solubilities, of the order of 1 to 2 *M*, of compounds such as $Li_4UO_2(CO_3)_3$ and $Mg_2UO_2(CO_3)_3$ can be obtained in the temperature range 25 to 60°C. However, they state that hydrolysis occurs above approximately 50 to 75°C, with subsequent precipitation of a uranium compound. Carbon dioxide gas pressure was used in the present investigation in an attempt to prevent this precipitation.

19.1.2 Experimental

Uranium trioxide was obtained from the Mallinckrodt Chemical Works. It was water-washed at room temperature and finally at 250°C in order to remove as much nitrate impurity as possible (NO_3^-, <24 ppm). Baker and Adamson reagent-grade sodium carbonate and lithium carbonate and Merck reagent-grade magnesium carbonate were used as starting alkali or alkaline-earth materials. Commercial-grade dry ice (carbon dioxide) was used for producing the CO_2 pressure on the system under study. Water-pumped, commercial-grade tank oxygen was used for oxygen addition; in some of the early work Baker and Adamson cp 30% H_2O_2 was used for oxygen addition. The use of H_2O_2 was discontinued, since it was observed to form highly colored soluble complexes

[1] H. W. Wright and J. S. Gill, *HRP Quar. Prog. Rep. Aug. 15, 1951*, ORNL-1121, p 120.

[2] C. A. Blake *et al.*, Oak Ridge National Laboratory, private communication (1951) (telephone conversation).

[3] R. W. Bidwell *et al.*, Los Alamos Scientific Laboratory, private communication (1951) (telephone conversation).

[4] C. A. Blake *et al.*, *Studies in the Carbonate-Uranium System*, AECD-3280 (Dec. 14, 1950), Y-794 (Aug. 20, 1951).

[5] K. B. Brown and J. M. Schmitt, *Studies in the Carbonate-Uranium System*, AECD-3229 (Oct. 20, 1950).

[6] M. Bachelet *et al.*, *Bull. soc. chim. France* 19, 55–60 (1952); 19, 565–569 (1952); 21, 173–179 (1954).

of questionable stability and thus to complicate the solubility relationships.

In aqueous solutions at low temperature the compounds $Mg_2UO_2(CO_3)_3$ and $Li_4UO_2(CO_3)_3$ were prepared according to the methods of Bachelet *et al.*[6] High solubilities at room temperature and up to approximately 100°C were obtained, and these values verified a few of the observations of Bachelet *et al.*

The soluble $Li_4UO_2(CO_3)_3$ did not crystallize when the solution was concentrated by evaporation to approximately 2.0 to 2.5 *M* in accordance with Bachelet's observations. However, the soluble $Mg_2UO_2(CO_3)_3$ did form clear yellow needle crystals after a dilute solution was concentrated, by evaporation at 75 to 80°C to approximately 2 *M*, and then cooled to room temperature when the resulting supersaturated solution was seeded.

The apparatus and thermostat controllers for solubility determination at high temperature are described in another report.[7] The present apparatus included a few modifications (Fig. 19.1). Commercial high-pressure stainless steel valves and other equipment were used exclusively. A second capillary tubing connection was added to the solubility bomb, thus providing both a capillary solution sampling tube and a tube opening into the vapor phase for addition or removal of gas and vapor.

Since the critical pressure of liquid carbon dioxide at the critical temperature (31°C) is only 1071 psi, whereas it was expected that there would be total pressures of 3000 psi in these investigations, the usual tank liquid CO_2 could not be used to obtain these pressures, at least not at room temperature. Therefore a bomb was constructed to which a weighed amount of dry ice was added, and the bomb was heated in a water bath above the critical temperature of CO_2. The bomb, containing a high pressure of CO_2 and connected to a pressure gage and to the thermostat bomb by a series of valves, was used to achieve the desired pressures on the system under consideration.

The procedure for making a run was as follows. Weighed amounts of UO_3 hydrate and either

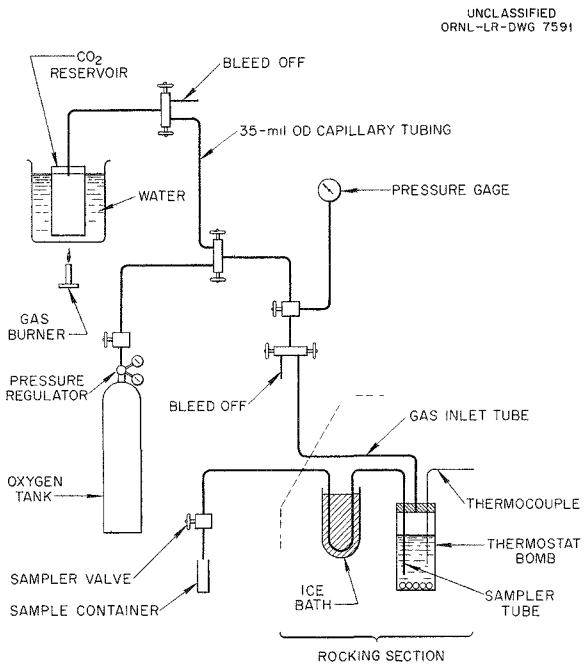

Fig. 19.1. Schematic Diagram of Solubility Apparatus.

Na_2CO_3, Li_2CO_3, or $MgCO_3$ were added to a 100-cc-capacity pressure bomb. A 60-cc volume of distilled water, which had been purified further by use of an ion-exchange column, was added to the bomb. The bomb head was screwed down and the unit placed in the thermostat, which was rocked by means of a hydrogenation apparatus rocker. The temperature was raised to 75 to 100°C, and 50 ± 5 psi oxygen pressure was added to the system from an oxygen tank and regulator. The temperature was raised to a given value, and the desired CO_2 pressure was placed on the system from the CO_2 bomb reservoir. The thermostat was rocked for a sufficient length of time, the unit stopped, the thermostat rotated from the horizontal to the vertical position, and a solution sample obtained in the manner described previously.[7] The total pressure on the system could be varied by adding additional CO_2 or bleeding off the vapor phase.

Uranium was determined in most samples colorimetrically by the basic peroxide method.[8] In the

[7] W. L. Marshall, *The pH of UO_3-H_2SO_4-H_2O Mixtures at 25°C and Its Application to the Determination of the Solubility of UO_3 in Sulfuric Acid at Elevated Temperature*, ORNL-1797 (Oct. 18, 1954).

[8] C. J. Rodden (Editor-in-Chief), *Analytical Chemistry of the Manhattan Project*, p 93, McGraw-Hill, New York, 1950.

case of UO_3 and UO_2CO_3 solubilities in H_2O the uranium concentrations were too low, and therefore the more sensitive method of Yoe, Will, and Black[9] was used. A few uranium samples were analyzed potentiometrically. Lithium was determined by use of a flame spectrophotometric method. Carbonate was determined by decomposition with acid and adsorption of the liberated CO_2 by Ascarite. An approximate method for estimating CO_2 in the liquid samples involved the trapping of the sample in a 3-mm pyrex tube 1 meter in length at 1-atm pressure. Comparison of the volumes of the liquid and gas phases permitted an estimation of the amount of CO_2 in excess of that which is in combined form in the liquid phase.

19.1.3 The Systems UO_3-H_2O and UO_2CO_3-H_2O

The solubility of UO_3 was determined at various temperatures on one batch of 3 g of solid oxide (Table 19.1). The average values for the indicated temperatures are listed in the last column of the table.

An attempt to measure the effect of CO_2 pressure on the solubility of UO_3 indicated that UO_3 was converted to a different solid phase, probably UO_2CO_3, at total pressures in excess of 860 psi (the minimum CO_2 pressure necessary for conversion was not determined). The solubility determinations were erratic but indicated that the solubility of the new phase is of the same order of magnitude as was the solubility of UO_3 in pure water.

19.1.4 The System (MO or M_2O)UO_3-CO_2-H_2O – General Discussion

The weight percentages of the components MO or M_2O, UO_3, and H_2O in the liquid phase (except

[9] J. H. Yoe, F. Will, III, and R. A. Black, *Anal. Chem.* 25, 1200 (1953).

TABLE 19.1. SOLUBILITY OF UO_3 IN WATER

Temperature (°C)	Initial Mixture (g of UO_3)	Initial Mixture (ml of H_2O)	Cumulative Stirring Time (hr)	Concentration of Uranium in Liquid Phase (ppm)	Concentration of Uranium in Liquid Phase (Average)
250	3	50	3	16.7	
			6	12.8	
			11	16.4	
			27	19.4	
*					
250		60	0.25	13.3	
			2.5	12.7	
			9	14.3	
*					
290		60	16	19.0	
			18	17.1	18.1 (290°C)
250			3	9.9	14.4 (250°C)
*					
200		60	4	5.3	
			7	5.2	5.3 (200°C)
*					
175		60	2.5	6.4	
			5.0	6.0	6.2 (175°C)
150			1.0	6.2	
			2.0	6.4	6.3 (150°C)

*Indicates interruption of run for washing of the solid.

when noted), the total mixture, and the solid phase are expressed – the CO_2 content being completely neglected. These data, therefore, represent points on a Jänecke projection of points in the quaternary isothermal, isobaric tetrahedron on the MO or M_2O-UO_3-H_2O face. The tie lines on this projection can be extrapolated to solid-phase compositions that express the true ratio of three of the components but do not give any information about the fourth component, CO_2. Some supporting observations provided the basis for an estimate of the CO_2 content of the liquid and solid phases. The composition of the vapor phase at a constant total pressure and temperature was assumed to be fixed, since the vapor pressure of water probably did not vary much.

In calculating the weight percentages in the liquid phase two assumptions were made. The first was that the CO_2 remaining in the liquid phase, after the solution was cooled and the pressure was reduced, as described in the discussion of the sampling procedure (Sec. 19.1.2), was stoichiometric to the M_2O and UO_3 in the liquid phase. This small weight of CO_2 was subtracted from the total weight of the sample, which was then analyzed for M and U. The second assumption concerned the densities of the liquid phase. Since a volumetric sample was analyzed, it was necessary, in the absence of density measurements, to assume that the density of the liquid was unity. Based on observations of UO_2SO_4 densities for similar molarities,[10] it is probable that these densities did not deviate more than 5% from unity.

In order to obtain the *absolute* weight percentages of the three components, MO or M_2O, UO_3, and H_2O, the absolute weight percentage of the fourth component, CO_2, would have to be determined in the system under equilibrium conditions. The Jänecke projection values given in Table 19.2 (and also in Table 19.7 in Sec. 19.1.7) and shown in Fig. 19.2 (and also in Fig. 19.7, Sec. 19.1.7) would then be multiplied by the factor $(1.0 - X)$, where X is the weight fraction of CO_2 at equilibrium. The true weight percentages for all four components would then be obtained. At 1500 psi total pressure and at 250°C the true weight fraction of CO_2 in the solution was found to be approximately 0.018 to 0.020 in the lithium

[10] W. L. Marshall, *HRP Quar. Prog. Rep. March 15, 1952*, ORNL-1280, p 188.

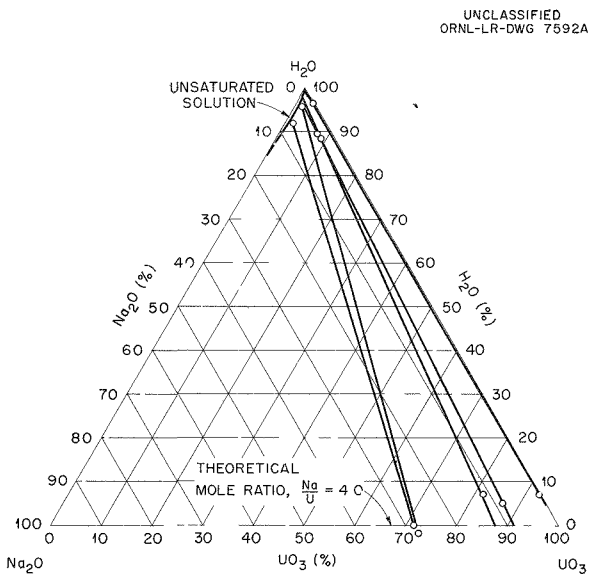

Fig. 19.2. The System Na_2O-UO_3-CO_2-H_2O at 250°C and at 1000 to 1600 psi CO_2 (Janecke Projection).

system by the gas-liquid volume ratio method at atmospheric pressure and by assumption of the residual and stoichiometric CO_2 contents in the liquid. Therefore, the correction factor $(1 - X)$ would produce only a 1.8 to 2.0% negative correction of the values reported in Table 19.7 and Fig. 19.7.

19.1.5 The System Na_2O-UO_3-CO_2-H_2O

Table 19.2 lists the data obtained thus far for the Jänecke projection. The solid-phase compositions were obtained by direct analysis of the solids which had been removed from the bomb after the final sampling of the liquid phase. The solids were separated from the liquid phase by filtration, washed with two or three small portions of distilled water, allowed to dry in air, and ground in a mortar until uniform. The complete analyses of the solids, including CO_2 determination, are listed in Table 19.3.

In constructing the Jänecke projection (Fig. 19.2) the liquid phase could not be corrected for residual CO_2 because the Na_2O content of the liquid had not been determined in most cases. The solubility curve in the projection was therefore fixed by drawing a tie line between the solid phase and total mixture points and terminating it

TABLE 19.2. THE SYSTEM Na_2O-CO_2-UO_3-H_2O

Data for Jänecke Projection on Na_2O-UO_3-H_2O Face at 250°C

Run No.	Total Mixture (%)		Liquid[a] Phase (%)		Solid[b] Phase (%)		Total Pressure (psi)	Stirring Time[c] (hr)
	UO_3	Na_2O	UO_3	Na_2O	UO_3	Na_2O		
II-44-1	3.06	0.265	0.00				580	1
2			0.00		92.48	0.00	1600	2
II-39-1[d]	8.78	2.53	0.135				820	3
2			0.192		83.36	11.05	1250	4
II-41-1	7.43	2.56	0.098	1.82			580	2
2			0.159	1.82	86.67	8.85	1100	3
II-31-1[d]	1.67	2.74	0.050				800	1
2			0.144				1000	3
3			0.169				1000	3
4			0.154				1400	4
5			0.179		73.57	28.79	1300	2
II-43-1	19.54	6.02	0.126				580	
2			0.166				1400	
II-35-1[d]	1.63	6.36	0.159				780	2
2			0.179		71.47	28.27	1000	3

[a] Analytical data uncorrected for residual CO_2.
[b] By analysis of washed, dried solids.
[c] Not cumulative.
[d] Initial pressure of O_2 introduced at 100°C was 200 psi; in all other runs it was 50 psi.

TABLE 19.3. ANALYSES OF DRIED WASHED SOLIDS

Run No.	Composition (%)		
	UO_3	Na_2O	CO_2
II-44-2	91.80	0.004	0.74
II-41-3	83.16	8.49	4.04
II-39-2	81.33	10.78	2.43
II-35-2	55.20	21.83	22.77
II-31-5	56.48	22.10	23.23

at the given value of the percentage UO_3 in the liquid phase.

Two of the solids obtained had compositions close to that of $Na_4(UO_2)(CO_3)_3$ (theoretical composition, wt %: Na_2O, 22.87; UO_3, 52.77; CO_2, 24.36). It appears probable, therefore, that this solid is one of the equilibrium phases at high temperature just as it is at room temperature. Two of the tie lines in the projection lie in what appears to be a two-solid-phase-eutectic region. If the two solid phases involved are $Na_4(UO_2)(CO_3)_3$ and UO_2CO_3, then the deep solubility well found by Blake and co-workers at room temperature apparently is absent at 250°C.

19.1.6 The System MgO-UO_3-CO_2-H_2O

An unsaturated solution of magnesium uranyl carbonate (0.2154 *M* in MgO and 0.07173 *M* in UO_3) was prepared at room temperature according to the directions given by Bachelet *et al.*[6] This solution was employed in run A IX 25. For run B IX 27,

solid $MgCO_3$ and UO_3 were mixed with water. The data for these runs are listed in Table 19.4. These two runs cover only a small portion of the dilute region of the phase diagram. Much more extensive investigation is planned for this system, although the apparently very low solubility of $MgCO_3$ seemed to indicate that there may not be any appreciable solubility of uranium at high temperatures.

19.1.7 The System Li_2O-UO_3-CO_2-H_2O

A preliminary measurement of solubility relations in the system Li_2O-CO_2-H_2O at various CO_2 pressures at 250°C was made; the data are recorded in Table 19.5 and are plotted in Fig. 19.3. It is seen that the rate of change of the solubility with pressure appears to fall off at about 1000 psi total pressure to a constant low value at higher pressures. Moreover, plots of the Li_2O and UO_3 contents in the liquid phase and of the Li/U mole ratio (Figs. 19.4, 19.5, 19.6) exhibit, with some scattering of points, a similar behavior.

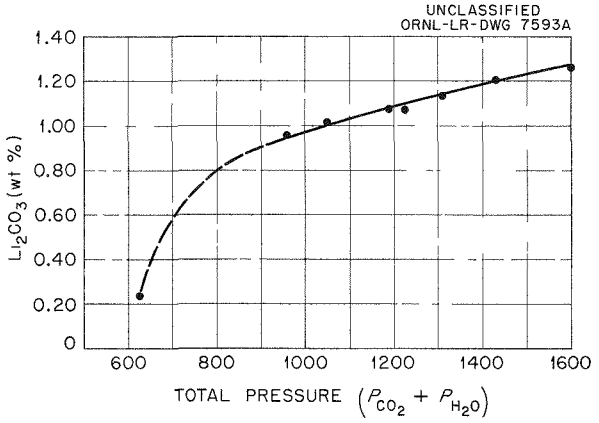

Fig. 19.3. Per Cent of Li_2CO_3 in Liquid Phase; System Li_2O-CO_2-H_2O.

Table 19.6 contains the data thus far obtained in this investigation. The solid-phase compositions are the Jänecke projections. The liquid-phase compositions as listed in the table and plotted in Figs. 19.4 and 19.5 have not been corrected for residual CO_2.

In considering Figs. 19.4 and 19.5, it is seen that the UO_3 and Li_2O content of the liquid phases

TABLE 19.5. THE SYSTEM Li_2O-CO_2-H_2O, SOLUBILITIES

Run No.	Total Pressure* (psi)	Weight Per Cent As Li_2CO_3	Weight Per Cent As Li_2O on Jänecke Projection
IX-38-1	625 (no CO_2)	0.241	0.0973
IX-38-2	625 (no CO_2)	0.235	0.0952
IX-38-3	1600	1.26	0.511
IX-38-4	1430	1.21	0.490
IX-38-5	1310	1.14	0.460
IX-38-6	1225	1.07	0.434
IX-38-7	1190	1.08	0.435
IX-38-8	1050	1.02	0.411
IX-38-9	960	0.964	0.390

*H_2O + CO_2 + 50 psi O_2.

TABLE 19.4. THE SYSTEM MgO-UO_3-CO_2-H_2O

Run No.	Total Mixture (%)		UO_3 in Liquid Phase (%)	Temperature (°C)	Total Pressure (psi)	Agitation Time* (hr)
	MgO	UO_3				
A IX 25	0.869	2.052	0.0039	250	1500	2
			0.0012	150	1000	2
			0.0015	100	880	2
			0.0026	100	220	2
B IX 27	0.438	3.107	<0.004	250	1600	2
			<0.004	250	720	2

*Not cumulative.

TABLE 19.6. THE SYSTEM Li_2O-UO_3-CO_2-H_2O AT 250°C

Run No.	Total Mixture[a] (%)		Liquid Phase[b] (%)		Total Pressure[c] (psi)	Agitation Time[d] (hr)	Mole Ratio Li/U in Liquid
	UO_3	Li_2O	UO_3	Li_2O			
II-48-1	3.043	0.9440	2.15	0.850	1600	1	7.57
2			1.91	0.743	1400	2	7.45
3			1.76	0.754	1350	2	8.20
			1.76	0.753	1350	1	8.19
II-50-1	3.043	0.9435	0.061	0.131	600	2	41.1
2			0.046	0.121	600	2	50.4
3			0.421	0.323	750	1	14.7
II-52-1	8.439	2.616		0.194		1	
2			2.21	0.861	1670	1	7.46
3			3.17	1.055	1590	1	6.37
4			2.42	0.840	1170	1	6.65
5			2.50	0.905	1140	3	6.93
6			2.51	0.881	1280	3	6.72
7			2.60	0.819	1060	2	6.03
8			2.36	0.819	1050	2	6.64
9			2.05	0.753	910	1	7.03
10			1.60	0.666	820	2	7.97
11			1.44	0.603	740	1	8.02
12			1.03	0.496	700	1	9.22
13			0.89	0.451	680	1	9.70
IX-33-1	10.385	2.169	3.83	1.16	1640	4	5.80
2			3.74	1.16	1530	1	5.94
3				0.990	1340	2	
4			2.75	0.947	1230	4	6.59
5			2.85	0.947	1190	1	6.36
6			2.68	0.926	1170	1	6.62
7			2.42	0.840	1080	2	6.65
8			2.22	0.80	990	2	6.9
9			1.73	0.69	790	2	7.6
10			1.18	0.54	690	1	8.8
11			0.96	0.45	650	2	9.0
12			0.75	0.43	640	2	11.0
13			0.70	0.39	640	1	10.7
II-63-1	5.184	0.5447	0.497	0.366		1	14.1
2			0.448	0.366		4	15.6
3			0.439	0.366		2	16.0
4			0.298	0.323		1	20.7
5			0.302	0.323		2	20.5
6			0.336	0.344		3	19.6
7			0.342	0.323		1	18.1
8			0.364	0.344		1	18.1
II-58-1	5.564	0.8480	2.17	0.797	1580	1	7.03
2			2.21	0.797	1560	2	6.90
3			2.01		1500	19	
4			1.84	0.732	1300	2	7.62
5			1.87	0.732	1250	1	7.50
II-61-1	5.204	5.206	2.234	0.797	1140		6.83

[a]Points on Jänecke projection on Li_2O-UO_3-H_2O face.
[b]Not corrected for residual CO_2 and are not points on the projection.
[c]50 psi of O_2 introduced at 100°C.
[d]Not cumulative.

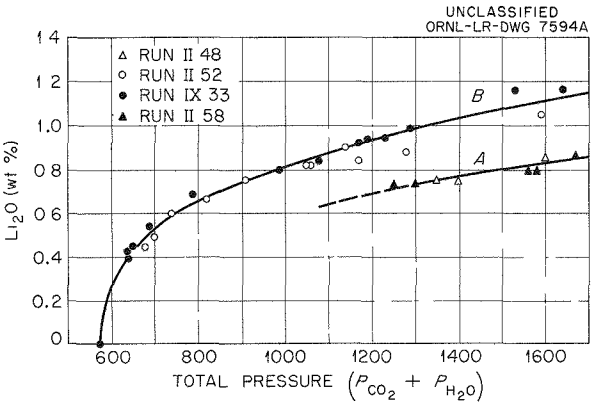

Fig. 19.4. Per Cent of Li_2O in Liquid Phase; System Li_2O-UO_3-CO_2-H_2O.

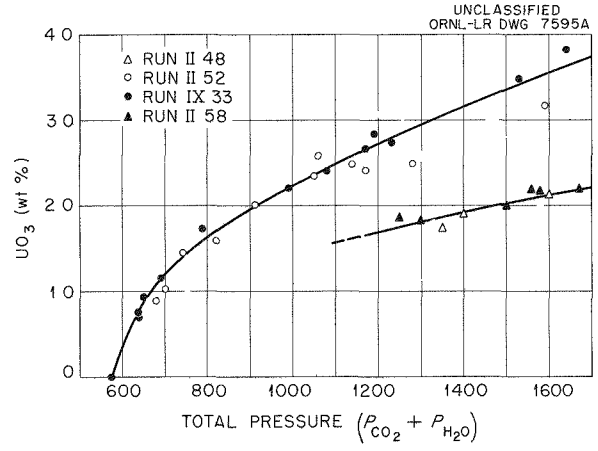

Fig. 19.5. Per Cent of UO_3 in Liquid Phase; System Li_2O-UO_3-CO_2-H_2O.

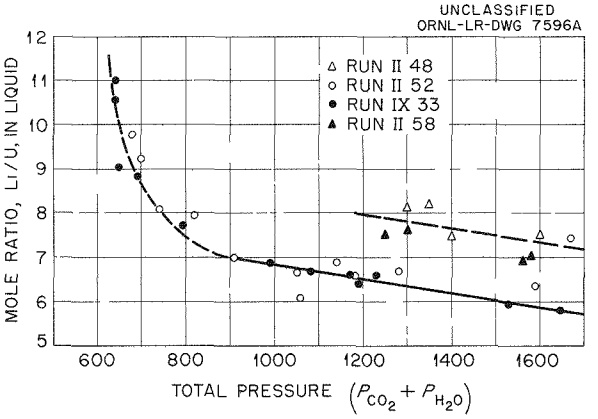

Fig. 19.6. Mole Ratios of Li to U in Liquid Phase; System Li_2O-UO_3-CO_2-H_2O.

at pressures above 1100 psi roughly appears to be one of two constant sets of values. For example, at 1500 psi for runs IX-33 and II-52, values of Li_2O = 1.80% and UO_3 = 3.37% may be read from the figure and, likewise, for runs II-48 and II-58, values of Li_2O = 0.80% and UO_3 = 2.04% may be obtained. These values may be corrected for residual CO_2, and they are listed in Table 19.7. The data in Table 19.7 are plotted in Fig. 19.7. The existence of three solid phases is tentatively postulated, and this is consistent with the experimental observations. The postulated solids may be: I = Li_2CO_3, II = a lithium uranyl carbonate with mole ratio of Li/U probably 2 or less, and III = UO_2CO_3. The existence of a whole series of complex solids, such as occurs in the Na_2O-UO_3-H_2O system,[11] is, of course, possible. If this were the case, then a corresponding number of very dilute solutions saturated with respect to two solids would exist in the system.

The relatively small region of unsaturation is bounded by rather steep solubility surfaces, and, if the liquid phase is to remain unsaturated, conditions have to be maintained within rather narrow limits. It is expected that this region of unsaturation will increase as the temperature is decreased. However, at 250°C it does not appear likely that a liquid phase containing more than 4% of UO_3 or about 30 to 40 g of uranium per liter will be obtained, at least at total CO_2-H_2O pressures up to 2000 psi.

19.1.8 Summary and Conclusions

Some preliminary solubility data for the systems Na_2O-UO_3-CO_2-H_2O, Li_2O-UO_3-CO_2-H_2O, and MgO-UO_3-CO_2-H_2O have been obtained at 250°C up to approximately 1000 psi CO_2. On the basis of these data some deductions about the solid phases in equilibrium with the solutions are made, and tentative phase diagrams are presented. In addition, the solubility of UO_3 or UO_2CO_3 as a function of CO_2 gas pressure and temperature from 150 to 290°C is mentioned, and an order of magnitude of solubility is given.

Several experiments indicate that a small pressure of oxygen of the order of 50 psi is necessary to stabilize the U(VI) in solution and thus prevent reduction to U(IV) in type 347 stainless steel and

[11] J. E. Ricci and F. J. Loprest, *J. Am. Chem. Soc.* 77, 2119 (1955).

TABLE 19.7. THE SYSTEM Li_2O-UO_3-CO_2-H_2O

Jänecke Projection on Li_2O-UO_3-H_2O Phases at 250°C and 1500 psi Total Pressure

Run No.	Total Mixture (%)		Liquid Phase[a] (%)		Extrapolated Value of Li_2O (%) (0 % H_2O)	Postulated[b] Solids
	UO_3	Li_2O	UO_3	Li_2O		
	0.000	4.49		0.505	4.40	I
IX-33	10.385	2.169	3.47	1.10	13.9	I + II
II-52	8.439	2.616	3.47	1.10	23.4	I + II
II-61	5.204	5.206	3.47	1.10	68.3	I + II
II-48	3.043	0.9440	2.07	0.81	*c*	II + III
II-58	5.564	0.8480	2.07	0.81	*c*	II + III
II-63	5.184	0.5447	0.338	0.325		III

[a]Corrected for residual CO_2 content of sample on the assumption of stoichiometry; see text.
[b]I = Li_2CO_3, II = a lithium uranyl carbonate (possibly with mole ratio Li/U = 2 or less), III = UO_2CO_3.
[c]Not precise enough for accurate extrapolation.

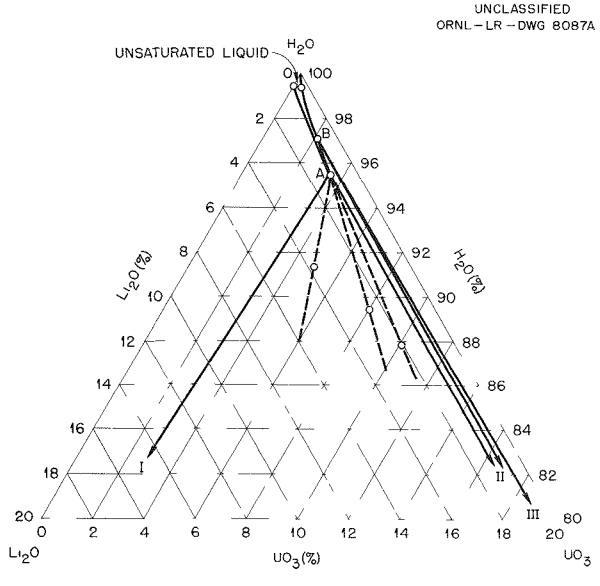

Fig. 19.7. The System Li_2O-UO_3-CO_2-H_2O at 250°C and at 1500 psi Total Pressure, Where $P_{Total} = P_{H_2O} + P_{CO_2}$ (Jänecke Projection). *A* and *B* are invariant points.

perhaps in titanium containers at 250°C. The use of 30% H_2O_2 for stabilization of these systems resulted in the formation of highly colored soluble complexes which do not precipitate as such and which interfere with a study of the four-component system MO-UO_3-CO_2-H_2O alone.

At 250°C there was negligible solubility of uranium in the magnesium system. The uranium solubility in the sodium system was of the order of 1.5 g of uranium per liter, and the Na/U ratio is probably unfavorable from neutron-absorption cross-section considerations. The lithium system seems most feasible at the present time for possible consideration as a fuel solution for an aqueous homogeneous reactor making use of the low-cross-section stable isotope (σ_{abs} = 0.033; 92.5%). Concentrations of uranium as high as 20 to 25 g/liter at a mole ratio of Li/U $\cong$ 6 can be attained at 250°C under 1500 to 2000 psi total pressure of CO_2 and H_2O.

The next objective is to make a rather extensive study of the Li_2O-UO_3-CO_2-H_2O system at high temperature as a function of temperature and CO_2 pressure before proceeding to a further evaluation of the other systems.

19.2 THE BASE-SATURATED REGION OF THE SYSTEM CuO-UO_3-SO_3-H_2O AT 100°C

F. E. Clark R. Slusher
C. H. Secoy

19.2.1 Introduction

Study of the solid-liquid phase equilibria in the four-component system CuO-UO_3-SO_3-H_2O at 100°C in the region in which the liquid is base-saturated was almost completed. Data embracing all but a small uranium-rich region of the phase diagram from total salt concentrations as low as about 4% up to salt concentrations as high as about 25% are presented for this system. Five points in the three-component system CuO-SO_3-H_2O were obtained, each corroborating and verifying the results of Posnjak and Tunell.[12] Observations made on experiments designed to cover the uranium portion of the phase diagram indicate that previous work done at 100°C on the three-component system UO_3-SO_3-H_2O is valid[13] and will be compatible with this four-component phase diagram.

19.2.2 Experimental Methods

Solutions of $CuSO_4 \cdot 5H_2O$ in a range of concentrations from 4% $CuSO_4$ through saturation at room temperature served as vehicles for adding the CuO and SO_3 components in the desired quantities; UO_3 was added, by weight, in the form of specially purified $UO_3 \cdot H_2O$.

The components, in the desired concentration, were sealed into 12-mm pyrex tubes. Approximately 7 ml of solution was found to fill each tube to not more than two-thirds its volume, including the addition of the solid component. Then, after equilibration, 4 to 6½ ml of liquid could be removed for analyses. The wet solids could be weighed readily in the tubes prior to their dissolution and dilution to volume; aliquots were removed for analyses. In those few instances where necessary, the tubes were centrifuged in order to effect a more complete separation of the liquid from the solid phase. The top of the tube was removed after scratching with a file and the liquid sample taken by decantation into a sample bottle, which was quickly stoppered with a rubber stopper. Every effort was made to maintain the temperature of each experiment at 100°C up to the time of opening the tube. Samples were equilibrated in a specially insulated Precision Unitherm constant temperature water bath, with Dow-Corning 550 fluid silicone used as the bath medium. Temperature control was maintained to ±1°C by the use of a Fenwal thermoregulator. Equilibration time varied from a minimum of 86 days for one experiment to 151 days for the majority of the tubes. This equilibration time was found necessary in past experience in this laboratory and by other workers.[12,14,15]

The analyses of the liquid samples were carried out as follows: The SO_3 analyses were made by weighing the sample aliquots in previously calibrated 500-μl pipettes and thus obtaining approximate specific gravity values. The aliquot was then eluted, with water, through Dowex 50 cation-exchange resin in the hydrogen form,[16,17] and the resultant quantitatively exchanged H_2SO_4 was titrated with approximately 0.1 *N* NaOH. This alkali solution had been standardized by titration against U. S. Bureau of Standards potassium acid phthalate to a pH of 8.6.

Cupric oxide was determined according to the short iodide method for copper as given in *Scott's Standard Methods of Chemical Analysis.*[18] The liquid sample was rinsed from the micropipette into a 100-ml beaker, rendered alkaline with NH_4OH, and acidified with glacial acetic acid plus six drops of excess acetic acid; 2 g of solid KI was added, and the liberated iodine was titrated with standardized sodium thiosulfate solution, a starch indicator being used for determining the end point. The sodium thiosulfate solution was standardized by titrating against weighed quantities of copper dissolved in H_2SO_4, and treating as outlined above.

A determination of UO_3 was made by the potentiometric titration method of employing $Ce(HSO_4)_4$

[12] E. Posnjak and G. Tunell, *Am. J. Sci.* 218, 1–34 (1929).

[13] C. H. Secoy *et al.*, *HRP Quar. Prog. Rep. Oct. 31, 1953*, ORNL-1658, p 90.

[14] F. E. Clark and C. H. Secoy, *HRP Quar. Prog. Rep. Oct. 31, 1954*, ORNL-1813, p 168.

[15] S. W. Young and A. E. Stearn, *J. Am. Chem. Soc.* 38, 1947–1953 (1916).

[16] O. Samuelson, *Ion Exchangers in Analytical Chemistry*, Wiley, New York, 1953.

[17] W. L. Marshall *et al.*, *Anal. Chem.* 26, 611 (1954).

[18] W. F. Scott, *Scott's Standard Methods of Chemical Analysis*, 5th ed., I, 371–372, Van Nostrand, New York, 1939.

as the oxidant; this is a modification of the method described by Furman and Schoonover.[19] The uranium-containing solution was made 10 vol % H_2SO_4 and then passed slowly through a Jones reductor; the reductor was thoroughly rinsed with 10% H_2SO_4, to assure quantitative recovery of the uranium, and the reduced solution was then aerated to oxidize trivalent uranium to the tetravalent form. The uranium was then titrated with standard ceric sulfate solution; the end point was detected with a Fisher titrimeter using a gold-platinum electrode system. The ceric sulfate solution was standardized against U. S. Bureau of Standards As_2O_3 and/or weighed portions of specially purified uranium metal.

A special technique was developed to enable both the CuO and UO_3 to be determined in the same weighed aliquot of each sample. The weighed sample was rinsed into a column of Dowex 1 anion-exchange resin in the sulfate form. The CuO was quantitatively eluted from the column with distilled water as $CuSO_4$ into a 100-ml beaker and determined as previously mentioned. The UO_3, which had been quantitatively held in the column, was then quantitatively eluted from the ion-exchange resin with warm (70°C) sulfuric acid and determined by the accepted potentiometric method for uranium.

A special technique was also employed for analyzing the solid phase obtained in experiments 1000, 1006, 1012, 1018, and 1024. In each case the total solid phase, after being separated from the liquid phase and being weighed, was slurried with Dowex 50 cation-exchange resin in the hydrogen form. The solid phase was slowly dissolved, and the free H_2SO_4 was eluted from the resin and titrated with standard NaOH solution. In order to accomplish the elution, it was necessary to transfer the resin quantitatively to a glass column containing several centimeters of clean Dowex 50 resin in the hydrogen form and to continue rinsing until at least four to six resin volumes of water had been used as rinse water. The Cu^{++} was held on the Dowex cation resin; it was then quantitatively eluted from the resin with about six column volumes of 10% H_2SO_4 and determined as previously mentioned for CuO.

In all cases except in experiments 1000, 1006, 1012, 1018, and 1024, the solid phase was weighed in the stoppered tube after decantation of the liquid phase and dissolved in a minimum amount of concentrated HCl. The solution was then diluted to a convenient volume, and pipetted aliquots were removed for the SO_3 determination and for the CuO and UO_3. No difficulties were encountered in separating the CuO from the UO_3 by utilizing the anion-exchange resin, unless the concentration of HCl was in excess of that required initially to dissolve the solid phase. The SO_3 content of the solid phases obtained in the remainder of the experiments in this study was determined by precipitating the SO_3 as $BaSO_4$ according to the conventional gravimetric procedure.

19.2.3 Data and Discussion

The results of the analyses of the saturated liquids and the wet residues are given in terms of weight per cent in Table 19.8. The compositions of the synthetic mixes, known in all cases, are not given, since the linearity of the three points was so good that the third point is superfluous. The synthetic mixes were prepared in five sets, as indicated in the arrangement of the table, each set consisting of variable additions, in increasing amounts, of solid $UO_3 \cdot H_2O$ to a fixed concentration of stoichiometric copper sulfate solution. The nominal concentrations of the starting $CuSO_4$ solutions were 4, 6, 8, 10, and 18% $CuSO_4$, respectively. The first member of each set contained no added $UO_3 \cdot H_2O$ and thus provided not only a starting point for each set in the quaternary system but also gave a value in the ternary system, $CuO\text{-}SO_3\text{-}H_2O$. It is of interest to note, as has already been shown by Posnjak and Tunell,[12] that stoichiometric copper sulfate solutions are not stable at 100°C over the concentration range studied and will yield a precipitate of the basic salt, $3CuO \cdot SO_3 \cdot 2H_2O$.

The nature of the liquid surface in the portion of the quaternary system studied is shown by the projections of Fig. 19.8. The isobaric, isothermal diagram for such a system is perhaps most completely shown in a regular tetrahedron or by various projections of surfaces and lines to the faces of the tetrahedron. In the system under discussion neither the usual orthogonal projection nor the Jänecke projection from the H_2O apex of the tetrahedron is satisfactory, because the surface to be projected is nearly parallel with the direction of

[19] N. H. Furman and I. C. Schoonover, *J. Am. Chem. Soc.* 53, 2561–2571 (1931).

TABLE 19.8. ANALYSES OF SATURATED LIQUID AND WET RESIDUES IN THE SYSTEM CuO-UO_3-SO_3-H_2O EQUILIBRATED AT 100°C

Sample No.	Saturated Liquid				Wet Residue (%)			Solid Phase
	Composition (%)			Specific Gravity (~25°C)				
	CuO	UO_3	SO_3		CuO	UO_3	SO_3	
1000	1.89	0	2.00	1.0374	19.46	0	7.92	$3CuO{\cdot}SO_3{\cdot}2H_2O$
1001	0.90	2.64	1.63	1.0468	25.20	0.95	9.49	$3CuO{\cdot}SO_3{\cdot}2H_2O$
1002	0.40	3.88	1.48	1.0532	19.41	35.82	6.85	Solid solution
1003	0.33	5.01	1.40	1.0627	10.68	49.27	4.01	Binary
1004	0.30	5.02	1.39	1.0621	6.37	52.38	2.61	Binary
1005	0.30	5.10	1.40	1.0626	4.60	57.76	1.49	Binary
1006	2.65	0	2.78	1.0541	28.89	0	11.00	$3CuO{\cdot}SO_3{\cdot}2H_2O$
1007	1.60	2.78	2.39	1.0639	17.41	2.61	7.36	$3CuO{\cdot}SO_3{\cdot}2H_2O$
1008	0.73	5.33	2.05	1.0759	19.39	13.06	7.69	Solid solution
1009	0.40	6.95	1.91	1.0889	14.56	35.05	5.66	Binary
1010	0.40	6.98	1.91	1.0894	8.10	42.78	3.49	Binary
1011	0.40	7.06	1.91	1.0892	6.76	51.83	2.86	Binary
1012	3.44	0	3.60	1.0708	41.14	0	15.81	$3CuO{\cdot}SO_3{\cdot}2H_2O$
1013	2.40	2.65	3.21	1.0800	23.66	3.23	9.60	$3CuO{\cdot}SO_3{\cdot}2H_2O$
1014	1.18	5.96	2.74	1.0968	25.05	3.90	10.28	$3CuO{\cdot}SO_3{\cdot}2H_2O$
1015	0.60	8.47	2.51	1.1122	21.80	31.85	8.33	Solid solution
1016	0.50	9.01	2.45	1.1185	12.36	40.90	5.14	Binary
1017	0.51	9.19	2.46	1.1195	9.67	51.98	4.02	Binary
1018	4.18	0	4.37	1.0877	32.77	0	12.63	$3CuO{\cdot}SO_3{\cdot}2H_2O$
1019	3.19	2.54	3.99	1.0983	17.55	2.76	8.04	$3CuO{\cdot}SO_3{\cdot}2H_2O$
1020	1.85	6.02	3.48	1.1128	16.25	3.72	7.91	$3CuO{\cdot}SO_3{\cdot}2H_2O$
1021	0.91	9.08	3.08	1.1316	23.24	24.44	9.26	Solid solution
1022	0.60	11.07	2.93	1.1478	19.80	39.72	7.61	Binary
1023	0.60	11.00	2.92	1.1478	12.55	49.12	5.18	Binary
1024	8.77	0	9.02	1.2019	27.72	0	10.77	$3CuO{\cdot}SO_3{\cdot}2H_2O$
1025	8.47	0.66	8.88	1.2044	34.59	0.38	13.64	$3CuO{\cdot}SO_3{\cdot}2H_2O$
1026	8.14	1.35	8.77	1.2070	51.67	0.33	21.67	$3CuO{\cdot}SO_3{\cdot}2H_2O$
1027	7.75	2.44	8.59	1.2117	29.76	1.33	12.83	$3CuO{\cdot}SO_3{\cdot}2H_2O$
1028	5.93	5.74	7.99	1.2245	26.32	3.59	12.28	$3CuO{\cdot}SO_3{\cdot}2H_2O$
1029	4.07	11.19	7.06	1.2476	31.33	5.99	13.70	$3CuO{\cdot}SO_3{\cdot}2H_2O$
1030	2.43	16.18	6.30	1.2807	31.30	8.86	13.68	$3CuO{\cdot}SO_3{\cdot}2H_2O$
1031	0.94	18.00	4.65	1.2644	15.17	41.49	9.40	Probably ternary

projection. Therefore, in Fig. 19.8, projection parallel to an edge of the tetrahedron, sometimes called the Schreinemakers projection, was employed. The data were then plotted with orthogonal coordinates rather than with trilinear ones. Weight per cents are read directly from the scales of the graph and the per cent H_2O at any pair of points (one in the UO_3-CuO projection and a corresponding point in the UO_3-SO_3 projection) may be readily obtained by subtracting the sum, UO_3 + CuO + SO_3, from 100.

The constant-SO_3 contour lines shown on the UO_3-CuO portion of the diagram were obtained by graphical interpolation in the following manner.

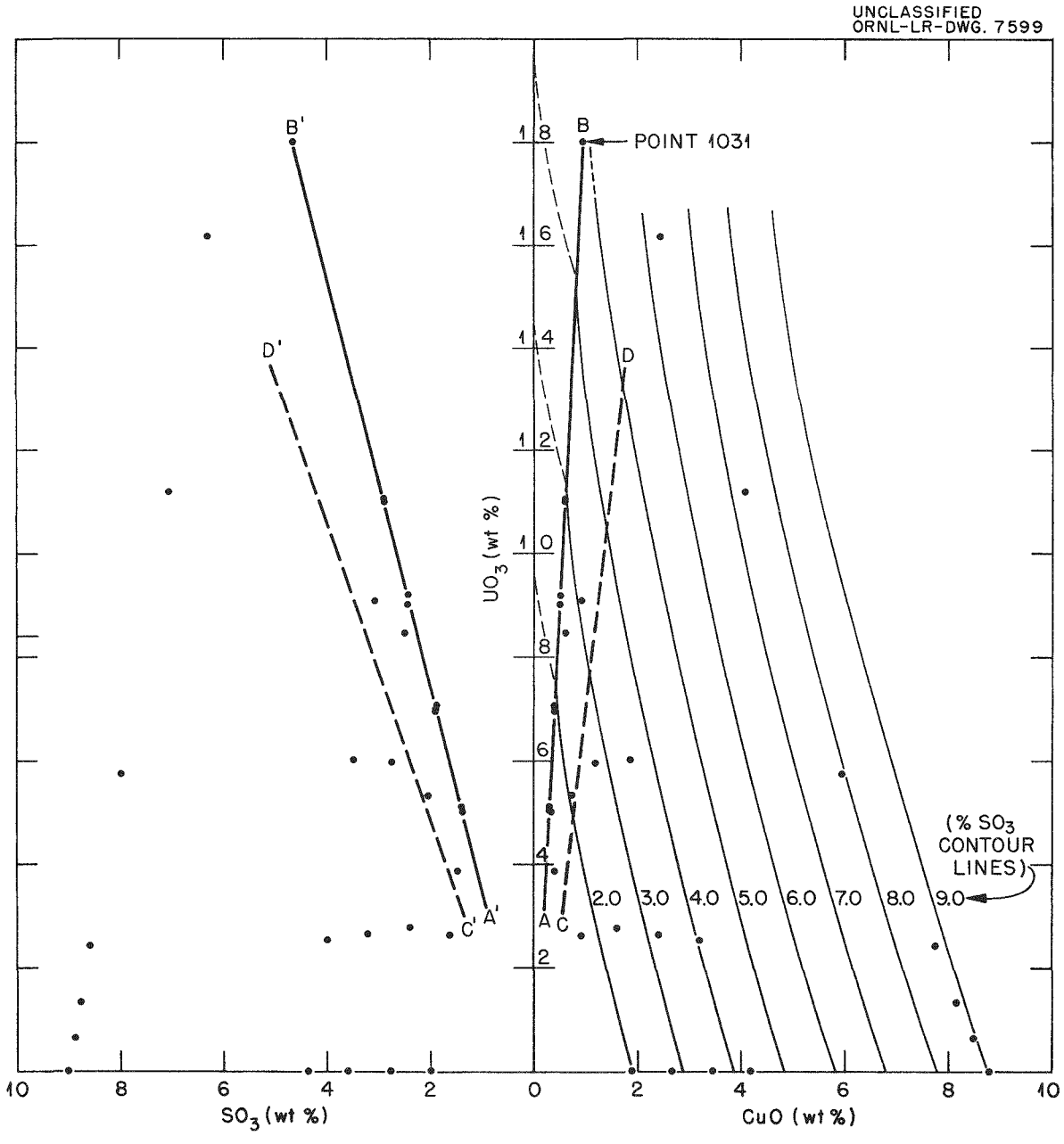

Fig. 19.8. Liquidus Surface in the System CuO-UO_3-SO_3-H_2O at 100°C.

Each set of data follows a smooth but arbitrary path across the liquid surface. For each set a smooth curve was drawn through the points obtained by plotting the per cent SO_3 against the UO_3 fraction of CuO + UO_3. Values for the per cent SO_3 at a constant UO_3 fraction read from these curves were found to give straight lines when plotted against the per cent total salt. This is equivalent to saying that the liquid surface has no curvature if a path of constant $UO_3/(CuO + UO_3)$ ratio is followed. Values of this ratio and of the per cent total salt at constant per cent SO_3 could therefore be obtained from the graphs and the per cent of each component readily calculated.

The identities of the solids were established by a study of projections of the tie lines. Tie lines for the first two or three points of each set and for all but the last point of the most concentrated set project close to the theoretical composition of the mineral, antlerite, $3CuO \cdot SO_3 \cdot 2H_2O$. Microscopic examination of these solids agreed with Posnjak and Tunell's description. Therefore the conclusion was reached that this compound is the stable solid phase in equilibrium with solutions over a major portion of the liquid surface. This conclusion should and will be verified or disproved by obtaining the x-ray diffraction pattern for the solids.

The fact was noted that the CuO-to-SO_3 mole ratio was nearly constant and was approximately 3 in all the wet residues except the residue from tube 1031. This suggested immediately that the remaining solids were either a mixture of antlerite and $UO_3 \cdot H_2O$ (known to be the stable solid phase along the UO_3-SO_3-H_2O side of the diagram) or a series of solid solutions whose compositions could be represented by a combination of varying amounts of these two compounds. It was also noted that the composition of the liquid phase in the last two or three points of each set except the fifth was essentially constant in spite of the fact that the synthetic mix varied markedly. Furthermore, these liquid points lie on a smooth curve, line *AB* in Fig. 19.8. This strongly suggests that the solid is a binary mixture. In order to prove that this is the case, the algebraic equation for each tie line was solved simultaneously with the algebraic equation for the line connecting the two compounds, antlerite and $UO_3 \cdot H_2O$. The calculated intersection points are given in Table 19.9, and the projections of these points are shown in Fig. 19.9. Obviously the compositions of all solids except the solid from tube 1031 can be accurately represented by combinations of antlerite and $UO_3 \cdot H_2O$.

Four of the liquid points falling in the region between lines *CD* (position not known accurately) and *AB* in Fig. 19.8 also gave solid compositions falling on the antlerite–$UO_3 \cdot H_2O$ line. These liquid points are scattered over an area and could not lie on any sensible continuous curve. The solid therefore must consist of a single phase, and the only reasonable interpretation is that it is a solid solution. The limit of solubility appears to be about 1.5 moles of $UO_3 \cdot H_2O$ to 1 mole of antlerite. Any $UO_3 \cdot H_2O$ in excess of this amount appears as a second solid phase, and the liquid points then fall on the binary line, *AB*. These conclusions must be checked by x-ray studies before they can be accepted without question.

Point 1031 does not follow the pattern established by the last points of each of the four more dilute sets in either the liquid phase or the solid. Microscopic examination of the solid indicated the probable presence of three solid phases. The liquid point 1031 probably represents a ternary in the system and therefore should lie at the intersection of three binary lines, one of which is the line *AB*. Visual observation of tubes containing compositions in this vicinity and now in the process of equilibration appears to support this interpretation. The third solid phase in the ternary may well be the basic uranyl sulfate, $5UO_3 \cdot 2SO_3 \cdot XH_2O$, previously found to exist at the higher concentrations in the three-component system, UO_3-SO_3-H_2O.[13]

Additional compositions, now in the process of equilibration, are designed to give information at lower concentrations (2% $CuSO_4$); in the $UO_3 \cdot H_2O$ region between the binary *AB* and the UO_3 axis in Fig. 19.8; concerning the exact position of the line *CD*; and at higher concentrations, particularly in the region beyond the point *B*.

19.3 PHASE VOLUMES IN THE TWO-LIQUID-PHASE REGION OF THE SYSTEM UO_3-SO_3-H_2O

D. W. Sherwood
G. M. Hebert
S. F. Clark[20]
C. H. Secoy

Measurement of the volumes of the liquid and vapor phases of uranyl sulfate solutions sealed in

[20] University of Mississippi.

TABLE 19.9. INTERSECTION POINTS OF EXTRAPOLATED TIE LINES WITH THE LINE REPRESENTING MIXTURES OF $UO_3 \cdot H_2O$ AND $3CuO \cdot SO_3 \cdot 2H_2O$

Sample No.	Composition (%)				Solid Phase
	CuO	UO_3	SO_3	H_2O	
$3CuO \cdot SO_3 \cdot 2H_2O$	67.27	0	22.57	10.16	Theoretical composition
1000	66.23	0	23.67	10.10	$3CuO \cdot SO_3 \cdot 2H_2O$
1001	68.37	−2.05	23.45	10.23	$3CuO \cdot SO_3 \cdot 2H_2O$
1006	66.94	0	22.92	10.14	$3CuO \cdot SO_3 \cdot 2H_2O$
1007	65.41	2.09	22.46	10.14	$3CuO \cdot SO_3 \cdot 2H_2O$
1012	66.04	0	23.88	10.08	$3CuO \cdot SO_3 \cdot 2H_2O$
1013	63.99	4.33	21.73	9.95	$3CuO \cdot SO_3 \cdot 2H_2O$
1014	66.26	0.34	23.30	10.10	$3CuO \cdot SO_3 \cdot 2H_2O$
1018	67.25	0	22.59	10.16	$3CuO \cdot SO_3 \cdot 2H_2O$
1019	67.10	−1.30	24.05	10.15	$3CuO \cdot SO_3 \cdot 2H_2O$
1020	70.07	−0.488	24.47	10.34	$3CuO \cdot SO_3 \cdot 2H_2O$
1024	74.33	0	15.06	10.61	$3CuO \cdot SO_3 \cdot 2H_2O$
1025	69.66	0.41	19.62	10.31	$3CuO \cdot SO_3 \cdot 2H_2O$
1026	64.51	0.29	25.21	9.99	$3CuO \cdot SO_3 \cdot 2H_2O$
1027	69.82	−0.69	20.55	10.32	$3CuO \cdot SO_3 \cdot 2H_2O$
1028	68.38	0.26	21.13	10.23	$3CuO \cdot SO_3 \cdot 2H_2O$
1029	68.15	−1.03	22.66	10.22	$3CuO \cdot SO_3 \cdot 2H_2O$
1030	67.23	−0.25	22.86	10.16	$3CuO \cdot SO_3 \cdot 2H_2O$
1008	49.01	25.33	16.65	9.01	$(3CuO \cdot SO_3 \cdot 2H_2O) \cdot 0.43(UO_3 \cdot H_2O)$
1021	40.83	36.54	14.04	8.49	$(3CuO \cdot SO_3 \cdot 2H_2O) \cdot 0.75(UO_3 \cdot H_2O)$
1015	34.39	45.73	11.79	8.09	$(3CuO \cdot SO_3 \cdot 2H_2O) \cdot 1.11(UO_3 \cdot H_2O)$
1002	29.58	52.92	9.72	7.78	$(3CuO \cdot SO_3 \cdot 2H_2O) \cdot 1.49(UO_3 \cdot H_2O)$
1022	28.98	53.42	9.85	7.75	Binary: solid solution* + $0.04(UO_3 \cdot H_2O)$
1009	26.00	57.75	8.69	7.56	Binary: solid solution* + $0.35(UO_3 \cdot H_2O)$
1016	21.13	64.48	7.13	7.26	Binary: solid solution* + $1.05(UO_3 \cdot H_2O)$
1023	18.50	68.10	6.31	7.09	Binary: solid solution* + $1.57(UO_3 \cdot H_2O)$
1003	15.95	71.79	5.33	6.93	Binary: solid solution* + $2.25(UO_3 \cdot H_2O)$
1010	14.72	73.58	4.85	6.85	Binary: solid solution* + $2.67(UO_3 \cdot H_2O)$
1017	14.38	73.98	4.82	6.82	Binary: solid solution* + $2.79(UO_3 \cdot H_2O)$
1011	10.66	79.30	3.45	6.59	Binary: solid solution* + $4.71(UO_3 \cdot H_2O)$
1004	9.93	80.19	3.33	6.55	Binary: solid solution* + $5.24(UO_3 \cdot H_2O)$
1005	6.79	84.64	2.22	6.35	Binary: solid solution* + $8.90(UO_3 \cdot H_2O)$
$UO_3 \cdot H_2O$	0	94.08	0	5.92	Theoretical composition
1031	24.05	56.15	12.36	7.44	Probably ternary

*Solid solution = $3CuO \cdot SO_3 \cdot 2H_2O \cdot 1.5(UO_3 \cdot H_2O)$.

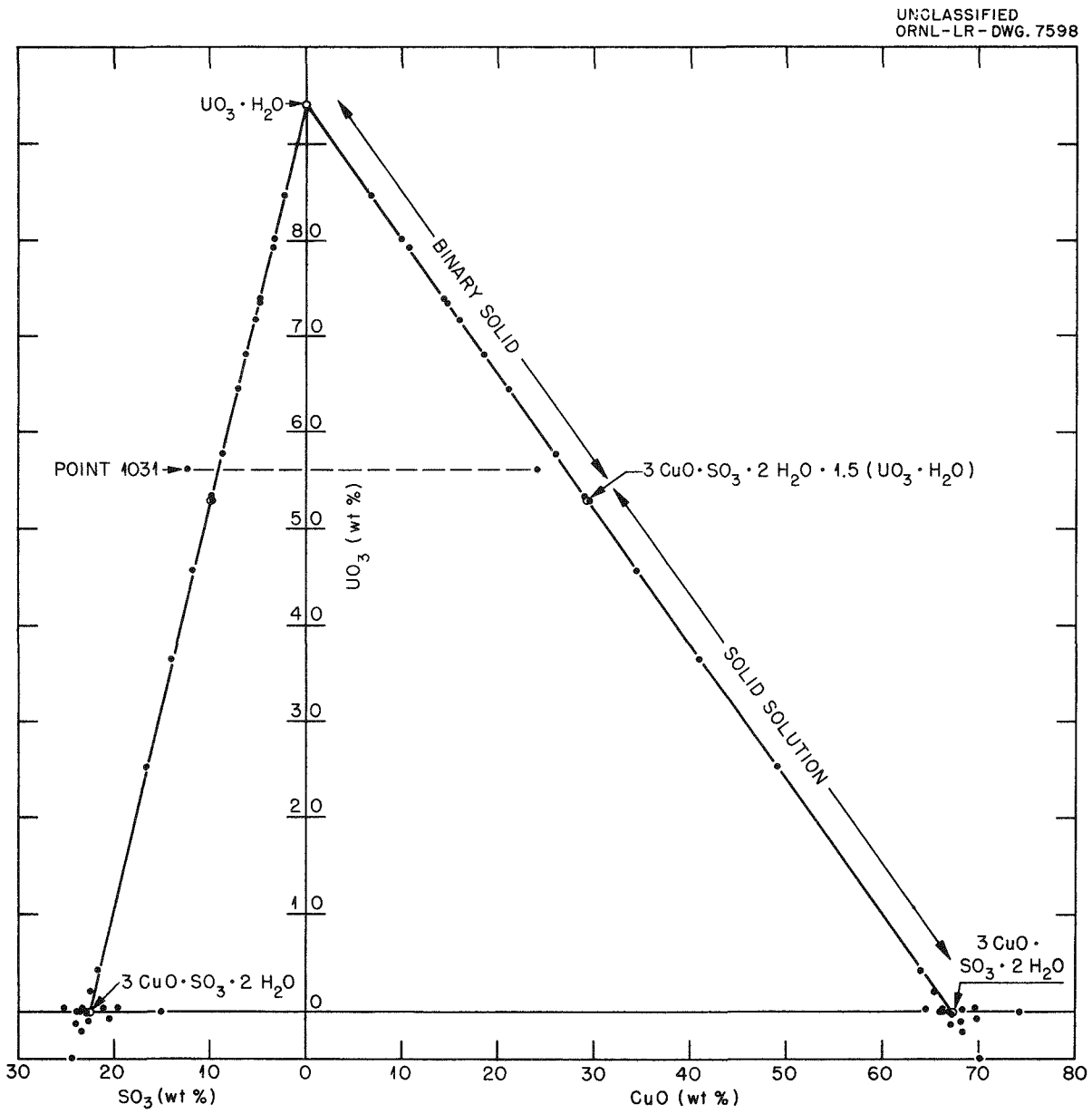

Fig. 19.9. Projection of the Intersection Points of the Extrapolated Tie Lines with the Line Connecting the Compositions $3CuO \cdot SO_3 \cdot 2H_2O$ and $UO_3 \cdot H_2O$.

quartz tubes continued.[21] Data are now available for 0.25, 0.50, 1.00, 2.00, and 3.00 *m* stoichiometric solutions over the temperature range 25 to 400°C. A sufficient number of fractional fillings (25°C) were employed for each concentration so that accurate interpolated volumes might be calculated for any fractional filling within the range of from about 0.25 to about 0.60.

Figures 19.10, 19.11, 19.12, and 19.13, in which the volume fraction of the total liquid and of the salt-rich liquid, respectively, is plotted against the temperature, illustrate the phenomena observed.

[21] D. W. Sherwood and G. M. Hebert, *HRP Quar. Prog. Rep. April 30, 1955*, ORNL-1605, p 149.

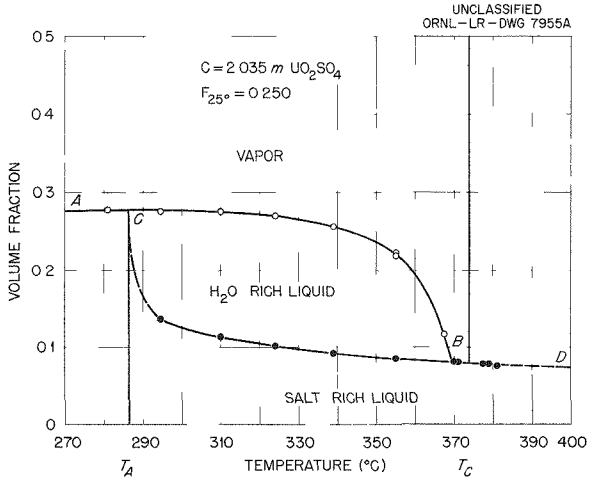

Fig. 19.10. Phase Volumes with High Concentration and Low Filling.

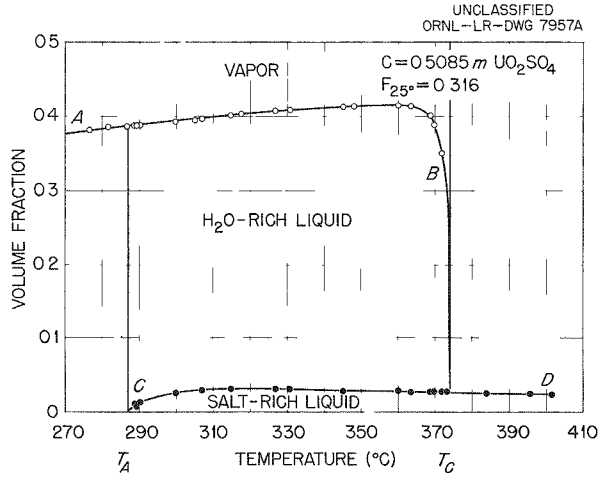

Fig. 19.12. Phase Volumes with Low Concentration and Low Filling.

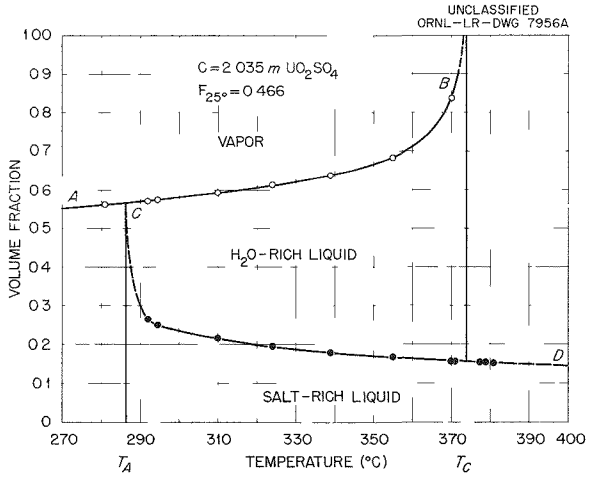

Fig. 19.11. Phase Volumes with High Concentration and High Filling.

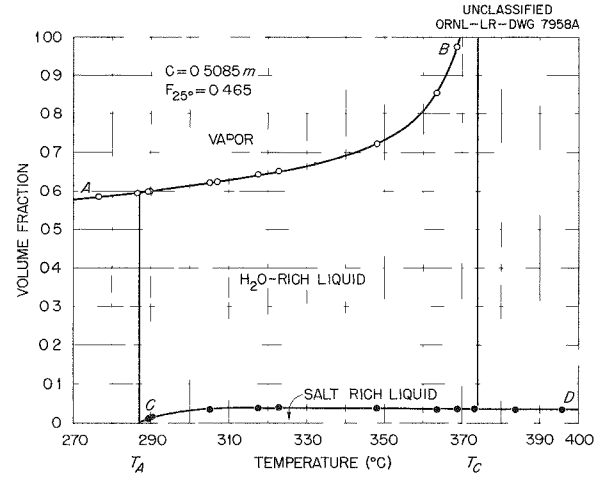

Fig. 19.13. Phase Volumes with Low Concentration and High Filling.

In each figure the total liquid volume curve is labeled *AB*, and the salt-rich liquid volume curve is labeled *CD*. The volume of the H_2O-rich liquid phase at any temperature is given by the difference between the curves at that temperature. The shape of the volume curves depends on two factors. First, the concentration of the solution determines the manner of appearance of the second liquid phase at the minimum critical temperature. Solutions more dilute than the consolute concentration (estimated to be 1.3 ± 0.2 *m*) yield the salt-rich phase as the new phase (Figs. 19.12 and 19.13), while more concentrated solutions yield the water-rich phase (Figs. 19.10 and 19.11). In the first case the volume of the salt-rich phase increases from zero to a maximum and then decreases very slightly with increasing temperature. In the second case the volume of the salt-rich phase is initially equal to the total liquid volume and drops very sharply at first as the new water-rich phase makes its appearance. It then decreases very slowly with rising temperature.

The second determining factor is the fractional filling of the tube. This determines the behavior of the volume of the water-rich phase as the liquid-vapor critical temperature is approached. If the fractional filling is greater than a critical value, the meniscus moves through the top of the tube before the critical temperature is reached (Figs. 19.11 and 19.13); if less than the critical value, the meniscus vanishes downward into the salt-rich liquid (Figs. 19.10 and 19.12)

Apparatus for the measurement of the system pressure as a function of solution composition, temperature, and fractional filling has just been received from the manufacturer. Although no serious difficulties are foreseen, the apparatus, being the first of its kind, will require considerable debugging and calibration before useful data can be obtained.

19.4 COLLOIDAL THORIUM OXIDE AS A REACTOR BLANKET

F. H. Sweeton

The possibility of using a sol of ThO_2 as a breeder blanket has been considered previously, but a few experiments failed to show stability of such sols at the elevated temperatures required by a homogeneous reactor system.[22-24] Because of the special advantages to be obtained from the use of sols, plans are being made to re-examine the system in more detail to see whether conditions can be found under which a sol is satisfactorily stable at elevated temperatures.

The potential advantages of a sol are due in part to the ThO_2 particles being small and in part to their being completely dispersed. Since the particles are small, they can be expected neither to settle out in stagnant regions of the blanket system nor to cause erosion when pumped around the system. Since the particles are dispersed, the viscosity of a sol is very low. If a sol can be found that is feasible for use as a reactor blanket, it would then be of interest to see whether a double sol of ThO_2 and UO_3 could also be found that is feasible for use in a single-region homogeneous breeding reactor. To be feasible for a reactor blanket, a sol must be stable to flocculation. This stability of a sol depends on many factors, some being based on the properties of the solid particles and the others on the properties of the solution.

One important aspect of the solid is the electrical potential built up on the surface by loss of ions to the solution and by adsorption of ions from the solution. The size of the particles is also important, as increasing the size tends to increase the mutual repulsion between neighboring particles (however, above a certain limit in size the particles, of course, tend to settle). The shape of the particles can also be expected to influence the repulsion.

The effect of the solution on the stability is in part tied up with the solid and in part independent of it. The nature and concentration of ions in the solution help to determine the surface potential of the particles. In addition, the ions in solution have an independent effect on the stability in that they tend to shield adjacent particles from the full effect of their surface potentials on each other, thus decreasing the stability. The ions of opposite sign to the charge on the particle surface are of primary importance in this respect, and their effectiveness increases greatly with valence.

The experimental work in studying the thorium oxide colloid system will be directed to finding the conditions that give greatest stability and thus showing whether or not this kind of blanket system is practical. The first work planned is the measurement of the flocculation temperature of ThO_2 sols as a function of the concentration of $Th(NO_3)_4$ used as peptizing agent.

19.5 ADSORPTION OF WATER BY ThO_2

D. M. Richardson

The adsorption of water on one sample of de-aerated ThO_2 has been measured by observing the pressure of water vapor at a series of temperatures after filling a bomb with the ThO_2 sample and a known amount of water. The pressures were measured by the method described earlier,[25] in which a single 0.005-in.-thick diaphragm with several annular corrugations was used. Observations were reproducible within 1 psi.

[22] A. S. Kitzes *et al.*, *HRP Quar. Prog. Rep. July 31, 1953*, ORNL-1605, p 149.

[23] A. S. Kitzes, *Peptized $Th(OH)_4$ Slurries*, ORNL CF-55-5-202 (May 6, 1955).

[24] K. A. Kraus *et al.*, *HRP Quar. Prog. Rep. April 30, 1955*, ORNL-1895, p 199.

[25] D. M. Richardson, *HRP Quar. Prog. Rep. April 30, 1955*, ORNL-1895, p 195–196.

The measurements were started at the lowest unsaturated steam temperature and continued at successively higher temperatures. At 360°C a slow rise in pressure occurred. Following this, the pressures measured at the lower temperatures were greater and had increased by greater amounts than the pressure rise observed at 360°C. Since the calculated mole fraction of adsorbed water decreased by approximately the same fraction at the several temperatures, the change occurring at 360°C would appear to be due to a decrease in the surface area of the thorium oxide. Several more samples will be studied in order that isotherms and isobars may be constructed.

20. ADSORPTION ON INORGANIC MATERIALS

K. A. Kraus

T. A. Carlson J. S. Johnson
D. J. Coombe H. O. Phillips

Study of adsorptive properties of inorganic materials for ions in aqueous solutions was continued. In the last progress report[1] it was pointed out that hydroxides of Zr(IV), Th(IV), Fe(III), and Cr(III), which are precipitated by bases, exhibited anion-exchange properties and that Zr(IV) hydroxide changed to a cation exchanger in the presence of 0.1 *M* NaOH, presumably because of amphoterism of the solid. Precipitates of W(VI) and Mo(VI), which are brought down by acids, adsorbed cations. Mixed precipitates of Zr(IV) and W(VI) and precipitates of zirconium thrown down by phosphate, or columns of zirconium hydroxide treated with solutions of tungstate or phosphate, also took up cations.

The greater part of the work during the last quarter can be conveniently grouped under three headings: characterization of the materials in terms of usual ion-exchange properties, such as determination of affinity for different ions in various media, capacities, reversibility of adsorption, stability in different chemical media, and effect of different conditions of preparation; study of how far properties of these materials can be described in terms of "ideal" ion-exchange behavior, that is, equivalence of exchange and adherence of distribution between phases to mass-action expressions written in terms of concentration rather than activities (organic ion exchangers frequently do not obey such restrictions); and demonstration of separations which appear to be feasible. Attention was centered on zirconium tungstate, zirconium phosphate, and zirconium hydroxide, although it should be remembered that these materials are but single examples of classes.[1] It should be emphasized that these materials are not necessarily stoichiometric compounds. Affinities are expressed in terms of the distribution coefficient, *D*, defined as the ratio of the amount of material adsorbed per kilogram of adsorber to the amount per liter of solution.

[1] K. A. Kraus *et al.*, *HRP Quar. Prog. Rep. April 30, 1955*, ORNL-1895, p 197–198.

20.1 CHARACTERIZATION OF MATERIALS

The general outline of properties of these materials given in the last progress report[1] was confirmed, and they were studied in more detail. A few observations of somewhat different aspects will be outlined here.

If adsorption of negative metal complexes on inorganic anion exchangers occurs, opportunities for the versatile separations achieved with organic exchangers would be indicated. Such adsorption on zirconium hydroxide was successfully demonstrated for Hg(II) from 0.1 *M* HCl; elution was readily effected by changing the acidity of the external solution to 0.01 *M*. However, Zn(II) was not taken up from solutions from which adsorption might have been expected (2 *M* chloride), and further study is necessary before the extent of possible applications analogous to organic exchangers is known.

The effect of conditions of preparation on adsorption was investigated for zirconium tungstate. Preparation was carried out by mixing a solution of $ZrOCl_2$ with a solution of Na_2WO_4 brought to a desired pH by addition of HCl. The effect of pH was investigated by comparing *D*'s of Ce(III) in 0.1 *M* HCl as a function of the pH of the solution after precipitation had occurred. The value of *D* was 10 for a final pH of 8 and rose to about 3000 for a pH of 1. It then declined sharply with further increase in acidity – to about 5 at an acidity of about 0.7 *M*. The ratio of moles zirconium to moles tungstate in the solutions which were mixed for precipitation also affected the adsorptive properties. A distribution coefficient of about 3000 for Ce(III) in 0.1 *M* HCl was observed for a ratio of 1 to 5, while for a 2 to 5 ratio the *D* was only 90. A 5 to 1 ratio gave a precipitate adsorbing anions only. Analysis showed that the mole ratio of Zr/W in the precipitate from solutions of ratio 1 to 5 was approximately 1 to 2. Preparations made under the conditions indicated here for maximum adsorption had properties reproducible to about 25%.

A slow change of *D* with time, which has been observed in strongly acidic solutions, indicates

that zirconium hydroxide, phosphate, and tungstate are all attacked by acid. For example, 1.7 hr after a solution of Ce(III) tracer in 0.2 *M* HCl was brought into contact with zirconium tungstate, the measured *D* was 225; after 72 hr, *D* had dropped to 90. In contrast, from 0.5 *M* KCl, *D* was 33 after 0.3 hr and 34 after 96 hr. In some cases an increase in *D*, rather than a decrease, was observed in acid solutions.

20.2 IDEALITY OF EXCHANGE

The question of whether or not exchange is ideal is obviously of interest. The occurrence of ideal exchange gives information about the nature of the exchanger, and, in the range of conditions where it is found, a few measurements suffice for selection of proper conditions for practical separations. One test of ideality can be made by measuring *D* for a tracer ion as a function of the concentration of another ion at macro concentration. If the macro ion has a charge of 1, ideal exchange will be indicated by a straight line for a plot of log *D* (tracer) vs the logarithim of concentration of the macro ion in the solution phase. The slope of the plot should be the charge on the tracer. Tests of this relation were made on all the exchangers discussed here; behavior approached ideality under most conditions for which acid attack on the exchangers was not great. Some examples are given in the figures. Figure 20.1 shows the exchange of tracer Br^- in KNO_3 on zirconium hydroxide. In the two experiments at lowest concentration of KNO_3, which are particularly sensitive to error in this concentration variable, the final KNO_3 concentration was established by conductivity measurements. The points are seen to fall on a straight line of slope close to unity. Figure 20.2 shows the exchange of tracer Ce(III) with HCl on zirconium phosphate, and Fig. 20.3, the exchange of tracer cesium with NH_4Cl on zirconium tungstate. Two sets of points taken at different times of equilibration are given in Fig. 20.2, since there was evidence of some attack on the exchanger with acid. In both cases, however, behavior appeared to approach ideality closely under these conditions.

At macro concentrations of both ions, mass-action equations may not hold. For example, in a study of the effect of loading on *D* for cesium exchanging with sodium on zirconium tungstate, the value of *D* obtained when the exchanger was 50% in the cesium form was only about 20% of the *D* predicted on the basis of tracer experiments.

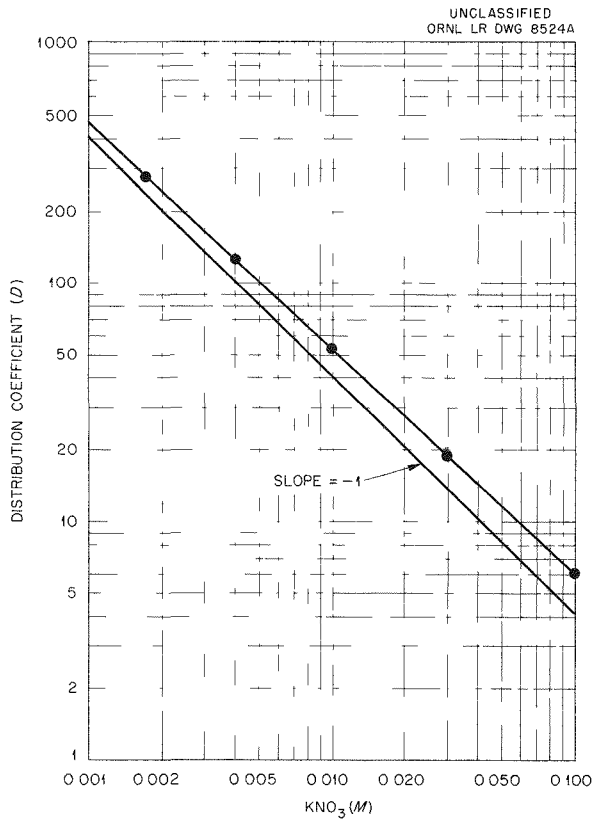

Fig. 20.1. Bromide–Nitrate Exchange on Zirconium Hydroxide (Drying Temperature 200°C).

20.3 SEPARATIONS

Differences of *D* for ions on zirconium tungstate and zirconium phosphate indicate that separations should be feasible. Separations of tracers have been demonstrated so far for rubidium and cesium on both tungstate (Fig. 20.4) and phosphate, for sodium and potassium on tungstate (Fig. 20.5), for Co(II) and Fe(III) on both phosphate (Fig. 20.6) and tungstate, and for sodium tracer from macro lithium on phosphate. These separations are on approximately 6-cm columns.

Conditions for some of these separations are given in the figures. Of the others, rubidium and cesium were put on a zirconium phosphate column in 0.5 *M* HCl; the rubidium was eluted with 3 *M* HCl, and the cesium with saturated KCl. About 0.01 meq of LiCl and tracer sodium in water were put on a zirconium phosphate column; the lithium came through immediately, and the sodium was eluted with 0.04 *M* HCl. Cobalt(II) and Fe(III) were put on a zirconium tungstate column in 0.1 *M*

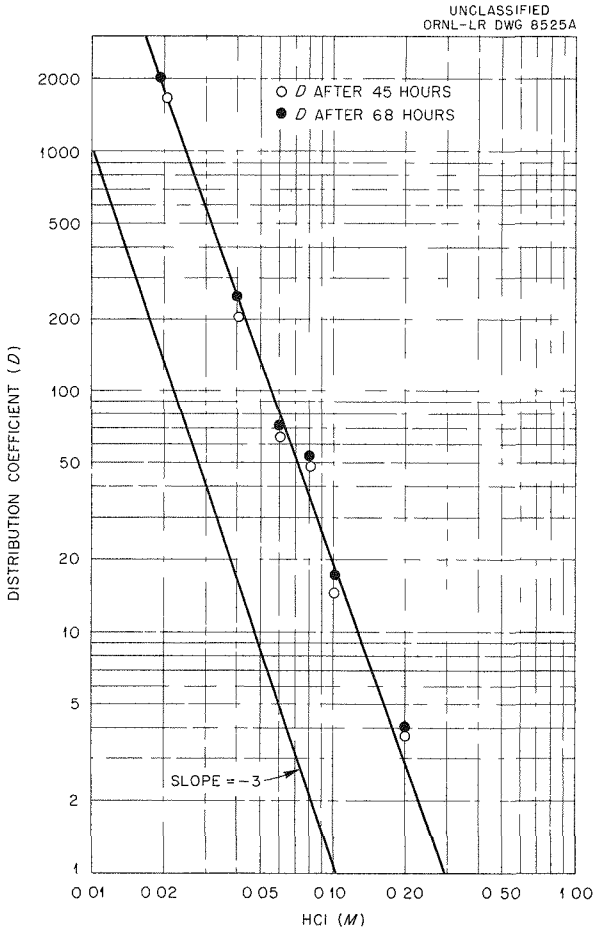

Fig. 20.2. Cerous–Hydrogen Ion Exchange on Zirconium Phosphate (Drying Temperature 78°C).

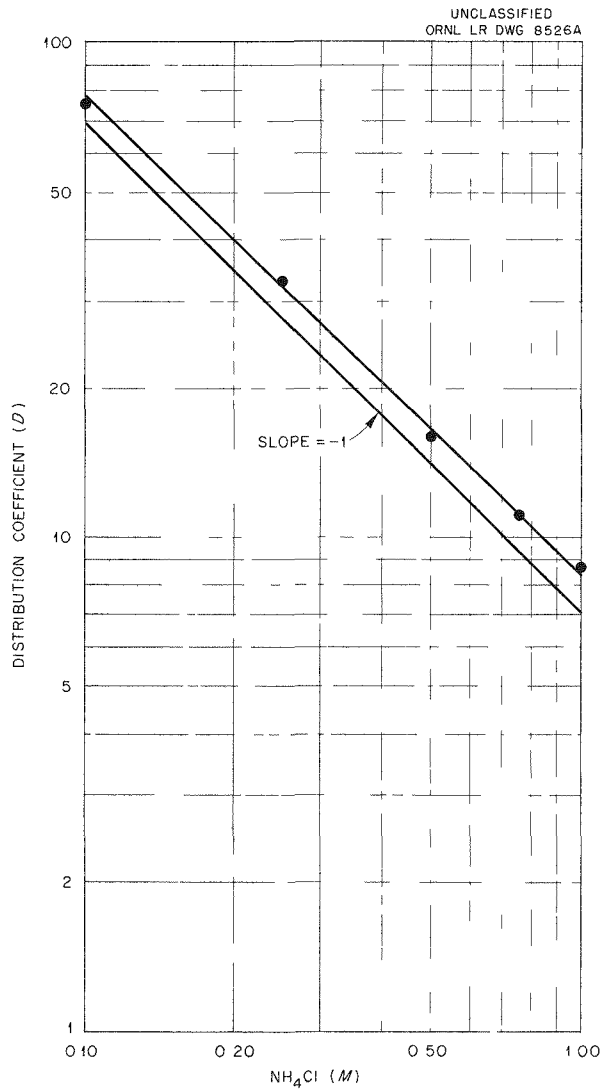

Fig. 20.3. Cesium–Ammonium Exchange on Zirconium Tungstate.

HNO_3; cobalt was eluted with 0.05 *M* HNO_3–0.5 *M* KNO_3, and iron was eluted with 8 *M* LiCl.

The shape of elution peaks indicated that no major trouble was encountered from slowness of reversibility of exchange. However, some caution is necessary; cesium adsorbed from a solution left in contact with zirconium phosphate overnight could be desorbed only with difficulty.

A separation of macro amounts (about 0.1 meq total) of terbium and cesium was effected on a column containing 1 g of zirconium tungstate by elution with NH_4Cl. The edges of the elution peaks overlapped slightly; however, on a column of this size, such an overlap was not surprising.

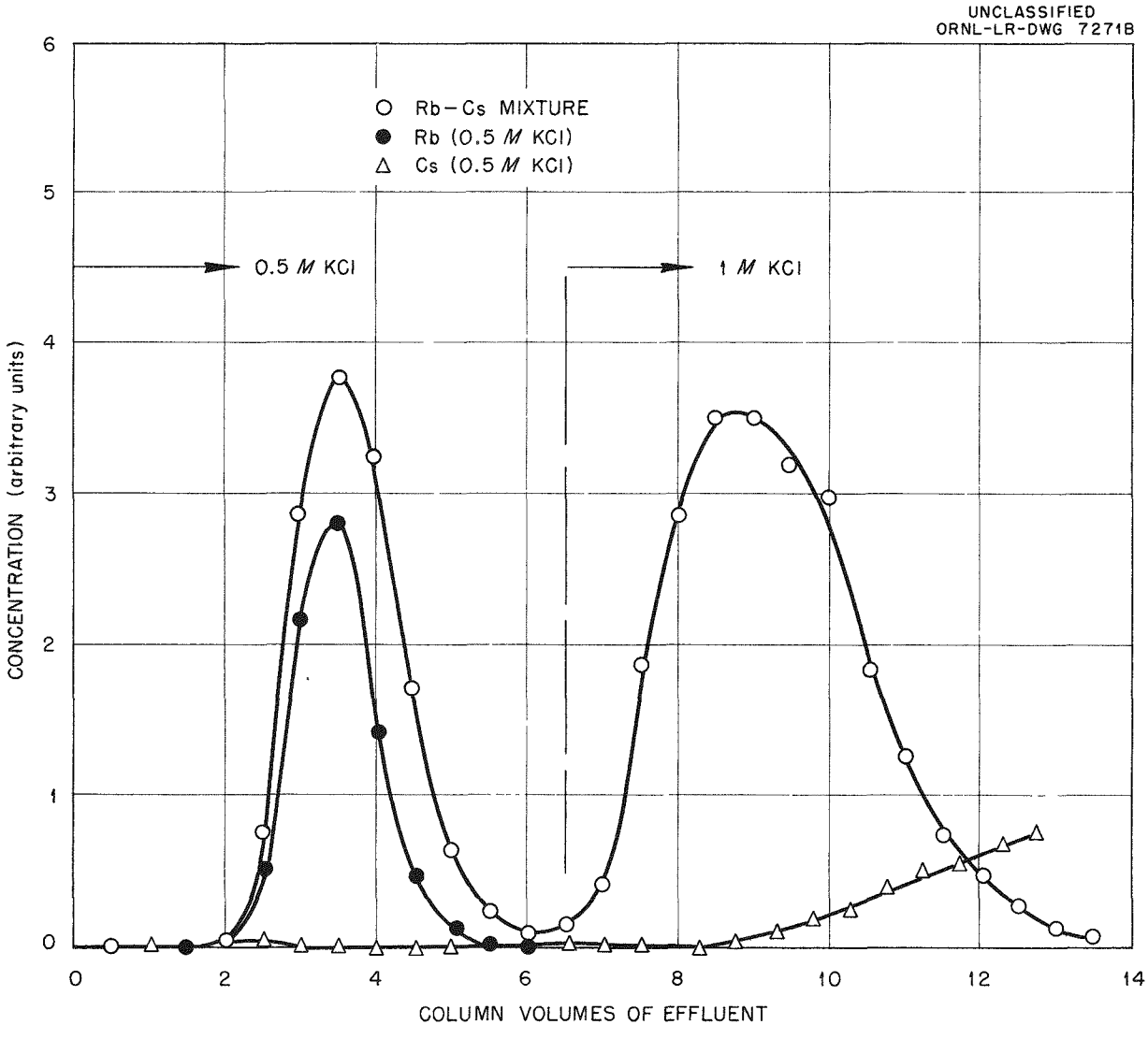

Fig. 20.4. Separation of Rubidium and Cesium on Zirconium Tungstate (Drying Temperature 25°C). Column 6.0 cm × 0.09 cm^2.

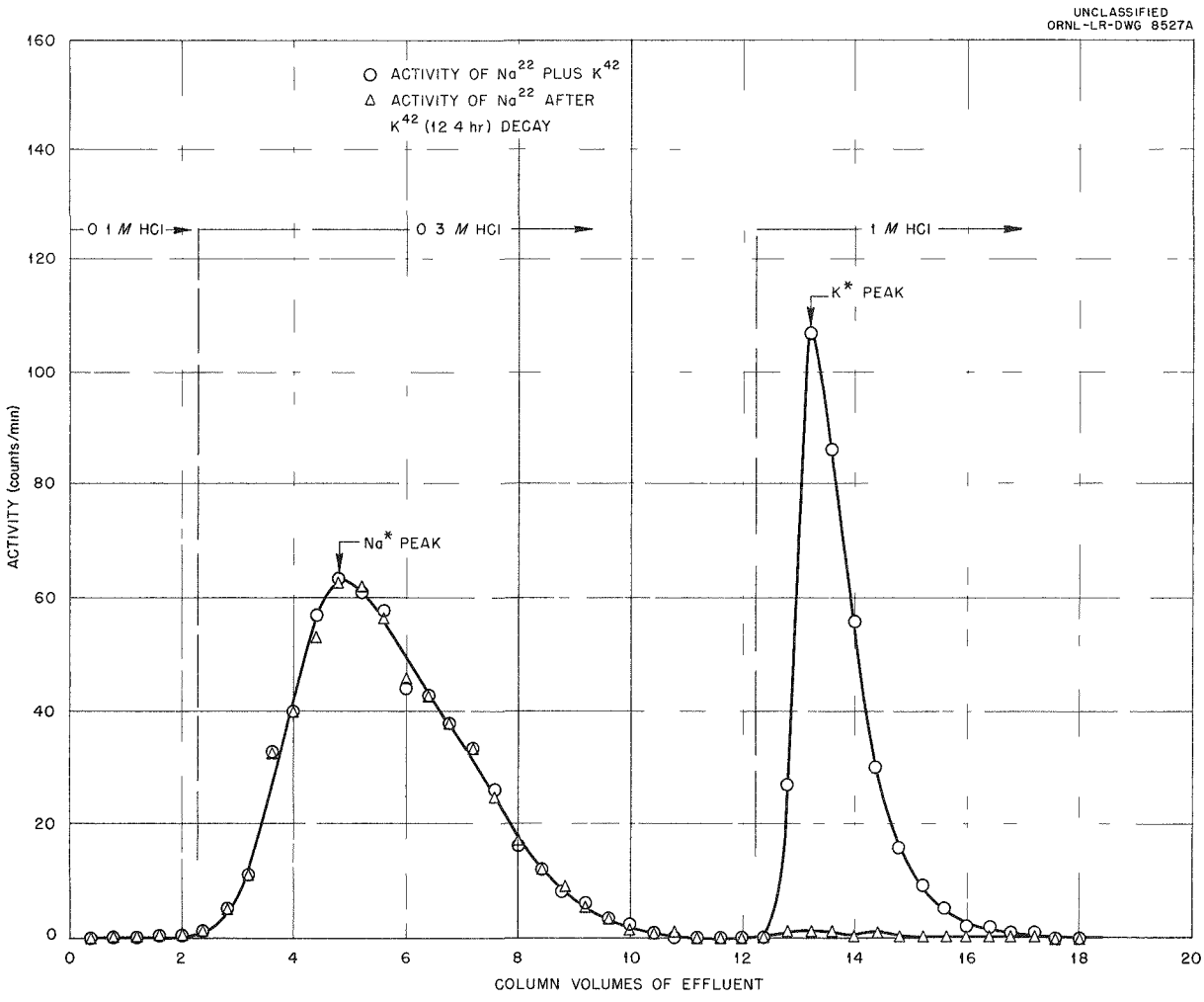

Fig. 20.5. Separation of Sodium and Potassium on Zirconium Tungstate (Drying Temperature 25°C). Column 5.0 cm × 0.2 cm^2.

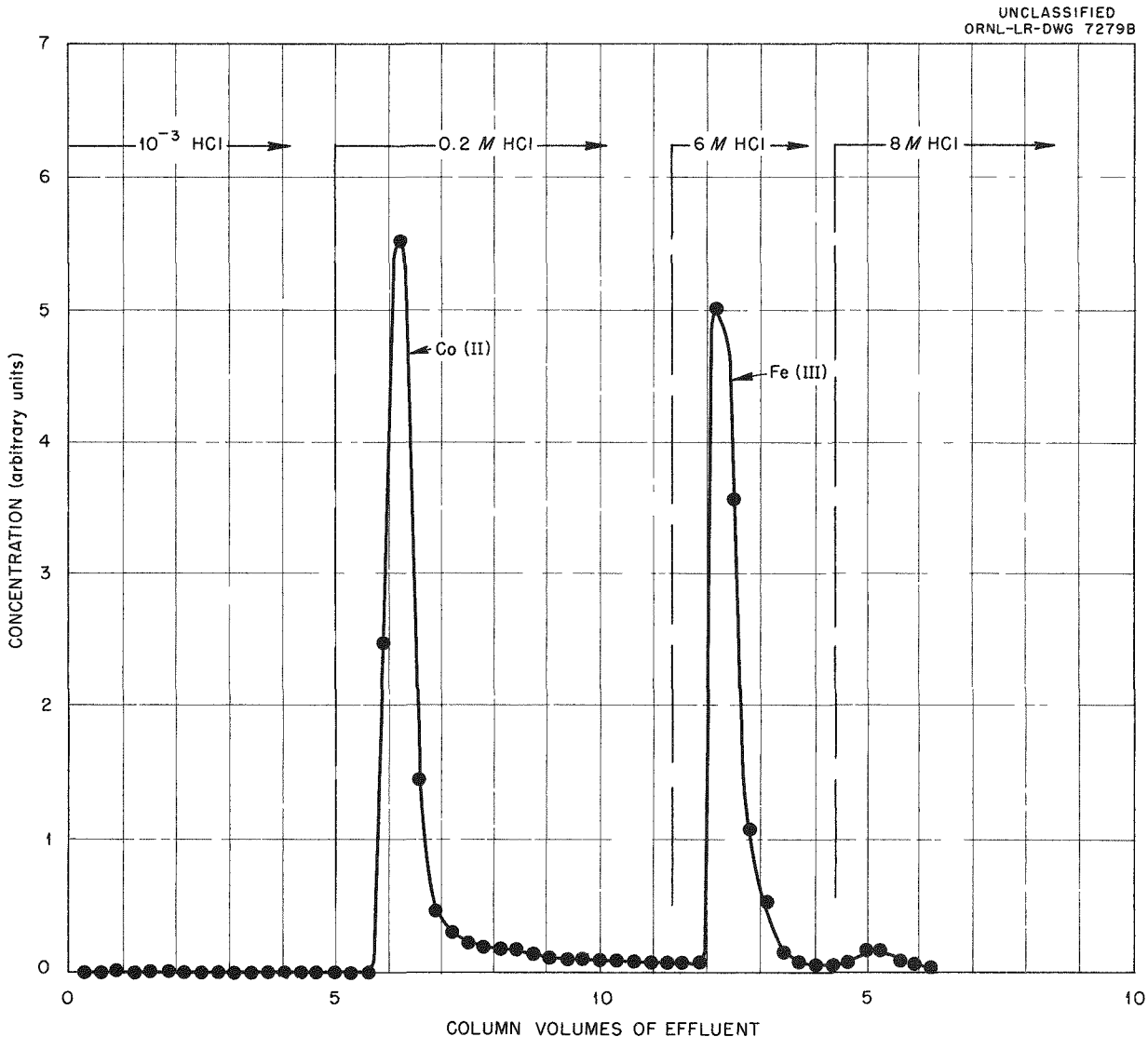

Fig. 20.6. Separation of Co(II) and Fe(III) on Zirconium Phosphate (Drying Temperature 78°C). Column 8 cm × 0.2 cm^2.

21. RADIATION STUDIES ON THORIUM NITRATE SOLUTIONS

C. J. Hochanadel

J. W. Boyle H. A. Mahlman

21.1 EFFECT OF TEMPERATURE

Studies of the radiation decomposition of thorium nitrate solutions containing enriched uranyl sulfate were extended[1] from 130 to 250°C. Samples contained in silica ampoules were thoroughly degassed before they were irradiated in beam hole 12 of the ORNL Graphite Reactor in an electrically controlled furnace. Each sample was preheated to the desired temperature before it was lowered into the reactor. The energy input was calculated from the thermal-neutron flux, which was monitored for each sample.

At elevated temperatures, thermal decomposition was evident from the deep-red color of the gas phase. The red color disappeared when the sample was cooled to room temperature. The intensity of the color at any given temperature was dependent on the $Th(NO_3)_4$ concentration. The red color probably does not indicate a very great increase in pressure over that from the vapor pressure of water. Within a probable uncertainty of 10 to 20 psi, the results from one measurement indicated the same pressure inside a stainless steel bomb containing 2.73 *m* $Th(NO_3)_4$ at 250°C as would arise from water alone.

Yields of hydrogen, nitrogen, and oxygen at elevated temperatures are listed in Table 21.1. The nitrogen yield appears to be independent of temperature at any fixed concentration and decreases slightly with increasing dose. As reported previously,[2] the nitrogen yield increases with increasing nitrate concentration.

The hydrogen yield appears to increase slightly with increasing temperature, but at any given temperature the yield decreases with dose. Examination of the table shows a poor material balance between the oxidants and reductants reported. Some of the discrepancy can be accounted for by

[1] J. W. Boyle and H. A. Mahlman, *Chem. Semiann. Prog. Rep. June 20, 1955*, ORNL-1940 (to be published).

[2] J. W. Boyle and H. A. Mahlman, *Chem. Semiann. Prog. Rep. Dec. 29, 1954*, ORNL-1832, p 69.

TABLE 21.1. IRRADIATION OF THORIUM NITRATE SOLUTIONS AT ELEVATED TEMPERATURES

$Th(NO_3)_4$ (*m*)	UO_2SO_4 (*M**)	Irradiation (min)	Temperature (°C)	Energy (ev per g of solution)	Fission Energy / Total Energy (%)	G_{H_2}**	G_{N_2}**	G_{O_2}**
7.59	0.0128	30	250	2.62×10^{20}	90.8	0.09	0.18	0.002
2.73	0.134	3	250	3.63×10^{20}	99.2	0.50	0.092	0.36
2.73	0.0128	15	250	1.77×10^{20}	92.7	0.54	0.10	0.30
2.73	0.0128	30	250	3.78×10^{20}	92.7	0.48	0.093	0.36
2.73	0.0128	45	250	5.76×10^{20}	92.7	0.44	0.078	0.37
2.73	0.0128	15	200	1.71×10^{20}	92.7	0.52	0.10	0.37
2.73	0.0128	30	200	3.45×10^{20}	92.7	0.46	0.090	0.37
2.73	0.0128	45	200	5.14×10^{20}	92.7	0.47	0.089	0.41
2.73	0.135	5	135	7.56×10^{20}	99.6	0.33	0.063	0.32
1.45	0.0125	30	250	4.55×10^{20}	93.1	0.78	0.054	0.40
1.57	0.135	10	135	17.0×10^{20}	99.6	0.51	0.035	0.34

*Molarity of $U^{235}O_2SO_4$ at room temperature (93.2% enrichment).

**Molecules per 100 ev.

the nitrous oxide and carbon dioxide found in each analysis. The amount of nitrous oxide was always low but measurable. The carbon dioxide usually was 3 to 10% of the total gas measured. The carbon dioxide apparently arose from the oxidation of some organic impurity present.

The solution 7.59 *m* in $Th(NO_3)_4$ had more carbon dioxide present than any other single component, which accounts for the very low oxygen yield observed. There also appeared to be a continuing evolution of acid gases after the gases had been pumped off and collected in the usual manner. The high nitrogen yield and the low hydrogen yield were in agreement with extrapolations of previous reports.[2]

21.2 EFFECT OF ACIDITY

Nitrite analyses of irradiated solutions of thorium nitrate have always been very low, a few micromoles per liter, or below the limits of detection. Studies with $NaNO_3$ solutions[1] showed that the production of nitrite is pH-dependent.

Table 21.2 gives hydrogen, oxygen, nitrogen, and nitrite (calculated and measured) yields for three samples that were irradiated in beam hole 10 of the ORNL Graphite Reactor.

The hydrogen yield appeared nearly constant over the pH range studied, as did the nitrogen yield. The fact that the molecular nitrogen yield remained constant as the nitrite yield increased indicates that the principal mode of molecular nitrogen formation was not from the nitrite ion. The calculated NO_2^- yield was obtained from the stoichiometry of the hydrogen and oxygen analysis.

TABLE 21.2. REACTOR IRRADIATION OF 5 *M* SODIUM NITRATE SOLUTIONS AT SEVERAL ACIDITIES

Sample	pH	G_{H_2}	G_{O_2}	G_{N_2}	$G_{NO_2^-}$ (Calculated)	$G_{NO_2^-}$ (Measured)
1	0.5 (H_2SO_4)	0.071	0.036	0.001	~0	
2	5.9	0.069	0.63	0.001	1.20	1.21
3	~11.0 (NaOH)	0.075	1.22	0.001	2.36	2.33